THE INFLUENCE OF MACROBENTHOS ON CHEMICAL DIAGENESIS OF MARINE SEDIMENTS

NOTICE

This report was prepared as an account of work sponsored by the United States Government. Neither the United States nor the United States Energy Research and Development Administration, nor any of their employees, nor any of their contractors, subcontractors, or their employees, makes any warranty, express or implied, or assumes any legal liability or responsibility for the accuracy, completeness or usefulness of any information, apparatus, product or process disclosed, or represents that its use would not infringe privately owned rights.

A Dissertation

Presented to the Faculty of the Graduate School

of

Yale University

in Candidacy for the Degree of

Doctor of Philosophy

by

Robert Curwood Aller

May 1977

DISTRIBUTION OF THIS DOCUMENT IS UNLIMITED

DISCLAIMER

This report was prepared as an account of work sponsored by an agency of the United States Government. Neither the United States Government nor any agency Thereof, nor any of their employees, makes any warranty, express or implied, or assumes any legal liability or responsibility for the accuracy, completeness, or usefulness of any information, apparatus, product, or process disclosed, or represents that its use would not infringe privately owned rights. Reference herein to any specific commercial product, process, or service by trade name, trademark, manufacturer, or otherwise does not necessarily constitute or imply its endorsement, recommendation, or favoring by the United States Government or any agency thereof. The views and opinions of authors expressed herein do not necessarily state or reflect those of the United States Government or any agency thereof.

DISCLAIMER

Portions of this document may be illegible in electronic image products. Images are produced from the best available original document.

ABSTRACT

THE INFLUENCE OF MACROBENTHOS ON CHEMICAL DIAGENESIS OF MARINE SEDIMENTS

Robert Curwood Aller
Yale University 1977

Diagenetic reactions involving the decomposition of organic matter and the dissolution, mobilization, and reprecipitation of metals sensitive to oxidation-reduction reactions, are most intense and rapid in the upper 1 m and especially the upper 10 cm of marine sediment. It is in this upper zone where most benthic organisms live and interact with sediments and where exchange rates of dissolved and particulate material between sediment and overlying water are largely determined. Knowledge of diagenetic processes taking place in this zone is therefore essential for understanding the chemistry of sediment, the chemistry of water overlying sediment, certain ecological interactions and adaptations of marine organisms, and the long term recording of historical information in marine deposits, for example: fossil preservation. Many investigators have recognized that the feeding, respiring, burrowing, and construction activities of marine bottom-living animals must influence early diagenesis but no systematic study of this possibility has been previously made. In this

thesis, the effects of animal-sediment interactions on selected aspects of early diagenesis are examined in detail.

Permanent tube-dwellings formed by sedentary benthos produce three dimensional gradients in pore water and solid phase chemistry of sediment and increase the flux of material into and out of a deposit. These tubes are hollow cylinders often extending several decimeters below the interface. There are specific effects on diagenesis created by the structure of a particular tube, the distribution of bacterial activity around it, and the way the burrow is maintained. There are also nonspecific effects which result simply from the change in the geometry of diffusion in the sediment created by the presence of a hollow tube held at close to sea water ion concentrations. Laboratory and field studies of Amphitrite ornata, a sedentary, surface deposit-feeding polychaete, and Clymenella torquata a sedentary, subsurface deposit-feeding polychaete, were used to investigate these processes in representative cases. The packing of mucus into tube walls and the providing of electron acceptors by irrigation promote bacterial metabolism, particularly sulfate reduction, around the burrow core. Direct or indirect products of decomposition in the wall: NH_4^+, $HPO_4^=$, HCO_3^-, HS^-, Fe^{++}, and Mn^{++} are either rapidly lost to overlying water by a combination of diffusion and irrigation or precipitated around the burrow. In the absence of irrigation the more stable of these ions rapidly build-up in burrow water. Reducing conditions and concentration

gradients around burrows result in migration of metals like Fe and Mn which are sensitive to oxidation-reduction reactions. The innermost lining of a burrow becomes rich in Fe, Mn-oxides which extract dissolved ions from sea water passed through the tube by irrigation. Fe-sulfides concentrate preferentially around this inner lining and because of repeated formation and oxidation, create conditions comparable in some ways to micro acid mine drainage in the burrow core. These concentration and migration processes cause the common occurrence of pyrite and hematite enveloped trace fossils.

Rather than constructing specific sediment structures which act as particular sites of diagenesis and exchange, mobile deposit feeders such as Yoldia limatula often homogeneously rework sediment. This results in a biogenically mixed layer near the sediment-water interface in which particles are transported at a rate faster than net sedimentation and pore water ions migrate more rapidly than can be accounted for by molecular diffusion. Because of this rapid exchange with overlying water, pore water ions produced by reactions in the sediment are lowered in concentration while those whose source is in overlying water are raised. Bacterial metabolism is stimulated as a result of this flushing and the rates of reactions associated directly or indirectly with the decomposition of organic matter are increased without a corresponding increase or decrease in standing concentrations of dissolved ions. As shown in laboratory experiments, this may mask the presence of certain reactions because of the lack of build-up of products or depletion of reactants in pore water. The

general effect of mobile deposit feeders is to speed the flow of material between chemical reservoirs within the sediment and overlying water. Different elements respond to the changes in the transport-reaction regime in accordance with their individual chemistry.

In Long Island Sound, U.S.A., both spatial and temporal trends in sediment chemistry and the flux of material out of the bottom, demonstrate the control of diagenesis by bottom fauna. Microbial metabolism dominates pore water chemistry during the late spring and summer, biogenic transport flushes the sediment during later summer and fall, and relict fall profiles altered by molecular diffusion and abiogenic reactions are characteristic of winter. This pattern is repeatable from year to year. The flux of NH_4^+, $HPO_4^=$, and Mn^{++} out of sediment varies seasonally and is higher than predicted by Fick's First Law (molecular diffusion, vertical dimension only) during the summer and fall. Fe^{++} is also released in abundance but its reactivity precluded accurate measurement and modeling of fluxes. High Mn^{++} and Fe^{++} fluxes aid in scavenging the water column of Fe, Mn-oxide seeking elements during reprecipitation on suspended particles. The NH_4^+ and $HPO_4^=$ fluxes supply $>$ 30% and 100% respectively of the daily N and P requirement of plankton. In winter, the fluxes of unreactive ions out of sediment generally agree with that predicted by molecular diffusion. It is shown that two dimensional diffusion based on an accurate consideration of the geometry of the system is a more conceptually correct (but less practically useful) description of pore

water transport in the bioturbated zone than the one dimensional model developed for use in anoxic basins or unbioturbated layers of sediment. Spatial patterns in pore water and solid phase chemistry and the magnitude of bottom fluxes reflect the composition of the bottom community in different regions of the Sound.

$^{234}Th/^{238}U$ disequilibrium studies demonstrate that particle reworking rates near the sediment-water interface vary both temporally and spatially in the Sound. The most rapid reworking occurs in protobranch-inhabited bottom areas as do the highest ^{234}Th inventories. Excess ^{234}Th profiles in the sediment allow determination of the rates of selected diagenetic reactions, such as Mn^{++} production, near the sediment surface. Both the ^{234}Th disequilibrium and flux measurements indicate that intra-estuarine redistribution of metals continually takes place.

ACKNOWLEDGEMENTS

Karl K. Turekian and Donald C. Rhoads encouraged and supervised this study. They influenced its development in many direct or subtle ways over the last five years. Robert A. Berner also played a dominant role in this work. I am grateful for the advice, tolerance, and friendship of each of these men.

When, as an undergraduate at the University of Rochester, I first became interested in the topics touched on in this thesis, Zeddie P. Bowen kindly accommodated in his laboratory the mud and worms I brought from the Genesee River. His early interest in me and his guidance eventually resulted in this thesis.

Martin B. Goldhaber presided over my baptism into pore water chemistry, aided in some of the crucial early work, and engagedme in many stimulating discussions. Josephine Y. Yingst worked with me on several projects in parts of this thesis and played an indispensable role in making things go. J. Kirk Cochran and Larry K. Benninger worked closely with me on radiochemical projects and offered up their valued opinions on many additional aspects of this work. G. Richard Holdren kindly let me use his computer program to calculate ion activities and constructively argued many hours with me. My thanks also to the geochemistry coffee-seminar group which, in addition to

those listed above, consisted over the years of the likes of: G. Brass, D. DeMaster, E. Dion, R. Dodge, W. Graustein, R. Kier, D. Lewis, C. Martens, Y. Nosaki, J. Rosenfeld, J. Thomson, and many others. They provided the general background murmurings or roar which make science fun and help one walk the straight and narrow.

H. Bokuniewicz, R. Gordon, and R. Hall made helpful comments on this work.

Robert Wells was an indispensable aid in the field and lab. He built many of the box cores used in this study, constructed the hot-point thermistor current meter, and drafted many of the early versions of figures used in the manuscript. J. Y. Yingst, William Ullman, and Mike Pimer were my major diving partners at one time or another on ~ 150 dives into Long Island Sound. J. Y. Yingst in particular accompanied me over two winter diving seasons. M. Pimer and Matt Reed were the able commanders of the boats in sampling.

Art Goodhue and Wally Phelps provided assistance in various construction or machining activities. Mrs. Dorothy Hildreth ably dealt with the bureaucratic machinery.

Many people have given of their time, in one way or another, in the actual preparation of the manuscript. These include: Ann Phelps, J. Yingst, Kokilam Subbiah, Dwight "Kee" Muschenheim, Nnenna Anigbro, Richard Dodge, Barbara Brockett, and William Sacco.

Ann Phelps typed the first drafts and the tables and Rosemary Garrison typed the final copy.

Financial support was provided predominately by ERDA grant EY-76-S-02-3573 (K. K. Turekian, principle investigator) and also by NSF grant GA-42-838 (D. C. Rhoads, principle investigator). Personal support was provided by an NSF Fellowship, a Yale Graduate Fellowship, ERDA grant EY-76-S-02-3573 and EPA grant R804-909-010 (D. C. Rhoads, principal investigator).

TABLE OF CONTENTS

	Page
ACKNOWLEDGEMENTS	ii
LIST OF TABLES	xi
LIST OF FIGURES	xiv
Chapter	
I. INTRODUCTION AND BACKGROUND	1
Patterns in animal-sediment interactions	2
Trophic groups	4
Life habit	5
Dependence of particle transport on tropic group and life habit	7
Biogenic fluid transport	9
Dependence of transport activity on life history, population structure, and temperature	12
Meiobenthos	15
Effect of macrobenthos on microorganisms	16
Diagenetic reactions related to biological activity	17
Study approach	18
II. BIOGEOCHEMISTRY OF THE TUBE-DWELLING OF A SEDENTARY POLYCHAETE: AMPHITRITE ORNATA (LEIDY)	32
The study animal	32
Study area	33
Sampling and methods	34
Solid phase analyses	35
Pore water analyses	38
Burrow water samples	39
Tidal flat water samples	40

TABLE OF CONTENTS--Continued

		Page
	Irrigation rate measurements	42
	Particle transport	43
	Results	43
	Burrow structure	43
	Irrigation, particle transport, and behavior	45
	Overlying water results	51
	Burrow water results	52
	Pore water concentrations around burrow	55
	Solid phase analyses	56
	Discussion	59
	Burrow structure	59
	Chemistry of water in the burrow	63
	Geochemical processes associated with the burrow wall	72
	Decomposition	72
	Mobilization of metals	86
	Summary	92
III.	EXPERIMENTAL STUDIES OF CHANGES PRODUCED BY DEPOSIT FEEDERS ON PORE WATER, SEDIMENT, AND OVERLYING WATER CHEMISTRY	118
	Methods	121
	Experiments with *Clymenella torquata*	121
	Experiments with *Yoldia limatula*	124
	Analytical techniques	126
	Results	129
	Clymenella experiment, pore water	129
	Clymenella experiment, overlying water	130
	Yoldia experiment, sediment description	131
	Yoldia experiment, pore water	132
	Yoldia experiment, solid phase properties	134
	Yoldia experiment, overlying water	135
	Discussion	136
	Clymenella experiment	136
	Iron and manganese distributions	138
	Transport rates by irrigation of permanent burrows	143
	Special features of the pore water profiles	148

TABLE OF CONTENTS--Continued

		Page
	Sediment-water exchange of NH_4^+ and $HPO_4^=$	149
	The effects of a mobile, deposit-feeder: *Yoldia limatula* on sediment diagenesis	151
	Production reactions in tank sediment	152
	Specific reactions following production	156
	Evaluation of equilibrium controls on tank pore water profiles	159
	Models of transport and kinetic controls on tank pore water profiles	161
	Alteration of transport mechanisms by the activities of *Yoldia*	166
	Specific effects of reworking on Mn	172
	Redistribution of organic matter	177
	Effects of reworking on Fe and Ca	178
	Influence of reworking by *Yoldia* on overlying water chemistry	183
	Summary	184
IV.	TRACKING PARTICLE ASSOCIATED PROCESSES IN A COASTAL ENVIRONMENT BY USE OF $^{234}TH/^{238}U$ DISEQUILIBRIUM	214
	Introduction	214
	Study areas	216
	Methods	218
	Results	221
	Core description	221
	Radiochemical results	222
	Discussion	223
	Particle mixing at NWC and DEEP	223
	Th inventories	235
	Uranium	236
	Summary	238

TABLE OF CONTENTS--Continued

		Page
V.	DIAGENETIC PROCESSES NEAR THE SEDIMENT-WATER INTERFACE OF LONG ISLAND SOUND, I: DECOMPOSITION AND NUTRIENT GEOCHEMISTRY (S, N, P)	249
	Introduction	249
	Location of study and station description	250
	Sampling	256
	Methods	258
	Treatment of cores	258
	X-ray samples	258
	Pore water and sediment samples	258
	Flux samples	261
	Decomposition experiments	263
	Analytical techniques	264
	General	264
	Pore water	265
	Solid phase	266
	Results	268
	Decomposition experiment	268
	Pore water results	272
	Gravity cores	272
	Box cores	273
	Flux measurements	276
	Solid phase analyses	277
	Discussion	279
	Decomposition reactions	280
	The supply of organic material	281
	Products of decomposition, solid phase	283
	Physically controlled transport processes	291
	Biogenic transport processes	292
	Biogenic particle reworking	293
	Biogenic fluid transport	298
	Seasonal dependence of biological and physical processes	299
	Seasonal and spatial variation in pore water profiles, general patterns	300
	Abiogenic reaction controls on profiles	306
	Modeling pore water distributions in the zone of bioturbation	319

TABLE OF CONTENTS--Continued

		Page
	Separate time dependence of D and R	321
	Horizontal and radial diffusion	327
	Material flux of N and P between sediment and overlying water in LIS	337
	Ammonia	342
	Phosphate	347
	Stoichiometry of decomposition	352
	Summary	356
VI.	DIAGENETIC PROCESSES NEAR THE SEDIMENT-WATER INTERFACE OF LONG ISLAND SOUND, II: Fe AND Mn	422
	Introduction	422
	Location and description of study area	423
	Sampling	424
	Treatment of cores	424
	Flux samples	427
	Excretion experiments	428
	Precipitation experiments	429
	Reduction-decomposition experiments	429
	Oxidation experiments	431
	Analytical techniques	433
	General	433
	Water analyses	434
	Solid phase analyses	435
	Results	436
	Pore water profiles, gravity cores	436
	Pore water profiles, box cores	437
	Solid phase	439
	Precipitation experiments	440
	Flux measurements	441
	Reduction-decomposition experiments	444
	Marsh sediment	444
	Mucus-limonite	444
	Oxidation experiments	445
	Excretion experiments	446

TABLE OF CONTENTS--Continued

	Page
Discussion	446
Production of dissolved Mn and Fe	447
Precipitation reactions and equilibrium controls	455
Seasonality of pore water profiles	462
Flux of Mn and Fe into overlying water	467
Solid phase distributions	478
Modeling Mn pore water profiles	493
Summary	497

Appendices

I.	DESIGN AND USE OF DIVER-TAKEN BOX CORES	534
II.	NOTES ON ANALYTICAL TECHNIQUES	541
III.	MACROFAUNA (> 1 mm) SIEVED FROM FLUX CORE BOXES	546
IV.	BOX CORE AND GRAVITY CORE DATA FROM LONG ISLAND SOUND	549
V.	FLUX CORE DATA	568

REFERENCES 573

LIST OF TABLES

Table I-1.	Particle Transport and Biodeposition Rates
Table I-2.	Fluid Transport Rates
Table I-3.	Fluid/solid Biogenic Transport Ratios
Table I-4.	Burrowing Rates
Table I-5.	Temperature Dependence of Macrofaunal Metabolic Activity
Table II-1.	Weight Percent Abundance of Particle Size Fractions in the Burrow Wall of Amphitrite ornata
Table II-2.	Fluid and Particle Transport Rates for Amphitrite ornata
Table II-3.	Tidal Flat Water Samples, Barnstable Harbor
Table II-4.	Burrow Water of Amphitrite ornata
Table II-5.	Pore Water Analysis Around Amphritite Burrows
Table II-6.	Burrow Solid Phase Analyses
Table III-1.	Clymenella Tank Experiment: Pore Water Results
Table III-2.	Clymenella Tank Experiment: Overlying Water
Table III-3.	Yoldia Tank Experiment: Pore Water and Sediment
Table III-4.	Yoldia Tank Experiment: Overlying Water
Table III-5.	Solubility Products at 25°C for Selected Compounds

LIST OF TABLES--Continued

Table III-6.	Yoldia Experiment Pore Water: Log(IAP/K) for Selected Phases
Table IV-1.	Deep ^{234}Th-^{210}Pb Core (October 23, 1975; T = 17°C) Radiochemical Results
Table V-1.	Long Island Sound Station Location and Description
Table V-2.	Sampling Schedule
Table V-3.	Flux Measurements, NH_4^+ and $HPO_4^=$
Table V-4.	Solubility Products at 25° for Selected Phosphate and Carbonate Compounds
Table VI-1.	Precipitation Rate Experiment, Fe and Mn
Table VI-2.	Flux Measurements, Fe and Mn
Table VI-3.	Decomposition Experiments--Marsh Sediment
Table VI-4.	Decomposition Experiments--Mud + Mucus + Limonite
Table VI-5.	Oxidation Experiment--Pyrite-FOAM
Table VI-6.	Oxidation Experiment--NWC Sediment
Table VI-7.	Solubility Products for Selected Sulfide and Carbonate Compounds
Table AI-1.	Dimensions of Box Cores
Table AIII-1.	Faunal Samples (≥ 1 mm)
Table AIV-1.	Box Core Data FOAM-1
Table AIV-2.	Box Core Data FOAM-2
Table AIV-3.	Box Core Data FOAM-3

LIST OF TABLES--Continued

Table AIV-4. Box Core Data FOAM-4

Table AIV-5. Box Core Data FOAM-5

Table AIV-6. Box Core Data NWC-1

Table AIV-7. Box Core Data NWC-2

Table AIV-8. Box Core Data NWC-3

Table AIV-9. Box Core Data NWC-4

Table AIV-10. Box Core Data NWC-5

Table AIV-11. Box Core Data NWC-6

Table AIV-12. Box Core Data DEEP-1

Table AIV-13. Box Core Data DEEP-2

Table AIV-14. Box Core Data DEEP-3

Table AIV-15. Gravity Core Data FOAM-G

Table AIV-16. Gravity Core Data NWC-G

Table AIV-17. Gravity Core Data DEEP-G

LIST OF FIGURES

Figure I-1. Schematic breakdown of functional types of animals present on or in marine sediments.

Figure II-1. Sampling locations in Barnstable Harbor, Massachusetts

Figure II-2. Diagrammatic representation of radial and vertical sample zones of a burrow for solid phase and pore water analysis.

Figure II-3. General shape of Amphitrite burrow, cross section of burrow wall, and blow-up of single layer of wall.

Figure II-4. X-radiograph of one leg of burrow.

Figure II-5. Grain size distribution in samples from radial and vertical sample zones for solid phase analysis. Weight percent abundance plotted.

Figure II-6. Illustrative velocity patterns of water flow into and out of burrows.

Figure II-7. Tidal flat water compositions during ebb as a function of Cl^- concentration.

Figure II-8. Burrow water concentrations of NH_4^+, $HPO_4^=$, and Fe as a function of time after exposure by tide.

Figure II-9. Radial and vertical patterns of pore water alkalinity and NH_4^+ around Amphitrite burrow.

Figure II-10. Radial and vertical patterns of dissolved Fe and Mn associated with burrow.

Figure II-11. Ignition loss (~ organic matter) patterns in burrow sample zones.

LIST OF FIGURES--Continued

Figure II-12. Acid volatile sulfur (~ FeS) and pyrite sulfur (FeS_2) in burrow wall zones and surrounding sediment.

Figure II-13. Fe, Mn, and Zn distributions in burrow wall and ambient sediment (< 74 μm size fraction) demonstrating enrichment patterns.

Figure II-14. NH_4^+ versus titration alkalinity plot used in calculations in text. Line determined by least squares method fit to data; surface not used.

Figure III-1. Sketches of Clymenella torquata and Yoldia limatula.

Figure III-2. Tank set-up used in Clymenella experiment (plan view).

Figure III-3. Pore water Fe and Mn profiles from tanks 1, 2, 3.

Figure III-4. pH profiles from tanks 1, 2, 3.

Figure III-5. pH, $HPO_4^=$, and NH_4^+ concentrations in overlying water in tanks used in Clymenella experiment. Clymenella added after 15 days to tanks 3 and 4.

Figure III-6. Fe and Mn concentrations in overlying water in tanks 1, 2, 3, 4. Clymenella added after 15 days to tank 3 and 4.

Figure III-7. Pore water sulfate, alkalinity, NH_4^+ and $HPO_4^=$ profiles from Yoldia experimental tanks.

Figure III-8. Pore water Ca, pH, Mn,and Fe profiles from Yoldia experimental tanks.

Figure III-9. ATP and % organic matter profiles from Yoldia experimental tanks.

Figure III-10. Solid phase Mn profiles in Yoldia experimental tanks.

Figure III-11. Alkalinity, Mn, NH_4^+, and $HPO_4^=$ concentrations in Yoldia experimental tanks with time.

LIST OF FIGURES--Continued

Figure III-12. X-radiograph of 2.5 cm thick sediment slab showing natural density of Clymenella and capitellid tubes at Calves Pasture Point, Barnstable Harbor, Massachusetts (June 29, 1974).

Figure III-13. Nonsteady state diffusion-reaction model fit to pore water NH_4^+ profile of Yoldia experiment control tank.

Figure III-14. Nonsteady state diffusion-reaction model fit to pore water $HPO_4^=$ profile of Yoldia experiment control tank.

Figure III-15. Composite layer, steady state model showing effect of increasing diffusion rates or changing both diffusion and reaction rates in a two layer system.

Figure III-16. Composite layer steady state model showing effect of an exponentially decreasing reaction rate in two layer system rather than constant reaction rates in each zone as illustrated in Figure III-15.

Figure III-17. Nonsteady state-equilibrium composite model showing hypothetical sequence of pore water Mn and alkalinity profiles which may have occurred through time in the tanks.

Figure IV-1. Location of stations NWC and DEEP in Long Island Sound.

Figure IV-2. Box core x-radiograph at NWC.

Figure IV-3. Box core x-radiograph at DEEP.

Figure IV-4. X-radiograph of sediment slab from DEEP analyzed radiochemically.

Figure IV-5. % H_2O, % ignition loss, $^{234}Th_{xs}$, and U/Th weight ratio profiles at NWC and DEEP.

LIST OF FIGURES--Continued

Figure V-1. Location of Long Island Sound and stations: FOAM, NWC, and DEEP in central basin.

Figure V-2. Cross-section of central basin through approximately 72° 53' with thickness of marine mud deposits outlined (after Bokuniewicz, Gebert, and Gordon, 1976). Stations are passed onto this single plane illustrating relative position with respect to bathymetry and long term deposition.

Figure V-3. Schematic drawing of major fauna at FOAM.

Figure V-4. Schematic drawing of major fauna at NWC.

Figure V-5. Schematic drawing of major fauna at DEEP.

Figure V-6. X-radiograph of vertical sediment section at FOAM.

Figure V-7. Parts of two vertically oriented x-radiographs taken at FOAM.

Figure V-8. Vertically oriented x-radiograph illustrating sedimentary features typical of NWC.

Figure V-9. X-radiograph of horizontal slab of sediment 10-15 cm deep from NWC.

Figure V-10. Vertical x-radiograph from DEEP.

Figure V-11. Large burrow formed by unknown organism is seen in center of this x-radiograph from DEEP.

Figure V-12. Seasonal temperature variation at NWC over three year period.

Figure V-13. $SO_4^{=}$ and NH_4^{+} concentration in sediment from discrete depths at NWC versus time of sampling (enclosure) in decomposition experiment.

Figure V-14. $SO_4^{=}$ and NH_4^{+} concentration in decomposition experiment samples from NWC versus time of enclosure. T = 4°C.

LIST OF FIGURES--Continued

Figure V-15. $SO_4^=$ and NH_4^+ concentration in decomposition experiment samples from DEEP versus time of enclosure. $T^o = 22\,^oC$.

Figure V-16. The rate of $SO_4^=$ reduction obtained from decomposition experiments as a function of depth in sediment.

Figure V-17. Rate of NH_4^+ production ($R_N/(1 + K)$) obtained from decomposition experiments as a function of depth in sediment at NWC and DEEP. Data uncorrected for adsorption.

Figure V-18. Ratio of $SO_4^=$ reduction rate to NH_4^+ production rate (no adsorption correction) as a function of $SO_4^=$ reduction rate.

Figure V-19. Pore water profiles of $SO_4^=$, NH_4^+, $HPO_4^=$, and alkalinity at FOAM, NWC, and DEEP (gravity cores).

Figure V-20. Ca^{++} concentration in pore water as a function of depth at FOAM, NWC, and DEEP (gravity cores).

Figure V-21. Seasonal pore water $SO_4^=$ profiles from box cores at FOAM.

Figure V-22. Seasonal pore water $SO_4^=$ profiles from box cores at NWC.

Figure V-23. Seasonal pore water $SO_4^=$ profiles from box cores at DEEP.

Figure V-24. Seasonal pore water alkalinity profiles from box cores at FOAM.

Figure V-25. Seasonal pore water alkalinity profiles from box cores at NWC.

LIST OF FIGURES--Continued

Figure V-26. Seasonal pore water alkalinity profiles from box cores at DEEP.

Figure V-27. Seasonal pore water ammonia profiles from box cores at FOAM.

Figure V-28. Seasonal pore water ammonia profiles from box cores at NWC.

Figure V-29. Seasonal pore water ammonia profiles from box cores at DEEP.

Figure V-30. Seasonal pore water phosphate profiles from box cores at FOAM.

Figure V-31. Seasonal pore water phosphate profiles from box cores at NWC.

Figure V-32. Seasonal pore water phosphate profiles from box cores at DEEP.

Figure V-33. Ca/Cl molar ratios during fall (solid lines) and winter (dashed lines) at FOAM, NWC, and DEEP.

Figure V-34. Plot of NH_4^+ and $HPO_4^=$ released versus time in flux cores from NWC.

Figure V-35. Ignition loss profiles from selected cores from FOAM (Goldhaber et al., 1977), NWC, and DEEP.

Figure V-36. Comparison of acid volatile sulfide (FeS) profiles at FOAM, NWC, and DEEP.

Figure V-37. Seasonal variation in acid volatile sulfide profiles at NWC. Lowest values near interface occur during winter.

Figure V-38. Total non-volatile sulfur ($FeS_2 + S^o$) profiles at FOAM, NWC, and DEEP.

Figure V-39. Seasonal profiles of total non-volatile sulfur ($FeS_2 + S^o$) at NWC. A possible minor decrease in interface sulfur during fall and winter is detectable.

Figure V-40. Total nitrate-nitrite profiles at FOAM, NWC, and DEEP at different times of year.

Figure V-41. Plot of the functions which describe the relative seasonal temperature dependence of macrofaunal and microbial activity.

Figure V-42. Plots of -logIAP versus depth at each station for selected solid phases: whitlockite ($Ca_3(PO_4)_2$) and vivianite ($Fe_3(PO_4)_2 \cdot 8H_2O$).

Figure V-43. Plots of -logIAP versus depth at each station for the phases: reddingite ($Mn_3(PO_4)_2 \cdot 3H_2O$) and $CaCO_3$.

Figure V-44. pPO_4 versus pS for upper 8 cm at FOAM, NWC, and DEEP where pS was detectable.

Figure V-45. Seasonal change in pore water NH_4^+ profiles predicted by numerical model discussed in text.

Figure V-46. Geometrical analogues for diffusion in the zone of biogenic reworking.

Figure V-47. Comparison of vertical pore water profiles predicted from steady state transport-reaction models where only radial diffusion into burrows at a given depth is considered (solid lines) and where only vertical diffusion is considered.

Figure V-48. The flux of NH_4^+ out of bottom sediment as a function of temperature (season) at FOAM, NWC, and DEEP.

LIST OF FIGURES--Continued

Figure VI-1. Pore water Fe^{++} and Mn^{++} profiles from gravity cores at FOAM, NWC, and DEEP.

Figure VI-2. Seasonal change in pore water Mn^{++} profiles in box cores from FOAM.

Figure VI-3. Seasonal change in pore water Mn^{++} profiles in box cores from NWC.

Figure VI-4. Seasonal change in pore water Mn^{++} profiles in box cores from DEEP.

Figure VI-5. Seasonal change in pore water Fe^{++} profiles in box cores from FOAM.

Figure VI-6. Seasonal change in pore water Fe^{++} profiles in box cores from NWC.

Figure VI-7. Seasonal change in pore water Fe^{++} profiles in box cores from DEEP.

Figure VI-8. Distribution of Mn and Fe in solid phase at NWC showing lack of seasonal variation for Mn and ability to repeat gross features of solid phase distribution in separate samples.

Figure IV-9. Fe and Mn solid phase distribution at FOAM and NWC. Dashed lines represent concentration on a $CaCO_3$-free basis at FOAM.

Figure IV-10. Examples of solid phase Cu profiles at FOAM (Goldhaber et al., 1977), NWC, and DEEP.

Figure IV-11. Semi-log plot of dissolved Fe in sea water versus time after collection (Lewin and Chen, 1973; T = 10°) or after separation of water from underlying sediment in flux core (T = 22°).

Figure IV-12. Amount of Mn^{++} and Fe^{++} released from flux core sediment versus time after collection.

Figure VI-13. Concentration of Mn^{++} (open circles) as a function of time in decomposition experiment using marsh sediment.

Figure VI-14. Concentration-time plots of $SO_4^{=}$ and Fe^{++} in the mucus + mud + limonite experiment.

Figure VI-15. Fe^{++} concentration in overlying water versus time of resuspension in pyrite--FOAM sediment oxidation experiment.

Figure VI-16. Fe^{++} concentration in overlying water versus time of resuspension of NWC sediment from 0-1 cm in oxidation experiment.

Figure VI-17. Alkalinity of overlying water versus time of resuspension of NWC sediment from different depth intervals.

Figure VI-18. Plots of -logIAP for solid phases: FeS and $FeCO_3$ as a function of depth in sediment at FOAM, NWC, and DEEP.

Figure VI-19. Plots of -logIAP for solid phases: MnS and $MnCO_3$ as a function of depth in sediment at FOAM, NWC, and DEEP.

Figure VI-20. Mn^{++} flux out of bottom sediment at each station as a function of temperature (season).

Figure VI-21. Solid phase distribution predicted by transport-reaction model (open circles) compared to Mn distribution of core NWC-2.

Figure VI-22. June-July Mn^{++} pore water profile predicted from transport-production model described in text.

Figure AI-1. The hand-held, diver-operated box corer with details of construction.

DEDICATION

This dissertation is dedicated to my parents:

James Curwood Aller and Mary Matilda Bramble Aller

CHAPTER I

INTRODUCTION AND BACKGROUND

In soft-bottom marine sediments, abrupt changes in mass properties and physical-chemical processes take place in the zone just beneath the sediment-water interface (Moore, 1931a, b). Biological activity shows equally abrupt changes in distribution near the sediment surface and has long been recognized as a major modifier of processes occurring there (Richter, 1927; Schwarz, 1932; Dapples, 1942; Hayes, 1964). Large (>1 mm), bottom-dwelling invertebrates contribute to these modifications by influencing fluid and solid phase transport within a sedimentary deposit. The resulting biogenic reworking or bioturbation of sediment by benthos has been well studied with respect to the changes it can produce in physical properties of a deposit (Rhoads, 1974); but, in part because of sampling and analytical problems, until recently little attention has been given to changes in chemical processes caused by animal-sediment interactions of this kind. In this study, I examine how large, bottom-dwelling animals, in concert with microbial activity, influence the distribution and rate of diagenetic reactions related to the decomposition of organic matter near the sediment-water interface and the exchange of material between sediment and

overlying water. The geochemical consequences and ecological significance of these effects are considered over several size scales: ranging from the sedimentary microenvironment surrounding an individual organism to the integrated effects of animal communities on diagenesis in associated sedimentary facies.

Patterns in animal-sediment interactions

Animals greater than 0.5-1.0 mm in size that live on the sea-floor are commonly referred to as macro or megabenthos. Invertebrate macrobenthos, the most abundant macroorganisms, can be differentiated into subgroups on the basis of either taxonomy or ecology. Both differentiations are useful in understanding or predicting the way in which a given animal or assemblage of animals interacts with sediment.

Morphology places limits on animal-sedimentary particle interaction. Types of appendages, body shape, and presence or absence of hard parts determine the potential of an animal to live in sediment of different kinds and to ingest or otherwise manipulate it (Yonge, 1954). These same qualities determine the kind of dwelling, such as a tube, an animal may require for protection and body support.

The physiological adaptations of a taxonomic group help determine its presence or absence in certain environments (Kinne, 1967), for example: transitional salinity regions such as estuaries or low oxygen habitats such as silled basins. Respiratory requirements in particular and the behavioral adaptations

developed for fulfilling those requirements are, as discussed below, important in influencing transport of fluids in sediment.

Ecological categorizations of marine benthos are often based on observed functional associations of an animal with the sedimentary habitat. The two major characteristics used to separate marine benthic invertebrates are: (1) trophic or feeding type and (2) life habit. The first refers to how and where an animal obtains food. The second, used in its broadest sense, refers to the relative mobility and the location-position of an animal in the sediment. Together these two characteristics qualitatively describe the ability of a given animal to process or redistribute sedimentary particles and, to an extent, fluids. If animals of a given feeding--group and life habit were randomly distributed in space and time, it would not be useful to interpret sedimentary processes in terms of the presence or absence of animals belonging to different ecological categories. In fact, these groups are not randomly distributed in either space (Sanders, 1956, 1958; Turpaeva, 1957; Rhoads and Young, 1970; Jumars and Fauchald, 1977) or time (Eagle, 1973; Myers, 1973; McCall, 1976). Because of this, it is useful to know how ecologically separable groups of benthos differ in their distribution and in their interaction with sediments in order to best interpret and generalize measurements of diagenetic processes related to their activities.

Trophic groups

Based on the way in which they obtain food, macrobenthos can be categorized into suspension feeders, deposit feeders, browsers, scavengers, and carnivores (e.g., Walker and Bambach, 1974). The differences between these groups are not always clear cut and many animals are facultative with respect to feeding-type, but the distinctions have been found to be relatively useful. Both suspension and deposit feeders are dependent on sedimentary particles and associated bacteria or plankton rich detritus for nourishment (e.g., Levinton, 1972). Suspension feeders are adapted to processing a high ratio of fluids to solids and feed on suspended particles in the water column proper by use of filtering or particle-capture mechanisms of various types. Suspension feeders are sometimes classed into subgroups based on how far above the sediment-water interface they feed (Turpaeva, 1957). Deposit feeders are adapted to processing a high ratio of solids to fluid and feed on particles deposited on the sediment surface or at depth. Both groups consume a high ratio of mineral to organic material and utilize particles much smaller than body size. On the basis of where they feed and how selective they are of particle sizes which are ingested, deposit feeders are sometimes classified into the self-explanatory categories of selective or non-selective surface or subsurface deposit feeders. The term browser refers to commonly herbivorous animals that crop surfaces which are large relative to the size of the animal. Scavengers are those animals that feed on parts of dead organisms and can be thought of as processing a high

ratio of organic matter relative to mineral particles compared to suspension feeders and deposit feeders. Carnivores feed directly on other living animals of relatively comparable size after active predation.

Life habit

Animals can live above or below the sediment-water interface and depending on where they spend the most time are referred to as epifaunal or infaunal respectively. In either location, an organism may be mobile (vagile), or relatively immobile (sedentary). The exact orientation of an animal with respect to the interface and the relative mobility of the animal describe its life habit.

The common combinations of trophic group and life habit together with the bottom type on or in which animals of each type usually occur are listed in Figure I-1 (based largely after Newell, 1970; Walker and Bambach, 1974). In Figure I-1, relative bottom stability refers both to physical disturbance such as current shifting of bottom sediments and biological distrubance such as reworking activities. Sand and mud deposits are the most important bottom types in the sense that they are the most abundant, all trophic groups are represented in these soft bottoms, and diagenetic reactions involving organic matter decomposition occur and are most readily studied there. Browsers are found on sands and muds only in the case where algal mats, grasses, or massive benthic algae are present and will not be considered further.

Within the general sand-mud facies complex, it has been found that under certain conditions particular combinations of suspension and deposit-feeding trophic groups, life habits, and life histories rarely occur together or that one functionally similar group of animals far outnumbers all others. The general patterns are as follows: (1) Suspension feeders are often more common than deposit feeders in well-sorted sands. (2) Deposit feeders are often more common than suspension feeders in regularly disturbed muds. (3) Mixed trophic groups occur in stable muddy sands or muds; if organic supply is low, surface deposit feeders are more plentiful than subsurface feeders and potential mobility of both types increases. (4) Mobile animals are more common than sedentary animals in mobile sediments. (5) Large, long-lived sedentary animals occur most commonly in regions of stable sediments or low sedimentation and resuspension. (6) Fluctuating populations of small, short-lived sedentary and mobile animals of mixed trophic type occur in muddy sands or muds which are intermittently and irregularly disturbed on the same time scale as time to reproduction. Explanations or documentations for some of these patterns have been put forth by many investigators (e.g., Sanders, 1956, 1958; Purdy, 1964; Seilacher, 1964; Nesis, 1965; Neyman, 1968; Rhoads and Young, 1970; Rhoads, 1974; Stanley, 1974; Stanley, 1970; Myers, 1973; Aller and Dodge, 1974; McCall, 1976; Jumars and Fauchald, 1977). Carnivores and scavengers are less abundant than either suspension or deposit feeders and are assumed to be ubiquitous.

Dependence of particle transport on trophic group and life habit

The redistribution of sedimentary particles by macrobenthos is one of the major biogenic processes occurring in or on a deposit. Particle transport takes place during feeding, burrow construction, and locomotion. Feeding involves: the extraction of particles from the zone of feeding, sorting and ingestion or rejection of the particles, and defecation of the particles, now packaged into a mucus-laden fecal pellet or mass, at the interface. Pellets may also be packed as waste stow in vacated burrow galleries (Seilacher, 1967). In the case of suspension feeders, feeding results in a net extraction of fine particles from the water and their sedimentation at the interface; a process referred to as biodeposition (Havens and Morales Alamo, 1966). The case of deposit feeders is more complex. Surface deposit feeders move particles horizontally at the interface; subsurface deposit feeders transport ingested particles vertically, and particles overlying the feeding zone fall downward to fill the resulting void. If a special size class of particles or particles of a particular property are transported in this way, inhomogeneities of various types can be created horizontally or vertically in the sediment (Darwin, 1894; Van Straaten, 1952; Schäfer, 1962; Rhoads and Stanley, 1966; Davis, 1974). If feeding is nonselective, the sediment is homogenized to the depth of feeding.

Members of all trophic groups may construct permanent or temporary burrows. Biogenic shafts can extend several meters into sediment as in the case

of some crustaceans but more generally are restricted to the upper 100 cm. These structures play two roles in particle transport: (1) once vacant they act as one-way conduits to depth for surface particles which fall in and (2) they are often formed of highly selected sedimentary material and represent an aggregation of sorted particles compared to ambient sediment. Excepting crustaceans, long-lived sedentary benthos form the deepest and largest burrows commonly found. Burrows may be highly specialized and geometrically intricate depending on the exact mode of feeding by the animal involved and the habitat in which they occur (Seilacher, 1964; Röder, 1971).

Mobile epifaunal benthos constantly form tracks, trails, and small scale depressions at the sediment surface. The effect is to plow and furrow sediment on a microscale (upper 0.5-1 cm). Mobile infauna such as errant polychaetes or naticid gastropods may continuously form new burrows by moving horizontally through sediment. The effect of this movement in the absence of other particle redistribution is to mildly randomize or sometimes homogenize sediment after a long period of steady burrowing (Schäfer, 1962). Other mobile infauna may form temporary burrows and periodically reestablish them in a new location or produce temporary extensions of a more permanent burrow. This group simulates the effects of both sedentary organisms and mobile in- and epifauna.

The dependence of biogenic particle transport on the type of animal present serves to illustrate that the abundance of organisms per se is not a good indicator of particle mixing rates. The presence of a key species, few in

number but great in effect, may radically alter biogenic reworking rates from what would take place in its absence (Rhoads, 1963; Rhoads and Young, 1970; Aller and Dodge, 1974).

Rates of particle reworking resulting from feeding (feces and pseudofeces) have been determined for many animals. Species representing major taxonomic, life habit, and trophic groups are listed with their measured reworking rates in Table I-1. Several patterns are evident: (1) suspension feeders have lower rates than deposit feeders, (2) mud dwellers have lower rates than sand dwellers, and (3) animals occurring at low population abundance have higher reworking rates than animals occurring at high abundance. The first two are due to the fact that richer food sources are available to the reworkers having the lower rates in each case and the third is related to size as discussed below.

Biogenic fluid transport

In addition to transport of particles animals also transport fluids into and out of sediments. This can occur in two ways: (1) regular transport of water related to predictable activity such as respiration, release of gametes, release of dissolved wastes, or feeding; or (2) irregular exchange of overlying water with sediment during random burrowing activity. All infauna engage in the first while only mobile infauna are important in the second type. Regular pumping activity by burrow-dwelling animals which exchanges burrow with overlying water is referred to as irrigation (Mangum, 1964) and has been studied quantitatively for many years by physiologists (e.g., Lindroth, 1938).

In this study both regular and irregular exchange of sedimentary water with overlying water will be termed irrigation; regular pumping activity will usually be referred to as respiratory irrigation or 'regular irrigation.'

Regular irrigation rates related to respiration, or fluid transport related to both feeding and respiration in the case of suspension feeders, have been listed by species in Table I-2. Common values are 10-100 ml/hr/individual for deposit feeders of all life habits and 100- >1000 ml/hr/individual for suspension feeders. Because regular irrigation is related to respiration and therefore the utilization of organic material, the rate of fluid transport has at least a partial relation to particle transport rates associated with feeding. The exact ratio of fluid to particle transport rates will depend on the oxygen content of overlying water, the respiratory adaptations of the animal, the food content of the particles, the turbidity of water in the case of suspension feeders and whether many more particles are manipulated than actually ingested (pseudofeces). Despite these complications the weight/weight ratios of regular fluid to solid transport vary within well defined bounds for deposit feeders at 100-500 (Table I-3). Suspension feeders seem to have ratios of ~100,000-1,000,000.

Irregular fluid, or particle, transport due to burrowing is much harder to estimate. A rough limit can be made by multiplying an average burrow cross-sectional area times the burrowing rate to obtain a volume per unit time.

This volume per unit time can be converted to either a particle reworking rate if bulk density is known (Howard and Elders, 1970; Myers, 1973) or a minimum fluid exchange rate due to new burrow formation. Examples of this type of calculation are given in Table I-4. Rates seem to lie within the range 0.01-1.0 cc/hr/individual or about a 100 to 10,000 times smaller than respiratory fluid transport. Locomotion alone is therefore not as important as respiratory irrigation in introducing large volumes of water into sediment; its chief effect will be in introducing irrigation water into fresh regions of the sediment along new burrow galleries. At bulk densities of ~0.5 g/cc particle displacement during burrowing is about 10 times that due to feeding (by weight), but the distance of particle transport differs greatly in the two instances. Except during occasional excavation of a large relatively permanent burrow, regular burrowing moves particles only a small distance ~0.1-1 cm while regular feeding transports particles 1- > 60 cm.

The potential influence of biogenic fluid transport on sediment pore waters depends strongly on taxonomy and life habit of the animals involved. Infaunal animals that bear hard parts or pump water predominately into and out of a tissue-enclosed body cavity (e.g., many bivalves) will effect little contact and exchange of overlying water with sediment except by indirect leakage out of body openings (e.g., pedal gape in some bivalves). Infaunal, soft-bodied animals such as polychaetes must circulate water over the exterior of the body and therefore all water passing over the body surface must also contact a

sediment surface. The effectiveness of this contact in producing exchange depends on the characteristics of the burrow wall, for example: is it sealed with an impermeable membrane or not? This must be determined in any given case. Nevertheless, as a general rule soft bodied animals will be more effective than shelled animals in exchanging overlying water with sedimentary water by regular irrigation. No such difference exists in the case of irregular irrigation due to burrowing.

Life habit and trophic group affect potential fluid exchange in several obvious ways: (1) Infaunal animals are more important than epifauna in exchanging pore waters with overlying water. (2) Mobile animals are more important than sedentary ones in homogeneously mixing and exchanging sediment by burrowing activity. (3) Sedentary animals are important in constructing specific long term sites of exchange, for example: burrow shafts, which may result in unique conditions around burrows. (4) Subsurface deposit feeders also transport pore fluids during feeding; this transport must be on the order of $F \cdot \frac{w}{1-w}$, where F = feeding rate in g dry wt/time and w = % water by weight, but information on ingestion of pore fluids by deposit feeders is lacking.

Dependence of transport activity on life history, population structure, and temperature

Animals having short life spans are often numerous ($>1{,}000/m^2$), small, and restricted to living and feeding near the sediment-water interface

(Grassle and Grassle, 1974; McCall, 1976). Their influence on sediments through biogenic reworking will tend to be intense but also restricted to near the interface (1-2 cm), (e.g., Myers, 1973). Longer-lived animals can be relatively large, few in number, and deep-burrowing; of course, there are exceptions (restricted mainly to the deep-sea) where very old animals are quite small (e.g., Turekian et al., 1975). In the case of large, deep burrowers, reworking of particles to the depth of burrowing is much more heterogeneous in space than for smaller, younger, and more numerous animals and may be quite slow when averaged over the total volume of inhabited sediment.

Young animals are commonly more active in reworking per unit body weight than older animals of the same species (Jørgensen, 1966; Budnova, 1972; Driscoll, 1975) and, during growth, the depth pattern of reworking or burrow formation may also undergo continuous change (Hertweck, 1970; Whitlatch, 1974). Young animals are usually more numerous and smaller than older ones as well. The relative effect of these intraspecific age-size distributions on reworking activity is then very similar to that described above for interspecific ones. This means that irrespective of other factors there will be a seasonality in the reworking patterns of sediment related to recruitment and growth of new year classes of animals; biogenic reworking will affect deeper sediment at a slower average rate as the mean age (size) of a given population increases. Seasonality in death patterns will also influence temporal changes in reworking.

Poikilothermic animals such as benthic invertebrates are less active at lower than at high temperatures (e.g., Prosser and Brown, 1961). A certain amount of acclimation can take place so that animals accustomed to a low temperature will tend to have a higher metabolic rate at that temperature than another group placed suddenly in a lower temperature environment than it is acclimated to. These hysteresis effects in temperature response based on history of temperature exposure complicate but do not greatly alter the basic pattern of low temperature--low metabolic rate, high temperature-high metabolic rate for a given species at a given latitude (e.g., Mangum, 1963). Temperature dependence of activity can be described by an apparent activation energy or Q_{10} (the number of times slower [faster] activity is for a drop [rise] in temperature of 10°C). Q_{10}'s for several species important for sediment reworking activity along the east coast of North America are listed in Table I-5. For the normal temperature range of ~ 20°C, found in estuaries along the northeast coast of North America, a rate decrease in reworking activity of about four times can be expected from late summer to late winter due to temperature alone.

In summary, feeding group and life habit influence the kind of biogenic transport processes taking place in sediment and the spatial (vertical and horizontal) distribution of these processes. Life history patterns, population abundance, age-size distributions, and temperature help determine the rate, depth in sediment, and temporal distributions of reworking. These features are

not random and can be correlated with depositional environment.

Meiobenthos

There is little information on the reworking activity of organisms smaller than macrobenthos but larger than bacteria, for example: nematodes. These meiobenthic organisms are in abundance only in the upper 1-2 cm of muds (Moore, 1931a; Mare, 1942) but may occur to depths of 50-60 cm in coarse sands (Swedmark, 1964). A range of trophic types equivalent to those described above for macrofauna are present (Swedmark, 1964). Because of their small size and interstitial habit, meiofauna are not as important as macrofauna in reworking particles great distances but tend to act as particle-agitators, producing a kind of biogenic Brownian motion of large, sedimentary particles. This agitation is capable of destroying features such as tracks and trails which rely on inter-particle cohesion for preservation (Cullen, 1973). Meiofauna may also breakdown aggregate particles such as fecal pellets by grazing and burrowing activity (Rhoads, Aller, and Goldhaber, 1976).

The magnitude of fluid transport by meiofauna, to my knowledge, is unknown. Interstitial burrowing activity must result in turbulent, eddy diffusion of pore fluids at a rate much faster than molecular diffusion. Cullen (1973) describes burrowing rates for meiofauna of 0.2-0.3 cm/sec; these compare to maximum expected molecular diffusion coefficients of $\sim 1 \times 10^{-5}$ cm^2/sec for ions dissolved in pore water. At these transport rates,

in one second an ion could move ~0.2-0.3 cm by burrowing activity or ~0.4×10^{-3} cm by molecular diffusion. This is not a completely appropriate comparison but demonstrates the relative potential of the two transport processes in a given volume of fluid.

Meiofauna are known to vary in abundance seasonally (low in winter), (Tietjen, 1969) and to be sensitive to temperature changes in the same manner as macrofauna (Prosser and Brown, 1961). A seasonal pattern of change in activity of meiofauna similar to that found for macrofauna in seasonal environments must occur.

Effect of macrobenthos on microorganisms

Macrobenthos influence the microbial community in several ways: (1) The gross horizontal and vertical distribution of different microorganisms may be continuously altered by biogenic transport and construction activity (e.g., Rhoads, 1974). (2) The creation of special surfaces or microenvironments such as fecal pellets and burrows by macrobenthos may produce especially favorable conditions for microbes (e.g., Driscoll, 1975). (3) Microfauna and flora are continuously consumed by deposit feeders during feeding (Newell, 1965; Frankenberg and Smith, 1967). (4) Biogenic transport may provide additional nutrients or flush metabolites from sediment at a rate faster than molecular diffusion. The net effect of these activities is to increase microbial metabolism above that found in the absence of macroorganisms (Hargrave,

1970; Fenchel, 1970) and to change the geometrical-spatial distribution of types of metabolism in near-interface sediment.

Diagenetic reactions related to biological activity

Diagenetic reactions associated with the decomposition of organic matter determine the pH and oxidation-reduction properties in earth surface environments (Baas Becking, Kaplan, and Moore, 1960; Berner, 1963; Ben Yaakov, 1973; Gardner, 1973). Elements composing the major fraction of organic material: C, H, N, O, P, S, and the electron acceptor complex: $N_wS_xC_yO_z$ (where w = 0, 1; x = 0, 1, 2; y = 0, 1, . . . ; z = 2, 3, 4, . . .) are involved in most reactions. The most studied, common, and important electron acceptors in marine sediments are O_2, NO_3, SO_4, and CO_2, and they are used, when available, in that order of preference by correspondingly changing populations of microorganisms (Richards, 1965; Thorstenson, 1970; Claypool and Kaplan, 1974).

Elements sensitive to oxidation-reduction conditions, pH, or reactive with products of decomposition, and relatively abundant in sediments, are intimately involved in diagenesis; examples are Fe, Mn, Ca, and Mg. Much of the chemistry of C, H, N, O, P, S, Ca, Mg, Fe, and Mn is therefore directly coupled by biogenic reactions taking place in marine sediments and other surficial environments (Berner, 1976a). Because of the special properties of Fe and Mn hydrated oxides in reacting with other elements and

compounds (Jenne, 1968) and the role of these oxides in controlling open marine and estuarine chemistry (Goldberg, 1954; Kharkar, Turekian, and Bertine, 1968; Turekian, 1976), the chemistry of many additional metals is coupled into these processes. Berner (1976a) was able to give examples of only a few strictly abiogenic reactions occurring in sediments: (1) silica dissolution, (2) $CaCO_3$ dissolution, (3) silicate (clay, feldspars, glass)--sea water reactions and (4) recrystallization. Because of biogenic control of pH, CO_2, and HCO_3^-, control of surface coatings on particles (organic, $Fe_xO_y(H_2O)_z$, $Mn_xO_y(H_2O)_z$), and biogenic control of the fluid-particle transport regime described above only (4) can be said to be strictly abiogenic in surface sediment.

The dependence of diagenesis on biogenic processes implies that chemical diagenesis near the sediment-water interface is subject to all the complexities of biological interactions. It is the purpose of the present study to investigate some of the diagenetic processes occurring in the surface zone of sediments and in particular the contribution of the activities of macrobenthos to these processes.

Study approach

The different chemistry and relative reactivity of the elements listed above, makes it possible to use them together to probe the complex reactions taking place in the near interface zone or zone of biogenic reworking.

One of the most sensitive indicators of diagenetic reactions is pore water chemistry (Emery and Rittenberg, 1952; Shiskina, 1964; Siever, Beck, and Berner, 1965), measurements of which, together with solid phase measurements and intuition, allow the deciphering of major chemical processes. In this study, the elements or molecules: Fe, Mn, Ca, NH_3, PO_4, SO_4, Cl, alkalinity ($\sim HCO_3^- + CO_3^=$) were chosen for common measurement in pore water; FeS, FeS_2, Fe and Mn were normally measured in the solid phase and bulk measurements of pH were also commonly made, all as a function of position in sediments of different types, times, and environments.

All chemical measurements are standing crop measures so it is necessary to have independent evidence on the relative rates of reactions of different types and the relative importance of possible transport mechanisms taking place in order to interpret the meaning of standing concentrations. In general, rate or transport measurements cannot be made at the same time or on the exact same sample as bulk property measurements without disturbance so that reaction and transport rates must be inferred from separate experiments. The geometry of the distribution of reactions with respect to overlying water and available transport mechanisms also determine the importance of reactions taking place in a given region of sediment for influencing conditions in overlying water. With these factors in mind, the approaches of this study are to: (1) examine the three dimensional distribution of representative diagenetic reactions in a deposit, (2) measure directly the magnitude and

distribution of organic matter decomposition rates in near surface sediment, (3) establish time scales for solid phase reactions and particle transport by use of natural radioactive tracers (^{238}U, ^{232}Th series nuclides), (4) measure directly bottom interaction with overlying water through particle scavenging reactions and material flux by use of natural radioactive tracers and direct flux measurement, (5) examine selected components of the near interface diagenetic system under simplified conditions, for example: comparison in the laboratory of changes in sediment chemistry produced by single species of macrobenthos representing particular ecological types, (6) utilize the natural cycle of temperature and mortality of animals so as to sample sediments during periods when biogenic influences are relatively low compared to higher activity periods, (7) utilize the differences in spatial distribution in animal types, adaptations, and depositional environment, to study the effects of different animal groupings and environment on sedimentary diagenesis, and (8) attempt to integrate these measurements into a preliminary but consistent description of the influence of macroorganisms on chemical diagenesis of sediments, overlying water chemistry, and ecological coupling between benthos and pelagic organisms.

Following these approaches, the chapters of this study progress from investigation of small scale diagenesis associated with a single type of permanent burrow structure produced by a sedentary, surface deposit feeder (Chapter II), to the integrated effects of single populations of a facultative-

mobile, subsurface deposit feeder and a mobile, subsurface deposit feeder (Chapter III), to spatial and temporal patterns of particle-reworking and particle-water reactions in an estuary (Chapter IV), and finally to a more general consideration of spatial and temporal patterns of diagenetic processes and sediment-water coupling as related to total animal communities and depositional environment in the same estuary (Chapters V, VI).

Table I-1. Particle Transport or Biodeposition Rates

Species	Taxon	Trophic Group - life habit	Bottom† type	Burrowing depth	Rate* (per individual)	Typical abundance (per m^2)	Reference
Macoma baltica	Bivalvia, Tellinacia	Infaunal, mobile deposit feeder (surface)	mud	4-6 cm	0.043 g/d	100-1000	Bubnova, 1972
Yoldia limatula	Bivalvia, Nuculacea	Infaunal, mobile deposit feeder (subsurface)	mud	2-4 cm	0.28 g/d	10-100	Rhoads, 1963
Nucula annulata	Bivalvia, Nuculacea	Infaunal, mobile deposit feeder (subsurface)	mud	1-2 cm	0.0033g/d	100-1000	Young, 1971
Pectinaria gouldii	Polychaeta, Pectinariidae	Infaunal, mobile deposit feeder (subsurface)	sand (poorly sorted)	1-6 cm	1.6 g/d	10	Gordon, 1966
Arenicola marina	Polychaeta, Arenicolidae	Infaunal, mobile deposit feeder (subsurface)	sand	15-60cm	4.5 g/d	10-100	Jacobsen, 1967
Clymenella torquata	Polychaeta, Maldanidae	Infaunal, sedentary deposit feeder(subsurface)	sand (poorly sorted)	20-30cm	0.9 g/d	100-1000	Rhoads, 1967
Amphitrite ornata	Polychaeta, Terribellidae	Infaunal, sedentary deposit feeder (surface)	sand (poorly sorted)	∿ 30 cm	4.6 g/d (field) 4.5 (lab)	1-10	Rhoads, 1967 Aller, Chapter II
Leptosnapta tenuis	Holothuroidea, Apoda	Infaunal, mobile deposit feeder (subsurface, non-selective)	sand (fine)	∿ 10 cm	5-14 g/d (4.5-11.5cc/d)	10-100	Myers, 1973
Parastichopus parvimensis	Holothuroidea, Aspidochirota	Epifaunal, mobile deposit feeder (surface, non-selective)	sand (carbonate)	surface	22 g/d (field)	0-1 (0.4)	Yingst, 1974

Table I-1. (continued)

Species	Taxon	Trophic Group - life habit	Bottom† type	Burrowing depth	Rate* (per individual)	Typical abundance (per m^2)	Reference
Caudina chilensis	Holothuroidea, Malpadonia	Infaunal, mobile deposit feeder (subsurface, non-selective)	sand (fine)	∿ 20 cm	158 g/d (field)	1-10	Yamanouchi, 1927
Uca pugliator	Crustacea, Brachyura	Infaunal-Epifaunal mobile, deposit feeder (selective)	sand	∿ 15 cm	9.6 g/d (feces only)	1-10	Kraeuter, 1976
Mya arenaria	Bivalvia, Myacea	Infaunal, sedentary suspension feeder	sand	10-20 cm	0.025g/d (.029g/d-g dry wt)	100	Havens and Morales-Alamo, 1966
Crassostrea virginica	Bivalvia, Ostreacea	Epifaunal, sedentary suspension feeder	sand	surface	0.18 g/d (0.20g/d-g dry wt)	100	Haven and Morales-Alamo, 1966

† All locations intertidal or shallow subtidal (< 30 m)

* All rates were determined in lab at ∿ 15-22°C unless otherwise noted and in general represent feces and pseudofeces.

Table I-2. Fluid Transport Rates

Species	Taxon	Tropic group - Life Habit	Irrigation Rate (per individual)	Typical abundance (per m^2)	Burrowing depth	Reference
Glycera dibranchiata	Polychaeta, Glyceridae	Infaunal, mobile deposit feeder*	32 ml/hr (25°C)	10	< 30 cm	Hoffman and Mangum, 1970; *Klawe and Dickie, 1957
Hyalinoecia tubicola	Polychaeta, Onuphidae	Epifaunal, mobile deposit feeder (surface)	3-4 ml/hr (18-21°C)	-	surface	Dales, Mangum and Tichy, 1970
Diopatra cuprea	Polychaeta, Onuphidae	Infaunal, sedentary deposit feeder (surface)	68 ml/hr (20°C)	10-100	50-60 cm	Mangum, Santos and Rhodes, 1968
Eupolymnia heterobranchia	Polychaeta, Terribellidae	Infaunal, sedentary deposit feeder (surface)	64 ml/hr(12-13°C) (117.4 ml/hr-g-dry wt)	-	-	Dales, 1961a(average wt estimated from data)
Thelepus crispus	Polychaeta, Terribellidae	Infaunal, sedentary deposit feeder (surface)	50 ml/hr(12-13°C) (59.7 ml/hr-g-dry wt)	-	-	Dales, 1961a(average wt estimated from data)
Neoamphitrite robusta	Polychaeta, Terribellidae	Infaunal, sedentary deposit feeder (surface)	51 ml/hr (12-13°C) (31.4 ml/hr-g-dry wt)	-	-	Dales, 1961a(average wt estimated from data)
Amphitrite ornata	Polychaeta, Terribellidae	Infaunal, sedentary deposit feeder (surface)	75 ml/hr (lab) 91 ml/hr (lab,22°C)	10	> 30 cm	Coyer and Mangum,1973 Aller,Chapter II
Clymenella torquata	Polychaeta, Maldanidae	Infaunal, sedentary deposit feeder (deep)	2-3 ml/hr	100-1000	20-30 cm	Mangum, 1964
Arenicola marina	Polychaeta, Arenicolidae	Infaunal, mobile deposit feeder (deep)	42 ml/hr	10-100	15-60 cm	Jacobsen, 1967

Table I-2. (continued)

Species	Taxon	Trophic Group -Life Habit	Irrigation Rate (per individual)	Typical abundance (per m^2)	Burrowing depth	Reference
Nereis virens	Polychaeta, Nereidae	Infaunal, mobile carnivore	10-50 ml/hr	-	-	Lindroth, 1938
Chaetopterus variopedatus	Polychaeta, chaetopteridae	Infaunal, sedentary suspension feeder	480 ml/hr (15°C)	1-10	20-30 cm	Dales, 1969
Schizobranchia insignis	Polychaeta, sabellidae	Epifaunal (Hard gravel)sedentary, suspension feeder	18-30 ml/hr(12-13°C)	-	surface	Dales, 1961b
Myxicola infundibulum	Polychaeta, sabellidae	Infaunal, sedentary suspension feeder	286 ml/hr(17-20°C) (100 ml/hr-g wet wt)	-	-	Dales, 1957
Spiroibis borealis	Polychaeta, serpulidae	Epifaunal, sedentary suspension feeder	0.23 ml/hr(17-19°C) (950 ml/hr-g wet wt)	-	-	Dales, 1957
Mya arenaria	Bivalvia, myacea	Infaunal, mobile suspension feeder	800-1200 ml/hr(17-18°C) (800 ml/hr-g dry wt)	100	10-20 cm	Allen, 1962
Venus streatula	Bivalvia, veneracea	Infaunal, mobile suspension feeder	50-200 ml/hr(17-18°C)	-	∿ 5 cm	Allen, 1962
Mytilus edulis	Bivalvia, Mytilacea	Epifaunal, sedentary suspension feeder	400-2,600 ml/hr (∿15°C)	-	surface	Jorgensen, 1966
Crassostrea Virginica	Bivalvia, Ostreacea	Epifaunal, sedentary (cemented) suspension feeder	10,000 ml/hr (∿2,400 ml/hr-g-dry wt assuming 80% water on fresh wt)	-	surface	Jorgensen, 1966

Table I-3.* Fluid/solid Biogenic Transport Ratios

Species	Trophic Group	Fluid/Solid Transport Rate (mass ratio)
Clymenella torquata	Deposit feeder	67
Amphitrite ornata	Deposit feeder	410
Arenicola marina	Deposit feeder	220
Mya arenaria	Suspension feeder	600,000
Crassostrea virginica	Suspension feeder	300,000

* See Tables I-1, I-2 for data and species descriptions.

Table I-4. Burrowing Rates

Species	Taxon	Trophic Group - Life Habit	Burrowing (cm)	Burrowing (cm/hr)	Burrow Production (cc/hr)	Reference
Nephtys incisa	Polychaeta, Nephytidal	Infaunal, mobile deposit feeder	∿ 20	10	1.3	Goldhaber et al, 1977
Glycera dibranchiata	Polychaeta, Glyceridae	Infaunal, mobile deposit feeder	< 30	4.2	0.5	Klawe and Dickie, 1957 (estimated from maximum burrowing distance per time)
Scoloplos robustus	Polychaeta, Orbiniidae	Infaunal, mobile deposit feeder	< 13	0.41	0.013	Myers, 1974
Nereis diversicolor	Polychaeta, Nereidae	Infaunal, mobile carnivore	< 30	3.2	0.1	Renfro, 1973
Nucula annulata	Bivalvia, Nuculacea	Infaunal, mobile deposit feeder	1-2	0.04	0.01	Stanley, 1970 (estimated from data, average of 7 p. 203)
Parahaustorius longimerus	Amphipoda	Infaunal, mobile deposit feeder	< 3	4.6	0.25	Howard and Elders, 1970
Lepidactylis dystiscus	Amphipoda	Infaunal, mobile deposit feeder	< 3	0.8	0.01	Howard and Elders, 1970 (5 other species lie within the range of these two)

Table I-5. Temperature Dependence of Macrofaunal Metabolic Activity

Species	Q_{10}*	Reference
Nucula annulata	∿ 2 (feeding rate)	Young, 1971 (estimated from data)
Yoldia limatula	∿ 5 (feeding rate)	Rhoads, 1963 (estimated from data)
Clymenella torquata	∿ 2 (metabolism)	Mangum, 1963
Amphitrite ornata	∿ 2 (metabolism)	Coyer and Mangum, 1973
Glycera dibranchiata	∿ 2 (metabolism)	Coyer and Mangum, 1973
Diopatra cuprea	∿ 2 (metabolism)	Coyer and Mangum, 1973

* Q_{10}'s vary somewhat over any given temperature interval for an animal; they are also history dependent and should be considered approximate as presented here.

Chapter I

Figure Caption

Figure I-1: Schematic breakdown of functional types of animals present on or in marine sediments.

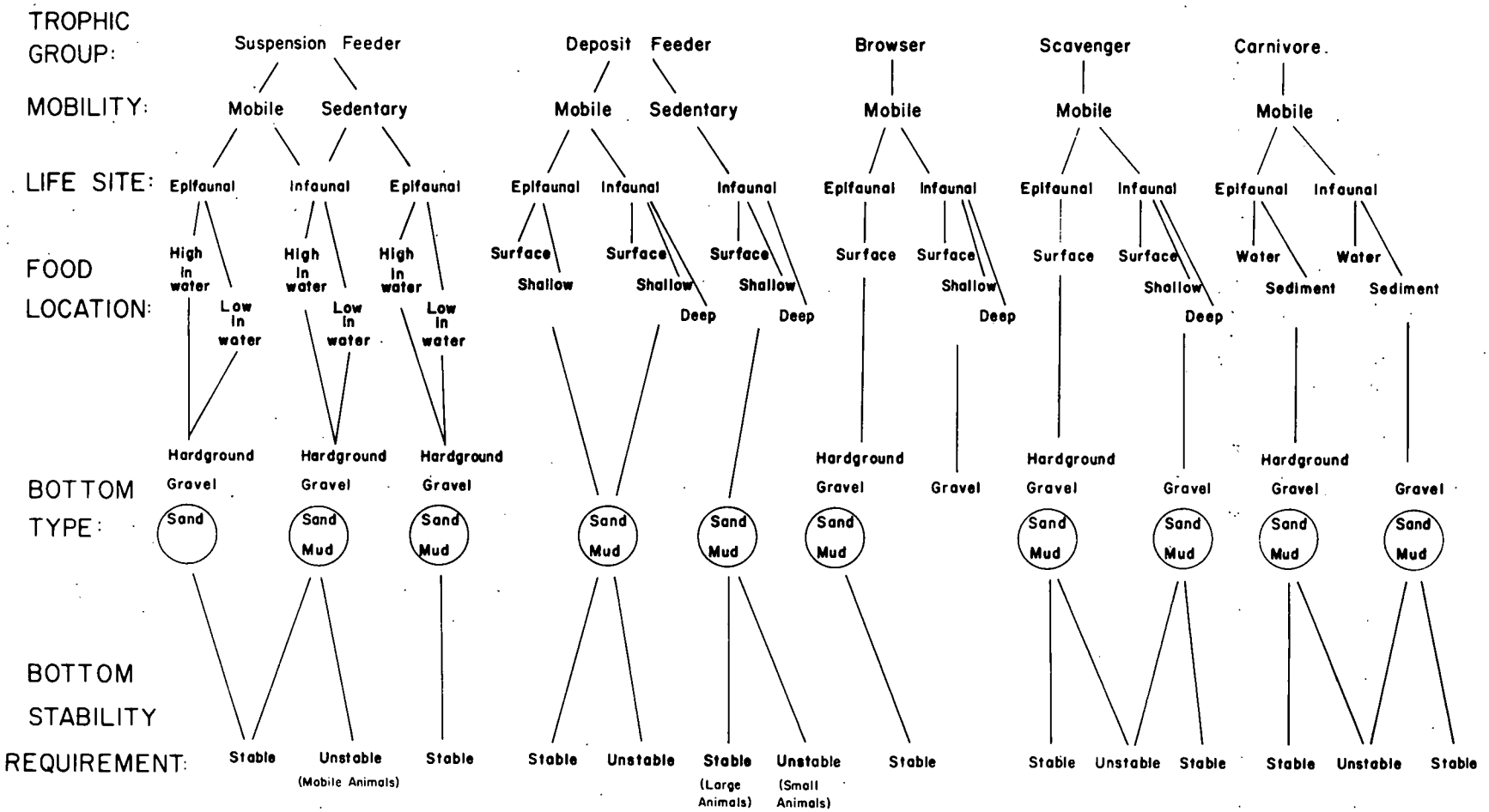

TROPHIC GROUP:
MOBILITY:
LIFE SITE:
FOOD LOCATION:
BOTTOM TYPE:
BOTTOM STABILITY REQUIREMENT:
Suspension Feeder
Deposit Feeder
Browser
Scavenger
Carnivore
Mobile
Sedentary
Epifaunal
Infaunal
High in water
Low in water
Surface
Shallow
Deep
Water
Sediment
Hardground
Gravel
Sand
Mud
Stable
Unstable
(Mobile Animals)
(Large Animals)
(Small Animals)

Figure 1-1

CHAPTER II

BIOGEOCHEMISTRY OF THE TUBE-DWELLING OF A SEDENTARY POLYCHAETE: *AMPHITRITE ORNATA* (LEIDY)

The formation of biogenic structures in marine sediments has been intensively studied by marine biologists and geologists for over a hundred years (for example: Dalyell, 1853; Watson, 1890; McIntosh, 1894; Richter, 1927; Schäfer, 1962). Permanent tube dwellings of sedentary benthic animals have been of particular interest because they often show features characteristic of feeding type, life habit, general ecology, and habitat of an organism (Seilacher, 1951; Zieglemyer, 1952, 1969; Schäfer, 1956; Myers, 1972; Frey, 1970a). These burrow structures are most readily recognized in sediments as physical discontinuities of one kind or another, but their common association with color discontinuities in soft-sediment or their preservation as sites of distinctive mineralization (e.g., Simpson, 1957; Hallam, 1960; Frey, 1970b; Hein and Griggs, 1972) suggest chemical discontinuity as well. The possibility that burrows are sites of geochemical processes not necessarily representative of conditions in surrounding sediment or overlying water is of considerable importance, both for understanding the habitat and adaptations of an animal

and for understanding geochemical cycles and diagenetic processes in sediments.

In this study the dwelling tube of Amphitrite ornata (Leidy) is examined in detail. Geochemical environment in and adjacent to the burrow as well as the physical structure of the tube are described. Behavioral adaptation to the burrow environment as expressed by irrigation activity is also investigated and the geochemical significance of irrigation evaluated.

The study animal

Amphitrite ornata is a sedentary, surface deposit-feeding polychaete worm of the family Terebellidae. Both large (often 8-20 cm long) and common, it occurs along the east coast of N. America from Cape Cod, Massachusetts to N. Carolina (Pettibone, 1963). A. ornata is normally present in intertidal sands or sandy muds where it usually forms a U-shaped tube (Linville, 1903; Scott, 1909), the internal diameter of which ranges from 0.5-1.0 cm. The burrow is often coinhabited by the scale worm Lepidometria commensalis and the crab Pinnixa chaetopterana. One or both ends of the tube are commonly surrounded by a small pile of sediment accumulated as a result of feeding or tube construction activity (e.g., Linville, 1903; Rhoads, 1967). The burrow is constantly ventilated by peristaltic movements of the worm's body; these movements generally travel as waves posterior to anterior and are important to the organism both for the supply of oxygen and for the release of gametes (Linville, 1903; Scott, 1909). Reproduction occurs at a low level from

June to August (Cape Cod region) and is most intense near times of spring tide and during July (Mead, 1897; Scott, 1909, 1911).

The life span of Amphitrite is apparently not known but other terebillids may live up to at least 5 years (Dales, 1964). In this study, the laboratory life of Amphitrite maintained in natural burrows was >1 year.

Study area

All animals and burrows sampled in this study were taken from intertidal locations in Barnstable Harbor, Cape Cod, Massachusetts along Calves Pasture Point (Figure II-1). The Point is characterized by sand and muddy sand deposits. Mud content increases away from shore into the channel area of both sampling locations I and II and is also generally higher south of the Point toward location II. Sediment in this area is intensively reworked by a variety of deposit-feeding infauna and exhibits a range of biogenic sedimentary structures such as biogenic graded bedding (Rhoads and Stanley, 1965; Rhoads, 1967). Surface sediment is rich in fecal material and generally oxidized but black sulfide-rich sediment occurs just beneath the surface (0.5-1.0 cm) and sometimes crops out in patches where it is colonized by films of the sulfide oxidizer: Beggiatoa spp. In areas of biogenic or otherwise graded bedding this black zone is restricted to a few centimeters thickness and is underlain by oxidized sediment corresponding to the feeding zone of Clymenella torquata or other deep-feeding invertebrates. Grey or less intensely black sediment underlies

the near-surface black zone in sediment not showing graded bedding.

In addition to Beggiatoa, surface sediment is also colonized by diatoms. Both these groups of organisms are constantly disturbed by surface grazing of dense aggregations of the gastropod Nassarius obseletus. These animals and water turbulence continually obliterate the feeding mounds of Amphitrite.

Both sampling locations I and II are exposed during low tide allowing convenient sampling of animals and burrows.

Sampling and methods

Sampling and field observations were made intermittently from 1970-1976. All samples for quantitative study were taken in the summers 1974, 1975, and 1976.

Burrows were sampled in the field using several types of plexiglas box cores (Appendix I). Large cores (inside dimensions 28.1 l x 20.5 w x 30.5 h cm) made of 0.95 cm thickness Plexiglas were used to sample entire burrows including surrounding sediment and the living, relatively undisturbed Amphitrite in each case. Smaller cores, 2.5 cm thick, were used for x-radiography. Box cores 7.5 cm thick were dissected for general observations of burrow shape and structure. Neither of the two smaller cores were usually deep enough (<25 cm) to contain an entire burrow.

After collection, samples were placed in insulated container boxes and transported to Yale (~ 4 hours). The large cores, containing one entire

burrow and living animal each, were placed into a plexiglas aquarium containing 180 liters of Long Island Sound sea water ~28‰ salinity at 22°C. One large core was also sampled for solid phase analyses as described below. The 2.5 cm thick cores were x-rayed immediately (60 KV, 4 min at 60 cm) and then stored at 4°C or frozen for later study.

Slabs of wet sediment carefully extruded from x-ray cores were impregnated with polyethylene glycol (6000-8000 M.W.) at 60°C for one week (Allman and Lawrence, 1972). Impregnated slices of burrow walls were polished or water etched and viewed under a microscope for burrow wall structure studies. Carefully dried burrows were also used for this purpose.

For study of burrow wall and lining features, several fresh or frozen burrows were stained using histological stains: periodic acid-Schiff test (carbohydrate), mercuric bromphenol blue (protein), and Sudan-Black B (lipid), and the general procedures for sediment staining described by Whitlach and Johnson (1974).

Solid phase analyses

One complete burrow taken from location II (Sept. 22, 1975) was sampled and analyzed in detail. Samples were taken radially outward away from the burrow wall at several different depth intervals. These represent concentric cylinders of successively large inner and outer radii away from the center of the tube. Samples were taken from only one branch of the

U-shaped tube. This is not significant as explained later. These burrow wall samples are coded by two numbers. The first number indicates the general depth interval of the sample in the sediment; the second represents the radial interval or zone away from the tube axis at a given depth. These radial intervals are: Zone (1) the inner 0-3 mm of the wall, commonly yellow-orange in color from 0-2 mm; Zone (2) the next 1 cm annular section away from the inner 3 mm (0.3-1.3 cm), it is usually black and will be referred to as outer burrow wall; Zone (3) the next 1 cm annular section (1.3-2.3 cm) away from the burrow center. These sample rings are shown schematically in Figure II-2A. Additional samples coded Zone (4): 0-1, 1-2, 2-3, and 14-15 cm were taken at given depth intervals between the two burrow openings which were 21 cm apart (10.5 cm from each).

Each sample was frozen immediately. After slight thawing, samples were homogenized then split into three portions. One portion, the largest, was analyzed immediately for acid volatile sulfide ($\sim$ FeS) using Goldhaber's (1974) method. Briefly, sulfide released upon addition of 10 ml of 12 N HCL under N_2 is passed through a pH 4 trap and then precipitated in $AgNO_3$. The precipitate (Ag_2S) is weighed and weight percent of labile solid phase sulfur in the sample calculated. The sample residue was dried and a portion analyzed for total remaining sulfur (pyrite and organic S) using a Leco induction furnace with a 3% H_2O_2 trap. The solution was filtered, acidified with HCl, heated, 10 ml of 10% $BaCl_2$ (w/v) added, the precipitate digested,

then filtered and weighed. Standards of pyrite (FeS_2) and galena (PbS) were also run and samples corrected to 100% yield based on 12 standard yields averaging 84 ± 5% for four different grain sizes.

A second portion of each sample was ashed at 475° for 12 hours to determine percent organic matter by weight loss. The ashed sample was sieved through a 74 μm (400 mesh) nylon sieve (SPEX) and the < 74 μm fraction was leached for 24 hours in scalding 12 N HCL (25 ml/sample). After taking to near dryness, each sample was picked up in 0.2 N HCl, filtered through Whatman 42 filters, and brought up to volume. This leachate was analyzed for Fe using Ferrozine (Stookey, 1970) and Mn and Zn using flame atomic absorption spectrometry. Total Fe, Mn, and Zn in each sample was calculated. Precision is ≤ 3%.

A third portion of each sample was used for particle size analysis by wet sieving. Sieve series 2 mm, 1 mm, 0.5 mm, 250 μm, 125 μm, and 62 μm were used. Particles were carefully filtered onto 25 mm preweighed Whatman 42 or Millipore (0.45 μm pore size) discs, dried and weighed. Percent dry weight in each size class was calculated, based on total accumulated weight on filters not on basis of initial sample weight. Yields were 96.2 ± 0.8%. Sample sizes were small (≤ 1 g) but represent a large percentage of the feature being analyzed so can be considered representative.

Pore water analyses

Two cylindrical cores were taken for pore water analysis near the relatively muddy sand of the tidal creek at location I on October 13, 1975. One core, 7.5 cm in diameter, was taken so that one branch of an Amphitrite burrow was at the center of the core. The second core, 4.78 cm diameter, was taken approximately 30 cm away, not any closer to large burrows. These were placed in a cooler and transported to Yale ($\sim$4 hours). The cores were placed in a N_2-flushed glove bag and sampled into acid-cleaned pyrex screw cap tubes. Except for the top 0-1 cm depth interval, which was taken in its entirety, the core containing the Amphitrite tube was sampled in two parts for a given interval. The inner part of the core containing the burrow proper (approximately the annular ring from the inner burrow wall to 1.5 cm away) and the remainder of the core were separated as shown in Figure II-2B. The second, thinner core was sampled in its entirety at any given depth interval. Punch-in pH measurements of the sediment were taken for each sample by insertion of a rugged electrode into each horizon and allowing it to come to equilibrium. The packed tubes were then centrifuged (particles $>$ 0.4 μm theoretically sedimented). The clear, overlying water was carefully removed using Eppendorf pipets and transferred to prewashed vials for analysis. 0.1 to 0.5 ml samples were used for ammonia analyses by a modification of the phenol hypochlorite method (Solorzano, 1969) after fixing with phenol

(Degobbis, 1973). Precision is < 3% except where noted. The remainder was used for alkalinity titrations using 0.1 N HCl and 2.0 ml or 0.2 ml cross-calibrated Gilmont burets, depending on sample size (Gieskes and Rogers, 1973). After sitting for several days, the acidified solutions (pH 1.5-2.0) from the alkalinity titrations were analyzed for Fe by a modified Ferrozine procedure (Stookey, 1970). Mn was determined by a modification of the leuco malachite green method (Strickland and Parsons, 1968) using two standard additions and a correction for non-linearity of the addition (Appendix II). Based on other analyses where duplication is possible, precision of Mn analyses is generally ≤30% for sample sizes used and levels found. Analyses of pore water from centrifuged Long Island Sound mud samples treated as above compare well with squeezed and filtered (<0.45 μm) samples of Long Island Sound mud for both NH_4^+ and Fe; Mn has not been compared (see Chapters V and VI). The use of samples acidified in their initial container during alkalinity titration for subsequent Fe and Mn analysis yields 100 ± 1% return of Fe and 100 ± 2% of Mn in the original sample if titration is performed within 1 week of collection (Chapter VI).

Burrow water samples

Samples of water remaining in burrows following the receding of the overlying water were taken at location I on August 12, 1975 (Figure II-1). Burrow water was sampled by inserting Tygon tubing attached to a syringe

into a burrow and withdrawing water. Sampling began at the water's edge at low tide and progressed up the tidal bank so that burrows exposed over a period of 10 to 283 minutes were sampled. Usually two or more complete burrows were sampled at a given time following the receding tide; these samples were combined. Sea water was poured back into each burrow so as not to kill the animal and the burrow marked so that mistaken resampling was not made. The withdrawn water was filtered immediately through 0.4 μm pore size Nuclepore filters in swinex holders. This was pipeted immediately in the field into cleaned vials and stored for later alkalinity titration in the same vial. Fe and Mn determinations were made on the acidified sample using the methods described previously. Samples were also taken for NH_4^+ (fixed with phenol within 2 hours, analyzed as above) and $HPO_4^=$ analysis (stored in refrigerator at 4°C). $HPO_4^=$ analyses were made using a slight modification of the molybdate method (Strickland and Parsons, 1968; Presley, 1971). Subsamples were taken for Cl^- titration ($AgNO_3$, starch--fluorescein indicator) and Ca and Mg determination (Atomic absorption spectrometry, K-La buffer used in both cases). Field measurement of the pH of burrow water, overlying water, and surface sediment was made (punch-in) on October 14, 1975.

Tidal flat water samples

Samples of water which successively overlies the study area as the tide recedes were taken on Sept. 1, 1976 (Figure II-1). These were obtained

~10 cm above the bottom at the water's edge just before a given area of the flat was exposed. They correspond in composition roughly to the last water overlying burrows on a given area of the flat just before exposure and, as will be shown, were necessary to interpret the results of the burrow water study. The location of these samples in relation to the burrow water samples is shown in Figure II-1. Samples were collected by inserting Tygon tubing, attached to a syringe, below the water surface and withdrawing water. The syringe was immediately attached to a Nuclepore in-line filter and the water filtered through a 0.4 μm pore-size Nuclepore filter directly into an acid-washed polyethylene container. A total of about 250 ml water was collected. Samples for Fe and Mn analysis were acidified with HCl; a separate container was used for storing samples for NH_4^+, $HPO_4^=$, alkalinity, and Cl^- analyses and placed in an ice water bath for storage. After transport to Yale, the samples were analyzed for a given property using the methods described previously but on 40 ml samples. $HPO_4^=$ analysis and the fixing of NH_4^+ with phenol were performed within 24 hours of collection after storage at 4°C. All analyses were completed within 5 days of collection.

A single overlying water sample obtained at the time of burrow water sampling, August 10, 1975, was also taken and analyzed in a similar way.

Irrigation rate measurements

Direct measurement of irrigation of the burrow was made both on animals brought to the lab in the large cores and on animals removed from their natural burrow and placed in artificial burrows constructed of U-shaped Tygon tubing. Animals collected on September 13, 1974, September 22, 1975, and June 10, 1976 were used. The velocity of water pumped into and out of the burrow was measured 0.5-1.0 cm above each burrow opening using micro-thermistor (hot point) current meters (Forstner and Rutzler, 1969). Velocities were recorded continuously on strip chart recorders. By integrating the velocity-time patterns obtained it is possible to obtain an average velocity and total volume of water pumped. If possible, it was noted if the meter was recording at the burrow opening corresponding to the head or tail end of the animal and if the animal was feeding or not. Sometimes only one meter was used and was occasionally switched from one opening to the other.

Current probes were standardized in a salt-water flume at known flow velocities. A 12 V battery source was used for maximum background stability. The useful detection range was 0.04-15 cm/sec with greatest sensitivity from 0.04-1.0 cm/sec. Water was 22°C, 28‰ salinity, and near air saturation during velocity determinations.

Particle transport

The weight of particles manipulated or ingested by one individual collected together with its burrow (September 13, 1974) and maintained in its box core was determined over a one week period at 22°C. Particles were removed by pipet as they accumulated around the tube openings, dried at 100°C, and weighed.

Results

Burrow structure

The burrow wall usually consists of several thin-walled, concentric cylinders (Figure II-3). There are commonly four or more such tubes or parts of tubes making up the burrow at any given depth. Each individual tube has a wall thickness of ~1.5-2 mm and is lined on its inner side with an organic sheet ≤5 μm thick. The total thickness of the multiple layers forming the wall is ~1-1.5 cm. Only the inner most tube is a perfect cylinder and acts as the burrow chamber; the outer layers are split lengthwise parallel to the tube axis and wrap partly around the circumference of the next inner cylinder. The arc length of an outer split tube can be smaller than the next inner one by a few millimeters or may be approximately the same.

The cylindrical organic sheet or sheets lining the tube and the successive sheets separating individual wall layers are strongly stained by the periodic acid-Schiff reaction for carbohydrate. The lining stains very

lightly with mercuric bromphenol blue (protein) and does not react with Sudan Black B (lipid stain). Particles in the wall layers also stain lightly for carbohydrate.

The tube wall is formed by successive packing of small parcels of sediment (Figure II-3). These brick-like structures are of variable size and fusiform in shape. They separate from one another upon drying of the burrow Ranging in length from 2-4 mm or greater with maximum thicknesses of 0.2-0.7 mm parallel to the tube axis, they may extend either partly or entirely through the ~2 mm burrow layer (Figure II-3). Small invaginations of burrow lining occasionally occur between bricks. There is no readily apparent organization of sediment grains internally in a single brick but the grains around the edges are commonly oriented with their long axes, if present, tangent to the brick surface.

The wall layers are formed from a higher percentage of small particles than found in the average surrounding sediment. The difference between particle size distributions in the burrow wall and ambient sediment can be easily seen in medium sand areas of Locality I (Figure II-4). In silty areas such as Locality II and low intertidal areas of Locality I, discontinuities in particle size are subtle and less easily seen. Three dimensional grain size distribution data for one burrow from Locality II, the particles of which were used in chemical analysis, are given in Table II-1 and Figure II-5. There is a consistently higher percentage of very fine sand and silt (< 125 μm) in the

sediment surrounding the burrow than in ambient sediment. This percentage increases in the burrow wall with depth. In Locality I where biogenic graded bedding is present, the discontinuity between particle sizes composing the burrow wall compared to surrounding sediment can be easily seen. At depths of 30 cm, burrows can often be found as silty pipes running through coarse sand and gravel.

The openings of each leg of the U-shaped tube may be as close as 15 cm or more than 60 cm apart. The base of the U is found at 30 cm $\pm$ 10 cm depth. Sometimes the U is more nearly a ⌊⌋ -shape rather than a curved base. The trough of the U is often reinforced with many of the primary tube layers, creating structures in cross section similar to spreite, although they are not caused by moving the entire burrow as a unit up or down the sediment column. Only burrows having two openings have been observed in the field but it is possible that single verticle burrows or multiple branched burrows also occur. During winter months the burrow openings to the surface are often not maintained and the animal can be found in the trough of the burrow, apparently hibernating. This requires further substantiation.

Irrigation, particle transport, and behavior

Amphitrite ornata, like many terebellids, is capable of turning around (end-for-end) in its burrow (Dalyell, 1854; Linville, 1903; Dales, 1955;

Schäfer, 1956). Observations in the laboratory through the sides of artificial burrows, show that A. ornata turns by first contracting its tentacles, then, tucking its head ventrally, it moves toward its posterior. The anterior ventral surface slides successively over posterior ventral segments; the final motion is the pulling through of the posterior while the head remains relatively stationary. Turning takes about 30 sec. in both artificial and natural burrows.

The ability to turn in its burrow allows Amphitrite to feed at both ends of the U-shaped tube. Tentacles are stretched radially (> 25 cm radius) over the interface and particles transported to the mouth (Linville, 1903). The dominant particle transport usually takes place by the pulling in of an entire tentacle once its underside is coated with particles rather than continual transport in a conveyer-like fashion along the ciliated groove.

Defecation of ingested particles takes place at the same end of the burrow as feeding. The animal doubles over, the tentacles remaining partially extended at the surface, and extrudes unconsolidated feces in a continual stream; it then resumes feeding at the same end.

Unless disturbed, in the lab the animal feeds continuously after a few days of no tidal activity. It feeds both in light and dark. The feeding rate of one individual in an undisturbed box core during the first week in the lab (20°C) was 4.5 g/d (seven day average). The daily rate was variable: 3.9 ± 1.9 g/d (Table II-2). Rhoads (1967) made field measurements of reworking by A. ornata at a temperature of ~17°C. Averaging his data and converting

to g/d, he found 4.6 ± 2.2 g/d. After finding this excellent agreement between lab and field, further measurements were not made.

In addition to turning end-for-end in the tube, A. ornata also rotates about its anterior-posterior axis, but the preferred orientation is with the ventral surface to the inner curve of the U. During rotation, the animal continually crops the burrow sides (of bacteria?) with its mouth. Rotation has been observed in animals placed in artificial burrows, but rotation is also known to take place during tube construction in natural burrows (Linville, 1903).

The burrow is continually irrigated with overlying water by peristaltic body waves and by the animal's moving up and down the burrow. Records of this activity were made on four individuals (10-15 cm long) two in undisturbed box cores and two in artificial burrows using the current meters previously described. Approximately 56 hours of records were made at a chart speed of 1.25-0.5 cm/min, 16 hours of which were integrated for the calculation of irrigation velocities. No significant differences between animals in natural and artificial (Tygon) burrows were found.

There are several different activity patterns of irrigation velocities. Because the average velocity and volume of water pumped were the primary objectives of the irrigation measurements no detailed explanation of the many small variations in activity patterns is attempted here, but some general observations can be made. The head-end patterns differ greatly from those

recorded over the tail-end and patterns recorded during feeding differ from those when the animal is retracted into the tube. Often, when the animal is withdrawn into the burrow, only one side of the burrow, the head-end, is irrigated for long periods of time (e.g., 1 hr.). Currents are detected over the head-end as regular pulses moving in and out of the burrow while no movement (<0.043 cm/sec) is detected over the tail end. An example of this is shown in Figure (II-6A, B). During this type of head-end pattern, the peaks correspond to times of regular peristaltic body wave movement. These waves start about 2/3 of the way down the body and move towards the head. The corresponding velocity valleys represent periods of quiescence during which the animal contorts slightly and a constriction of the body occurs just behind the anterior 1/3 of the animal before the regular waves begin again. The current records and direct observation show this pattern repeated ~ 3 times a minute with wave generation occurring for about 15-20 second periods and quiescence for shorter periods between. Head-end velocity patterns during feeding are shown in Figure II-6C; a tail-end pattern during feeding is shown in Figure II-6D. Animals in box cores sometimes exhibited patterns such as Figure II-6E, showing large single velocity spikes of $>$ 10 cm/sec. with lower velocity regions and periods of quiescence in between. Single velocity spikes interspersed with long periods of quiet are common at the tail end.

An estimate of the average velocity, calculated as a continuous stream, and the total volume of water pumped were made by first dividing the recordings into four types: head-end (animal withdrawn), tail-end (animal withdrawn), head-end (during feeding), and tail-end (during feeding). Velocity peaks were integrated over numerous short time periods and a time-weighted average velocity calculated for each type. Velocities at the background were assigned a value of zero rather than 0.04 cm/sec, the detection limit. The average irrigation velocities found in this way are given in Table II-2. Because the velocity probe does not distinguish direction, these average velocities represent the sum of the absolute values of velocities into and out of the burrow. To calculate a unidirectional current velocity into or out of the burrow for a given state of the animal, withdrawn or feeding, the head and tail-end contributions must be summed and then divided in half. This gives:

$$\bar{V}_{\text{withdrawn}} = \frac{\text{Head + tail (withdrawn)}}{2} = 0.056 \text{ cm/sec}$$

$$\bar{V}_{\text{feeding}} = \frac{\text{Head + tail-end (feeding)}}{2} = 0.059 \text{ cm/sec}$$

These are the same within error and illustrate constancy of total irrigation regardless of current pattern within the burrow. To calculate a volume pumped the above velocities are averaged to give: $\bar{v} = 0.0575$ cm/sec. The burrow openings used had an average diameter of 0.75 cm. The water volume pumped, V, is then:

$$V = \bar{v}A = (.057 \text{ cm/sec})(0.44 \text{ cm}^2)$$

$$= .025 \text{ cc/sec} = 91 \text{ cc/hr}$$

where A is the area of the burrow opening. This number probably has an uncertainty of at least ± 25%. The inability to detect currents below 0.043 cm/sec may make this a minimum and must also influence the magnitude of the observed asymmetry between irrigation velocities at different burrow openings.

In the field, burrows are observed always to have an inner oxidized halo, usually the inner layer of 1-2 mm thickness, extending the entire distance of the burrow. This may be slightly thinner in the deepest parts of the tube. Since it was found that the burrow was asymmetrically irrigated, in order to maintain the approximate evenness in the halo depth from one side of the burrow compared to the other (and to keep the tube clear) the animal must periodically reverse in its tube. By knowing how fast the oxidized halo is destroyed it is possible to estimate the minimum number of times an animal turns around in its burrow under field conditions. Sections of burrows (5-8 cm long) were collected and placed in an aquarium with air saturated sea water ($T = 22^{\circ}C$) circulating above. In 12 hours the oxidized rind was reduced from a bright orange layer $\geq$ 1 mm thick to a dull orange layer $\sim$0.5 mm thick, in 36 hours it was $\sim$0.1 mm thick. It remained at 0.1 mm after 60 hours in all but one sample (in which it was totally absent), after which the experiment was terminated. A reasonable estimate based on these data is that in nature A. ornata turns in its burrow at least once a day.

Overlying water results

Analyses of overlying water at Location I show that as the tide recedes, water of variable salinity flows over or past the flat (Table II-3). The sampling transect down the flat is at right angles to the primary direction of tidal flow so that samples taken at the water's edge during ebb represent water which had resided farther up the embayment a short time before. Ayers (1959) gives an upper salinity for the main body of the harbor as 32.5 ‰ (Cape Cod Bay water) which, as the tide recedes, is reduced to lower values as marsh water is drawn out into the harbor; a low value of $\leq$20‰ is not unreasonable in this cycle. The data given in Table II-3 agree well with Ayers' description of the hydrography of the harbor. The samples taken lowest on the flat and representing the innermost harbor are lowest in Cl^- concentration. The time of sample collection in relation to Cl^- concentration shows that Cl^- changes rapidly during the final ebb stages but otherwise changes slowly in a simple mixing sequence of inner marsh and Cape Cod Bay water and is generally high in salinity.

Both $HPO_4^=$ (1 -2 μM) and NH_4^+ (0.5 - 1 μM) concentrations are similar to coastal water values reported elsewhere. Plotting $HPO_4^=$ versus Cl^- demonstrates that the inner marsh has a high standing concentration of $HPO_4^=$ and that this high $HPO_4^=$ water mixes rapidly and in a fairly conservative way with the lower $HPO_4^=$ water of Cape Cod Bay salinity (Figure II-7).

NH_4^+ concentrations are too low to accurately assess its behavior but the inner marsh water is clearly higher in NH_4^+ than outer harbor water.

Fe and Mn concentrations (~1 μM) are 10-100 times higher than typical coastal sea water concentrations determined by the same sampling and analytical methods. There are too few data to define an exact relation but the pattern of Fe and Mn concentrations in relation to Cl^- shows that regions of the marsh at $Cl^- < 0.4$ M and tidal flats are sites of high standing concentrations of Fe and Mn and that these concentrations decrease as salinity increases. The supply of Fe is high enough and mixing with high Cl^- sea water rapid enough that non-conservative behavior typical of Fe (Boyle et al., 1974) is not revealed with the few data available (Figure II-7). Mn is thought to plot linearly against salinity in many cases (Holliday and Liss, 1976; Graham, Bender, and Klinkhammer, 1976) as it does here for $Cl^- > 0.4$ M. The standing crop of Fe and Mn appears to be constant or go through a maximum at $Cl^- < 0.4$ M implying the major source (as determined by standing concentration only) for these elements contacts waters of $Cl^- < 0.4$ M.

The alkalinity to Cl^- molar equivalent ratio increases steadily from $4.32 - 4.97 \times 10^{-3}$ in the overlying water as the tide recedes.

Burrow water results

Analyses of water collected from burrows at Location I are given in Table II-4. The length of time the sampled burrows had been exposed after

the tide receded is also given. If it is assumed that the initial concentrations of the measured substances were within the range of values found for overlying water, then time related changes in burrow water concentration values which exceed the range of possible initial concentrations are indicative of loss or supply of dissolved material to the burrows. The sources of these changes are internal to the burrow and are due either to the inhabitants of the burrow or to diffusion-precipitation processes in surrounding sediment.

Measurements of Cl^-, Mg, Ca, alkalinity, NH_4^+, $HPO_4^=$, Fe, and Mn were made. Cl^- shows substantial variation between the burrows sampled after different times of exposure. Burrows sampled after the shortest time of exposure were lowest on the flat while burrows sampled after the longest exposure were highest on the flat. The Cl^- variation could then be due to evaporation trends related to time of exposure or the variation may simply reflect the last water which overlay a given burrow just before exposure. The burrow water Cl^- range of 0.364-0.560 M is comparable to the range found in overlying water. The high value of 0.560 M (~35‰) is indicative of slight evaporation since 32.5‰ is the highest salinity reported for Barnstable Harbor. This percentage evaporation is not important for the treatment of the data. The interpretation of the Cl^- variation accepted here and used in the data analysis is that variable salinity water passes over the flat as the tide recedes. Animals low on the flat pump lower salinity water into their burrows just before exposure than do individuals slightly higher

on the flat. This variable salinity source causes the differences in Cl^- in burrow water.

pH measurements of burrow water by insertion of a combination microelectrode into burrows on October 14, 1975 gave values of 7.09 ± 0.43. Surface sediment (0-1 cm) was 7.10 ± 0.13 and overlying water 8.19 on the same day.

Alkalinity varies regularly between sample sets. When normalized to Cl^-, four of the samples cluster around a molar equivalence ratio of $\sim 4 \times 10^{-3}$ or lower. Sample 6 is much higher (5.8×10^{-3}) and sample 4 is much lower (2.9×10^{-3}) than this ratio. Most samples have lower alkalinity /Cl^- ratios than expected for sea water at 35‰ ($\sim 4.25 \times 10^{-3}$ at 0.550 M Cl^-) or that found in the overlying water if the ratio were assumed conservative. The Mg/Cl and Ca/Cl ratios are typical of sea water in all cases showing that alkalinity is not lowered by carbonate precipitation in the burrow.

NH_4^+, $HPO_4^=$, and Fe concentration trends during the time of burrow exposure are much greater than can be explained by source water variation. Therefore the differences in concentration of NH_4^+, $HPO_4^=$, and Fe between burrow samples is taken as a real index of rate of increase or flux of material into the burrow. The measured concentrations are plotted against time of exposure in Figure II-8. Lines have been fit to these data by least squares methods. The slopes of these lines which will be used in later calculations, are: NH_4^+: $m = 0.31 \pm 0.06$ μM/min; $HPO_4^=$: $m = 0.66 \pm .022$ μM/min;

Fe: m = 0.10 ± .007 μM/min. In each case, the errors can be greatly reduced by the elimination of one point which is clearly an outlier but no points have been thrown out since the slopes are not greatly influenced.

Variations in Mn concentration in burrow water are largely masked by changes in the source water. By comparing Mn and Cl^- relationships in the overlying water (Figure II-7) with Mn and Cl^- values from burrow water samples (Table II-4), it is evident that burrow samples 1, 2, and 3 contain Mn concentrations appropriate to their Cl^- levels. At the higher Cl^- concentration and lower Mn background for samples 4, 5, and 6 there is an apparent increase in Mn with time. With the large analytical uncertainty in the Mn burrow water values (~ 30%) this apparent increase is only suggestive and will not be treated quantitatively. The net, internal supply of Mn to burrow water is lower than that for NH_4^+, $HPO_4^=$, and Fe.

Pore water concentrations around burrow

Analyses for water centrifuged from sediment at different distances from the burrow and depth intervals are given in Table II-5. The sampling code and positions are given in methods. The spatial patterns of concentrations for each set of analyses are plotted in Figures II-9-10. These show several distinct trends. In the sediment core taken away from the burrow, alkalinity and NH_4^+ concentrations increase with depth to the 3-6 cm interval then decrease very slightly (Figure II-9). Concentration profiles associated with

burrow core also show increased values with depth but values are higher in the burrow wall (Zone I) and immediately around the burrow (Zone II) than in the surrounding sediment. The highest concentrations are found in the burrow wall and are sustained at these high levels relative to surrounding sediment at all depths. The pore water immediately surrounding the burrow has concentration levels intermediate between burrow wall and sediment from the flat.

In both the core away from the burrow and Zone II, dissolved Fe is highest at the surface and decreases to undetectable values, given sample size, at depth (Figure II-10). The burrow halo concentrations (Zone II) are consistently higher than the ambient sediment values. Water from the burrow wall shows an entirely different distribution; concentrations are consistently higher than surrounding sediment and increase with depth.

Dissolved Mn is very low and near the detection limit (for sample size) in all cores but shows a tendency to be higher in the burrow wall samples at depth (Figure II-10).

Solid phase analyses

Samples analyzed for solid phase chemistry are splits of samples used for grain size analysis given in Table II-1. The results of analyses are listed in Table II-6; the sample coding is described in the methods section.

The spatial distribution of organic matter (loss on ignition) around the sampled burrow is shown in Figure II-11. The inner wall (Zone 1, 0-3 mm) is highest in organic matter and increases with depth. Organic matter decreases regularly away from the inner burrow wall at all depths in both the older sublayers of the burrow and in surrounding sediment. The deepest sample of Zone 3 annular ring (1.3-2.3 cm) intersects old burrow wall or spreite-like reinforcement and shows high values typical of burrow wall. Above this depth, sample values for Zone 3 are low and more similar to ambient sediment.

Acid volatile sulfide, predominantly mackinawite and greigite (Berner, 1964, 1970; Goldhaber and Kaplan, 1974) is higher in sediment associated with the burrow than in surrounding sediment (Figure II-12). Values for Zone 3 (Table II-5) have not been plotted for clarity but are intermediate between Zone 2 and ambient sediment. The layer just outside the inner oxidized wall, Zone 2,has the highest concentration of acid volatile sulfide and is often colored black. The orange burrow wall has measurable concentrations of FeS. All profiles show a tendency to lower values at depth. Ambient sediment has a slight maximum $S_{a.v.}$ in the second centimeter.

Non-volatile sulfur (pyrite and organic) is also higher in sediment near and part of the burrow than ambient sediment. The highest levels are found in the black burrow Zone 2. The oxidized inner wall also has relatively high concentrations of pyrite sulfur. The profiles show increased

values with depth. The third sampling ring (Zone 3) has intermediate values, except for the deepest sample, which as stated above is burrow wall, and is not plotted. Assuming organic matter has 1% S (Kaplan, Emery, and Rittenberg, 1963) and given the organic matter values of Table II-5 more than half of the measured non-volatile sulfur is mineralized sulfur. In the case of the black burrow zone having the highest sulfur values, 90% of the fixed S is probably pyrite.

Analyses of the < 74 μm size fraction for Fe, Mn and Zn are given in Table II-5 and spatial distribution plotted in Figure II-13. The use of the < 74 μm fraction greatly reduces random dilution by large sand particles and the effect of slight differences in particle size which would affect comparison between samples. The samples as given should reflect diagenetic differences rather than particle size differences.

The inner burrow wall is enriched in Fe relative to all other samples. Zone 2, outer burrow wall, is enriched in Fe relative to surrounding sediment but slightly and consistently depleted in Fe relative to the innermost wall layer. Surrounding sediment shows a slightly enriched surface but otherwise low, relatively constant values. There is a consistent trend toward higher Fe with depth in the burrow samples, including the bottom most (2-3 cm) sample of Zone 3 which as mentioned before is also old burrow wall.

Solid phase Mn shows depletion in the surface sample of the inner burrow wall but is enriched at depth with respect to other samples. All

other samples show Mn enrichment at the interface with decreasing concentrations at depth. Burrow wall levels are consistently higher than ambient sediment.

Zn is enriched in the burrow relative to ambient sediment and is consistently slightly enriched in the innermost burrow oxidized layer relative to the remainder of the burrow (Figure II-13).

Discussion

Burrow structure

The microbrick structure of each burrow layer is similar to the tube structure of Neoamphitrite figulus described by Reis (1909) and Schäfer (1956). By analogy with tube formation by other terebellids (Watson, 1890; Schäfer, 1956; Ziegelmeyer, 1969), the descriptions given for Amphitrite by Linville (1910), and direct laboratory observation, the burrow wall is formed as follows. Mucus coated particles procured by the tentacles are taken between the outer lips, worked into a small parcel with additional mucus, then packed and shaped by the lower lip into the edge of the accreting end of the tube. The animal then rotates slightly in the tube and repeats the procedure; each packing episode represents a brick and the result is the structure shown in Figure II-3C. Adult Amphitrite taken from Barnstable Harbor can actively extend their tube in this way at $\geq$ 1 cm/hr but when removed entirely from the burrow are not capable of constructing a new one. This inability to reburrow is not uncommon in adult sedentary animals

inhabiting relatively stable sediment.

The multiple layer structure of the burrow wall represents several episodes of tube construction. Only the innermost tube and its lining act as the primary dwelling structure. The outer layers result either from slight movement of the burrow or perhaps represent the walls of older smaller diameter tubes which have been split by the animal after a period of growth, much like molting. The arc length of the outer layers taken in cross section is sometimes successively smaller than the next inner one, lending support to the latter possibility; however, the two explanations are not mutually exclusive. Multiple layers give added protection from disturbance by other burrowing animals and in sandy beaches must help prevent loss of burrow water in the high intertidal zone during drainage at low tide.

The polysaccharide burrow lining found on the inner side of each wall layer is presumably similar to that reported for other dwelling burrows. These have been variously described as sulphated or phosphate-rich mucopolysaccharides (Zolz, 1967; Muzii, 1968) and can have a fibrous substructure (Muzii, 1968). Zottoli and Carriker (1974) suggest that these linings may also contain bound enzymes such as protease to prevent colonization by other organisms. High ATP concentrations found throughout the length of the innermost tube wall (J. Yingst, pers. comm.) and the presence of several tube commensals in Amphitrite burrows, show that such an antifouling mechanism cannot be pervasive away from the lining surface itself. As stated previously, Amphitrite

grazes the inside of the tube periodically, thereby helping to prevent excessive colonization of the burrow lining. The permeability of this lining to diffusion of ions from surrounding sediment is not accurately known, but it is not highly impermeable like some burrow linings, e.g., Cerianthus americanus. A dialysis effect on molecular diffusion is possible.

In many cases, the small particles from which the burrow wall is made are available in abundance only at the sediment surface. This fact together with the fact that the outer (older) burrow wall layers are not destroyed when a new inner layer is formed, demonstrate that only particles obtained at the sediment-water interface are used to form the tube. When animals in artificial burrows in the lab were allowed access to sediment, they quickly formed a single burrow wall layer throughout the entire inside length of the plastic tube. This shows that Amphitrite is capable of forming a tube layer at depth using only surface sediment and in conjunction with the above observation is added proof that normally only surface particles are used.

The apparent use of particles obtained only at the interface for burrow construction may explain the regular increase in the abundance of small particles in the burrow wall with depth. If the animal adds a new layer rapidly, beginning first in the deeper sections of the burrow and building up (as was observed in the lab with Tygon burrows), then small particles may become progressively depleted in the surface sediment immediately around the burrow during construction, forcing use of progressively larger

building material as the surface is approached. Current action and biogenic reworking would later restore the steady state grain size distribution at the interface around the burrow. The difference between the grain size distributions in the burrow wall at 24-30 cm depth compared to ambient surface sediment (Zone 4) must represent the maximum particle size selectivity exercised by Amphitrite in tube construction.

In sandy areas of the flat where the maldanid polychaete Clymenella torquata or similar deposit feeders are present, fine particles are selectively transported vertically to the surface creating biogenic graded bedding (Rhoads and Stanley, 1965). Amphitrite then further selects a subclass of these particles and transports them horizontally into a small mound; as just shown, a portion of this material is transported back to depth, this time as a distinct shaft. This represents a commensalistic-like interaction of Amphitrite with Clymenella mediated through biogenic sediment transport. Acting in concert these two organisms radically reorganize the fine particle fraction of otherwise sandy deposits into surface layers of fines and shaft-like invaginations of those layers into the bottom to depths of > 30 cm.

Although the burrow is U-shaped, Amphitrite uses its tube much of the time as two separate verticle burrows. The ability to turn around, defecation out the same end as feeding, and asymmetrical irrigation of the tube support this contention. Other teribellids also turn in their burrows, defecate out the feeding side, and may construct U-shape, multibranched,

or vertical tubes (e.g., Dalyell, 1853; Seilacher, 1951; Ziegelmeyer, 1952; Schäfer, 1956). These facts suggest a different functional significance to the U-shaped tubes of terebellids than that described for other tube dwellers such as Chaetopterus (MacGinitie, 1939). The U-shape obviously increases the options available to the animal for either escape, switching feeding areas, or changing respiratory position. The 'redundant' tube may be particularly valuable in the often physically unstable intertidal regions. Use of a general tube type and dependency on its shape or structure may vary greatly within genera or different populations of the same species (see comments of Linville, 1903; Dales, 1955; Schäfer, 1956).

Chemistry of water in the burrow

The properties of the water found in the burrow are different from overlying sea water and, in the absence of irrigation, are subject to rapid change. The concentrations of NH_4^+, $HPO_4^=$, and Fe quickly become higher than expected for the possible sea water sources (Tables II-3, II-4). In contrast, except for sample 6, the alkalinity / Cl ratio is lower than overlying sea water. These low alkalinites are associated with pH values: 7.09 ± 0.43, also lower than overlying sea water: 8.19. Although CO_2 production could cause these low pH values, the fact that alkalinity ($\sim HCO_3^- + CO_3^=$) is also lowered requires that CO_2 not be the only acid involved in the lowering of pH. As will be shown below, the changes observed in burrow water chemistry

are consistent with diagenetic reactions taking place in the tube wall.

There are two sources of NH_4^+ and $HPO_4^=$ increase in the burrow water: excretion by Amphitrite and diffusion from the surrounding burrow wall. Apparently no data exist on NH_3 excretion by Amphitrite but the related terebellid Pista is known to be ammonotelic and to excrete NH_3 at a rate of 3.3 µmoles/g-worm/d (O'Malley and Terwilliger, 1975). Using this value and assuming a generous average weight of ~3 g for Amphitrite in the field (animals in lab were ~1 g dry wt, a 30% conversion was used (Dales, 1961a), ~10 µmoles NH_3/burrow/day could be supplied by direct excretion. Over the time interval used for sampling (4.6 hours), this would give a rate of increase of 0.35 µM/min in the burrow (assuming an average burrow water volume of about 13 ml (see below)). There are at least two reasons why this rate is too high: (1) At rest (i.e., during intertidal periods), Amphitrite's metabolic rate is about 15% of its active rate ($T = 20^\circ$) (Mangum and Burnett, 1975). (2) Previous studies of oxygen content of tidal flat burrow water (e.g., Arenicola, Jones, 1955) have revealed lowered oxygen concentrations during intertidal periods. This same change can be expected in the Amphitrite burrows and should result in a further reduction in metabolic activity (Mangum and Burnett, 1975). Both these facts suggest that during intertidal periods Amphitrite's NH_3 excretion rate will be ~1/10 of its normal rate, which, if the above rate can be applied, should not greatly influence the rate of increase, 0.31 µM

NH_4^+/min, actually measured. The conclusion is that the major source of increase in burrow water concentrations of NH_4^+ and $HPO_4^=$ during the intertidal period is diffusion or production from the burrow walls and not the animal itself. This conclusion is shown later to be consistent with calculation of fluxes into the burrow based on concentration gradients across the burrow wall. The source of Fe and Mn is also surrounding sediment.

By using a simple mass balance model, it is possible to show that the laboratory measurement of irrigation rate, the observed rate of change of dissolved substances in burrow water during the intertidal period, and the earliest burrow water sample (10 minutes after exposure), represent mutually consistent data.

Let:

$\left(\frac{dC}{dt}\right)_{supply}$ = rate of concentration change due to internal input of a substance to burrow water, e.g., due to diffusion from walls, excretion, etc.

$\left(\frac{dC}{dt}\right)_{loss}$ = rate of concentration change (negative) due to internal loss of a substance from burrow water, e.g., precipitation on walls, uptake of metabolites bacteria, etc.

C_{sw} = concentration of substance in sea water

C_B = concentration of substance in water leaving burrow.

V_o = volume of water in burrow

v = irrigation rate in volume of water pumped per unit time.

Then for constant burrow conditions (i.e., C_B = constant):

$$(1) \quad V_o \left(\frac{dC}{dt}\right)_{supply} + C_{sw} = - V_o \left(\frac{dC}{dt}\right)_{loss} + C_B v$$

$$(2) \quad \left(\frac{dC}{dt}\right)_{supply} + \left(\frac{dC}{dt}\right)_{loss} = \frac{(C_B - C_{sw})\, v}{V_o}$$

Of the substances measured in the burrow water, NH_4^+ is the least subject to abiogenic reactions. If it is assumed that photosynthetic fixation of NH_4^+, nitrification, adsorption, and precipitation can be ignored in the water itself, then letting C refer to NH_4^+:

$$(3) \quad \left(\frac{dC}{dt}\right)_{loss} \sim 0$$

and

$$(4) \quad \left(\frac{dC}{dt}\right)_{supply} = \frac{(C_B - C_{sw})\, v}{V_o} = m$$

where m = the slope of the line of increase of NH_4^+ concentration during burrow exposure as shown in Figure II-8. Approximating the average burrow

by a tube of 0.75 cm diameter and whose length is bent into a semicircle shape of diameter 30 cm (a good average distance between burrow openings in the field) then: $V_o \sim 13$ cc. The average laboratory irrigation rate calculated in this study from current meter records is 91 cc/hr and that found by Coyer and Mangum (1973) using hydrostatic head methods (Wells and Dales, 1951) is 75 ml/hr. Taking the mean of these values as v(83 cc/hr) and letting: $m = 0.31$ μM/min and $C_{sw} = 0.9$ μM (average of overlying water concentrations, Table II-3), then the steady state concentration of NH_4^+ in burrow water is predicted as $C_B = 3.8$ μM. This compares well with the NH_4^+ concentration, 4.5 μM, in the burrow water sample taken 10 minutes after exposure of the flat, suggesting several conclusions: (1) The concentration of dissolved substances in burrow water samples taken shortly after exposure of the flat represent a good approximation to those present when the flat is covered and irrigation is taking place. (2) If conclusion (1) is correct, then the water to which Amphitrite is normally exposed differs from overlying sea water. These differences include higher concentration of metabolites such as $HPO_4^=$ and NH_4^+ and lower pH and alkalinity. (3) The laboratory and field data are mutually consistent. If, for example, the burrow water concentration of NH_4^+ at 10 minutes after exposure had been initially accepted as a good approximation of C_B, then the calculated irrigation rate using $C_B = 4.5$ μM is v = 67 cc/hr, in good agreement with laboratory measurements. The burrow volume (V_o) is the least substantiated value of the data used in the

calculation but is a reasonable estimate based on field observations of tube size and the amount of water easily extracted from burrows; it probably tends to err on the low side.

A slight expansion of the above model allows estimation of loss or precipitation rates of reactive species like $HPO_4^=$ from burrow water. For short time periods, $HPO_4^=$ exchange reactions may be described by first order kinetics (Pomeroy, Smith, and Grant, 1965; Li et al., 1972) and Fe precipitation, with which $HPO_4^=$ can be expected to coprecipitate (e.g., Stumm and Morgan, 1970), can also be described by first order kinetics under conditions of constant pH and O_2 concentration (Stumm and Lee, 1961). By assuming that removal of $HPO_4^=$ in burrows will tend to be first order, a rate constant can be calculated as follows:

Let:

J = constant flux of $HPO_4^=$ from tube walls (the concentration change during exposure is small enough to not effect the flux)

A = inner surface area of tube

V_o = tube volume

k = first order rate constant

C = $HPO_4^=$ concentration.

then, ignoring excretion,

$$(5) \qquad \left(\frac{dC}{dt}\right)_{supply} = \frac{AJ}{V_o} = F$$

$$(6) \qquad \left(\frac{dC}{dt}\right)_{loss} = - kC$$

From equation (1), at constant burrow conditions:

$$(7) \qquad F = \frac{v}{V_o} (C_B - C_{sw}) + k C_B$$

During the period of exposure, the burrow water $HPO_4^{=}$ concentration is given by:

$$(8) \qquad \left(\frac{dC}{dt}\right)_{total} = F - kC$$

therefore,

$$(9) \qquad C = \frac{F}{k} + (C_B - \frac{F}{k}) e^{-kt}$$

and

$$(10) \qquad \left(\frac{dC}{dt}\right)_{total} = (F - k C_B) e^{-kt}$$

$$= \frac{v}{V_o} (C_B - C_{sw}) e^{-kt}$$

from equation (7). This gives:

$$(11) \qquad \frac{v}{V_o} (C_B - C_{sw}) e^{-kt} \sim m$$

It was shown previously that C_B is approximately the concentration found 10 minutes after exposure. In the case of $HPO_4^{=}$, this is 3.9 μM. Taking:

v = 83 cc/hr (as discussed above), C_{sw} = 1.2 μM (average of overlying water values), V_o = 13 cc, m = 0.066 μM/min, and t = 278 min, then k ~ 0.005/min. A similar value of k, 0.004/min, is obtained if a polynomial of the form: $C = a_o + a_1 t + a_2 t^2$ is fit to the $HPO_4^=$ data of Figure II-8, the series expansion $e^{-kt} \sim 1 - kt$ employed in equation (10), and $2a_2$ taken as equivalent to $\frac{v}{V_o}(C_B - C_{sw})\,k$. If coprecipitation with Fe were controlling $HPO_4^=$ loss, this k would also represent a minimum reaction rate for Fe^{++} loss. In fact, it is in the general range but somewhat smaller than the k values expected for Fe precipitation in the pH range of burrow water and at atmospheric O_2 levels (Stumm and Lee, 1961).

The Fe supply and loss terms within the burrow are nearly equal. The supply rate is only slightly in excess of loss due to precipitation. Net supply is 0.01 μM/min, which with a burrow volume of 13 cc, implies a source of Fe equal to 1.3×10^{-4} μmoles/min or ~0.2 μmoles/day from an average burrow. At population densities up to ten individuals per m^2 (Rhoads, 1967), fluxes as high as 2 μmoles/m^2 - d from Amphitrite burrows alone are possible. This value may be too high and could even change sign if during active irrigation the oxygen content of the burrow water increases to a level where Fe is precipitated from the Fe-rich overlying water onto the reactive oxide burrow wall. Similar flux calculation for $HPO_4^=$ and NH_4^+ give 1.2 and 5.8 μmoles/d respectively. These fluxes, which include only Amphitrite burrows, are just 10-100 times smaller than total fluxes measured from

muddy sediments of Long Island Sound (Chapter V), suggesting the importance of burrow microenvironments in remobilization processes.

Geochemical processes associated with the burrow wall

Decomposition

The selection of small, organic-rich particles for burrow construction and the packing of mucus into the tube walls by Amphitrite, enrich the walls in organic matter relative to surrounding sediment (Figure II-11, Tables II-1, and II-4). Irrigation of the core of this organic-rich cylinder with sea water supplies an abundance of electron acceptors (e.g., O_2, $SO_4^{=}$) and flushes out possible inhibiting metabolites. The result of these conditions is an increase in microbial activity around the burrow relative to ambient sediment. This increase in the intensity of decomposition is the direct or indirect cause of changes in both fluid and solid phase chemistry near the burrow.

Both the sediment color distribution and the excess fixed sulfur in the burrow wall demonstrate that much of this decomposition is associated with sulfate reduction. This is clearly not the only decomposition process taking place in the burrow wall but by assuming it is a major pathway and using established conventions for describing decomposition by sulfate reducers, it is possible to demonstrate some of the characteristics of organic matter breakdown taking place there. A general stoichiometric equation for the breakdown of organic matter by sulfate reduction can be written (Richards, 1965):

(This page is blank)

approximately the same as at 30 cm distance, it is assumed for purposes of calculation that the outer radial boundary of Zone II is held at the NH_4^+ concentration of surrounding sediment. The equations describing the radial distribution of pore water NH_4^+ concentrations away from the central axis of the tube are then (no compaction or net addition of particles):

Zone I

$$(13) \quad \frac{\partial C_I}{\partial t} = \frac{D}{(1+K)r} \frac{\partial}{\partial r}\left(r \frac{\partial C}{\partial r}\right) + \frac{R}{(1+K)}, \qquad a < r < b$$

Zone II

$$(14) \quad \frac{\partial C_{II}}{\partial t} = \frac{D}{(1+K)r} \frac{\partial}{\partial r}\left(r \frac{\partial C}{\partial r}\right), \qquad b < r < d$$

Where:

r = radial distance from tube axis

t = time

C_I = concentration of NH_4^+ in Zone I (burrow wall)

C_{II} = concentration of NH_4^+ in Zone II

R = constant average rate of NH_4 production in Zone I, production in Zone II is ignored

K = Langmuir adsorption coefficient (reversible) in linear range of adsorption.

a = inner radius of Zone I (radius of hollow tube)

b = outer radius of Zone I (outer radius of distinct burrow wall,

$$(12) \quad 6(CH_2O)_x\ (NH_3)_y\ (H_3PO_4)_z + 3(SO_4^{=})_x \rightarrow$$

$$6x(HCO_3^{-}) + 6y(NH_3) + 6z(H_3PO_4) + 3x(H_2S)$$

where, after Sholkovitz (1973), the stoichiometry of C, N, and P in the source organic material have not been explicitly defined and have been left as the subscripts x, y, and z; carbon is written as having an average carbohydrate oxidation state (Richards, 1965).

The gradients in pore water concentrations of NH_4^+ and alkalinity around the burrow are maintained over the short distances involved by metabolic reactions like equation (12). By assuming steady state concentration distributions, these gradients can be used to model the rate of metabolism in the tube wall. The radial symmetry of the burrow suggests that the geometry of pore water diffusion around it can be approximated by a hollow cylinder (annulus) having its axis fixed vertically in the sediment; this symmetry was assumed during sampling. In the case of NH_4^+, no great depth dependent concentration gradient in the burrow wall exists below the top few centimeters which, together with the ~20 cm axial length and ~1.5 cm wall thickness, implies that the end boundaries of the cylinder can be considered to be at infinite distance. The average concentration of pore water NH_4^+ is known in two discrete sampling zones around the tube axis and also at a distance of ~30 cm from the burrow. Because Zone II pore water NH_4^+ values are

$$(22) \quad \bar{C}_{II} = \frac{2\pi \int_b^d C_{II}\, r\, dr}{2\pi \int_b^d r\, dr}$$

Solving these equations simultaneously and using the values: $C_I = 0.98$ mM (average concentration below 0-1 cm), $C_{II} = 0.43$ mM (average concentration below 0-1 cm), $C_a = 0.0045$ mM ($= C_B$), $C_d = 0.35$ mM (average surrounding sediment below 0-1 cm), $a = 0.375$ cm, $b = 1.875$ cm, and $d = 3.75$ cm, results in:

$$\frac{R}{D} = 0.80 \ \frac{\mu M}{cm^2}$$

Taking $D = 7 \times 10^{-6}$ cm^2/sec for NH_4^+ (based on Li and Gregory, 1974; with tortuosity correction of 0.37 based on Goldhaber et al., 1977, and temperature correction to 22°), then $R = 5.6 \times 10^{-6}$ mM/sec = 180 mM/yr. This rate of NH_4^+ production is about 4 times the highest rates of production (corrected for adsorption) found in the top few centimeters of muds from Long Island Sound (Chapter V), demonstrating the high reactivity of the burrow wall and the importance of burrow microenvironments in decomposition.

The assumptions and data used in the diffusion-reaction model can be checked in part by comparing the model predicted flux of NH_4^+ into burrow water with that actually measured on the flat. The flux of NH_4^+, J, across the inner burrow wall is given by:

b - a = thickness of Zone I) and inner radius of Zone II

d = outer radius of Zone II sample zone

Adsorption can be ignored because only the steady state case will be considered (see Berner, 1976b).

At steady state ($\frac{\partial C}{\partial t} = 0$), the general solutions are:

Zone I

(15) $C_I = A + B \ln r - \frac{Rr^2}{4D}$

(16) $C_{II} = A_2 + B_2 \ln r$

The constants A, B, R, A_2, and B_2 must meet the boundary conditions:

(17) $C_I = C_a$, $r = a$ (burrow water concentration)

(18) $C_{II} = C_d$, $r = d$ (average surrounding sediment concentration)

(19) $\left(\frac{\partial C_I}{\partial r}\right)_{r=b} = \left(\frac{\partial C_{II}}{\partial r}\right)_{r=b}$

(20) $C_I = C_{II}$, $r = b$

and in addition the average analytical concentration, $\bar{C}$, in each zone is known, giving:

(21) $\bar{C}_I = \frac{2\pi \int_a^b C_I \, r \, dr}{2\pi \int_a^b r \, dr}$

state distribution of NH_4^+ and $HPO_4^=$ in Zone I due to diffusion and production only, is given by (adsorption cancels out at steady state, no advection):

$$(24) \quad C_N = A_N + B_N \ln r - \frac{R_N r^2}{4D_N}$$

$$(25) \quad C_P = A_P + B_P \ln r - \frac{R_P r^2}{4D_P}$$

C_N = NH_4^+ concentration

C_P = $HPO_4^=$ concentration

A_N, B_N, A_P, B_P = constants

R_N = rate of NH_4^+ production

R_P = rate of $HPO_4^=$ production

If, like NH_4^+ and alkalinity, the average $HPO_4^=$ concentration is highest in Zone I and decreases in Zone II, then for both NH_4^+ and $HPO_4^=$ there is a distance $r = f_{N,\,P}$ away from the burrow axis where:

$$(26) \quad \left(\frac{\partial C_N}{\partial r}\right)_{r = f_N} = 0$$

$$(27) \quad \left(\frac{\partial C_P}{\partial r}\right)_{r = f_P} = 0$$

The use of this condition in the solution of equations (24) and (25) results in

$$(23) \quad J = \varphi D \left.\frac{\partial C}{\partial r}\right|_{r=a} = \varphi D \left(\frac{B}{a} - \frac{Ra}{2D}\right)$$

φ = porosity at r = a

Taking φ = 0.5 (approximate porosity of sediment just outside the inner organic lining of burrow) and all other values as listed previously, then the predicted flux is 9.8×10^{-6} μmoles/cm^2/sec. With a standard burrow of diameter 0.75 cm and length 30 cm (V_o = 13 cc), then the rate of increase of NH_4^+ in burrow water should be 3.1 μM/min. The actual measured value is 0.31 μM/min. Agreement between the predicted and measured flux is not especially good but considering the large number of assumptions it is as good as could be expected. The comparison assumes that : (1) no NH_4^+ consumption occurs in the oxidized portion of the burrow wall; (2) the organic sheets periodically present in the tube wall do not hinder diffusion; (3) that no significant change in pore water concentrations took place between August, when the burrow water measurements were made, and October when the pore water NH_4^+ concentrations were determined; (4) that uncertainties in the value of D and analytical concentrations are insignificant; and (5) that exact agreement of data from a single burrow with average data from many burrows is expected.

The flux and pore water measurements allow limits to be placed on the stoichiometry of decomposition as represented by x, y, and z in equation (12). From the above hollow cylinder model (equations 13-15), the steady

an especially simple form for comparison of fluxes as will be demonstrated. From the model and boundary conditions used previously (equations 13-22) one expression for f is:

$$(28) \quad f = \left(\frac{2D z}{R} + b^2 \right)^{1/2}$$

where

$$(29) \quad z = \frac{\bar{C}_{II} - C_d}{\frac{d^2 \ln d - b^2 \ln b}{d^2 - b^2} - \ln d - 0.5}$$

With the values used for the NH_4^+ model, $f_N = 1.66$ cm and lies in Zone I. Assuming that f_P also is in Zone I then:

$$(30) \quad B_N = \frac{R_N f_N^2}{2 D_N}$$

$$(31) \quad B_P = \frac{R_P f_P^2}{2 D_P}$$

Letting J_N and J_P correspond to the flux of NH_4^+ and $HPO_4^=$ across the inner burrow surface r = a, results in:

$$(32) \quad J_N = \varphi D_N \left(\frac{R_N f_N^2}{2 D_N a} - \frac{R_N a}{2 D_N} \right)$$

$$(33) \quad J_P = \varphi D_P \left(\frac{R_P f_P^2}{2 D_P a} - \frac{R_P a}{2 D_P} \right)$$

If the stoichiometry of N to P release during decomposition is relatively constant, then by equation (12):

$$(34) \quad R_P = \frac{z}{y} R_N$$

The ratio y/z (average N/P ratio) can be obtained directly from the ratio of the fluxes only if $f_N \sim f_P$. The equivalency of f_N and f_P depends on both D_N, D_P, and on the concentration differences on the boundaries of Zone I (equations 28, 29); assuming that $f_N \sim f_P$ (not unreasonable, see for example Figures V-28, 31; Chapter V) in the absence of pore water $HPO_4^=$ data, gives

$$(35) \quad \frac{J_N}{J_P} = \frac{y}{z} \left(\frac{f_N^2 - a^2}{f_P^2 - a^2} \right) \sim \frac{y}{z}$$

The ratio of fluxes obtained from burrow water samples results in an N/P ratio of 4.7; use of equation (7) to correct the $HPO_4^=$ flux for precipitation lowers the ratio to ~ 1. Because of the uncertainty, listed previously, in the correspondence of measured fluxes across the inner burrow surface to metabolic reactions in the wall, these ratios could be low by a factor of 10. If the calculated ratios are accepted, then the N/P content of the decomposing fraction of organic matter is lower than average planktonic material where N/P ~ 16 (Richards, 1965). Preferential release of P relative to N is typical of the earliest stages of decomposition (e.g., Vacarro, 1965, Table 4; Grill and Richards, 1964) where autolysis and excretion by microbes other than bacteria

may also play a role (Johannes, 1968).

An average C/N (x/y) ratio for the decomposing organic matter in the burrow wall can also be derived by use of the master decomposition equation (12) and the alkalinity models of Berner, Scott, and Thomlinson (1970) and Sholkovitz (1973). Titration alkalinity is predominantly carbonate alkalinity in muds (Berner, Scott, and Thomlinson, 1970) and it should be a good approximation to carbonate alkalinity in the relatively organic-poor sediment studied here. Given this and initially ignoring adsorption of NH_4^+, then by equation (12): $(Alk) = (Alk)_{initial} + 2\Delta SO_4^= + \Delta NH_4^+$, assuming no change in Ca^{++} or Mg^{++}. Since:

$$(36) \qquad \Delta NH_4^+ = \frac{2\Delta SO_4^=}{x/y}$$

then:

$$(37) \qquad C/N = x/y = \frac{\Delta Alk - \Delta NH_4^+}{\Delta NH_4^+}$$

is the carbon/nitrogen ratio of the organic matter being broken down. The ratio $\Delta NH_4^+/\Delta Alk$ can be obtained by plotting NH_4^+ vs. Alk and computing the slope (Figure II-14). Data from all samples have been plotted on the same graph; this assumes that the same fraction of organic matter is being broken down initially in each sample zone and that only the intensity and not kind of breakdown differs between burrow wall and surrounding sediment.

Surface values (0-1 cm) were excluded in the calculation because of the possible influence of diatoms. The calculated C/N (molar) ratio by use of the slope and equation (35) is 2.7. If the concentrations are not at steady state then adsorption of NH_4^+ affects this calculation (Berner, 1976b; Rosenfeld and Berner, 1976); based on a Langmuir adsorption coefficient $K \sim 1$ (for muds, Rosenfeld, in preparation), the calculated C/N ratio would be lowered to 0.9.

Because of the possible low N/P ratio, H_3PO_4 production, depending on its speciation at formation, may also influence alkalinity. Assuming $PO_4^{\equiv}$ is formed first and that after reaction $HPO_4^{=}$ is the predominant species at pH ~ 7.2 (see Kester and Pytkowitz, 1968), then:

$$(38) \quad \frac{\Delta Alk - \Delta NH_4^+}{\Delta NH_4^+} = \frac{C}{N} - 2\frac{P}{N}$$

Unfortunately no $HPO_4^{=}$ concentration measurements were made around the burrow but the N/P ratios calculated previously can be used. This changes the calculated C/N ratio from 2.7 to 3.1 - 4.8 by use of N/P = 4.7 - 1 respectively, or if adsorption is considered with K = 1, the range is C/N = 1 - 2.9. Both the calculations with and without considering the effects of $HPO_4^{=}$ formation or adsorption result in determination of a C/N ratio lower than the 6.6 average ratio accepted for planktonic material (Richards, 1965).

The high rate of metabolism in the burrow wall is reflected in the relatively greater abundance of fixed sulfur: acid volatile (~FeS), pyrite (FeS_2), and elemental (S^o), in the wall than in ambient sediment (Figure II-12). The increase in pyrite and acid volatile sulfur from the inner burrow wall (Zone 1) to the outer (Zone 2) demonstrate that the sulfur is fixed by reduction in the wall and cannot result from selection by Amphitrite of sulfur rich particles at the interface during burrow construction. It is possible to show that not all sulfur reduced in the wall may remain there by the following considerations. The outer burrow wall (Zone 2) is formed by addition of layers which once formed the inner wall (Zone 1, Figures II-4B, C). These are added to Zone 2 in single construction events so that initially Zone 2 layers have the same organic matter content as did the inner wall. Because Zone 1 usually shows some evidence of the presence of black FeS on its outside edge and Zone 2 is exclusively black, it can be assumed that further breakdown of organic matter once in Zone 2 is by sulfate reduction. The difference in organic matter content over the depth intervals 0-7, 7-11, 11-18, and 24-30 cm is 1.09%, 0.51%, 0.97&, and 0.99% respectively. Percent organic matter can be roughly converted to %C values by dividing by the factor 2 (e.g., Dean, 1974) Assuming the 2C/1 S stoichiometry of sulfate reduction, the corresponding %S at each depth is: 0.7, 0.3, 0.6, and 0.7%. The measured total %S (FeS, FeS_2, S^o, org. S) in each interval is: 0.12, 0.15, 0.16, and 0.17%. This suggests that: (1) other

The calculations of C/N ratio made above assume complete oxidation of carbon by sulfate reducers and its appearance as bicarbonate (e.g., Goldhaber, 1974). If, for example, part of the carbon fraction is oxidized to short chain acids rather than CO_2, the C/N ratio will be underestimated because of the use of titration alkalinity. Metabolic pathways other than that described by equation (12) which influence either alkalinity or NH_4^+ also compromise this calculation. The stoichiometric ratios for both P/N and C/N release are therefore suspect but are consistent with the known tendency for preferential breakdown of N and P-rich fractions of organic matter during early decomposition (e.g., Krause, 1959; Johannes, 1968).

Knowledge of the C/N ratio allows conversion of the rate of NH_4^+ production in the burrow wall to an equivalent rate of $SO_4^=$ reduction for purposes of comparison. In this case:

$$(39) \quad \frac{d(SO_4)}{dt} = \frac{1}{2} \frac{C}{N} \frac{d(NH_4^+)}{dt}$$

which from C/N ~ 1 - 2 gives R_s ~ 100 - 200 mM/yr. This rate is similar to that found in surface sediment (0-1 cm) of Long Island Sound where R_s ~ 100 mM/yr at 22°C (Goldhaber et al., 1977; Chapter V). This general agreement is evidence that the metabolic rates and stoichiometric ratios calculated are not unreasonable and that the range of the rates, at least, is indicative of fresh organic material as substrate.

forms of bacterial metabolism have broken down the utilized organic matter, (2) HS^- has been lost from the system by diffusion and oxidation in a relatively Fe poor environment (Berner, 1969), (3) labile solid phase sulfides or pyrite have been oxidized, (4) the stoichiometry of 2C/1 S is not valid (Goldhaber, 1974), (5) the assumption of steady state organic content in the burrow wall is incorrect, (6) the conversion factor of organic matter determined by ignition loss to C is incorrect due to water loss from minerals. None of these is mutually exclusive but #4 is unlikely because of the high selectivity and predictability in burrow construction and #6 is minimized in sandy sediment and by the use of differences in organic content between layers rather than absolute values. Because of the many possible errors involved in the above sulfur balance calculation, it cannot conclusively demonstrate oxidation and loss of sulfide from the burrow wall but the results are not inconsistent with loss. This is discussed in more detail later.

Before further discussing diagenetic processes associated with the burrow an interesting observation on diagenesis in surrounding sediment can be made. Despite the presence of a large number of living shell bearing animals in the sands of Barnstable Harbor there is sometimes little evidence that shell debris is preserved at depth. Shells of one of the most abundant animals, Nassarius obseletus, can often be found in various stages of destruction throughout the top few decimeters of sediment. There are several possibilities for this lack of preservation: transport, biogenic

destruction, or shell dissolution. The last case can be shown to be a distinct possibility by simple equilibrium calculations. Assuming the apparent K_{sp}'s at 25°C for calcite and aragonite of Berner (1976c), the carbonic acid apparent dissociation constants of Lyman (1965), assuming Ca^{++} concentration of 10 mM, using titration alkalinities as equivalent to carbonate alkalinity, and punch-in pH's of Table II-5, then it is found that pore water samples from every zone are undersaturated with respect to both calcite and aragonite. The assumptions of high temperature, high calcium concentration, and use of total alkalinity make the calculated ion products/K_{sp} maxima. The highest IAP/K_{sp} calcite is 0.9 (burrow wall); ambient sediment $\sim$0.2-0.8. It seems likely that the paucity of preserved shell debris in these sands is due to carbonate dissolution.

Mobilization of metals

The pore water Fe and Mn profiles show mobilization of both metals at the sediment-water interface and in the burrow wall. Dissolved Fe and Mn concentrations in the burrow wall increase with depth while those of the ambient sediment decrease rapidly away from the interface. This demonstrates, just as the earlier considerations on decomposition in the burrow wall, that the burrow retains along its entire length diagenetic properties typical of, or more intense than, the sediment-water interface. The decrease in Fe and Mn concentrations with depth in sediment away from the burrow is presumably

the result of precipitation of insoluble compounds such as iron or manganese sulfides (e.g., Troup, 1974; Holdren, 1977) or irrigation and reworking of surrounding sediment by animals like Clymenella torquata resulting in transport of dissolved Fe and Mn out of the sediment (Chapter III).

Both Fe and Mn occur as oxide coatings on particles and under reducing conditions are dissolved and mobilized as Fe^{++} and Mn^{++} (e.g., Krauskopf, 1957). The reduction of Fe and Mn-oxides may be mediated directly by bacteria, catalyzed by their metabolic by-products, or may be the indirect result of the reducing conditions created by their metabolic activity (Mann and Quastel, 1946; Trimble and Ehrlich, 1968; Bromfield and David, 1976). Iron can also be mobilized as Fe^{++} by the oxidation of FeS and FeS_2, as occurs in acid mine drainage. Although under oxidizing conditions at near neutral pH the resulting Fe^{++} is quickly converted to Fe^{+++}, in the presence of additional iron sulfide the Fe^{+++} becomes an active agent in the further oxidation of solid phase sulfide and is rapidly reduced once again (e.g., Singer and Stumm, 1970; Stumm and Morgan, 1970). Pyrite oxidizes slowly in sea water (Harmsen, 1954); a rough estimate of pyrite oxidation in surface muds of Long Island Sound gives rates of ~ 50 μmoles s/g-sediment/year (Chapter VI). Water-logged soil also shows relatively slow rates of pyrite oxidation (Bloomfield, 1972). On the other hand, labile FeS (acid volatile S) is rapidly oxidized on a time scale of a few days and results in the release of Fe^{++} and a lowering of alkalinity, but with only minor

changes in pH (Bloomfield, 1972; Chapter VI). This suggests that in the burrow wall and in near-interface sediment, Fe^{++} can be produced by both the reduction of $Fe(OH)_3$ and by the oxidation of FeS and FeS_2 resulting in high standing concentrations of Fe^{++} along boundaries between O_2-rich and HS^--rich regions of sediment. Little is known about the role of oxidation in the mobilization of Mn. The chemistry of Fe and Mn near the sediment water interface is discussed in more detail in Chapter VI.

The possibility that in addition to reduction of Fe-oxides, oxidation of solid phase sulfides takes place in the burrow wall, is consistent with a number of observations: (1) the low alkalinity/Cl^- ratios in the burrow water, (2) the low pH of burrow water, (3) high dissolved Fe in burrow water, and (4) an apparent imbalance between organic matter utilized and fixed S in the burrow wall. Each of these suggest that conditions in the dwelling tube of Amphitrite can in some ways be described as micro-acid mine drainage. A slow rate of oxidation, irrigation of the burrow, and the buffer capacity of sea water keep the burrow from becoming very acid and thereby more favorable for marine Thiobacilli (Vishniac and Santer, 1957) and a resulting acceleration in oxidation (Singer and Stumm, 1970). It should be emphasized that the reduction of $Fe(OH)_3$ and production of FeS_x is also taking place, tending to counteract the effects of oxidation and also mobilizing Fe as Fe^{++}.

Mobilization of Fe and Mn in the pore water lead to their redistribution in the solid phase. Zn is also clearly solubilized and concentrated in the inner burrow wall (Figure II-13). When the burrow is first constructed of surface material and packed with mucus it presumably consists only of the innermost layer (Figure II-3). If the surrounding sediment contained reactive metal oxide surfaces, those metals, for example Fe, capable of being mobilized by reduced ion diffusion (not HS^-) from the wall would counterdiffuse toward the organic rich burrow wall and become enriched there (Berner, 1969). Because of the low pore water concentrations of either Fe or Mn at depth in the sediment and because in this case the surfaces of particles are low in metals and have probably been previously reacted with sulfide, it is unlikely that most of the enrichment of the burrow wall in Fe, Mn and Zn occurs in the above way. A more likely explanation in the present case is that initially the innermost burrow lining becomes enriched to a small extent in Fe and Mn-oxides which accumulate by diffusion from the more reduced portions of the burrow wall (0-2 mm thick at this point). These oxides are known to scavenge many metals such as Cu, Zn, Co, Ba, Ra (e.g., Goldberg, 1954; Krauskopf, 1956; Jenne, 1968; Kharkar, Turekian and Bertine, 1968; Murray, 1975). Metal rich sea water released from marsh areas in the inner harbor is constantly cycled over this surface by irrigation, which, together with active precipitation of Fe and Mn diffusing into the burrow

water from the burrow wall, acts to scavenge the cycled water of some of its dissolved metals. The inner burrow layer becomes increasingly enriched in Fe and Mn oxide-scavenged metals such as Zn as well as additional Fe and Mn. When a new inner burrow layer is formed the initial one moves outward and is reduced; a portion of its enriched metal content becomes mobilized and diffuses both back toward the new inner burrow wall and into surrounding sediment (Sensu: Murray and Irvine, 1895; Bender, 1971; Holdren, 1977) but much of the excess metal is fixed as sulfide in the metabolically active burrow wall thereby permanently enriching the older burrow wall layers. A portion of the sulfides may also be subject to oxidation and acid production as previously described. Deeper regions of the burrow which are subject to slightly longer residence times of burrow water because of asymmetric irrigation, should tend to accumulate rapidly precipitated metals such as Fe. The data support this contention (Figure II-13).

It was shown earlier that there is a measurable flux of Fe out of the average burrow of ~ 0.2 μmoles/d. This is a small loss compared to the total Fe passed through the burrow by irrigation per day of ~ 2 μmoles/d (assuming irrigation rate = 83 cc/hr, Fe = 1 μM --see Table II-2, 3). Approximately the same quantity of Mn is also cycled through and is subject to capture. These calculations indicate that the above explanation for enrichment is possible from the standpoint of supply. Zn content of overlying

water was not determined but literature data show that salt marshes may be a source for this and other metals as well (Turekian, 1976). It should be noted explicitly that Zn is shown to be diagenetically mobile, a factor sometimes ignored in many recent investigations of sedimentary trace element distributions.

Many permanent dwelling-tubes constructed in sediment can be expected to exhibit similar chemical processes as documented for Amphitrite ornata. When these burrows are near an overwhelming source of supply of dissolved metals such as a salt marsh they may accumulate excess metal in the burrow wall as in the case of Amphitrite. Normal diagenetic migration related to gradients in the distribution of metabolizable organic matter around the burrow and associated decomposition will also tend to enrich the inner burrow surface in metals like Fe and Mn. My own observations plus those of many others in the literature indicate that these processes are common in both recent and preserved burrows. In the fossil record, dwelling structures and feeding traces occupied by an animal for a considerable period, commonly show pyrite envelopes or are centers of concretions (e.g., Simpson, 1957; Hallam, 1960; Frey, 1970b; Hein and Griggs, 1972). Hematite cylinders ringing the inside of the inner burrow lining can often be seen in Skolithos burrows common in quartzites (e.g., Hoffman, 1970). This study shows that the migration processes responsible for these features occur during the life of the organisms involved and result from their activities. The occurrence of similar features in fossil structures demonstrates the geologic continuity

in these processes. It also suggests the use of trace fossils as diagenetic markers during lithification and as indicators of late stage migration of elements in a deposit where these concentrations are destroyed.

Teal and Kanwisher (1963) estimated that at least 22% of the surface area of a Georgia salt marsh was represented by burrow walls. The illustration in this study of the importance of burrow environments to sediment-water interaction and the long geologic history of biogenic structures such as permanent tube-dwellings, suggests that an understanding of diagenetic processes associated with burrows is essential for elucidating sediment and overlying water interaction.

Summary

1. The U-shaped tube of Amphitrite ornata is formed of particles obtained at the sediment surface and transported to depth. The tube consists of five or more multiple layers 1-2 mm thick composed of small mucus cemented particles of sediment. Each layer is lined on its inner side with an organic membrane ~5 μm thick.

2. Amphitrite transports particles at a rate of ~4.5 g/d at 22°C. Fluid transport into the burrow is ~91 cc/hr based on microthermister current meter readings made in the laboratory. This is in good agreement with hydrostatic head measurements of irrigation rate of ~75 ml/hr made by Croyer and Mangum (1973).

3. Chemical properties of water contained in the burrows of Amphitrite change rapidly during the intertidal period. The rate of change can be modeled to obtain the flux of Fe, NH_4^+, and $HPO_4^=$ out of the burrow walls. Together with irrigation rate measurements, the rate of change of burrow water properties can be used to determine the steady state concentration of different ions normally present in the burrow and to show that burrow water is higher in certain metabolites (e.g., NH_4^+, $HPO_4^=$) than overlying sea water. $HPO_4^=$ flux can be corrected for precipitation and a precipitation rate constant calculated. Expressed as a first order constant, a value of ~ 0.005/min is obtained.

4. The burrow wall is the site of intense decomposition. Expressed as a rate of $SO_4^=$ reduction a modeled rate of ~100-200 mM SO_4/yr at 22°C is obtained. The modeled N/P and C/N ratios of the decomposing organic material are low and indicative of the rapid initial stages of decomposition of organic material.

5. The intense decomposition processes in the burrow wall result in the concentration of iron sulfides immediately around the tube possibly creating micro-acid mine-drainage conditions in the burrow.

6. Decomposition also results directly or indirectly in the mobilization of Fe, Mn, and Zn in the wall and their concentration along the inner burrow surface. Irrigation of the chemically reactive Fe-Mn oxide rich burrow wall results in scavenging of some elements from sea water into the wall and

further metal enrichment of the burrow.

7. Similar diagenetic structures around trace fossils demonstrate the geologic antiquity of the processes described.

Table II-1. Weight Percent Abundance of Particle Size Fractions in the Burrow Wall of *Amphitrite ornata*

Sample		Size fractions						
Radial sample zone	Vertical depth interval	<62μm%	>62μm%	125μm%	250μm%	500μm%	1000μm%	2000μm%
1	0-7 cm	11.6	28.1	31.0	22.8	6.8	-	-
1	7-11 cm	20.1	38.9	22.9	7.8	7.4	2.9	-
1	11-18 cm	26.0	39.3	19.1	9.5	6.0	-	-
1	24-30 cm	30.7	32.1	19.8	11.5	2.4	3.4	-
2	0-7 cm	11.0	23.1	22.6	24.4	14.6	4.4	-
2	7-11 cm	27.0	40.3	18.3	8.3	4.6	1.5	-
2	11-18 cm	28.8	38.3	18.0	10.8	4.0	0.1	-
2	24.30 cm	37.8	35.6	14.6	6.7	2.8	2.5	-
3	0-7 cm	15.8	27.4	25.1	21.3	8.8	1.7	-
3	7-11 cm	16.0	33.6	25.8	15.6	5.8	3.3	-
3	11-18 cm	20.2	35.6	20.7	15.6	6.0	1.8	-
3	24-30 cm	37.6	19.6	13.2	15.4	11.1	2.9	-
4	0-1 cm	16.2	26.0	23.0	20.8	11.1	2.0	0.9
4	1-2 cm	11.7	23.7	24.2	25.9	13.8	0.6	-
4	2-3 cm	14.1	21.6	22.3	25.7	13.5	2.7	-
4	14-15 cm	16.9	22.6	18.7	26.3	11.3	4.1	-

Table II-2. Fluid and Particle Transport Rates for *Amphitrite ornata*

Fluid Transport

Burrow Opening	Average Continuous Velocity
Head (withdrawn)	0.094 cm/sec
Head (feeding)	0.075 cm/sec
Tail (withdrawn)	0.018 cm/sec
Tail (feeding)	0.043 cm/sec

Velocity range: $\leq$ 0.043 cm/sec - 10 cm/sec; usually < 1 cm/sec

Particle Transport

Measurement Period	Rate	Average Rate (short period average)	Average Rate (integrated 7 day)
1 (2 days)	2.6 g/d		
		3.9 $\pm$ 2 g/d	4.5 g/d
2 (5 days)	5.2 g/d		

Table II-4. Burrow Water of Amphitrite ornata

Sample No.	t (minutes exposed)	Number of burrows sampled	Cl^- (M)	Ca (mM)	Ca/Cl	Mg	Mg/Ca	Alk (meq/ℓ)	Alk/Cl x 10^3	$PO_4^{\equiv}$ (μM)	NH_4^+ (μM)	Fe (μM)	Mn (μM)
1	10	1	0.364	6.58	.0181	34.1	5.18	1.46	4.01	3.9	4.5	1.3	1.3
2	47	2	0.412	7.42	.0180	38.6	5.20	1.58	3.83	8.4	25.2	1.6	1.3
3	80	2	0.408	7.39	.0181	37.9	5.13	1.74	4.26	3.7	27.6	5.6	1.2
4	141	2	0.480	8.61	.0179	44.5	5.17	1.38	2.88	15.5	15.8	1.4	0.2
5	198	2	0.560	10.07	.0180	51.4	5.10	2.22	3.96	25.8	62.8	3.2	0.5
6	278	3	0.452	8.30	.0184	43.3	5.19	2.62	5.80	16.3	96.3	5.2	0.9

Table II-3. Tidal Flat Water Samples, Barnstable Harbor

Sample (see Fig. 1)	Cl^- (M)	Alk(meq/ℓ)	Alk/Clx10^3	$PO_4^{\equiv}$ (μM)	NH_4^+ (μM)	Fe(μM)	Mn(μM)
1 (Sept. 1,1976)	0.499	2.16	4.32	0.74	0.6	0.87	0.72
2	0.468	2.08	4.44	0.96	0.4	1.18	0.98
3	0.456	2.04	4.47	1.07	0.3	1.21	0.97
4	0.440	1.98	4.50	1.32	0.9	1.46	1.11
5	0.302	1.50	4.97	1.87	2.2	1.26	1.07
A (Aug. 12,1975) (random sample incoming water)	0.410	1.99	4.85	0.93	-	-	-

Table II-5. Pore Water Samples Around Amphitrite Burrows

SAMPLE						
Ambient Sediment						
Core Sample No.	Vertical Depth Interval	Alk (meg/ℓ)	pH (punch in)	NH_4^+ (mM)	Fe (μM)	Mn (μM)
1	0-1 cm	2.40	6.8	0.090	16.5	1.5
2	1-3 cm	2.51	6.9	0.306	4.1	0,6
3	3-6 cm	3.25	7.1	0.462	3.0	0.5
4	6-9 cm	2.48	7.2	0.4	2.9	-
5	9-12cm	2.26	7.2	0.3	$\leq$ 2.0	0.6
6	12-15cm	2.10	7.2	0.3	$\leq$ 1.4	0.7
Burrow Core						
Radial Zone						
I + II	0-1 cm	2.59	6.9	0.082	23.5	1.2
I	1-3 cm	3.70	7.1	0.87	25.0	1.2
I	3-6 cm	4.27	7.2	0.86	31.2	0.5
I	6-9 cm	5.37	7.0	1.27	48.3	9.9
I	9-13cm	5.07	7.0	0.963	48.3	4.3
I	13-17cm	5.15	7.1	0.943	156	8.0
II	1-3 cm	3.23	7.1	0.398	10	0.46
II	3-6 cm	3.04	7.3	0.399	6.8	0.2
II	6-9 cm	2.87	7.2	0.473	6.6	0.1
II	9-13cm	3.10	7.2	0.513	3.4	0.4
II	13-17cm	2.70	7.3	0.380	$\leq$ 0.9	1.7

Table II-6. Burrow Solid Phase Analysis

Sample					< 74 μm size fraction					
					Fe		Mn		Zn	
Radial Zone	Depth Interval	Ignition Loss	S_{av} (FeS) μm/g*	$S(FeS_2)$ μm/g	mg/g-ash	mm/g**	μg/g-ash	μm/g-ash	μg/g-ash	μm/g-ash
1	0-7	2.28	2.2	22	12.1	0.217	231	4.21	41.8	0.639
1	7-11	2.47	1.1	27	12.4	0.222	255	4.64	41.7	0.638
1	11-18	2.85	2.5	24	13.3	0.238	270	4.91	43.8	0.638
1	24-30	3.61	0.2	27	15.2	0.272	258	4.70	51.6	0.789
2	0-7	1.19	1.9	34	11.6	0.208	287	5.22	39.6	0.606
2	7-11	1.96	5.99	41	12.0	0.215	230	4.19	35.7	0.546
2	11-18	1.88	5.14	44	12.8	0.229	242	4.41	39.7	0.607
2	24-30	2.62	4.21	50	14.4	0.258	238	4.33	48.9	0.748
3	0-7	1.48	1.7	17	12.2	0.218	305	5.55	38.4	0.587
3	7-11	1.56	1.6	23	10.2	0.183	255	4.64	34.3	0.525
3	11-18	1.13	1.4	18	9.44	0.169	228	4.15	34.8	0.532
3	24-30	2.17	0.62	53	14.5	0.260	258	4.70	50.7	0.776
4	0-1	1.60	1.0	15	10.4	0.186	237	4.31	36.7	0.561
4	1-2	0.83	1.7	15	9.18	0.164	246	4.48	29.3	0.448
4	2-3	1.03	0.31	18	9.46	0.169	217	3.95	33.2	0.508
4	14-15	1.05	0.2	18	9.89	0.177	216	3.93	35.1	0.537

*μm = μmoles

**mm = mmoles

Chapter II

Figure Captions

Figure II-1: A. Cape Cod, Massachusetts showing location of Barnstable Harbor.

B. Barnstable Harbor, Calves Pasture Point lies in square.

C. Sampling locations I and II at Calves Pasture Point. Arrow indicates direction of current past sample locations at ebb.

D. Diagramatic cross section at location I during low tide, ebb current out of plane of page. Numbers in circles indicate position of burrow water samples; numbers in squares represent position of tidal flat water samples as described in text.

Figure II-2: A. Diagramatic representation of radial and vertical sample zones of a burrow for solid phase analysis.

B. Sampling zones for pore water analysis (done on entirely separate burrow).

Figure II-3: A. General shape of burrow; dimensions I and II are variable often (~ 30 cm each, see text).

B. Cross section of a section of one side of burrow illustrating multiple layer structure.

C. Blow-up of a single layer showing small parcels of mucus-cemented sediment which act as fusiform bricks of which the wall is constructed.

D. Enlargement of section of single layer showing polysaccharide lining on inner side and schematic packing of grains and sediment parcels.

Figure II-4: X-radiograph of one leg of a burrow from the relatively sandy high intertidal at location I showing particle size discontinuity between burrow wall and ambient sediment (scale bar = 3 cm).

Figure II-5: Grain size distributions in samples from radial and vertical sample zones (Figure II-2A) for solid phase analysis (burrow from location I). Weight percent abundance plotted.

Figure II-6: Illustrative velocity patterns of water flow into and out of burrows. A. Head end (withdrawn). B. Tail end (withdrawn). C. Head end (feeding). D. Tail end (feeding). E. Animal (withdrawn) quiescent with occasional velocity spikes up to, in some cases (not shown) 10 cm/sec.

Figure II-7: Tidal flat water compositions during ebb as a function of Cl^- concentration. Cl^- decreases during ebb (see text). $HPO_4^=$ = circles, Fe = triangles, Mn = squares.

Figure II-8: Burrow water concentrations of NH_4^+, $HPO_4^=$, and Fe as a function of time after exposure by tide. Lines determined by least squares analysis fit to data.

Figure II-9: Radial and vertical patterns of pore water alkalinity and NH_4^+ around Amphitrite burrow. Note radial gradients are greater than vertical. Zone I (burrow wall) = dots; Zone II = dashes; surrounding sediment = solid lines.

Figure II-10: Radial and vertical patterns of dissolved Fe and Mn associated with burrow. Zone I (burrow wall) = dots; Zone II = dashes; surrounding sediment = solid lines.

Figure II-11: Ignition loss (~ organic matter) patterns in burrow sample zones. Zone 1 = dots; Zone 2 = dashes; Zone 3 = solid; Zone 4 = diagonal slashes.

Figure II-12: Acid volatile sulfur (~ FeS) and pyrite sulfur (FeS_2) in burrow wall zones and surrounding sediment. (Zone 3 not plotted for clarity). Zone 1 = dots; Zone 2 = dashes; Zone 4 = diagonal slashes.

Figure II-13: Fe, Mn, and Zn distributions in burrow wall and ambient sediment (<74 μM size fraction) demonstrating enrichment patterns (Zone 3 not plotted for clarity). Zone 1 = dots; Zone 2 = dashes; Zone 4 = diagonal slashes.

Figure II-14: NH_4^+ versus titration alkalinity plot used in calculations in text. Line determined by least squares methods fit to data; surface values not used. Zone I = open circles; Zone II = open triangles; surrounding sediment core = solid circles; surface value is boxed in.

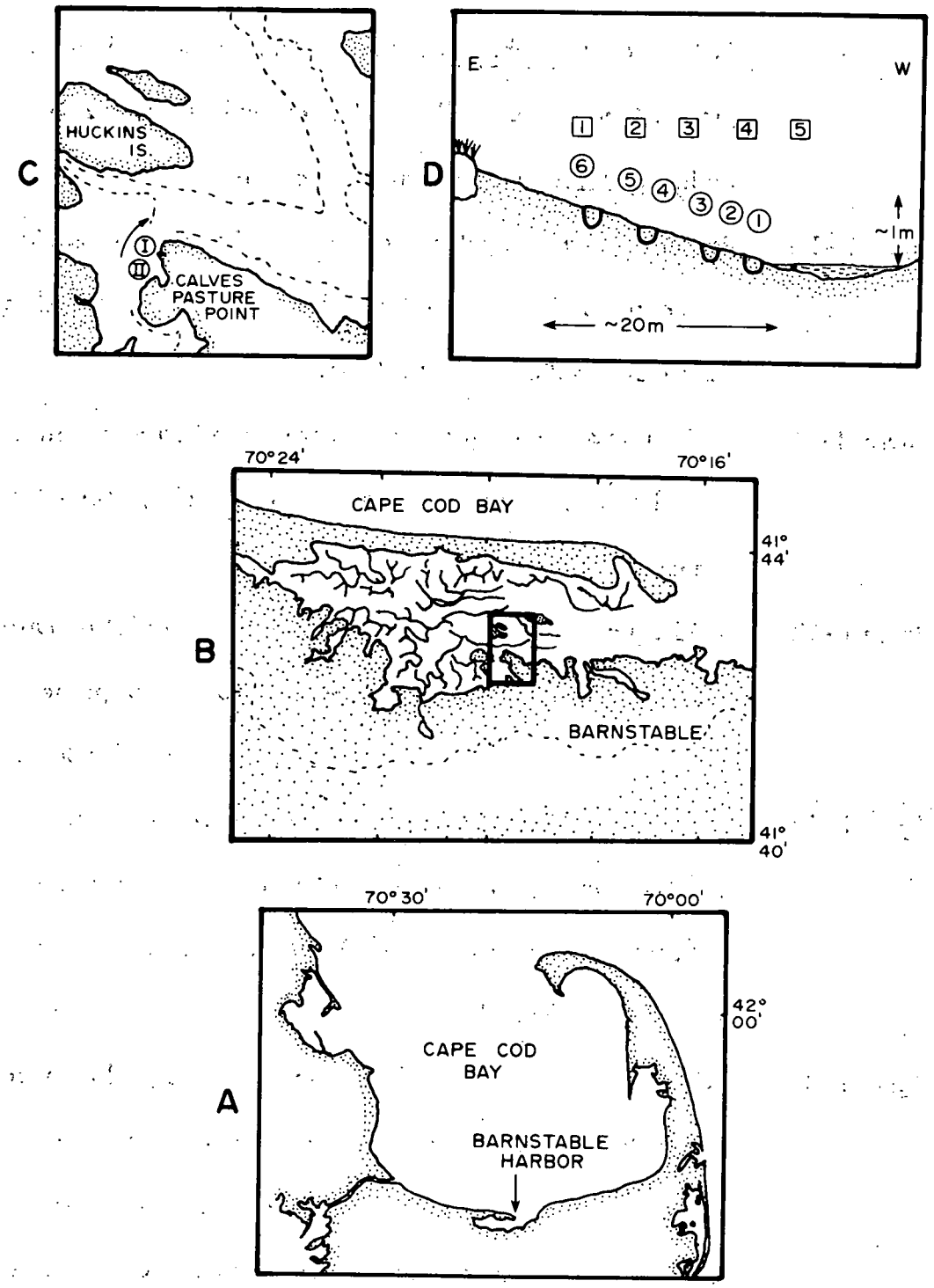

C
HUCKINS IS.
I
II
CALVES PASTURE POINT
D
E
W
1
2
3
4
5
6
~1m
~20m
B
70°24'
70°16'
CAPE COD BAY
41° 44'
BARNSTABLE
41° 40'
A
70°30'
70°00'
42° 00'
CAPE COD BAY
BARNSTABLE HARBOR

Figure II-1

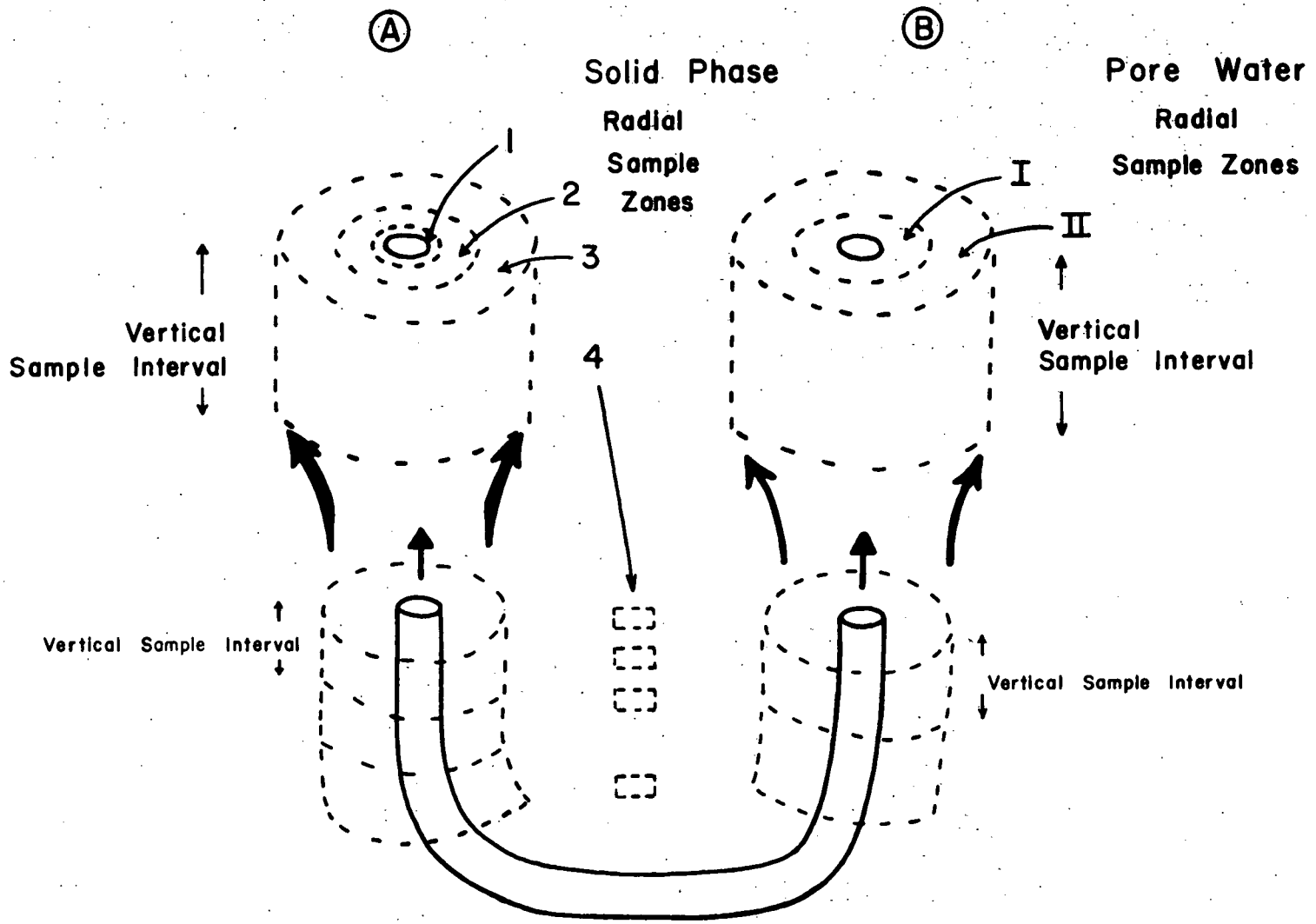

A
B
Solid Phase
Radial
Sample
Zones
Pore Water
Radial
Sample Zones
1
2
3
4
I
II
Vertical
Sample Interval
Vertical Sample Interval
Vertical Sample Interval
Vertical Sample Interval

Figure II-2

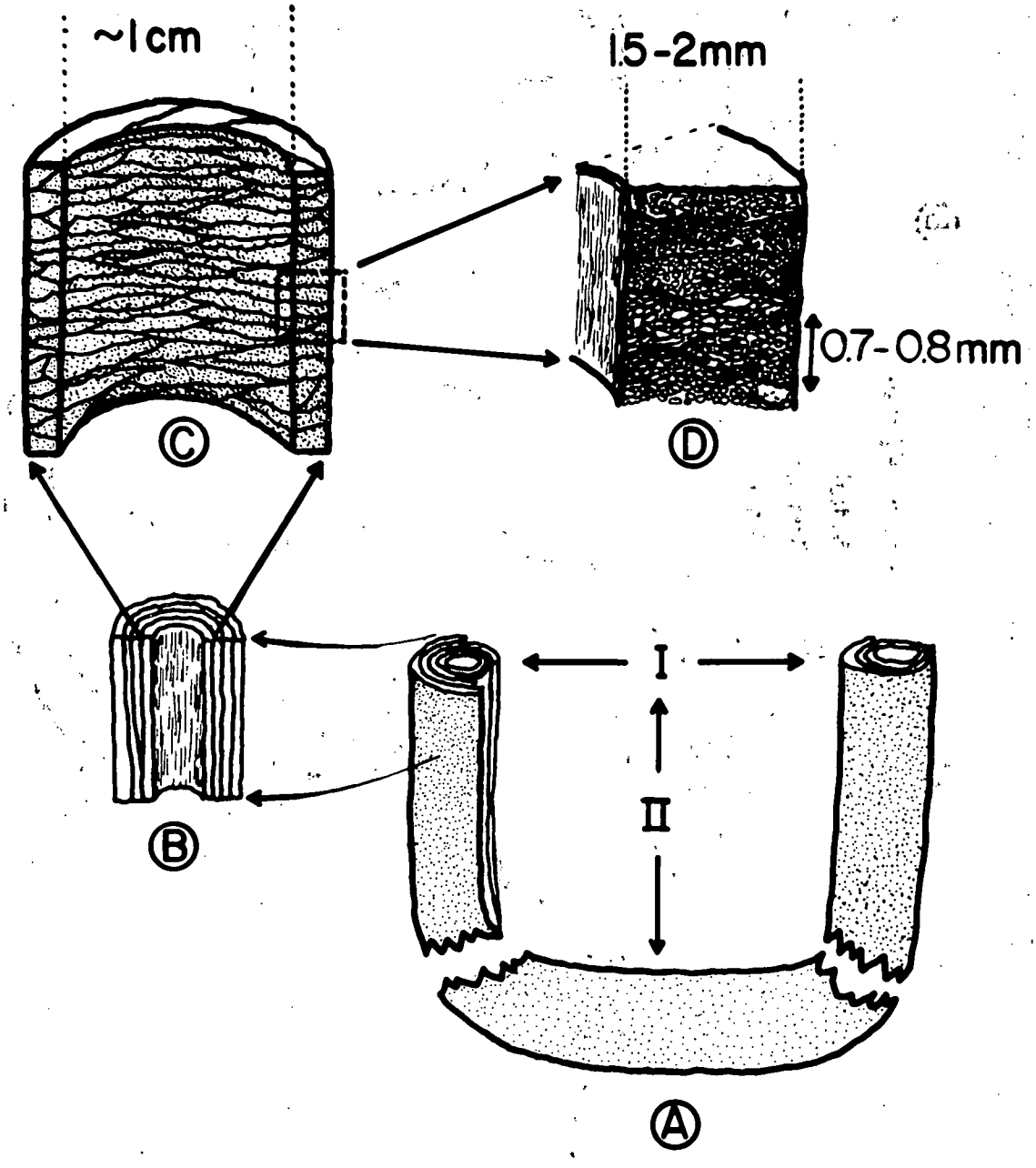
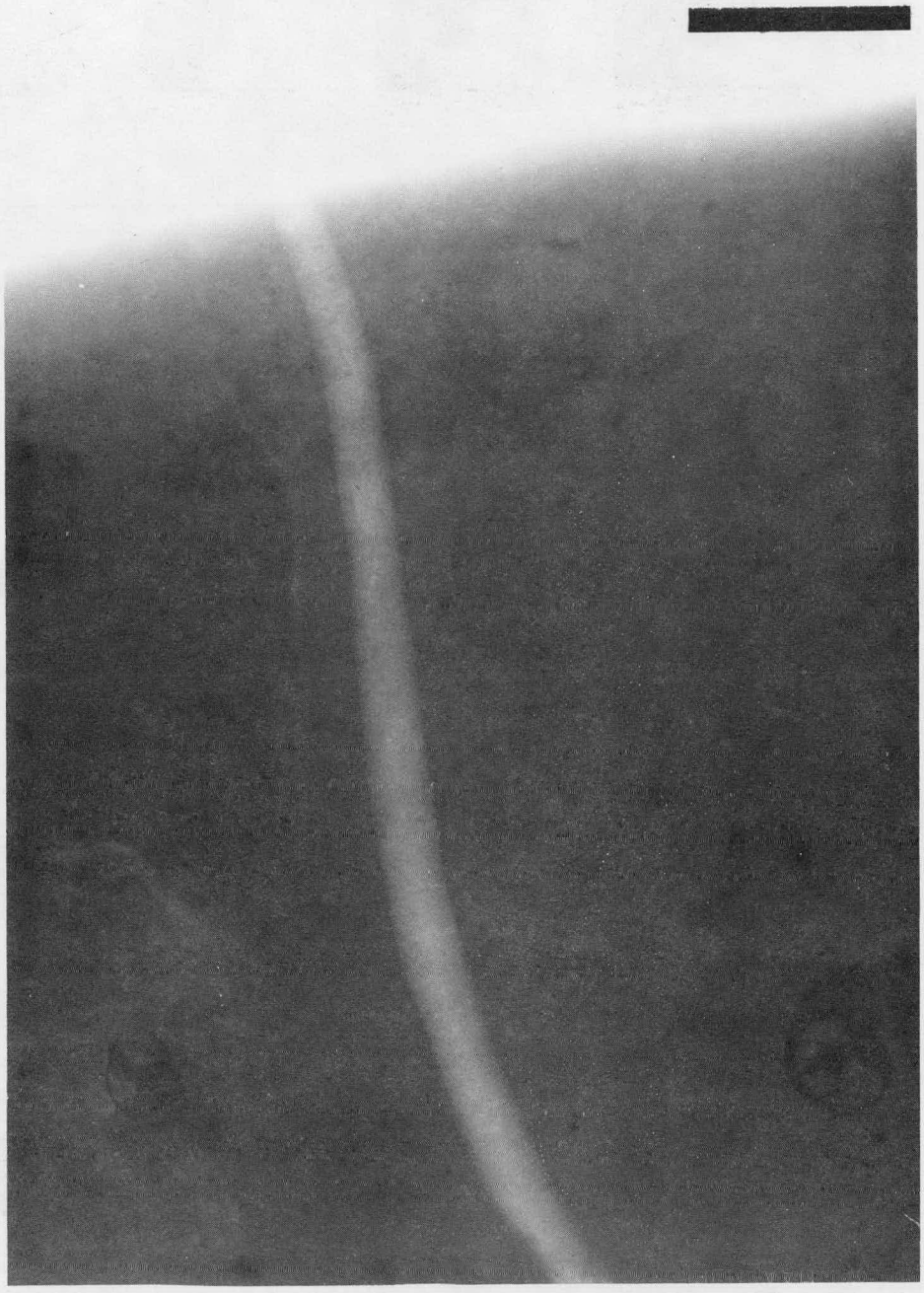


Figure II-3



11-4

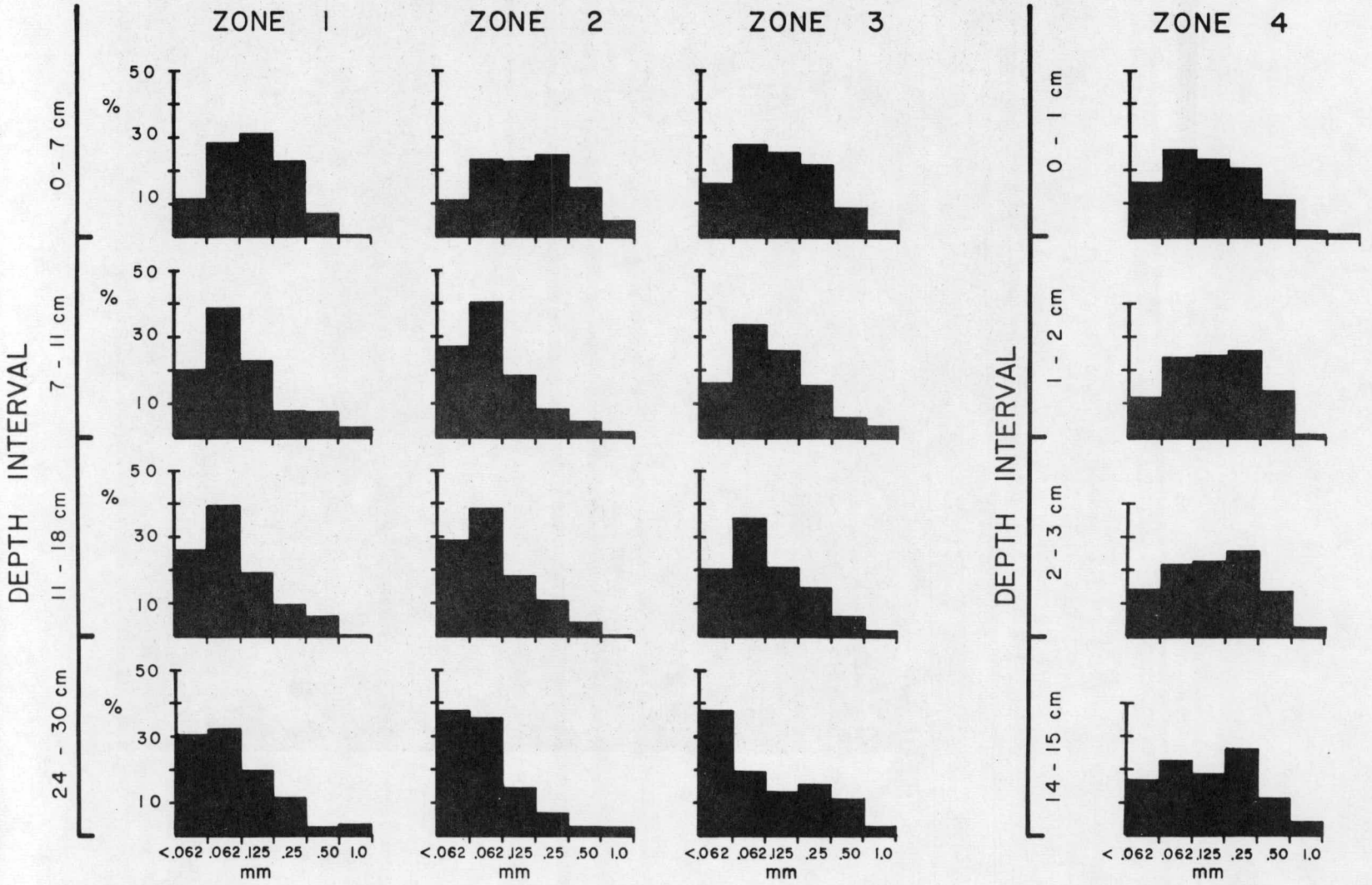

ZONE 1
ZONE 2
ZONE 3
ZONE 4
DEPTH INTERVAL
0 - 7 cm
7 - 11 cm
11 - 18 cm
24 - 30 cm
0 - 1 cm
1 - 2 cm
2 - 3 cm
14 - 15 cm
%
50
30
10
<.062 .062 .125 .25 .50 1.0
mm

Figure II-5

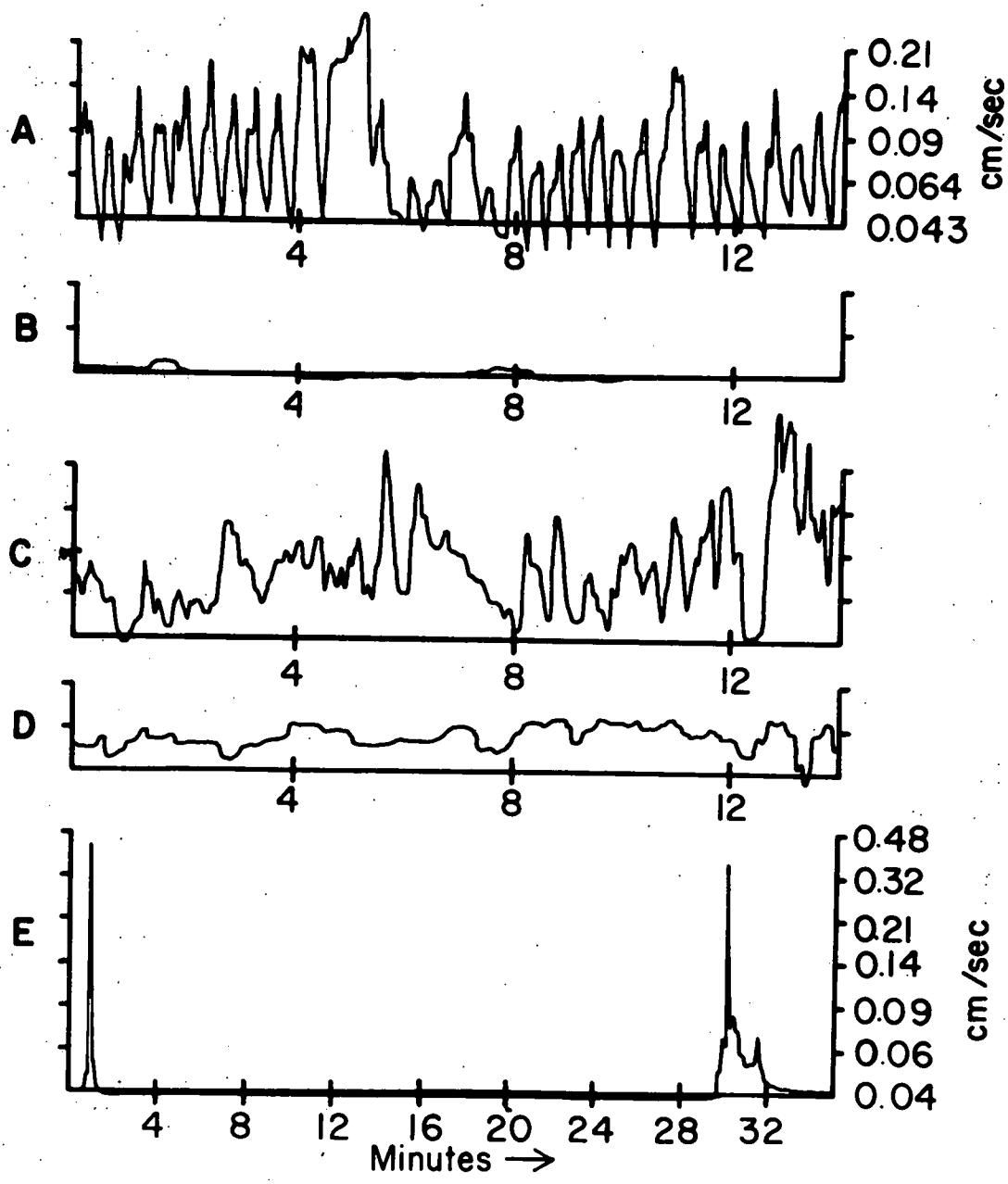

A
0.21
0.14
0.09
0.064
0.043
cm/sec
4
8
12
B
4
8
12
C
4
8
12
D
4
8
12
E
0.48
0.32
0.21
0.14
0.09
0.06
0.04
cm/sec
4
8
12
16
20
24
28
32
Minutes →

Figure II-6

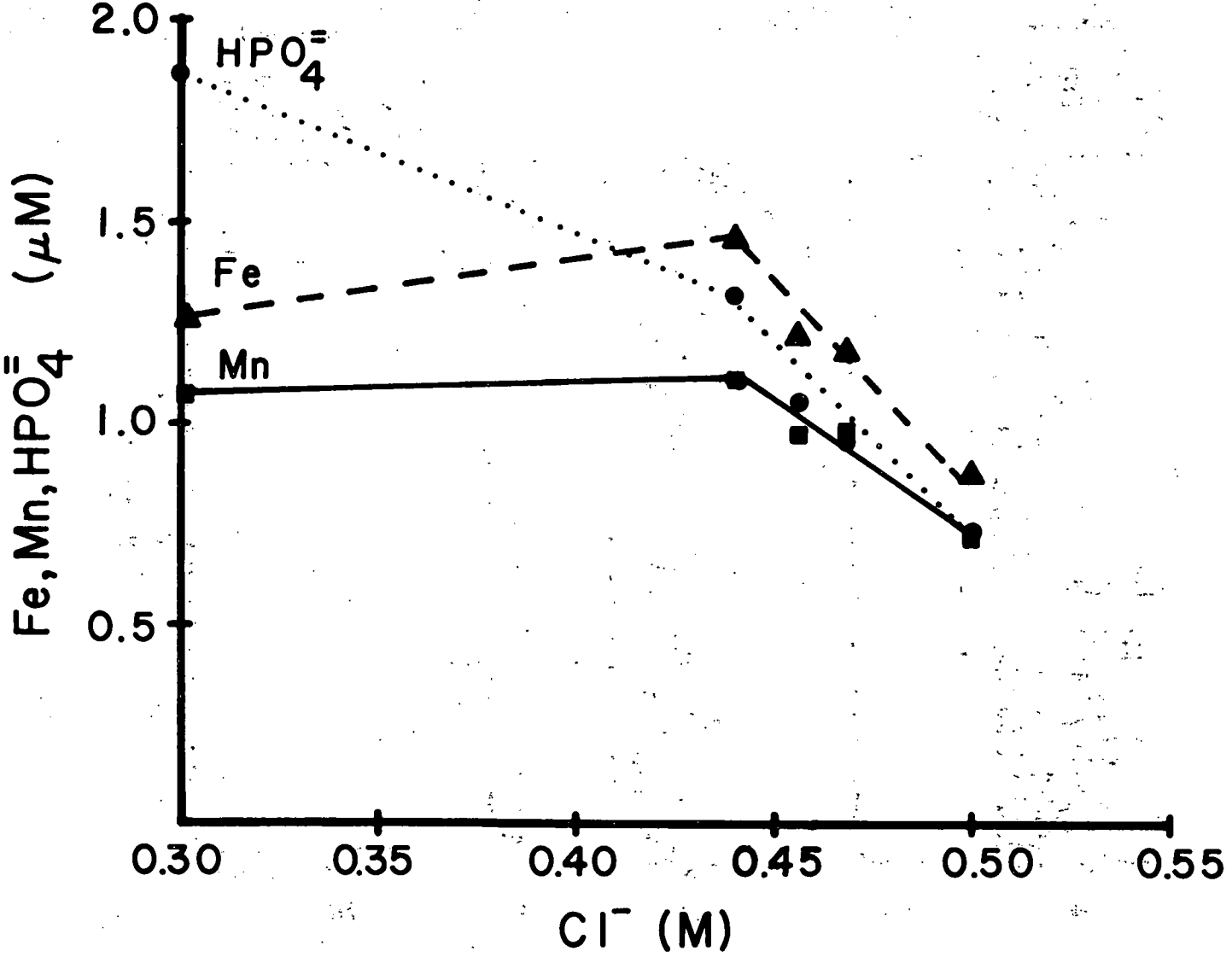


Figure II-7

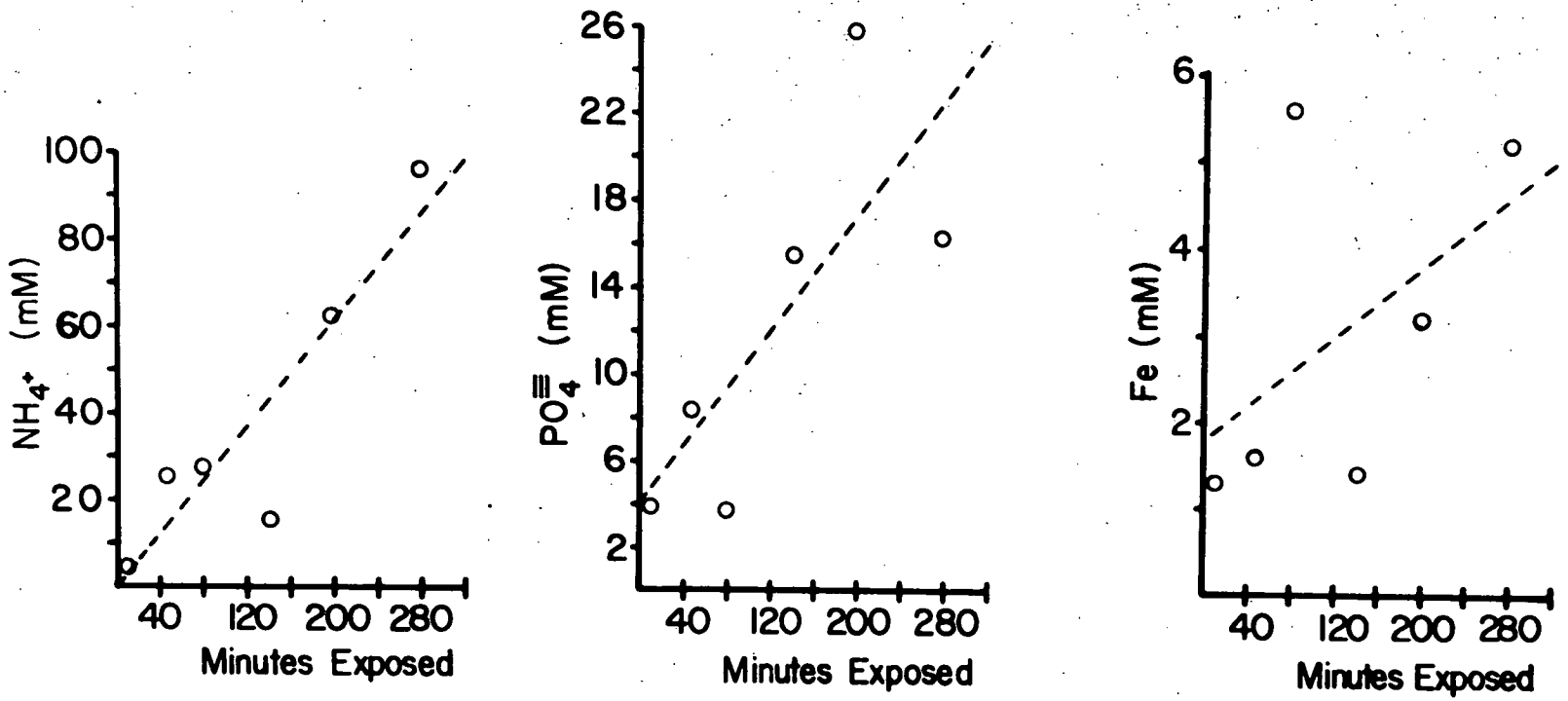

100
80
60
40
20
NH_4^+ (mM)
40 120 200 280
Minutes Exposed
26
22
18
14
10
6
2
$PO_4^{\equiv}$ (mM)
40 120 200 280
Minutes Exposed
6
4
2
Fe (mM)
40 120 200 280
Minutes Exposed

Figure II-8

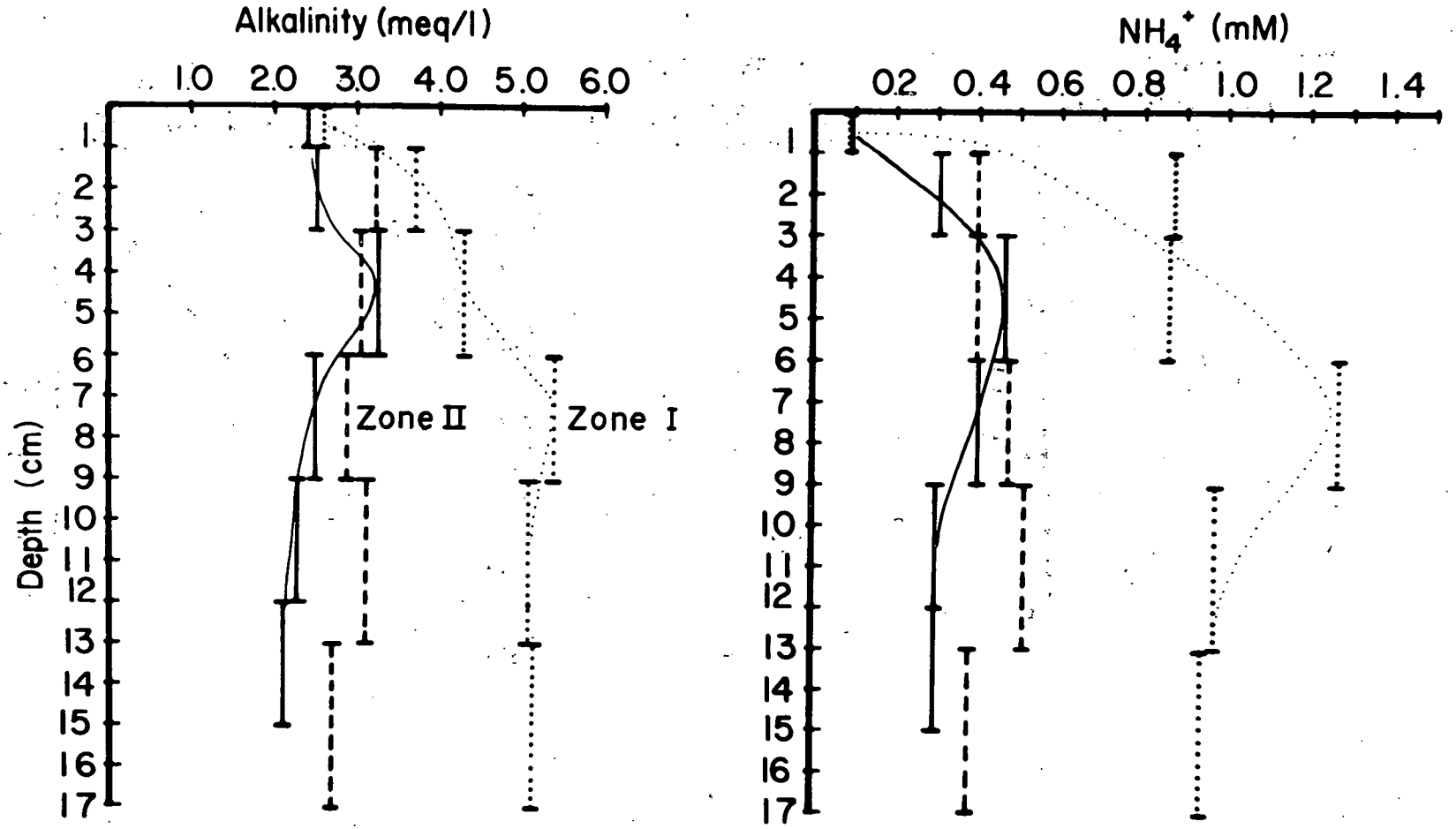

Alkalinity (meq/l)
1.0 2.0 3.0 4.0 5.0 6.0
Depth (cm)
1 2 3 4 5 6 7 8 9 10 11 12 13 14 15 16 17
Zone II
Zone I
NH4+ (mM)
0.2 0.4 0.6 0.8 1.0 1.2 1.4
1 2 3 4 5 6 7 8 9 10 11 12 13 14 15 16 17

Figure II-9

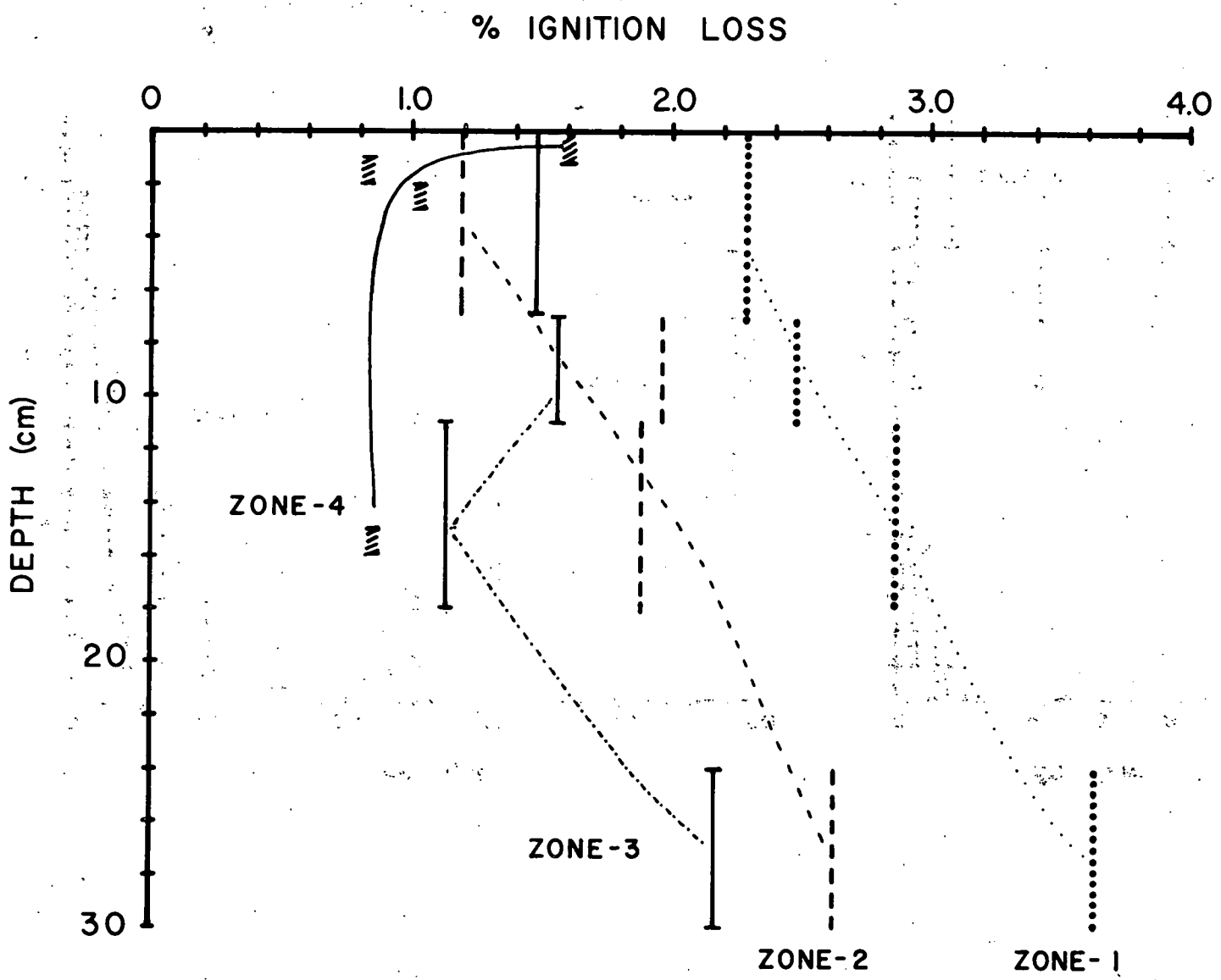

% IGNITION LOSS
0
1.0
2.0
3.0
4.0
DEPTH (cm)
10
20
30
ZONE-4
ZONE-3
ZONE-2
ZONE-1

Figure 11-11

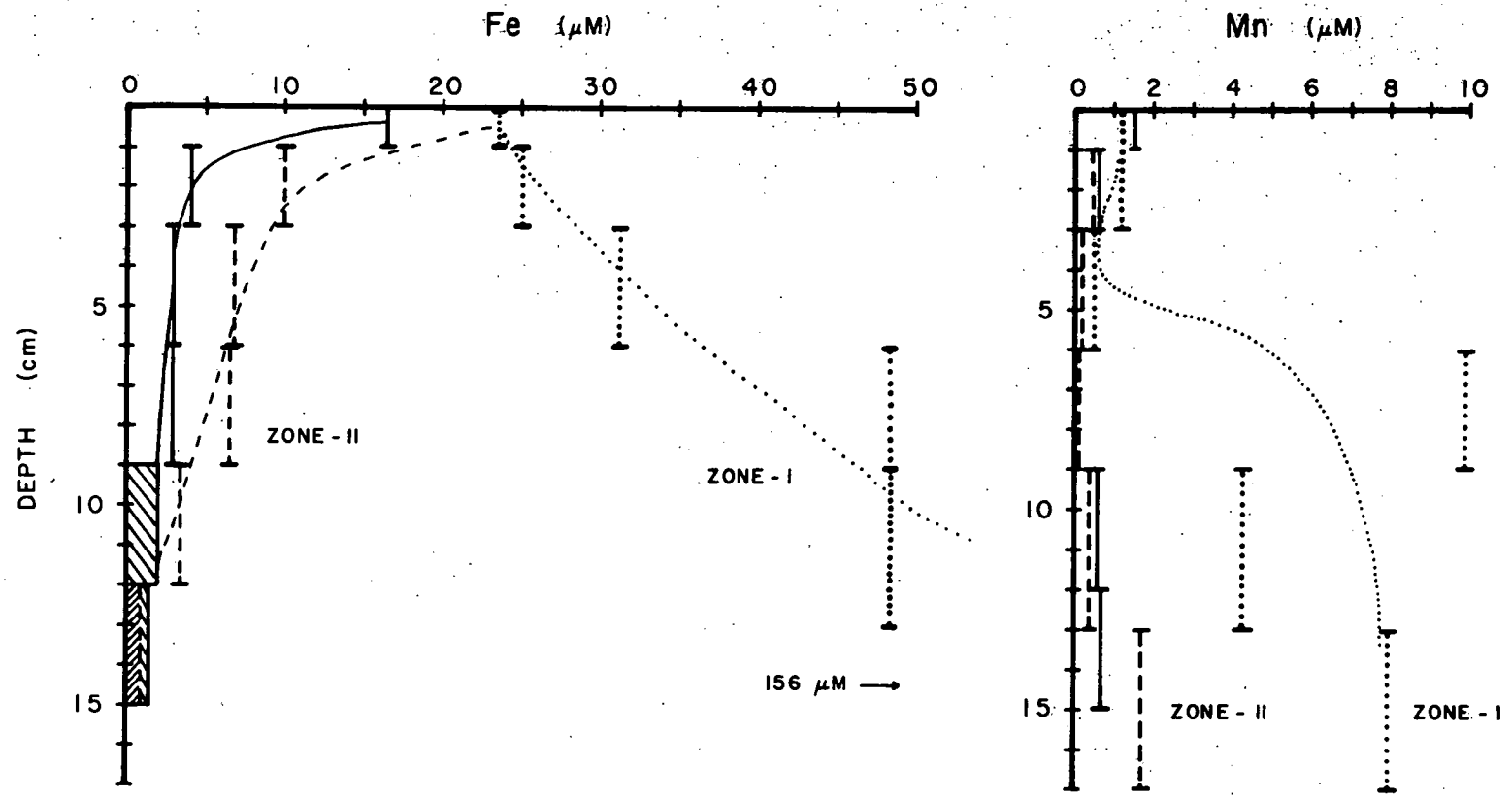

Fe (μM)
0
10
20
30
40
50
DEPTH (cm)
5
10
15
ZONE - II
ZONE - I
156 μM
Mn (μM)
0
2
4
6
8
10
5
10
15
ZONE - II
ZONE - I

Figure II-10

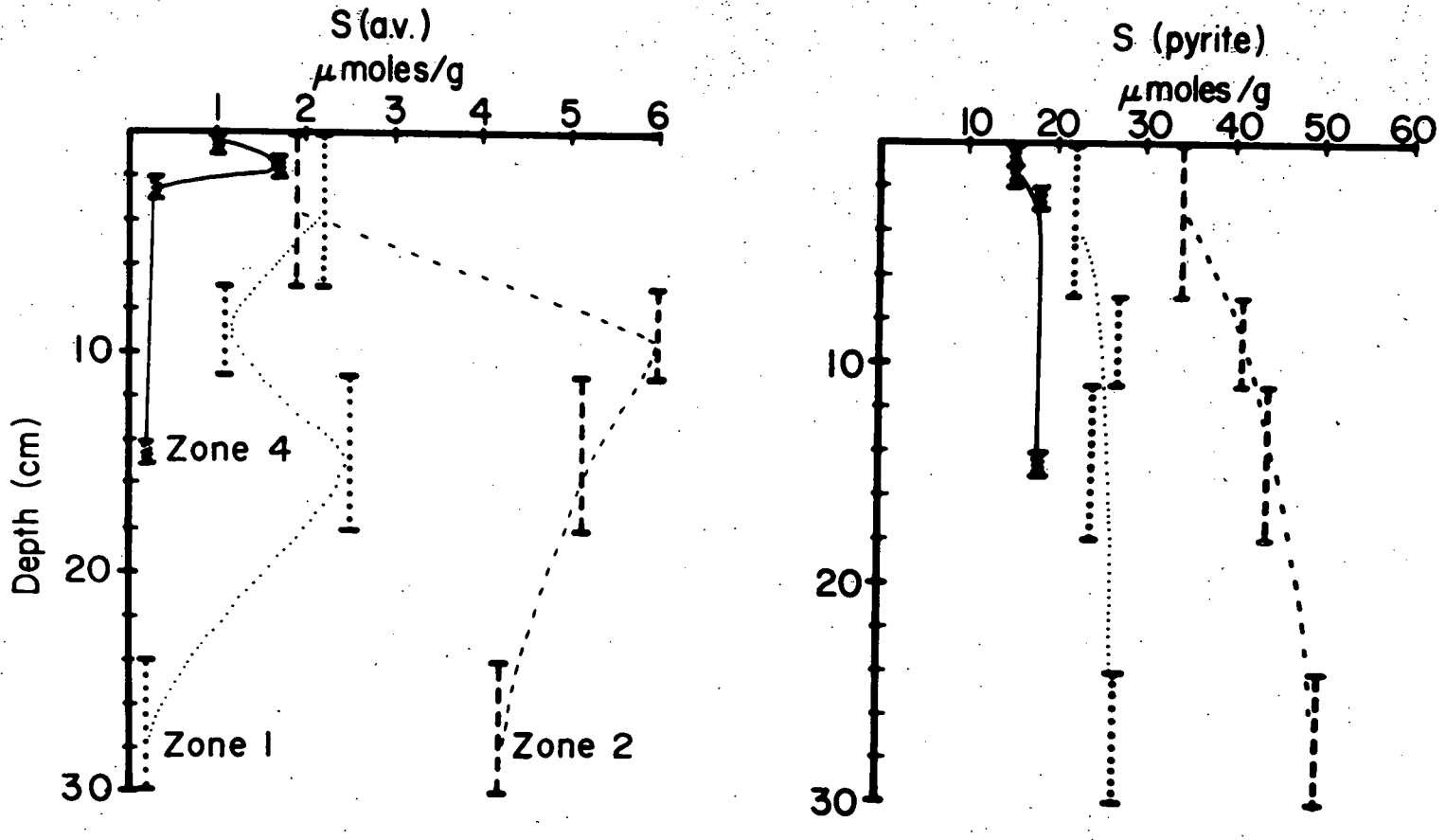

S(a.v.)
μmoles/g
1
2
3
4
5
6
10
20
30
Depth (cm)
Zone 4
Zone 1
Zone 2
S (pyrite)
μmoles/g
10
20
30
40
50
60
10
20
30

Figure II-12

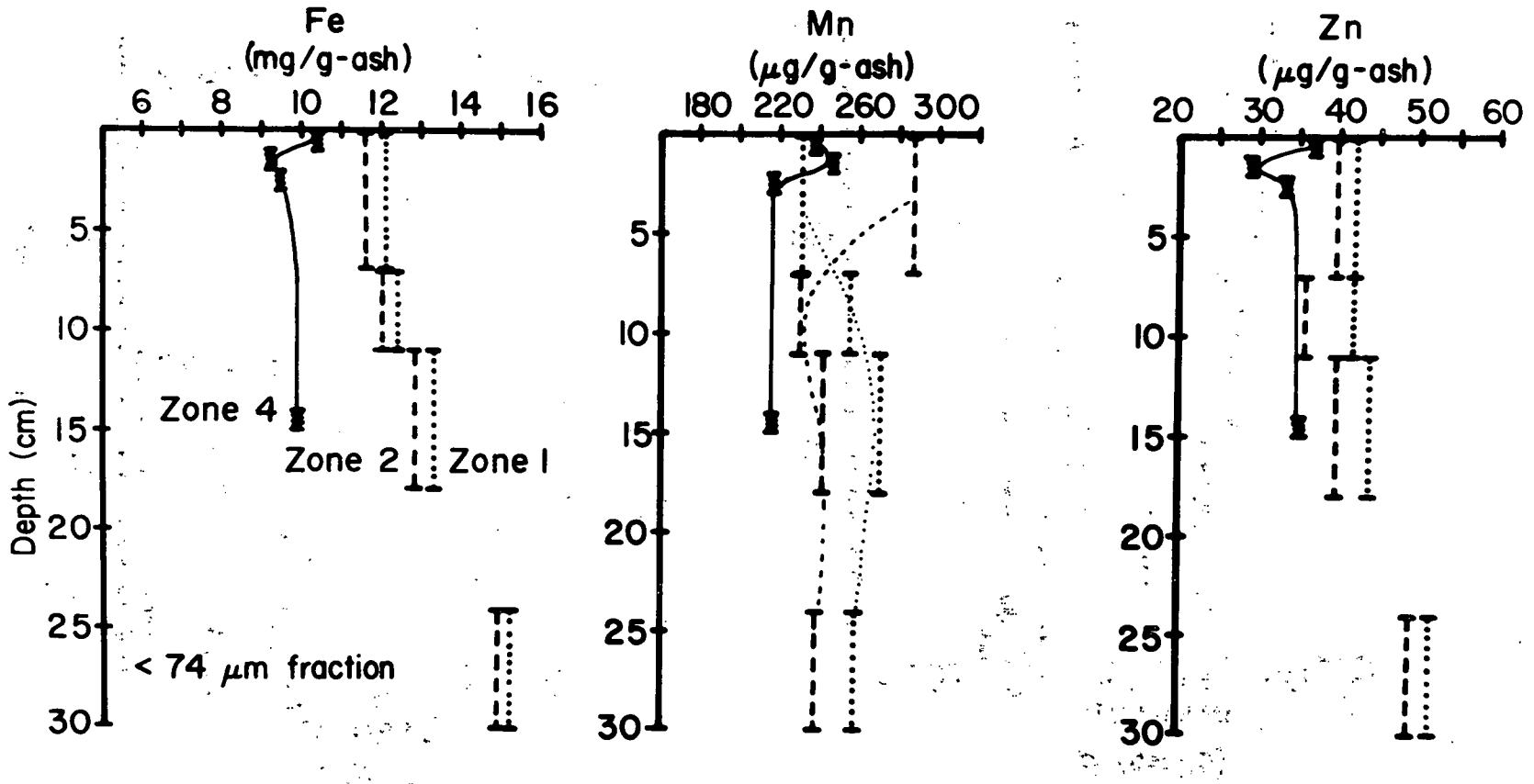

Fe
(mg/g-ash)
6
8
10
12
14
16
Mn
(μg/g-ash)
180
220
260
300
Zn
(μg/g-ash)
20
30
40
50
60
Depth (cm)
5
10
15
20
25
30
Zone 4
Zone 2
Zone 1
< 74 μm fraction

Figure II-13

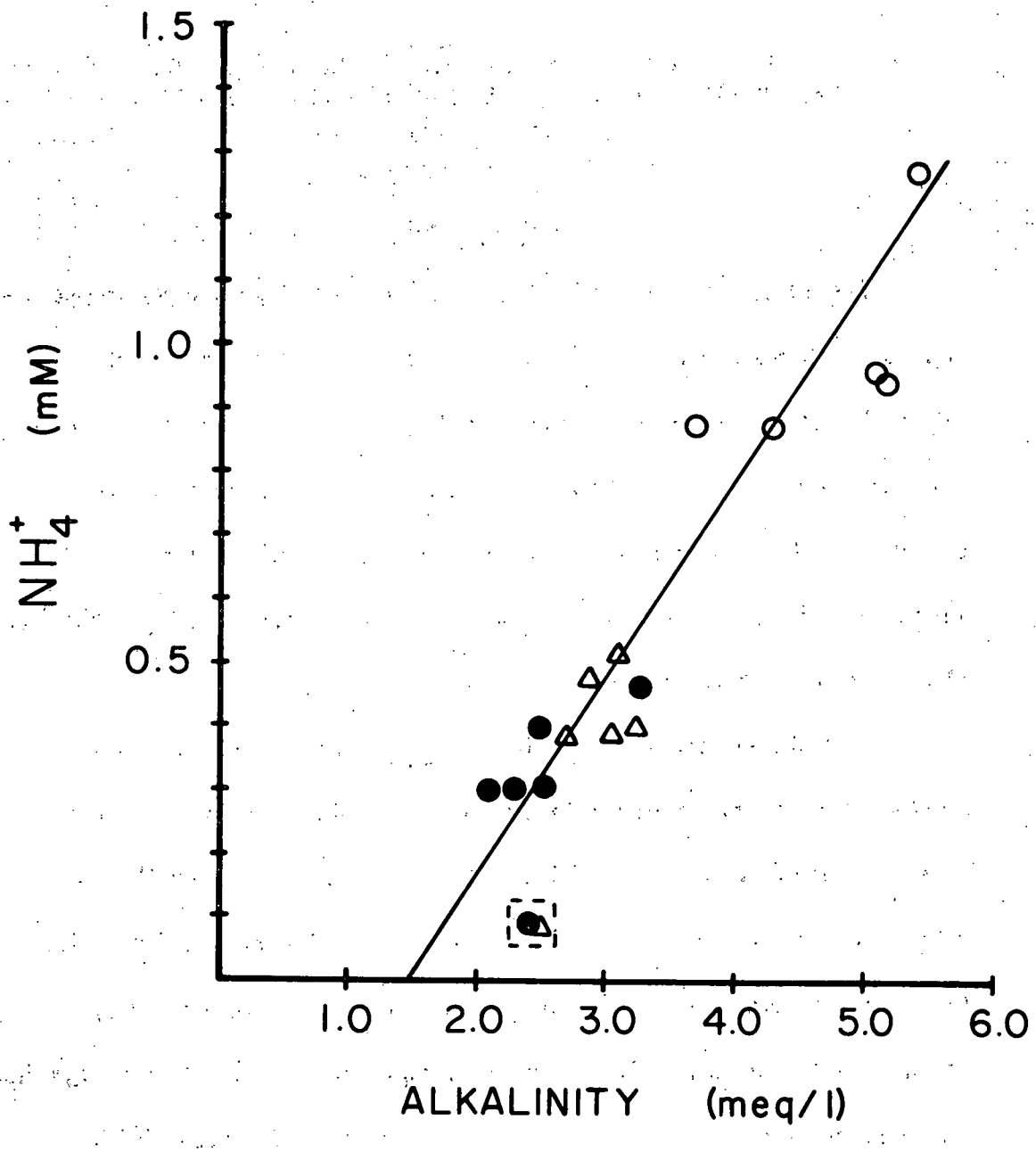


Figure II-14

CHAPTER III

EXPERIMENTAL STUDIES OF CHANGES PRODUCED BY DEPOSIT FEEDERS ON PORE WATER, SEDIMENT, AND OVERLYING WATER CHEMISTRY

Introduction

The influence of a given deposit-feeding species on sediment properties depends on its taxonomic group, size, mobility, life habit, particle size selectivity, depth and rate of feeding, and the population densities in which it normally occurs. In this chapter, two species, representing two very different and important functional groups of marine deposit-feeding organisms, were studied in the laboratory for their effects on selected aspects of chemical diagenesis near the sediment-water interface.

One of these species is Yoldia limatula, a siphonate, protobranch bivalve which commonly occurs in shallow sub-tidal muds off the northeast coast of North America (Figure III-1). The protobranchs are small (0.1-4 cm) highly mobile, shell-secreting organisms, which generally feed below the sediment-water interface but within the top 2-4 cm (Stanley, 1970; Levinton and Bambach, 1975). They are conspicuous and abundant enough that a protobranch species is sometimes used as a characteristic species in the

classification of bottom communities, for example, the Yoldia limatula-Nephtys incisa community of Long Island Sound (Sanders, 1956). They are active, which together with population densities of several hundred per m^2, results in high rates of particle reworking in bottoms where these animals are present (Rhoads, 1963; Young, 1971; Aller and Cochran, 1976). Because of this biogenic activity and the resulting changes in mass properties and physical stability of the bottom, protobranchs are thought to play a significant role in determining the distribution of other organisms (Rhoads and Young, 1970).

The other species investigated in this study is Clymenella torquata, a maldanid polychaete which normally inhabits muddy sands along the east coast of North America (Figure III-1). Maldanids orient vertically in the sediment, ingest particles at depths from 10-30 cm, and pass them vertically to the sediment surface (Mangum, 1964; Rhoads, 1966). In this respect they are functionally representative of many deposit-feeding polychaetes which orient and feed in a similar way. Clymenella are capable of reburrowing if exumed but under normal conditions tend not to be highly mobile. Maldanids are tube-dwellers; Clymenella constructs a permeable, lined-tube of poorly sorted sand grains while other maldanids such as Maldanopsis may form less permeable, firmly packed tubes of mud. Maldanids are common members of near-shore and deep-sea bottom communities.

Many of the effects of deposit-feeding organisms on sediment chemistry result from the changes that animals produce in the transport processes occurring in a deposit. The changes can be divided into those predominately involving the transport of either particles or fluid. Feeding, burrowing, and construction activity influence particle transport while fluid transport is affected mostly by irrigation (respiration) and burrowing. Changes in selected aspects of average sediment chemistry which accompany biogenic transport activity are investigated in this study. Changes resulting from the formation of tube microenvironments (Chapter II) or indirect changes caused by synergistic interaction between macro and microfauna are also considered but given less emphasis.

Fe and Mn were chosen for special study for several reasons: (1) These metals are believed to have a dominant role in determining the distribution and mobility of many other metals such as Cu, Zn, Co, and Ra (e.g., Goldberg, 1954; Krauskopf, 1956; Jenne, 1968). (2) Both Fe and Mn are highly sensitive to oxidation-reduction conditions and the presence of sulfide and are thereby particularly sensitive to diagenetic processes involving the destruction of organic matter by O_2 or $SO_4^=$ reduction. Reactions of this type are especially rapid in the near interface zone inhabited by benthos and can be expected to be influenced by the activities of the animals dwelling there. (3) As a result of the conditions mentioned above, Fe and Mn are present in sufficient concentrations in sediment pore water to be

readily measured without extensive preconcentration.

In addition to Fe and Mn: NH_4^+, $HPO_4^=$, $SO_4^=$, pS, and alkalinity were also measured in some cases. These constituents are useful indicators of decomposition--metabolic processes, are potential reactants with Fe and Mn, and are important nutrients. The similar sources (organic material) but different reactivity and chemistry of NH_4^+ and $HPO_4^=$ also allow the tracing in certain cases of reactions involving their precipitation or other mechanisms of removal such as adsorption.

Methods

Experiments consisted basically of comparing pore water profiles, sediment, and overlying water chemistry in sea water aquaria containing animals, with aquaria in which macroorganisms were absent (controls).

Experiments with Clymenella torquata

Clymenella and sediment from their natural habitat were collected at Calves Pasture Point, Barnstable Harbor on Cape Cod, Mass., and transported to Yale. Collections during 1972 and 1973 showed that these organisms were easily maintained alive in the laboratory for periods longer than six months. Individuals collected on June 29, 1974 were used within one day of capture in the experiments described below.

The muddy sand from the collecting site was dried, sieved through a 2 mm mesh sieve, then mixed with mud from New Haven Harbor (Long Wharf),

Connecticut in a ratio of 15 parts sand: 1 part mud in order to increase the organic matter content of the sediment and raise the concentration of the elements measured to detectable levels in the sediment pore water. Sediment layers 15 cm deep were deposited in each of four plexiglas aquarium tanks and covered with sea water for 12 days prior to the start of the experimental run. These aquaria had dimensions of 33.3 x 29.1 x 33.3 cm for length, width and height and were each connected by latex rubber tubing to separate 50 ℓ polyethylene carboys, the outside of which were painted black (Figure III-2). The carboys acted as sea water reservoirs for each tank and water was continually circulated between the reservoir and its associated tank using a centrifugal pump (no metal parts in water contact) and a gravitational return. Sheet-like flow over the sediment surface was maintained by using perforated, pyrex glass tubes at each end of the tank for uptake and return of water. Both the carboys and aquaria were surrounded by a water bath which kept the temperature at 19 ± 1°C. The entire system was placed under a polyethylene tent to prevent contamination by dust.

After an initial equilibration period of 12 days, the water over the tanks was changed. Water was then circulated and monitored for pH, Cl^-, $HPO_4^=$, NH_4^+, Fe and Mn for a two week period in each tank. At the end of this two week period, tanks 1 and 2 were designated controls and tanks 3 and 4 designated to receive Clymenella; tank 2 was drained at this time and the sediment cored using a PVC coring tube. The core was

immediately placed in a glove bag and the bag flushed repeatedly with N_2. The core was then extruded in 1 cm intervals into specially constructed plastic squeezers made from syringes. These squeezers were sealed and then mounted into vises and pore water mechanically squeezed out directly through 0.4 μm pore size Nuclepore membrane filters, which had been previously flushed with N_2, into 3 cc syringes. Syringes were weighed and pore water expressed into 10 ml volumetric flasks where it was immediately acidified with 0.1 ml of HCl and diluted to 10 ml. Syringes were reweighed and the amount of pore water obtained by difference. Great care was taken to prevent air contact with pore water during handling and squeezing prior to acidification. This minimizes loss of Fe due to oxidation and precipitation (Troup, Bricker, and Bray, 1974).

On the same day as Tank 2 was sampled, 30 Clymenella torquata (a natural density of 300/m^2) were placed in both tanks 3 and 4; tank 1 continued as a control tank. Overlying water was sampled during the following two week period at the end of which tanks 1 and 3 were cored and sampled as described above for tank 2. Sediment from tank 4 was not sampled.

Overlying water samples were taken by inserting a piece of Tygon tubing below the water surface in each tank and drawing water directly into a syringe. An inline filter holder was attached and water filtered directly through a 0.4 μm pore size Nuclepore filter into acid-cleaned polyethylene

sample bottles. Water used for Fe and Mn determinations was acidified to 0.1 N HCl immediately. Filtered samples for $HPO_4^=$ and NH_4^+ analyses were placed in a refrigerator (4°C) and either analyzed, or fixed in the case of NH_4^+, within 24 hours. Samples for Cl^- analysis were titrated immediately.

Experiments with Yoldia limatula

Yoldia limatula and sediment were collected at station NWC in Long Island Sound, 6 km south of the New Haven Harbor entrance on October 21, 1975 (see Rhoads, Aller and Goldhaber, 1977). Samples of the upper ~ 10 cm of sediment were taken by grab and placed in polyethylene containers. Yoldia were removed as they came near the surface of the samples and placed temporarily into a holding tank. The wet sediment, which is > 75% silt-clay, was then forcibly passed through a 1 mm sieve to remove other macrofauna and large shell debris. No additional water beyond that naturally in the sediment was added. (An initial attempt to wash a small portion of the sediment through the sieve using sea water proved unsuccessful; a small quantity of water may have been added to the subsample at that time but no detectable increase in the water content of the bulk sample resulted.) This sieved sediment was homogenized and placed as a 10 cm deep layer in each of two plexiglas tanks having dimensions of 28.7 w x 29.7 l x 30.5 h cm. The tanks were then carefully filled with water, 30 Yoldia added to one tank, aerators inserted, and then the top partially sealed with a glass plate.

This was all completed on the same day as collection. Temperature was subsequently maintained at 22°C.

A sample of the starting sediment was taken and processed for pore water analysis as follows. Sediment was packed into a 10 cm long section of butyrate tubing (4.5 cm I.D.) then squeezed using the method of Kalil and Goldhaber (1973). Pore water was expressed first through glass fiber filters followed by 0.45 μm pore size Millepore filters directly into plastic syringes without air contact. Water was analyzed for $SO_4^=$, NH_4^+, $HPO_4^=$, alkalinity, Ca, Cl^-, Fe and Mn. ($Si(OH)_4$ was also measured but the results will not be described in this report.) $SO_4^=$ analyses were made on 10 ml samples. A 10 ml sample was taken for alkalinity, Fe, and Mn determination as follows. Immediately after filling of the sample syringe the pore water was transferred through a short section of tygon tubing into a 10 ml pipet. This pipet was drained directly into an acid-cleaned and thoroughly rinsed 2 oz. polyethylene wide-mouthed bottle; total transfer time was approximately 30 sec. Alkalinity titrations were then made directly in this vial and the samples acidified to pH ~ 1.5-2. After sitting for at least a week following acidification, these samples were analyzed for Fe and Mn as described under analytical techniques below. No significant Fe or Mn blank or loss (recovery 100 ± 1 to 2% for Fe and Mn respectively) is incurred by this method if titration and acidification is performed within about 1 week after transfer

(Chapter VI). Samples for $HPO_4^{=}$, NH_4^{+}, and Cl^{-} were taken in 3 cc syringes and analyzed as described below.

Overlying water in each tank was changed at approximately one week intervals. This water was monitored for Cl^{-}, $HPO_4^{=}$, NH_4^{+}, Fe and Mn concentration in the same way as for the Clymenella experiment.

After five weeks the tanks were drained and inserted directly into a glove bag. The bag was pumped down with a vacuum pump and flushed with N_2 several times. Sediment was carefully removed at 1 cm or 2 cm intervals by use of plastic spoons and placed in precut 10 cm sections of butyrate tubing (4.5 cm I.D.). The pH and pS were taken then measured by insertion of electrodes directly into the upper portion of the sample, and the tube then sealed with end caps. A portion of sediment from each depth was taken for H_2O content and ATP determination. When all intervals had been sampled and tubes sealed, the glove bag was opened and the samples were removed and placed into a refrigerator (4°C) for storage prior to squeezing. Pore water was removed by the method of Kalil and Goldhaber (1973) and samples treated as described previously. Squeezing was completely within 12 hrs of sampling; sediment was allowed to come to room temperature and was squeezed at 22°C.

Analytical techniques

pH was determined by direct insertion of a rugged, combination electrode into either a sediment or overlying water sample after standardization of the

electrode in 7.414 buffer followed by rinsing. pS measurements were made by insertion of a standardized Ag_2S electrode (Berner, 1963) into sediment using the calomel portion of the pH electrode as reference. In the case of sediment, these measurements were made directly in the glove bag by passing the lines through a sealed port in the side of the bag. The portion of sediment in which the electrodes were inserted in the squeezing tubes was eventually removed just before squeezing during the emplacement of glass fiber filters and squeezing caps.

All Fe analyses were made with the colorimetric reagent Ferrozine using a modification of the procedure of Stookey (1970); samples were not boiled but were reacted at room temperature for 1 hr prior to color development. Mn analyses were made using three different methods: formaldoxime colorimetric method (Goto, Komatsu, and Furukawa, 1962), a modified leuco malachite green colorimetric method (Strickland and Parsons, 1968; Appendix II) and atomic absorption spectrometry. Intercomparison of these methods on tap water and standard rock samples gave results within 5% of one another. Formaldoxime was used for analysis of overlying water samples, leuco malachite green for pore water samples in the Clymenella experiment, and atomic absorption was used for Mn pore water analysis in the Yoldia limatula experiment. All $HPO_4^{=}$ (reactive) determinations were made using a modified version of the molybdate method (Strickland and Parsons, 1968; Presley, 1971). NH_4^{+} was analyzed by use of the phenol hypochlorite method after

initial fixing with phenol (Solorzano, 1969; Degobbis, 1973). Cl^- was determined by $AgNO_3$ titration using chromate or starch-fluorescein indicators. Alkalinity was determined by titration with 0.1 N HCl (Gieskes and Rodgers, 1974). $SO_4^=$ was analyzed gravimetrically following precipitation of acidified samples with $BaCl_2$.

Estimates of % organic matter were made by ignition of sediment at 475°C after drying to constant weight at 100°C. Percent H_2O was determined by drying sediment to constant weight at 80°C.

Mn determinations were made on aliquots of ashed sediment by refluxing for 24 hrs in 12 N HCl (30 ml), taking to near dryness, picking up in 0.2 N HCl, and filtering through Whatman 42 paper. The resulting leachate was diluted to known volume and analyzed for Mn by use of AA.

ATP analysis was done on wet sediment by J. Yingst. Sediment samples, with and without the addition of standard, were extracted in boiling bicarbonate buffer (Christian, Bankroft, and Wiebe, 1975) and ATP leached from the samples was determined by reaction with luciferin-luciferase (luminescence assay). Extraction efficiency was determined using the standard addition; average yield and total precision for this analysis are 108 ± 24% (Yingst, 1977).

pH showed a decrease with depth in all tanks and the average pH in both the control and Clymenella tanks also increased with time. In the presence of Clymenella, however, pH increased beyond the control values in the top 5 cm of sediment (Figure III-4).

Clymenella experiment, overlying water

Cl^- concentrations in the overlying water remained relatively constant throughout the experimental period; a minor increase in chlorosity of ~0.015 M (3% of starting value) took place over the 29 day period of measurement due to evaporation. There is no significant difference between tanks (Table III-2).

The pH of overlying water decreased from ~8.2 to ~7.4 in all tanks during the experimental run. The pattern of change is similar in all cases (Figure III-5).

Reactive PO_4 ($HPO_4^=$) decreased initially in all tanks and remained at constant low values in control tanks 1 and 2. After addition of Clymenella in tanks 3 and 4, reactive PO_4 increased and then dropped slightly in the last sampling (Figure III-5).

NH_3 (NH_4^+) was low and essentially constant or decreasing in each tank. Following the addition of Clymenella in tanks 3 and 4 a radical increase in NH_3 concentration in tank water took place (Figure III-5) and this increase continued, but at a decreasing rate, until the end of the experiment.

Results

Clymenella experiment, pore water

Pore water concentration profiles of both Fe and Mn underwent radical change in the presence of Clymenella. Prior to addition of animals, both metals had pore water concentrations which increased steadily with depth (Figure III-3, Table III-1); this increase can be roughly approximated by a simple straight line. Comparisons of tank 2 with tank 1 data, show that control tank profiles of dissolved Fe and Mn remained relatively stable over the fourteen day period between samplings, but there is a tendency for somewhat lower values in tank 1. After addition of Clymenella in tanks 3 and 4, pore water concentrations became low at depth and high near the interface compared to the control tanks (Figure III-3). Fe reaches a maximum in the second cm while Mn continues to increase or stay the same in the top one cm. The deepest sampling interval, 9-10 cm, indicates that pore water values begin to increase again below that depth.

The measured dissolved Fe concentrations are high but not out of the range found in naturally accreting sediments (Bricker and Troup, 1975; Troup, 1974; Chapter VI). Mn concentrations are well within the range found in natural sediments. The Fe/Mn ratio of $\sim$ 100 is higher than the 10-20 found normally in sediment pore waters from Barnstable Harbor (Chapter II).

Dissolved Fe and Mn ($\leq$ 0.4 μm) was initially near or below the detection limits for the analytical methods used in all tanks. It remained low in the control tanks but after addition of Clymenella to tanks 3 and 4 both Fe and Mn in overlying water increased (Figure III-6). Like reactive PO_4, dissolved Fe decreased in the last sampling period after an initial large jump in concentration. Mn, like NH_3, continued to increase.

Yoldia experiment, sediment description

The sediment surface in the tank containing Yoldia was flocculent and watery (Table III-4) compared to the control. Protobranchs are known to increase the water content of sediment during reworking (Rhoads and Young, 1970).

Except for some very minor disturbance by meiofauna, the control tank maintained surface features which were formed when sediment was laid down in each tank. In comparison, the Yoldia tank surface sediment was composed of gently sloping fecal mounds and loosely aggregated pellets with no hint of original surface features. In profile, the control tank sediment was capped by an orange-yellow oxidized layer 0.3-0.4 cm in depth underlain by black colored sediment. The color stratigraphy of the Yoldia tank was similar except that the surface yellow zone was 2-3 cm thick.

Yoldia experiment, pore water

Analytical results of pore water and solid phase analyses in the Yoldia and control tanks are listed in Table III-4 and graphed as depth dependent concentration profiles in Figures III-7-10; initial values, when available, are usually graphed for comparative purposes. Differences between Yoldia and control tanks are subtle in some instances but dramatic in others. Sulfate profiles show definite depletion of sea water sulfate with depth in both tanks; normalization to Cl^- does not significantly change this observation. The Yoldia tank has slightly higher sulfate concentrations in the upper 5 cm and slightly lower values from 5-9 cm depth interval compared to the control but these differences are not analytically significant. Decreasing $SO_4^=$ is mirrored by decreasing pS values with depth in both tanks, with slightly higher $S^=$ levels in the Yoldia tank than control below 5 cm (Table III-3).

Associated with decreases in sulfate are increases in interstitial concentration of alkalinity, ammonia, and phosphate (Figure III-7). These trends are predictable results of sulfate reduction (e.g., Richards, 1965; Goldhaber and Kaplan, 1974). Alkalinity concentrations are lower at all depths in the tank containing Yoldia than in the control. The profile in the Yoldia tank shows a break in concentration gradient at ~3-4 cm; while the control tank profile is slightly bowed from a smoothly increasing profile to lower values in the region from 2-4 cm, yielding a similar profile shape

to that present in the Yoldia tank. The ammonia profiles are superficially quite similar in both tanks but some distinct differences do occur. Above 3 cm, NH_4^+ concentrations are the same or lower in the Yoldia side than the control, below 3 cm the Yoldia tank invariably has higher concentrations. This results in a slight break in the depth trend of concentration at ~3 cm in the Yoldia tank. Phosphate concentrations show the same trends and differences between tanks as ammonia except a definite bowing or concavity in the profiles of both tanks can be noticed above 4 cm.

Dissolved Mn profiles are similar in shape in both tanks in the sense that in both the concentration of Mn increases to a maximum at 4-5 cm and then decreases below that interval. The tanks differ in that Mn concentrations are lower at every depth in the tank containing Yoldia than in the control (Figure III-8).

In the same way, dissolved Fe profiles are similar in basic depth trends: increasing to a maximum followed by decreasing concentration at depth, but concentrations are higher in the control (Figure III-8). This is especially true in the region of the maximum value from 2-3 cm where dissolved Fe is dramatically higher in the control.

Like Fe and Mn, Ca in the control increases to a maximum concentration at a depth of 3-4 cm then decreases below that interval (Figure III-8). Ca values have been normalized to Cl^- to show that Ca increases beyond sea water

Ca/Cl ratios (~ .0187) at all depths in the control tank and in the upper 3 cm in the Yoldia tank.

The depth dependence of pH differs considerably in the two tanks (Figure III-8). In the control, pH reaches a very low minimum value of 7.02 at 3-4 cm with sharply increasing values above and below. pH is relatively low and constant in the upper 3 cm of the Yoldia tank and increases at depth.

Yoldia experiment, solid phase properties

The distribution of organic matter differs in the two tanks and, in both, underwent change from the initial value (Figure III-9). In the Yoldia tank the organic matter profile was changed from initially constant with depth to one which decreases steadily from a surface maximum to a low at 3-4 cm, then jumps to a higher value which is maintained to depth. This higher value at depth is greater than the initial starting value. The control tank increases, below the interface to a relatively high value similar to that found below 4 cm in the Yoldia tank.

ATP distribution (no correction for yield, see Methods) is similar in the upper few centimeters in the two tanks but shows distinct differences below 3 cm (Figure III-9). In the Yoldia tank ATP reaches a local minimum at 3-4 cm and then increases to a relatively constant level independent of depth. The control profile reaches a slight maximum in the second cm and then decreases steadily to depth. No ATP values for the homogenized starting

sediment were measured; typical ATP profiles at the sediment collection site are given in Yingst (1977).

Solid phase Mn (Figure III-10) underwent a radical redistribution in the sediment during the 45 day experiment. Again, similarities and differences can be found between the tanks. Both have maximum Mn concentration in the top 0-1 cm, minimum levels at 1-2 cm, and then mild increases to a second maximum at depth followed by a decrease in concentration at the lowest sampling interval. Mn concentration profiles differ in that at most sampling intervals Mn is lower in the Yoldia than the control tank and that the interval in which the second maximum occurs is deeper in the Yoldia tank than control.

Yoldia experiment, overlying water

A number of differences were found in overlying water properties and chemistry of the two tanks. The water in the Yoldia tank was continuously turbid throughout the experiment and the sediment surface could not be seen from above. In the control, the overlying water was clear at all times.

Time dependent change in the concentration of total alkalinity, ammonia, phosphate, and Mn is plotted in Figure III-11 and additional data given in Table III-4. Plots are discontinuous at intervals because water was changed at that time. In general, NH_4^+, $HPO_4^=$, and Mn concentrations increase after each water change. The rate of increase after each successive

change, decreases throughout the experiment in both tanks so that, in the case of Mn, little change occurs in overlying water concentrations toward the end of the experiment. The amount of increase of NH_4^+ and Mn is greater in the tank with Yoldia than in the control but $HPO_4^=$ increase is often greater in the control.

Changes in alkalinity levels of overlying water differed in general trends from NH_4^+, $HPO_4^=$ and Mn. At all times alkalinity decreased after each water change in the Yoldia tank, the magnitude of the decrease decreased through time. In the control tank, alkalinity decreased at first, then increased during all successive time intervals but at a decreasing rate. No associated change in Ca/Cl^- concentrations were found (Table III-4).

Discussion

Clymenella experiment

The experiment with Clymenella shows that in the presence of this organism, pore water profiles and overlying water concentrations are changed relative to control conditions when Clymenella is absent. Clymenella did not feed during the experiment, as evidenced by the lack of fecal mound formation, so that changes produced by these animals resulted from burrow construction, fluid transport associated with irrigation activity, excretion, and alteration of microbial populations in the sediment rather than particle transport during feeding.

In the case of Fe and Mn, direct excretion by Clymenella is not an important source of these metals to overlying water (see Chapter VI). Microbial activity influences the rate of transfer of Fe and Mn from particles to surrounding pore water and the distribution of these rates with depth in sediment, but, as illustrated by the control tanks it is unlikely that microbial activity can account for the kinds of changes observed. This suggests that, at least for Fe and Mn, the changes in overlying water concentrations and pore water distributions are due in large part to burrow construction and fluid transport during irrigation. Mangum (1964) showed that individual Clymenella pump from 50-100 ml of sea water/animal/day into and out of their burrows for respiratory purposes; this irrigation rate lies well within the range reported for other infaunal, deposit feeders (Chapter I). It can readily be shown in the laboratory that irrigation results in the oxidation of the sandy sediment surrounding tubes inhabited by Clymenella (e.g., Rhoads, 1967). Oxidation to a maximum distance of a few centimeters away from stationary animals can take place in a period of days depending on the organic content of ambient sediment; if animals are actively burrowing, sediment may become more generally oxidized rather than only in the vicinity of burrows. Together, tube construction and burrow irrigation offer a transport mechanism which, in some cases, could result in considerable exchange of pore water from overlying water with a minimum of particle movement.

Iron and manganese distributions

Both Fe and Mn are known to rapidly precipitate from oxygenated solution as hydrated oxides over the pH range found in sediment pore water and overlying sea water. At pH 7-8, Fe has homogeneous precipitation rates many times faster than Mn but both can be described by first order or, for Mn in the presence of abundant surface area: pseudofirst order kinetics (e.g., Stumm and Lee, 1961; Lewis, 1976). In the absence of catalytic surface area such as that provided by sediment particles, Mn precipitation is autocatalytic (Morgan, 1964, 1967; Hem, 1964). This means that during transport from the reducing conditions of sediment to oxygenated sea water, neither metal need act as a conservative tracer of exchange but of the two, Mn should behave more conservatively than Fe (e.g., Boyle et al., 1974; Holliday and Liss, 1976; Graham, Bender, and Klinkhamer, 1976). The rate of transfer must also be more rapid than precipitation. With these similarities and differences in the precipitation kinetics of Fe and Mn in mind, a simple mass balance calculation can be made to demonstrate: (1) that the observed increase in Fe and Mn in overlying water can be accounted for by pore water supply consistent with simple exchange by irrigation (2) differences between Fe and Mn behavior can be explained by differences in precipitation kinetics during oxygenation and (3) deviation from theoretical precipitation rates suggest a complexed speciation for Fe.

In order to calculate the supply of Fe and Mn from sediment in the Clymenella tank to overlying water, the pore water concentrations in each depth interval of the Clymenella tank 3 are subtracted from the initial control tank 2 values (Table III-1), this difference is multiplied by the volume of sediment involved (1 liter) and an assumed porosity of 0.5, and then the sum of these products over the core length is taken to obtain a minimum of 5.6 mmoles of Fe and 48 μmoles of Mn lost for pore water. This is a minimum loss because no production of new Fe and Mn in the pore water during the experiment is taken into account. There are three possible sinks for dissolved Fe and Mn lost from pore water in this system: (1) upon the introduction of oxygen into pore water by irrigation activity Fe or Mn may precipitate at depth in the sediment either randomly or at preferred sites such as burrow walls (Chapter II), (2) if exchange is rapid relative to precipitation rates both dissolved Fe and Mn will be advected out of the sediment body along the tube conduits and into overlying water, where, if soluble, they will remain or (3) once introduced into overlying water either Fe or Mn can precipitate onto environmental surfaces. These possibilities are not exclusive and the data indicate that each occurs to some extent. Evidence that possibly (1) takes place comes from the changed Fe/Mn ratios in pore water after the introduction of Clymenella. Data in Table III-1 show that the Fe/Mn ratio drops from ~ 100/1 to 20/1-5/1. Since there is no reason to believe that Fe would be transported out of sediment preferentially to Mn,

this change implies that Fe is precipitated preferentially to Mn at depth during the initial introduction of sea water by irrigation and that water advected out of burrows during irrigation has a Fe/Mn ratio less than initial pore water.

The increase in Fe and Mn in overlying water is proof that (2) occurs. Ignoring precipitation, the minimum quantity of Fe and Mn transferred to overlying water can be calculated by taking the maximum increase in overlying water concentration and multiplying by $\sim 60\,\ell$, the quantity of water involved. This gives for Tank 3: $\Delta Fe \sim 0.4$ mmoles and $\Delta Mn \sim 22$ μmoles after addition of Clymenella; Tank 4, for which no pore water profiles are available, has similar increases of: $\Delta Fe \sim 0.5$ mmoles and $\Delta Mn \sim 16$ μmoles. It is then possible to account for ~ 50% (46%) of the Mn (calculated previously) lost from pore water as standing concentration in overlying water while only ~ 10% (7%) of the Fe found missing from pore water occurs as standing concentration in overlying water.

There are several types of evidence that possibility (3), precipitation out of overlying water, takes place. The most quantitative is the obvious decrease in Fe concentration with time (Figure III-6); this decrease takes place preferentially to Mn so that Fe/Mn ratios drop through time in overlying water. Qualitatively it was observed that in tanks with Clymenella an orange-yellow precipitate, soluble in dilute HCl, began to form at the

sediment-water interface, around burrow openings and on tank walls a day or so after introduction of animals and that this precipitate increased through time. No precipitate formed in control tanks, although a similar precipitate would form if the surface oxidized layer were gently scraped away in a small area. This precipitate is most probably $Fe(O)_x(H_2O)_y$ with various coprecipitates including Mn. Hem (1964) states that above pH $\sim$ 6, Mn coprecipitates with Fe but in the present experiments, although some coprecipitation does take place, a large percentage of the Mn remains in solution while Fe precipitates. Additional evidence that precipitation takes place is the fact that mass balances for both Fe and Mn in overlying water tend to the low side; it is not possible to determine whether this is due to precipitation at the site of irrigation or after advection into the water column.

Because Fe precipitation kinetics are known to be first order (Stumm and Lee, 1961), it is possible to place limits on the rate constant acting in the present experiment. If it is assumed, for the sake of calculation, that a minimum of 5.6 mmoles Fe was released into overlying water at a uniform rate during the 13 day experimental period (with Clymenella present) and that the average overlying water concentration was held at ~ 4 μM (average of Tank 3 values at 22 and 29 days) during that time, then a first order rate constant of $\sim 1 \times 10^{-3}$/min is calculated. This is about two orders of magnitude lower than expected at pH $\sim$ 7.4 and normal O_2

contents (Stumm and Lee, 1961). If Fe were precipitating at the theoretical rate, then the release rate would have to be 560 mmoles over the 13 day period to maintain the overlying water concentration. The most reasonable alternative is that Fe is not present as a free ion, but as a complex having a retarded precipitation rate. Fe is known to readily complex with natural organics and to be held in solution by them, often as colloidal sols (e.g., Moore and Maynard, 1929a, b, c; Rashid and Leonard, 1973; Picard and Felbeck, 1976); it seems likely that this kind of Fe speciation is responsible for the lowered precipitation rates in the present instance. This need not always be true but presumably depends on the kinds and concentrations of complexing agents in the sediment source. In the present case, the addition of organic and metal-rich sediment from inner New Haven Harbor (see Applequist, Katz, and Turekian, 1972) to the tank sediment may have aided the formation of complexed-iron.

A similar calculation for Mn results in a $k \sim 1 \times 10^{-4}$/min assuming first order reaction. This is much greater than expected theoretically (Morgan, 1964) but agrees well with field calculations of Lewis (1976) for the Susquehanna River (5×10^{-4}/min) where abundant catalytic surfaces (suspended particles) were available. In the present case the large k almost certainly reflects partial coprecipitation with Fe.

It has been shown to this point that the changes in pore water profiles and overlying water chemistry which took place after introduction of Clymenella can be consistently explained by irrigation transport and exchange of overlying water with pore water, that material balances between components are reasonable, and that differences in the relative behavior of Fe and Mn are in accordance with known differences in their properties. It is also possible to put limits on the rate of pore water transport by use of simple diffusion models and to demonstrate that it is not unusually rapid transport when the geometry of the system is considered.

Transport rates by irrigation of permanent burrows

The distribution of a pore water species, C, in a one dimension Cartesian coordinate system with no compaction or adsorption can be described by the equation:

$$(1) \quad \frac{\partial C}{\partial t} = D \frac{\partial^2 C}{\partial x^2} - w \frac{\partial C}{\partial x} + R$$

where t is time, x is the dimension variable, D is the molecular diffusion coefficient modified for tortuosity, w is the velocity of advection term, and R represents specific reactions (Berner, 1976b). In the present case of the tank experiments w = 0 and R can be taken as = 0 for the purposes of calculation. The pore water concentration distribution in one dimension is then given by:

$$(2) \qquad \frac{\partial C}{\partial t} = D \frac{\partial^2 C}{\partial x^2}$$

Assuming that the tank sediment can be approximated by a slab of thickness $0 \leq x \leq L$ having boundary conditions $x = L$, $C = 0$; $x = 0$, $(\frac{\partial C}{\partial x})_{x=0} = 0$ (the origin of this coordinate system is at the tank bottom, positive up) and that in the case of Fe or Mn the initial concentration distribution is linear with depth: $C \cong M(L - x)$. Then, the solution for C at a given time and position is (after Carslaw and Jaeger, 1959, p. 97):

$$(3) \qquad C = \frac{8LM}{\pi^2} \sum_{n=0}^{\infty} \frac{1}{(2n+1)} \cos \frac{(2n+1)\pi x}{2L} \; e^{-D(2n+1)^2 \pi^2 t/4L^2}$$

Because Mn behaves more conservatively than Fe it will be used in calculation. Ignoring the fact that Mn concentration increases in the top 2 cm after irrigation (discussed below) i.e., $x = L$, $C = 0$ does not really hold, the question asked is: what would D have to be in order to lower Mn concentration in the interval 8-9 cm from 29 μM to 1.8 μM in 13 days by vertical diffusion. Calculation shows that $D = 2\text{-}3 \times 10^{-4}$ cm^2/sec with $M = 2.3$ μM/cm, $L = 11$ cm.

The diffusion coefficient required to accomplish transport can be lowered significantly by more realistically approximating the experimental transport geometry. In the real case the sediment slab $0 \leq x \leq L$ is drilled by ~30 vertical cylinders (burrows) ~15 cm in length and 0.3 cm

diameter. Diffusion occurs horizontally around these cylinders in addition to vertically. In general, the distribution of cylinders (burrows) is not known and is time dependent, although time dependence in position is minimal in the case of sedentary animals. For the sake of illustration a number of additional approximations can be made in order to demonstrate how the required diffusion coefficient changes when a more realistic geometry of diffusion is used. The case of random burrow orientation is treated in Chapter V. Assume that Clymenella distribute themselves equal distances from their nearest neighbors so that looking down on the sediment the tube openings (30) would be hexagonally packed at the maximum distance possible in the 0.1 m^2 area allowed. Any three tubes now act as the vertices of equilateral triangles the sides of which are 7.9 cm long, so that burrow axes are all 7.9 cm apart from each other. If each burrow (tube) is imagined to be the central axis of a vertically oriented hollow cylinder (annulus of sediment) having inner radius 0.15 cm and outer radius 3.95 cm (half the distance between tube axes) then most of the sediment in the tank can be assigned to one burrow or another; only the center of each triangle of sediment described by any three burrow openings and associated cylindrical shells is unaccounted for and is ignored here. Because all burrows are identical in this arrangement, the transport problem can now be further approximated to the case of diffusion in the wall of a single infinite hollow

cylinder with uniform initial concentration C_o, the inner boundary $r_1 = 0.15$ cm of which is held at $C = 0$ by irrigation and at the outer boundary $r_2 = 3.95$ cm the condition $(\frac{\partial C}{\partial r}) = 0$ is required because of intersection with a neighboring cylinder zone. This problem is solved for the general case by Muskat (1934, pp. 82-85) and in this instance the solution is:

$$C(r, t) = -\pi C_o \sum_{1}^{\infty} \frac{J_o(\alpha_n r_1) J_1(\alpha_n r_2) U(\alpha_n r) e^{-D\alpha_n^2 t}}{J_o^2(\alpha_n r_1) - J_1^2(\alpha_n r_2)}$$

α_n = roots of

$$U(\alpha r_1) = Y_1(\alpha_n r_2) J_o(\alpha_n r_1) - J_1(\alpha_n r_2) Y_o(\alpha_n r_1) = 0$$

where $J_v(x)$ and $Y_v(x)$ are the appropriate Bessel functions in standard notation. Manipulation of the solution for different D values using the appropriate roots ($\alpha_1 = 0.223$, $\alpha_2 = 0.527$) of the cylinder function ($U(\alpha_n r)$) produces a $D \sim 4.5 \times 10^{-5}$ cm^2/sec required to change the average concentration from ~ 29 µM to ~ 2 µM over the annulus in ~ 13 days. This value is still slightly larger than most molecular diffusion coefficients calculated for sediments (Goldhaber et al., 1977) suggesting that precipitation took place, that animals were somewhat mobile thereby increasing the effective number of tubes and decreasing r_2 or that, in sands at least, some advection away from the burrows also occurs during irrigation.

Because of the form of the transport equations and solution, the diffusion coefficient required to effect a given amount of exchange in sediment by this mechanism will decrease as the factor L^2 decreases where L = half the average distance between burrows. This demonstrates that in natural situations where mixed populations of tube-dwelling species occur and the average distance between burrows may be quite small (Figure III-12), the diffusion coefficient required to effect exchange at any given depth will decrease radically from that required by equivalent vertical diffusion. As illustrated in Figure III-12, which shows natural densities of Clymenella and capitellid polychaete tubes at Calves Pasture Point where collections were made, an ion need diffuse only about 0.5-1.0 cm horizontally to escape into overlying water although its vertical distance from the interface is 10-15 cm.

The effect of permanent burrows and burrow irrigation can in some ways be viewed as decreasing the net distance to the interface for a diffusing molecule but more generally viewed as changing the geometry of diffusion paths. Unfortunately, permanent dwelling burrows also become sites of preferential microbial activity and associated diagenetic reactions (Chapter II) greatly complicating modeling of even the most simple geometries. Where most animals are mobile rather than relatively sedentary like Clymenella, their spatial distribution becomes less important and the use of vertical diffusion coefficients more appropriate, as discussed below for Yoldia.

Special features of the pore water profiles

Several additional features of the pore water profiles remain to be explained, in particular the increase in the concentration of pore water Fe and Mn near the interface which took place after the introduction of Clymenella. One possible cause is direct pumping of pore water extracted from depth by irrigation into the top two centimeters. This injection could occur on the way out of the burrow or during a drawing-in of recently ejected water which had only partially mixed with overlying water. Another, more likely, possibility is that Fe and Mn which has freshly precipitated out of the overlying water onto or slightly below the sediment surface becomes subject to reduction and remobilization. A third possibility is that the distribution of microbial activity may have been altered after the addition of Clymenella in a way which increased the production rate of dissolved Fe and Mn in the near interface zone. The fourth possibility, which can be important in muds, is that oxidation of sulfides is increased near the interface resulting in some increased release of Fe or Mn (see Yoldia section). Because the newly precipitated Fe-Mn-oxides can be expected to be highly labile to reduction and because solid phase sulfides available for oxidation are in relatively low abundance in the sandy sediment used in the experiment, the second possibility listed above is considered the dominant contributor to the increase in the present experiment.

The observed increase in pH may also have several causes similar to those responsible for the increase in Fe and Mn: a greater pumping of water in and out of this zone, change in the microbial population, or precipitation of HS^- with freshly formed Fe-oxide. The low pH of the sediment in general may result from lack of sulfide precipitation (Ben Yaakov, 1973) resulting from the iron complexing described above or may be an artifact of drying the sediment, rewetting it and oxidizing during the process original iron sulfides or other potential acid producing components.

Sediment-water exchange of NH^+ and $HPO_4^=$

Both NH_4^+ and $HPO_4^=$ increased in tank water after Clymenella was added (Figure III-5). These are excreted by Clymenella so their source need not be sediment pore water. To supply the increased NH_4^+ levels excretion rates would have to be ~ 4 μmoles/worm/day. Typical literature values for NH_4^+ excretion rates of polychaetes are ~3-6 μmoles/g-worm/day by wet weight (Harris, 1959; Hult, 1969; O'Malley and Terwillinger, 1975). Clymenella torquata can be expected to have wet weights ≤ 0.1 g (see Mangum, 1964) implying that only about 10% of the observed NH_4^+ flux out of tank sediment can be accounted for by excretion from Clymenella. In addition, NH_4^+ is not conservative in tank water as demonstrated by controls so that like Mn and Fe, measured fluxes are minima. The conclusion is that pore water NH_4^+ is supplied by irrigation and radial diffusion in quantities

higher than the background supply from excretion.

Phosphate is subject to coprecipitation with Fe-oxides (e.g., Einsele, 1938; Mortimer, 1941; Tessenow, 1974). This effect is demonstrated in the present experiment by the slight decrease in phosphate during Fe precipitation in the tanks while NH_4^+ continues to increase. This effect cannot be quantitatively dealt with using the present experiment but it does illustrate one important aspect of irrigation and burrow construction. By increasing the flux out of sediments of elements like Fe and Mn, known to scavenge other dissolved constituents during precipitation, irrigation aids in the stripping of otherwise soluble elements from the water column overlying sediments.

Because Clymenella did not feed during the period of experiment and because resuspension of the sediment surface did not take place, the present results allow examination of a system without particle flux in either the water column or in underlying sediment. This greatly simplifies the sediment system since surface particles are not subducted and transport geometry can be simplified as discussed earlier. If sediment were reworked by Clymenella, oxide-coated particles would have rapidly dropped into the reducing zone, Fe and Mn remobilized in part, and then a fraction refluxed out of the sediment by irrigation. Sulfide-rich particles placed at the interface may also release Fe during oxidation. Once in the overlying water at higher pH and O_2 levels, Fe and Mn act as particle-philes and rapidly precipitate in

a system of high particle flux (e.g., Asten and Calvert, 1975; Lewis, 1976; Turekian, 1976); these particles fall back to the sea floor to complete the cycle. The role of irrigation is to increase both the rate and magnitude of this flux. Specific examples of the combined role of biogenic particle and fluid fluxes are given below.

The effects of a mobile, deposit-feeder: Yoldia limatula on sediment diagenesis

The sediment used in the mobile, deposit feeder or Yoldia experiment was obtained from a station in central Long Island Sound which has been particularly well studied over a several year period for biological, physical, and chemical properties (Rhoads and Michael, 1974; Gordon and Pilbeam, 1974; Rhoads, Aller, and Goldhaber, 1977; Chapter IV, V, VI). The results of the Yoldia experiment can therefore be used in conjunction with field data for understanding diagenetic processes and animal-sediment interaction in central Long Island Sound sediments. Indeed, the pore water profiles which formed in the tank can be directly compared to those found in the sediment at NWC as discussed later (Chapter V, VI). Control tank profiles, particularly for Fe, Mn, and Ca, resemble natural profiles found during the winter when macrobenthos are least active while those found in the Yoldia tank, except Mn, resemble Fall profiles when macrobenthic activity is known to be the highest of the year. Differences in tank profiles from natural ones can in most cases be accounted for by differences in the depth

distribution of the rates of reactions associated with organic matter decomposition, which, because of homogenization of sediment as discussed below, were altered from their normal exponential depth dependence. Processes which contributed to the formation of the profiles observed in each tank will first be considered and then the role of the deposit-feeder: Yoldia, in altering these processes from what occurs in its absence will be evaluated.

Pore water profiles in the tanks result, like their natural counterparts, from competition between transport and reaction. In the present experiment, biogenic transport has been greatly simplified by restricting the macrobenthos present to a single species known to limit its activities to the upper 4 cm. Physical transport has been greatly simplified as well; as in the Clymenella experiment, advection (i.e., net sedimentation) can be considered unimportant and physical transport predominantly diffusive.

Production reactions in tank sediment

Decomposition of organic matter by sulfate reduction results in the production of interstitial metabolites such as NH_4^+, $HPO_4^=$, H_2S, and alkalinity (e.g., Richards, 1965; Goldhaber and Kaplan, 1974). The reactions can be described in a general way by the equation (Richards, 1965):

$$(4) \quad 6(CH_2O)_x (NH_3)_y (H_3PO_4)_z + 3x(SO_4^{=}) \rightarrow 6x(HCO_3^{-}) + 6y(NH_3) + 6z(H_3PO_4) + 3x(H_2S)$$

The stoichiometry of C:N:P (x/y/z) in the metabolized fraction depends on the stage of decomposition and varies as a function of depth and time in sediments (Sholkovitz, 1973; Chapter V). In the free state and at normal pH values of sediments, reaction products are present predominately as NH_4^+, $HPO_4^{=}$, HS^-, and HCO_3^- (Berner, Scott, and Thomlinson, 1970; Kester and Pyt kowicz, 1967; Goldhaber and Kaplan, 1975a).

The rate and depth dependence of organic matter decomposition and therefore the production of metabolites is related to the quantity of metabolizable organic matter present in a given sediment depth interval (Zobell and Anderson, 1936; Waksman and Hotchkiss, 1938) and in the case of decomposition of organic matter by SO_4 reduction is thought in many instances to decrease sharply with depth (e.g., Zobell and Rittenberg, 1948; Oppenheimer, 1960; Sorokin, 1962; Goldhaber et al., 1977). At NWC, where sediment was collected for the present experiment, the rate of sulfate reduction decreases exponentially with depth and is quite low at depths as shallow as 10 cm (Chapter V). In the tanks, sediment was thoroughly homogenized before beginning the experiment so that both quality and quantity of source organic matter was initially constant with depth. This means

that to a first approximation the rate of sulfate reduction or production of NH_4^+, $HPO_4^=$, HS^-, and alkalinity is also constant.

Several kinds of reactions produce dissolved Mn and Fe in marine sediment. Under reducing conditions, strictly inorganic processes are capable of solubilizing the oxides of Fe and Mn and releasing Fe^{++} and Mn^{++} (e.g., Krauskopf, 1957). Because of this, the rate of supply of Fe^{++} and Mn^{++} to solution may be related to the quantity of oxide readily available for reduction. This relation is sometimes approximated by a first order reaction where production rate is proportional through a rate constant to the quantity of oxide (e.g., Robbins and Callender, 1975; Holdren, Bricker, and Matisoff, 1976). Because the absence of oxygen in near surface sediment is maintained by microbial metabolic activity this superficially inorganic reaction is tied indirectly to biological activity.

There are several other mechanisms by which dissolved Mn and Fe can be produced which are not necessarily related to the quantity of oxide. Reduction of oxide may be specifically or catalytically a part of bacterial metabolic pathways (Mann and Quastel, 1946; Trimble and Ehrlich, 1968; Bromfield and David, 1976). In this case, the rate of production, like the rate of sulfate reduction, would be determined by the quality and quantity of metabolizable organic matter available until the quantity of reducible oxides became limiting (see Chapter VI).

Along or near the oxidizing-reducing boundary, the oxidation of solid phase or interstitial sulfide may aid in increasing the quantity of dissolved Fe^{++} in particular. The oxidation of FeS and FeS_2 is known to produce dissolved Fe^{++} as a transient intermediate in addition to $SO_4^{=}$ (Stumm and Morgan, 1970; Bloomfield, 1972; Chapter VI). The rate of production of Fe^{++} relative to the rate of its further oxidation to Fe^{+++} will determine whether this production reaction will contribute significantly to the standing concentration of Fe^{++} at any given horizon of sediment. The oxidation of dissolved HS^- alone will also tend to raise the level of Fe^{++} through mass action influence on the reaction:

(5) $\quad Fe^{++} + HS^- = FeS + H^+$

since HS^- is oxidized at a lower Eh than Fe^{++}. Of course, this mechanism could operate only over the restricted depth range where it would be a controlling reaction but oxidation could still take place. None of these production reactions are exclusive in the present experiment but their relative contributions and importance can be expected to change as a function of position in the sediment column.

The formation of dissolved Ca may take place by the dissolution of $CaCO_3$ present in the solid phase when $CaCO_3$ becomes undersaturated in solution. This reaction may be inhibited by surface poisoning, particularly by $HPO_4^{=}$ (Morse and Berner, 1972).

Specific reactions following production

Each of the dissolved ions produced by the above reactions are subject to specific interactions, appropriate to their chemistry with sediment particles or other dissolved ions. NH_4^+ can be considered the least reactive in terms of precipitation out of solution as an insoluble phase but is known to absorb strongly to organic and clay particles abundant in sediment (Mortland and Wolcott, 1965; Nommek, 1965). Rosenfeld (in preparation) has shown that for marine sediments adsorption of NH_4^+ is reversible and can be described by Langmuir isotherms. At low levels present in sediment, the amount adsorbed is proportional to the amount in solution through a proportionality constant of ~ 1. Except for biological consumption in the overlying tank water, adsorption will be considered the dominant reaction affecting NH_4^+.

Phosphate is more reactive than NH_4^+ and is involved in both irreversible and reversible adsorption (Carritt and Goodgal, 1954; Li et al., 1972; Syers, Harris, and Armstrong, 1973) and the formation of specific inorganic phases with major to minor sedimentary metals such as Fe, Ca, and Mn (Nriagu and Dell, 1974). Under oxidizing conditions adsorption of phosphate is large, and often specifically related to interaction with Fe-oxide present on particle surfaces (Mortimer, 1941; Carritt and Goodgal, 1954; Li et al., 1972; Parfitt, Atkinson, and Smart, 1975); in reducing conditions phosphate adsorption is lower (Olsen, 1964). Expressed as a reversible linear

adsorption coefficient, K, the data of Li et al. (1972) imply that in lake sediment, K ranges from ~0.3-7 under anoxic conditions with most values at ~5. In oxygenated conditions K ~25-50. At low sulfide levels but in reducing sediments, phosphate may precipitate and its concentration in solution be controlled by the formation of phases similar to vivianite ($Fe_3(PO_4)_2 \cdot 8H_2O$) or reddingite ($Mn_3(PO_4)_2 \cdot 3H_2O$) (Bray, 1973; Nriagu, 1972; Nriagu and Dell, 1974; Norvell, 1974). Study of precipitation reactions and equilibrium relationships of this kind between dissolved and solid phases is greatly complicated by kinetics of reaction, solid solutions or otherwise impure phases, and in some instances a lack of reliable thermodynamic data on the pure compound which is most likely to form.

Titration alkalinity is predominately carbonate alkalinity in pore waters of near surface marine sediments (Berner, Scott, and Thomlinson, 1970). Two major types of reactions consume HCO_3^- and lower the alkalinity levels: precipitation of Ca and Mg carbonates (Abd-el-Malek and Rizk, 1963; Berner, Scott, and Thomlinson, 1970) and production of acids which titrate HCO_3^- (Chapter VI). The formation of carbonates by precipitation from marine sediment pore water has been demonstrated by several investigators (Berner, Scott, and Thomlinson, 1970; Ben Yaakov, 1973; Sholkovitz, 1973) and normally occurs at depth in sediment where supersaturation with respect to $CaCO_3$ occurs. Titration of alkalinity by acid production has been less

emphasized but can be shown to take place in the upper oxidized zone of sediment during the oxidation of sulfides (Chapter VI).

Dissolved Fe and Mn are subject to precipitation at variable rates under oxidizing conditions as discussed earlier. Under reducing conditions, the formation of their respective phosphates, carbonates, or sulfides is likely to take place (Troup, 1974; Holdren, 1977). Where sulfide is in plentiful supply, variably stable forms of Fe-sulfides: mackinawite (FeS), greigite (Fe_3S_4), and pyrite (FeS_2), are readily formed and have been well studied (Berner, 1967, 1970; Rickard, 1969, 1974; Sweeney and Kaplan, 1973). Iron sulfides are abundant in NWC sediment (Chapter V, VI). Sedimentary manganese sulfides have been much less studied and their thermodynamic properties poorly documented but alabandite (MnS) and hauerite (MnS_2) are possible phases. Precipitation of Mn as a rhodochrosite-like carbonate ($MnCO_3$) is thought to be an important control on sedimentary Mn (Li, Bischoff, and Mathieu, 1969; Holdren, Bricker, and Matisoff, 1976) and the formation of siderite ($FeCO_3$), together with vivianite ($Fe_3(PO_4)_2 \cdot 8H_2O$), is thought to control Fe^{++} levels in pore waters of sulfide-poor sediments (Troup, 1974). A reddingite-like ($Mn_3(PO_4)_2 \cdot 3H_2O$) phase may also enter into Mn precipitation (Tessenow, 1974; Nriagu and Dell, 1974).

Evaluation of equilibrium controls on tank pore water profiles

The likelihood of specific phase formation and equilibrium controls on sediment pore water chemistry in each tank can be evaluated by calculating the state of saturation of dissolved ions with respect to a range of pure solid phases likely to form. This is done by determining the activity of a given ion in solution and comparing ion activity products (IAP) for different phases with predicted equilibrium activity products. To calculate dissolved ion activities in sea water both nonspecific and specific (ion pairing) effects must be taken into account; techniques for doing this are outlined in detail by Garrels and Christ (1965) and Berner (1971). In the present study a computer program developed and written by R. Holdren (Holdren, 1977) was used for calculation of activities. Ion pairing for HCO_3^-, $CO_3^{\equiv}$, $SO_4^=$, $H_2PO_4^-$, $HPO_4^=$, HS^-, OH^-, Cl^-, H^+, Na^+, K^+, Ca^{++}, Mg^{++}, Fe^{++} and Mn^{++} is calculated using accepted values for association constants at 25°C (Sillen and Martel, 1964; Morgan, 1967), the choice of which are discussed in detail by Holdren (1977) and will not be repeated here. The formation of complexes with organic material is ignored. Activity coefficients are estimated using the extended Debye-Huckel equation for the appropriate ionic concentrations. This results in an error of ~ 10-20% which becomes insignificant compared to other uncertainties such as the value chosen for the K_{sp} of a given phase (see below). Charge balances for the data are $\pm$ 0.1 in the Yoldia tank and

-0.1 to 0.5% in the control assuming Mg/Cl, Na/Cl, and K/Cl ratios of sea water. The calculated γ_T's (total activity coefficient) by the model are 0.16-0.17 for Fe, 0.11 for Mn, and 0.21-0.22 for Ca at the tank conditions and are within the expected range (Berner, 1971).

Selected reactions involving some of the solid phases likely to form and a representative K_{sp} for each are given in Table III-5. Saturation indices (log IAP/K_{sp}) for individual depth intervals are calculated and listed in Table III-6. These indicate that, within error, Fe is in equilibrium below 4 cm depth with various iron sulfides, a finding consistent with the black color and known presence of these compounds in NWC sediment. In the control tank, a zone of saturation with respect to vivianite occurs just above the sulfide zone. Mn could be in equilibrium with either a rhodochrosite-like or reddingite-like phase; the measured activities of $CO_3^{=}$ and $PO_4^{\equiv}$ lie very close to the equilibrium boundary for the two phases. This may be a fortuitous result of the chosen K_{sp} for reddingite as a range of values has been reported; the value chosen is in reasonable agreement with the results of Tessenou (1974) at 5°C and low a_{Fe}/a_{Mn} ratio, but not with ΔG_f° of Latimer (1952) which predicts a significantly higher solubility. The range of reported K_{sp}'s for Mn sulfides is so large that it is not possible to rule out a role for these phases. The salient conclusion is that below ~4 cm depth in each tank, Mn is at saturation or supersaturation with respect to several reasonable solid phases. Because of its common geologic occurrence, $MnCO_3$ can be

considered the most likely of the possible pure phases to form and, in addition, its K_{sp} is the least contested and the calculation most valid.

Both calcite and aragonite are undersaturated at selected horizons of sediment with undersaturation occurring in zones of low pH. Supersaturation takes place in intervals of high pH or high alkalinity. These calculations agree, very well with similar calculations using the raw data and apparent dissociation constants for carbonic acid (Lyman, 1965) and apparent solubilities of calcite and aragonite (Berner, 1976c) in sea water, giving added confidence to the model used here to determine activities.

Models of transport and kinetic controls on tank pore water profiles

Simple transport models and knowledge of the specific reactions taking place can be used together to help explain similarities and differences in the pore water and solid phase properties of the Yoldia and control tanks. NH_4^+ is the least reactive in terms of specific phase formation and its distribution will be considered first in order to substantiate or disprove assumptions about transport and decomposition in each tank. As in the case of the Clymenella experiment there is no net sedimentation during the course of the experiment so that, ignoring compaction, the NH_4^+ concentration distribution, C(x, t), in pore water is described by the equation (Berner, 1976b):

$$(6) \qquad \frac{\partial C}{\partial t} = \frac{D}{1+K}\left(\frac{\partial^2 C}{\partial x^2}\right) + \frac{R_N}{1+K}$$

where: t = time

x = dimension variable, origin at sediment-water interface and positive axis into sediment

K = Langmuir adsorption coefficient for NH_4^+ in linear adsorption range

D = Molecular diffusion coefficient modified for tortuosity

R_N = rate of NH_3 production as a function of depth and time.

In the present experiment the sediment was initially homogenized so that, as discussed above, the concentration of metabolizable organic matter is constant and R_N will be assumed constant with depth. Decomposition experiments on sediments from NWC show that R_N is unlikely to be a strong function of time over the length of the present experiment as long as temperature is held constant (Chapter V). The initial conditions to be included in the solution are:

$$t = 0, \quad C = C_o, \quad 0 \leq x \leq \ell$$

where ℓ = thickness of sediment layer. The boundary conditions, with overlying water at $x = 0$ and the bottom of the tank $x = \ell$ sealed, are:

$$t > 0, \; C = C_1, \; x = 0 \; ;$$

$$\left(\frac{\partial C}{\partial x}\right)_{x = \ell} = 0$$

The solution is obtained by a minor modification of the problem solved by Nelson (1952) giving:

(7)

$$C = C_1 + \frac{D}{R} x (\ell - x) - \frac{8D\ell^2}{R\pi^3} \sum_{n=1}^{\infty} \frac{e^{-(2n-1)^2\pi^2 Dt/4\ell^2(1+K)} \sin[(2n-1)\pi x/2\ell]}{(2n-1)^3}$$

$$- \frac{4}{\pi}(C_1 - C_o) \sum_{n=1}^{\infty} \frac{e^{-(2n-1)^2\pi^2 Dt/4\ell^2(1+K)} \sin[(2n-1)\pi x/2\ell]}{(2n-1)}$$

From Rosenfeld (in preparation), $K \cong 1$. $D \sim 7.0 \times 10^{-6}$ cm^2/sec based on the theoretical ratio of $D_{NH_4^+}/D_{SO_4}$ (corrected to 22°C) (Li and Gregory, 1974) multiplied by $D_{SO_4} = (4 \times 10^{-6}$ $cm^2/sec)$ for Long Island Sound sediment (Goldhaber et al., 1977). This $D_{NH_4^+}$ also agrees well with measured $D_{NH_4^+}$ in sediment in the laboratory (Rosenfeld, in preparation). There are two independent ways of estimating or placing limits on R_N. Since in diffusive transport, the mean distance x affected in a defined time is: $x = (2Dt)^{1/2}$ then in 44.9 days with the above $D_{NH_4^+}$ a depth of x = 7.4 cm in the tank would be greatly influenced by diffusion. This means a minimum R_N can be estimated by using the measured NH_4^+ concentration at 7-9 cm, C, compared to the starting value, C_o, to give $\frac{R_N}{1+K} = \frac{C - C_o}{t}$ with t = 44.9 days. This gives for the control tank: $R_N/1+K = 7.2 \times 10^{-8}$ mM/sec (a minimum value). An independent check comes from decomposition experiments at NWC (Chapter V) which give an average $\bar{R}_N/1+K$ for the upper 10 cm of sediment of $1.8 - 0.4 \times 10^{-7}$ mM/sec (22°C); since the grab sampler used to obtain sediment for the tanks may

have captured the upper portion of sediment in a somewhat different proportion than exactly 0-10 cm, these R_N values can be considered in fairly good agreement.

Using $R_N/(1+K) = 7.2 \times 10^{-8}$ (lower limit), the model generated profile for t = 44.9 days is given in Figure (III-13. The case where $R_N/(1+K) = 8 \times 10^{-8}$ mM/sec is also graphed for even better agreement. Agreement between the observed data and the simple production, adsorption, and transport model is excellent indicating that the assumptions of the model are reasonable and represent a basically adequate description of the processes affecting NH_4^+ in the tank. Precipitation of NH_4^+ as part of an insoluble phase at depth in the tank would not be illuminated by this treatment of the data but the relatively narrow range of independently estimated R_N's suggest that this is not a serious problem. Slight changes in R_N near the interface do not greatly affect the profile, while, as shown below, changes in D do, so that the assumption of constant R_N need really hold only below the upper few centimeters. The model is highly sensitive to values chosen for D and K.

Phosphate data in the control tank were modeled in a similar way but with $D = 2.6 \times 10^{-6}$ cm^2/sec (assume $HPO_4^=$ form, estimated as for $D_{NH_4^+}$) and $R_p/1+K_p = 1.2 \times 10^{-8}$ mM/sec estimated from concentration changes in the 7-9 cm interval. No independent estimate of $HPO_4^=$ production other than that obtained from the tank is available. However, the ratio $[R_N/(1 + K_N)]/[R_p/(1 + K_p] \sim 7$ calculated from the above estimates is

consistent with limits on N/P release ratios estimated from flux measurements at NWC (Chapter V). This suggests that if K_P and K_N are either small or approximately equal, the $R_P/(1 + K_P)$ estimated here is reasonable. K_P is assumed to be ~ 1 for purposes of the present calculations; at higher K_P's the fit becomes worse. The $HPO_4^=$ data deviate strongly from simple diffusion-production control, particularly near the interface (Figure III-14). This demonstrates the greater chemical reactivity of $HPO_4^=$ compared to NH_4^+ in the oxygenated zone. The marked upward concavity in the concentration profile presumably results from interaction with Fe, either through precipitation as a distinct phase or irreversible adsorption on oxides as noted previously. The Yoldia tank profile shows similar effects but is complicated by reworking as discussed below.

It is possible to fit a similar diffusion-production curve to the Yoldia tank NH_4^+ data as was done for the control using a slightly higher R_N; but there are several clues that transport-reaction conditions are not the same in the Yoldia and control tanks: (1) The flux of Mn out of Yoldia tank sediment is three times the control tank during the first three days when $(\frac{\partial C}{\partial x})_{Yoldia} \sim (\frac{\partial C}{\partial x})_{control}$ must roughly be true (Figure III-11, Table III-4). This means the effective diffusion coefficient for Mn must be at least three times higher near the sediment-water interface in the Yoldia tank than control. Since the precipitation rate of Mn is pseudofirst order at high reactive-particle concentrations (Lewis 1976) like that present in the Yoldia

tank, the discrepancy in flux must be even greater when precipitation is considered. (2) Both the Mn and alkalinity profiles in the Yoldia tank are lower in concentration level than the control despite apparently higher rates of organic matter decomposition in the Yoldia tank. These higher rates are indicated by slightly higher concentrations of NH_4^+, $HPO_4^=$, HS^-, and ATP in Yoldia tank sediment below 4 cm depth (Figures III-7, III-10; Table III-4). (3) The dissolved Fe maximum is greatly lowered in the tank with Yoldia compared to the control (Figure III-8).

These differences, and also similarities between tanks, can be explained by considering the effects of sediment reworking by Yoldia on pore water distributions. Two distinctly different kinds of effects can be expected: (1) changes which result from simply altering the rate of transport of fluid and particles in the inhabited zone relative to underlying sediment, and (2) the effects of specific chemical reactions which result when particles are transferred from one diagenetic zone to another during reworking.

Alteration of transport mechanisms by the activities of Yoldia

Reworking by Yoldia is restricted to the upper 3-4 cm so that transport in the Yoldia tank can be described by a composite system where the upper 3 cm has an effective, biogenic diffusion coefficient D_1 and the zone 3-10 cm is controlled by a molecular diffusion coefficient D_2. Because Yoldia is

mobile and its activities restricted to a thin zone near the interface, the geometry of diffusion, unlike the case of the sedentary, tube-dweller Clymenella, can be adequately described by an average, vertical diffusion coefficient. The use of a diffusion analogue for biogenic reworking and of an average diffusion coefficient in particular, assumes that the sample of sediment taken at any given depth integrates over a large enough area (or individual animals) to eliminate heterogeneities in rates and depth of reworking (e.g., Hanor and Marshal, 1971; Chapter IV). It is not necessary to solve the transient state in order to illustrate the effect of this composite system on pore water profiles; the steady state equations to be solved, using the same basic form and assumptions as previously, are:

Zone I: (8) $$\frac{\partial C_1}{\partial t} = 0 = D_1\left(\frac{\partial^2 C_1}{\partial x^2}\right) + R_1 \qquad 0 \leq x \leq L_1$$

$$x = 0, \quad C = C_o$$

Zone II: (9) $$\frac{\partial C_2}{\partial t} = 0 = D_2\left(\frac{\partial^2 C_2}{\partial x^2}\right) + R_2 \qquad L_1 \leq x \leq L_2$$

$$\left(\frac{\partial C_2}{\partial x}\right)_{x = L_2} = 0$$

with the added continuity condition that at the boundary (L_1) between the upper and lower zones:

(10) $$D_1\left(\frac{\partial C_1}{\partial x}\right)_{x = L_1} = D_2\left(\frac{\partial C_2}{\partial x}\right)_{x = L_1}$$

The solutions with R_1, R_2 constants are:

$$(11) \quad C_1 = -\frac{R_1}{2D_1} x^2 + \frac{R_2}{D_1} L_2 x + \frac{R_1}{D_1} L_1^2 + \frac{R_2}{D_1} L_2 L_1 + C_o$$

$$(12) \quad C_2 = -\frac{R_2}{2D_2} x^2 + \frac{R_2}{D_2} L_2 x + \frac{R_1}{D_1} L_1^2 + \frac{R_2}{D_1} L_2 L_1 + C_o$$

The ratio D_1/D_2 can be estimated in the present case from the alkalinity profile in the Yoldia tank by assuming $L_1 = 3$ cm, fitting second order polynomials to the data in each zone, and calculating $\left(\frac{\partial C}{\partial x}\right)_{x = L_1}$ for each function. This gives $D_1/D_2 = 3.3$ by the continuity relation above. Taking $D_2 = 3 \times 10^{-6}$ cm^2/sec for HCO_3^- then $D_1 \sim 1 \times 10^{-5}$ cm^2/sec. Unfortunately alkalinity is also destroyed by sulfide oxidation (Chapter VI) in the near interface zone as demonstrated in the present experiment by the concavity in the alkalinity profile in the control tank (Figure III-7) so that this estimate of D_1 may err on the high side. There are two reasons to believe that it is in fact accurate: (1) destruction of alkalinity occurs in the low pH zone of sediment, which due to mixing as discussed below is at the interface in the Yoldia tank. It therefore acts as a pseudo-boundary condition in the present case rather than internally disrupting the profile within zone I and should not influence the calculation and (2) the initial flux of Mn out of the Yoldia tank, as pointed out earlier, requires a D_1 of $>6 \times 10^{-6}$ cm^2/sec

if $D_{Mn} = 2 \times 10^{-6}$ cm^2/sec normally. The effect of the higher D_1 than D_2 is illustrated for steady state in Figure III-15A. Similar results have been obtained for a composite system of this type but with different reaction and boundary conditions by Vanderborght, Wollast, and Billen (1977). It is obvious that even with Yoldia present, if the molecular diffusion coefficient of an ion is $\sim 1 \times 10^{-5}$ cm^2/sec, reworking will not affect transport of that ion but as in the case of alkalinity, if $D_1 > D_2$, the concentration is lowered throughout the sediment column. The model curves compare well in relative shape with the observed differences between Yoldia and control tanks even though the actual steady state values have not yet been attained (Figures III-7, 15A). The greater the disparity between D_1 and D_2 for a given ion, other things equal, the greater the effect of mixing on its entire profile. For example, NH_4^+ has a $D_{NH_4^+} \sim 7 \times 10^{-6}$ cm^2/sec so that changes in its profile due to a mixed zone become more subtle: the break between Zone I and II is less evident but concentrations in Zone II can still be generally lowered as illustrated in Figure III-15A for the case where $D_1 \rightarrow D_2$.

Changes in R_1 relative to R_2 do not influence the observed profiles very much as long as L_1 is much less than L_2 and R_1 and R_2 are both positive (Figure III-15B). When R_1 becomes negative, that is, the ion under consideration is consumed uniformly in the upper layer, the profile can become significantly affected without any change in diffusion coefficients.

In this case, the upper zone profile takes on an increasingly concave shape, like that of $HPO_4^{=}$, as R_1 becomes greater than $|-2R_2|$ (Figure III-15B). An example where both R_1 and D_1 differ from D_2 and R_2 is given in Figure III-15A illustrating the effect of increasing D_1 on the shape of the concavity produced by consumption in Zone 1. The curves where R_1 is 1/10 R_2 and $D_1 = 3/2\ D_2$ demonstrate that it is not possible to easily recognize changes in R and D near the interface from the shape of profiles alone, although a significant lowering of concentrations takes place in each instance.

Changing the functional form of R to $R = R_o e^{-\alpha x}$ does not alter the basic conclusions of the composite model. In this case, a break in the concentration profile at the mixing depth is harder to see but the general lowering of concentration still takes place. The solutions, with the same boundary conditions as above, are:

$$(13)\quad C_1 = -\frac{R_o}{D_1\alpha} x\, e^{-\alpha L_2} + \frac{R_o}{D_1\alpha^2} + C_o - \frac{R_o}{D_1\alpha^2} e^{-\alpha x}$$

$$(14)\quad C_2 = -\frac{R_o}{D_2\alpha} x e^{-\alpha L_2} - \frac{R_o}{D_2\alpha^2} e^{-\alpha x} - \frac{R_o}{D_1\alpha} L_1 e^{-\alpha L_2} + \frac{R_o}{D_1\alpha^2} - \frac{R_o}{D_1\alpha^2} e^{-\alpha L_1} + \frac{R_o}{D_2\alpha} e\, L_1^{-\alpha L_2} + \frac{R_o}{D_2\alpha^2} e^{-\alpha L_1} + C_o$$

and solutions have been graphed for the case where $\alpha = .33$, as found normally for rates of sulfate reduction at NWC (Chapter V), with R_o evaluated so that the average R over 10 cm is equivalent to the constant R_2 used in the previous examples (Figure III-16). The significance of the depth dependence of R in controlling the final concentrations obtained is illustrated by comparison of the two examples with R = constant and $R = R_o e^{-\alpha x}$ (Figures III-15, 16).

The general lowering of concentration produced by a mixed layer illustrates that in order for NH_4^+ and $HPO_4^=$ levels to remain greater at depth in the Yoldia than control tanks the discrepancies in rates of decomposition in the two tanks must be much greater than at first indicated. Stimulation of microbial metabolic activity by macrofauna has been noted in several cases (Hargrave, 1970; Fenchel, 1970; Chapter II). There are a number of reasons why this may take place: high turnover of microbes due to grazing by macrofauna, stimulation of microbes by mucus secretions from macrofauna, formation of favorable hibitats such as tube walls, and the flushing of metabolites from sediment by irrigation. In the present case, where metabolism and biomass (ATP) is apparently increased below the feeding zone, the most probable effect of macrofauna is to lower the concentration of some inhibiting by-product of metabolic activity by the transport mechanism outlined above or to increase the supply of a depleted nutrient available only in overlying water by the same means.

The rate of particle transport by Yoldia when expressed as a vertical diffusion coefficient has been shown by dimensional analysis of reworking

data (Rhoads, 1963) to be $\sim 2 \times 10^{-6}$ cm^2/sec for a feeding depth of 3 cm (after Guinasso and Schink, 1975). This is much lower than the effective biogenic diffusion coefficient of $\sim 1 \times 10^{-5}$ cm^2/sec calculated above for pore water. The discrepancy arises for several reasons: (1) Yoldia pumps water for respiration into its mantle cavity. Although many shelled animals would be effectively sealed from their environment (Chapter I) the relatively low degree of mantle fusion in protobranchs together with the use of labial palps helps to irrigate sediment with respiratory water during feeding. Irrigation rates are volumetrically ~ 100 times greater than particle reworking rates (Chapter I) so that even at low efficiency of exchange out of the mantle cavity it will be an effective transport mechanism. (2) Yoldia is highly mobile. Burrowing does not result in a great deal of particle transport relative to feeding (Chapter I) but does greatly increase the exchange of pore water as shown previously for one particular geometry in the case of Clymenella tubes. Burrowing and irrigation during respiratory pumping can easily account for the increase in the effective, vertical diffusion coefficient beyond that accounted for by feeding alone.

Specific effects of reworking on Mn

When coupled with the specific chemistry of a given element, the relatively simple change in transport regime brought about by Yoldia has some very important and permanent effects on sediment diagenesis and overlying water chemistry. Mn is a good example in the present experiment. The general

features of the Mn pore water profiles in both tanks can be explained by assuming that initially like NH_4^+, Mn is produced at a constant rate R_{Mn} with depth and is subject to the same kind of initial and boundary conditions as used for solving the NH_4^+ distribution above (equation 7). But, because it was shown earlier that Mn becomes saturated with respect to a number of solid phases below 4 cm, at some point Mn concentration reaches a level at depth where precipitation as a reduced phase becomes likely. For illustrative purposes this phase will be arbitrarily taken as rhodochrosite. If for simplicity a constant pH = 7.4 is assumed and $\gamma_{T,\,Mn} = 0.11$, then at saturation with respect to $MnCO_3$:

$$(15) \qquad C_{Mn} \sim \frac{0.6}{C_{Alk}}$$

where C_{Mn} = total concentration of Mn;

C_{Alk} = total alkalinity, assumed to be HCO_3^- + $CO_3^=$ only.

It is possible to produce a time series of Mn concentration curves by assuming that both Mn and alkalinity increase initially in the same way as does NH_4^+ so that an equation of the type:

$$(16) \qquad \frac{\partial C}{\partial t} = D\,\frac{\partial^2 C}{\partial x^2} + R; \qquad \begin{array}{l} t + 0,\ C = C_o,\ 0 \le x \le L; \\ t > 0,\ x = 0,\ C = C_1 \\ x = L,\ \left(\frac{\partial C}{\partial x}\right)_{x=L} = 0 \end{array}$$

would describe their profiles until concentration levels at a given time and

depth had reached values where supersaturation with respect to $MnCO_3$ took place. At this time, C_{Mn} becomes controlled by the equilibrium condition (15) (or a constant supersaturation due to kinetic constraints (e.g., Holdren, 1977) at and below that depth. Because of its much greater abundance than C_{Mn}, C_{Alk} continues to increase according to (16). Above the depth where (15) is met, Mn concentration is still described by (16) except the lower boundary L is now determined by where equilibrium (or supersaturation + kinetic) control begins and becomes a function of time. In the present example, this boundary change was found by trial and error manipulation of the solution to (16), equation (7), to not be quantitatively important.

For evaluation of the model, D_{Mn} and $D_{HCO_3^-}$ can be estimated by the same method used for finding $D_{NH_4^+}$, yielding $D_{Mn} = 2 \times 10^{-6}$ cm^2/sec and $D_{HCO_3^-} = 3 \times 10^{-6}$ cm^2/sec. R_{Mn} (2×10^{-5} $\mu M/sec$, no adsorption correction), was determined by fitting the solution to (16) so that the interface concentration gradient in the control tank would be produced at the assumed D_{Mn}, and, R_{Alk} (1.34×10^{-6} mM/sec) was found by the method used for NH_4^+. Using these values, a hypothetical time series of Mn concentration was generated and is shown in Figure III-17. The basic features of the final Mn profile at time of sampling the control tank are well described except that the Mn maximum is at a lower depth in the real case because of the depression of alkalinity near the interface (probably by sulfide oxidation). The maximum in the dissolved Mn profile requires

diffusion of Mn both toward the interface and toward the tank bottom. This predicts a redistribution of solid phase Mn, a prediction substantiated by the measured solid phase Mn levels (Figure III-10). The time series of Mn pore water profiles suggests that a maximum appeared only after a few weeks and that because of the nature of the production distribution and the relative rates of Mn and alkalinity production, once formed, the maximum Mn concentration rose rapidly from the tank bottom to a depth of 4-5 cm in just a few days. Ignoring other reactions the maximum theoretically would rise to a depth where production rate is balanced by diffusive loss to the overlying water.

The flux of dissolved Mn to any part of the tank is determined by $\partial C/\partial x$ of the profile at a given time and depth; the modeled gradient can be seen in Figure III-17 to exponentially decrease below the pore water maximum. This predicts that most downward diffusing Mn will be precipitated just below the maximum rather than at the tank bottom, a prediction born out by the solid phase distribution which shows the lower solid phase Mn maximum occurring above the tank bottom (Figure III-10).

Sediment reworking by Yoldia affects this pattern of Mn redistribution in several ways. Because biogenic diffusion induced by Yoldia is greater than D_{Mn} or D_{Alk}, the concentration of both components are lowered in pore water as demonstrated previously. This means that the dissolved Mn concentration maximum will appear at the tank bottom later in time and that it will reside at a lower depth in the tank longer than in the control before rising to a higher

level such as 4-5 cm. The result is that the solid phase Mn maximum should occur lower in the Yoldia tank than in the control and, in fact, it does (Figure III-10).

Although the assumption of constant R_{Mn} with depth explains many of the features of the present experiments it is clear that the R_{Mn} value chosen, 2×10^{-5} μM/sec, is a minimum. This can be shown by considering the sediment interval 1-2 cm where Mn concentrations dropped by 28 μg/g and 79 μg/g relative to starting values in the control and Yoldia tanks during the experiment . This drop predicts an R_{Mn} of 1.3×10^{-4} to 2.4×10^{-4} μM/sec for that interval, using the appropriate water contents for calculation (Table III-3). The discrepancy between the estimate of R_{Mn} from pore water and solid phase Mn profiles may result for several reasons: (1) The pore water gradient near the interface is not adequately described by equation (16). (2) The second centimeter interval may have a uniquely high R_{Mn} resulting from the particular conditions, either microbial or physical, which exist there. (3) R_{Mn} may be a strong function of time. In any case, the presence of Yoldia apparently results in a higher rate of dissolved Mn production than when they are absent.

The rapid redistribution of solid phase Mn during the 45 day period of these laboratory experiments substantiates field observations where, based on ^{234}Th ($t_{1/2}$ = 24.1 d) time scales (Aller and Cochran, 1976), it was shown that Mn profiles must form and reform on time scales of the order of at most months (Chapter IV, V).

Reworking increases the flux of Mn out of the Yoldia tank as discussed previously. Because the overlying water was changed repeatedly, Mn was removed from the system. The higher flux and higher suspended particle concentration onto which precipitation took place in the Yoldia tank resulted in a higher loss of Mn during water changes than in the control. This explains the general lowering of Mn levels in the solid phase of the Yoldia tank compared to the control (Figure III-10). More importantly it demonstrates that under natural conditions, Yoldia helps maintain a higher proportion of sedimentary Mn in the overlying water than would occur in its absence.

Redistribution of organic matter

The percent organic matter (ignition loss) profiles demonstrate redistribution of sediment particles directly by feeding. Organic matter decreases from the interface to 4 cm in the Yoldia tank, then increases sharply and remains relatively constant below that depth. The increase at the surface presumably results from the selection of small or organic-rich particles relative to ambient sediment at depth (3-4 cm) and placement of these particles at the interface during defecation. The increase of percent organic matter above the starting value at depth in the sediment of both tanks may result from an increase in bacteria by chemosynthesis or may reflect an inaccurate measure of the starting value.

Effects of reworking on Fe and Ca

In the process of reworking particles for feeding, Yoldia transport labile, reduced compounds such as FeS from depth directly to the sediment-water interface. The surfaces of these particles rapidly oxidize and are subsequently subducted back to the base of the feeding zone. Particles are constantly refluxed between reducing and oxidizing conditions. The steady reoxidation of labile sulfides which results, helps to lower alkalinity and pH of surface sediment and overlying water (Chapter VI; Figure III-7, 8). This process must play a role in keeping alkalinity lower in the Yoldia tank water than in the control despite the greater flux of HCO_3^- out of sediment due to reworking. Two additional processes may also lower alkalinity: organic acid excretion by Yoldia and shell formation. If shell formation were the only cause then Ca should show minor depletion below Ca/Cl ratios present in sea water but it does not. All these processes are nonexclusive and together with increased biogenic diffusion can be expected to lower alkalinity in pore water; this lowering of alkalinity helps to keep the saturation state of $CaCO_3$ low at the reduced pH levels of sediment.

Dissolved Ca concentrations above the sea water background demonstrate the production of Ca^{++} in sediment near the interface of the control tank (Figure III-8). This production presumably results from the dissolution of $CaCO_3$ (probably aragonite, the most abundant shell debris; see Table III-6 for IAP calculation). Undersaturation and dissolution are

caused in turn by the lowering of pH and alkalinity during the oxidation of sulfides. There are at least two possible reasons why, despite the apparently higher overall oxidation of sulfide evidence for $CaCO_3$ dissolution is not found in the dissolved Ca profile of the Yoldia tank: (1) Reworking presumably causes the maximum oxidation of sulfide to occur at or very near the sediment-water interface rather than below it. This is due to the direct placement of reduced material at the surface during feeding. Because of the proximity to overlying water, the reaction products from oxidation or dissolution do not build-up in the sediment pore water. (2) The increase in the effective diffusion rate due to irrigation and burrowing may prevent build-up of reaction products into distinct, easily detected concentration maxima. These considerations demonstrate, as did the earlier modeling, that although reactions may be more rapid in the Yoldia than control tank, specific and nonspecific effects of reworking can act to mask their presence. Reactions like $CaCO_3$ dissolution in sediment from the Yoldia tank must be largely inferred from control tank pore water profiles, knowledge of how Yoldia rework sediment, changes in overlying water chemistry, or separate experiments such as determining the effect of sulfide oxidation on alkalinity (Chapter VI).

It is possible to obtain an estimate of Ca^{++} production rate in the control tank by using equation (16) and then fitting the observed gradient in the upper 3 cm of the control tank by trial and error to calculate a best $R_{Ca^{++}}$, the average production rate. L is chosen as 3 cm since this is

the depth of the maximum in the Ca profile and the boundary condition $(\frac{\partial C}{\partial x})_{x = L} = 0$ is met. It is assumed that L is not changing rapidly with time. Taking at t = 0, Ca/Cl = C_o = .0195, C_1 = .0183, $D_{Ca^{++}}$ = 2.7 x 10^{-6} cm^2/sec (estimated in the same way as $D_{NH_4^+}$ above); then the best $R_{Ca^{++}}$ obtained in this way is 1.5 x 10^{-6} mM/sec using an average Cl^- of 0.533 M and t = 44.9 days. The value chosen for t is not especially important since at the chosen L and D values, the gradient is set up in about two weeks and a steady state solution can be used. Because of the model used, the $R_{Ca^{++}}$ should be a reasonable estimate of $R_{Ca^{++}}$ in the interval 2-3 cm but probably overestimates the production rate closer to the interface. With D ~ 1 x 10^{-5} cm^2/sec, as occurs in the upper 3 cm of the Yoldia tank, almost no evidence of a Ca increase would be detected with the R_{Ca} calculated above. In addition, in the Yoldia tank the greatest dissolution probably takes place at the interface where undersaturation is highest rather than several centimeters below (Table III-6). The calculated dissolution rate predicts a loss rate of $CaCO_3$ of about 2 mg/g sediment/yr (0.9 mg Ca/g-yr) assuming a 50% water content. If an adsorption coefficient of K_{Ca} = 1.8 (Li and Gregory, 1974) is included in the calculation, the $CaCO_3$ loss is reduced to 2.7 µg/g sediment/yr (R_{Ca}/ 1 + K = 2 x 10^{-9} mM/sec).

Ca produced by dissolution, like Mn, diffuses both out of the sediment and down. At depth, Ca should reprecipitate as a carbonate but is clearly capable of maintaining a high degree of oversaturation with respect to these

phases once it has been released into solution (Table III-VI). (See also Ben Yaakov, 1973, Table 2 for illustration of this supersaturation phenomena even after precipitation). Ca profiles of this type, observed in the control tank case, occur during winter months in Long Island Sound.

The maximum in dissolved Fe in the control tank occurs at the same depth interval as the high Ca, low pH, and depressed alkalinity. These data, together with pS data (Table III-3), imply that Fe is produced along the boundary between oxygenated and reduced sediment where it could be formed by oxidation of sulfides on one side of the boundary and by reduction of oxide on the other as discussed earlier. Production by oxidation or reduction could continue for some distance away from the boundary but in the reduced zone the rate of precipitation by sulfide becomes greater than production and in the oxidized zone the rate of loss by diffusion or oxide precipitation also becomes greater than production. The spike in Fe concentration represents a unique zone where production of the transient intermediate, dissolved Fe^{++}, outstrips loss. In the Yoldia tank this spike is greatly lowered. This lowering in concentration presumably results from the alteration of the relative rates of several processes: (1) higher rates of diffusion, (2) the zone of production by oxidation of solid phase sulfide is moved to the interface because Yoldia places sulfide rich particles obtained at depth there during feeding as discussed earlier (see Figure III-1),

(3) precipitation rates may be increased by higher O_2 levels in the pore water below the interface and (4) once oxidized at the surface, particles are subducted downward but with a critical change, their surfaces are oxidized so further oxidation of interior sulfides does not take place and acid production below the interface is now minimal unlike the control tank. Fe^{++} which results from reduction of this oxide coating is presumably rapidly diffused out of the system by reworking.

Using the control tank profile, an Fe production rate can be estimated as was done for Ca. In this case precipitation is a serious problem. A range of minimum R_{Fe} values was found by fixing the base of the production zone with the Fe^{++} concentration measured at 2-3 cm but allowing L to vary from either 2 or 3 cm. This is equivalent to raising or lowering the interface by 1 cm and should offset the effect of precipitation in the top 0-1 cm interval somewhat. Taking $D_{Fe^{++}} = 2.4 \times 10^{-6}$ cm^2/sec (estimated in the same way as $D_{NH_4^+}$) the range found for $R_{Fe^{++}}$ is 6×10^{-5} - 1.2×10^{-4} $\mu M/sec$; on a molar basis this is lower than but close to the estimated R_{SO_4} = from the sulfate profile (- 3.5×10^{-7} mM/sec) so that reduction of oxide alone would be capable of producing the observed spike and subsequent precipitation of Fe as FeS easily accommodated by the amount of HS^- generated. The titration of alkalinity and dissolution of $CaCO_3$ suggests, as noted above, that oxidation also contributes to $R_{Fe^{++}}$.

Influence of reworking by Yoldia on overlying water chemistry

The ejection of feces into the water column and reworking of the interface by protobranchs increases the turbidity of water overlying bottom areas where these organisms live (Rhoads and Young, 1970) and, in the present case, the water in the tank containing Yoldia relative to the control. Elements which are subject to scavenging by particles, for example, Fe, Mn, and P should be preferentially removed over bottom areas inhabited by these organisms as found for ^{234}Th (Chapter IV). Molecules like NH_4^+ will tend to be released from particles by desorbtion after being reworked upward and deposited at the interface during feeding. The scavenging effect is illustrated in the tank experiment by the fact that dissolved $HPO_4^=$ levels in water overlying sediment in the Yoldia tank are lower than in the control (Figure III-11, Table III-4). Since the flux of $HPO_4^=$ should be greater in the Yoldia tank because of reworking and excretion, as demonstrated by NH_4^+, the most reasonable explanation for the observed lowering of concentration is scavenging by particles rich with surface Fe-oxides. Together with the previous observations on the increased fluxes and transport of material throughout the sediment column and increased microbial metabolic activity in sediment containing Yoldia, this observation of increased scavenging in overlying water illustrates that the general effect of Yoldia is, like a catalyst, to increase the rate and magnitude of diagenetic

processes of all kinds taking place near the sediment-water interface and in overlying water.

Summary

(1) Two separate sets of experiments were performed in the laboratory in order to study under relatively controlled and simplified conditions the changes produced by deposit-feeding organisms on marine sediment and overlying water chemistry. The organisms used: Clymenella torquata and Yoldia limatula, are representative of two important and distinctive types of deposit feeders. Clymenella, a maldanid polychaete, is a relatively sedentary tube-dweller, lives in sediment containing sand, and normally feeds below 10 cm. Yoldia, a protobranch bivalve, is highly mobile, lives in muds, and feeds below the surface but in the upper 4 cm.

(2) The construction and irrigation of tubes by Clymenella alters the rate and geometry of pore water diffusion in sediment. This results in rapid exchange of pore water constituents such as Fe, Mn, NH_4^+, and $HPO_4^=$ with overlying water. When modeled as a strictly vertical diffusion process, a diffusion coefficient of 2-3 x 10^{-4} cm^2/sec is required to produce the observed changes. A horizontal diffusion coefficient of 4.5 x 10^{-5} cm^2/sec, calculated for an ideal arrangement of tubes, is capable of explaining the observed changes. The required coefficient becomes lower when the system is more accurately described. In natural bottom sediments, populations of tube dwellers will consist of several kinds of species with relatively closely

packed burrows. The horizontal diffusion coefficient required to produce deep vertical exchange of sediment pore waters by irrigation decreases dramatically as the average distance between burrows decreases. This decrease depends on the square of the distance between burrows.

(3) Both Fe and Mn are advected out of sediment into overlying water by irrigation, where they precipitate, scavenge additional elements such as P from the water, and return to the sediment surface. In the presence of feeding, the entire cycle would represent a constant refluxing of Fe and Mn between sediment, keeping Fe-Mn oxides in a continual, fresh and highly reactive state.

(4) Because of its mobility and restriction to a zone near the interface, transport of pore water by Yoldia can be adequately described by a vertical diffusion coefficient of $\sim 1 \times 10^{-5}$ cm^2/sec. Biogenic transport near the interface lowers the concentration of ions and, under some conditions, the shape of profiles of ions which have diffusion coefficients less than $\sim 1 \times 10^{-5}$ cm^2/sec in sediment beneath the reworked zone. Correspondingly greater changes in the rates of production or consumption in the near interface zone relative to deeper sediment are required to produce alterations in profiles similar to those generated by small changes in rates of diffusion.

(5) Particle reworking results in the oxidation of sulfides at the interface. This lowers pH, consumes alkalinity, and dissolves $CaCO_3$. Particle reworking also redistributes organic matter and contributes to the formation of profiles or organic matter where concentration is high at the

interface and falls off with depth.

(6) Interstitial water profiles of Fe, Mn, Ca, $HPO_4^=$, alkalinity, and NH_4^+ are altered by reworking in accordance with their individual chemistry and physical properties. Modeling of the pore water or solid phase distributions allows the calculation of average rates of production, R_i, of these ions in the sediment in general or in selected horizons.

(7) Mn is shown to rapidly form solid phase concentration profiles similar to natural ones over time scales of a month.

(8) The rate of microbial metabolism, biomass, and associated production of decomposition products is increased in the presence of Yoldia. Because these increases take place away from the actual zone inhabited by Yoldia, these increases probably result as a by-product of changes in the transport of metabolites into or out of sediment as illustrated by models.

(9) The increased flux of Fe and Mn, as well as particles, in the presence of Yoldia results in the scavenging of particle and Fe-Mn oxide-seeking elements from the water column. As in the case of Clymenella, reworking maintains the Fe-Mn oxide scavenging system in a highly reactive state and increases the rates of many reactions in the diagenetic system near the sediment-water interface and in overlying water.

Table III-1. *Clymenella* Tank Experiment: Pore Water Results

Depth (cm)	pH				Fe(μM)			Mn(μM)		
	Tank 1 (control t = 29)	Tank 2 (control t = 15)	Tank 3 (*Clymenella* t = 29)		Tank 1 (control t = 29)	Tank 2 (control t = 15)	Tank 3 (*Clymenella* t = 29)	Tank 1 (control t = 29)	Tank 2 (control t = 15)	Tank 3 (*Clymenella* t = 29)
			duplicate cores							
0-1	7.00	6.96	7.22	7.20	122	310	1190	4.0	4.6	22
1-2	6.93	6.89	7.22	7.24	657	757	2010	4.2	4.6	20
2-3	6.93	6.85	7.15	7.26	962	1340	160	5.3	9.5	2.7
3-4	6.93	6.83	7.00	7.15	1650	1060	110	11	13	2.4
4-5	6.92	6.82	6.96	7.04	1750	1574	150	14	16	2.7
5-6	6.91	6.80	6.94	6.95	1650	2220	39	14	16	< 1.8
6-7	6.91	6.80	6.93	6.92	1950	2150	20	16	20	< 1.8
7-8	6.89	6.78	6.91	6.89	2170	2600	9	18	24	1.8
8-9	6.89	6.76	6.91	6.90	1770	2360	160	21	29	1.8
9-10	6.88	6.72	6.90	6.90		3010	636		22	6.0
10-11	6.88	6.72	6.87	6.89		3800			25	
11-12	6.83	6.63		6.85						

Table III-2. *Clymenella* Tank Experiment: Overlying Water

Time (days)	Measurement	Tank 1 (Control)	Tank 2 (Control	Tank 3 (*Clymenella*)	Tank 4 (*Clymenella*)
0	pH	8.16	8.16	8.16	8.16
	Cl^- (M)	0.488	0.490	0.486	0.491
	PO_4 (μM)	1.39	1.39	1.39	1.39
	NH_3 (μM)	1.22	1.22	1.22	1.22
	Fe (μM)	≤ 0.05	≤ 0.05	≤ 0.05	≤ 0.05
	Mn (μM)	≤ 0.14	≤ 0.14	≤ 0.14	≤ 0.14
9	pH	7.60	7.62	7.68	7.62
	Cl^- (M)	0.490	0.487	0.489	0.491
	PO_4 (μM)	0.09	0.16	0.17	0.17
	NH_3 (μM)	0.92	-	-	1.29
	Fe (μM)	≤ 0.05	≤ 0.05	≤ 0.05	≤ 0.05
	Mn (μM)	≤ 0.14	≤ 0.14	≤ 0.14	≤ 0.14
15	pH	7.80	7.80	7.92	7.78
	Cl (M)	0.496	0.497	0.497	0.497
	PO_4 (μM)	0.13	0.17	0.22	0.07
	NH_3 (μM)	1.00	0.57	0.84	1.35
	Fe (μM)	0.16	≤ 0.05	0.13	0.14
	Mn (μM)	≤ 0.14	≤ 0.14	≤ 0.14	≤ 0.14
16	Add *Clymenella* to tanks 3 and 4				
22	pH	7.53	-	7.38	7.38
	Cl (M)	-	-	-	-
	PO_4 (μM)	0.19	-	0.54	0.47
	NH_3 (μM)	0.76	-	22.4	15.6
	Fe (μM)	0.11	-	6.21	0.20
	Mn (μM)	≤ 0.14	-	0.22	0.20
29	pH	7.40	-	7.39	7.38
	Cl (M)	0.502	-	0.507	0.503
	PO_4 (μM)	0.10	-	0.51	0.43
	NH_3 (μM)	0.82	-	26.1	18.9
	Fe (μM)	0.11	-	1.95	5.17
	Mn (μM)	< 0.14	-	0.51	0.40

Table III-3. Yoldia Tank Experiment: Pore Water and Sediment

Depth (cm)	%H_2O	pH	pS	Cl^- (M)	Alk (meq/ℓ)	$SO_4^=$ (mM)	NH_4^+ (mM)	$PO_4^{\equiv}$ (μM)	Ca (mM)	Mn (μM)	Fe (μM)	% Ignition loss	ATP (μg/g)	Mn (μg/g-ash)
Blank														
0-1	61.6	7.45	-	0.539	4.45	28.3	.062	5	10.75	33.5	1.1	5.99	0.503	694
1-2	57.0	7.14	-	0.534	4.80	27.3	.135	20	11.56	72.8	55.9	6.08	1.67	589
2-3	56.2	7.03	-	0.526	5.47	26.5	.208	34	11.92	91.0	91.5	6.30	1.32	600
3-4	54.2	7.02		0.515	6.11	24.3	.256	49	11.83	105	61.8	6.52	1.43	620
4-5	54.4	7.15	14.2	0.509	7.49	23.6	.372	86	10.78	109	7.31	6.35	0.685	631
5-7	54.2	7.27	12.4	0.501	8.28	23.5	.420	97	10.36	101	4.28	6.47	0.812	615
7-9	53.8	7.40	13.2	0.494	8.93	22.3	.497	112	9.82	81	2.9	6.37	0.23	603
Yoldia														
0-1	69.3	7.16	-	0.546	3.07	28.5	.063	6.9	10.12	17.5	0.91	6.23	0.552	647
1-2	60.3	7.19	-	0.543	3.60	28.1	.133	20	10.09	48.9	4.06	5.92	1.84	538
2-3	56.6	7.15	-	0.534	4.15	27.0	.183	32	10.39	61.3	4.62	5.89	1.29	608
3-4	53.4	7.27		0.519	4.21	25.2	.290	65	9.40	67.5	2.3	5.65	1.01	605
4-5	53.7	7.36	12.5	0.515	5.94	24.1	.374	90	9.31	74.4	2.1	6.44	1.51	607
5-7	53.5	7.35	11.5	0.505	6.74	23.5	.453	114	9.25	69.2	2.1	6.33	1.50	637
7-9	53.5	7.37	11.9	0.493	7.48	22.2	.507	113	8.75	66.4	1.8	6.17	1.34	596
Start														
-	-	7.49	*	0.457	3.72	22.8	.217	65.2	8.89	73.5	1.7	(5.92)	-	617

* not measured

Table III-4. Yoldia Tank Experiment: Overlying Water

Sample time (cumulative days)	Sample time (after water changes) days	Cl^- (M)			Alk (meq/ℓ)			Ca (mM)			NH_3 (μM)		
		source water	Yoldia	blank	source water	Yoldia	blank	source water	Yoldia	blank	source water	Yoldia	blank
0	0	0.521			2.60			9.18			0.0		
3.6	3.6(change)		0.520	0.523		2.20	2.45		8.98	8.96		50	32
4.6	1.0		0.521	0.524		2.48	2.65		9.08	9.06		18.8	9.98
6.9	3.3		0.524	0.528		2.24	3.05		9.13	9.18		30.3	15.9
15.9	12.3(change)		0.536	0.529		1.96	5.02		9.41	9.58		70	32
33.9	18 (change)		0.559	0.546		2.43	4.58		9.86	10.2		30.8	5.9
44.9	11 (end)		0.548	0.540		2.74	3.66		9.91	9.91		11	0.7

		$PO_4^{\blacksquare}$ (μM)			Mn (μM)		
		source water	Yoldia	blank	source water	Yoldia	blank
0	0	3.23			<0.14		
3.6	3.6(change)		3.92	4.79		3.63	1.18
4.6	1.0		3.72	3.74		1.0	<0.14
6.9	3.3		5.46	8.40		1.2	<0.14
15.9	12.3(change)		4.17	10.1		3.2	<0.14
33.9	18 (change)		3.54	6.33		0.16	<0.14
44.9	11 (end)		3.6	5.0		0.15	<0.14

Table III-5. Solubility Products at 25°C for Selected Compounds

Reaction	Solubility product	Reference
$Mn_3(PO_4)_2 \cdot 3H_2O \rightleftarrows 3Mn^{++} + 2PO_4^{\equiv} + 3H_2O$	$K_{sp} = 10^{-34.6}$	(1)
$Fe_3(PO_4)_2 \cdot 8H_2O \rightleftarrows 3Fe^{++} + 2PO_4^{\equiv} + 8H_2O$	$K_{sp} = 10^{-36.0}$	(2)
$FeS_{mack.} \rightleftarrows Fe^{++} + S^{=}$	$K_{sp} = 10^{-17.5}$	(3)
$Fe_3S_4 \rightleftarrows 3Fe^{++} + 3S^{=} + S^{\circ}$	$K_{sp(FeS)} = 10^{-18.2}$	(3)
$FeS_{amorph} \rightleftarrows Fe^{++} + S^{=}$	$K_{sp} = 10^{-16.9}$	(3)
$FeCO_3$ siderite $\rightleftarrows Fe^{++} + CO_3^{=}$	$K_{sp} = 10^{-10.2}$	(4)
$MnCO_3$ Rhod. $\rightleftarrows Mn^{++} + CO_3^{=}$	$K_{sp} = 10^{-10.4}$	(5)
$MnS_{alab.} \rightleftarrows Mn^{++} + S^{=}$	$K_{sp} = 10^{-12.9}$	(6)
	$K_{sp} = 10^{-15.2}$	(7)
	$K_{sp} = 10^{-17.8}$*	(8)
MnS_2 hauerite $\rightleftarrows Mn^{++} + S^{=} + S^{\circ}$	$K_{sp} = -20.6$	(8)
$CaCO_3$ calc. $\rightleftarrows Ca^{++} + CO_3^{=}$	$K_{sp} = 10^{-8.42}$	(9)
$CaCO_3$ arag. $\rightleftarrows Ca^{++} + CO_3^{=}$	$K_{sp} = 10^{-8.25}$	(10)

(1) Nriagu and Dell, 1974 - ΔG_f° data

(2) Nriagu, 1972

(3) Berner, 1967

(4) Stumm and Singer, 1966

(5) Morgan, 1967

(6) Robie, 1966

(7) Kolthoff, 1931

(8) Mills, 1974 - ΔG_f° data (*= one (7) used in calculation

(9) Jacobsen and Langmuir, 1974

(10) ($1.48 \times K_{sp}$ calcite) e.g. Berner, 1976c

Table III-6

Yoldia Experiment Pore Water: Log (IAP/K) for Selected Phases

	Reddingite $Mn_3(PO_4)_2 \cdot 3H_2O$		Vivianite $Fe_3(PO_4)_2 \cdot 8H_2O$		Mackinawite FeS		Greigite Fe_3S_4		Alabandite MnS	
Depth	Yoldia	Blank	Yoldia	Blank	Yoldia	Blank	Yoldia	Blank	Yoldia	Blank
0-1	-5.83	-4.62	-7.74	-7.17	-	-	-	-	-	-
1-2	-3.50	-3.09	-4.77	-1.46	-	-	-	-	-	-
2-3	-2.87	-2.59	-4.28	-0.59	-	-	-	-	-	-
3-4	-1.82	-2.09	-4.28	-0.78	-	-	-	-	-	-
4-5	-1.22	-1.24	-3.93	-2.77	-1.4	-2.6	-0.70	-1.9	0.23	-2.9
5-7	-1.12	-0.96	-3.72	-3.09	-0.40	-1.0	0.30	-0.3	1.20	0.46
7-9	-1.11	-0.82	-3.87	-3.20	-0.10	-2.0	0.60	-1.3	-1.6	-0.43

	Rhodochrosite $MnCO_3$		Siderite $FeCO_3$		Calcite $CaCO_3$		Aragonite $CaCO_3$	
Depth	Yoldia	Blank	Yoldia	Blank	Yoldia	Blank	Yoldia	Blank
0-1	-1.27	-0.55	-2.58	-2.06	-0.22	.26	-0.39	0.087
1-2	-0.73	-0.48	-1.82	-0.60	-0.12	.021	-0.29	-0.15
2-3	-0.60	-0.43	-1.74	-0.43	-0.078	-0.017	-0.25	-0.19
3-4	-0.43	-0.32	-1.91	-0.55	-0.010	.023	-0.16	-0.15
4-5	-0.15	-0.093	-1.72	-1.27	0.25	.20	0.075	0.033
5-6	-0.13	0.038	-1.67	-1.34	0.29	.35	0.12	0.18
6-7	-0.079	0.11	-1.67	-1.36	0.34	.49	0.17	0.32

Chapter III

Figure Captions

Figure III-1:A. *Clymenella torquata* in tube. Unstipled sediment represents oxidized zone; arrows indicate transport direction of particles.

B. Sketch of *Yoldia limatula* in feeding position, labile palps extended. Unstipled region represents visually oxidized sediment. Arrows indicate direction of particle transport. Scale= 1 cm.

Figure III-2: Tank set up used in *Clymenella* experiment. H_i = holding tanks, T_i = aquaria, F_i = refrigerating units, WB = water bath (stipled), PP = pump. Path of water circulation is shown only for tank 1.

Figure III-3: Fe and Mn pore water profiles form tanks 1, 2, 3. *Clymenella* present in tank 3 (circles). [Tank 1 = dashed; tank 2 = solid lines.]

Figure III-4: pH profiles from tanks 1, 2, 3. (Tank 1 = dashed lines; tank 2 = solid lines; tank 3 (*Clymenella*) = circles.)

Figure III-5: pH, $HPO_4^{=}$, and NH_4^{+} concentrations in overlying water in tanks used in *Clymenella* experiment. *Clymenella* added after 15 days to tanks 3 and 4.

Figure III-6: Fe and Mn concentrations in overlying water in tanks 1, 2, 3, and 4. *Clymenella* added after 15 days to tank 3 and 4.

Figure III-7: Pore water sulfate, alkalinity, NH_4^+ and $HPO_4^=$ profiles from Yoldia experimental tanks. Control tank = dashed lines; Yoldia tank = solid; starting profile = large dots.

Figure III-8: Pore water Ca, pH, Mn, and Fe profiles from Yoldia experimental tanks. Control tank = dashed lines; Yoldia tank = solid; starting profile = large dots.

Figure III-9: ATP and % organic matter profiles from Yoldia experimental tanks. Control tank = dashed lines; Yoldia tank = solid lines.

Figure III-10: Solid phase Mn profiles in Yoldia experimental tanks. Control tank = dashed lines; Yoldia tank = solid lines.

Figure III-11: Alkalinity/Cl^-, Mn, NH_4^+, and $HPO_4^=$ concentrations in Yoldia experimental tanks with time. Control tank = open triangles, dashed lines; Yoldia tank = open squares, solid lines; source water used in each water change = open circles.

Figure III-12: X-radiograph of 2.5 cm thick sediment slab showing natural density of Clymenella and capitellid tubes at Calves Pasture Point, Barnstable Harbor Mass. (June 29, 1974). Note biogenic graded bedding resulting from selective particle transport during feeding (Rhoads and Stanley, 1965). Scale = 3 cm.

Figure III-13: Nonsteady state diffusion-reaction model fit to NH_4^+ pore water profile of Yoldia experiment control tank. Control tank data = dashed vertical lines. Model fit with $D = 7 \times 10^{-6}$ cm^2/sec,

$K = 1$, $R/(1 + K) = 7.2 \times 10^{-8}$ mM/sec is represented by the dotted line. The solid line is with $R/(1 + K) = 8 \times 10^{-8}$ mM/sec. Time = 44.9 days.

Figure III-14: Nonsteady state diffusion-reaction model fit to $HPO_4^=$ pore water profile of control tank. Poor fit probably results from precipitation or adsorption reactions in the upper few centimeters. Control tank data = dashed vertical lines. Model fit (dotted line) is with $D = 2.6 \times 10^{-6}$ cm^2/sec, $K = 1$, and $R/(1 + K) = 1.2 \times 10^{-5}$ μM/sec. Time = 44.9 days.

Figure III-15: A. Composite layer, steady state model showing effect of increasing diffusion rates or changing diffusion and reaction rates in a two layer system. With $R_1 = R_2 = 1.34 \times 10^{-6}$ meq/l/sec then the dash-dot line is with $D_1 = D_2 = 3 \times 10^{-6}$ cm^2/sec; the solid line is with $D_1 = 4.5 \times 10^{-6}$, $D_2 = 3 \times 10^{-6}$ cm^2/sec; the dashed line is with $D_1 = 9 \times 10^{-6}$ cm^2/sec, $D_2 = 3 \times 10^{-6}$ cm^2/sec. The dotted line represents the case where $R_1 = -2.68 \times 10^{-6}$, $R_2 = 1.34 \times 10^{-6}$ meq/l/sec, $D_1 = 9 \times 10^{-6}$, $D_2 = 3 \times 10^{-6}$ cm^2/sec.

B. Curves illustrate effect of changing only the relative rates of reaction in the two layers without change in diffusion coefficients as probably occurs in the case of $HPO_4^=$ and HCO_3^- control tank profiles. With $D_1 = D_2 = 3 \times 10^{-6}$ cm^2/sec then the

line of open circles is $R_1 = R_2 = 1.34 \times 10^{-6}$ meq/l/sec, this corresponds to the dash-dot line of part A. Letting the lower zone reaction rate R_2 remain at 1.34×10^{-6} meq/l/sec and varying R_1 gives $R_1 = 1.34 \times 10^{-7}$ (dash-dot line), $R_1 = -1.34 \times 10^{-6}$ (solid line), $R_1 = -2.68 \times 10^{-6}$ (dashed line), $R_1 = -4.02 \times 10^{-6}$ meq/l/sec (dotted line).

Figure III-16: Composite layer steady state model showing effect of an exponentially decreasing reaction rate in two layer system rather than constant reaction rates in each zone as illustrated in Figure III-15. $R = R_o \exp(-\alpha x)$, $\alpha = 0.33$, $\bar{R}$ (0-10 cm) = 1.34×10^{-6} meq/l/sec. Dashed line: $D_1 = D_2 = 3 \times 10^{-6}$ cm^2/sec. Solid line: $D_1 = 4.5 \times 10^{-6}$, $D_2 = 3 \times 10^{-6}$ cm^2/sec. Dotted line: $D_1 = 9 \times 10^{-6}$, $D_2 = 3 \times 10^{-6}$ cm^2/sec.

Figure III-17: Nonsteady state-equilibrium composite model showing hypothetical sequence of pore water Mn and alkalinity profiles which may have occurred through time in the tanks. See text for detailed explanation. $D_{Mn} = 2 \times 10^{-6}$, $D_{HCO_3^-} = 3 \times 10^{-6}$ cm^2/sec. $R_{Mn} = 2 \times 10^{-5}$ μM/sec, $R_{alk} = 1.34 \times 10^{-6}$ meq/l/sec. Solid = 7 days, open circles = 14 days, dashes = 21 days, dots = 28 days, dash-dots = 45 days. The starting profile (0 days) is $C_{Mn} = 73.5$ μM, x = 0-10 cm.

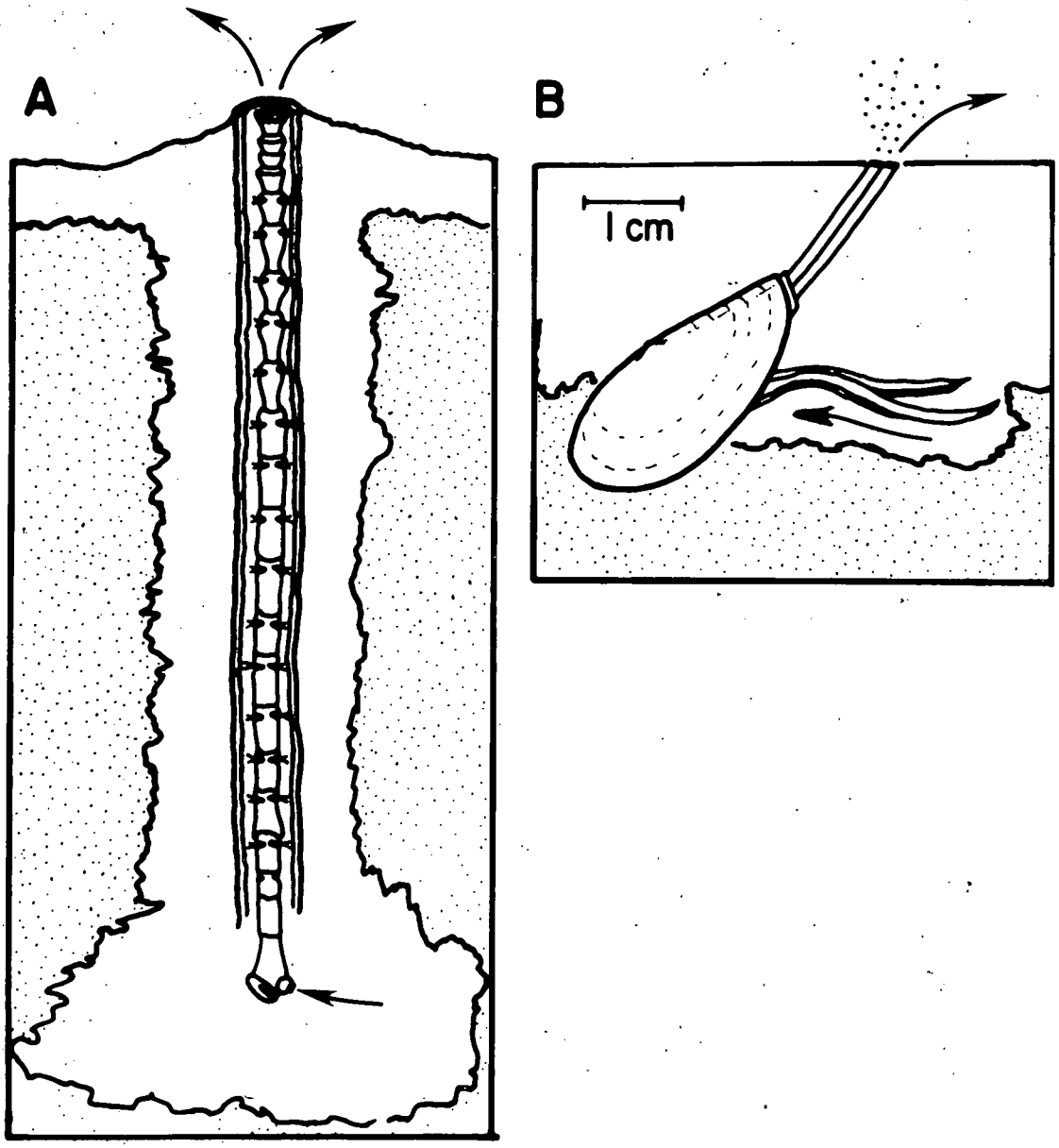


Figure III - 1

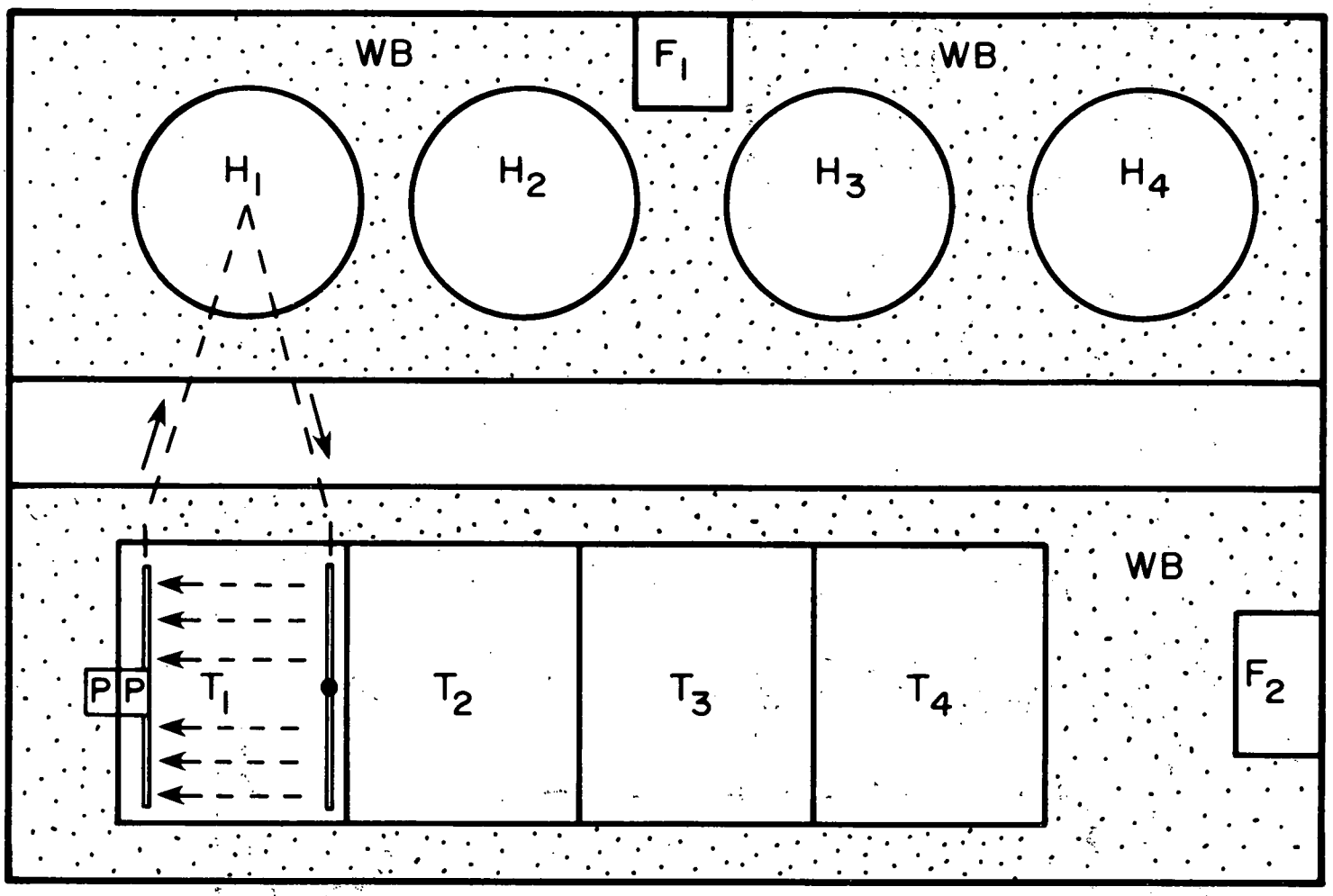


Figure III-2

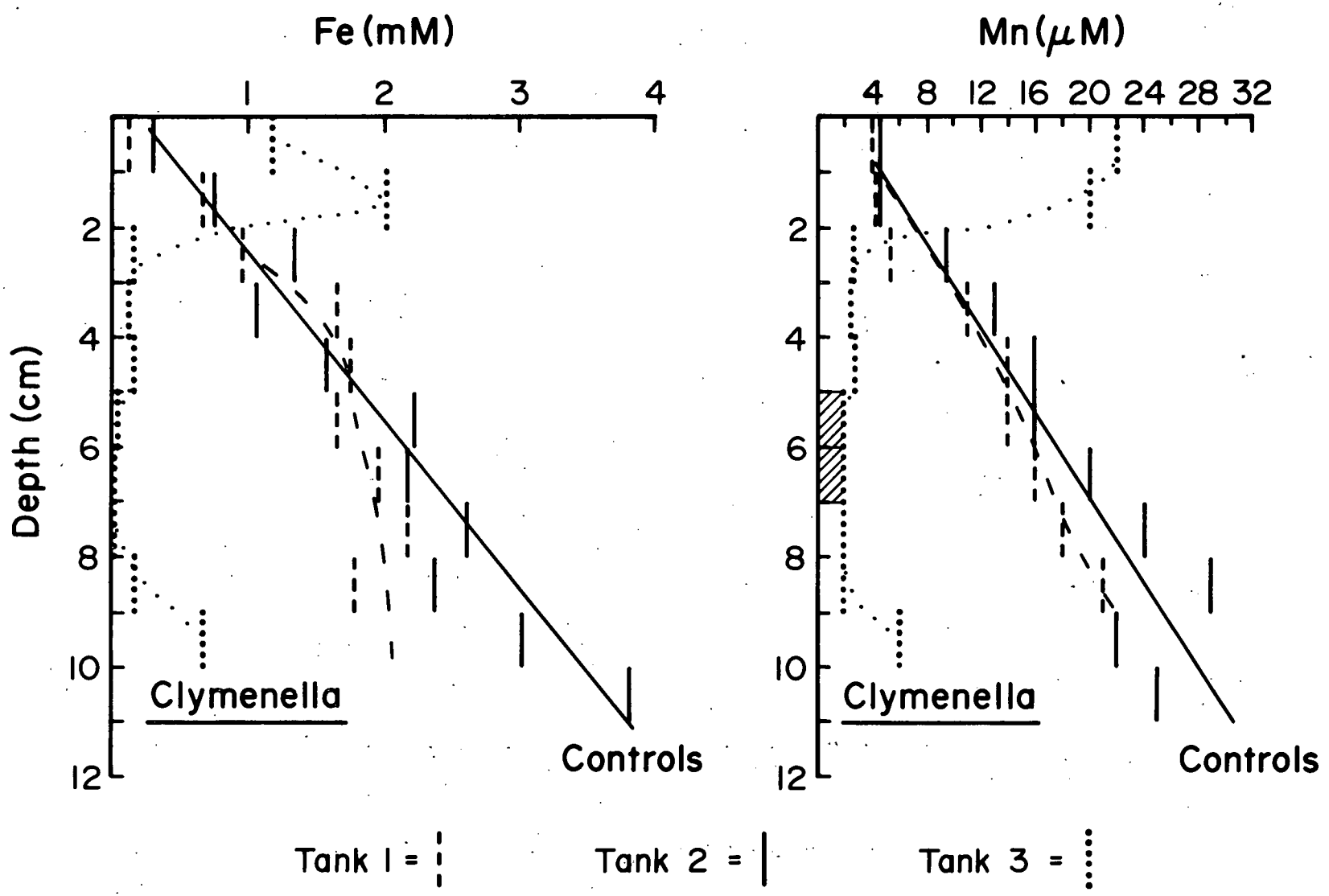


Figure III-3

1999

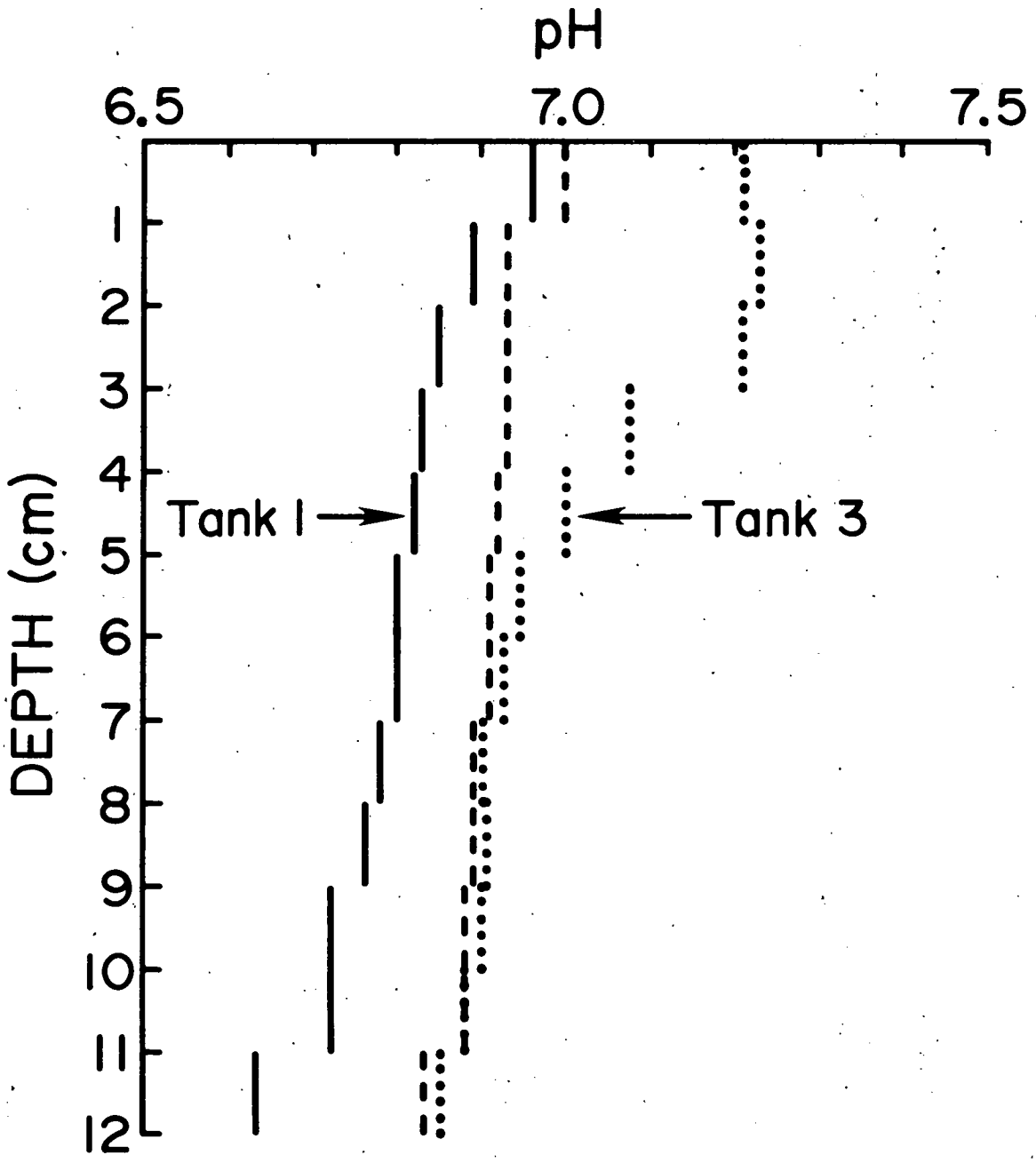


Figure III-4

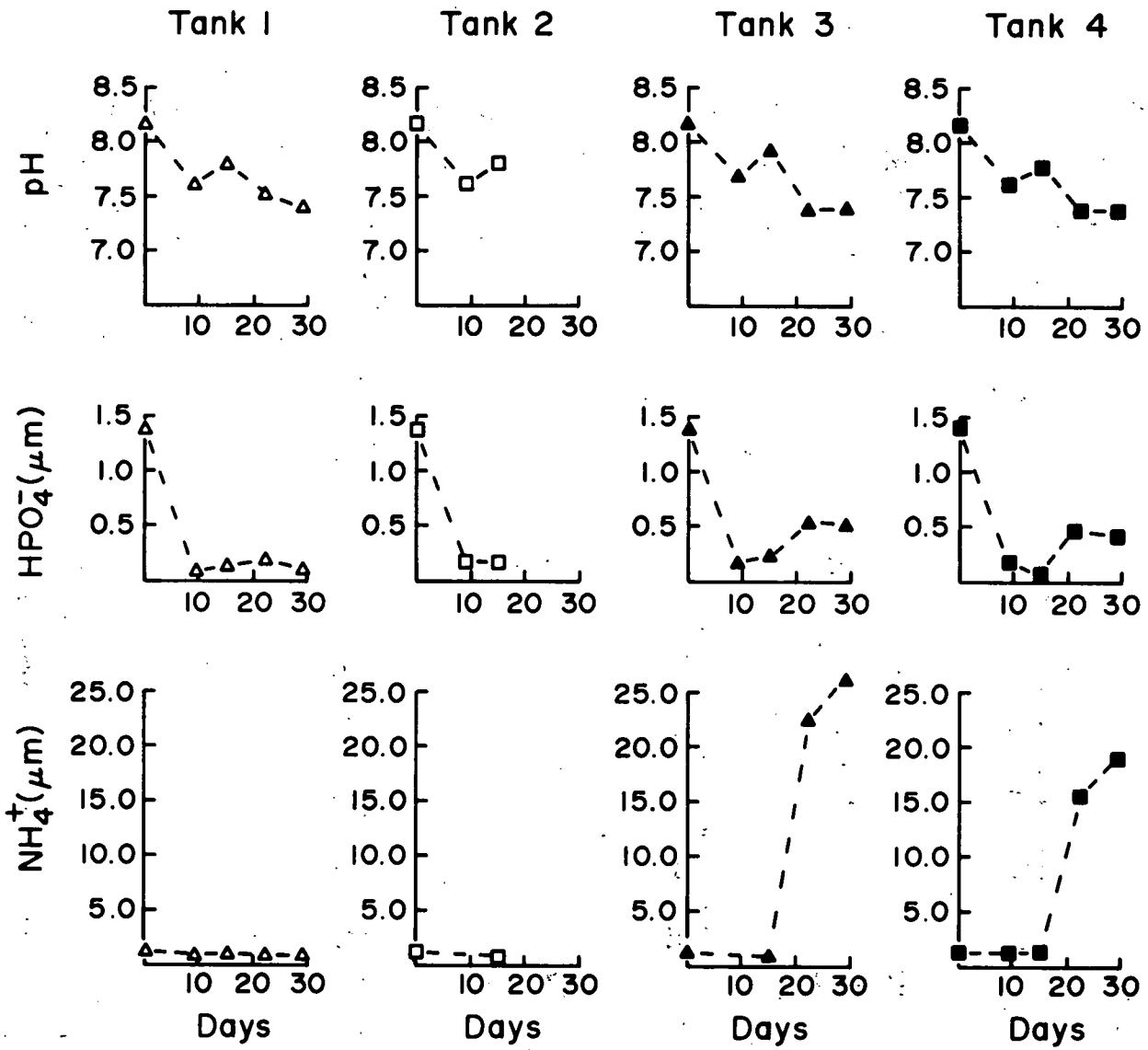

Tank 1
Tank 2
Tank 3
Tank 4
pH
8.5
8.0
7.5
7.0
10 20 30
$HPO_4^-(\mu m)$
1.5
1.0
0.5
$NH_4^+(\mu m)$
25.0
20.0
15.0
10.0
5.0
Days

Figure III-5

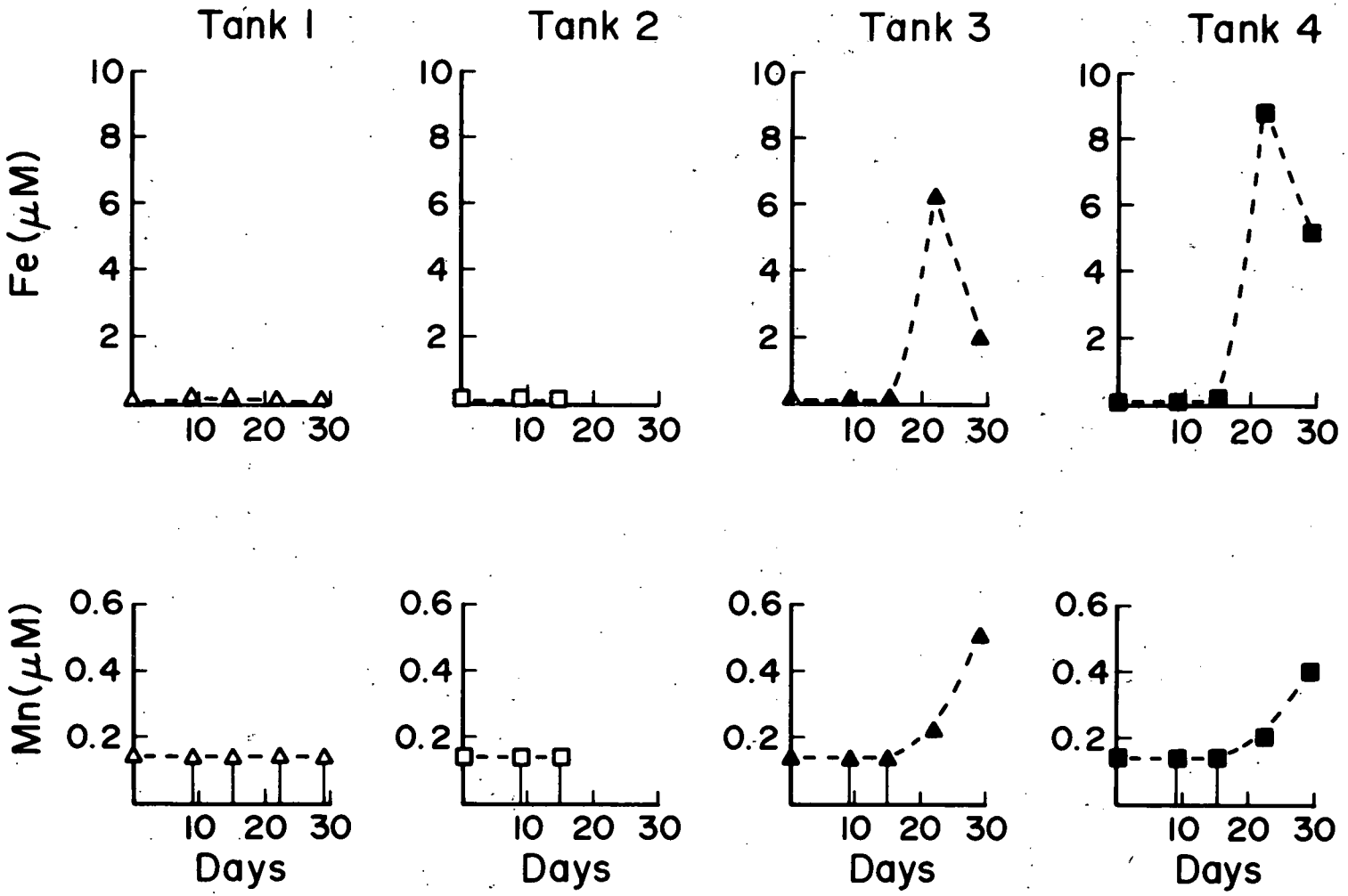

Tank 1
Tank 2
Tank 3
Tank 4
Fe (μM)
Mn (μM)
10
8
6
4
2
0.6
0.4
0.2
10 20 30
Days

Figure III-6

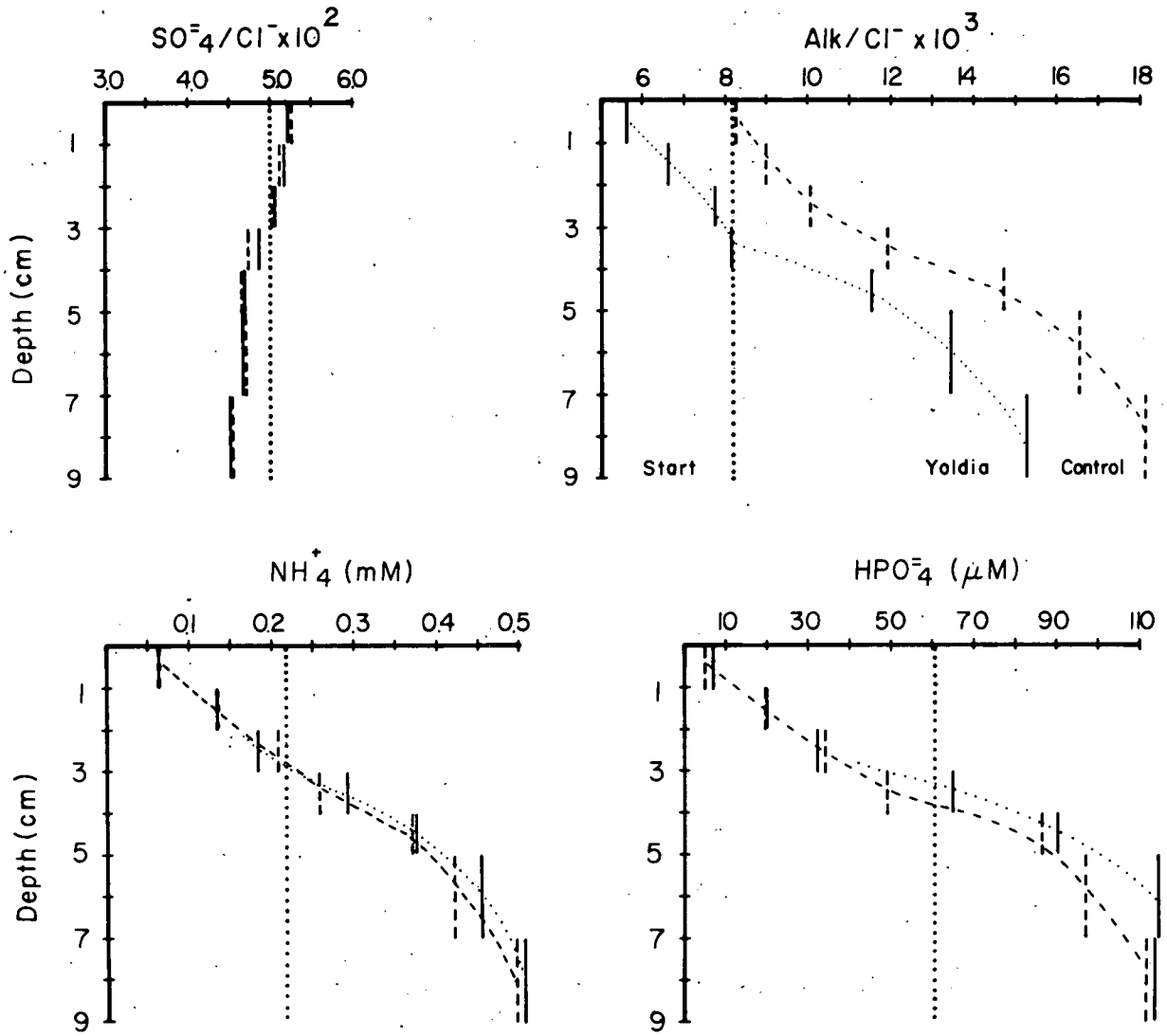

$SO^{=}_4/Cl^{-}x10^{2}$
3.0
4.0
5.0
6.0
Depth (cm)
1
3
5
7
9
$Alk/Cl^{-}x10^{3}$
6
8
10
12
14
16
18
Start
Yoldia
Control
NH^{+}_4 (mM)
0.1
0.2
0.3
0.4
0.5
$HPO^{=}_4$ (μM)
10
30
50
70
90
110

Figure III-7

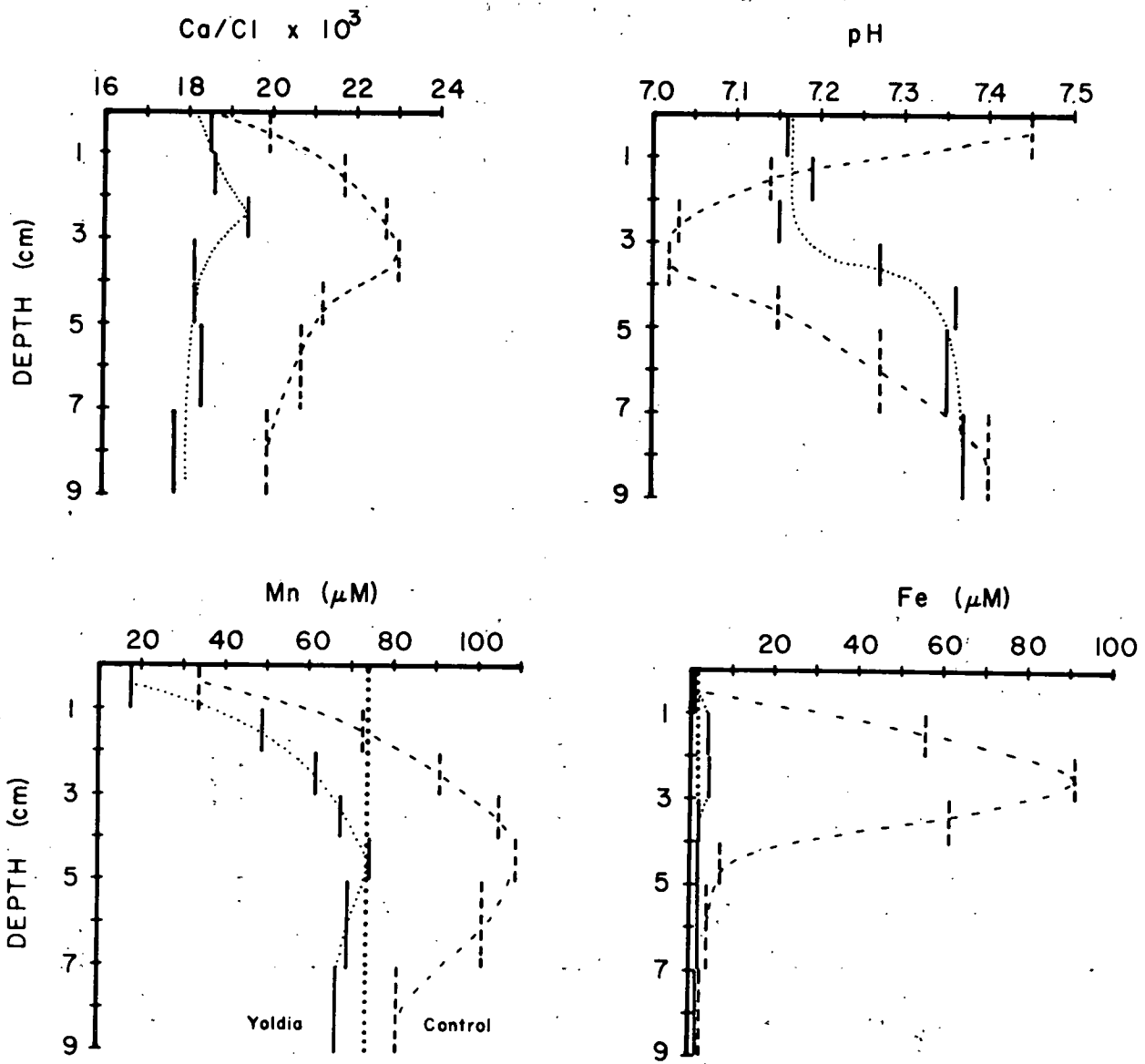

Ca/Cl x 10³
16
18
20
22
24
pH
7.0
7.1
7.2
7.3
7.4
7.5
DEPTH (cm)
1
3
5
7
9
Mn (μM)
20
40
60
80
100
Fe (μM)
Yoldia
Control

Figure III-8

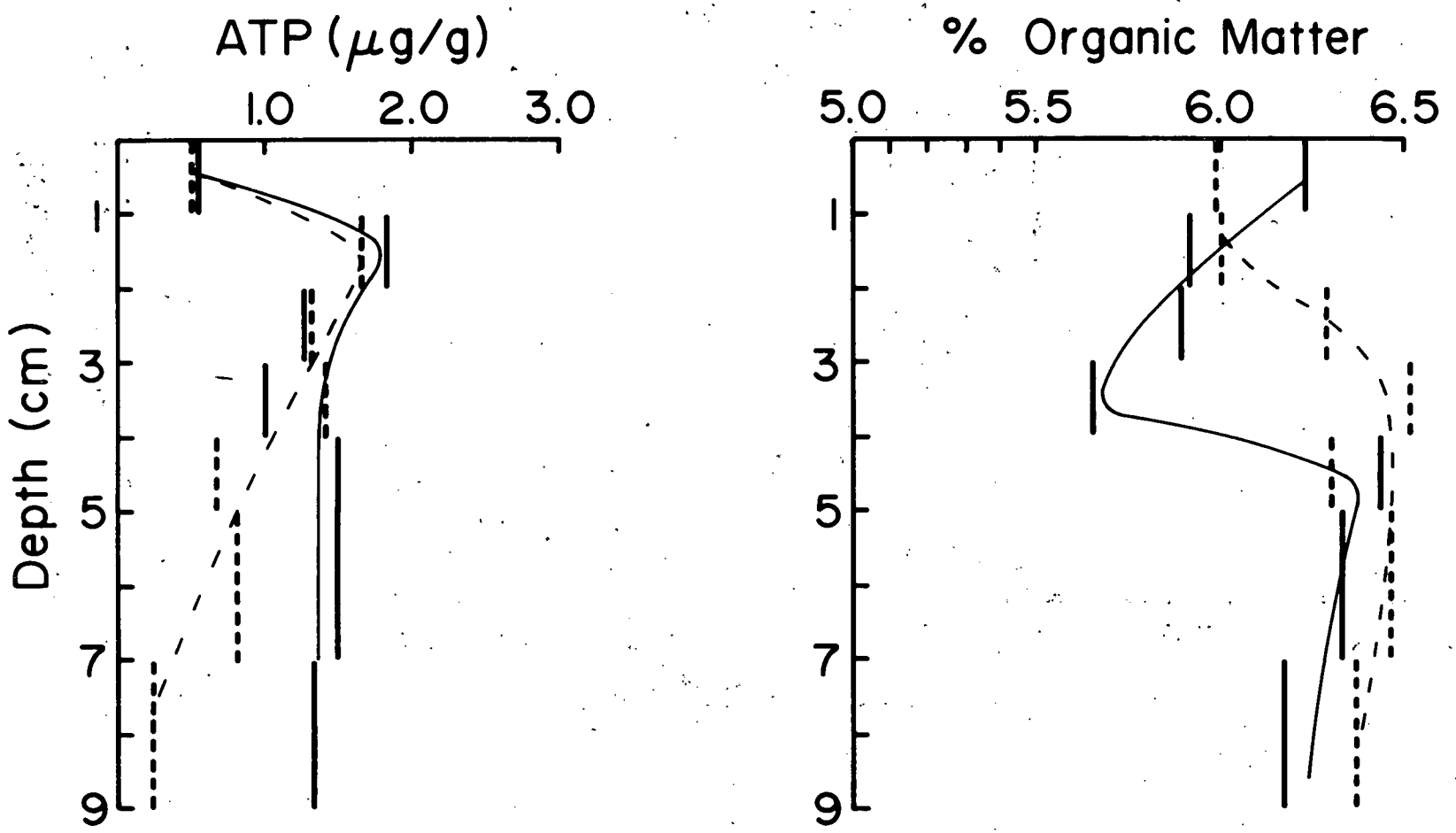

ATP (μg/g)
1.0
2.0
3.0
Depth (cm)
1
3
5
7
9
% Organic Matter
5.0
5.5
6.0
6.5
1
3
5
7
9

Figure III-9

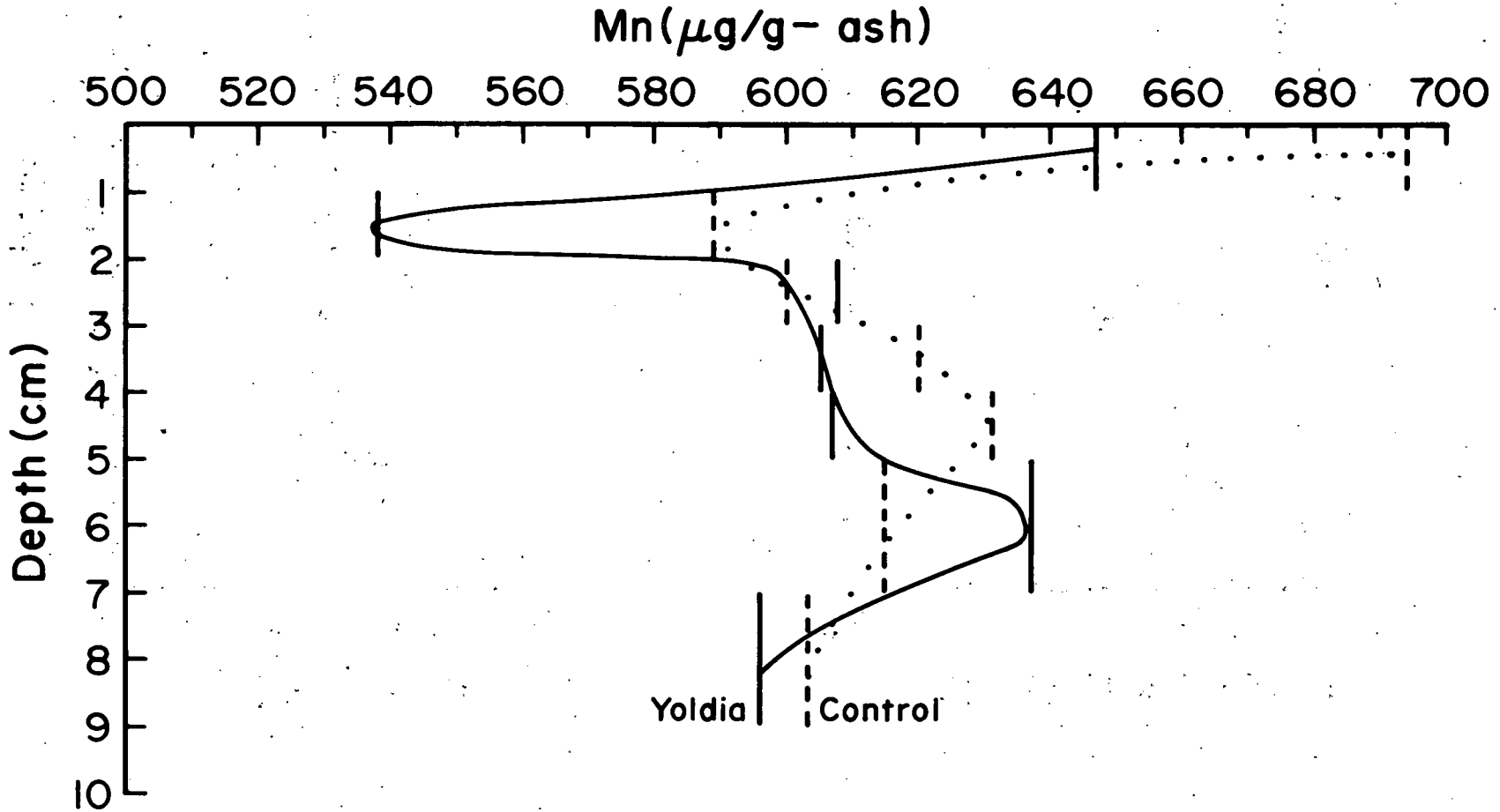


Figure III-10

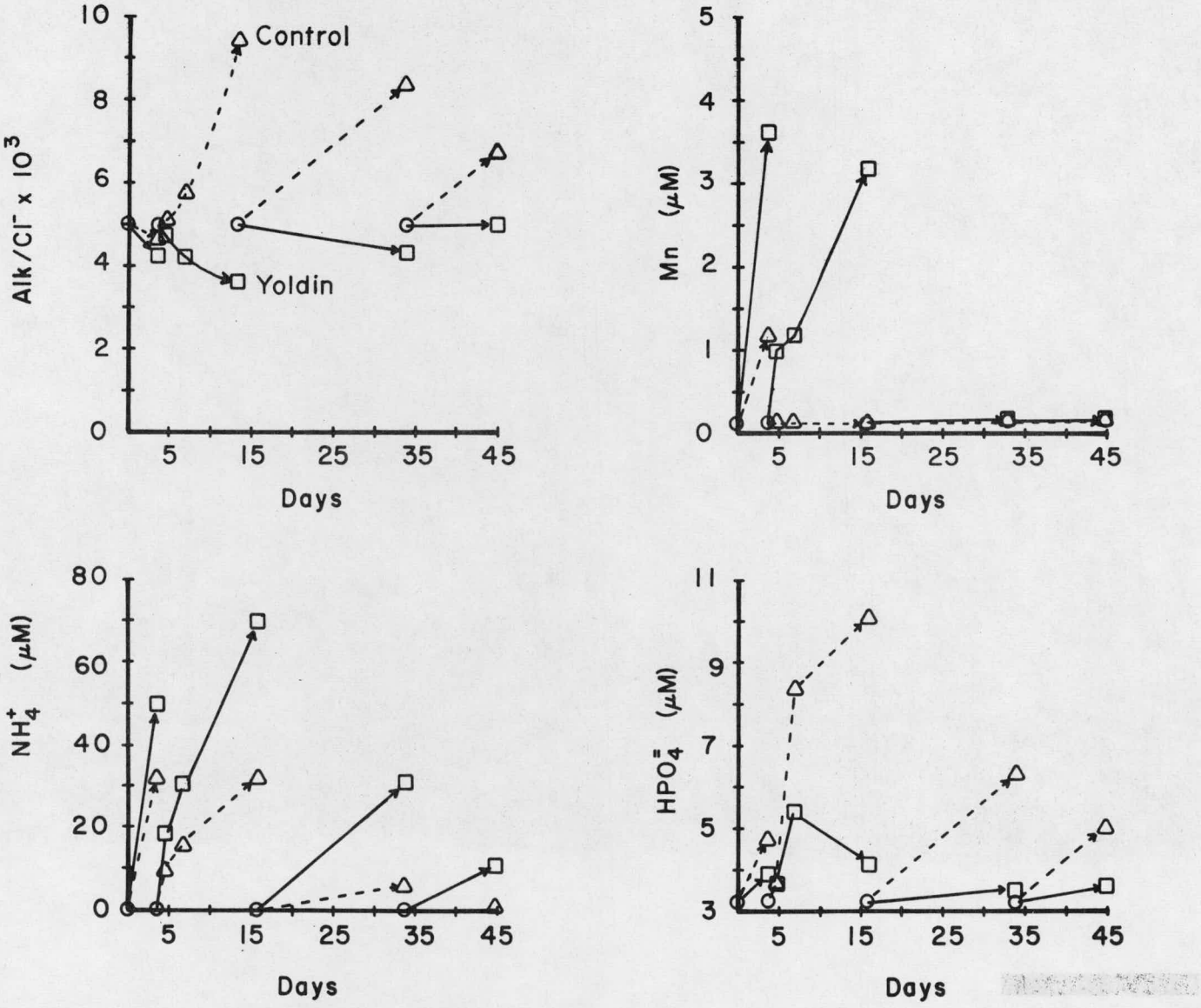
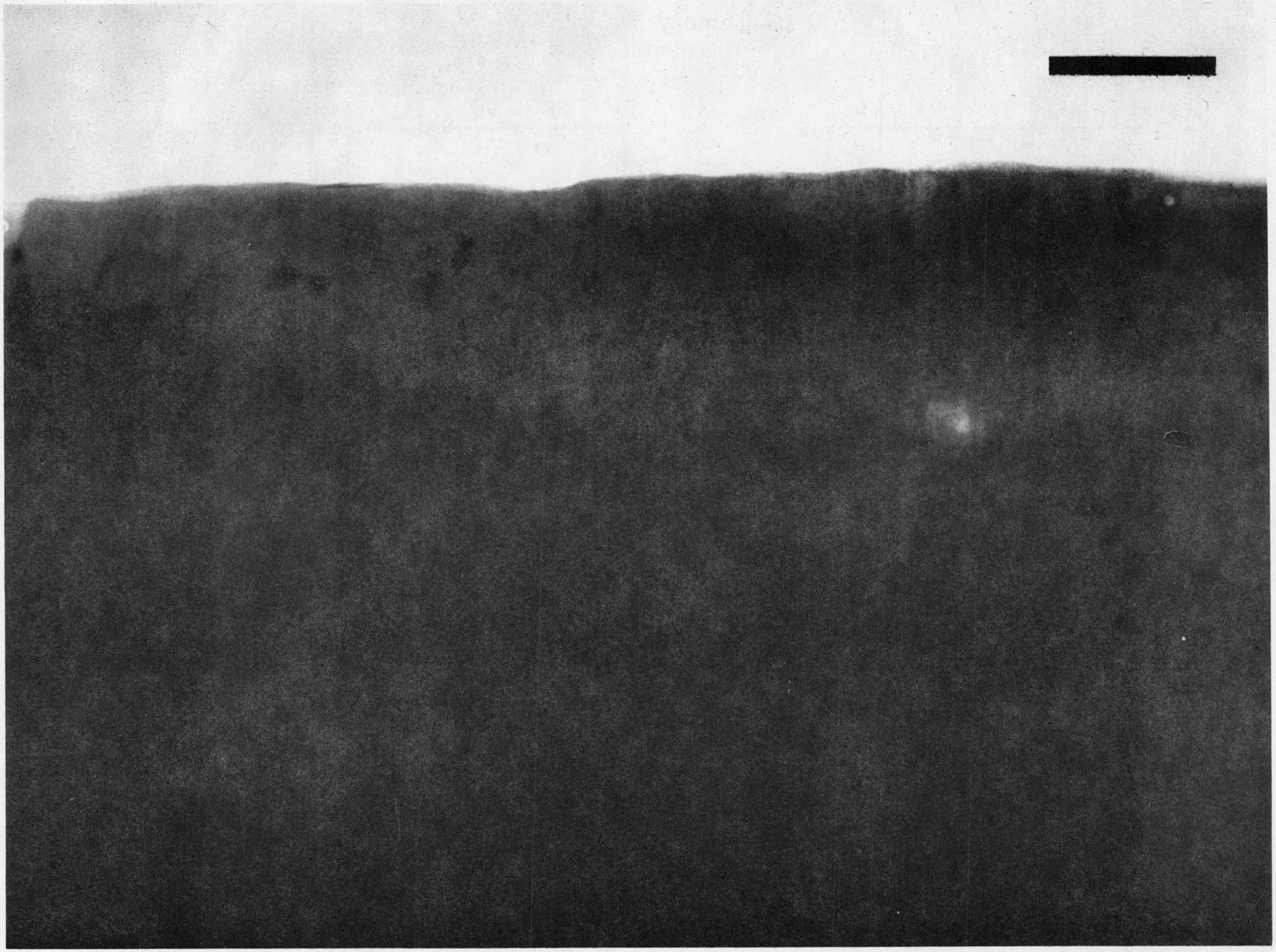


Figure III-11



III-12

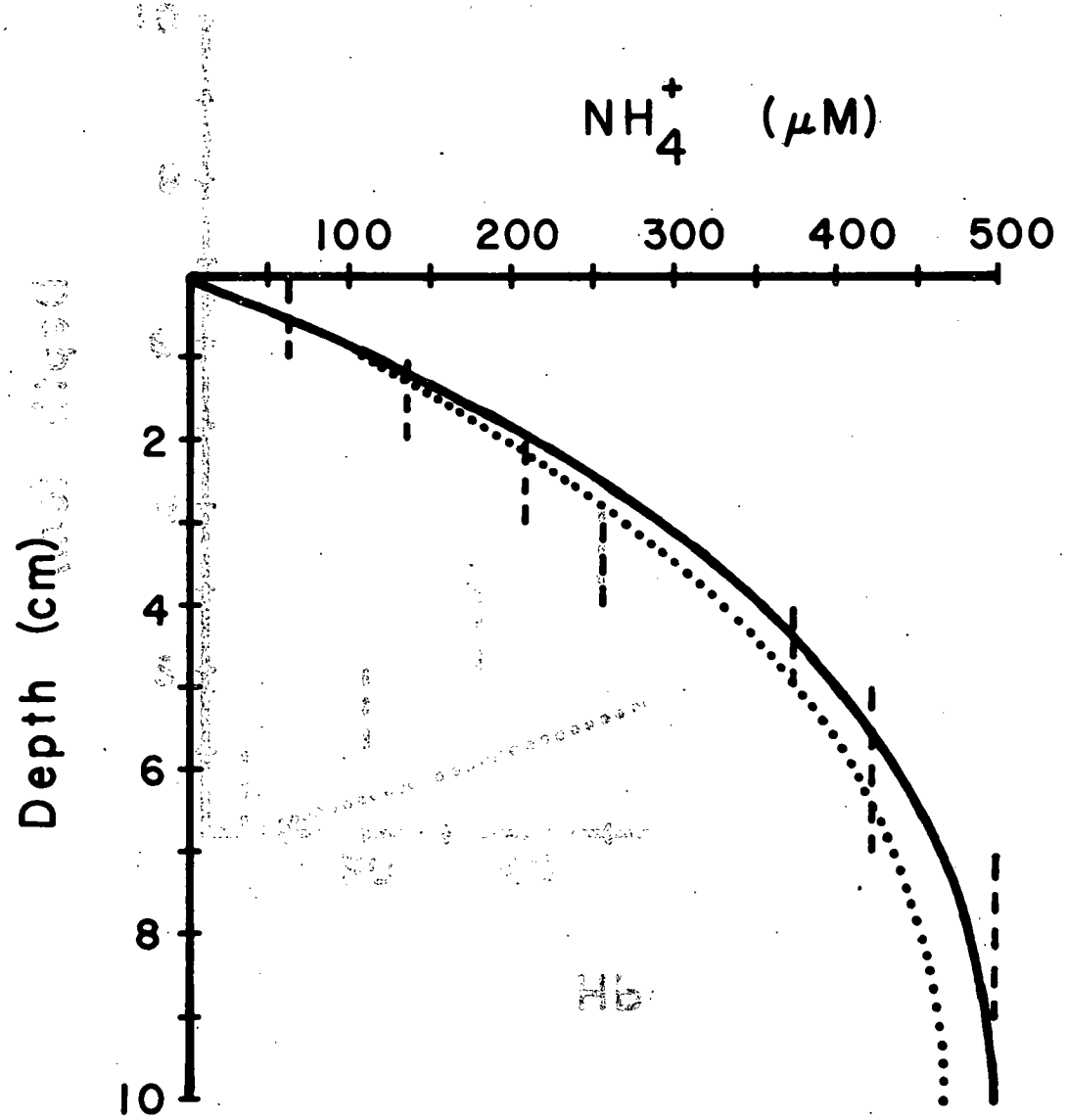


Figure III-13

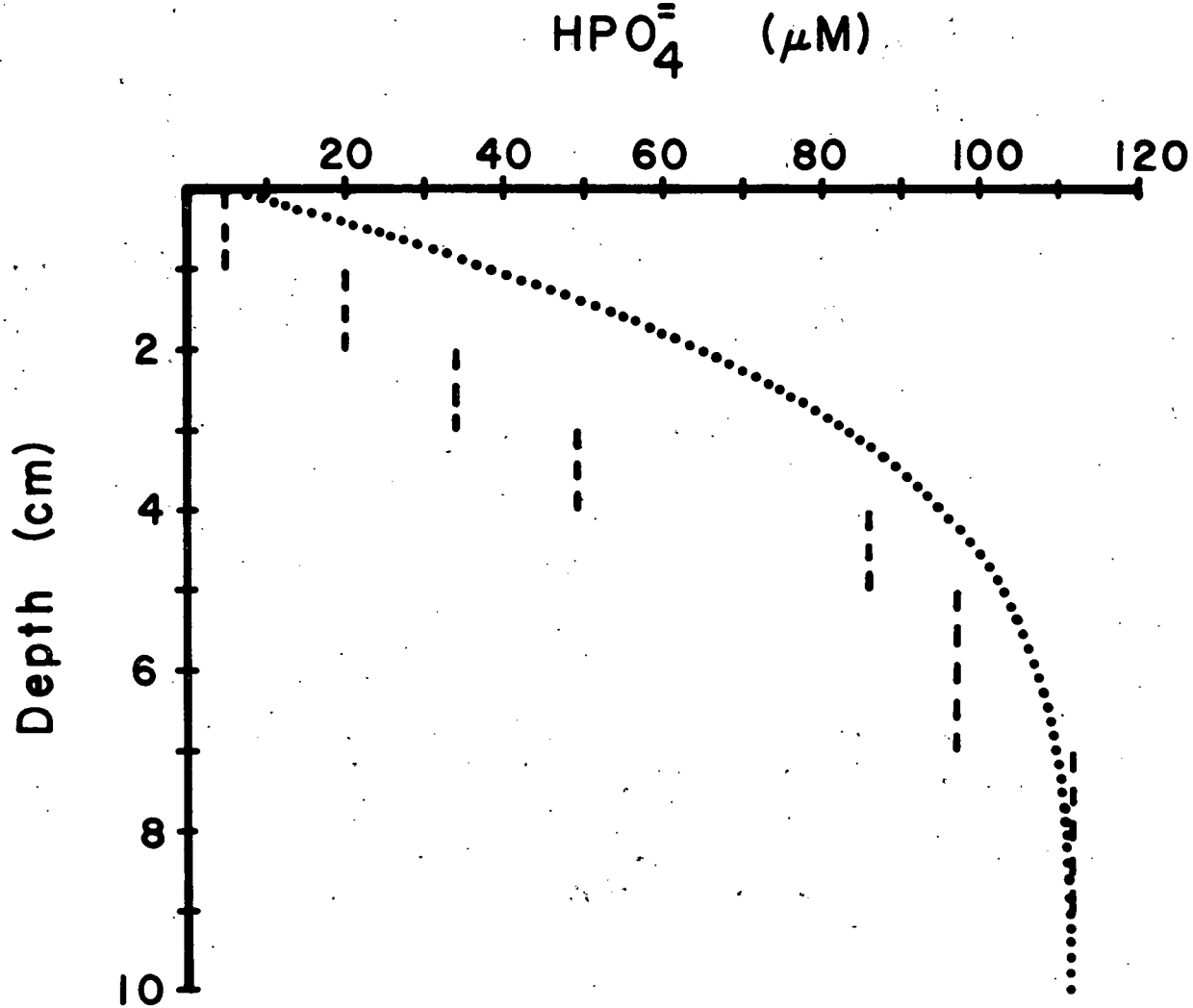


Figure III-14

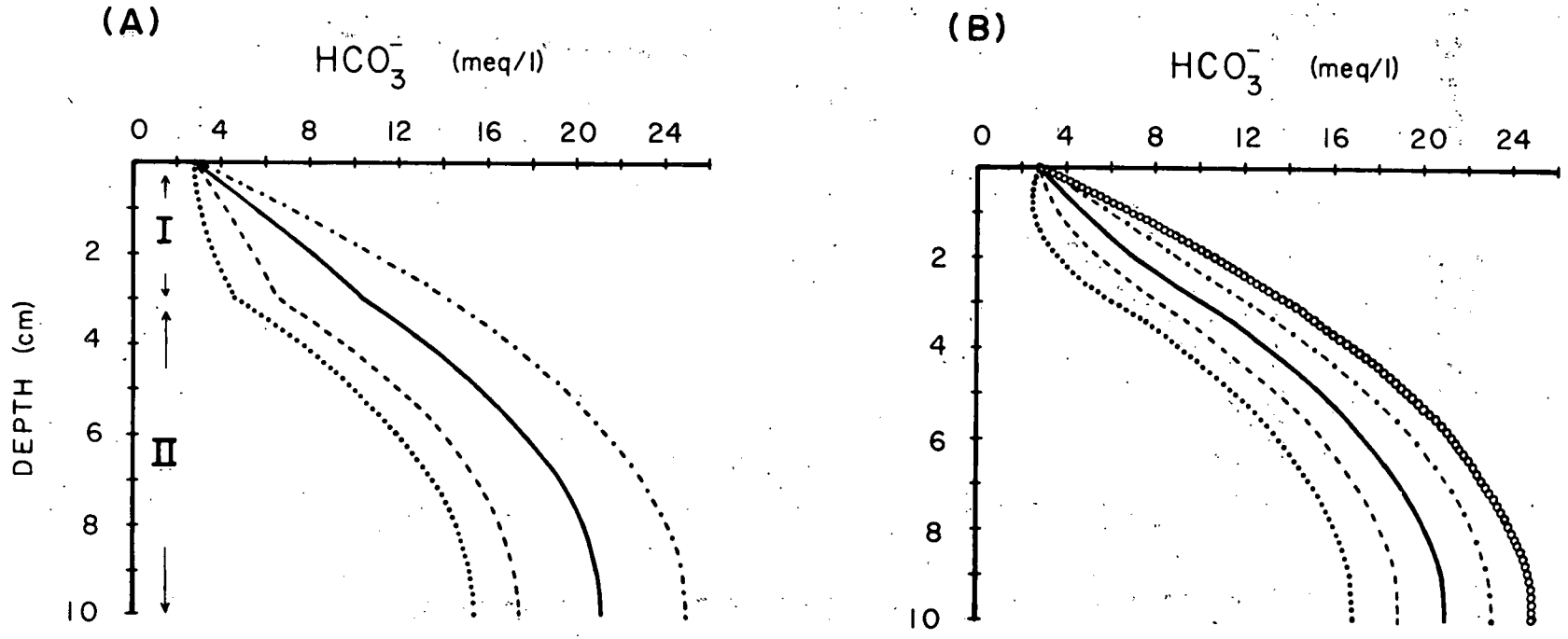


Figure III-15

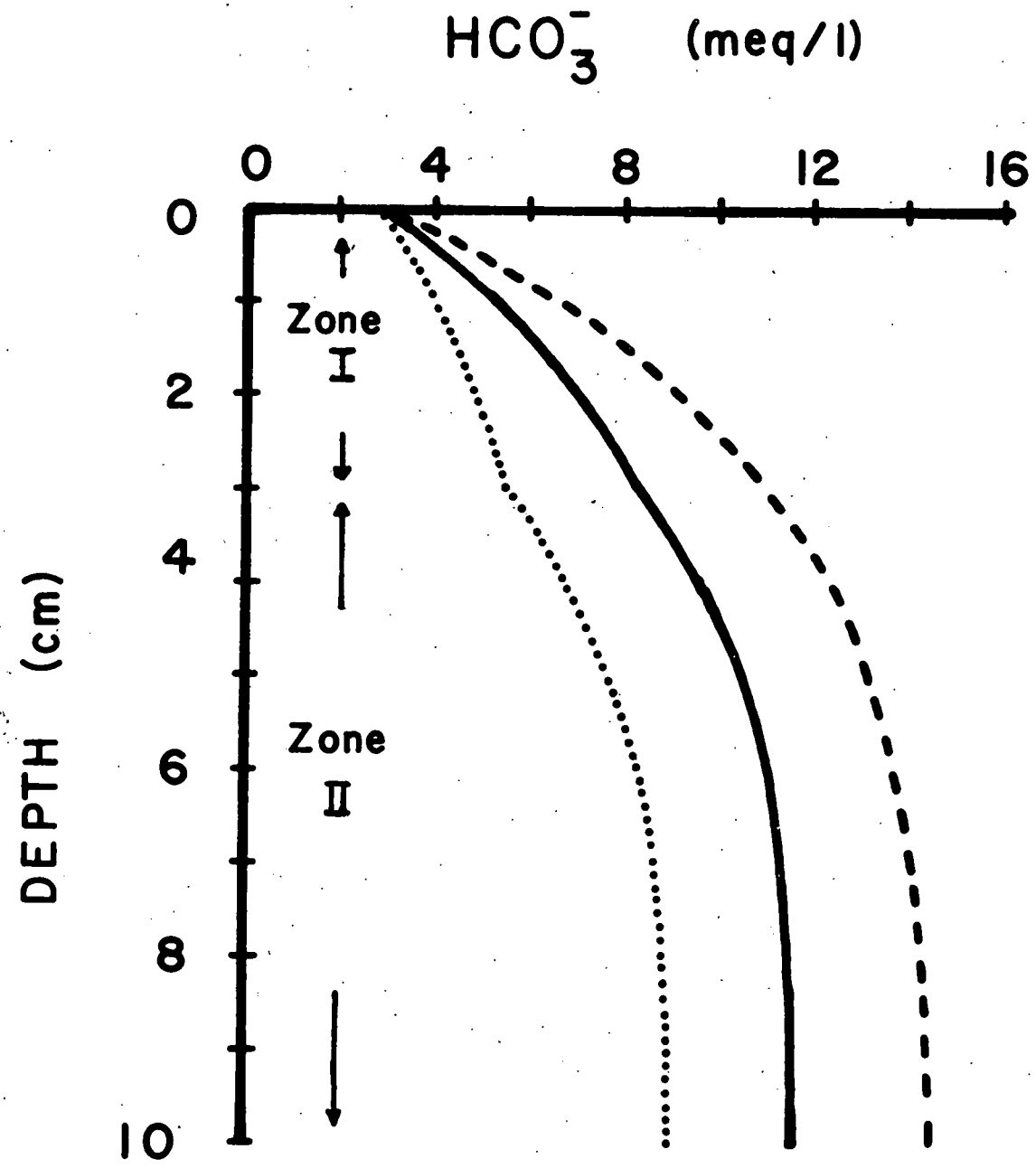


Figure III-16

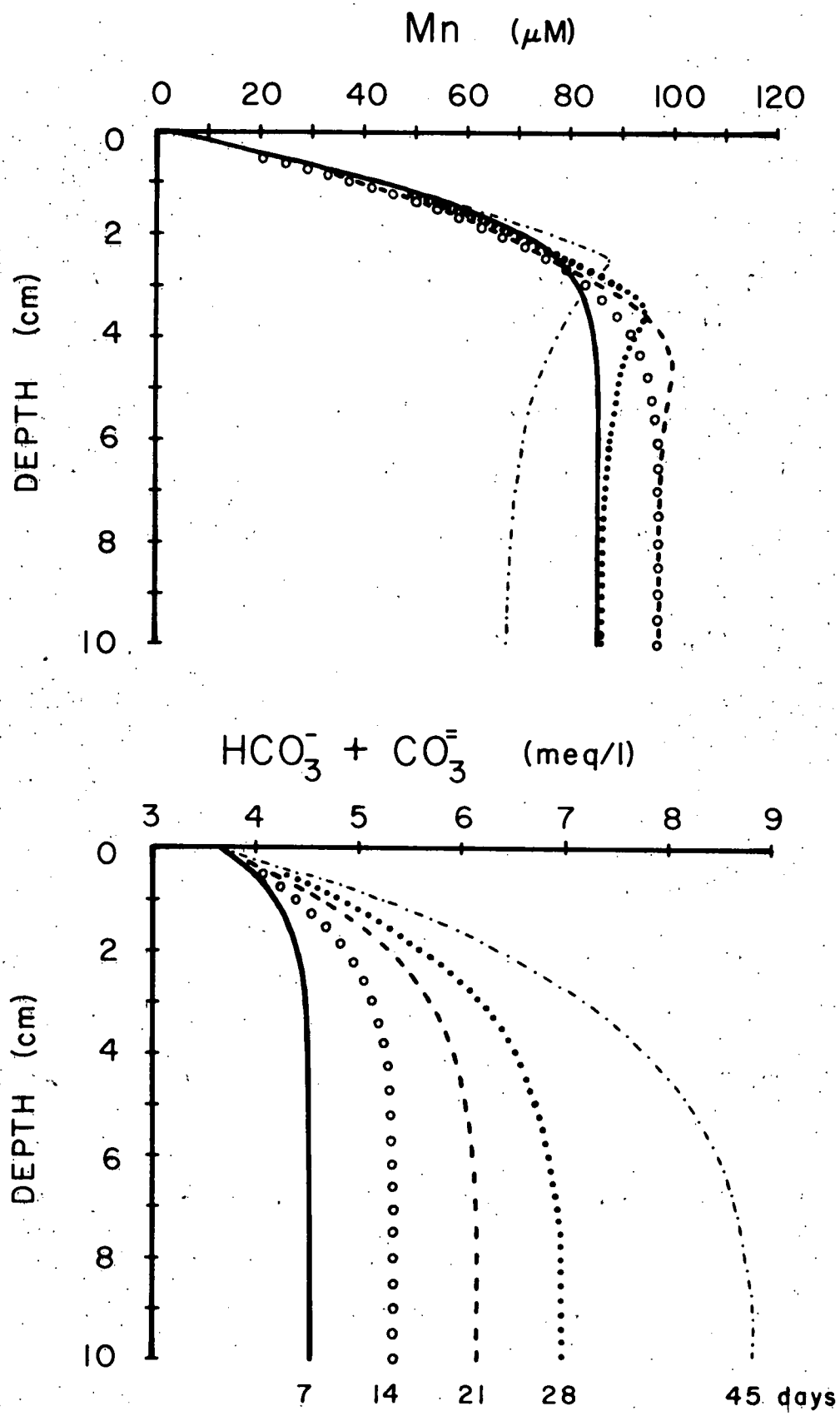


Figure III-17

CHAPTER IV

TRACKING PARTICLE ASSOCIATED PROCESSES IN A COASTAL ENVIRONMENT BY USE OF $^{234}TH/^{238}U$ DISEQUILIBRIUM

Particle transport near the sediment-water interface results from both physical and biogenic reworking of sediment. It is possible to describe this transport quantitatively in a deposit by using the disequilibrium activity distribution of ^{238}U or ^{232}Th series nuclides of varied half-lives, for example: ^{230}Th, ^{210}Pb, ^{228}Th and ^{234}Th as indicators of particle mobility (e.g., Koide and Goldberg, 1962; Bruland, 1974; Shokes, 1976; Aller and Cochran, 1976). Except in basins which are permanently or frequently anoxic (Calvert, 1964), or have especially high rates of sedimentation ($>$ 4 cm/yr) (Moore and Scruton, 1957), recent marine deposits are characterized by a predominance of sedimentary structures that are biogenic rather than physical in origin. This means that in general the distribution of a short-lived nuclide will be determined not by the net sedimentation rate but by the more rapid processes of sediment redistribution: interface resuspension and biogenic reworking. These nuclides then become important for investigating rapid diagenetic and particle-associated, redistribution processes within a given depositional environment rather than for documenting rates of net sedimentation.

Within the ^{238}U series, the thorium isotopes and ^{210}Pb are known to be rapidly extracted from coastal sea water onto particles (^{228}Th: Broecker, Kaufman, and Trier, 1973; ^{234}Th: Bhat et al., 1969; Aller and Cochran, 1976; ^{210}Pb: Benninger, Lewis, and Turekian, 1975; Benninger, 1976). These particles fall to the sea floor where they become available for either reworking into surface sediment or resuspension. The shortest-lived and highest in the decay series of these isotopes is ^{234}Th; its half life is 24.1 days. This short half life makes the activity distribution of ^{234}Th in sediment responsive to seasonal changes in particle reworking as well as short term lateral redistribution of particles within a sedimentary basin.

^{234}Th was first investigated successfully in sediments at a single station in central Long Island Sound (Aller and Cochran, 1976). Seasonal variation in its distribution was shown to be interpretable in terms of the physical and biological processes occurring there. Although similar in bottom type and faunal composition with large areas of the Sound and other estuaries or embayments of the northeastern U.S., this station (or any one station) is not representative of all major regions of the Sound. In order to evaluate our earlier results in terms of particle associated processes operating in the central Sound, a second station from a different bottom type was also chosen for ^{234}Th analysis (Figure IV-1). In this report, $^{234}Th_{excess}$ (^{234}Th activity above ^{238}U supported background) distributions at the two stations are compared and the significance of the similarities and differences between the two stations

evaluated in terms of intra-Sound material redistribution processes.

Study areas

Two sampling stations were designated for ^{234}Th analysis in central Long Island Sound. One of these, NWC, lies in 14 m of water 6 km south of the New Haven, Connecticut, harbor entrance in an area of topographically flat silty-clay bottom. During the course of sampling, this station was marked by a permanent buoy. The second station, DEEP, is in 34 m of water and also characterized by silt-clay deposits but with occasional sand layers. Both stations are undisturbed in any direct way by large-scale human activity such as dumping.

The macrofauna present at the two stations differs greatly. The infauna at NWC is dominated by dense populations of mobile deposit feeders (Rhoads, Aller and Goldhaber, 1976). These consist predominately of the highly active protobranch bivalves: Yoldia limatula and Nucula annulata, and the errant polychaete Nephtys incisa. Other fauna less abundant and less reliably present at this station include the suspension-feeding bivalves: Pitar morrhuana and Mulinia lateralis, the suspension-feeding polychaete Spiochaetopterus oculatus and surface deposit-feeding polychaete Melinna cristata, and surface deposit-feeding amphipods Ampelisca sp.

The DEEP station is characterized by larger, deeper burrowing, more sedentary benthos than NWC (Chapter V). Pherusa afinis, a large flabelligerid

surface deposit or suspension feeder and deposit-feeding maldanids are the characteristic polychaete species. Nephtys incisa, a cosmopolitan species in the Sound, is present in abundance. Protobranch bivalves are effectively absent and bivalves are largely represented by the suspension feeders: Pitar and Mulinia (small). Other common polychaetes include surface deposit feeders Melinna cristata, Pista palmata, and suspension feeder Spiochaetopterus oculatus.

Large Cerianthus americanus and evidence of the deep burrowing shrimp Squilla emposa are present at both NWC and DEEP.

Intensive resuspension of bottom sediment occurs at NWC. Stations in shallow regions (< 15 m) of the Sound have yielded the highest subtidal resuspension rates (100-300 mg/cm^2-day at 15 cm above bottom) ever reported for the northeastern U.S. (McCall, 1976). Despite these high flux rates, only the top 1 mm of sediment is thought to be affected by normal tidal and wave activity at NWC depths (Bokuniewicz, 1976). No resuspension data are available for DEEP type depths but qualitative evidence suggests that resuspension is much lower than at NWC. During diver descents, beginning at a depth of about 20 m, the water becomes noticeably less turbid. At the bottom, visibility (with a light) is good at DEEP, often 3 m or more, while at NWC 1 m visibility is considered extraordinary.

The surface sediment at both stations is rich in fecal material composed mostly of fusiform and rod-shaped pellets. NWC surface sediment is more

flocculent than DEEP and contains more abundant molluscan shell debris. In cross-section, NWC sediments show a distinct color stratigraphy: a surface yellow-orange oxidized cap of 1-5 cm thickness depending on the time of year, an underlying black, FeS rich zone 2-3 cm thick, and a bottom grey zone several meters thick. Only the surface 0.5 cm is orange-yellow in color at DEEP, this layer is underlain by a yellow and black mottled zone about 10-15 cm thick, below which the sediment is predominately grey.

Bottom water temperature follows the regional seasonal cycle with maxima ($\sim 22^{\circ}C$) and minima ($\sim 2^{\circ}C$) normally in August-September and February-March respectively (Riley, 1956; Chapter V).

Methods

In order to recover the sediment-water interface intact, bottom sampling was done by SCUBA divers. At NWC two types of hand-held plexiglas box cores, one measuring 25 cm wide x 30 cm deep x 2.5 cm thick and the other 25 cm wide x 30 cm deep x 7.5 cm thick were used (Appendix I). At DEEP a coring device copied from a corer in use in the laboratory of E.D. Goldberg, Scripps Institution of Oceanography was used. This consists of a five-foot length of PVC sewer pipe 10.2 cm I.D. modified for use as a corer and sharpened for insertion into the bottom. A diver was used in conjunction with a surface winch to obtain the core. Communication between diver and surface crew was maintained by use of an underwater microphone system. At the

diver's command and with his guidance the corer was allowed to free fall through the last ~0.5 m. The corer was gently pushed into the sediment by the diver as far as possible, the upper tube opening capped, and, after withdrawing the corer from the sediment by use of the winch, the bottom was capped as well. A second core, in this case a hand-held plexiglas box core (2.5 cm thick) was also taken at DEEP. Cores were taken at NWC on August 5, 1975; December 5, 1974 and April 15, 1975; and at DEEP on October 23, 1975. Both coring techniques, when properly employed, obtain an undisturbed interface.

At each station the thinner of the two box cores was x-rayed within several hours of collection to obtain an x-radiograph of sediment structure. At NWC the thicker box core was sampled for radiochemical analysis. The sewer pipe core taken from DEEP was sampled for both x-ray and radiochemical analyses as follows. After slow removal of the overlying water in the core, the upper unfilled section of pipe was gently removed by use of a pipe cutter. The fluid upper 10 cm of core was subcored for x-radiography by using a 2.5 cm thick subcorer of 0.16 cm plexiglas. Below this zone the sediment was cohesive enough to be cut without disturbance of structures by using a band saw. The core was sawed into 25 cm long sections, halved along each section's long axis, and from one of these halves, a slab 2.5 cm thick was painstakingly removed into specially constructed plexiglas trays. The slab was cut using thin stainless steel wire. This slab was then x-rayed.

The result of this processing was a continuous 2.5 cm thick slab down the middle of the core which could be x-rayed and also sampled without distrubance or freezing. After x-raying, these slabs were then carefully sampled for radiochemical analysis the day following collection. It should be noted that the fluid upper 10 cm of core was never turned from vertical in this procedure and no visual disturbance of the samples was evident.

Water content, ignition loss, and dry bulk sediment densities were determined from weight losses of known volumes of wet sediment dried at 100°C and then ashed at 475°C in a muffle furnace.

Ashed sediment samples (8–20 g) were spiked with a ^{232}U–^{228}Th tracer and leached in 300 ml of scalding hot 6 N HCl for 4 hours. U and Th were separated by ion exchange following slight modifications of the U procedure of Ku (1966) and the Th procedure of Bhat et al. (1969). The purified U and Th fractions were extracted into 0.4 M thenyltrifluoroacetone (TTA), and thin sources were prepared by evaporating the TTA phase onto stainless steel planchets. The ^{234}Th activity in the samples was determined immediately after plating by counting its daughter ^{234}Pa ($t_{1/2}$ = 6.1 min, 2.31 Mev β) on a Sharp LOW BETA anticoincidence counting system (^{234}Th counting efficiency = 0.50 ± 0.01). Because of ingrowth from ^{228}Th of ^{224}Ra ($t_{1/2}$ = 3.64 days) and its short-lived β-emitting daughters (^{212}Pb, ^{212}Bi, ^{208}Tl) only the first few hours of a count were used to calculate the activity. ^{238}U, ^{234}U, ^{230}Th, and ^{232}Th activities were determined by α spectrometry. The

$^{228}Th/^{232}Th$ activity ratios determined on unspiked aliquots of sediment were used to correct for natural ^{228}Th contribution to the ^{228}Th peak of the spiked sample.

Sample purity and cross-system calibration were checked by monitoring ^{234}Th decay of selected samples and by determining the ^{238}U activity by β counting the ingrown ^{234}Th (Aller and Cochran, 1976).

Results

Core description

Cores taken at NWC have been described and x-radiographs presented in Aller and Cochran (1976). One of these x-radiographs is shown again for comparative purposes (Figure IV-2). The upper few centimeters are intensely burrowed by protobranch bivalves. Beneath this upper zone, diffuse shell layers occur at intervals of about 4-6 cm but are absent below about 20 cm; these layers probably represent lag deposits formed during feeding. Tubes and burrows formed by soft-bodied fauna are irregularly preserved at depth. Bioturbate structure predominates.

DEEP station x-radiographs contrast with NWC in several significant ways. Shell debris occurs only at the interface and is conspicuously absent beneath a few centimeters depth. Biogenic structures result predominately from permanent tube dwellings, represented here by maldanid tube fragments of varied diameters and large dwelling burrows (Figure IV-3, 4), rather

than the homogenizing effect of mobile deposit feeders. And, as shown by water content and ignition loss profiles (Figure IV-5), the gradients in these properties are not as great near the interface at DEEP as at NWC. Water content and ignition loss are higher in the top samples from NWC than from DEEP, while samples from deeper in the cores are generally higher at NWC than DEEP for percent H_2O but lower in percent ignition loss (~ organic matter).

Radiochemical results

Radiochemical data for the DEEP core are given in Table IV-1. Data from NWC cores are reported in Aller and Cochran (1976). Excess ^{234}Th ($^{234}Th_{xs}$) activities are corrected to the time of collection of each core. Errors listed are 1σ and are based solely on counting statistics. The ^{234}Th errors reflect both the β counting error and the uncertainty in the Th yield.

At both stations $^{234}Th_{xs}$ decreases rapidly away from the interface. Of the three NWC cores analyzed only the summer (August 5, 1974) core has been plotted for visual comparison with the DEEP core. The differences shown are either similar or more exaggerated between the other NWC cores and DEEP. The major differences are that $^{234}Th_{xs}$ activities are lower at DEEP than NWC and that $^{234}Th_{xs}$ is mixed more deeply at NWC than DEEP. This deeper mixing is seen as irregular high activity regions in the NWC cores. The $^{234}Th_{xs}$ background of about 0.20 $\pm$ .10 dpm/g is apparently a leaching (Kogoshi, 1971; Cherdyntsev, 1971) or calibration effect.

The $^{234}Th_{xs}$ inventory (total integrated excess Th in sediment column) differs for the two stations. The inventories for the upper 5 cm alone at NWC are 3.7, 7.7, and 5.3 dpm/cm^2 for summer, fall, and winter cores (Aller and Cochran, 1976). $^{234}Th_{xs}$ inventory at DEEP (5 cm) is 1.9 dpm/cm^2.

Except for one sample the U/Th weight ratios at DEEP are fairly constant with depth at a value of ~ 0.20. This is higher than near interface sediment at NWC but not as high as deep NWC sediment (Figure IV-4).

Discussion

Particle mixing at NWC and DEEP

Because of the abundance of large, deep-burrowing benthos at DEEP, the sampling intervals for $^{234}Th_{xs}$ were chosen to outline patterns of deeper biogenic reworking than found at NWC. In fact, the $^{234}Th_{xs}$ pattern found shows that all excess activity is restricted to the upper 3 cm. This leaves only two data points from which to derive any quantitative measure of mixing for comparison with NWC. Several approaches to quantitatively describing biogenic particle transport are used in the literature. Particle movement is generally expressed in terms of a diffusion-type mixing coefficient or as an advective transport coefficient such as an apparent sedimentation rate (Koide and Goldberg, 1962; Guinasso and Schink, 1975; Aller and Cochran, 1976).

The use of diffusion as an analogue to biogenic particle transport in a sediment sample assumes: (1) that particle transport resulting from the

activities of individual organisms represent random walks or eddies of sediment within a deposit, and , (2) the scale of particle eddies is small compared to sample size so that the number of transport events represented in a sample is large. When the distribution of a time dependent property of the transported particles is considered, particle diffusion can be used in the description of its distribution only if the mixing rate is rapid enough relative to the time dependence to fulfill condition (2).

In some special cases, the initial stage of sediment mixing by deposit feeders is also similar to an advective process. For example, early stages of sediment mixing by populations of deep-feeding deposit feeders such as Clymenella torquata (marine) or the tubificid Tubifex tubifex (fresh water) advect the sediment surface relatively uniformly downward toward the feeding zone (e.g., Figure 3 of Aller and Dodge, 1974). On long time scales the particles become recycled toward the interface and this type of mixing becomes comparable to diffusion but on short time scales transport resembles unidirectional advection. The distribution near the sediment-water interface of a short-lived nuclide attached to particles might therefore be adequately described by an advective transport model under certain circumstances. This would depend largely on the kinds and relative abundance of animals present in the sediment and on the half-life of the nuclide in question.

The distribution in the sediment column of a non-exchangeable radionuclide attached to sediment particles subject to diffusive and advective

transport, can be described in one dimension (Cartesian coordinates) by the equation (ignoring compaction):

$$(1) \quad \frac{\partial A}{\partial t} = \frac{\partial}{\partial x}\left(D \frac{\partial A}{\partial x} \right) - v \frac{\partial A}{\partial x} - \lambda A$$

where,

t: time

x: space coordinate, origin fixed at sediment-water interface, positive axis into sediment

A: activity of nuclide on particles

λ: decay constant of nuclide

v: advection coefficient

D: diffusion coefficient

In the case of biogenic reworking, $D = D_B + D_C$ where D_B = biogenic diffusion or mixing coefficient and D_C = chemical diffusion along particle surfaces. In general, D_C can be ignored and $D = D_B$. The advection coefficient is $v = v_B + \omega$, where v_B = biogenic advection and ω = net sedimentation rate.

Assuming a steady state activity distribution ($\frac{\partial A}{\partial t} = 0$), then the general solution to equation (1) when $D = D_B$ is constant with depth is:

$$(2) \qquad A = B_1 \exp \frac{v - (v^2 + 4\lambda D_B)^{1/2} x}{2 D_B} + B_2 \exp \frac{v + (v^2 + 4\lambda D_B)^{1/2} x}{2 D_B}$$

where B_1, B_2 are constants determined by the boundary conditions. With the boundary conditions: $x = 0$, $A = A_o$; $x = \infty$, $A = 0$, then equation (2) becomes:

$$(3) \qquad A = A_o \exp \frac{v - (v^2 + 4\lambda D_B)^{1/2} x}{2 D_B}$$

Two end number cases where biogenic transport controls the activity distribution will be considered; one where biogenic particle transport is due predominantly to diffusion-like mixing and the second less general case, where biogenic advective transport is more important than biogenic diffusion. Assuming only diffusion-like transport then at steady state, equation (1) becomes (D_B constant with depth):

$$(4) \qquad D_B \frac{\partial^2 A}{\partial x^2} - \lambda A = 0$$

It is permissible to ignore net sedimentation in equation (4) if $\omega^2 << 4\lambda D_B$ (from application of L'Hospital's rule to equation (3), $v_B = 0$). The solution is:

$$(5) \qquad A = B_1 \exp\left(-\left(\frac{\lambda}{D_B}\right)^{1/2} x\right) + B_2 \exp\left(\left(\frac{\lambda}{D_B}\right)^{1/2} x\right)$$

B_1, B_2: constants

The second end member case is where biogenic advection controls the activity distribution ($v_B >> \omega$, $D_B = 0$), equation (1) becomes:

$$(6) \qquad - v_B \frac{\partial A}{\partial x} - \lambda A = 0$$

The solution is:

$$(7) \qquad A = B_3 \exp\left(-\frac{\lambda}{D_B} x\right) + B_4$$

B_3, B_4 : constants

With the boundary condition $x = 0$, $A = A_o$; $x = \infty$, $A = 0$, then the solutions to (5) and (6) become:

$$(8) \qquad A = A_o \exp\left(-\left(\frac{\lambda}{D_B}\right)^{1/2} x\right) \qquad \text{diffusion only}$$

$$(9) \qquad A = A_o \exp\left(-\frac{\lambda}{v_B} x\right) \qquad \text{advection only}$$

In the absence of any information on exactly what kind of particle transport was taking place in the sediment, either equation (8) or (9) could be used to describe an activity distribution which decreased exponentially with depth. If the equations were used to describe the same data, the numerical relationship between the exponents requires:

$$(10) \qquad \frac{\lambda}{v_B} = \left(\frac{\lambda}{D_B}\right)^{1/2} \longleftrightarrow D_B = \frac{v_B^2}{\lambda}$$

(It should be noted explicitly that no conceptual relationship between D_B and v_B is implied here; this discussion merely illustrates numerical relations between the two brought about by the mathematical formalism of considering the end member cases).

In deriving a mixing coefficient from ^{234}Th activity profiles at station NWC, Aller and Cochran (1976) approximated a D_B value equivalent to v_B (v_B was called an apparent sedimentation rate in that paper) by using a dimensional analysis approach similar to one employed by Guinasso and Schink (1975). The latter authors converted values of reworking rates (in units of length/time) compiled for individual animal species into corresponding diffusion coefficients by multiplying by a scale factor, L_B, representing the particular feeding depth of the animal involved. Aller and Cochran (1976) estimated a L_B at station NWC from knowledge of the feeding depths of the fauna and the shape of the $^{234}Th_{xs}$ profiles found there and calculated D_B from v_B (apparent sedimentation rate) using the relation:

$$(11) \quad D_B = L_B v_B$$

In general, equation (11) is incorrect as it was employed since:

$$(12) \quad L_B \neq \frac{v_B}{\lambda}$$

as required by equation (10). Equation (10) results from the assumption that biogenic reworking is not a function of depth whereas the use of a L_B implies that it is.

The rapid drop-off of infaunal abundance with depth in a deposit (e.g., Mare, 1942; Myers, 1973) requires that biogenic reworking rates for the deposit as a whole must eventually decrease as well. It is not possible from the ^{234}Th data alone to determine the dependence of reworking on depth in the sediment (this dependence will be treated in a later report, Benninger et al., in preparation); however, as implied by the introduction of L_B, it is possible to place limits on reworking rates which show depth dependence by use of a composite layer mixing model. Such a model assumes that discrete intervals of the sediment column are mixed at constant rates but that these rates differ between layers (e.g., Berger and Heath, 1968; Guinasso and Schink, 1975; Shokes, 1976; Chapter III). For purposes of the remaining discussion on mixing only the diffusion analogue to particle reworking will be considered.

Let the sediment column be divided into two layers, the upper layer (zone 1) of thickness L_B is mixed at a uniform rate described by D_B and the lower layer (zone 2) is not subject to reworking. Transport in zone 2 is controlled by net sedimentation only. Assuming that $\omega^2 << 4\lambda D_B$ then the activity distribution at steady state of a non-exchangeable radionuclide attached to particles is given for zone 1 by equation (5). In this case the boundary conditions on zone 1 are:

$$x = 0, \quad A = A_o$$

$$x = L_B, \quad D_B \left(\frac{\partial A}{\partial x}\right)_{x = L_B} = 0$$

The diffusive flux across the lower boundary must be zero since by definition D_B in zone 2 was set at zero. This gives:

$$(13) \quad B_1 = \frac{A_o \exp\left(2\left(\frac{\lambda}{D_B}\right)^{1/2} L_B\right)}{1 + \exp\left(2\left(\frac{\lambda}{D_B}\right)^{1/2} L_B\right.}$$

$$(14) \quad B_2 = \frac{A_o}{1 + \exp\left(2\left(\frac{\lambda}{D_B}\right)^{1/2} L_B\right.}$$

so that the activity at $x = L_B$ is:

$$(15) \quad A_{L_B} = \frac{2 A_o \exp\left(\left(\frac{\lambda}{D_B}\right)^{1/2} L_B\right.}{1 + \exp\left(2\left(\frac{\lambda}{D_B}\right)^{1/2} L_B\right.}$$

If: (16) $\exp\left(2\left(\frac{\lambda}{D_B}\right)^{1/2} L_B\right. >> 1$

then,

$$(17) \quad A_{L_B} \approx 2 A_o \exp\left(-\left(\frac{\lambda}{D_B}\right)^{1/2} L_B\right)$$

therefore

$$(18) \quad D_B \approx \lambda \left(\frac{L_B}{\ln 2 A_o - \ln A_{L_B}} \right)^2$$

If $A_{L_B} \neq 0$, then $\ln A_{L_B}$ and $\ln A_o$ can be determined by fitting a curve to the activity profile data and calculating values for A at $x = 0$ and $x = L_B$. It is necessary to know L_B independently to evaluate D_B.

Use of the composite layer model results in calculation of a smaller D_B for a given activity profile than for the case of infinitely deep mixing described previously or than when mixing at a rate greater than zero is also allowed in zone 2. This can be demonstrated by substituting $x = L_B$ in equation (8) yielding:

$$(19) \qquad D_B = \lambda \left(\frac{L_B}{\ln A_o - \ln A_{L_B}} \right)^2$$

which predicts a higher D_B than equation (18). Clearly as $A_{L_B} \rightarrow$ small, the D_B values calculated by the two models (infinite mixing, finite mixed layer) become equivalent. Calculation of D_B by application of both models to a profile will result in a range of values representing upper and lower limits on D_B. Note that choice of an L_B in the composite layer model requires a considerably greater quantity of information about mixing processes in the sediment than naive use of the infinitely deep mixing model.

To obtain a mixing rate from the ^{234}Th activity distribution at DEEP it is necessary to assume that activity decreases exponentially with depth, that is, $A = A_o e^{-\alpha x}$. Since the average values for A are known over the intervals 0-1 cm and 1-3 cm, α can be computed by integration. The value

for α at DEEP is 1.71/cm . It is not possible to estimate a L_B at DEEP from the ^{234}Th profile alone but the kinds of animals present there indicate that reworking takes place to at least several decimeters. Unlike NWC, there are no conspicuously active deposit feeders present near the interface which would allow the ready choice of a smaller value of L_B for modelling the distribution of short-lived nuclides like ^{234}Th. Therefore only the infinitely deep mixing model can be used in this case and an upper limit on D_B obtained; if L_B is greater than ~ 2 cm this limit will be very near the value calculated for the upper few centimeters using a more complicated composite layer model. Equation (8) with $\alpha = (\frac{\lambda}{D_B})^{1/2}$ gives $D_B = 0.1 \times 10^{-6}$ cm^2/sec. Since estimates of the net sedimentation rate at DEEP and other areas of the Sound indicate an upper bound on ω (net sedimentation) of ~ 0.5 cm/year (Thompson, Turekian, and McCaffrey, 1975; Bokuniewicz, Gebert, and Gordon, 1976; Benninger et al., in preparation) then $\omega^2 << 4 \lambda D_B$ holds and the use in the calculation of equation (8) rather than (3) is justified.

For comparison, the ^{234}Th data from NWC can also be fit by equations of the form $A = A_o e^{-\alpha x}$ over the top few centimeters. In previous calculations the measured activity values were assigned to the midpoint depth of the sampling interval (Aller and Cochran, 1976) but for the present purposes the finite interval approach of Robbins and Edgington (1975), as employed above

for DEEP, is used instead. The appropriate equations describing the NWC data from 0-4 cm are $A = 11.4\ e^{-1.107x}$; $A = 8.84\ e^{-0.352x}$; and $A = 17.1\ e^{-1.295x}$ for summer, fall and winter.

At NWC, the fall case has a visual discontinuity in the ^{234}Th activity profile at x = 4 cm which corresponds with the expected basal depth of the feeding zone for Yoldia limatula, a very mobile and highly active deposit-feeding bivalve abundant at this station. Assuming that this is a true mixing discontinuity depth that holds year round then taking $L_B = 4$ cm and using equation (18) yields D_B's for summer, fall, and winter of: 0.2×10^{-6}, 1.2×10^{-6}, and 0.15×10^{-6} cm^2/sec. Since the summer and winter profiles show no definite lower discontinuity at 4 cm the infinitely deep mixing model might also be used. Equation (8) yields D_B's of 0.3×10^{-6} and 0.2×10^{-6} cm^2/sec for summer and winter; these represent upper limits on D_B as discussed above and are in close agreement with the composite layer model. The similarity in the calculated summer and winter D_B's probably reflects symmetry in the integrated mixing effects (over ~ 5 half-lives of ^{234}Th) during the rising and falling legs of the yearly temperature distribution.

The summer, fall, and winter values for D_B at NWC estimated by Aller and Cochran (1976) using equation (11) and $L_B = 4$ cm were 1×10^{-6}, 3×10^{-6}, and 1×10^{-6} cm^2/sec (finite sampling interval ignored in pervious calculation). Although these are not terribly inaccurate, use of the D_B's as calculated in this report is more consistent mathematically and

meaningful than those done previously.

The fall (1975) D_B at DEEP (infinitely deep mixing model) and the fall (1974) D_B at NWC (composite layer model) differ by an order of magnitude at 0.1 and 1.0×10^{-6} cm^2/sec respectively. This difference is a minimum because the D_B for DEEP is a maximum and that for NWC is a minimum due to the different models used in calculation. Fall mixing as measured by $^{234}Th_{xs}$ at DEEP is lower than the lowest value at NWC. These calculations demonstrate that vertical particle reworking near the interface is more rapid in shallow, protobranch inhabited areas than in deeper areas of Long Island Sound inhabited by larger, more sedentary benthos. Mixing over time scales integrated by longer-lived nuclides such as ^{210}Pb may not show this difference in reworking rate and in fact could reveal an opposite pattern (although the D_B's calculated would be lower than found using ^{234}Th). Over longer time scales the cumulative effect of the in-filling of large dwelling burrows becomes more important relative to the intense short-term turnover of particles near the sediment-water interface.

The relative importance of horizontal mixing at the two stations cannot be quantitatively compared but the mobility of protobranchs coupled with surface resuspension at NWC must more than equal the effect of surface deposit feeders at DEEP, such as Pista, in homogenizing sediment horizontally.

Th inventories

There is a significant difference in the $^{234}Th_{xs}$ inventories at DEEP and NWC. The theoretical inventory at DEEP based on a water depth of 34 m and a Long Island Sound sea water uranium value of 1.80 dpm/kg (low in range of U values) is 6.12 dpm/cm^2 ; only 1.9 dpm/cm^2 is found. At NWC the theoretical inventory is 2.5 dpm/cm^2 and up to 8.4 dpm/cm^2 (fall-integrated to 8 cm) is found (Aller and Cochran, 1976). These discrepancies show clearly that in Long Island Sound the shallow bottom muddy areas play a significantly greater role in scavenging the water column and capture of Th-like metals than deeper regions and that these differences are ongoing and rapid. It is known that protobranch bivalves increase the susceptibility of bottom sediments to resuspension as a result of their feeding activity (Rhoads and Young, 1970). This effect plus the high particle reworking rates characteristic of protobranch inhabited areas, which serve to increase ^{234}Th inventories (Aller and Cochran, 1976) suggest that bottom areas of the Sound inhabited by these organisms are especially active environments for the transfer of chemical species between sediment and overlying water.

The difference in inventories has far-reaching consequences for the distribution of certain elements in sediments in the estuary. Some elements, such as Fe and Mn have high flux rates out of Long Island Sound sediment (Chapter VI). Both Fe and Mn precipitate rapidly on reactive particle

surfaces and can be expected to have residence times in the water column comparable to ^{234}Th of about $\leq$ 1 day. These elements are also important in scavenging many additional metals through coprecipitation or by adsorption onto the freshly precipitated Fe, Mn-oxide surfaces (Jenne, 1968; Kharkar, Turekian, and Bertine, 1968). The significance of the ^{234}Th inventories together with the measurable fluxes of particle-seeking metals from Long Island Sound sediments is that rapid, intraestuarine redistribution of metals like Fe and Mn may continually be taking place and that on short time scales preferential accumulation in areas like NWC occurs. Any initially soluble but particle-seeking pollutants dumped into the sound can be expected to at first preferentially accumulate in NWC-like bottom areas. This scavenging-capture pattern may differ on longer time scales depending on differences in mixing as discussed above or additional diagenetic processes in a particular deposit (see Chapters V, VI).

Uranium

The uranium profile at DEEP obviously differs from that at NWC. Represented as a U/Th weight ratio, U is nearly constant at DEEP while NWC shows a steady increase in U away from the interface (Figure IV-5). Low U in the upper few centimeters of Long Island Sound deposits has been attributed to oxygenation of surface sediment by biogenic reworking which together with the high carbonate alkalinity of sea water probably results in formation of a

soluble uranyl carbonate complex and U loss (Thompson, Turekian, and McCaffrey, 1975; Aller and Cochran, 1976). Beneath the oxidized zone, sea water U is subject to reduction and precipitation causing an increase in U/Th and $^{234}U/^{238}U$ ratios with depth (Aller and Cochran, 1976). Following these arguments, the higher rates of particle transport and the deeper extent of the yellow oxidized zone at NWC is consistent with the lower U/Th ratios found near the interface there than at DEEP. Differences at depth must result from differences in the distribution of reducing effects of bacterial activity and pore water transport mechanisms such as irrigation at the two stations.

It is shown in Chapter V and VI that biogenic irrigation and reworking takes place to a greater depth in the sediment and is more extensive at DEEP than NWC. In the presence of burrows, diffusion of pore water constituents is both vertical and horizontal. The result is that the average distance of a parcel of sediment from sea water is greatly decreased and determined by the abundance of open, irrigated burrows in the deposit. The U/Th profile at DEEP could then result from the fact that in the upper few decimeters of sediment the effective distance from the sediment-sea water interface is on the average just a few centimeters (i.e., half the distance between burrows). The solid phase U/Th ratio in the entire upper portion of the deposit would then be appropriate for that average distance and associated reducing conditions. This results in a relatively constant U/Th depth profile. Additional information

on U/Th ratios at depth in the sediment and perhaps U in pore water are required to substantiate this explanation.

Summary

(1) Modeling of $^{234}Th_{xs}$ profiles from two stations in Long Island Sound show that vertical mixing of particles near the sediment-water interface varies both in time and space. Mixing over ^{234}Th time scales is higher in shallow (14 m) areas inhabited by protobranch bivalves than at a deeper water (34 m) station where larger, more sedentary benthos are prominent. When expressed as a diffusion-like mixing coefficient D_B particle mixing rates in the protobranch-inhabited bottom vary from $0.2 - 1 \times 10^{-6}$ cm^2/sec, depending on the assumed boundary conditions, and are highest in the fall. The D_B value derived for the deep water station is 0.1×10^{-6} cm^2/sec (fall) and is ten times smaller than the fall shallow water value.

(2) The $^{234}Th_{xs}$ inventories show that the protobranch station retains up to four times the theoretically predicted inventory while the deep water station is three times lower than it should be. This illustrates that, on short time scales, some bottom areas are more effective than others in scavenging the water column of particle-seeking metals. Protobranch inhabited bottoms are especially interactive with overlying water. When the fact that some metals, such as Fe and Mn, are constantly released from the bottom and precipitated in the water column is considered, it is clear that differences in

the scavenging ability of bottom areas should result in intraestuarine redistribution of metals.

(3) Differences in the uranium profiles at the two stations show that the intensity and depth distribution of processes affecting uranium differ at the two stations. The depletion of U in the upper few centimeters at the protobranch station relative to the deep water station is probably caused by more rapid mixing and oxygenation at the protobranch station and results in U loss. Differences in the profiles at depth require more U data for explanation but are probably associated with differences in the depth distributions of bacterial reduction rates and intensity of irrigation.

Table IV-1. Deep ^{234}Th-^{210}Pb Core (October 23, 1975; T = 17°C) Radiochemical Results

Depth	^{232}Th dpm/g	$^{228}Th/^{232}Th$	$^{234}Th_{xs}$ dpm/g	^{238}U	$^{234}U/^{238}U$	U/Th	ρ g/cc	% H_2O	% Organic matter	$^{230}Th/^{232}Th$
0-1 cm	2.29 ±.12	.973 ±.023	3.93 ±.22	1.358 ±.035	1.04 ±.03	0.197 ±.012	.355	70.8	6.87	.741 +.023
1-3 cm	2.40 ±.14	.967 ±.016	0.42 ±.16	1.776 ±.044	1.07 ±.03	0.246 ±.016	.452	63.1	6.09	.734 ±.026
3-5 cm	2.59 ±.10	.793 ±.021	0.20 ±.10	1.607 ±.031	1.04 ±.02	0.206 ±.009	.473	61.5	6.47	.706 ±.018
5-8 cm	2.50 ±.08	.838 ±.013	0.15 ±.08	1.634 ±.033	1.07 ±.02	0.217 ±.008	.572	56.5	6.07	.725 ±.016
8-11cm	2.39 ±.07	.869 ±.012	0.17 ±.07	1.417 ±.027	1.03 ±.03	0.197 ±.007	.515	56.1	7.12	.723 ±.014
11-15cm	2.49 ±.07	.794 ±.016	0.16 ±.07	1.481 ±.028	1.02 ±.02	0.198 ±.007	.594	54.9	6.58	.703 ±.01
15-19cm	2.55 ±.08	.800 ±.016	0.17 ±.07	1.532 ±.019	1.03 ±.02	0.200 ±.007	.554	54.5	6.53	.718 ±.020
19-24cm	2.40 ±.08	.813 ±.019	0.14 ±.08	1.509 ±.029	1.08 ±.02	0.209 ±.008	.557	53.5	6.07	.725 ±.016

* 6N HCl 4 hrs. hot leach

Chapter IV

Figure Captions

Figure IV-1: A. Northeast U.S.A. showing location of Long Island Sound.

B. Long Island Sound.

C. Central Long Island Sound illustrating positions of NWC and DEEP.

Figure IV-2: Box core x-radiograph at NWC (August 5, 1974). Yoldia limatula in life position at left. Cerianthus americanus burrow in center. Bioturbate structure at depth. Scale = 3 cm.

Figure IV-3: Box core x-radiograph at DEEP (October 23, 1975). Dwelling burrows of Pherusa affinis center and left. Scattered maldanid tubes near interface and right hand side. Shells of Mulinia lateralis present, but shell debris conspicuously absent in general. Bioturbate structure throughout (crack at bottom during sampling). Scale = 3 cm.

Figure IV-4:A,B X-radiograph of sediment slab at DEEP analyzed radiochemically. Maldanid dwelling tubes conspicuous at interface (top of IV-4A) and below 16 cm. Large crustacean burrow present on left side of IV-4B. A = 0 to 8 cm, B = 8 to 33 cm. Scale = 3 cm.

Figure IV-5:A. % H_2O profiles at NWC and DEEP. (NWC = triangles + dashed line, DEEP = circles + dotted line).

B. % ignition loss profiles at NWC and DEEP.

C. $^{234}Th_{xs}$ profiles at NWC and DEEP.

D. U/Th weight ratio profiles at NWC and DEEP.

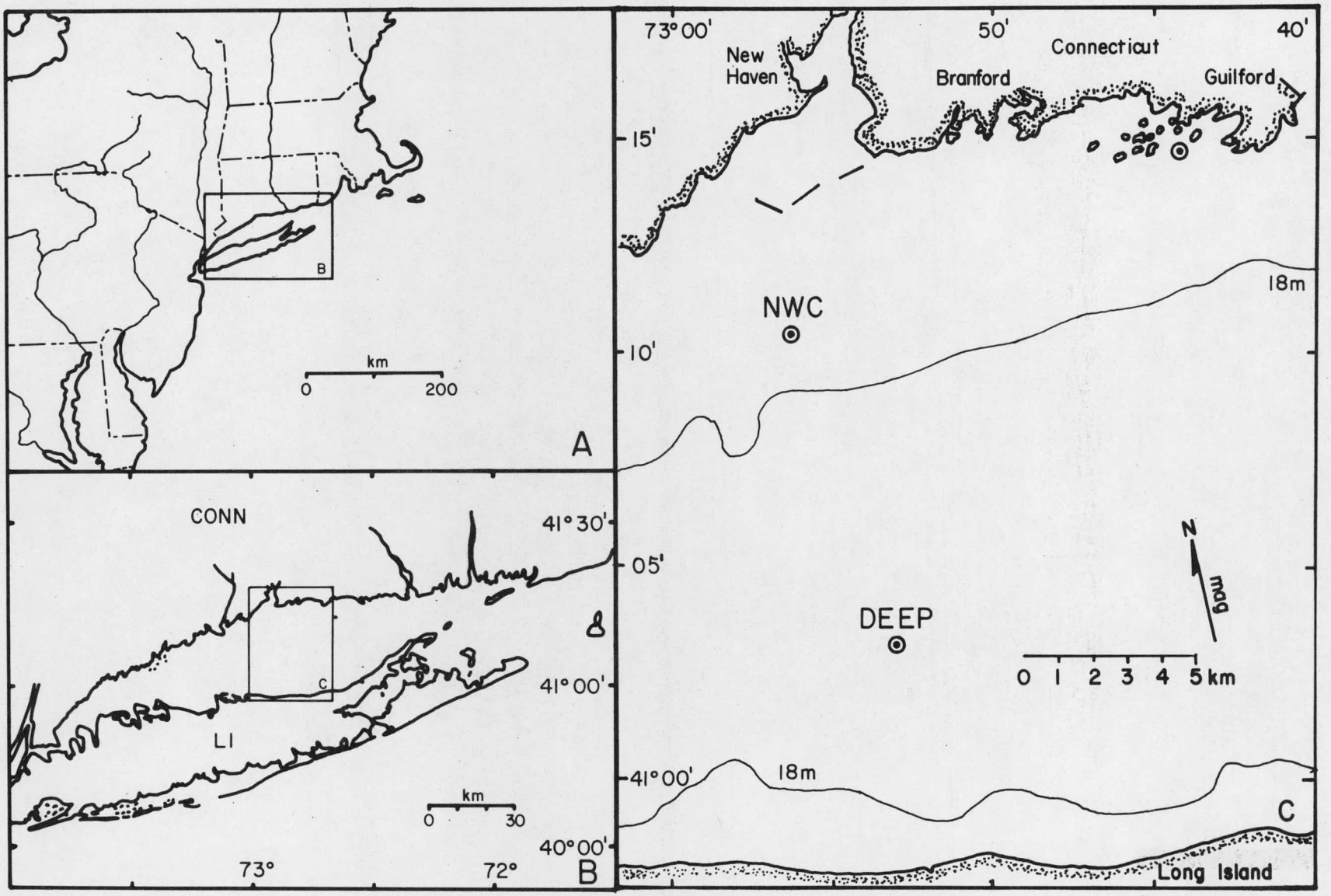
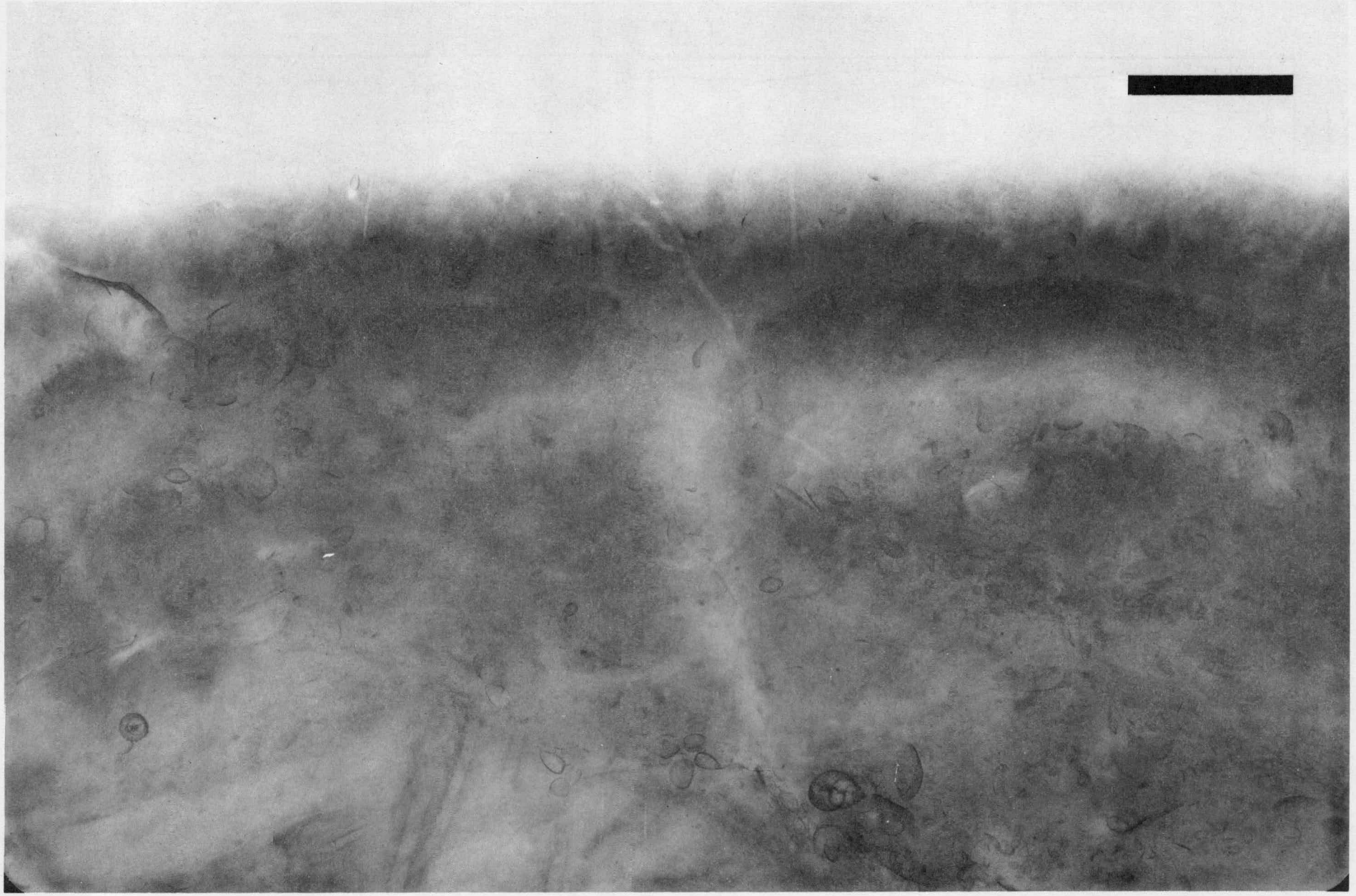

B
km
0
200
A
CONN
41°30'
C
LI
41°00'
km
0
30
40°00'
73°
72°
B
73°00'
50'
40'
New
Haven
Connecticut
Branford
Guilford
15'
18m
NWC
10'
05'
DEEP
N
mag
0 1 2 3 4 5 km
41°00'
18m
C
Long Island

Figure IV-1



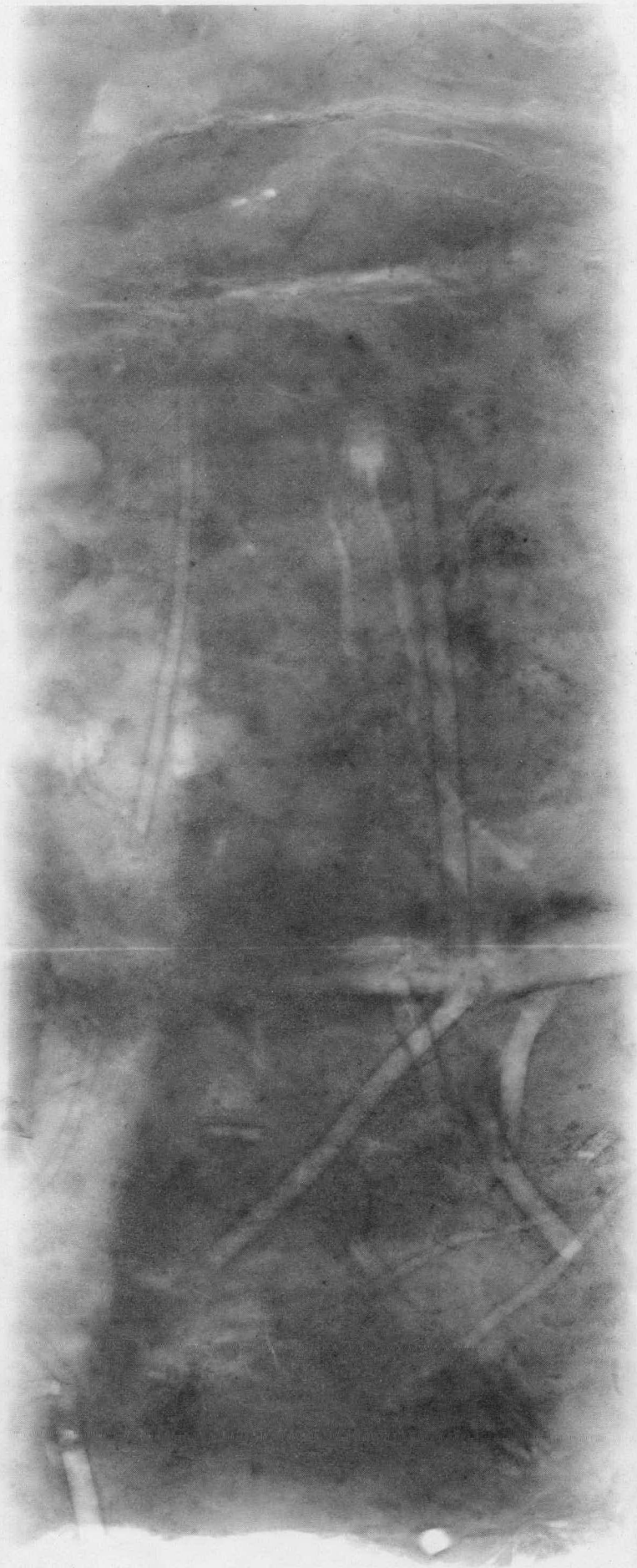
IV-2



IV-3



IV-4A



IV-4B

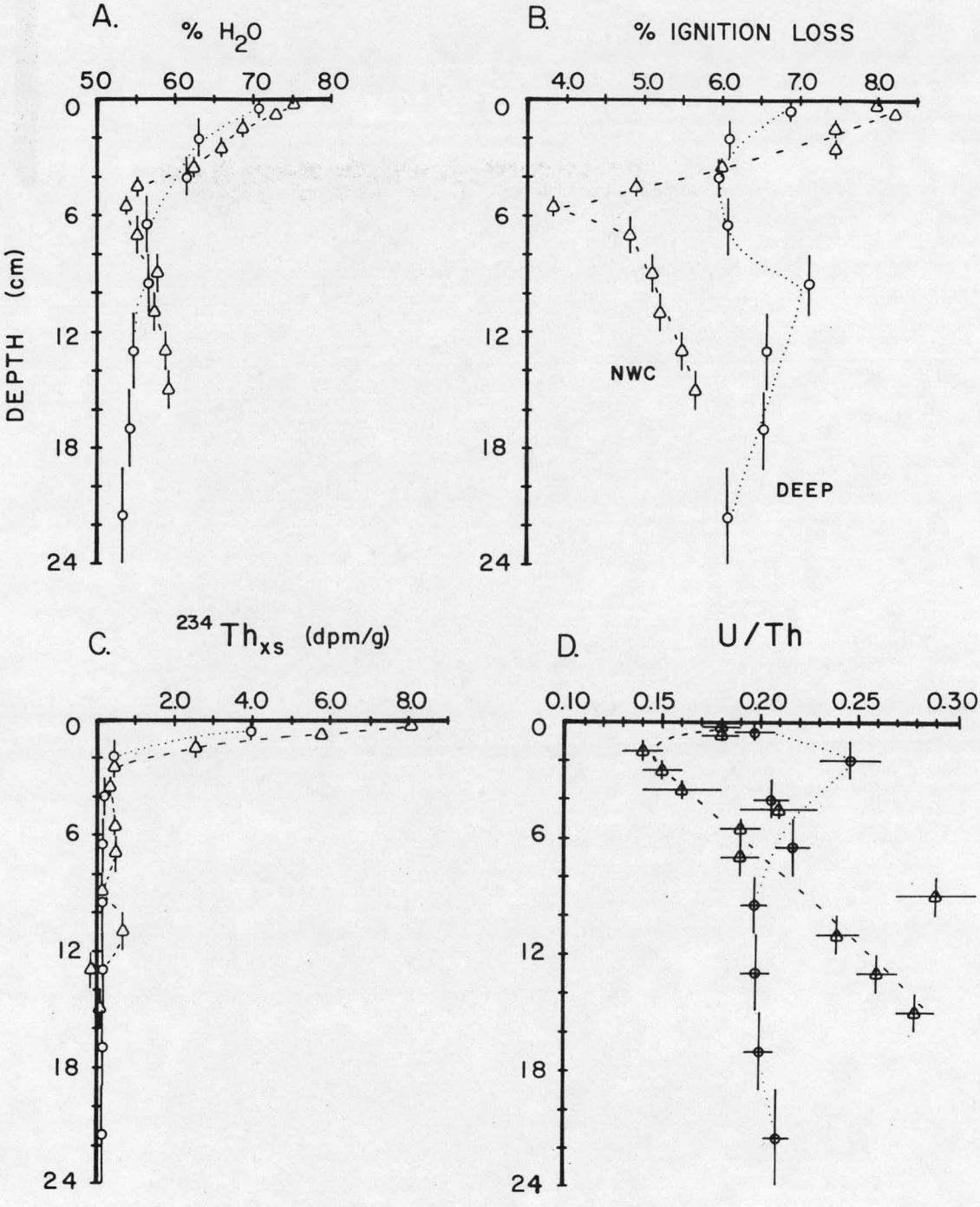

A.
% H_2O
50
60
70
80
0
6
12
18
24
DEPTH (cm)
B.
% IGNITION LOSS
4.0
5.0
6.0
7.0
8.0
NWC
DEEP
C.
$^{234}Th_{xs}$ (dpm/g)
2.0
4.0
6.0
8.0
D.
U/Th
0.10
0.15
0.20
0.25
0.30

Figure IV-5

CHAPTER V

DIAGENETIC PROCESSES NEAR THE SEDIMENT-WATER INTERFACE OF LONG ISLAND SOUND, I: DECOMPOSITION AND NUTRIENT GEOCHEMISTRY (S, N, P)

Chemical diagenesis near the surface of marine sediment is associated directly or indirectly with the decomposition of organic matter. The type, rate, and extent of many diagenetic reactions near the surface zone are thereby influenced by the activities of organisms which live there and utilize the available organic material. Microbial metabolism largely determines limits on the type of compounds available for reaction and the oxidation-reduction properties of the sediment (Baas-Beckling, Kaplan, and Moore, 1960; Berner, 1963). Limits on the rate and extent of reactions may be set by factors external or internal to a deposit. External factors include the delivery of particles and decomposible organic debris to the surface and depend on depositional environment (e.g., Goldhaber and Kaplan, 1975b). Internal factors include transport and supply of electron acceptors or organic material within a deposit (Berner, 1974a). Near the sediment-water interface, macrobenthos are of major importance in either directly or indirectly determining material transport within the sediment body or between sediment and overlying water and also influence the distribution, metabolic rate, and abundance of

micro-organisms (Fenchel, 1970; Hargrave, 1970; Rhoads, 1974; Chapter II, III). Because of this, macrobenthos can be expected to greatly affect diagenetic processes in the near surface zone and reactions in immediately overlying water (e.g., Carriker, 1967). In this report, diagenetic reactions near the sediment-water interface are examined in estuarine deposits of Long Island Sound, U.S.A. Particular emphasis is placed on the role of benthic macro-organisms and on depositional environment in controlling sedimentary diagenesis and sediment-water exchange rates.

The study has been broken into two parts, the first concentrates on describing diagenetic processes involving organic matter decomposition and production or consumption of $SO_4^=$, NH_4^+, alkalinity, and $HPO_4^=$. The second emphasizes the chemistry of Fe and Mn (Chapter VI). Several types of measurements were made: (1) seasonal pore water and solid phase analyses, (2) direct measurement of fluxes out of the sediment, (3) rates of decomposition as a function of depth and temperature and (4) the abundance and composition of the fauna at each station.

Location of study and station description

Three stations from three distinctly different depositional environments in central Long Island Sound were chosen for study (Figure V-1). The stations represent an inshore-offshore environmental and depth sequence. A concise description of these stations is given in Table V-1. The stations have been

passed onto a north-south plane cross-section (Figure V-2) showing both the thickness of marine sediment in this section of the Sound and the relative bathymetry of the stations (Bokuniewicz, Gebert, and Gordon, 1976). No stations were located in the region of highest long term sedimentation rate between NWC and DEEP but the average long term rate is so low, ~0.02 - .06 cm/yr (Bokuniewicz, Gebert, and Gordon, 1976), as to be unimportant in this study.

All stations in less than about 20 m of water are subject to constant resuspension of surface sediment creating highly turbid conditions. During major storms the upper few centimeters at these stations may be eroded and redeposited (Aller and Cochran, 1976; McCall, 1976) but normally only the top 1 mm or so is subject to resuspension (Bokuniewicz, 1976). DEEP station is also subject to resuspension but only through tidal scour and it is considerably lower in turbidity than either FOAM or NWC (Chapter IV).

The bottom fauna in the central Sound have distinct bathymetric patterns in distribution. These patterns are delineated by changes in the relative abundance of animals of certain sizes, life habits, life history, and feeding types in different regions of the bottom and reflect depositional environment and severity--frequency of physical disturbances (McCall, 1976). This allows comparison, in an inshore-offshore transect, of diagenetic processes in sediment inhabited by animals of different feeding groups, life habits and life histories all of which determine the ways in which animals interact with sediment (Chapter I).

Based on direct observation of the bottom on numerous occasions and sieve analyses (≥ 1 mm mesh) of box cores taken at FOAM, NWC, and DEEP (Rhoads, Aller and Goldhaber, 1977; Appendix III) a composite description of the fauna at each station can be made. The fauna at each station are shown schematically in Figures V-3, V-4, and V-5.

FOAM contains a diverse assemblage of infaunal benthos consisting of mixed trophic groups but mostly of deposit feeders. Large numbers of the surface deposit-feeding amphipod Ampelisca sp. are characteristic of this station. During the summer and fall they form dense mats of dwelling tubes at the interface which bind the sediment surface; these are eroded into irregular clumps during the winter at which time the population levels are greatly reduced (Appendix III). Other surface deposit feeders present are the tellinid bivalves: Tellina agilis and Macoma tenta. Deep-feeding bivalves are represented by small numbers of Nucula annulata and Yoldia limatula. Other deep feeders or burrowers are the sedentary maldanid polychaete Clymenella sp. and the highly mobile polychaete Nephtys incisa, both of which burrow to depths > 12 cm. The gastropods: Nassarius trivitatus (deposit feeder) and Retusa sp. (predator) together with the hermit crab Paguris sp. (scavenger) comprise the easily captured mobile epifauna. Suspension feeders include the bivalve Mulinia lateralis and the deep-burrowing (> 25 cm), sedentary polychaete Spiochaetopterus oculatus. FOAM is characterized by the presence of both mobile and sedentary tube dwellers

and dominated by deposit feeders. Most animals are very small in size and, on the basis of direct inspection by diving, vary greatly from year to year in their occurrence. These observations, together with the physical setting, the large numbers of the typical opportunist Ampelisca, and the high diversity of apparently short-lived (small) benthos, all suggest that the FOAM site is highly physically disturbed and in a state of constant colonization by a wide variety of organisms (see criteria of McCall, 1976).

NWC has a relatively stable, low diversity assemblage of organisms characterized by large numbers of the highly active protobranch bivalves Yoldia limatula and Nucula annulata and the errant polychaete Nephtys incisa. These organisms were always present during this study at fairly constant levels (Rhoads, Aller, and Goldhaber, 1977). All are deep-feeding deposit feeders. Other less reliably present fauna include the suspension feeding bivalves: Pitar morrhuana and Mulinia, the suspension-feeding polychaete Spiochaetopterus, and the surface deposit feeders: Melinna cristata (ampharetid polychaete) and small numbers of Ampelisca. Permanent tube-dwelling polychaetes other than Spiochaetopterus are not common but the infaunal anemone Cerianthus americanus, seldom recovered by grabs or samples, is plentiful as observed by diving. Evidence of the deep-burrowing shrimp: Squilla, is also found by diving. Easily captured epifauna are the same as FOAM.

The polychaete fauna at DEEP are generally larger, more sedentary, and deeper burrowing than at either FOAM or NWC. Many form permanent

dwelling tubes. Pherusa affinis, a flabelligerid polycheate, is conspicuous and abundant. Maldanids are also plentiful and are represented by Maldanopsis elongata (not recovered live because of burrow depth > 25 cm but tubes present in abundance) and a Clymenella species which forms Fe-encrusted silt-sand tubes. The teribellid, Pista palmata and the ampharetid Melinna cristata, both sedentary surface deposit feeders, are present. Suspension-feeding polychaete Spiochaetopterus is also present. An occasional proto-branch or tellinid is found but these are rare. Very large, infaunal anemones: Cerianthus are plentiful as is the hydroid Corymorpha . Burrowing activity by Squilla is evident.

Representative x-radiographs of samples taken at each station employing the techniques described under methods are shown in Figures V-6-V-11. These illustrate sedimentary features indicative of the physical and biological conditions effective at each station. The small size and transitory nature of the fauna at FOAM and the intensity of its physical setting is demonstrated by the presence of dense and massive shell lag layers and preservation of physically formed laminations at depth. These layers have been subject to only minor biogenic particle reworking. Dwelling burrows and burrows of vagile fauna, the construction of which at low abundance does not homogenize sedimentary particles, are evident but at low density compared to NWC and DEEP. The shell layers probably obscure many biogenic sedimentary features. Many

of the shells are quite large and are composed of species not common at FOAM, suggesting that physical processes tend to accumulate shell debris in the FOAM area.

At NWC, shell debris is less plentiful and is often aggregated into distinct layers which probably represent biogenic lag layers resulting from feeding (e.g., Van Straaten, 1952; Schäfer, 1962; Rhoads and Stanley, 1965; Aller and Dodge, 1974). No evidence of physically produced sedimentary structure is found and storm laminations which do form are known to be rapidly destroyed by biogenic particle reworking (Aller and Cochran, 1976). The protobranch bivalves present at NWC are responsible for much of the particle homogenization. Despite extensive homogeneous, particle reworking, a high degree of biogenic and physical heterogeneity is present in sedimentary structures as shown by horizontal x-radiographs taken at NWC; an example of which, in addition to a vertical x-radiograph, are given in Figures V-8, V-9. Permanent and temporary dwelling burrows create a complex geometry of biogenic shafts through the upper few decimeters of sediment. Construction of these features together with physical processes make it necessary to average measurements, especially solid phase measurements, over as large an area as possible (e.g., Hanor and Marshall, 1971).

DEEP also lacks evidence of many sedimentary structures formed by physical processes. Dwelling burrows, often at high abundance, extend great distances into sediment and are characteristic of this station (Figures

V-10, V-11). Despite the presence of living shell-bearing animals at DEEP, little shell debris is preserved.

All stations are subject to a sinusoidal variation in temperature during the year with a low temperature of about 2°C in February-March and a high of about 22° in August-September (Riley, 1956a). A summary of bottom temperatures at NWC, taken by inserting a thermometer into the top 1 cm of diver-taken box cores, for the two year sampling period is given in Figure V-12.

Sampling

In order to obtain undisturbed samples of consistently high quality most bottom samples were obtained by SCUBA divers. Three types of hand-held plexiglas box cores were commonly taken. These varied in size and dimension according to the type of analyses for which they were used. One type, termed "chem box," wereused for studying interstitial water and sediment chemistry and has dimensions 25 cm high, 30 cm long, and 7.5 cm wide. Thinner cores, called "x-ray boxes," were used to study biogenic and other sedimentary structures and measured 25 cm high, 30 cm long, and 2.5 cm wide. The third type, "flux boxes," were 30 cm high, 30 cm long and 10 cm wide. All cores are constructed of clear plexiglass and are essentially boxes having removable tops with vent holes and removable bottoms (Appendix I). The bottom edges of the box are sharpened for easy insertion into sediment.

Coring is done by gently pushing the bottomless corer into the sediment to a depth of 10-22 cm in the case of x-ray and chem boxes or 10-15 cm for flux boxes. The vent holes in the top are then sealed with rubber stoppers. After removing sediment from the exterior of one side of the core, the bottom plate is slid under the core and locked into place. Large rubber bands are then strapped around the corer to permanently secure the bottom and the core returned to the surface. If done correctly an undisturbed vertical section of the bottom and its immediately overlying water is obtained. Water overlying the core is clear and surface sediment not resuspended; animals in the cores continue their activity unperturbed. The sealed top and overlying water prevent disturbance of the core during transport by eliminating sloshing action. After recovery, cores were placed in large cooler boxes and returned to the lab for analysis. A specifically designed corer which allowed the taking of horizontal samples in the lab was used to obtain the horizontal x-radiographs (Appendix I).

Gravity cores of ~ 1 m length were taken on one or more occasions at FOAM, NWC, and DEEP. Acetate-butyrate liners 4.5 cm I.D. were used in all cases.

The sampling dates and types of cores taken at each station, for which data are presented, are given in Table V-2. Often more than one core of each type was taken and only the best (e.g., longest, straightest insertion) was used for analysis. In general, box cores were taken in summer, fall and

winter-spring periods at each station and represent times of warmest, intermediate, and coldest water temperature. Sampling was carried out over two year periods at FOAM and NWC and for one year at DEEP.

Methods

Treatment of cores

X-ray samples.--After storing at 4°C, x-ray box cores were x-rayed within several hours of collection by placing an 8" x 10" sheet of Kodak AA Industrial x-ray film on the back and exposing it for ~2.5 min using 60 Kv x-rays at a distance of 60-75 cm. A dental x-ray unit was used. Positive prints of the x-ray negatives were then made. Because of gradients in water content near the surface, positives were often printed so as to reduce the resulting gradient in exposure density in the negative. This does not affect interpretation of structures except by giving better resolution near the interface.

Pore water and sediment samples.--Chem cores were stored in the dark at 4°C for a period of 3-5 hours after collection. Before processing the core, the color stratigraphy, general sediment features, and readily identified animal life were described and recorded. The sides of the box were ruled, using a marking pen, at 1 cm intervals from the sediment-water interface to within 3 cm of the base of the particular core being sampled. Water overlying the core was then rapidly removed using a vacuum line, the core top and fasteners removed, and the entire core placed in a glove bag. This bag was

pumped down and purged several times with N_2 (O_2 free) and subsequent sampling of the core done under a nitrogen atmosphere.

Sediment was removed at 1 cm intervals using plastic spoons, then packed into 10 cm long sections of butyrate tubing (4.5 cm I.D.). Subsamples of sediment were saved for percent H_2O determination. pH and Eh or pS measurements were then made as described below and the tubes sealed with plastic end caps. Care was taken to avoid entrapment of N_2 in the sediment taken from each interval. Degassing is not a problem as shown by comparing values of H_2S concentrations (methylene blue analysis) obtained by this sampling procedure with other methods (Goldhaber et al., 1977). The sediment in these sections is squeezed within a few hours for removal of interstitial water as described below. Samples were stored at 4°C at times when they were not being processed.

Most samples were squeezed within 12 hours but occasionally a few samples were squeezed as late as 24 hours after collection. The method of Kalil and Goldhaber (1973) was used in all cases. After removal from the storage cooler, the 10 cm long butyrate sections were quickly uncapped, approximately 1 cm of sediment scooped out from each end, and glass-fiber filter paper inserted against the sediment. O-ring-sealed end pistons constructed of plexiglas and teflon were seated against the paper. A series of holes and channels allowed passage of pore waters through the piston. The entire assembly was placed in a mechanical press. Water was forced out of both ends

of the section at pressures $\geq$ 200 psi and passed through in-line Millipore filters (0.45 μm pore size) directly into syringes. The first $\sim$5 ml of expressed water at each end was discarded to avoid air contamination. In the case of summer and fall samples, the sediment was allowed to warm to room temperature before squeezing. The winter 1975 samples were squeezed immediately after removal from the refrigerator; winter 1976 samples were squeezed at 4°C using the cooling units described by Kalil and Goldhaber (1973).

Gravity cores were processed in the same way with two differences. The core was sectioned into 10 cm intervals in a miter box using a hack saw. When sections were squeezed, water taken from each end was either kept separate and assigned to different 5 cm intervals or combined into a single sample.

Pore water samples were treated in the following way: 10 ml of water was passed from a syringe through a short section of tygon tubing into a 10 ml pipet. This pipet was drained into a beaker and the water acidified for $SO_4^=$ analysis. A second 10 ml sample from the same depth interval was immediately passed into the same pipet and this sample was drained into an acid washed and H_2O rinsed 2 oz polyethylene wide-mouth bottle. The total transfer time was only slightly greater than the drain time of the pipet ($\sim$30 sec). This sample, which was sometimes 15 ml in size as well (a separate pipet used), was titrated for alkalinity and acidified within 48 hours (occasionally

72 hours) in the same 2 oz container. After acidification it was used for Fe and Mn analysis as described in Chapter VI, and in some cases Ca. A 2 ml sample for Cl^- was taken in the same way (1975-1976 samples only) and pipeted immediately into a glass vial for later titration in that same vial. Separate samples were taken for $HPO_4^=$, NH_4^+, and in some cases H_4SiO_4 (not discussed in this report) and H_2S analysis. Samples for $HPO_4^=$ and NH_4^+ were kept in sealed, air-free syringes and placed immediately into a 4°C refrigerator for storage. These were analyzed, or fixed in the case of NH_4^+, within 24 hours. Extra pore water was stored in sealed syringes in the refrigerator for possible use in any later analyses.

The sediment cake which resulted from squeezing was retained in its butyrate tube, sealed with end caps and placed in a freezer for later analysis of the solid phase. Ignition loss, percent $CaCO_3$, acid volatile sulfide, and total non-volatile sulfur were measured on many samples. Fe, Mn, and Cu determinations were also made (Chapter VI).

Flux samples.--Two flux boses were always taken (1975-1976 only); one contained only bottom water and acted as a blank, the other was filled with 10-15 cm of undisturbed bottom sediment and its overlying water. Both summer (1975) boxes were kept at 22°C, fall flux boxes at 15°C, and winter at 4°C. The original FOAM fall flux box developed a leak so that a second flux core was taken 12 days later as a replacement. Processing of these boxes consisted of withdrawing water samples from each box at successive

times and following the change in overlying water concentrations of selected, dissolved ions. The total initial overlying water volume was determined and volumes removed at each sampling were measured. By correcting the concentration changes for volume differences between one sampling and the next, a flux of a given ion out of the sediment could be calculated as described below. The summer and fall boxes were periodically aerated. Sampling of overlying water was continued for up to 2 days in the summer and fall cores and for up to 7 days in the case of winter cores.

Water samples were obtained by inserting a section of tygon tubing attached to a syringe into a box and withdrawing a sample. This water was immediately filtered through 0.4 μm pore size Nuclepore filters directly into acid cleaned sample bottles. The contents of one bottle was acidified with HCl and one bottle was left unacidified and placed immediately into a refrigerator at $4^{o}C$. The acidified samples were later analyzed for Fe and Mn and the unacidified samples for NH_4^+ and $HPO_4^=$. pH and Eh of the water were occasionally checked by insertion of the appropriate electrode into a water sample.

After water sampling was complete, sediment in the flux boxes was sometimes sieved through a 1 mm mesh sieve for the contained animals. This was done at DEEP and FOAM for fall 1975 and winter 1976 samples and at NWC for winter 1976. Regular sampling of fauna at NWC (Rhoads, Aller, and Goldhaber, 1977; Rhoads, 1976) made sieving of most flux boxes at

that station unnecessary. Based on this regular sampling, fall and winter samples should give the maximum ranges found in the abundance and kinds of animals at a given station.

Decomposition experiments

Rates of decomposition as measured by rate of sulfate reduction or ammonia production were estimated as a function of depth in the sediment. This was done by sealing sediment samples from a given depth interval into a number of glass containers and incubating these samples under an anoxic (N_2) atmosphere. The progressive changes in sulfate and ammonia pore water concentration, as measured by opening containers and analyzing samples from a given depth serially through time, is used to calculate rates of utilization. This approach has been employed by many investigators (e.g., Gunkel and Oppenheimer, 1963; Nakai and Jensen, 1974; Martens and Berner, 1974; Goldhaber et al., 1977).

At FOAM, these experiments were done by Goldhaber et al. (1977) and were carried out at a temperature of 22°C. At NWC, sediment collected using two Chem boxes was sampled in a glove bag at depth intervals of 0-1, 1-2, 2-3, 5-6, and 9-10 cm. The samples from the two boxes were then combined for a given interval, and sealed into large screw cap culture tubes. Macrofauna were removed from the sediment samples. These tubes were placed into larger, nitrogen-filled containers for incubation. One set of

samples was stored (in dark) at 22°C and another set at 4°C. A similar set of samples was obtained for DEEP and incubated at 22°C.

At various times, tubes representing different depth intervals were placed in a centrifuge and the pore water separated out. This water was removed using calibrated Eppendorf pipets and analyzed for sulfate and ammonia; usually 5-10 ml of water were available for analysis. These experiments were set up and carried out in conjunction with Dr. J. Yingst who assayed for ATP and organic matter contents in the sediment samples.

Analytical techniques

General.--Weight percent water was determined by drying samples to constant weight at 80°C. No salt correction was made.

pH and pS or Eh measurements were made in the glove bag by inserting the appropriate electrode directly into one end of the 10 cm squeezing section; electrodes were passed into the bag through a sealed port. The sediment immediately surrounding the electrodes was discarded before squeezing. A rugged, combination glass electrode with calomel reference was standardized at pH 7.414 and 7.0 and used for pH. Platinum (cleaned) and silver sulfide electrodes were used for Eh and pS measurements relative to the calomel reference of the pH electrode. The sulfide electrode was calibrated as described by Berner (1963). Both pH and pS came to stable readings in the time allowed; Eh did not, but it was not changing rapidly when readings were taken.

Pore water.--The acidified sample for $SO_4^=$ analysis was diluted with 50-75 ml of distilled water and heated to scalding hot. Ten ml $BaSO_4$ (10% w/v) was added and the resulting precipitate was allowed to cool and digest for at least 24 hours. The precipitate was filtered onto preweighed 25 mm Millipore filters (0.45 μm pore size), dried under a heat lamp, and weighed. The molarity of $SO_4^=$ in the original sample was then calculated from the appropriate gravimetric factor. Precision of analysis is ± 0.5 mM.

Reactive phosphate was determined by a slightly modified molybdenum blue method (Strickland and Parsons, 1968; Presley, 1971). Precision of analysis was better than 3%. Standards were periodically made up and absorbance readings of these standards were the same throughout this study.

The phenol hypochlorite (Indophenol blue) method was used for ammonia analysis (Solorzano, 1969). Appropriate sample sizes were fixed with phenol within 24 hours of collection (Degobbis, 1971) and stored at all times at 4°C. Analyses were made within 2 weeks of collection. The reagent dilutions given by Presley (1971) were used but the quantity added was doubled. All reaction and color development was done in polyethylene scintillation vials. Color development was allowed for 6-8 hours to obtain a straight line standardization curve; blanks (always < 0.010 absorbance with respect to distilled water) were insignificant compared to sample absorbances and precision better than 3%. Standards were diluted immediately before use.

Total alkalinity was determined by titration with standardized 0.1 N HCl (Fisher) using a Gilmont micrometer buret and a micro-combination electrode (Gieskes and Rodgers, 1973). The sample was titrated to pH = 5 and allowed to degas until pH drift was minor or absent. At high alkalinities, titration to pH ~5 was sometimes done more than once. After degassing the sample was titrated to the end point (0.002 ml steps) and the alkalinity determined by curve inflection which was always exceedingly sharp. Precision of analysis was ~ 1% based on overlying water samples.

Chloride was done by titration with $AgNO_3$ using starch-fluorescine indicator. $AgNO_3$ was initially gravimetrically standardized and inter-calibration between sample sets checked by titration of standard Long Island Sound sea water which had been sealed in glass ampules (courtesy L. Benninger).

Ca analyses were made using atomic absorption spectrometry. A K-La buffer was used. Total precision is about 3%.

Solid phase

Weight loss on ignition at 475°C for 6 hours was measured on sediment samples after drying to constant weight at 80-100°C.

$CaCO_3$ was estimated on ashed sediment samples by measuring weight loss after leaching with dilute HCl (e.g., Molnia, 1974).

Acid volatile sulfide was determined on sediment cakes as follows. The frozen sample was thawed slightly and a portion of the center of the

cake away from any oxidized exterior taken for analysis. This was weighed, placed in a reaction vessel and covered with distilled water. Nitrogen was passed through the chamber to clear out oxygen; gas passed successively through the sample vessel, into a pH = 4 buffer trap, and then into a $AgNO_3$ trap. After clearing the line of air, 10 ml of 12 N HCl was slowly added to the sediment sample by use of a syringe mounted on the reaction vessel. The sample was vigorously agitated throughout by use of a vortex mixer. H_2S released from the sample was precipitated as Ag_2S in the $AgNO_3$ trap. The precipitate was filtered onto preweighed Millipore filters (0.45 μm pore size) and weighed. The percent or μmoles/g acid volatile S in the sample was then calculated. A separate sample of the cake was used to find percent H_2O of the sediment and correct the measurements to dry weight. Both Pruden and Bloomfield (1968) and Berner (1974b) have suggested that Fe^{+++} released from the sample will greatly decrease (up to 50%) the amount of released H_2S due to oxidation of H_2S to S^o. Pruden and Bloomfield found no significant effect up to Fe^{+++} concentrations of 50 mg in a sample. They suggest adding 2 g of $SnCl_2$ to samples to prevent this reaction. Unfortunately, before discovering their work, initial experiments with hematite and CdS showed no difference between samples with or without added $SnCl_2$ so it was thought any interference by Fe^{+++} would be minimal and $SnCl_2$ was not used in the natural samples. It is possible that the use of cold reaction conditions and hematite decreases interference because of lower Fe^{+++} release. In any

case, $SnCl_2$ was not added to the samples and the results may be low. Standard yields were > 90% and results precise to within ~10%.

Total sulfur, expressed as pyrite, was determined on the rinsed and dried samples left from the acid volatile sulfur runs. A Leco Induction furnace was used. Sulfur oxide gases released from the burning samples were trapped in 3% H_2O_2 solution, the solution filtered, and $SO_4^=$ content determined as described previously for pore water samples. Yields of 84 ± 5% were obtained by twelve determinations of natural FeS_2 and synthetic PbS having four different grain sizes; all samples were corrected to 100% yield using this factor.

Results

Decomposition experiment

The rate of sulfate utilization as a function of depth in the sediment was obtained by first plotting the sulfate concentration found in each decomposition jar series versus time and then calculating the slope of the line which fit the data by least squares methods. Plots of sulfate concentration versus time for each depth interval are shown in Figures V-13, V-15 and the slopes of the lines plotted against depth in Figure V-16. The earlier results of Goldhaber et al. (1977) for the FOAM site are also plotted for comparison. Only the top three depth intervals at NWC gave measurable rates of decrease at 4°C

over a one year period; these rates are plotted together with results obtained at 22°C.

Both FOAM and NWC are characterized by exponentially decreasing rates of sulfate reduction with depth. DEEP has an initial drop in rate in the first few centimeters then levels off and even shows an increase in rate by the 9-10 cm interval. Rates near the interface are lower at DEEP than either NWC or FOAM while rates at depth are higher than either NWC or FOAM. NWC experiments produced the highest rates found at any of the stations.

In the 0-1 cm interval experiments from both NWC and DEEP, an initial gestation period was found during which no detectable reduction of sulfate concentration took place followed by an extremely rapid decrease. This period may correspond to initial consumption of remaining O_2 prior to the start of sulfate reduction or to reoxidation of H_2S. This illustrates that in the top 0-1 cm at least; these experiments may not be representative of in situ rates.

According to the ATP data of J. Yingst, after an initial rapid drop in ATP concentration during the first few days in samples from 0-1 cm and a less precipitous drop in ATP from samples taken from 1-2 cm both of which can be attributed to death of mieiofauna, the ATP concentrations stay constant in all samples from each depth through time. The 4°C experiments show a very slow decrease in ATP over a one year period. These data indicate that bacterial populations remain representative at least in biomass, of in situ

conditions during the course of the experiment.

Because of the smooth form of the decrease with depth at FOAM and NWC, an exponential function can be used to describe the depth dependence of the data. An exponential function which fits the data at NWC (22°) is:

(1) $R_s = 129\, e^{-0.33x}$

where R_s = rate of sulfate reduction in mM/yr at a given depth in the upper 10 cm. Goldhaber et al. (1977) found at FOAM that:

(2) $R_s = 81\, e^{-0.24x}$

At DEEP, the data can be reasonably represented by a function similar to that often used to describe porosity:

(3) $R_s = 27.3 + 26.6\, e^{-0.71x}$

The temperature dependence of sulfate reduction has been shown to be exponential (Vosjan, 1975). Using the NWC data from 4° and 22° an apparent activation energy or coefficient of temperature dependence can be calculated. Apparent activation energies of 20, 18, and 18 Kcal/mole (Q_{10} = 3.4, 3, 3) are calculated for the depth intervals 0-1, 1-2, and 2-3 cm, respectively. NWC sediment was collected at 4°C. Goldhaber et al. (1977) found 25 Kcal/mole for salt marsh sediment (collected at 20°C) and Vosjan (1975) calculated 22 Kcal/mole from data obtained from isotopic measurements in North Sea sediments. These are all in reasonable agreement and are in the

appropriate range for enzymatic reactions (e.g., Hoar, 1966).

Ammonia production is also linear with time in the decomposition experiments and has a depth dependence similar to sulfate reduction (Figures V-13, V-15, V-17). Because of adsorption of NH_4^+ on particles these rates must be corrected to account for adsorption loss (e.g., Rosenfeld and Berner, 1976). NH_4^+ adsorption can be described adequately by linear adsorption isotherms with an adsorption coefficient: $K \sim 1$ (Rosenfeld, in preparation). The rates of NH_4^+ production, R_N, as determined are actually $R_N/(1 + K)$. When NH_4^+ production rates are referred to as R_N in this study it is assumed that an adsorption correction using $K = 1$ has been made, otherwise $R_N/(1 + K)$ will be used to describe the raw data.

The ratio of R_s/R_N changes with depth at NWC and DEEP, becoming higher in samples taken from deeper intervals. This phenomena appears to correlate both with R_s and depth in sediment as can be shown by comparing sulfate reduction/ammonia production rate ratios from the 4° experiments at NWC and from the 22°C data at DEEP with the ratios from 22° at NWC. Slower rates of sulfate reduction are associated with high rate ratios regardless of depth. Data from NWC 22° are plotted in Figure V-18 to illustrate this correlation. Because of the high scatter in rate ratios at low rates of sulfate reduction, data from the other experiments have not been plotted.

The depth dependence of ammonia production rates in the upper 10 cm at NWC can be described by the equation:

(4) $R_N/(1 + K) = 23\, e^{-0.405x}$ mM/yr (22°C)

At DEEP the form of this equation must be modified as done above for R_s, to give:

(5) $R_N/(1 + K) = 1.7 + 6.9\, e^{-0.55x}$ mM/yr (22°C)

The production rates of NH_4^+ at DEEP, like $SO_4^=$ reduction rates, are generally lower than at NWC but less sharply attenuated with depth in sediment.

Pore water results

Gravity cores.--Sulfate, ammonia, phosphate, and alkalinity profiles over the top meter or more of sediment at each station are shown in Figure V-19. Note that season of collection may differ between stations (Table V-2). The FOAM site has the greatest decrease in sulfate concentration with depth and the expected associated increases in ammonia, phosphate, and alkalinity. [Many additional gravity core data from this station are given in Goldhaber et al., 1977.] Evidence for sulfate reduction and mineralization of organic matter becomes less evident from gravity core pore water data with distance offshore. NWC has a minor decrease in sulfate and regular minor increases in ammonia, phosphate, and alkalinity with depth. DEEP has no evidence of sulfate decrease and no increase in alkalinity, phosphate, or ammonia with depth after an initial increase above sea water values. Both NWC and DEEP have minima in the alkalinity and phosphate profiles which occur at depths

of 15-20 cm at NWC and 20-30 cm at DEEP. Ammonia does not show a definite minimum at the same depths but is nearly constant on either side of the respective depth interval at each station. In addition, at DEEP a slight decrease in concentrations of alkalinity, phosphate, and ammonia below 80 cm occurs.

Ca^{++} levels are on the average at sea water values except at FOAM where there is an unambiguous decrease in dissolved Ca^{++} with depth (Figure V-20). This decrease was documented previously by Graber (1975) using different analytical techniques.

Box cores.--All stations are characterized by an upper zone of approximately constant sulfate concentration (Figures V-21-V-23). At FOAM this zone varies seasonally, ranging from a few centimeters to greater than 16 cm, and is deepest in the fall. At NWC and DEEP, the zone runs essentially the length of the cores at all times with a possible exception during summer at DEEP. Summer samples from NWC-1 are irregular and are considered bad data due to faulty analysis.

A regular pattern of seasonal change in alkalinity, ammonia, and phosphate concentration profiles occurs at all stations (Figures V-24-V-32). Seasonal changes are most easily delineated at NWC and will be examined first. During the summer, the concentrations of alkalinity, ammonia and phosphate at NWC are the highest of the year (Figures V-25, V-28, V-31). Concentrations at this time show a tendency to increase rapidly as the interface is

approached then drop suddenly in the top one to a few centimeters as sea water concentrations are intersected, producing a maximum value a few centimeters beneath the interface. Fall concentrations are lower at all depths sampled than summer but remain higher than sea water values even in the top centimeter. The winter profiles show a steady decrease in concentrations as the interface is approached and in the upper few centimeters become closest to sea water values of any time of the year.

There are some minor but important differences between the profiles of the three properties at NWC. Structure in the alkalinity profile is small because the values are very close to sea water in magnitude, nevertheless the seasonal pattern described is evident. Ammonia most clearly follows the seasonal pattern of change. Concentration maxima are produced in summer cores NWC-1 and NWC-4; these are absent and concentrations uniformly low with depth in fall cores NWC-2 and NWC-5. Convex-upward profiles decreasing smoothly toward the interface occur in winter cores NWC-3 and NWC-6. In all summer and fall cores, the ammonia concentrations are about 100 times sea water in the top 0-1 cm interval giving the impression of a discontinuity between sediment and overlying water concentrations; this discontinuity effect is absent in winter cores. Phosphate profiles follow the general seasonal pattern but differ from ammonia profiles in that phosphate concentrations decrease regularly near the interface in fall cores and during the winter decrease with a linear or slightly concave-upward profile rather

than convex-upward as does ammonia (NWC-2, 3, 5, 6).

FOAM follows the same general time sequence and pattern of change in pore water concentration profiles as NWC but with several important differences (Figures V-24, V-27, V-30). The high pore water concentrations at FOAM allow alkalinity to more clearly reflect seasonal patterns. These high values also obscure any summer increases near the interface; no distinct maxima occur in summer FOAM cores except for phosphate in FOAM-1 (ammonia was not measured in FOAM-1). FOAM-3, the second summer core, more closely resembles a winter core than the previous summer core FOAM-1, but it does have the summer characteristic of relatively high values of alkalinity and ammonia in the upper few centimeters compared to later times of the year. The fall core, FOAM-4, has low, constant values in the upper 0-13 cm; a feature typical of fall cores at NWC. Concentrations begin to increase below this zone of relatively constant concentration. Both alkalinity and ammonia have convex-upward concentration profiles during winter (FOAM-2, FOAM-5) which decrease smoothly to low values near the surface, while phosphate profiles are distinctly concave-upward.

At DEEP, the highest concentrations of alkalinity, ammonia, and phosphate near the sediment surface occur during summer (Figures V-26, V-29, V-32). These drop to lower values throughout the profile during the fall and remain low near the interface in the winter but increase in the deeper sections of the profile at that time. Like NWC, alkalinity is near sea water

values at DEEP. The discontinuity between ammonia concentration in the upper few centimeters at DEEP is not as great as either NWC or FOAM. Phosphate profiles, like the FOAM site, are concave-upward during winter and at this station also in fall.

At all three stations Ca^{++} increases during the winter above sea water Ca^{++}/Cl^{-} ratios near the interface (Figure V-33). This is particularly evident at FOAM where a distinct Ca^{++} maximum is found. At other times of the year Ca^{++} is not distinguishable from sea water background levels at any station except possibly NWC.

Flux measurements

No significant change in concentration of NH_4^+ and $HPO_4^=$ in the flux boxes without sediment (blanks) relative to flux boxes with sediment were found at any time so fluxes were calculated as follows. The concentration of either ammonia or phosphate at time of first measurement in the blank box, C_o, was determined. The volume of water overlying the sediment in the sediment flux box at a given time, V_t, and the concentrations, C_t, of ammonia or phosphate in that water at the same time were also measured. The quantity $V_t(C_t - C_o)$ was then plotted versus time, t, a line fit to the data by least square methods and the amount of material entering the water per unit time determined as the slope. This number was divided by the surface area sampled by the flux box to calculate the flux of material out of the sediment per unit area--time. The error is taken as the

standard deviation of the slope. Usually four or more points were used.

In general, ammonia followed the straight line fit rather well. Phosphate did not in all cases; when iron flux was high or iron precipitation took place in the box (Chapter VI), phosphate levels showed little or negative change.

Tabulations of the flux data are in Appendix V. Plots of the NWC measurements are shown in Figure V-34 to illustrate the trends and the calculated fluxes for each station during the year are listed in Table V-3 together with the temperature at which they were determined. The highest fluxes were found in the summer boxes and the lowest in the winter. Winter fluxes are an order of magnitude lower than those found in summer or fall. The N/P flux ratio varies at the three stations; it is highest at FOAM and lowest at DEEP. Seasonal variation in the ratio also occurs with the lowest ratio during the fall at any given station.

Solid phase analyses

Ignition loss measurements for the three stations are plotted in Figure V-35. FOAM is lowest in percent ignition loss even when corrected on a carbonate free basis. DEEP is next with values between 5-6% with most about 6%. Neither FOAM nor DEEP have much depth dependence in ignition loss profiles. NWC has the highest values near the interface of any of the stations. The profiles at NWC also show depth dependence with decreasing

values at deeper levels in the sediment. Ignition loss is proportional to organic matter content but may not be readily converted to percent organic matter values in fine grained sediment due to water loss from hydrated particles,although Dean (1974) demonstrates a good direct comparison between ignition loss and percent organic matter in silt-clay sediments.

Acid volatile sulfide profiles at each station all show maxima 4-6 cm below the interface then decrease to background values at depth (Figure V-36). DEEP has the largest maximum of any of the stations at about 30 μmoles/g. Three cores were analyzed at NWC. All three have maximum acid volatile sulfide at 4 cm and appear to decrease in a similar way at depth (Figure V-37). The main differences between the three cores is in the upper 3 cm samples. The winter core contained no acid volatile sulfide in the 0-1 cm sample; the silver nitrate trap did not show even a hint of discoloration. The 1-2 cm sample from the winter core is also lower than that found in either of the others. The fall core has the highest near interface values of acid volatile sulfide of any time of the year.

Non-volatile (pyrite) sulfur profiles differ at the three stations. FOAM (after Goldhaber et al., 1977) has the highest values of pyrite sulfur, followed by NWC, and the lowest values at DEEP (Figure V-38). At all three stations pyrite increases away from the interface and, at all three, measurable levels are found at the interface. Pyrite sulfur shows little evidence of seasonal change as determined at NWC although there is a

possibility of slight decreases near the interface in fall and winter relative to summer (Figure V-39). Profiles over the upper meter of sediment from the offshore central Sound show little increase in pyrite sulfur after the top 10 cm (Berner, 1970), so these data can be considered representative of the fixed sulfur concentrations and profiles at each station.

Discussion

The pore water, solid phase, and flux data indicate that diagenesis is non-steady state on an annual basis but predictable at each station and that an annual pattern of change occurs in many properties which is repeatable in major features from year to year. There are many similarities between areas both in the general type of diagenetic reactions taking place and in the sequence of change in sediment properties through time. There are major differences as well, particularly in the way in which the products of organic matter decomposition: HS^-, $HPO_4^=$, HCO_3^-, and NH_4^+, build up in the sediment and the magnitude of release of these products into overlying water. These similarities and differences reflect similarities and differences in physical, chemical, and biogenic processes of production, consumption, and transport influencing the decomposition and remineralization of organic material in each region. By considering the relative contribution of these processes at different times of year and in different bottom areas, it is possible to derive a consistent explanation for the temporal and spatial patterns observed.

Decomposition reactions

The abundance of fixed sulfur in the solid phase and the presence of dissolved sulfide (Appendix IV) are evidence that sulfate reduction is taking place at each station. Sharp decreases in NO_3^- concentration in the upper 1-3 cm (Figure V-40, Rosenfeld, personal communication) also demonstrate denitrification. Because of the low concentration of NO_3^- in overlying water (1-15 μM) and the restriction of denitrification predominantly to the top 0-1 cm, the products of this reaction are rapidly lost from sediment and do not greatly influence the standing concentration of decomposition products in pore water. Additional decomposition reactions involving aerobic metabolism, sulfide oxidation or specific interaction with Fe-Mn oxides near the interface almost certainly occur (Chapter VI) but, like denitrification, should not greatly influence the build up of nutrients below the surface. Fermentation must also take place as argued for other sedimentary environments (e.g., Presley and Kaplan, 1968). Despite this range of possibilities, sulfate reduction is probably the chief pathway of organic matter breakdown in the sediment zone under consideration as argued previously for the FOAM site alone (Goldhaber et al., 1977). This conclusion is consistent with the observed diagenetic trends and previous studies of marine sediments (Goldhaber and Kaplan, 1974; Jorgenson and Fenchel, 1974; Jorgenson, 1977).

Decomposition of organic material by sulfate reducers can be described in a general way by the reaction (Richards, 1965):

$$(6) \quad 6(CH_2O)_x (NH_3)_y (H_3PO_4)_z + 3x(SO_4^{=}) \rightarrow 3x(H_2S) + 6x(HCO_3^{-})$$

$$+ 6y(NH_3) + 6z(H_3PO_4)$$

where the subscripts x, y, and z define the stoichiometry of the metabolized fraction of organic matter at any given time or depth in sediment (Sholkovitz, 1973). At normal pH values of sediment, the products of this reaction exist as HS^{-}, HCO_3^{-}, NH_4^{+}, and $HPO_4^{=}$ (Kester and Pytkowicz, 1967; Berner, Scott, and Thomlinson, 1970; Goldhaber and Kaplan, 1975a). As mentioned above, HCO_3^{-}, NH_4^{+}, and $HPO_4^{=}$ may be released by decomposition pathways other than sulfate reduction; additional complications of this model equation are that the assumed oxidation states of C in products and reactants need not always apply (e.g., Goldhaber, 1974). Despite these possible problems, the reaction as written is a useful conceptualization of decomposition and will be used as a basis for interpreting the general features of the three stations.

The supply of organic material

Of the three environments, the near shore station FOAM shows the greatest evidence of sulfate reduction as expressed by depletion of sulfate pore water concentrations and the production of high concentrations of alkalinity, phosphate and ammonia (Figures V-19, V-24, V-32.

Evidence for sulfate depletion and mineralization of C, N and P as expressed in pore water profiles (Figure V-19) decreases with distance from the Connecticut shore and with depth. This trend could quite reasonably be due to a change in the supply of organic material to bottom sediments, either quantity or quality, as a function of depositional environment. Ignition loss measurements demonstrate that the quantity or content of organic matter at each station in any given sediment depth interval does not greatly differ and if anything is lowest at FOAM where evidence of sulfate reduction is greatest (Figure V-35).

The susceptibility or quality of the organic matter present at each station for use by sulfate reducers can be compared by considering the laboratory decomposition rates as an assay for metabolizable organic matter and comparing rates between stations. Since the depth distribution of particle-associated metabolizable organic matter is determined by particle transport processes at each station (Chapter II, III and as discussed below), the average value for sulfate reduction rate over the top 10 cm rather than the surface value is most appropriately compared. These values are obtained by integrating the functions describing the rate distributions (22°C): FOAM: $R_s = 81\, e^{-.24x}$ (Goldhaber et al., 1977); NWC: $R_s = 129\, e^{-.33x}$; and DEEP: $R_s = 27.3 + 26.6\, e^{-.71x}$; giving average rates of $\bar{R}$ = 30, 36, and 31 mM/yr respectively over the top 10 cm at each station. These are very similar, suggesting that the type of organic matter, in the sense of its ability to

support sulfate reduction, is not greatly different in different regions of the central Sound. (The entombment of meiofauna in the experimental jars may influence the exact rate that is calculated but would not change the conclusion that the quality of available organic material is similar at all stations.)

These considerations lead to the conclusion that to a first approximation the quantity (standing crop) and quality of organic matter at each of the three stations is nearly the same. The rate of supply of organic material also cannot differ much if it is assumed that a constant proportion of the flux of organics hitting the interface at each station must remain as refractory residue and therefore is reflected in the standing crop. Taken at face value, the data indicate that if anything FOAM is the least productive of the three stations.

Products of decomposition, solid phase

The sulfide produced by reaction (6) reacts rapidly with iron rich particles to form the acid volatile sulfides: mackinawite and greigite (Berner, 1967; Rickard, 1974). These labile sulfides represent transient intermediates which, if conditions are appropriate, commonly convert through several possible mechanisms to pyrite (Berner, 1970; Sweeney and Kaplan, 1973; Rickard, 1975). Acid volatile sulfides (FeS) readily oxidize back to Fe^{++} and $SO_4^{=}$ if exposed to oxygen (e.g., Bloomfield, 1972; Chapter VI), while pyrite oxidizes much more slowly in sea water (Harmsen, 1954) but

is also lost at a measurable rate of ~ 50 μmoles S/g-yr from oxidized LIS surface sediment (Chapter VI). (This means that assuming a constant loss rate, roughly half of the standing pyrite content of LIS surface sediment could be lost each year due to oxidation.)

The standing crop of FeS at any given depth in sediment represents the balance of the relative rates of formation (HS^- production, reaction with Fe) and loss (conversion to pyrite, oxidation to Fe^{++}, $SO_4^=$) taking place at that depth. The similarity in the general shape in depth distributions of FeS at the three stations (Figure V-36) indicate that the ratio of formation to loss rates as a function of depth at each station is similar.

There are several important differences as well. FOAM has a higher concentration of FeS at the interface than either NWC or DEEP (Figure V-36). This occurs despite the similarity with NWC in the depth distribution of potential sulfate reduction rates and the obvious presence of O_2 as shown by the general orange-yellow color of surface sediment at FOAM. The reason for this difference can be seen immediately by looking at x-radiographs taken at the three stations (Figures V-6 -V-11). Because of physical and chemical processes operating at FOAM, shell debris is abundant there but not at NWC or DEEP. These shells promote protective microenvironments for the formation and preservation of FeS right to the interface. This can be substantiated qualitatively by removing articulated bivalve shells (e.g., Mulinia) from near surface sediment, opening them and noting the characteristic black color

indicative of FeS in the entrapped sediment.

The seasonal change in near interface levels of FeS at NWC (Figure V-37) demonstrates that loss outstrips supply of FeS in the top 1-2 cm during the winter. It also demonstrates that FeS is formed in or supplied to this same near interface zone during other times of the year. Net loss during the winter probably occurs for several reasons: (1) rate of formation of FeS is lowered because of lowered production of HS^- during cold periods, (2) rate of supply of FeS-rich particles from depth by biogenic reworking is also reduced during the winter (Aller and Cochran, 1976; Chapter I), and (3) oxidation of FeS, which can take place inorganically, continues at a rate which, although slower than during warmer times, is still capable of lowering the standing crop of FeS. These same changes presumably occur in all regions of the Sound during the winter. Small changes in the shape of the profile at NWC will be discussed under biogenic transport below.

The acid volatile sulfide profiles provide an added check on the previous assertion that rates of sulfate reduction are not greatly different at the three stations and if anything are higher in deeper water. Evidence for similar rates of HS^- production comes from the approximately equal maximum value (4-8 cm) and standing crop of FeS in the top 0-10 cm in each area. Reactive iron does not differ significantly between the three stations (Chapter VI) and is in excess so that the rate of FeS formation should be determined for the most part by HS^- production. Of the three stations, DEEP appears

to have the highest rate of FeS formation based on standing crop arguments only; this is in contrast to its pore water profiles which show little evidence for sulfate reduction. Comparison of standing crops of FeS is not entirely valid because loss terms due to conversion to pyrite or reoxidation may differ at the three stations. As shown below, examination of loss terms indicate that the above conclusion of equal or only slightly higher rates of FeS formation offshore compared to FOAM is conservative.

The similarity in FeS profiles spatially in the Sound is in contrast to obvious differences in FeS_2 distributions in the shallow to deep water transect (Figure V-38). The basic form of the FeS_2 distribution at each station is nearly the same: a zone of relatively low, constant FeS_2 values overlies a zone of relatively high, constant values, but, the quantity of pyrite present is not the same. DEEP, which has the highest standing crop of acid volatile sulfide, has the lowest pyrite content.

Pyrite is present at the sediment-water interface at all stations as found in previous studies (Harmsen, 1954; Berner, 1970; Sweeney and Kaplan, 1973; Goldhaber and Kaplan, 1974). Because of the slow oxidation rates of pyrite in sea water (Harmsen, 1954; Chapter VI), the presence of pyrite at the interface is not necessarily indicative of formation there; biogenic particle transport, as discussed later, is fully capable of redistributing pyrite. The rapidly mixed zone at NWC is ~ 4 cm (Aller and Cochran, 1976; Chapter IV) a thickness which is quite similar to the zone of relatively constant

pyrite values overlying the region of higher concentration at that station. The slight decrease which occurs in this homogeneously reworked zone (Figure V-39) is added evidence of a small amount of continuous reoxidation of pyrite.

The discrepancy between the relative rates of sulfate reduction, FeS standing crops, and the resulting quantity of pyrite formed at each station may be due to several processes acting alone or in concert: (1) the rate of conversion of FeS to FeS_2 may differ, (2) FeS may be reoxidized prior to pyrite formation, or (3) FeS_2 may be oxidized after formation. Rickard (1975) demonstrated that the initial rate of formation of pyrite in aqueous solution at low temperatures could be described by the equation:

$$(7) \qquad \frac{d(FeS_2)}{dt} = k\,(FeS)^2\,(S^o)\,(P_{H_2S})$$

Assuming that a similar relation roughly describes pyrite formation in the upper 10 cm of sediment at the three stations, it is concluded that rates should be approximately equal at NWC and DEEP. FOAM should have higher rates only in sediment deeper than ~8 cm where P_{H_2S} increases rapidly (see pS data Chapter VI, Appendix IV; H_2S data of Goldhaber et al., 1977 at FOAM). Rate of conversion of FeS to FeS_2 alone is unlikely, therefore, to account for the observed differences.

As argued previously, oxidation of both FeS and FeS_2 occurs. This is demonstrated by the seasonality and form of FeS and FeS_2 profiles at NWC and by laboratory oxidation experiments (Chapter VI). Loss of sulfide, by

oxidation of HS^-, FeS, or FeS_2 can also be demonstrated by mass balance calculations based on the decomposition experiments. The relative loss of sulfide produced at each station can be calculated as follows. Sulfide production is a function of temperature and has an apparent activation energy of about 20 Kcal/mole (Vosjan, 1975; Goldhaber et al., 1977, this work). The temperature (T) of water in the Sound is approximately a sinusoidal function of time (t) with maximum and minimum of 22° and 2°; this variation can be described analytically as $T = 12 + 10 \cos\omega t$ with $\omega = 2\pi/yr$. The Arrhenius rate law describing the temperature dependence of the rate of sulfate reduction can then be converted to a time dependent function A(t), by replacement of temperature with the above expression for T. Since temperature dependence is not a function of depth in sediment this means R_s, the rate of sulfate reduction is given by:

$$(8) \qquad R_s(x, t) = R_s(x)\, A(t)$$

$$\sim R_s(x) \exp(34.12) \exp\left(\frac{-10{,}065}{285 + 10 \cos 2\pi t}\right)$$

where R(x) is the rate at depth x at 22°C, exp(34.12) is the preexponential factor of A(t) adjusted to set A(t) = 1 at 22°; the remainder of A(t) is determined by the apparent activation energy of sulfate reduction and temperature (time of year). The yearly average of A(t) is ~ 0.4 by numerical evaluation, so the yearly average $\bar{R}_s$ is $0.4\, R_s$ (R_s at 22°C). The total sulfur, S_T, fixed

at a depth of 10 cm assuming steady state R(x) is given by:

$$(9) \qquad S_T = \frac{0.4}{w} \int_0^{10} R(x)\,dx$$

where w is the sedimentation rate and $R_s(x)$ is the 22° rate distribution. This assumes that the depth interval considered represents an appropriately long span of time so that an average A(t) can be used. Taking as an approximation w = 0.5 cm/yr at NWC and DEEP and w = 0.3 at FOAM (these are the approximate ^{210}Pb rates found at FOAM, NWC, DEEP, and an additional offshore station by Thomson, Turekian, and McCaffrey, 1975; Benninger et al., in preparation; Dion, personal communication; and although not a true sedimentation rate (Chapter IV) it will be used as one in the model), then S_T = 400, 320, and 284 mM S at FOAM, NWC and DEEP. The average water content is about 45%, 55%, and 55% at FOAM, NWC and DEEP giving an expected S_T of 320, 342, and 307 μmoles S/g-sediment at a depth of 10 cm at each. This corresponds to an actual measured S_T of 278, 152 and 137 μmoles/g at 10 cm at the three stations. Almost all, 87% of the sulfide produced at FOAM can be accounted for by this model while only 45% of the sulfide produced at NWC and DEEP can. Goldhaber et al. (1977) had previously calculated, using the same method but without temperature correction, that only 43% of the sulfide produced at FOAM was retained; the difference arises because of the previous lack of temperature correction.

Because of the uncertainty in exactly what value for w should be used, for example: take very low long term rates documented by Bokuniewicz, Gebert, and Gordon (1976) or the ^{210}Pb rates which clearly contain a mixing term, the values of percent loss, even with the temperature correction, must be considered minima. (Since sulfate reducers presumably respond to supply rate of organic material (e.g., mixing) rather than net sedimentation per se, the ^{210}Pb rate is probably the appropriate term to be used in the comparison rather than the long term rate; see for example: Shokes, 1976.) The important conclusion from this calculation is that a portion of the sulfide produced at each station is lost and that this loss is greater at the offshore stations than at FOAM. The similar HS^- production rates at each station as measured experimentally and the similar standing crops of FeS indicate that most loss probably, but not necessarily, takes place after sulfide has reacted with the solid phase rather than before.

To this point, analysis of the data has demonstrated that the average rates of sulfate reduction of sediment in the upper 10 cm are comparable in different areas of the Sound but that the ultimate fate of at least one of the products of reduction, HS^-, differs from one region to the next. Because the reactivity of the sediment toward sulfide and subsequent conversion of solid phase sulfide is not significantly different between stations, these findings suggest that transport processes are responsible for the observed variations in the standing crops of different forms of solid phase sulfur in LIS sediment.

Physically controlled transport processes

Molecular diffusion along concentration gradients created by consumption or production reactions is a major form of material transfer in sedimentary decomposition reactions (Berner, 1964a; 1974a). Diffusion coefficients show dependence on porosity and tortuosity of sediment (Manheim, 1970). Although there are changes in porosity and grain size between sedimentary environments of the central Sound, these mass property differences are not large enough to cause significant differences between areas in rates of diffusion near the sediment surface. Diffusion is temperature dependent and, at the 20°C range found in the Sound, can be expected to be 1.5-2 times slower during cold periods than warm (Lai and Mortland, 1961; Li and Gregory, 1974; Goldhaber et al., 1977). These changes are relatively uniform over the Sound bottom.

Physical advection of particles and pore water by net sedimentation and compaction is also approximately the same at each station. This is demonstrated by the restricted range of net sedimentation rates found either seismically or radiometrically (Bokuniewicz, Gebert, and Gordon, 1976; Benninger et al., in preparation) and the similar water contents and lithologies over the depth interval considered.

Mixing of sediment by current and wave action occurs at shallow water stations during storms. As shown by x-radiography studies (not included here), short term storm events such as hurricane Belle [1976] are capable of

resuspending at least the upper 2-3 cm of sediment in depths of water of 10 m or less; this ability attenuates rapidly offshore and at depths of 15 m only the upper ~0.5 cm is influenced. During longer Northeastern storms, whose wind fetch is down the axis of the Sound, the upper 2-3 cm of sediment at NWC depths (~ 15 m) can be mobilized (Aller and Cochran, 1976). It is unlikely that sediment at DEEP (35 m) is ever directly influenced by wave activity. These physical mixing events are most important at FOAM and least important at DEEP; they are capable of directly affecting only the upper few centimeters of sediment and are relatively random single events. They cannot account for regular ongoing transport processes or differences between stations other than by indirectly influencing other types of sediment transport such as biogenic reworking as discussed below.

Biogenic transport processes

Unlike physical transport processes, biogenic transport shows significant variations between stations. The distribution of meiofauna, which are important for particle aggitation, the breakdown of aggregate particles, and advection of pore fluids (Chapter I), does not differ greatly at FOAM, NWC, and DEEP and these organisms are restricted predominately to the upper 0-2 cm in their activity (Yingst, 1977). Macrofauna, as described earlier, are quite different (Figures V-3-V-5). Variations in the trophic types, life habits, life histories, and size of macrofauna occur in the inshore-

offshore transect. These characteristics determine the kinds and rate of biogenic transport which can take place (Chapter I).

Biogenic particle reworking

There are three independent lines of evidence that biogenic particle reworking is different at FOAM, NWC, and DEEP: sedimentological, radiochemical, and biological. X-radiographs (Figures V-6-V-11) demonstrate the presence of biogenic structures at all stations but preserved, physically formed laminations only at FOAM. Preservation of this kind occurs only in physically distrubed environments where animals cannot establish themselves long enough to thoroughly rework sediment (Schafer, 1962; Howard, 1975), animals are in low abundance for other reasons, e.g., lack of food and oxygen (Calvert, 1964) or where sedimentation rates are extremely high (e.g., Moore and Scruton, 1957). Sedimentation rates, food source, and water characteristics do not differ significantly between stations, while, as discussed above, physical disturbance does. McCall (1976) suggested that in shallow water regions of LIS, physical disturbance maintained benthic communities in a constant state of recolonization due to increased mortality. This results in a high, transient diversity of small animals having short life spans, many of which are restricted in their activities to near the sediment-water interface. The resulting short residence time of individual populations at FOAM allows the partial preservation of physical structures produced by major storms.

Laminations at a depth of ~ 12 cm underwent little disturbance over the two year sampling period at FOAM (Figures V-6-V-7). X-radiographs of sediment structures at NWC and DEEP demonstrate a dominance of bioturbate structure at both with a greater importance of homogeneous reworking relative to dwelling structures at NWC than DEEP.

Profiles of the particle-associated radionuclides ^{234}Th and ^{210}Pb document differences in the rate and type of particle redistribution processes at each station. ^{234}Th ($t_{1/2}$ = 24.1 d) profiles are available at NWC and DEEP. These show that homogeneous particle reworking on ^{234}Th time scales is more rapid and slightly deeper, 4 cm versus 3 cm, at NWC than at DEEP (Aller and Cochran, 1976; Chapter IV). This reworking can be described by particle diffusion coefficients of ~ 1×10^{-6} cm^2/sec and 0.1×10^{-6} cm^2/sec at NWC and DEEP respectively. Irregular reworking over ^{234}Th time scales can be resolved at a depth of about 12 cm at NWC (Aller and Cochran, 1976). ^{210}Pb ($t_{1/2}$ = 22 yrs) profiles demonstrate that homogeneous particle reworking over ^{210}Pb decay time scales is greatest at DEEP with excess ^{210}Pb decreasing smoothly to a depth of about 40 cm (Benninger et al., in preparation). Smoothly decreasing decay curves extend to only about 15-20 cm at NWC (Benninger et al., in preparation) and FOAM (Dion, personal communication). In addition, excess ^{210}Pb is found to a depth of ~ 30 cm at a station situated between NWC and DEEP (Thomson, Turekian, and McCaffrey, 1975). Modeling of

of these distributions indicates that homogeneous particle reworking on ^{210}Pb time scales increases offshore in the inshore-offshore transect. Zones of irregular reworking on ^{210}Pb time scales extend to depths of >1 m and are due to infilling of solitary crustacean burrows rather than homogeneous mixing (Benninger et al., 1976 and in preparation).

The sedimentological and radiochemical evidence for trends in the type and extent of particle reworking in the central Sound are consistent with the kinds of animals present in each case. Deep burrowing, sedentary, long-lived, surface deposit or suspension feeding benthos increase in abundance offshore in deeper water (McCall, 1976; Figures V-3-V-5). These animals form permanent or temporary dwelling structures in which they reside for considerable periods of time, probably up to 3-5 years based on life spans of similar species. Maldanid polychaetes present at DEEP feed at depths of 15-30 cm and pass particles vertically to the interface (e.g., Rhoads, 1974). Most other organisms at DEEP are surface deposit or suspension feeders and their chief effect on particle transport at depth will be due to burrow construction and the subsequent filling-in of burrows when they are vacated rather than particle reworking during feeding. For the case of teribellid or other tube-building polychaetes present at DEEP, for example Pista, burrow formation can result in the construction of biogenic shafts lined with surface sediment rich in organic matter; these represent invaginations of surface material up to depths of 30-40 cm (Chapter II). Deep burrowing animals, including those

such as Pherusa, which do not build thickly-lined tubes of surface sediment, will also supply organic matter to deep sediment by the secretion of mucus into burrow walls. These kinds of particle reworking activities are relatively slow on monthly time scales (^{234}Th) but are significant when integrated over many generations (^{210}Pb time scales).

Animals at NWC are generally more mobile and shallow burrowing than at DEEP. The characteristic species are the protobranch bivalves Yoldia limatula and Nucula annulata and the errant polychaete Nephtys incisa. Yoldia and Nucula intensively rework the upper 3-4 cm of sediment (Rhoads, 1963; Young, 1971) and are largely responsible for the differences in ^{234}Th profiles at NWC, and DEEP (Chapter IV; Aller and Cochran, 1976). During reworking Yoldia, at least, is capable of aiding the formation of exponentially decreasing profiles of organic matter found at NWC (Figure V-35; Chapter III). Nephtys does not homogeneously rework sediment but tends to form temporary dwelling burrows with a characteristic Y-shape. It moves often enough that the in-filling of its burrows becomes important for irregular particle reworking on short time scales. Maximum burrowing depth of most common benthos at NWC is 15-20 cm although Spiochaetopterus builds slender burrows to ~25 cm. The number of active or open burrows decreases rapidly below the interface. At both NWC and DEEP, large crustacean burrows are found to depths greater than 1 m but as shown by ^{210}Pb profiles

these are not especially important for particle reworking over the period in which data were gathered for this study.

As described above, FOAM is characterized by small, short-lived animals representing many species living in the Sound. The most common and predictably present species is the surface deposit-feeding amphipod Ampelisca sp. which restricts tube-building and feeding activity to the upper 0-2 cm. Maldanid polychaetes which were not present during the first year of sampling at FOAM (Goldhaber et al., 1977) appeared in fair abundance in Fall 1975. Sediment remained laminated at depths $>$ 10 cm indicating no extensive, rapid particle reworking by these animals deep in the sediment column. Nephtys incisa is important for irregular reworking of particles as noted above but like many vagile species probably does not greatly disrupt sediment laminations (Schäfer, 1962).

Just as shells protect FeS from oxidation near the interface, enclosure of sediment by shells aids in protecting particles from reworking by animals at FOAM. Physical processes at FOAM apparently have two indirect roles in reducing biogenic particle reworking: disturbance decreases the residence time of given animal populations and therefore efficiency and depth of reworking, and, shell accumulations brought about by the current regime hinder homogeneous reworking by the species normally present in Long Island Sound.

Biogenic fluid transport

Irrigation of burrows or body cavities for purposes of respiration, excretion, or reproduction results in the biogenic transport of sea water into and out of marine sediment. Compilations of fluid and particle transport rates by various kinds of animals show that the weight ratio of fluid to solid transport rates by deposit feeders is ~ 100-500 (Chapter I). Suspension feeders have much higher ratios: $\sim 10^5$-10^6 but in many cases fluid pumped by suspension feeders does not intimately contact sediment. Irrigation is capable of maintaining burrow water at near sea water concentrations for many ions even in the face of high fluxes of material from surrounding sediment (Chapter II). Exchange of pore water with burrow water can be greatly complicated by specific microchemical environments which can form around burrows (Chapter II). Nevertheless, even in the absence of particle reworking by animals such as maldanid polychaetes, extensive exchange of pore water with overlying water can take place across tube walls (Chapter III). This exchange is brought about by a combination of horizontal diffusion and vertical advection (irrigation) and because of the geometry of diffusion does not require diffusion rates much higher than ordinary molecular diffusion ($\sim 1 \times 10^{-5}$ cm^2/sec) (Chapter III). The distance an ion must diffuse to escape sediment is approximately half the distance between burrows so that even at depths of 1 m in sediment, if the average distance between active burrows is 20 cm, the

distance that an ion need travel for escape (or to be supplied from overlying water) is ~ 10 cm depending on burrow packing geometries and wall effects. Vagile infauna have the effect of decreasing the average distance between burrows when their activities are integrated over a period of time.

From the previous considerations on particle reworking and the types of animals present at each station it is clear that biogenic fluid transport will vary in intensity and depth of influence in the Sound. Based on density and depth of burrowing, the deepest exchange by irrigation will occur at DEEP and the shallowest at FOAM. It is important to note that fluid and particle transport need not be coupled in the same way at all stations because of the dependence of these transport mechanisms on animal type and the geometry of exchange (Chapter I, III). Because fluid exchange is much more rapid than particle mixing, ($\geq 1 \times 10^{-5}$ cm^2/sec versus $\leq 1 \times 10^{-6}$ cm^2/sec), irrigation is capable of affecting pore water profiles in a short period of time without disturbing physically-formed sediment laminations such as occur at FOAM (Chapter III).

Seasonal dependence of biological and physical processes

Biological activity is strongly temperature controlled. The calculated temperature dependence of sulfate reduction suggests that the rate of decomposition by microorganisms may be 6-8 times lower during the coldest times of year ($\sim 2^{\circ}$) than during the summer ($\sim 22^{\circ}$). Based on published

Q_{10} values complied in Chapter I for macrofauna common in LIS, macrofaunal activity should be decreased by a factor of ~4 over the same 20° temperature range. Molecular diffusion, on the other hand, will be lowered by a factor of only 1.5-2.0 as noted previously. Mixing of sediment by storm activity, important mostly at FOAM increases during winter periods. Together with the biogenic transport processes discussed above, this large seasonal dependence in biological relative to physical activity is crucial in the interpretation of pore water profiles.

Seasonal and spatial variation in pore water profiles

General patterns.--The observed seasonal and spatial variation in pore water profiles and solid phase sulfides can be interpreted in terms of the different relative contributions of biogenic and physical-chemical processes at different times of year and in different bottom areas. The basic seasonal pattern at all stations is as follows: Production (NH_4^+, $HPO_4^=$, HCO_3^-, HS^-) and consumption ($SO_4^=$, etc.) of interstitial nutrients predominates during initial warming of overlying water during spring and early summer. This produces high standing concentrations of NH_4^+, $HPO_4^=$, and HCO_3^- in the pore water and increases or replenishes the standing crop of FeS near the sediment water interface after winter lowering by oxidation. Increases in NH_4^+ and $HPO_4^=$ at FOAM, NWC, and DEEP, which are most easily detected

because of the relatively low background concentrations, mirror the depth dependence of production predicted by the decomposition experiments. Concentrations at FOAM (FOAM 1) and NWC (NWC 1) increase exponentially toward the interface before decreasing to sea water values; concentrations at DEEP (DEEP 1) increase much less sharply as expected from the lower depth dependence of decomposition at that station (Figures V-27-V-29). The intensity of this early summer increase was not exactly the same in the two sampling years at NWC and FOAM. This may result from slight offsets in the sampling dates from the actual sequence of change in the sediment or may reflect a longer term cycle in sediment chemistry since a general lowering of concentrations occurred at both NWC and FOAM in the second year of sampling.

Riley (1956b) noted a steady two year decrease in the intensity of the spring flowering of phytoplankton during 1952-1954. This type of change may result in cyclical patterns of supply of decomposible organic material to bottom sediments and influence pore water compositions near the interface accordingly. These differences in supply would not affect the general temporal pattern of change in pore water profiles but would alter the magnitude of excursions in concentration levels from one season to the next.

During the late summer and fall (August, September, October) when water is the warmest of the year, biogenic reworking reaches its highest level (Aller and Cochran, 1976). This maximum in the rate of reworking

results not only from the increased temperature which increases activity at this time but from the fact that macrofaunal populations tend to be near their highest abundance and diversity of the year due to earlier recrutiment and growth (e.g., Rhoads, Aller, and Goldhaber, 1977; Appendix III). The increase in biogenic transport flushes the sediment at a rate faster than would occur by simple one dimensional molecular diffusion in a homogeneous body. The resulting decrease in standing concentration of NH_4^+, $HPO_4^=$, and HCO_3^- or corresponding replenishment of $SO_4^=$ occurs down to at least the deepest depth intervals sampled by the box cores at NWC and DEEP (16-18 cm) and to about 11-13 cm at FOAM 4 (Figures V-24-V-32). If it is assumed that the minima in the gravity core NH_4^+, $HPO_4^=$, and alkalinity profiles at NWC and DEEP correspond to the base of this exchanged zone and that the increased concentrations above these minima represent increased production rates resulting from the depth dependence of R_s, then the zone is about 15-20 cm deep at NWC and 20-40 cm deep at DEEP. This is in remarkable correspondence with the depth to which excess ^{210}Pb is found and the known burrowing depth of animals at these stations. The transport process itself does not involve a great deal of particle reworking, as demonstrated by the slopes of ^{234}Th and ^{210}Pb profiles and the laminations at FOAM which put limits on the rate of particle mixing, but is due to pore water exchange across burrows formed by sedentary and vagile organisms. The rate of production is probably also decreased at this time due to depletion of organic material from earlier

plankton blooms (Riley, 1956b; Conover, 1956) or to lower temperatures.

The winter-early spring profiles collected at close to the coldest temperatures of the year represent profiles having minimum biological contribution. NH_4^+ and alkalinity profiles appear to be simply diffusion altered relicts of the fall profiles. $HPO_4^=$ concentrations decrease with a concave-up form (Figures V-30-V-32) indicative of consumption, probably as a result of increased adsorption or reaction with Fe-oxides as the interface is approached. This consumption is hidden in most profiles taken at other times of the year by production; at DEEP, where production does not increase so radically near the interface as at FOAM and NWC, evidence for $HPO_4^=$ consumption near the interface also occurs in the fall profile where production is lowered somewhat from summer.

Additional reactions not evident from concentration profiles at other times of year also become noticeable at the lowered transport rates which act during the winter. An example of this is Ca. Winter calcium profiles show concentration increases above the sea water Ca/Cl ratio in a zone just beneath the sediment water interface (Figure V-33). Profiles of this type have been recreated in the laboratory by simply removing macrofauna and reducing the high biogenic diffusion coefficient which prevents Ca from building up to levels detectable above sea water background (Chapter III). This example leads to two very important conclusions: (1) $CaCO_3$ is dissolving in near interface sediment in all regions of the Sound; this will

be discussed more thoroughly below, and (2) when biogenic influence is reduced during cold periods of the year, inorganic reactions become evident and play a relatively greater role in controlling near interface pore water profiles than during warmer times. The transition between predominately biologically-controlled periods which represent ~2/3 of the year and predominately physically-controlled is smoothly varying and determined by the oscillation of temperature.

The shifting domination of pore water profiles from biogenic production and consumption reactions (summer) to biogenic transport control (summer-fall), to physically-controlled (winter) results from the relative temperature dependence of sulfate reduction, macrofaunal activity, and molecular diffusion and from the manner in which organic matter is supplied to the bottom. The spring phytoplankton bloom provides a pulse of organic material to underlying sediment. As the water warms, fresh organic material, which will become mixed into the top few centimeters of sediment, is available for rapid breakdown. Nutrients released from this as well as organics already present in the sediment begin to accumulate in pore water. Assuming that during warm times of the year, biogenic fluid transport can be described by an effective diffusion coefficient in the upper few centimeters of $\sim 1 \times 10^{-5}$ cm^2/sec (Goldhaber et al., 1977; Chapter III; and below) then with a temperature dependence represented by a Q_{10} of ~2 (Chapter I), this would be decreased to $\sim 3 \times 10^{-6}$ cm^2/sec during the winter. The result is that for certain ions, molecular diffusion will be

more rapid than biogenic transport during the winter; for example, the molecular diffusion coefficient of NH_4^+ is $\sim 7.0 \times 10^{-6}$ cm^2/sec at 25° and $\sim 4 \times 10^{-6}$ cm^2/sec at 2°. [The diffusion coefficient is computed from the theoretical infinite dilution value for NH_4^+, see below (Li and Gregory, 1974) corrected for tortuosity by use of the ratio of the observed sulfate diffusion coefficient at FOAM (Goldhaber et al., 1977) to the theoretical value.] There will be a period of time, for example when water temperature is about 12°C, during which molecular and biogenic diffusion rates are nearly the same for some ions such as NH_4^+. At the same time, production at 12°C, for the example of NH_4^+, will be increased by a factor of 3–4 above its winter background based on the observed temperature dependence in the decomposition experiments. Since the winter profiles represent a relatively balanced diffusion-inorganic reaction profile, this increase in the reaction term (production) with little increase in the rate of diffusion is readily expressed in the pore water profile above the winter diffusion-controlled background concentrations. Once biogenic diffusion becomes much greater than molecular diffusion it quickly begins to control the shape of the profile despite changes in reaction terms as shown by model considerations in Chapter III.

To illustrate the time dependence of these processes, the relative rates of transport (= macrofaunal activity) and metabolite production (= sulfate reduction) are plotted as a function of season in Figure V-41. The curves

in Figure V-41 are simply the Arrhenius rate function A(t) (equation 8) described previously in which the appropriate activation energy (Q_{10}) for macrofaunal activity ($Q_{10} = 2$) and sulfate reduction ($Q_{10} = 3$) have been used. The function is normalized so that it is 1 (maximum) at 22°C in each case. If it is assumed that the maximum biogenic diffusion coefficient is $\sim 1 \times 10^{-5}$ cm^2/sec, the horizontal line in Figure V-41 indicates what times of year the biogenic fluid transport coefficient would be greater than the molecular diffusion coefficient of NH_4^+ at 22°C (7×10^{-6}).

Abiogenic reaction controls on profiles

During the winter, abiogenic reactions become more apparent and are expressed by distinct changes in the form of individual profiles, for example: $HPO_4^=$ and Ca^{++}, at that time. The types of changes which take place can be shown to be consistent with the expected chemical behavior of the elements involved. The role of particular solid phases in these reactions during the winter or at other times can also be inferred by examining the disequilibrium state of pore water with respect to selected compounds.

NH_4^+ is involved mostly in adsorption reactions with sedimentary particles rather than in the formation of specific insoluble phases (e.g., Norvell, 1974). Adsorption may be reversible (exchangeable) or irreversible (fixed) and occurs on both clay and organic material (Mortland and Wolcott, 1965; Nõmmik, 1965). Ammonium-aluminum-phosphates (taranakite) have

been reported to form under relatively acid soil conditions (Nõmmik, 1965) but reports of similar compounds have not appeared in the marine literature. Adsorption of NH_4^+ on sediments from Long Island Sound and other areas is predominately reversible and follows a linear isotherm having proportionality constant $K \sim 1$ where $C_s = KC$; C is concentration in solution, C_s is concentration on solids (Rosenfeld, in preparation). It is assumed in this report that reversible adsorption is the chief abiogenic reaction of NH_4^+.

Phosphate is subject to both reversible and irreversible adsorption reactions (e.g., Li et al., 1972; Syers, Harris, and Armstrong, 1973) and is known to form a wide range of relatively insoluble Ca, Fe and Mn compounds in marine and lake sediments (Bray, 1973; Troup, 1974; Nriagu and Dell, 1974; Tessenow, 1974). Specific adsorption on Fe-oxides (Parfitt, Atkinson, and Smart, 1975) is thought to greatly influence $HPO_4^=$ mobility and concentrations in surface sediment (Hayes, 1964; Mortimer, 1971). Expressed as an adsorption isotherm, phosphate can be shown to be much more strongly absorbed under oxygenated ($K \sim 25$-50) than anoxic ($K \sim 0.5$-8) conditions, probably as a result of a reduction of Fe-oxides and a lowering of strong, specific Fe^{+3}-PO_4 interaction in the anoxic relative to the oxygenated case (Olsen, 1964; Li et al., 1972).

Distinct, end-member phosphate phases which are likely to form in anoxic marine sediments include: $Ca_5(PO_4)_3OH$ (Hydroxyapatite), $Ca_3(PO_4)_2$ (Whitlockite), $Fe_3(PO_4)_2 \cdot 8H_2O$ (Vivianite), and $Mn_3(PO_4)_2 \cdot 3H_2O$

(Reddingite). (Martens, Berner, and Rosenfeld (in preparation) have suggested that $MgNH_4PO_4 \cdot 6H_2O$ (Struvite) may also occur in inshore LIS sediments; this phase is highly undersaturated at the stations examined in this study). The presence of a pure phase is the exception rather than the rule in low temperature disgenesis but considerations of saturation states with respect to such end members has been demonstrated to give useful insights into the likelihood of a given type of reaction in controlling pore water chemistry (e.g., Bray, 1973; Troup, 1974; Emerson, 1976; Holdren, 1977).

In order to calculate the disequilibrium or equilibrium state of pore water with respect to a given phase, it is necessary to determine individual ion activities. This requires calculation of specific (ion pairing) and non-specific interactions influencing the solution activity of a given ion. Techniques used in the calculation of total activities are discussed in Garrels and Christ (1965) and Berner (1971). In the present study, a computer program developed and written by R. Holdren (Holdren, 1977) was employed to calculate activities. Specific interactions involving ion pairs of: Na^+, K^+, Ca^{++}, Mg^{++}, Fe^{++}, Mn^{++}, H^+, OH^-, Cl^-, HCO_3^-, $CO_3^=$, SO_4^+, H_2PO_4, $HPO_4^=$, and HS^- are taken into account, using stability constants (25°C) tabulated in the literature (Sillen and Martel, 1964; Morgan, 1967). After iteration to obtain the free ion concentration and a constant ionic strength, activity coefficients are determined by use of the extended Debye-Huckel equation. At the ionic strengths (0.40-0.55) present, the use of this

equation introduces an error of ~ 10-15% in divalent ion activities but as will become apparent this is not an important influence on the conclusions to be drawn. A detailed presentation of this model is given in Holdren (1977) and will not be repeated here. The Fe^{++} and Mn^{++} data used are discussed in detail in Chapter VI and listed in Appendix IV. Total alkalinity was assumed equivalent to carbonate alkalinity, a reasonable approximation based on previous studies (e.g., Berner, Scott, and Thomlinson, 1970). Na^{+}, K^{+}, and Mg^{++} were calculated from Cl^{-} by use of sea water concentration ratios. The model gives reasonable total activity coefficients at FOAM, NWC, and DEEP, for example: $\gamma_T (Fe^{++}) = 0.14\text{-}0.19$, $\gamma_T (Mn^{++}) = 0.11\text{-}0.14$, $\gamma_T (Ca^{++}) = 0.21$ and also agrees well in its predictions when compared to calculations using apparent solubility products in the case of $CaCO_3$ as shown below and in Chapter III. Charge balances were found to be $\pm$ 0.1% of neutrality except in the case of the FOAM-gravity core in which case balance was + 0.1% below ~ 90 cm. No correction for temperature variation has been made.

The solubility products and reactions used to determine saturation states are given in Table V-4. In comparing the pore water concentrations to these solubility products it is assumed implicitly that the kinetics of attainment of equilibrium are rapid with respect to transfer or production. The results of the calculations for phosphate compounds are plotted as -log IAP (IAP = ion activity product) as a function of depth at each station (Figures V-42-V-43).

Only box cores collected during the second year and some selected horizons from the gravity cores were used. Hydroxyapatite was supersaturated by a factor of 10^3-10^{10} at all stations and is not plotted; precipitation of this phase is known to be kinetically hindered in sea water (Martens and Harris, 1970). Whitlockite ($Ca_3(PO_4)_2$) (a common low temperature mineral in dental caries; also a secondary mineral in pegmatites (P.B. Moore, personal communication)) is very close to saturation, particularly at FOAM, DEEP 1 and DEEP 3. At depth, the FOAM and NWC gravity cores maintain a constant ion product for this phase even as Ca^{++} decreases (at FOAM) and $HPO_4^{=}$ increases, this is suggestive evidence that a compound of this type may be forming and aiding in the determination of standing $HPO_4^{=}$ concentrations below the upper few centimeters. Bray (1973) inferred that pore waters in southern Chesapeake Bay sediments are in equilibrium with whitlockite but used a $pK_{sp} = 26$; his inference is even more justified if the $pK_{sp} = 28.5$ based on the ΔGf determined by Duff (1971) is used. Norvell (1974) also found evidence of $Ca_3(PO_4)_2$ formation in experiments with anoxic lake sediments.

Saturation with respect to vivianite occurs in a thin band, 2-8 cm, just beneath the interface at all stations during the summer (Figure V-42). Saturation also occurs during the winter at FOAM and DEEP. Otherwise pore water is undersaturated with respect to pure vivianite. The band of saturation is caused by greatly increased Fe^{++} concentrations produced by

the reduction of Fe-oxides or oxidation of sulfides in this zone (Chapter VI). Fe-sulfides are forming in this zone as demonstrated previously (Figures V-36-V-39). In general, if sulfide is present, FeS forms in preference to vivianite (Nriagu, 1972). At equilibrium between FeS (Mackinawite) and $Fe_3(PO_4)_2 \cdot 8H_2O$

$$(10) \quad 3FeS + 2PO_4^{\equiv} + 8H_2O = Fe_3(PO_4)_2 \cdot 8H_2O + 3S^{=}$$

giving: $$(11) \quad \frac{(S^{=})^3}{(PO_4^{\equiv})^2} = 10^{-22.2} \text{ or } pPO_4 = \frac{3}{2} - 11.1$$

Data from the upper 8 cm at all stations where both pS and pPO_4 were detectable are plotted together with the equilibrium line calculated above. The pS for summer box cores was estimated from Eh measurements using the conversion equation of Berner (1963) for sediments with sulfide present; these are considered highly approximate but give reasonable values. These data indicate that a thin band of variable thickness just beneath the interface is capable of having both vivianite-like phosphates and Fe-sulfides forming. Based on the IAP/K_{sp} ratios calculated for vivianite, this should occur, if at all, during summer and winter. Diffusion of HS^- toward the interface will tend to move points to the left of the equilibrium line. Beneath this zone, pS decreases substantially and Fe-sulfides are formed preferentially to pure Fe-phosphates which become undersaturated (Figure V-44). Above this zone vivianite-like compounds are undersaturated but the presence of abundant Fe-oxides or

Fe-rich particles which scavenge $HPO_4^=$, and, diffusion into overlying water, maintain $HPO_4^=$ at low levels. During the fall when both Fe (Chapter VI) and $HPO_4^=$ are lowered in concentration by increased biogenic transport, vivianite-like compounds are also undersaturated in the sediment interval in which they might normally form at other times of the year. Scavenging of $HPO_4^=$ by Fe-oxides can be expected at all times thereby aiding in the formation of concave $HPO_4^=$ profiles near the interface.

Because of large discrepancies in reported values for $Mn_3(PO_4)_2 \cdot 3H_2O$ stabilities, it is hard to evaluate the role of a reddingite-like mineral in controlling $HPO_4^=$ levels. Using the ΔG_f reported by Nriagu and Dell (1974) (the calculated K_{sp} is similar to that of Tessenow, 1974), then reddingite is undersaturated at all stations except DEEP, where possible saturation occurs below 4 cm in summer and winter box cores. The possibility that solid solution with Fe lowers the solubility cannot be ruled out but according to Tessenow (1974) at the low $(Fe^{++})/(Mn^{++})$ present in Long Island Sound pore water, the solubility of (Mn^{++}) should approximate the solubility with respect to the pure reddingite phase.

In summary, the equilibrium calculations suggest that $HPO_4^=$ could be involved in the formation of Fe (vivianite) and Ca (whitlockite) phosphates and at one station, DEEP, Mn phosphate as well. Vivianite-like compounds should form only in a thin band just below the interface (2-8 cm). Whitlockite may form anywhere from 2-125 cm at FOAM, below 15 cm at NWC, and in

irregular horizons at DEEP but is generally undersaturated there. Because of biogenic transport and seasonal changes in phosphate production, saturation states change seasonally, particularly in the top 15 cm at FOAM, 20 cm at NWC, and probably 40 cm at DEEP. Undersaturation occurs to the greatest extent in the late summer and fall when extensive pore water exchange with overlying water takes place. Winter conditions depend in part on pore water chemistry underlying the fall exchange zone. If high concentrations of $HPO_4^=$ underlie this zone as in the case of FOAM, diffusion from below during the winter may increase the concentration of $HPO_4^=$ without a high production rate and bring the system closer to saturation or supersaturation with respect to end member phosphate phases. If, as at NWC, underlying pore water is low in $HPO_4^=$, then little change in the saturation state may occur in the exchanged zone during the winter. DEEP has low $HPO_4^=$ at depth but as shown by the decomposition experiments it has higher rates of production away from the near-interface than either FOAM or NWC so that production may replenish $HPO_4^=$ at this station in the upper $\sim$ 20 cm during the winter thereby increasing the state of saturation. During periods of undersaturation, for example the fall, dissolution or desorption of phosphates formed earlier in the summer may take place and aid in replenishing $HPO_4^=$ levels in the pore water of the upper 10-30 cm. At all times and particularly near the interface, $HPO_4^=$ is involved in adsorption reactions.

It was pointed out earlier that Ca^{++} is released into solution near the interface during the winter. The calculated saturation states of the pore waters with respect to calcite and aragonite at the three stations are shown in Figure V-43. Total alkalinity was used so that saturation is overestimated. The trends are clear: both calcite and aragonite are undersatruated near the sediment water interface at all stations; this zone of undersaturation is restricted to the upper 10 cm at FOAM below which supersaturation is reached. The thickness of the zone of undersaturation as well as the degree of undersaturation increases offshore. These calculations indicate that from an equilibrium standpoint, $CaCO_3$ should be subject to dissolution until it has passed into a lower sedimentary interval of supersaturation by either net sedimentation or biogenic transport, for example, the infilling of deep dwelling burrows. There are several additional lines of evidence consistent with the equilibrium calculations that $CaCO_3$ is undergoing dissolution. The increase of Ca^{++} above sea water Ca/Cl values near the interface during the winter is strong evidence for dissolution. Dissolution may be related to the lowering of pH and titration of alkalinity by the oxidation of FeS-FeS_2 near the interface (Chapter VI). Driscol (1975) documented a decrease of $CaCO_3$ during winter in sediments from Buzzards Bay suggesting that when animals were not actively bringing in $CaCO_3$ by recruitment of new populations there was a net loss of sedimentary $CaCO_3$.

Sedimentological evidence that dissolution is taking place can be seen in the x-radiographs discussed earlier. There is essentially no $CaCO_3$ present as shells below 1 cm at DEEP or below 15 cm at NWC. Shell bearing animals live at this station as demonstrated quantitatively by sieve analyses of samples in this study (Appendix III, Figure V-5). The appearance of shell bearing animals at DEEP is not a recent phenomena as can be readily shown by examining the species lists of Sanders (1956) from his station 5 (a similar depth (28 m) and position in the Sound), which demonstrate the presence of a number of bivalve and gastropod species in this region. The effects of dissolution can also be seen on the umbro areas of living bivalves at DEEP, where, when the periostracum becomes scrapped off, there is clear evidence of dissolution pits. At FOAM, the abundance of shell debris concentrated by physical processes as well as the relatively low degree of undersaturation and small extent of the undersaturated zone allow the preservation of a great deal of shell material. $CaCO_3$ may be precipitating in the deeper parts of FOAM sediment as suggested by the Ca^{++} decrease (Figure V-20). This has also been suggested by Graber (1975) on the basis of saturometry and equilibrium calculations made at FOAM. The Ca^{++} decrease may also be related to Ca-phosphate precipitation as argued earlier.

The paleontological significance of these inshore-offshore trends in preservation is that incorrect interpretations of the animal communities

inhabiting these bottoms would be made from fossil evidence. There would be little preserved evidence of molluscan bottom fauna at either NWC or DEEP. In some cases where surface shells were transported to depth by falling into deep crustacean (Squilla) burrows which often extend into zones of supersaturation, shells would be preserved as burrow fillings and appear as shell-filled vertical pods or chambers in later exposed outcrops, but with no evidence of shell bearing fauna in the ambient sediment. Examples of this have been found in recent Long Island Sound sediment (Benninger et al., 1976 and in preparation) but can also be observed in fossil examples such as the Maryland Miocene outcrops along the Chesapeake Bay and other areas.

It is important to recognize that preservation or lack of preservation is determined by biological activity. Reworking of bottom sediments near the interface rapidly depletes sediment of metabolizable organic matter. In cases such as DEEP, some organic surface material is transported to depth as burrow lining or fill and tends to increase the rate of decomposition at depth (Figure V-16). However, as long as decomposition occurs in the irrigated zone, alkalinity (from $SO_4^=$ reduction, reactive Fe present) will not build up in sediment pore water to bring $CaCO_3$ into saturation at low sediment pH levels. Once organic material has left the biogenically reworked zone it may be so depleted in metabolizable organic fractions that little additional production of HCO_3^-, $HPO_4^=$, NH_4^+, or HS^- by sulfate

reducers takes place and sediment remains undersaturated to depths significantly lower than the mixed zone. Models and experimental studies of mixing processes also show that the presence of a biogenically exchanged zone will lower alkalinity in sediment underlying the mixed layer (Chapter III; Vanderborght; Wollast, and Billen, 1976). All these facts suggest that biogenic reworking of particles and fluids act together to reduce the chance of shell preservation in sediments. Where net sedimentation is low and there is abundant burrowing infauna, particularly large sedentary burrowers such as occur in quiet water, there should be greatly reduced preservation of shell-bearing species in fossil communities.

The production of organic matter in LIS is generally capable of directly or indirectly supplying the acids required for total shell dissolution. Riley (1956b) estimated that 64 gC/m^2-yr is delivered to the benthos. Assuming for the sake of calculation that 50% of this appears as CO_2 in sediment pore water, then roughly 250 g $CaCO_3/m^2$-yr could be dissolved. At a maximum sedimentation rate of ~ 0.5 cm/yr and a maximum bulk sediment density of ~ 0.8 g/cc, this corresponds to eliminating $CaCO_3$ equivalent to 6 weight percent of the sediment. The exact amount lost will depend on many chemical, physical, and biological (e.g., decomposition pathway) factors, but this calculation demonstrates the feasibility of dissolution from the standpoint of organic matter supply .

There are several reasons why the FOAM site differs from offshore

stations with respect to shell preservation. The depth and extent of biogenic reworking is lowest at FOAM so that the products of decomposition build up in the pore waters of this station allowing supersaturation to be reached at a shallow depth. The reduced effects of reworking are caused by the severity and frequency of physical disturbance which prevents the establishment of a long-lived, deep-burrowing infauna. These physical disturbances also concentrate shell material at FOAM increasing the probability of perservation since for a given amount of dissolution (i.e., a set residence time of material in the zone of undersaturation) the chance of some shells surviving is increased. Shells also tend to protect organic material from biogenic reworking by actual physical enclosure of particles. This may cause a lower attenuation of decomposition rate with depth, for example $R = R_o e^{-.24x}$ at FOAM compared with $R = R_o e^{-.33x}$ at NWC. As discussed earlier, certain kinds of animals are also capable of lowering the attenuation coefficient by specific reworking activities which result in organic matter transport to depth (e.g., DEEP, Chapter II) but in this case irrigation prevents buildup of decomposition products whereas in the physical case it does not. These considerations show that the physical attributes of a depositional environment in setting limits on the kinds of animals present, influence the nature of biogenic transport processes which take place, and, together with normal diagenetic processes, determine whether shell material will or will not be preserved. It is ironic that from the standpoint of fossil preservation

the most physically controlled environments of Long Island Sound will preserve the most abundant evidence of a diverse, shell-bearing fauna in addition to lebensspuren, while offshore regions will leave evidence, except in the special microenvironments discussed above, in the sediment structure, only of soft-bodied organisms.

Modeling pore water distributions in the zone of bioturbation

Diffusion-advection-reaction models, like pure equilibrium models, can be used to check for consistency in understanding and interpretation of diagenetic processes near the sediment surface. The transport-reaction equation describing these processes in sediment pore water can be written in one dimension (cartesian coordinate system) as:

$$(12)\quad \frac{\partial C}{\partial t} = \frac{\partial}{1+K}\,\frac{\partial}{\partial x}\left(D\,\frac{\partial C}{\partial x}\right) - w\,\frac{\partial C}{\partial x} + \frac{R}{1+K}$$

where: C = concentration of pore water constituent being considered

x = vertical dimension, origin at sediment-water interface, positive axis into sediment

w = sedimentation rate

D = molecular or effective diffusion coefficient modified for tortuosity

R = reaction term with functional form to be described

K = Langmuir adsorption coefficient in linear range.

This is analogous to the equation of Berner (1976b) where compaction is ignored, adsorption is expressed as a simple linear isotherm, and diffusion is molecular. As discussed previously, because of biogenic control of both reaction and transport near the sediment-water interface, in general both D and R are functions of depth and time in sediments subject to temperature fluctuations. The dependence of D on x will be ignored initially. It was shown earlier that the temperature and depth dependence of R in Long Island Sound sediment led to a time dependent function of the form:

(13) $R \sim R(x)\, A(t)$

where: $A(t) = A_o e^{-\frac{E}{B + z \cos \omega t}}$

and E was determined by the apparent activation energy or temperature response (Q_{10}) of microbial activity. Macrofauna do not have the same Q_{10} and as was suggested earlier, this leads to the dominance of reaction terms during early summer. If macrofauna did have the same temperature dependence and D could be described as: $D = D_o A(t)$, where D_o = effective biogenic diffusion coefficient at 22°C, then ignoring advection for a short time such as one year and assuming no adsorption, the appropriate transport-reaction equation becomes:

(14) $$\frac{\partial C}{\partial t} = D_o A(t) \frac{\partial^2 C}{\partial x^2} + R(x)\, A(t)$$

Letting: (15) $t' = \int_0^t A(t^*)\,dt^*$

where t* is a dummy integration variable (Crank, 1956), then equation (13) reduces to an equation in t':

(16) $\frac{\partial C}{\partial t'} = D_o \frac{\partial^2 C}{\partial x^2} + R(x)$

If at $t' = 0$, $C = a_o + a_1 x$, a_o, a_1 = constants

$t' > 0$, $x = 0$, $C = 0$

$x = L$, $\frac{\partial C}{\partial x} = 0$

it can be shown that the system goes to near steady state in about one year (in t not t') in the upper 15 cm of sediment using $D_o = 1\text{-}3 \times 10^{-5}$ cm^2/sec, and $R_N/(1 + K) = 23e^{-.4x}$, values which are reasonable for NH_4^+ production and biogenic diffusion (see below, flux section) at station NWC. This means that assuming the initial and boundary conditions are appropriate, D and R cannot have the same functionality of time and still maintain the observed oscillatory behavior of the system.

Separate time dependence of D and R

If it is assumed that the time dependence of D and R are different but that the time and depth dependence are still separate functions so that:

(17) $D = D_o f(t)$

(18) $R = R(x)g(t)$

then proceeding as before and again ignoring compaction, advection, and adsorption:

$$(19) \quad \frac{\partial C}{\partial x} = D_o f(t) \frac{\partial^2 C}{\partial x^2} + R(x)g(t)$$

Letting: $(20)\ t' = \int_0^t f(t^*)dt^*$

gives: $(21) \quad \frac{\partial C}{\partial t'} = D_o \frac{\partial^2 C}{\partial x^2} + R(x)R(t')$

Taking $R(x) = R_o e^{-\alpha x}$ and approximating the geometry by a semi-infinite solid such that:

$t' = 0,\ C = a_o + a_1 x,\ a_o,\ a_1$ = constants

$t' > 0,\ x = 0,\ C = 0$

then the solution by application of Duhamel's theorum (see Carslaw and Jaeger, 1959, p. 79) is:

(22)

$$C(x,t') = a_o \operatorname{erf}(x/2/(D_o t')^{1/2}) + a_1 x + \int_0^{t'} \frac{R_o R(\tau)}{D_o \alpha^2} (x/2/(\pi D_o (t'-\tau)^3)^{1/2} \exp(-x^2/(4D_o(t'-\tau))))\, d\tau$$

$$+ \int_0^{t'} \frac{R_o R(\tau)}{2} \exp(D_o \alpha^2 (t'-\tau) - \alpha x) \operatorname{erfc}(\alpha (D_o (t'-\tau))^{1/2} - x/2/(D_o (t'-\tau))^{1/2})\, d\tau$$

$$- \int_0^{t'} \frac{R_o R(\tau)}{2D_o \alpha^2} \left(\frac{\alpha}{\pi^{1/2}} \left((D_o/(t'-\tau))^{1/2} + x/4/(D_o(t'-\tau)^3)^{1/2} \right) \exp(D_o \alpha^2 (t'-\tau) - \alpha x) \right.$$

$$\left. \cdot \exp\left(-(\alpha(D_o(t'-\tau))^{1/2} - x/2/(D_o(t'-\tau))^{1/2})^2\right) d\tau \right.$$

$$- \int_0^{t'} \frac{R_o R(\tau)}{2} \exp(D_o \alpha^2 (t'-\tau) + \alpha x) \operatorname{erfc}(\alpha(D_o(t'-\tau))^{1/2} + x/2/(D_o(t'-\tau))^{1/2}) \, d\tau$$

$$+ \int_0^{t'} \frac{R_o R(\tau)}{2D_o \alpha^2} \left(\frac{\alpha}{\pi^{1/2}} \left((D_o/(t'-\tau))^{1/2} - x/4/(D_o(t'-\tau)^3)^{1/2} \right) \exp(D_o \alpha^2 (t'-\tau) + \alpha x) \right.$$

$$\left. \cdot \exp\left(-(\alpha(D_o(t'-\tau))^{1/2} + x/2/(D_o(t'-\tau))^{1/2})^2\right) d\tau \right.$$

Use of the semi-infinite solid approximation is valid since with the values of α to be used in R(x) the first moment of R with respect to depth (x) is just a few centimeters below the interface. For small times this solution can be integrated directly by use of a computer or the problem can be solved sequentially for new initial conditions. In the present case direct integration was used to

approximate the solution at successive times. Using the temperature-time dependent functions for diffusion (f(t)) and reaction (g(t)) given earlier (e.g., Figure V-41), assuming $R(x)/(1 + K) = 23\ e^{-4x}$ mM/yr as found for NH_4^+ production in the decomposition experiments at NWC, and taking the maximum (22°C) effective diffusion coefficient for NH_4^+ corrected for adsorption to be: $D/(1 + K) = 1 \times 10^{-5}$ cm^2/sec (315 cm^2/yr, based on flux measurements, see below and Chapter III), then a sequence of curves can be generated for the actual time t over a period of a year or more. In order to eliminate diffusion from below from masking the seasonal pattern, the initial condition: $C_{NH_4^+}$ = 0.1 mM was used and the starting time taken as fall. This means cos ωt is changed to sin ωt in f(t) and g(t) (equation 13). In the real case the depth dependence of D cannot be ignored since it influences the depth and shape of the seasonal concentration maximum. In addition the depth and time dependence of D are not really separable functions since at deeper depths the time dependence of D is determined by physical rather than biological response to temperature so that f(t) is also a function of depth. The diffusion of heat into the sediment will also complicate the time dependence in deep regions of sediment. All of these complications are ignored here.

The model sequence of change in pore water concentration profiles of NH_4^+ at NWC through the year is shown in Figure V-45. Some of the basic features of the time dependence are reproduced by the model as can be demonstrated by comparison with actual data given in Figure V-28. The

maximum concentration is at ~5 cm. The major discrepancy occurs in the top 0-1 cm interval where the predicted concentration is always less than observed. An additional problem is that the early fall is the predicted time of greatest concentration. This latter problem may be related to a misrepresentation of the transport geometry as discussed below under radial diffusion. The former discrepancy may be related to underestimating NH_4^+ production, for example, ignoring denitrification, in the top few centimeters.

The depth of the concentration maximum and the NH_4^+ concentration predicted for the 0-1 cm interval can be altered by taking denitrification into account. Assuming that all NO_3^- is eventually reduced to NH_4^+ (this is a maximum estimate since N_2 and N_2O are more likely products) then ammonia production from this source at NWC can be roughly estimated as follows. NO_3^- is at background (~0.5 μM) by ~3 cm at all times of year (Rosenfeld, personal communication; Figure V-40, Appendix IV) and in particular during the fall when overlying water levels of NO_3^- are ~10 μM. The concentration of NO_3^- in the 1-2 cm interval is ~1 μM above background. Assigning this concentration to a depth of 1.5 cm and assuming a one dimensional, steady state transport-reaction equation which describes NO_3^- pore water distribution to be (no compaction, adsorption, notation as in equation 12):

$$(23)\quad \frac{\partial C}{\partial t} = 0 = D\,\frac{\partial^2 C}{\partial x^2} - R_o e^{-\alpha x}$$

where: $x = 0;\ C \sim 10\ \mu M$

$x = 1.5,\ C \sim 1\ \mu M$

$x = 3;\ C \sim 0\ \mu M$

then $R \sim 5e^{-1.6x}$ mM/yr. D was estimated to be 6×10^{-6} cm^2/sec (the infinite dilution diffusion coefficient for NO_3^- given by Li and Gregory (1974) was modified by a factor of 0.37 for tortuosity based on the ratio of the measured D for $SO_4^=$ found for Long Island Sound sediment relative to the infinite dilution D for $SO_4^=$ (see Goldhaber et al., 1977)). This calculation suggests that denitrification could result in about a 20% increase (maximum) in ammonia production near the interface during the fall. At other times of year when overlying water is lower in NO_3^- (Harris, 1959) this contribution will also be lower. Taking denitrification into account, a new $R(x) = 28e^{-.5x}$ mM/yr was used in the time dependent model and the new warm period concentration profiles given in Figure V-45. The maximum in the profile, as expected, is more skewed toward the interface and the 0-1 cm concentrations increased slightly.

The basic temporal pattern of change in concentration profiles is reasonably well described by this simple model suggesting that the description of the processes involved is not grossly inadequate. In addition to ignoring the more complicated nature of time and depth dependence of D, which is an obvious shortcoming, the model calculations indicate that the production

rates of constituents like NH_4^+ are probably underestimated and that the pore water transport rates estimated for the fall are too low to entirely eliminate the concentration maximum. This latter point is discussed further below. Note that the periodic oscillations of concentration in the upper few centimeters will result in a damped oscillation at depth in the sediment similar to that found for Cl^- concentrations in estuarine deposits (e.g., Matisoff et al., 1975; Holdren, Bricker, and Matisoff, 1975).

Horizontal and radial diffusion

The one dimensional, Cartesian coordinate model used above and the qualitative arguments made previously indicate that the basic features of time dependence in profile shape can be produced by the temperature dependence of reworking and metabolic activity. The one dimensional model cannot adequately describe transport in the bioturbated zone however, because the presence of burrows alters the geometry of diffusion (Chapter III). A model using only vertical diffusion can be shown to be conceptually incorrect as a description of transport in a burrowed interval as follows.

The relative importance of vertical (x) versus horizontal (y) diffusion can be compared by simple scale analysis. Assuming transport is approximately equal in both dimensions then:

$$(24) \qquad D_x \frac{(\Delta C)}{(\Delta x)} = D_y \frac{(\Delta C)}{(\Delta y)}$$

D_x = diffusion coefficient in x dimension

D_y = diffusion coefficient in y dimension

To account for the same reduction in concentration by transport in the x or y dimension requires either a difference in D_x relative to D_y or a difference in transport distance so that:

$$(25) \quad \frac{D_x}{D_y} = \frac{(\Delta x)}{(\Delta y)}$$

Further assuming that only molecular diffusion will be allowed and that sediment properties are homogeneous in the two dimensions, then $D_x = D_y$ and the relative importance of horizontal and vertical diffusion will depend predominately on the distance required for diffusion. In the bioturbated zone of marine sediment the distance Δy is simply half the distance between burrows (Chapter III) while Δx is the distance from the interface. Examination of x-radiographs and faunal analysis from, for example, station NWC indicates that where Δx = 0-2 cm, $\Delta y \sim 0.25$-0.5 cm; Δx = 2-5 cm, $\Delta y \sim 0.5$-1 cm; x - 5-20 cm, $\Delta y \sim 2$-3 cm; Δx = 20-100 cm, $\Delta y \sim 5$-15 cm. These distances are defined more exactly below for purposes of calculation. The Δy for the depth interval 20-100 cm was roughly estimated from four 10 cm diameter cores, two of which had open crustacean burrows running most of the core length and two of which had horizontal sections of open or recently infilled

(watery) burrows (see Benninger et al., 1976 and in preparation). These cores were taken randomly suggesting that crustacean (Squilla) burrows average between 10-30 cm apart at depth; even if burrows were 50 cm apart $\Delta y \sim 25$ cm would still be considerably smaller than Δx at a depth of ~ 1 m. These estimates of Δy at depths below 20 cm are also reasonable based on distance between surface openings of large burrows. This simple analysis shows that because of the presence of burrows in the upper ~ 20 cm of sediment an ion never has much farther than ~ 2 cm to travel in order to contact overlying sea water. Sea water concentrations or near sea water concentrations are maintained in burrows by irrigation activity (Chapter II).

Because animals which form burrows are often mobile as occurs at NWC, rather than sedentary as at DEEP, and because these animals are of different sizes it is not possible to describe the exact geometry of burrow position, particularly near the interface, as was done for the single species case in Chapter III. Instead it is possible to imagine a geometrical analogue to the average geometry of diffusion in the bioturbated zone. Because burrows are tubes, diffusion can be envisioned as taking place in a system of cylindrical symmetry, where ions diffuse toward the hollow center (the actual burrow) of a cylinder of sediment. If ℓ = the average length of burrow/unit volume of sediment in a given vertical depth interval, then all sediment in that interval can be assigned to be within a certain average radial distance r_2 to a burrow where $r_2 = 1/(\pi\ell)^{1/2}$. If the average burrow radius in that same

interval is r_1 then transport exchange resulting from burrows can be modeled as a single hollow cylinder (an annular section of sediment) having r_1 as inner boundary and r_2 as outer boundary. There must be no flux across the outer boundary since ions at radial distance $r_2 + \Delta r$ are assigned to diffuse to the center of another section of the average hollow cylinder, that is, another burrow (see Chapter III for specific case). This type of approach has been used previously to model water transport in soil profiles in the presence of roots (Gardner, 1960; Cowan, 1964).

In general, r_1 and r_2 are functions of depth and time. During periods of high activity and high populations (summer, fall) r_2 will decrease (ℓ increase) and then increase during periods of low activity and low populations (winter) or at depth in sediment at all times. The inner boundary r_1 increases with depth since larger animals burrow deeper than smaller and also increases through time because seasonal growth may increase the size of the average animal. It will be shown that it is actually change in r_1 and r_2 with time and space which alters transport, not a deviation of diffusion from the molecular rate.

The average geometrical analogue for diffusion paths envisioned in the bioturbated zone is shown in cross section in Figure V-46A. This analogue clearly becomes better as animals become less mobile, or burrows more permanent and therefore will be most useful for describing transport a few

centimeters below the interface or in bottom areas where animals are mostly sedentary. Both vertical and radial diffusion are allowed in the exact case and diffusion takes place across both the plane $x = 0$ and the inner boundary at r_1. Because r_1 and r_2 are functions of depth, the solution to this problem is quite complicated. But, it is possible to demonstrate the importance of radial transport into burrows by considering a greatly simplified case. Consider a series of sediment intervals represented by hollow cylinders stacked vertically, each having the average r_1 (burrow diameter) and r_2 $(1/(\pi \ell)^{1/2})$ found in that interval. The geometrical analogue is shown in Figure V-46B. Ignoring vertical diffusion so that each section can be treated as an infinite hollow cylinder it is possible to solve for the average concentration in each section. These average concentrations can be plotted as a function of depth in the sediment to obtain the vertical pore water concentration profile which would be produced by diffusion into burrows only. Since many burrows are vertical the radial component can be considered predominately horizontal diffusion.

For any sediment interval (vertical) $L_1 \leq x \leq L_2$, the equation:

$$(26) \quad \frac{\partial C}{\partial t} = \frac{D}{r} \left(\frac{\partial}{\partial r} \left(r \frac{\partial C}{\partial r} \right) \right) + R$$

C = concentration

r = radial dimension

D = molecular diffusion coefficient modified for tortuosity

R = average term in the interval; i.e., constant.

must be solved for: $r_1 \leq r \leq r_2$

$$t = 0,\ C = C_o$$

$$t > 0,\ \left(\frac{\partial C}{\partial r}\right)_{r_2} = 0$$

$$,\ C(r_1) = C_1$$

This equation has been solved by Muskat (1934, p. 82) if the initial conditions in his solution are defined to account for R and the appropriate steady state solution added. Because of the rough nature of the present calculations and the short distance for diffusion (small time to steady state) only the steady state case will be considered here. This case serves to illustrate much of the behavior of the model.

At steady state, ignoring adsorption,

$$(27)\quad \frac{\partial C}{\partial t} = 0 = \frac{D}{r}\left(\frac{\partial}{\partial r}\left(r\,\frac{\partial C}{\partial r}\right)\right) + R$$

Therefore:

$$(28)\quad C = A + B\ln r - \frac{Rr^2}{4D}$$

Since: $C = C_o,\ r = r_1$

$$\left(\frac{\partial C}{\partial r}\right)_{r_2} = 0,\ r = r_2$$

then: $$(29)\quad A = C_o - \frac{Rr_2^2}{2D}\ln r_1 + \frac{Rr_1^2}{4D}$$

$$(30) \quad B = \frac{Rr_2^2}{2D}$$

For any given depth interval for which the values of r_1, r_2, D and R are known, the average concentration due strictly to radial diffusion is given by:

$$(31) \quad \bar{C} = \frac{2\pi \int_{r_1}^{r_2} Crdr}{2\pi \int_{r_1}^{r_2} rdr}$$

Likewise the flux of material from any given zone can be calculated and summed over the entire depth interval to obtain an estimate of the flux due to burrows as discussed later.

In order to see whether radial diffusion could have a quantitatively important effect compared to vertical diffusion it was necessary to determine r_1 and r_2 as a function of depth in the sediment. This was done for NWC as follows. Approximately 15 x-radiographs were examined for obvious open burrows at different depths of sediment, r_1 was recorded and r_2 calculated from the burrow length and the known thickness (2.5 cm) of the x-rayed slab. In addition, macrofaunal samples taken at NWC July 16, 1975, October 29, 1975 (courtesy D. Rhoads), and March 19, 1976 (Appendix III) were examined and the cross sectional area of each specimen collected was measured. The average cross sectional area for each species was determined to obtain r_1

for each. Meiofaunal samples taken at the same time (Yingst, 1977) were also examined with the aid of J. Yingst and average r_1 for several of the species also represented in the macrofauna was determined. The species considered and their average burrowing depths are: Nucula (0-2 cm), Yoldia (0-4 cm), Macoma (0-2 cm), Tellina (0-3 cm), Pitar (0-2 cm), Nephtys (0-12 cm), Owenia (0-3 cm), Pectenaria (0-2 cm), Strebilospio (0-3 cm). Many of the deeper burrowing fauna known to be present from diver observation and x-radiographs are absent from the faunal samples so that open burrows determined from the x-radiographs are important in determining r_1 and r_2 below $\sim$3 cm depth. The average minimum r_1 and r_2 for a given sediment interval based on the number and size of animals only (not on the number of burrows constructed per day or any measure of activity) is: 0-1 cm, $\bar{r}_1$ = .014 cm, $\bar{r}_2$ = .24 cm; 1-2 cm, $\bar{r}_1$ = .077, $\bar{r}_2$ = .79; 2-3 cm, $\bar{r}_1$ = .14, $\bar{r}_2$ = 1.3; 3-4 cm, $\bar{r}_1$ = .21, $\bar{r}_2$ = 2.7, 4-5 . . . 11-12 cm, $\bar{r}_1$ = .17, $\bar{r}_2$ = 4. From x-radiographs the average r_2 below 3 cm depth is $\sim$2 cm and this latter r_2 together with the average r_1 values, and r_2 values above 3 cm depth, from the faunal data were also used in calculations.

NH_4^+ is used as an example; for illustration the values $D = 7 \times 10^{-6}$ cm^2/sec and $R = 46e^{-.4x}$ mM/yr for the appropriate diffusion coefficient and reaction terms. Adsorption does not enter the calculation for steady state with no advection (Berner, 1976b) so the value taken for R is approximately

twice the value found in the decomposition experiments (equation 4 with K = 1). The average R for a given depth interval for use in the radial model is:

$$(32) \quad \bar{R} = \frac{\int_{L_1}^{L_2} R\,dx}{\int_{L_1}^{L_2} dx}$$

Using the appropriate average R, r_1, and r_2 values for the intervals 0-1, 1-2, 2-3, 3-4, 4-5, 5-6, 6-8, and 8-10 cm, equation (31) predicts the concentration profile resulting only from radial diffusion shown in Figure V-47. The sea water value for NH_3 is taken as 1 μM. For comparison the solution to the steady state Cartesian coordinate case where (notation as in equation 12):

$$(33) \quad \frac{\partial C}{\partial t} = 0 = D\left(\frac{\partial^2 C}{\partial x^2}\right) + R$$

$$x = 0, \; C = 1\ \mu M$$

$$x = L \text{ (L large)}, \; \left(\frac{\partial C}{\partial x}\right)_L = 0$$

$$R = 46e^{-.4x}$$

is plotted for $D = 7 \times 10^{-6}$ cm^2/sec and $D = 3 \times 10^{-5}$ cm^2/sec. It is necessary to increase the effective D to approximately 3×10^{-5} cm^2/sec to obtain concentrations at depth by vertical diffusion comparable to those obtained by radial diffusion into burrows at the same depth by simple molecular diffusion.

These calculations illustrate several extremely important points. Radial diffusion into burrows is capable of significantly lowering pore water concentrations below that predicted by only vertical molecular diffusion. This lowering of concentration is particularly great when the average reaction term, R, is small as is generally true at depth in a deposit (note 8-10 cm interval, Figure V-17). When both vertical and horizontal (radial) diffusion are considered together it is clear that at observed burrow densities the pore water profiles found at stations such as NWC or DEEP or during the fall at all stations, which superficially result from extraordinary exchange rates, can be readily accounted for by molecular diffusion and an appropriate description of the geometry of diffusion.

Although conceptually useful the radial model requires a considerably greater quantity of information about the sediments under study than does the use of stochastic diffusion coefficients and the usual one dimensional, Cartesian coordinate model. As noted above and in Chapter III, near the interface and when animals are mobile it is impossible to accurately determine r_1 and r_2. Below this region the radial model is useful in explaining the apparent rapid exchange of pore water observed by many investigators in the upper $\sim$ 1 m of sediment underlying oxygenated water (e.g., Sholkovitz, 1973; Thorstenson and Mackenzie, 1974; Goldhaber, 1974). Of these investigators only Goldhaber (1974) attributed exchange to biogenic reworking.

Material flux of N and P between sediment and overlying water in LIS

The sea floor is an important site for nutrient regeneration and acts as a source of continual supply of remineralized material to overlying water (Rittenberg, Emery, and Orr, 1955). Direct measurement of fluxes of nitrogen and phosphorus compounds from marine or fresh water bottom sediments have been made by many investigators (e.g., Tessenow, 1972; Hartwig, 1973; Kamp-Nielsen, 1974; Hale, 1975; Rowe et al., 1975). Pore water concentration profiles have also been used to calculate theoretical fluxes by measuring the concentration gradient, assuming a diffusion coefficient, and employing Fick's First Law to obtain a flux (e.g., Bray, Bricker, and Troup, 1973; Billen, 1975; Norton and Sasseville, 1975). In some cases measured fluxes and concentration gradients have been used to obtain effective diffusion coefficients assuming a Fick's Law relation (e.g., Tessenow, 1972; Fanning and Pilson, 1974; Kamp-Nielsen, 1974). In this study both pore water profiles and flux measurements were made seasonally and it is possible to determine how well molecular diffusion, in conjunction with pore water gradients, predicts the observed fluxes at any given time. Deviation from or agreement with theoretical expectations can be used to substantiate or disprove conceptions about transport-reaction processes near the sediment-water interface which were developed earlier. The relative importance of different depositional environments in central LIS in nutrient regeneration and

sediment-water interaction can also be assessed and together with earlier studies of nutrient budget in LIS (Riley, 1956b; Harris, 1959), the role of bottom sediments as a nutrient source determined.

If one dimensional (vertical) diffusion in Cartesian coordinates is assumed then Fick's First Law gives in noncompacting sediments:

$$(34) \quad F_x = -\varphi D \left(\frac{\partial C}{\partial x}\right)_x$$

F: flux of dissolved material across plane x

φ: porosity at x

D: molecular diffusion coefficient

C: concentration of the constituent under consideration

In compacting sediments (e.g., Imboden, 1975):

$$(35) \quad F = -\varphi D \left(\frac{\partial C}{\partial x}\right) - \varphi v C$$

v: advection velocity of pore water with respect to the interface

Advection, which might also include a biogenic transport term, is assumed to be zero in the following calculations. As discussed in the last section, the presence of burrows can result in a radial geometry for transport. In general this geometry changes with depth (e.g., Figure 46) but assuming an average burrow size and density in sediment and ignoring vertical diffusion entirely, then diffusion can be described as purely radial and on the average

is equivalent to transport into the interior cavity of an infinite hollow cylinder having inner radius r_1 equal to the average burrow radius and outer r_2 determined by burrow density (ℓ). There is no flow across the outer cylinder boundary. In this case:

$$(36) \quad F_{r_1} = \varphi D \left(\frac{\partial C}{\partial r}\right)_{r_1}$$

If: $\frac{\partial C}{\partial t} = 0 = \frac{1}{r} \frac{\partial}{\partial r} \left(r \frac{\partial C}{\partial r}\right) + \frac{R}{D}$ $\qquad r_1 < r < r_2$, $\left(\frac{\partial C}{\partial r}\right)_{r_2} = 0$

R: constant average production or consumption term in burrowed sediment

Then from equations (28-30):

$$(37) \quad F_{r_1} = -\varphi D \left(\frac{Rr_2^2}{2Dr_1} - \frac{Rr_1}{2D}\right)$$

$$= -\varphi \left(\frac{Rr_2^2}{2r_1} - \frac{Rr_1}{2}\right)$$

These two approaches, pure vertical diffusion and pure radial diffusion allow different options if the measured flux deviates from the predicted. In the case of vertical diffusion the value of D may be increased or decreased to fit the flux to the calculated gradient. For pure radial diffusion it is necessary to have some independent information on average R in the burrowed zone, average r_1 or average r_2 ($r_2 = 1/(\pi \ell)^{1/2}$), ℓ = burrow density in cm/cc) but D is fixed at the molecular value. If the average cylinder model is used then the measured flux allows calculation of R, r_1, or ℓ if any two are fixed by independent means.

The theoretical flux predicted by vertical diffusion can be calculated by fitting the concentration curve with an equation and differentiating to obtain the gradient. Evaluating at $x = 0$ and use of equation (34) with an appropriate D and φ results in the calculated flux at the sediment-water interface. The $\lim_{x \to 0} \varphi$ is taken as 1; this is arguable but in muddy sediments $\varphi = 0.8$-.9 in the top 0-1 cm in any case. The chief problem in estimating the flux is the fact that sampling is made only over finite intervals, in this case 1 cm. Particularly at NWC, the majority of the concentration change between sea water and sediment takes place in the top 0-1 cm and the functional form of C in that centimeter is unknown. Assuming that $C = a_o + a_1 x + a_2 x^2 \ldots$ (a_0, a_1, $a_2 \ldots$ can be positive or negative) then over any finite sampling interval x_1 to x_2 the average concentration $\bar{C}$ is:

$$(38) \qquad \bar{C} = \frac{\int_{x_1}^{x_2} C\,dx}{\int_{x_1}^{x_2} dx}$$

Because of the shape of the profiles a_1 is determined almost entirely by the first sampling interval and the addition of polynomial terms beyond x^2 does little to change a_1 if only the top few data points in a profile are fit to the equation. If concentration values below the top few centimeters are included in the polynomial fit, however, a_1 is significantly lowered. In this study the simplest possible approach was taken, C was assumed to be given by

$C = a_o + a_1 x + a_2 x^2$, a_o was fixed at the seawater value (~ 0) and the top two 1 cm sampling intervals used to solve the simultaneous equations:

$$(\bar{C} - a_o) = \left(\frac{a_1 x^2}{2} + \frac{a_2 x^3}{3}\right)\Big|_0^1$$

$$(\bar{C} - a_o) = \left(\frac{a_1 x^2}{2} + \frac{a_2 x^3}{3}\right)\Big|_1^2$$

(For DEEP-3 the intervals 0-2, and 2-3 cm were used.)

In general, this procedure maximizes the calculated flux; it is important to realize that other approaches to calculating the concentration gradient for example: inclusion of deeper profile points or not accounting for the finite sampling interval, significantly lower the calculated flux. The use of only near surface samples is consistent with the fact that most decomposition is thought to take place at or just below the interface.

The diffusion coefficient for NH_4^+ at different temperatures was estimated by first obtaining a correction factor for sediment diffusion relative to the infinite dilution coefficient using the ratio of the SO_4 coefficient (20°) determined for LIS sediment by Goldhaber et al. (1977) relative to infinite dilution (Li and Gregory, 1974) and then applying this correction factor (0.37) to the theoretical NH_4^+ diffusion coefficient calculated from the values and temperature dependence determined by Li and Gregory (1974). This gives for D_N: 7.0×10^{-6}, 6.0×10^{-6}, and 4.3×10^{-6} cm^2/sec at 22°, 15°, and 4° respectively. For $HPO_4^=$, the same sediment--tortuosity factor was used

and temperature correction of 2.19/25° predicted by the Stokes-Einstein relation employed (Li and Gregory, 1974) to give D_p: 3.0×10^{-6}, 2.4×10^{-6}, 2.0×10^{-6} cm^2/sec at 22°, 15°, and 4°. The calculated NH_4^+ and $HPO_4^=$ fluxes are tabulated underneath the measured fluxes in Table V-3.

Ammonia.--There are several interesting trends in the data; NH_4^+ will be considered first. At FOAM the calculated NH_4^+ flux is in good agreement with measured flux at all times of the year; in fact, the predicted flux is slightly greater in all cases by about 10%. The measured flux at NWC is higher than predicted at all times. In order to account for the discrepancy by transport processes only, the effective diffusion coefficients must be: 1.2×10^{-5}, 1.0×10^{-5}, and 6.2×10^{-6} cm^2/sec during the summer, fall, and winter respectively. This is about 1.7 times molecular diffusion relative to normal NH_4^+ transport rates. The same pattern as occurs at NWC is also present at DEEP except that predicted NH_4^+ fluxes are quite close to measured fluxes even during the summer and fall. The effective diffusion coefficients needed to bring the measured fluxes at DEEP into agreement with predicted fluxes are: 8×10^{-6}, 7×10^{-6} and 4.8×10^{-6} cm^2/sec.

Part of this disagreement may result from direct excretion of NH_4^+ by animals rather than biogenic alteration of transport processes. Harris (1959) determined NH_4^+ excretion rates for Yoldia limatula and Nephtys incisa, the predominant macrofauna at NWC, and found these to be 0.059

and 0.049 μmoles/mg-drywt./day. The average dry weight (decalcified) per individual at NWC is 0.048 g and 0.036 g for Yoldia and Nephtys respectively (Rhoads, personal communication). Using the average population densities of these animals at NWC of $\sim 300/m^2$ and $\sim 170/m^2$ (Rhoads, Aller, and Goldhaber, 1976; Rhoads, personal communication; and Appendix III) this predicts an excretion flux due to Yoldia of 0.84 mmoles/m^2/day and due to Nephtys of 0.3 mmoles/m^2/day during warm periods ($\sim 17^{\circ}$) or a total excretion flux $\sim$ 1.1 mmoles/m^2/day. This estimate is about double the estimate made by Harris (1959) as to the amount of excretion by total bottom fauna. In the case of summer NWC flux, subtraction of this calculated contribution due to excretion lowers the required D to $\sim 9.5 \times 10^{-6}$ cm^2/sec to explain the data. At all other times and stations, addition of excretion to NH_4^+ predicted flux values brings the measured fluxes into such close agreement with the predicted that a D value different from the molecular values used cannot be discerned. It was demonstrated earlier, based on laboratory experiments, that the effective biogenic D due to Yoldia is $\sim 1 \times 10^{-5}$ cm^2/sec (Chapter III) which is in excellent agreement with the effective D $\sim 0.95 \times 10^{-5}$ cm^2/sec calculated above. This effective biogenic transport D is close enough to the molecular D_N of NH_4^+ of $\sim 7 \times 10^{-6}$ cm^2/sec that assumptions used in calculating the flux become significant with respect to determining transport effects of infauna. Additional problems which tend to make the measured fluxes minima are the lack of current or wave effects in the cores

(Hale, 1975), the fact that biological activity may become lower at low O_2 concentrations which become effective in the flux cores (e.g., Mangum and Van Winkle, 1973), and the possibility that nitrification may take place. The second problem was minimized by periodic oxygenation of the water.

Several important conclusions concerning NH_4^+ flux measurements can be made on the basis of these data and analysis: (1) Calculation of NH_4^+ flux to within a factor of 2 at all times, may be made using Fick's Law, the above molecular diffusion coefficient, and the concentration gradient determined from the value of NH_4^+ pore water concentration in the top 0-1 cm (assign to depth ~ 0.5 cm) relative to overlying water. During the winter and at stations which lack intense near interface mixing by animals such as protobranchs, the predicted NH_4^+ flux will be the same as that measured by the present techniques. (2) The effective biogenic pore water diffusion coefficient for NH_4^+ is $\sim 1 \times 10^{-5}$ cm^2/sec at NWC and $\leq 1 \times 10^{-5}$ cm^2/sec at all stations in the Sound. This compared with an effective biogenic particle diffusion coefficient at NWC of $\sim 1 \times 10^{-6}$ cm^2/sec (Aller and Cochran, 1976; Chapter IV) and indicates pore water transport of $\sim 10 \times$ particle transport. This relation is consistent with experimental and literature data which show true irrigation rates of about 100 x particle transport data (Chapter I, II, III). (3) NH_4^+ flux is seasonal; it is highest in summer and lowest in winter as found in previous studies (Hartwig, 1973; Hale, 1975; Rowe et al., 1975). NH_4^+ flux also varies spatially in the central Sound.

It is highest at NWC, a protobranch dominated area, and lowest at DEEP. During the winter, all stations have essentially the same flux rates. These increase exponenitally with temperature so that in summer NWC has almost 5x the NH_4^+ flux of DEEP (Figure V-48). Assuming that the winter is a time of physically controlled flux sustained by molecular diffusion while at other times of year biological production and transport dominate, then it is theoretically invalid to apply a single temperature relation such as an Arrhenius-type equation to the entire yearly cycle since the temperature dependence of the processes involved change. Nevertheless, such equations are useful analytical expressions if yearly average nitrogen fluxes are desired for large regions of the Sound. The relatively short period of physical control should reduce problems resulting from changing T dependence.

If $F = F_o \exp(-E/(RT))$, where F = flux, T = absolute temperature, E = apparent activation energy, R = 1.987, then:

$E = 19.2$ Kcal/mole; $F_o = e^{33.3}$ FOAM

$E = 26.2$ Kcal/mole; $F_o = e^{46.0}$ NWC

$E = 16.2$ Kcal/mole; $F_o = e^{27.5}$ DEEP

The apparent activation energy is quite similar to that found for sulfate reduction and suggests production rather than transport control on the absolute value of the fluxes in the case of NH_4^+. This can be easily demonstrated to be reasonable mathematically in the end-member steady state case, since if

for pore water (same symbols used previously):

$$(39) \quad \frac{\partial C}{\partial t} = 0 = D \frac{\partial^2 C}{\partial x^2} + Re^{-\alpha x}$$

$$C = 0; \quad x = 0$$

$$x = L \; (L >> \frac{1}{\alpha}); \quad (\frac{\partial C}{\partial x})_L = 0$$

then at steady state: $F = \frac{R}{\alpha}$

and the flux is production controlled.

Taking $T = 285 - 10 \cos 2\pi t$, (where t = time in years, $\omega = 2\pi/yr$) and averaging the time dependent flux functions by numerical integration, the resulting yearly average NH_4^+ fluxes are: 0.90, 1.8, and 0.49 mmoles/m^2 for FOAM, NWC, and DEEP. Protobranch inhabited bottom areas like NWC are the most important source regions of NH_4^+ to overlying water. Because of the possibility of nitrification at the sediment-water interface which might lower the measured NH_4^+ flux, these average values must be considered minimum measures of N regeneration rates at each station; but, based on standing crop measurements of pore water NO_3^- in LIS sediments (Figure V-40) and studies of NO_3^- fluxes in similar environments (Hale, 1975), sediments can be considered a sink rather than a source for NO_3^- in LIS.

Harris (1959) estimated the average daily N requirement of plankton in the central Sound for 1952 to 1954 to be 6.1 (1952-3)--5.1 (1953-4) moles/m^2/day of which he could account for roughly 4.0--2.2 mmoles/m^2/day

respectively by zooplankton excretion. The remainder was believed to come from bacterial regeneration in the water column or sediments. Depending on how average areas of bottom are assigned to corresponding flux rates like that of FOAM, NWC, or DEEP it is apparent that bottom regeneration alone can account for most of the remainder, assuming continuity in N utilization between the 1952-1954 period and 1975-1976. The very similar range of values obtained for the required bottom regeneration rates (Harris, 1959) and the actual measured values of this study is good evidence that the N budgets for the central Sound were well described by the calculations of Harris (1959) and Riley (1956b).

Phosphate.--Comparison of phosphate flux with predicted flux based on Fick's Law (Table V-3) show that measured fluxes are higher than predicted at all stations during summer. During the winter the measured fluxes are close to or slightly lower than predicted at NWC and DEEP and can be considered in good agreement. At FOAM, the winter flux was below the detection limit. The fall flux measurements and possibly the winter FOAM sample, are minimum values because of problems with the technique of measurement. During the fall the flux of Fe^{++} is quite high (Chapter VI) and dissolved Fe and Fe-colloids build-up rapidly in water overlying the flux core. These colloids either strip $HPO_4^{=}$ out of the water overlying the core as Fe precipitates, or, when water is filtered, Fe-oxide which builds up on the filter may strip $HPO_4^{=}$ out of water as it passes through. This was apparently

not a problem at NWC but was at FOAM and DEEP because of particularly high Fe^{++} fluxes at those stations. In the latter two cases, the measured fluxes are slightly lower than predicted by molecular diffusion while at NWC the actual flux is much higher than predicted.

Correction of the fluxes for $HPO_4^=$ excretion by macrobenthos was made as follows. Harris (1959) gives $HPO_4^=$ excretion rates for Yoldia and Nephtys as 0.0049 and 0.0039 µmoles/mg-dry wt./day. Using the average population densities for NWC given above results in a $HPO_4^=$ excretion flux for summer and fall of 0.093 mmole/m^2/day at NWC and a winter value of 0.026 mmoles/m^2/d assuming a $Q_{10} = 2$ (see Chapter I). Fall and winter faunal data at FOAM and DEEP are given in Appendix III. At DEEP, the species: Pherusa, Clymenella, Nephtys, Mulinia, and Pitar were considered abundant enough to affect the flux measurements. Taking the average individual weights given for these animals (15, 3.9, 5.7, 0.27, 3.3 mg respectively) at nearby station 5 of Sanders (1956) and assigning all bivalves the excretion rate for Yoldia and all polychaetes that of Nephtys, the resulting fall and winter values are: 0.023 and 0.0039 mmoles/m^2/day. Winter values were decreased by 3.5x assuming a $Q_{10} = 2$. The same calculation was made for FOAM for the species: Ampelisca, Clymenella, Yoldia, Nucula and Nephtys (individual weights = 0.3, 3.9, 48, 1, 36 mg) which, assuming Ampelisca has an excretion rate ~ 0.004 µmoles/mg/day, yields fall and winter values of 0.012 mmoles/m^2/day and 0.008 mmoles/m^2/day. The summer value is

taken as equivalent to fall for the sake of calculation.

After subtraction of the excretion corrections from the summer measurements at all stations and from the fall flux measurement at NWC, it is found that the observed flux is still much higher than predicted. The effective diffusion coefficients required to account for the discrepancy are for FOAM: 0.5×10^{-5}, for NWC: 0.9×10^{-5} (summer), 4×10^{-5} (fall); DEEP: 1.2×10^{-5} cm^2/sec. In all cases these are higher than the assumed molecular diffusion coefficient for $HPO_4^=$ at the appropriate temperature and are similar to the values used for NH_4^+. The fall NWC effective value is excessively high suggesting that either the excretion correction is too low or more likely that the measured concentration gradient is too low, i.e., the analytical concentration for $HPO_4^=$ in the top centimeter is lower than actually present. Because of the susceptibility of $HPO_4^=$ to oxidation effects and coprecipitation with Fe during processing (Bray, Bricker, and Troup, 1973) an analytical error is not unlikely. In all other cases, the effective diffusion coefficients are consistent with biogenic transport of pore water at a rate $\sim 1 \times 10^{-5}$ cm^2/sec during summer.

This is consistent with the previous inability to see a strong influence of biogenic transport on the flux of NH_4^+ since the effective coefficient is very close to the actual molecular D_N values. The calculated values are also consistent with previous estimates of rates of biogenic pore water transport.

These calculations indicate that the magnitude of the $HPO_4^=$ flux during summer and fall is controlled by biogenic reworking.

If the calculated macrofaunal excretion contributions are correct, than the winter flux of $HPO_4^=$ at NWC can be entirely explained by excretion. At both FOAM and DEEP, the measured value is either undetectable or lower than predicted by pure diffusion. It was shown earlier that the concavity in HPO_4 pore water profiles during the winter reflects the dominance of inorganic adsorption or precipitation reactions characteristic of phosphate--iron interactions at that time. Earlier investigations have suggested that $HPO_4^=$ diffusion out of sediments may be hindered by Fe-oxides near the interface (e.g., Mortimer, 1941; 1971; Hayes, 1964). Both the pore water profiles and the low $HPO_4^=$ flux suggest that this is what is happening at all stations during the winter. This is indicative of the general increase in dominance of physically controlled reactions in cold periods. At other times of the year these reactions are masked by high production rates of dissolved $HPO_4^=$ by bacteria and higher biogenic transport.

Riley (1956b) estimated bottom phosphate regeneration rates using oceanographic data (also used by Harris, 1959, for N budget calculation). Average seasonal bottom fluxes for 1952-1954 were calculated as: 0.25, 0.24, and -0.02 mmoles/m^2/day for summer, fall, and winter. The negative winter value suggests net extraction by bottom sediments; this is not

unreasonable given the nature of $HPO_4^=$ pore water profiles and the lower than predicted fluxes measured in this study. The values estimated by Riley (1956b) are quite close, within a factor of ~2, to the actual measured values although measured fluxes tend to be somewhat higher. The entire daily $HPO_4^=$ requirement of plankton (Riley, 1956b) can be supplied by the bottom fluxes measured in this study, however, nitrogen not phosphorus is a probable limiting nutrient in LIS (Conover, 1956; Harris, 1959) so that this supply may be considered excess.

One measure of the utilization rate of P and N in overlying water is the residence time, τ, where $\tau = \frac{C_{sw}\, d}{F}$; C_{sw}: sea water concentration, F: flux, d: water depth. Maximum residence times in days can be calculated from the measured fluxes and sea water concentrations for summer, fall and winter (Table V-3, Appendix IV; C_{sw} for DEEP-1 taken as 3 μM):

FOAM:	τ_n = 7.2, 1.8, 3.0;	τ_p = 173, 181, –
NWC:	τ_n = 8.0, 1.7, 51.4;	τ_p = 53, 93, 800
DEEP:	τ_n = 85, 25, 125;	τ_p = 465, 630, 3700

This is not an entirely appropriate calculation but it does indicate the fact that N is limiting rather than P and that maximum N turnover times are on the order of a few days. When excretion and rapid water column decomposition are considered (≥ bottom flux), water column residence time for dissolved N must be less than 1 day.

Because most decomposition takes place near the interface where vertical diffusion is most important and knowledge of the density of burrows is least, and, since simple vertical diffusion explained many features of the fluxes, the radial diffusion model was not applied to these data. Radial diffusion processes can be expected to greatly influence sediment well below the interface and as an end member model is best applied there rather than at the interface. In addition, because of lower rates of decomposition in deeper sediment, radial diffusion may radically alter pore water profiles but only minimally influence the flux of material out of a steadily accreting sediment body. This approximation of only vertical diffusion is least appropriate at DEEP.

Stoichiometry of decomposition

The measured fluxes, standing pore water concentrations, and the decomposition experiments can all be used to obtain information on the relative composition of decomposing organic matter at different stages of the breakdown process and in different regions of LIS. Limits on the N/P ratio in the metabolized portion of organic material near the sediment-water interface are obtained from the flux measurements. Because $HPO_4^{=}$ is more strongly adsorbed to particles than NH_4^{+} and because the method of flux measurement allowed $HPO_4^{=}$ loss by coprecipitation with or sorption by Fe-colloids in water overlying the flux core, these ratios can be considered upper limits due to lowering of measured $HPO_4^{=}$ concentrations. Denitrification ($NO_3^{-} \rightarrow N_2$, $N_2O \rightarrow$ protein $\rightarrow NH_4^{+}$)

will also tend to make these ratios upper limits with respect to the N/P ratio in the decomposing organic fraction but as calculated earlier, it is unlikely this would alter the ratios by more than a maximum of 20%.

The calculated N/P ratios at each station at different times of the year are given in Table V-3. These vary between 4.3-22. Because of the dominance of adsorption reactions during the winter, the high N/P ratios at all stations at that time reflect capture of $HPO_4^=$ by particles near the interface rather than decomposition release. As noted earlier, analytical problems resulting from high Fe flux during the fall almost certainly make the fall ratios at FOAM and DEEP larger than actual values. This leaves summer ratios at all stations and the fall ratio at NWC as most representative of the true N/P release. At NWC and DEEP, the ratio varies between 4-10 while at FOAM the ratio is 17. Assuming that because of the nature of the measurement the lowest values are most nearly correct than the range 4-10 is accepted as the best estimate of the upper limit for the N/P ratio in the metabolized organic fraction.

Harris and Riley (1956) determined that the average N/P ratio of LIS plankton was 16.7 (phytoplankton)--24 (zooplankton). Harris (1959) later determined that excretion of NH_4^+ and $HPO_4^=$ by zooplankton and bottom fauna in LIS varied in ratio between 2.6-21.4 but was mostly between 7-15. The measured limits on N/P ratios determined from the fluxes are lower than

the source of organic material, are in the range of the expected contributions from excretion (Harris, 1959; Johannes, 1968) and in the lower range, are also in accordance with the expected preferential release of P relative to N during early stages of breakdown (e.g., Grill and Richards, 1964; Johannes, 1968). This release will leave an organic substrate greatly depleted in P relative to N for later diagenesis occuring deeper in the sediment body (e.g., Sholkovitz, 1973).

Many studies have shown the preferential release of N relative to C during early decomposition in marine waters or sediments (e.g., Waksman, 1933; Anderson, 1939; Kaplan, Emery, and Rittenberg, 1963; Krause, 1959). Assuming that the carbon stoichiometry of decomposition is roughly represented by $SO_4^=$ reduction rates through equation (6) so that $SO_4^=$ reduced is related to C (HCO_3^-) release through a factor of ~ 2 (Abd-el-Malek and Rizk, 1963; Berner, Scott, and Thomlinson, 1970), then the ratio of NH_4^+ production to $SO_4^=$ reduction rates measured in the decomposition experiments is representative of the N/C ratio of the metabolized organic fraction. At both NWC and DEEP this ratio becomes lower with depth in the sediment as expected from the previously cited studies.

If the ratio of the average $SO_4^=$ reduction rate (R_s) to the average NH_4^+ production rate ($R_N/(1 + K)$) obtained from the decomposition experiments for the upper 10 cm of sediment is compared at NWC and DEEP it is found that $R_s/R_N(1 + K)$ is smaller at NWC (6.5) than DEEP (10.5). Krause (1959) has

demonstrated that a large percentage of the N fraction in zooplankton is released within the first week of decomposition; about 30% is released during the first day of decomposition and a similar percentage is lost almost immediately after death but before true decomposition. These early losses are so fast that they probably do not enter into the sediment inventory of decomposition measured here but it is possible that the slightly greater (~ 2X) the water depth at DEEP may result in a greater N-depletion of source organic material delivered to the interface than at NWC. Higher biogenic particle transport rates at NWC than DEEP in the upper 4 cm may also aid in the capture of highly reactive, N-rich debris into the sediment and away from the resuspended layer. It is also likely as mentioned previously that waters overlying bottom areas like NWC are particularly productive and it is possible that the plankton species composition or physiological state is such that the nitrogen content of their tissue is somewhat different than in other areas (see Harris and Riley, 1956).

Because of the domination of transport, adsorption, and precipitation reactions in controlling the forms of the pore water profiles it becomes very hard to determine from standing concentrations what the source material might be. Since the general trends and limits on N/P and N/C stoichiometry are evident from the previous considerations no further modeling will be done here. These trends are demonstrated qualitatively by noting that the N/P ratio

of standing concentrations increases below the biogenically reworked zone from a value of ~2 to ~9 at FOAM where precipitation of distinct $HPO_4^=$ phases or depletion of P-source may become increasingly important. The N/P standing concentration ratio decreases offshore and is lowest at DEEP, 1-2, where transport (irrigation) dominates pore water profiles.

Summary

(1) Pore water profiles of $SO_4^=$, alkalinity, $HPO_4^=$, and NH_4^+ differ radically in different depositional environments of Long Island Sound. The greatest evidence for extensive sulfate reduction and organic matter decomposition as measured by standing concentrations of pore water metabolites is found in shallow water along the north coast of the Sound; in deeper water sediments the build-up of decomposition products or depletion of $SO_4^=$ in pore water is greatly lowered.

(2) In contrast to pore water data, analysis of the solid phase shows extensive and comparable production of sulfide fixed as FeS (acid volatile sulfide) in all areas. Deep water stations show extensive loss of solid phase sulfide either prior to or after conversion of FeS to FeS_2 (pyrite). All stations have comparable standing crops of organic matter and all stations are capable of supporting approximately the same rate of sulfate reduction in the upper 10 cm of sediment where most decomposition takes place.

(3) All stations show similar seasonal variation in pore water profiles near the sediment-water interface. These are periodic and repeatable from year to year. During the late spring and summer, microbial activity results in high production of NH_4^+, $HPO_4^=$, and alkalinity throughout the sediment column but particularly near the interface. Because decomposition rates often show exponential decrease with depth below the interface, seasonal production results in maxima in pore water concentrations a few centimeters below the sediment surface. In late summer and in the fall, biogenic reworking, particularly fluid transport, results in extensive exchange of sediment pore water with overlying water and a general lowering of NH_4^+, $HPO_4^=$, and alkalinity concentrations or raising of $SO_4^=$. During the winter, pore water profiles become controlled predominately by simple molecular diffusion. The year can then be divided into a relatively warm period (spring, summer, fall) of different types of biogenic control of diagenesis followed by a shorter cold period (winter) when processes are predominately physically controlled.

(4) The oscillatory behavior of pore water profiles near the interface can be accounted for by the different temperature dependence of microbial and macrofaunal activity which control production (consumption) and biogenic transport processes respectively. A nonsteady state model is used to show this is the case.

(5) A conceptually correct description of transport in the zone of bioturbation requires inclusion of horizontal or radial transport of pore water into burrows. Model calculations show that at natural burrow densities molecular diffusion rates can readily explain the observed changes in pore water concentration occurring over short periods of time. When modeled as vertical diffusion only, stochastic diffusion coefficients much greater than molecular must be used.

(6) Equilibrium calculations suggest that $HPO_4^{=}$ is sometimes saturated with respect to a vivianite-like phase near the sediment surface and saturated with respect to whitlockite ($Ca_3(PO_4)_2$) at depth at all stations. Both aragonite and calcite ($CaCO_3$) are undersaturated near the interface at all stations and also in deeper sediment at offshore stations. $CaCO_3$ is lost from sediment and the reworking activities of macrobenthos aid this loss.

(7) The flux of NH_4^+ and $HPO_4^{=}$ out of the bottom varies seasonally and is highest in summer, lowest in winter. NH_4^+ flux measurements can be predicted within a factor of 2 at all times by use of Fick's First Law and knowledge of the pore water concentration in the top 0-1 cm. Deviations from predicted can be accounted for by including direct excretion by macrofauna and by use of an effective biogenic diffusion coefficient of $\sim 1 \times 10^{-5}$ cm^2/sec during the summer. $HPO_4^{=}$ fluxes are complicated by adsorption reactions and interaction with Fe^{++} flux. During the summer, the use of an effective biogenic diffusion coefficient of $\sim 1 \times 10^{-5}$ cm^2/sec was also

found to account for discrepancy between observed pore water gradients and predicted and measured $HPO_4^=$ fluxes. The highest bottom fluxes occurred at NWC, a station of intermediate depth dominated by protobranch bivalves; the lowest fluxes occurred at DEEP, the deepest station. Bottom fluxes are capable of supplying ~30-50% of the daily N requirement of plankton and >100% of the P.

(8) The flux measurements show that P is released preferentially to N during early diagenesis. Decomposition experiments demonstrate that N is released preferentially to C near the sediment surface. These observations are in agreement with previous studies on decomposition.

(9) Many of the diagenetic differences between stations are readily explained in terms of the characteristic macrofauna present in each depositional environment and the associated differences in the types of biogenic transport processes operating.

Table V-1 Long Island Sound Station Location and Description

Station	Location Latitude	Longitude	Depth	Relative Depositional Environment	Sediment Type	Color Stratigraphy	Comments
FOAM	41°14.5'	72°44.8'	∿8 m	Shallow, partially protected near-shore	Silt-clay, sand present, fecal-pelleted surface $\lesssim$ 30% $CaCO_3$ shell debris present in massive layers	Top 0∿3 cm yellow-orange, 3∿10 cm black, olive at > 10 cm	H_2S smell strong below 10 cm
NWC	41°10.4'	72°56.3'	∿15m	Intermediate depth unprotected off-shore	Silt-clay, sand pockets at depths $\gtrsim$ 1 m fecal-pelleted surface $\lesssim$ 10% $CaCO_3$ shell debris present in discrete, thin layers	Top 0∿3 cm yellow-orange, 3-8 cm black, grey at >8 cm. Yellow layer is seasonal in thickness: thin in early summer, thickest in fall. (Rhoads et al, 1977)	H_2S smell absent or faint at all depths sampled
DEEP	41°03.0'	72°53.1'	∿34m	Deep, unprotected, offshore	Silt-clay, thin sand layers present fecal-pelleted surface $\lesssim$ 5% $CaCO_3$ shell debris absent or very scattered	Top 0-0.5 cm orange-yellow. Mottled black & orange from 0.5-10 cm. Grey at $\gtrsim$ 10 cm.	H_2S smell absent or faint at all depths sampled

Table V-2

Sampling Schedule

Station	Date	Chem Box	Flux Box	X-Ray Box	Gravity Core
FOAM-1	08/5/74	X		X	
FOAM-2	03/13/75	X		X	
FOAM-3	07/8/75	X	X	X	
FOAM-4	11/5/75	X	X	X	
	11/17/75		X		
FOAM-5	03/18/76	X	X	X	
FOAMG	07/8/75				X
NWC-1	07/21/74	X		X	
NWC-2	11/11/74	X		X	
NWC-3	03/18/75	X		X	
NWC-4	07/16/75	X	X	X	
NWC-5	10/29/75	X	X	X	
NWC-6	03/23/76	X	X	X	
NWCG	11/11/74				X
DEEP-1	07/23/75	X	X	X	
DEEP-2	11/12/75	X	X	X	
DEEP-3	04/13/76	X	X	X	
DEEPG	11/12/75				X

Table V-3

Flux Measurements (mmoles/m^2/day)

NH_4^+ and $HPO_4^=$

Station	Summer (22°)			Fall (15°)			Winter (4°)		
	NH_4^+	$HPO_4^=$	N/P	NH_4^+	$HPO_4^=$	N/P	NH_4^+	$HPO_4^=$	N/P
FOAM	2.2 ±0.2	0.13±0.01	17±2	0.88±0.08	0.053±.004	17±2	0.26±0.02	-	-
predicted:	2.4	0.07		0.95	0.082		0.37	0.055	
NWC	4.9±0.3	0.48±0.04	10±1	1.87±0.07	0.43±0.03	4.3±0.3	0.28±0.01	0.021±.001	13±0.8
predicted:	2.8	0.13		0.93	0.019		0.17	0.026	
DEEP	1.2±0.3	0.19±0.01	6.3±2	0.42±0.02	0.019±.002	22±3	0.19±0.01	0.011±.001	17±2
predicted	0.99	0.045		0.37	0.024		0.16	0.017	

Table V-4

Solubility Products at 25°C for Selected Phosphate and Carbonate Compounds

Reaction	Solubility Product	Reference
$Ca_3(PO_4)_2 \rightleftarrows 3\,Ca^{++} + 2\,PO_4^{\equiv}$	$K_{sp} = 10^{-28.5}$	1
$Fe_3(PO_4)_2 \cdot 8H_2O \rightleftarrows 3Fe^{++} + 2PO_4 + 8H_2O$	$K_{sp} = 10^{-36.0}$	2
$Mn_3(PO_4)_2 \cdot 3H_2O \rightleftarrows 3Mn^{++} + 2PO_4 + 3H_2O$	$K_{sp} = 10^{-34.6}$	3
$CaCO_{3\,calcite} \rightleftarrows 2Ca^{++} + CO_3^{=}$	$K_{sp} = 10^{-8.42}$	4
$CaCO_{3\,arag.} \rightleftarrows 2Ca^{++} + CO_3^{=}$	$K_{sp} = 10^{-8.25}$	5

References: (1) Duff (1971); (2) Nriagu (1972); (3) Nriagu and Dell (1974); (4) Jacobsen and Langmuir (1974); (5) (1.48 x K_{sp} calcite, e.g. Berner,1976c)

Chapter V

Figure Captions

Figure V-1:A. Location of Long Island Sound along N.E. United States.

B. Long Island Sound showing central basin where stations were established.

C. Location of stations FOAM, NWC, and DEEP in the central Sound.

Figure V-2: Cross-section of central basin through approximately $72^{\circ}53'$ with thickness of marine mud deposits outlined (after Bokuniewicz, Gebert, and Gordon, 1976). Stations are passed onto this single plane illustrating relative position with respect to bathymetry and long term deposition.

Figure V-3: Schematic drawing of major fauna at FOAM. A = Ampelisca; C = Clymenella sp.; M.l. = Mulinia lateralis; M.t. = Macoma tenta; N.A. = Nucula annulata; N.i. = Nephtys incisa; N.t. = Nassarius trivitatus; P. = Pagurus; T.a. = Tellina agilis; S.o. = Spiochaetopterus oculatus.

Figure V-4: Schematic drawing of major fauna at NWC. C.a. = Cerianthus americanis; P.m. = Pitar morrhuana; S. = Squilla. All other abbreviations as in Figure V-3.

Figure V-5: Schematic drawing of major fauna at DEEP. C.p. = Corymorpha pendula. M.c. = Melinna cristata; M.e. = Maldanopsis elongata (drawn with some segments missing); P.a. = Pherusa affinis; P.p. = Pista palmata; All other abbreviations as in Figures V-3 and V-4.

Figure V-6: X-radiograph of vertical sediment section at FOAM. The upper 10-12 cm are characterized by abundant shell debris. A laminated layer at ~4 cm is disrupted irregularly by shells and biogenic reworking activity. Parts of two vertical maldanid tubes can be seen in the center at a depth of 8-10 cm. Below 10-12 cm, the sediment begins to become laminated. This laminated zone begins at 8 cm in most x-radiographs from FOAM (see Figure V-7). Scale = 3 cm.

Figure V-7: Parts of two vertically oriented x-radiographs taken at FOAM. A massive shell layer of varied thickness (6-8 cm) overlies a well laminated zone in both cases. There is relatively little evidence of biogenic structures although burrows can be made out in the shell layer. Beneath the laminated zone are additional shell layers down to at least 50 cm. Scale = 3 cm.

Figure V-8: Vertically oriented x-radiograph illustrating sedimentary features typical of NWC. The upper 4-6 cm is intensely

burrowed. Yoldia limatula can be seen at the far left and right of the radiograph. Abundant vertical burrows, due most probably to Owenia can be made out near the interface. A shell lag layer commonly found at this station occurs ~6 cm and results from both feeding and storm activity. Bioturbate structure dominates at depth; burrows coming out of plane of radiograph appear as light holes. Scale = 3 cm.

Figure V-9: X-radiograph of horizontal slab of sediment 10-15 cm deep from NWC. The irregular distribution of shell debris can be seen with most shell material restricted to the right side of the radiograph. Remnants of maldanid tubes can be made out as can a single large crustacean burrow (left) passing vertically down into the sediment. Maldanids are not presently a common, permanent faunal component at NWC but occur irregularly. Scale = 3 cm.

Figure V-10: Vertical x-radiograph from DEEP. Maldanid dwelling-tubes are abundant on right side. These commonly extend 20 cm into sediment. Shell debris is generally absent below a few centimeters. Where dwelling burrows are absent the sediment is characterized by a mottled, bioturbate texture (right side). Scale = 3 cm.

Figure V-11: Large burrow formed by unknown organism is seen in center of this x-radiograph from DEEP. The wall is lined with clods of sediment and small pebbles. Surrounding sediment shows bioturbate structure typical of sediment that is not part of a contemporary dwelling structure. Scale = 3 cm.

Figure V-12: Seasonal temperature variation at NWC over three year period. Data of Gordon and Pilbeam (1974) by thermistor all other by direct insertion of thermometer in surface of diver-taken sediment cores.

Figure V-13: $SO_4^=$ and NH_4^+ concentration in sediment from discrete depths at NWC versus time of sampling (enclosure) in decomposition experiment. T = 22°C. Solid circles = $SO_4^=$, open circles = NH_4^+.

Figure V-14: $SO_4^=$ and NH_4^+ concentration in decomposition experiments samples from NWC versus time of enclosure. T = 4°C. Solid circles = $SO_4^=$, open circles = NH_4^+.

Figure V-15: $SO_4^=$ and NH_4^+ concentration in decomposition experiment samples from DEEP sediment intervals versus time of enclosure. T = 22°C. Solid circles = $SO_4^=$, open circles = NH_4^+.

Figure V-16: The rate of $SO_4^=$ reduction obtained from decomposition experiments as a function of depth in sediment. Data from FOAM after Goldhaber et al. (1977).

Figure V-17: Rate of NH_4^+ production ($R_N/(1 + K)$) obtained from decomposition experiments as a function of depth in sediment at NWC and DEEP. Data uncorrected for adsorption.

Figure V-18: Ratio of $SO_4^=$ reduction rate/NH_4^+ production rate (no adsorption correction) as a function of $SO_4^=$ reduction rate (NWC, T = 22°C). The rate of $SO_4^=$ reduction decreases both with depth in sediment and temperature.

Figure V-19: Pore water profiles of $SO_4^=$, NH_4^+, $HPO_4^=$, and alkalinity at FOAM, NWC, and DEEP. (Gravity cores) Profiles from a given station are arranged horizontally.

Figure V-20: Pore water Ca^{++} concentrations as a function of depth at FOAM, NWC, and DEEP. (Gravity cores)

Figure V-21: Seasonal pore water $SO_4^=$ profiles from box cores at FOAM. FOAM-1 and FOAM-2 after Goldhaber et al. (1977).

Figure V-22: Seasonal pore water $SO_4^=$ profiles from box cores at NWC. NWC-1 scatter results from analytical problems.

Figure V-23: Seasonal pore water $SO_4^=$ profiles from box cores at DEEP.

Figure V-24: Seasonal pore water alkalinity profiles from box cores at FOAM.

Figure V-25: Seasonal pore water alkalinity profiles from box cores at NWC.

Figure V-26: Seasonal pore water alkalinity profiles from box cores at DEEP.

Figure V-27: Seasonal pore water ammonia profiles from box cores at FOAM.

Figure V-28: Seasonal pore water ammonia profiles from box cores at NWC.

Figure V-29: Seasonal pore water ammonia profiles from box cores at DEEP.

Figure V-30: Seasonal pore water phosphate profiles from box cores at FOAM.

Figure V-31: Seasonal pore water phosphate profiles from box cores at NWC.

Figure V-32: Seasonal pore water phosphate profiles from box cores at DEEP.

Figure V-33: Pore water Ca/Cl molar ratios during fall (solid lines) and winter (dashed lines) at FOAM, NWC, and DEEP.

Figure V-34: Plot of NH_4^+ and $HPO_4^=$ released versus time in flux cores from NWC. Circles = summer; squares = fall; triangles = winter. Slopes of lines drawn (mmoles/hour) correspond to flux values given in Table V-3.

Figure V-35: Ignition loss profiles from selected cores from FOAM (Goldhaber, et al., 1977), NWC, and DEEP.

Figure V-36: Comparison of acid volatile sulfide (FeS) profiles at FOAM, NWC, and DEEP.

Figure V-37: Seasonal variation in acid volatile sulfide profiles at NWC. Lowest values near interface occur during winter.

Figure V-38: Total non-volatile sulfur ($FeS_2 + S^o$) profiles at FOAM, NWC, and DEEP.

Figure V-39: Seasonal profiles of total non-volatile sulfur ($FeS_2 + S^o$) at NWC. A possible minor decrease in interface sulfur during fall and winter is detectable.

Figure V-40: Total nitrate-nitrite profiles at FOAM, NWC, and DEEP at different times of year. Overlying water NO_3^- is highest during late fall-early winter ($\sim$ 10 μM) and low ($\sim$ 1 μM) at all other times. Overlying water had just become low prior to winter-spring sampling, which, in addition to a small amount of nitrification, results in the maximum values below the interface at this time (courtesy J. Rosenfeld).

Figure V-41: Plot of the functions which describe the relative seasonal temperature dependence of macrofaunal and microbial activity. If the effective, vertical biogenic diffusion coefficient reaches a maximum value of 1×10^{-5} cm^2/sec it will exceed the molecular diffusion coefficient of NH_4^+ (0.7×10^{-5}) only after approximately June (horizontal line represents value of D_N). Other ions with lower coefficients will be influenced for a longer period. Immediately after water begins to warm, the production rate starts to change profiles from the diffusion-production balance reached during winter at the lowest temperature.

Figure V-42: Plots of -logIAP versus depth at each station for selected solid phases: whitlockite ($Ca_3(PO_4)_2$) and vivianite ($Fe_3(PO_4)_2 \cdot 8H_2O$). Box cores: open circles = summer (1975); open squares = fall (1975); open triangles = winter (1976). Gravity cores: filled circles = FOAM; filled squares = NWC; filled triangles = DEEP.

Figure V-43: Plots of -logIAP versus depth at each station for the phases: reddingite ($Mn_3(PO_4)_2 \cdot 3H_2O$) and $CaCO_3$. Symbols as in Figure V-42.

Figure V-44: pPO_4 versus pS for upper 8 cm at FOAM, NWC, and DEEP where pS was detectable. Line drawn is equilibrium relation between vivianite and mackinawite (FeS). Squares = FOAM; circles = NWC; triangles = DEEP. All seasons plotted. The formation of sulfides is generally favored but a zone where both phases can coexist is present.

Figure V-45: Seasonal change in pore water NH_4^+ profiles predicted by numerical model discussed in text. Both production and diffusion rates are time dependent. Dashed line = maximum diffusion coefficient of 2×10^{-5} cm^2/sec; solid line = maximum diffusion coefficient of 1×10^{-5} cm^2/sec. Production rate is that predicted by decomposition experiment data. Dotted line is model seasonal change in pore water profiles when maximum possible effect of denitrification is included in production rate of NH_4^+ near the interface. Maximum diffusion coefficient = 1×10^{-5} cm^2/sec.

Figure V-46:A. Geometrical analogue of diffusion in the zone of biogenic reworking. Average burrow diameter (r_1) increases with depth in sediment but the total abundance which determines r_2 also decreases. Diffusion can occur both vertically and radially.

B. Approximation to geometry of A by a series of stacked hollow cylinders representing different vertical intervals of sediment having an average burrow size r_1 and half the distance between burrows of r_2 over any given depth interval. Vertical diffusion is ignored in the text model in order to evaluate effects only of diffusion into burrows.

Figure V-47: Comparison of vertical pore water profiles predicted from steady state transport-reaction models where only radial diffusion into or only vertical diffusion burrows at a given depth is considered. Two cases are plotted in the vertical model: curve A, $D = 7 \times 10^{-6}$ cm^2/sec and curve B, $D = 3 \times 10^{-5}$ cm^2/sec. The radial model is solved for $D = 7 \times 10^{-6}$ cm^2/sec. This model generates average concentrations in discrete intervals of sediment and is plotted as vertical lines with a continuous curve sketched in. Two cases are plotted in the radial model: curve C, sizes (r_1) and densities of burrows ($1/\pi r_2^2$) determined only by sizes and abundances of animals captured at NWC (see text); curve D, same as C except that below 3 cm, r_1 and r_2 were estimated from x-radiographs. The reaction rate function is the same in both the vertical and horizontal models and is that determined by the decomposition experiments at NWC with K = 1 (Figure V-17).

Figure V-48: The flux of NH_4^+ out of bottom sediment as a function of temperature (season) at FOAM, NWC, and DEEP.

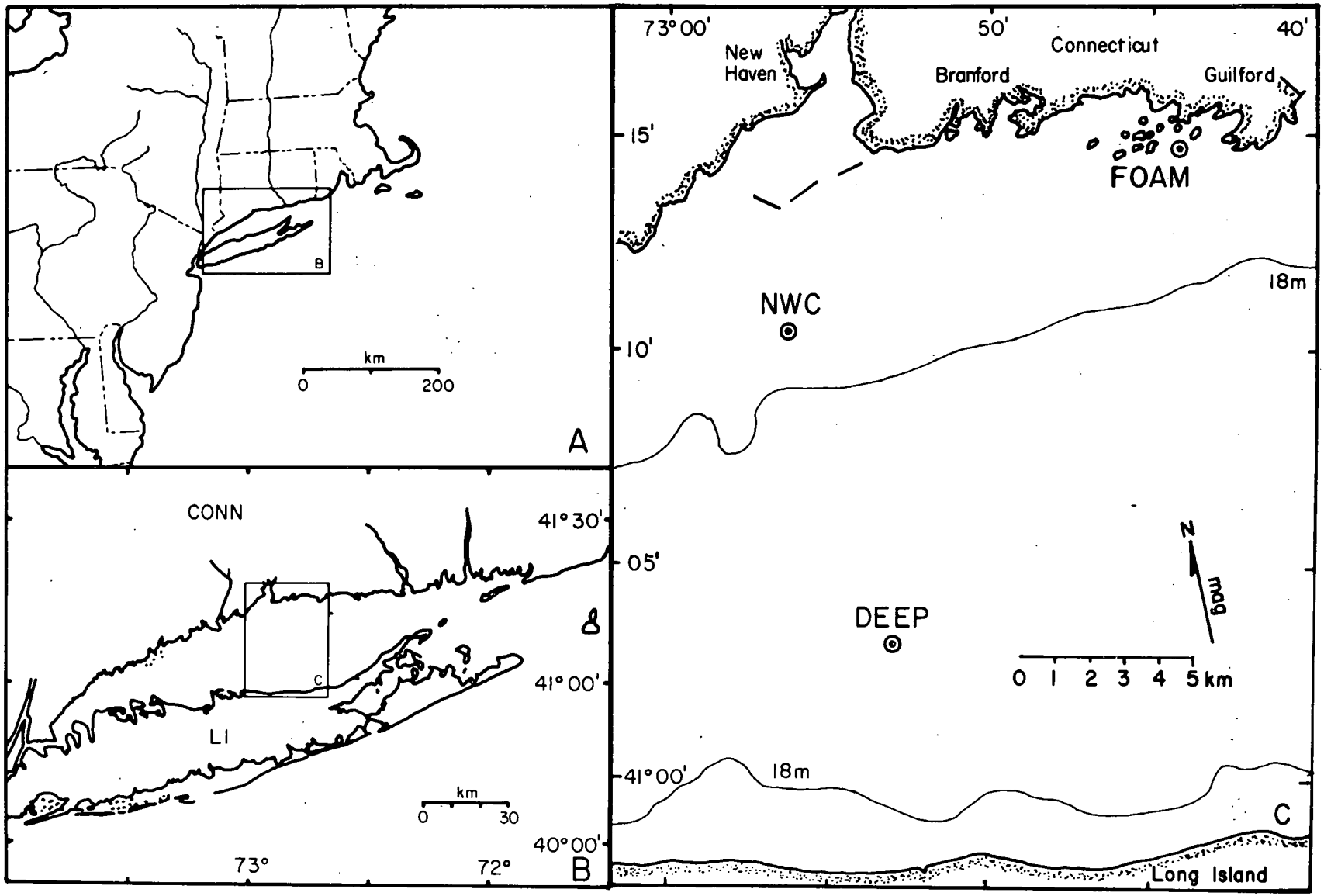

A
B
km
0
200
CONN
41°30'
41°00'
LI
C
km
0
30
73°
72°
40°00'
B
73°00'
50'
40'
New Haven
Connecticut
Branford
Guilford
15'
FOAM
NWC
18m
10'
05'
DEEP
N
mag
0 1 2 3 4 5 km
41°00'
18m
C
Long Island

Figure VI

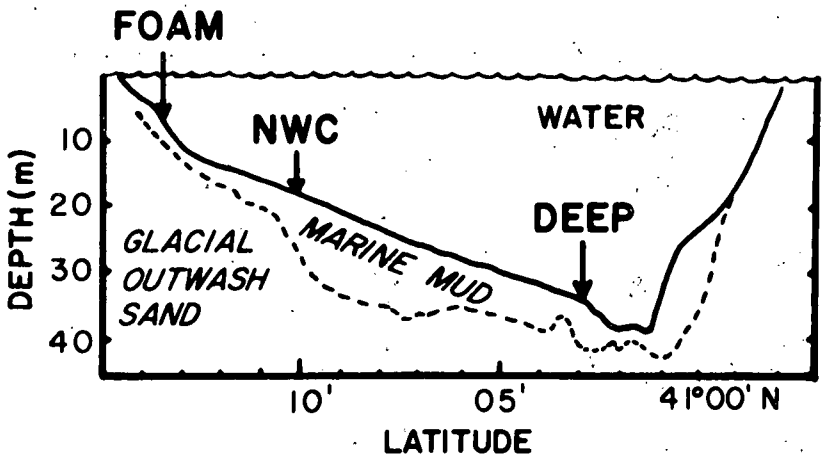

FOAM
NWC
WATER
DEEP
MARINE MUD
GLACIAL
OUTWASH
SAND
DEPTH (m)
10
20
30
40
10'
05'
41°00' N
LATITUDE

Figure V-2

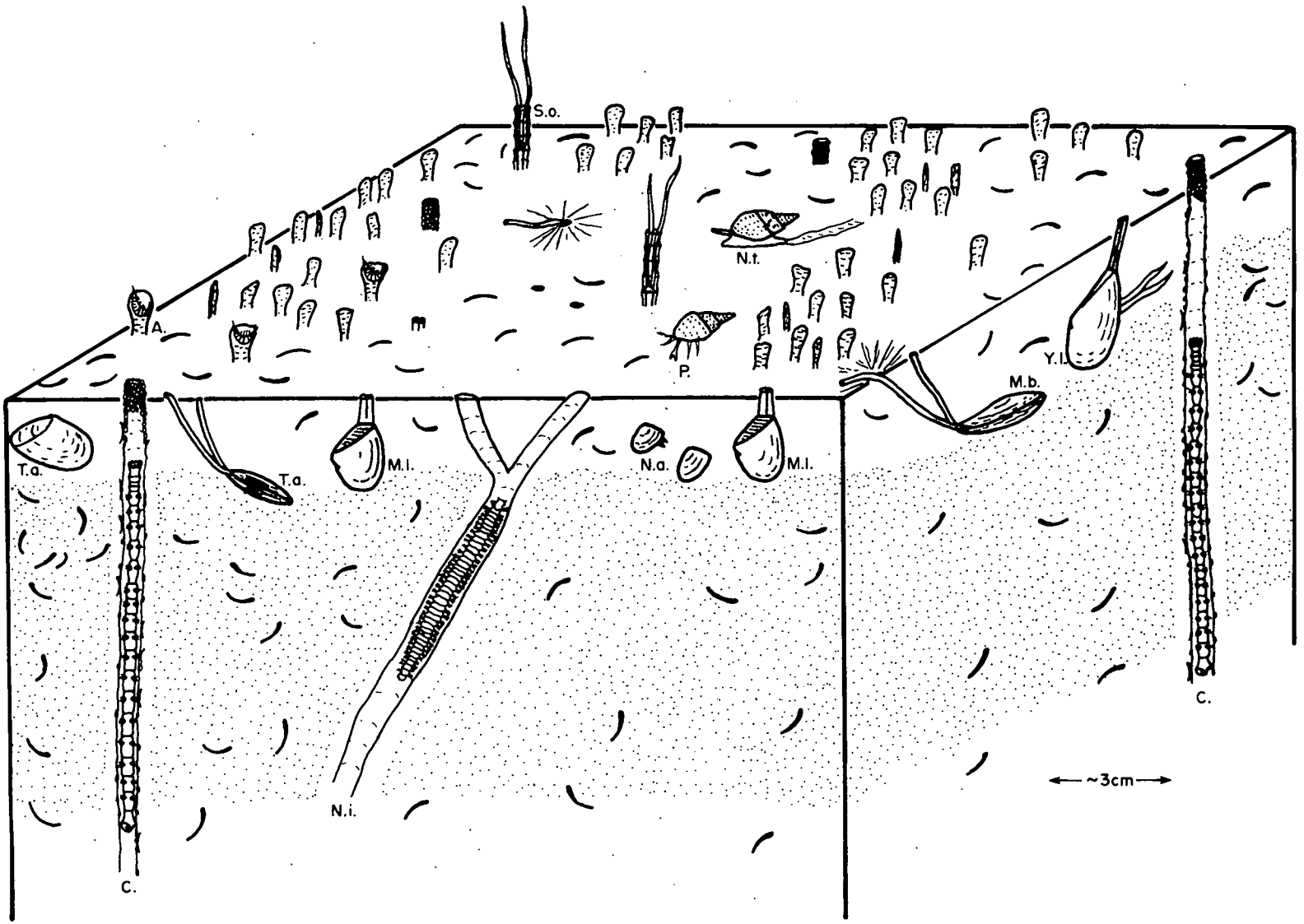


Figure V-3

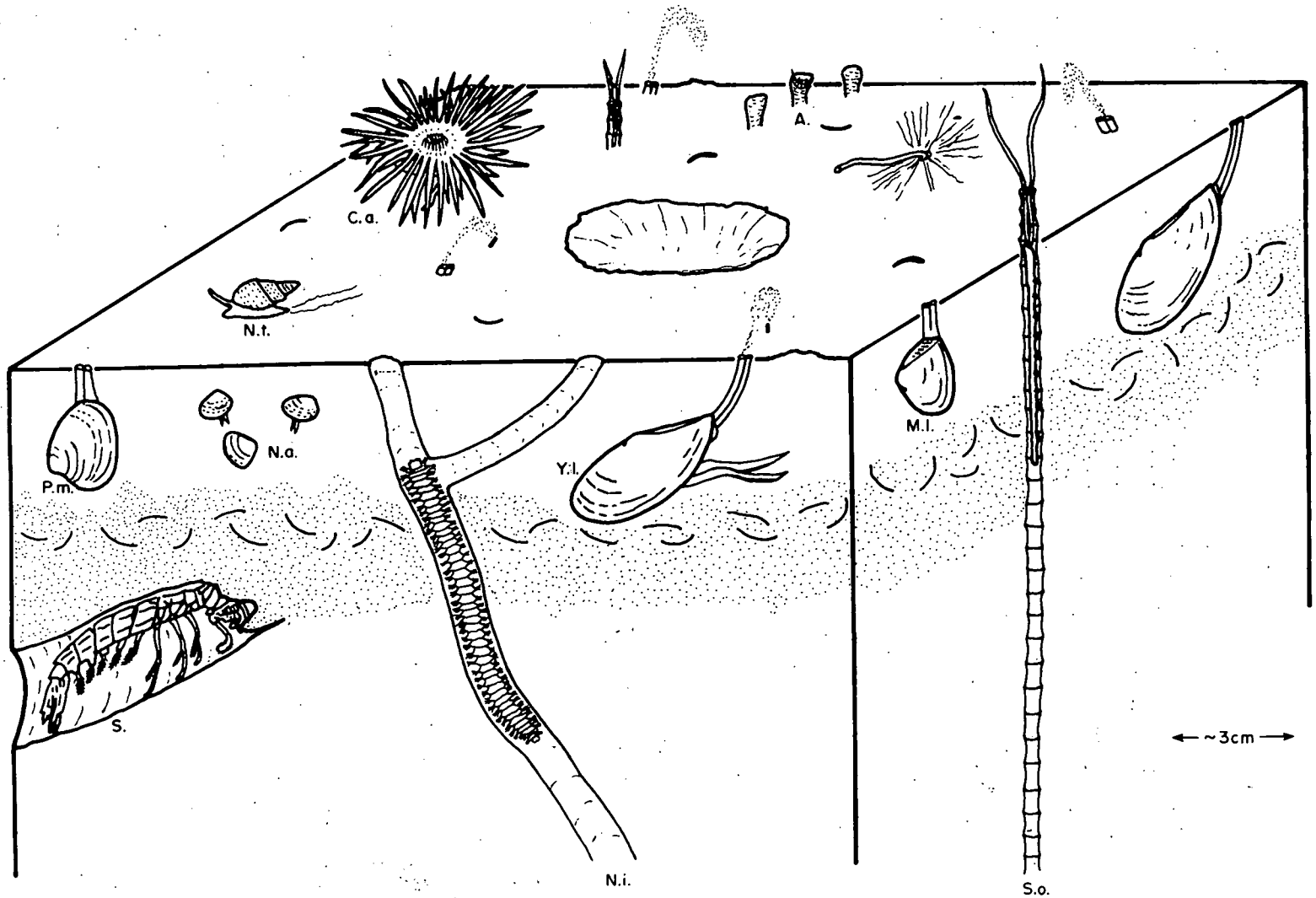


Figure V-4

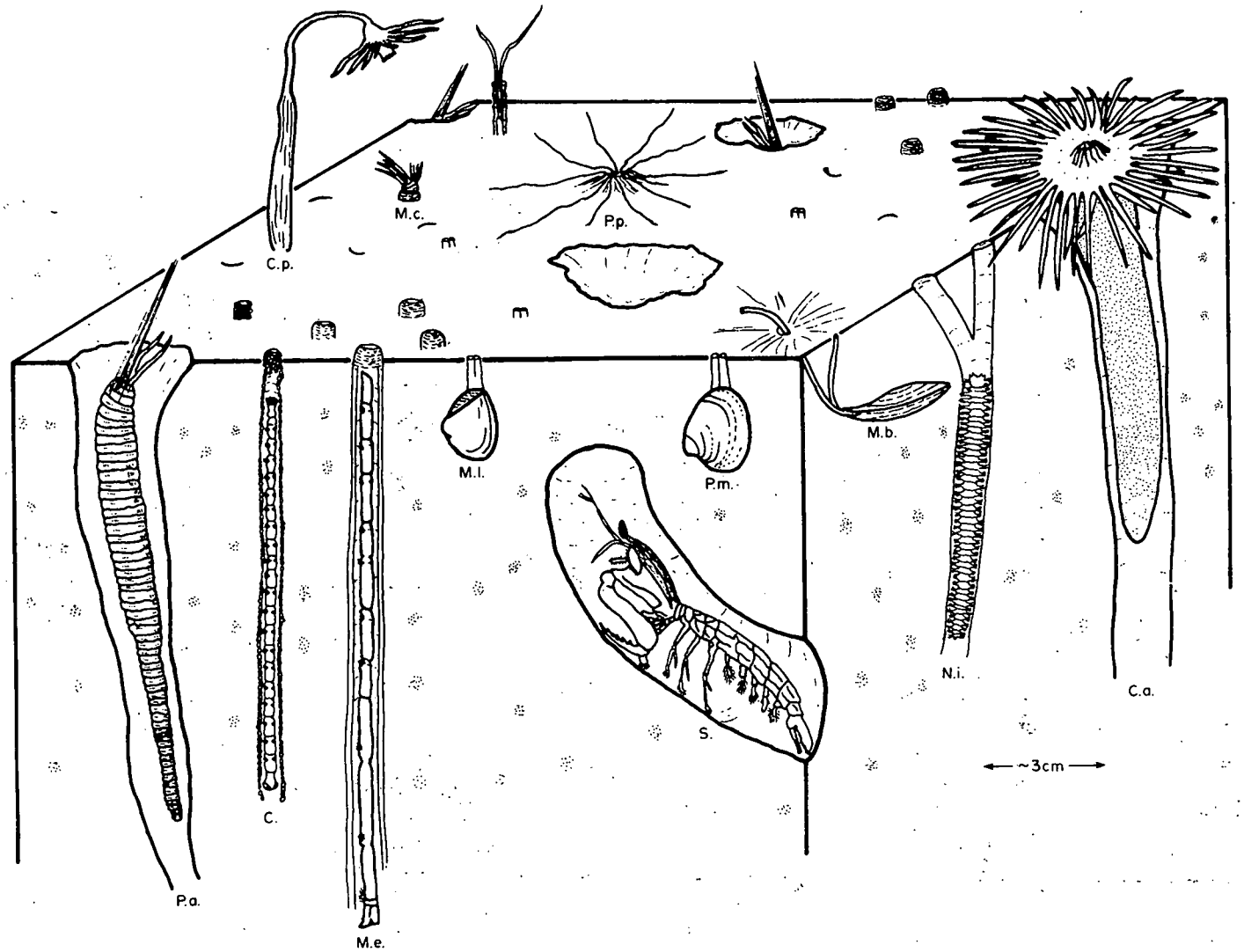
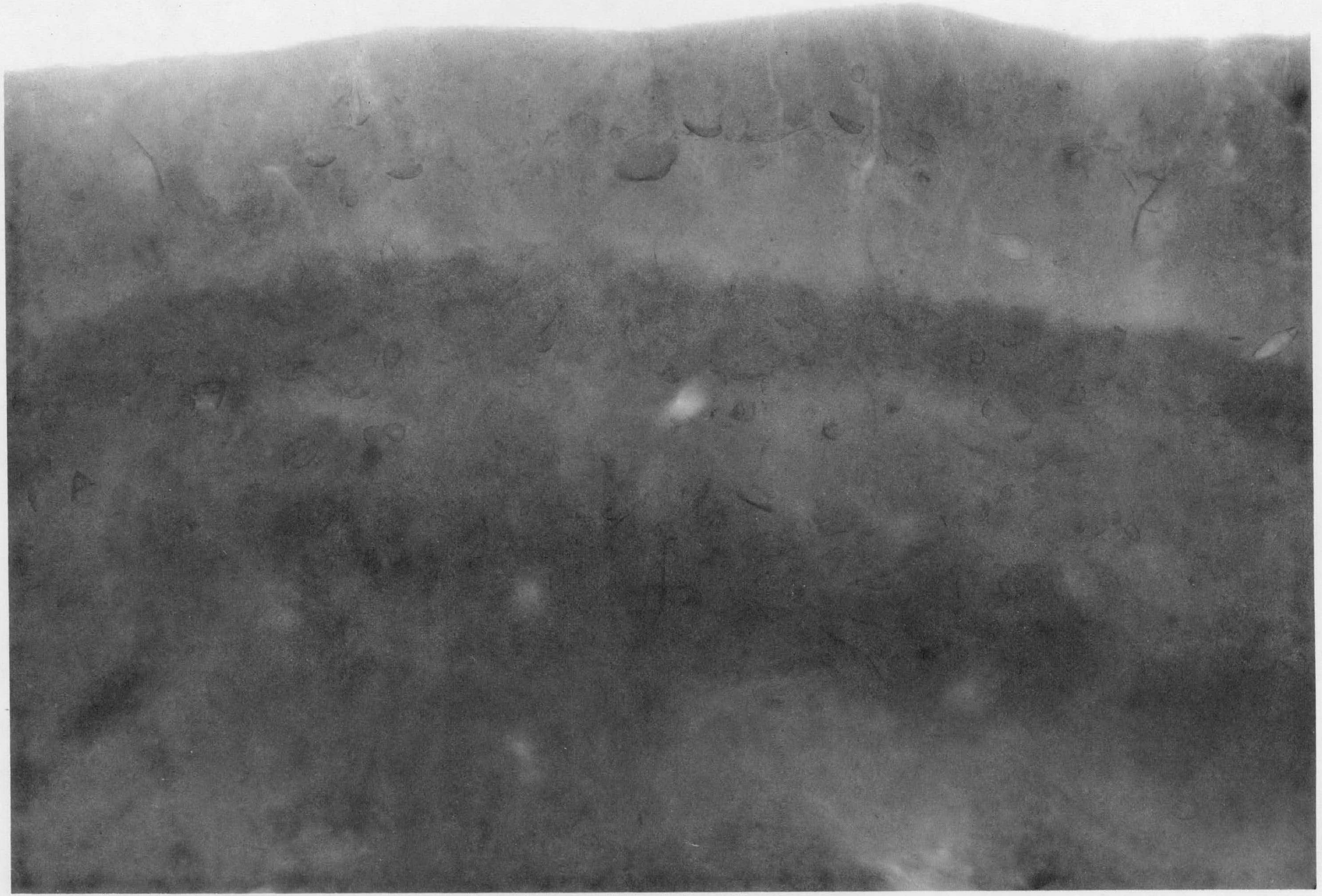


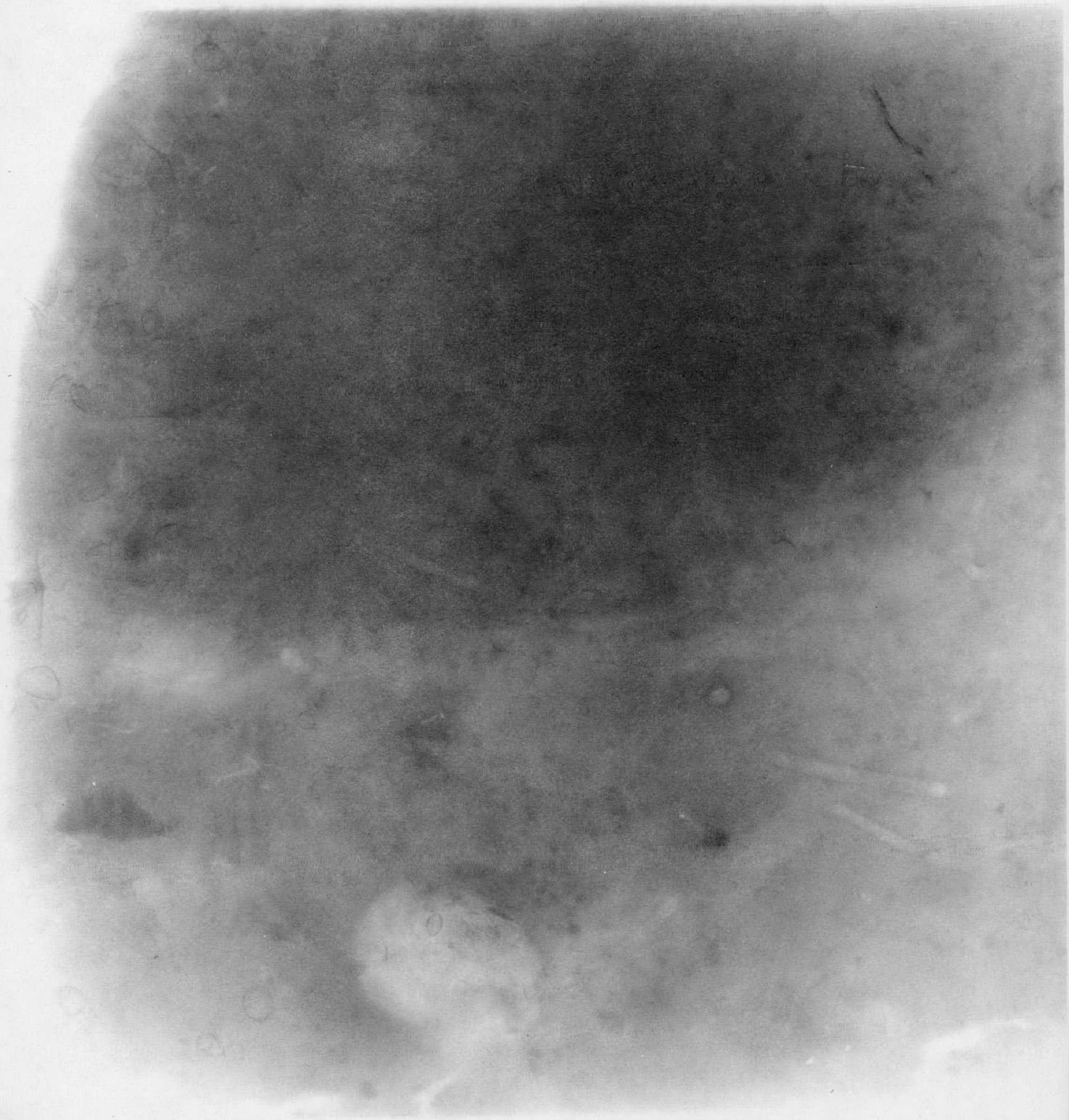
Figure V-5



V-6

V-7







V-10



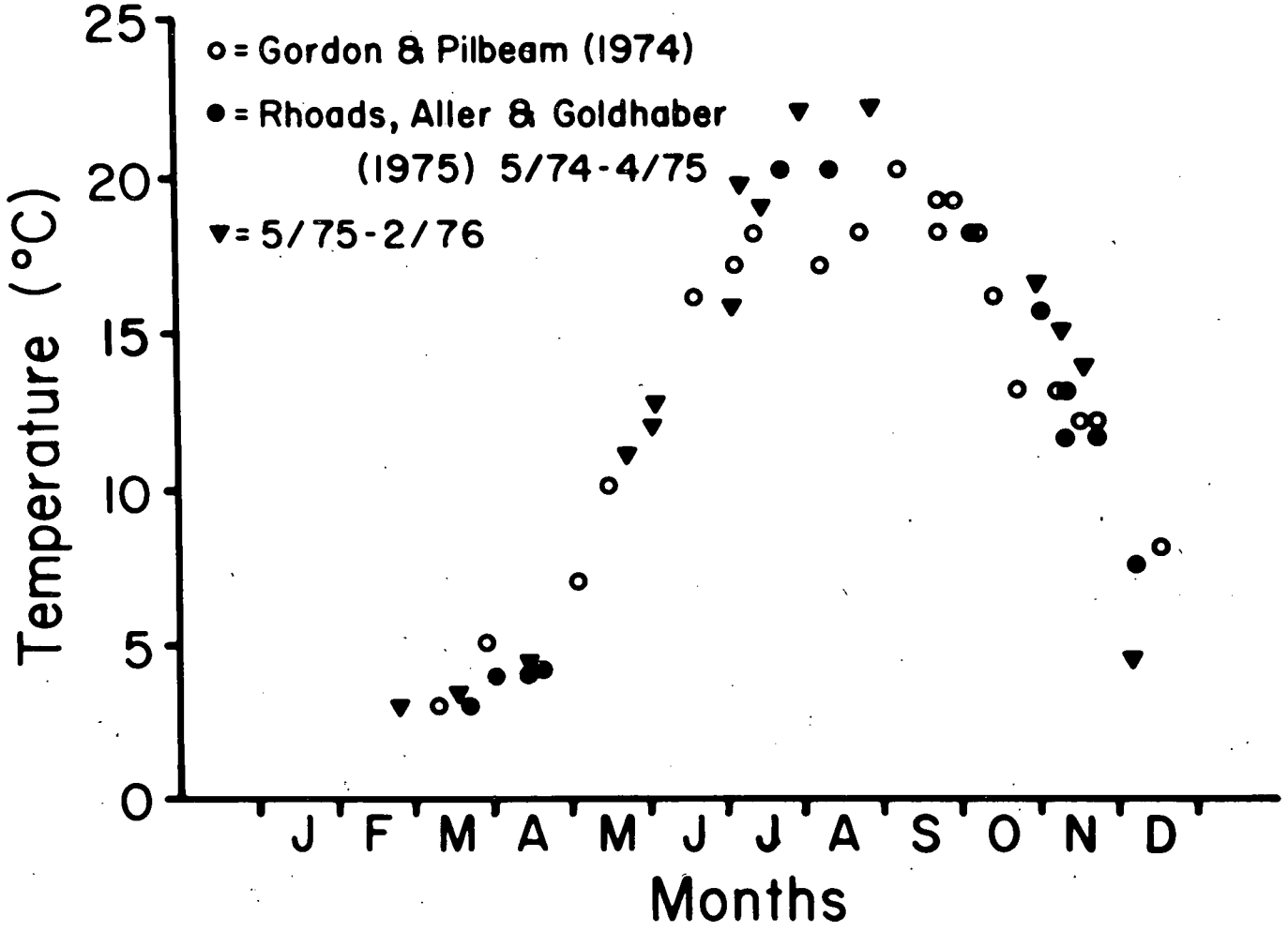

o = Gordon & Pilbeam (1974)
● = Rhoads, Aller & Goldhaber (1975) 5/74-4/75
▼ = 5/75-2/76
Temperature (°C)
25
20
15
10
5
0
J F M A M J J A S O N D
Months

Figure V-12

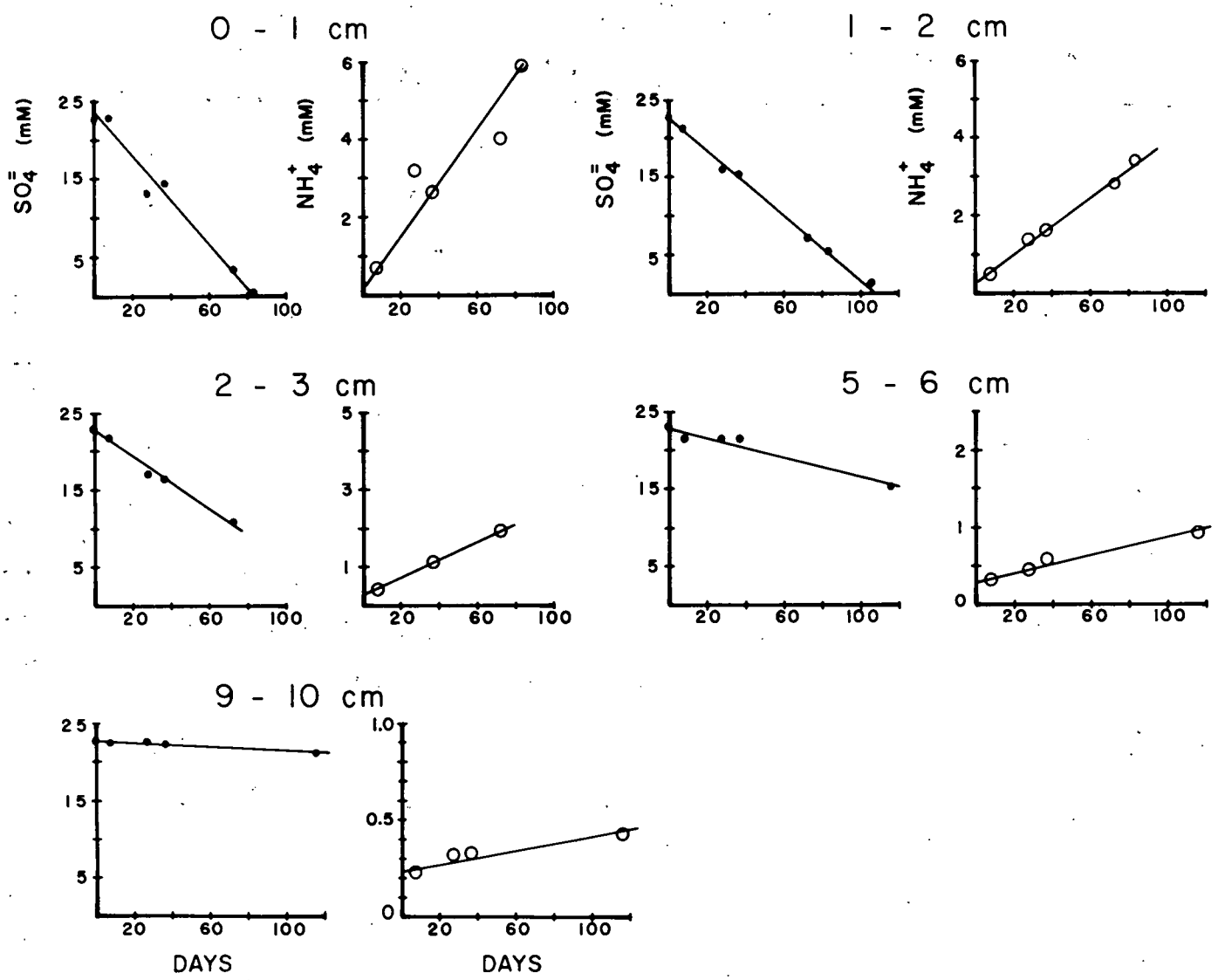
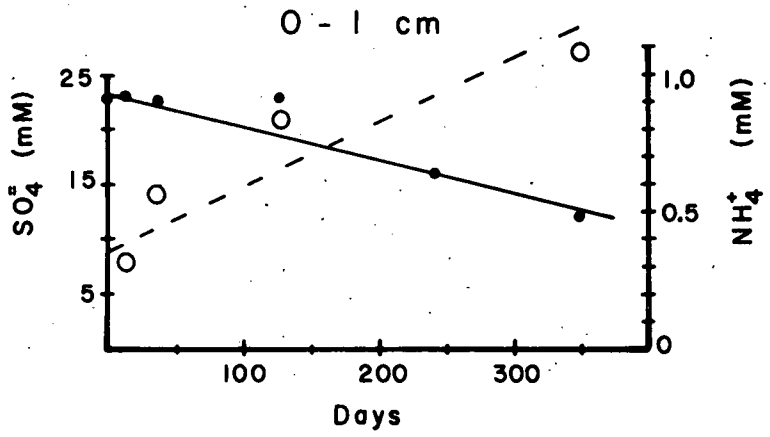
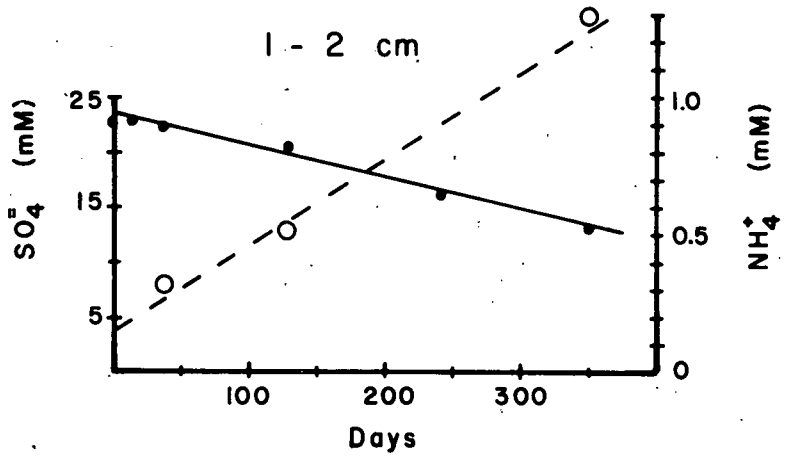


Figure V-13


0 - 1 cm
$SO_4^=$ (mM)
25
15
5
1.0
0.5
0
NH_4^+ (mM)
100
200
300
Days


1 - 2 cm
$SO_4^=$ (mM)
25
15
5
1.0
0.5
0
NH_4^+ (mM)
100
200
300
Days

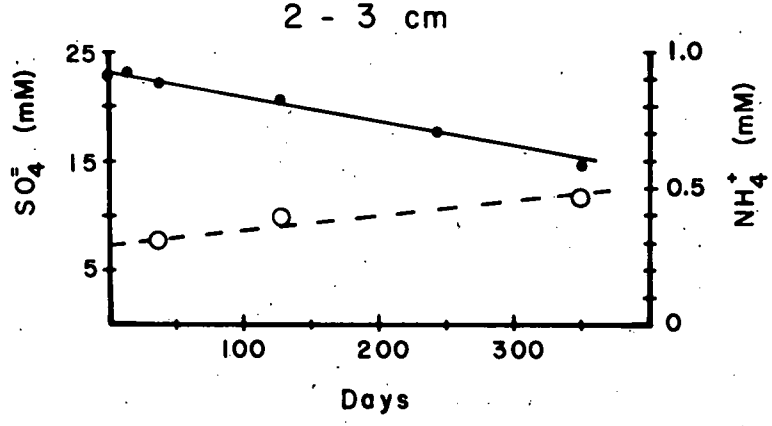

2 - 3 cm
$SO_4^=$ (mM)
25
15
5
1.0
0.5
0
NH_4^+ (mM)
100
200
300
Days

Figure V-14

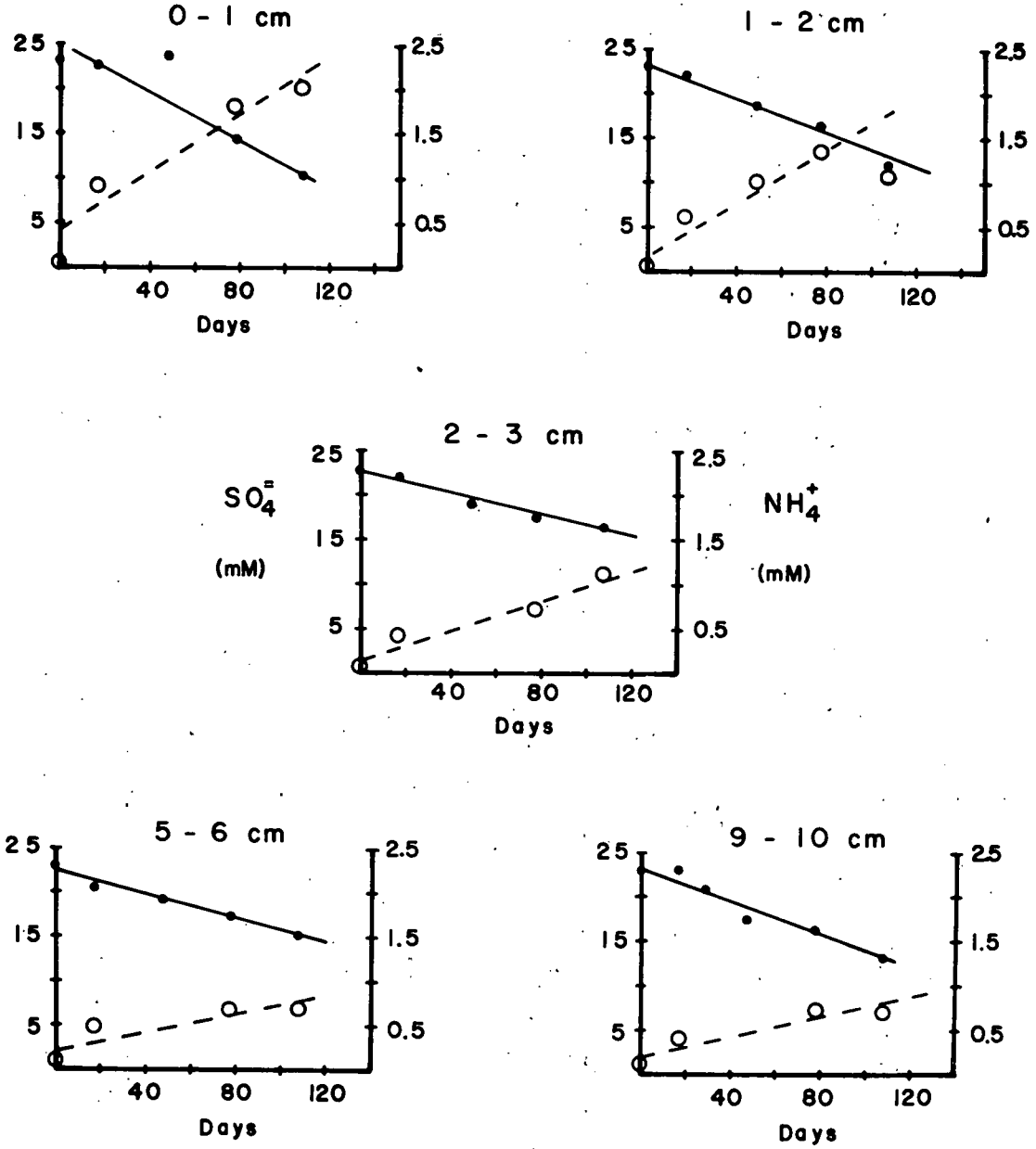

0 - 1 cm
1 - 2 cm
2 - 3 cm
5 - 6 cm
9 - 10 cm
$SO_4^=$
(mM)
NH_4^+
(mM)
25
15
5
2.5
1.5
0.5
40
80
120
Days

Figure V-15

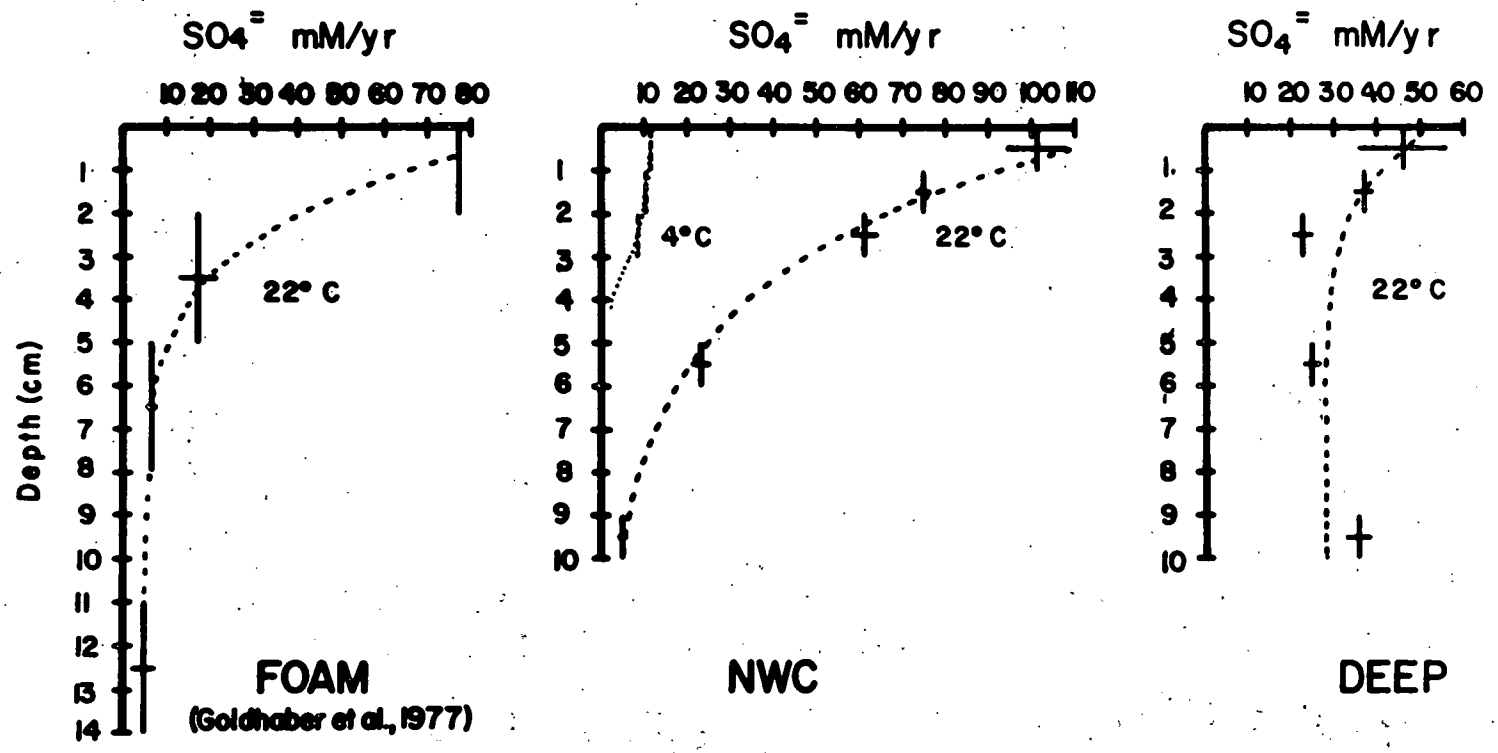

SO4= mM/yr
10 20 30 40 50 60 70 80
Depth (cm)
22° C
FOAM
(Goldhaber et al., 1977)
SO4= mM/yr
10 20 30 40 50 60 70 80 90 100 110
4°C
22° C
NWC
SO4= mM/yr
10 20 30 40 50 60
22° C
DEEP

Figure V-16

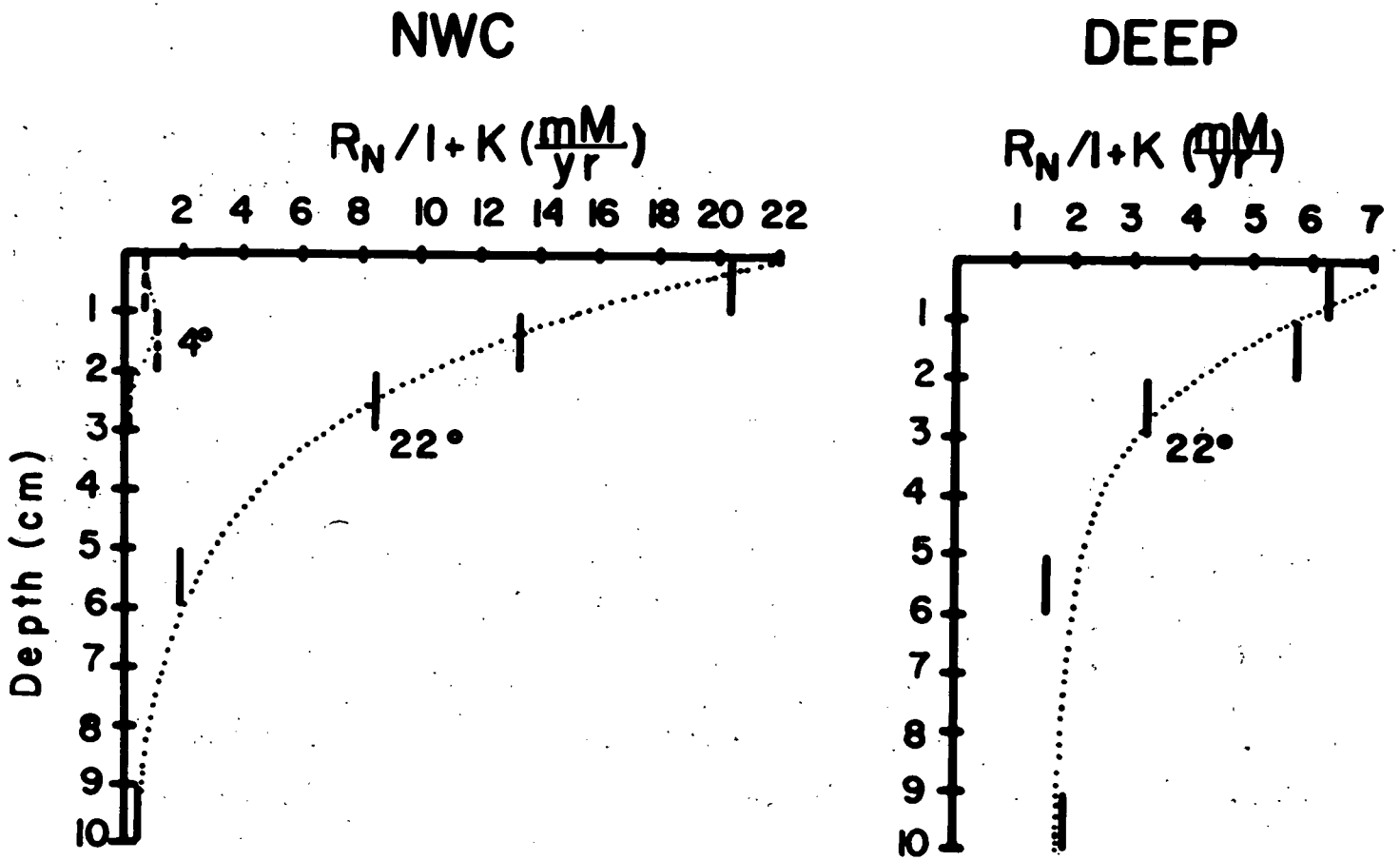

NWC
$R_N/1+K\left(\frac{mM}{yr}\right)$
2 4 6 8 10 12 14 16 18 20 22
Depth (cm)
1 2 3 4 5 6 7 8 9 10
4°
22°
DEEP
$R_N/1+K\left(\frac{mM}{yr}\right)$
1 2 3 4 5 6 7
1 2 3 4 5 6 7 8 9 10
22°

Figure V-17

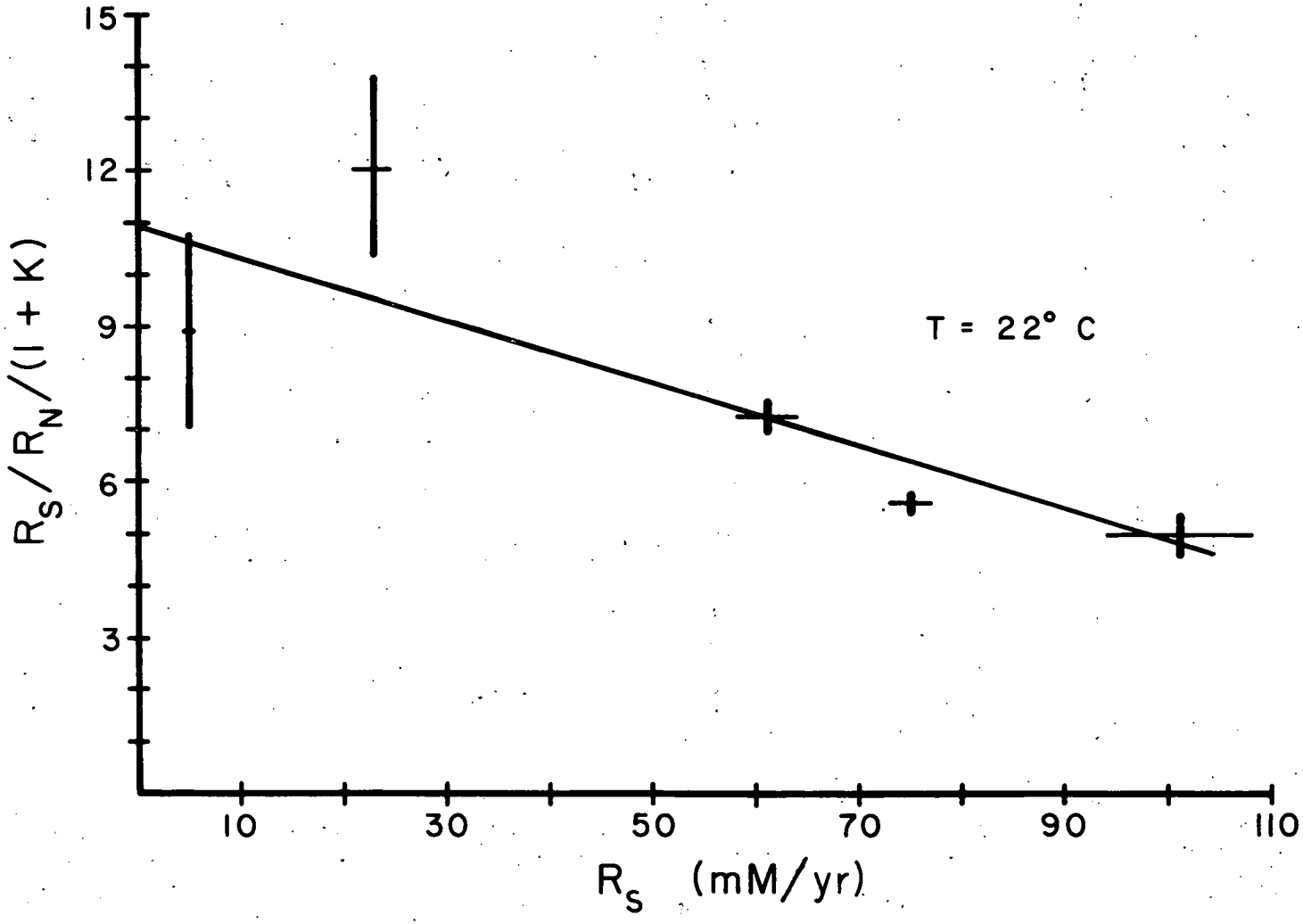


Figure V-18

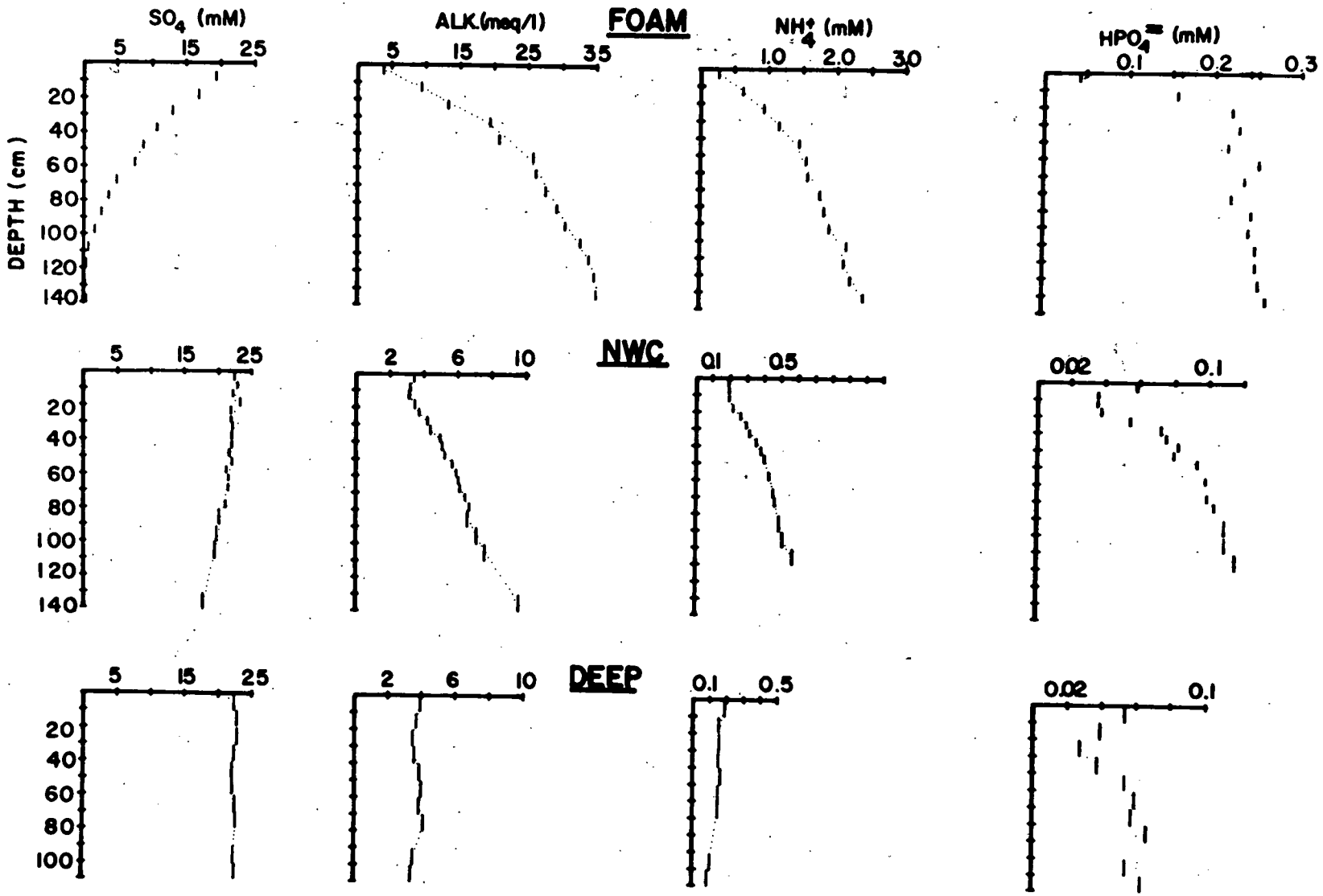


Figure V-19

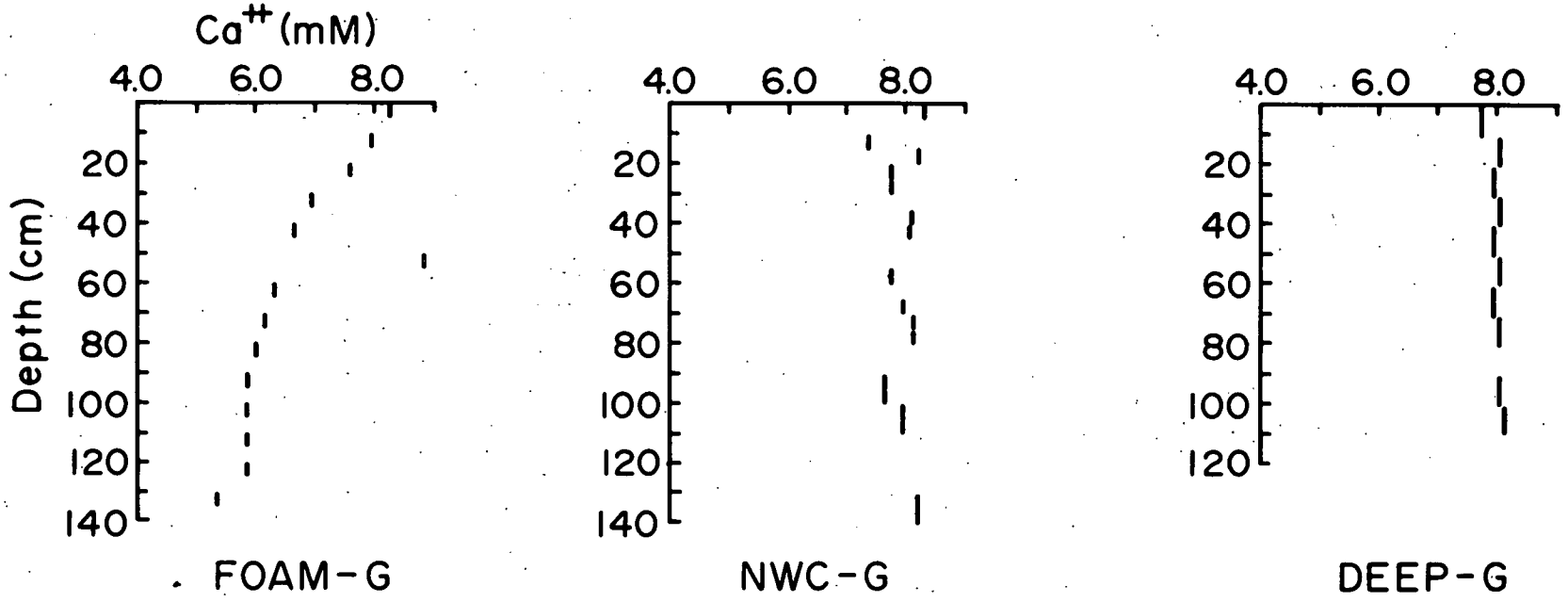


Figure V-20

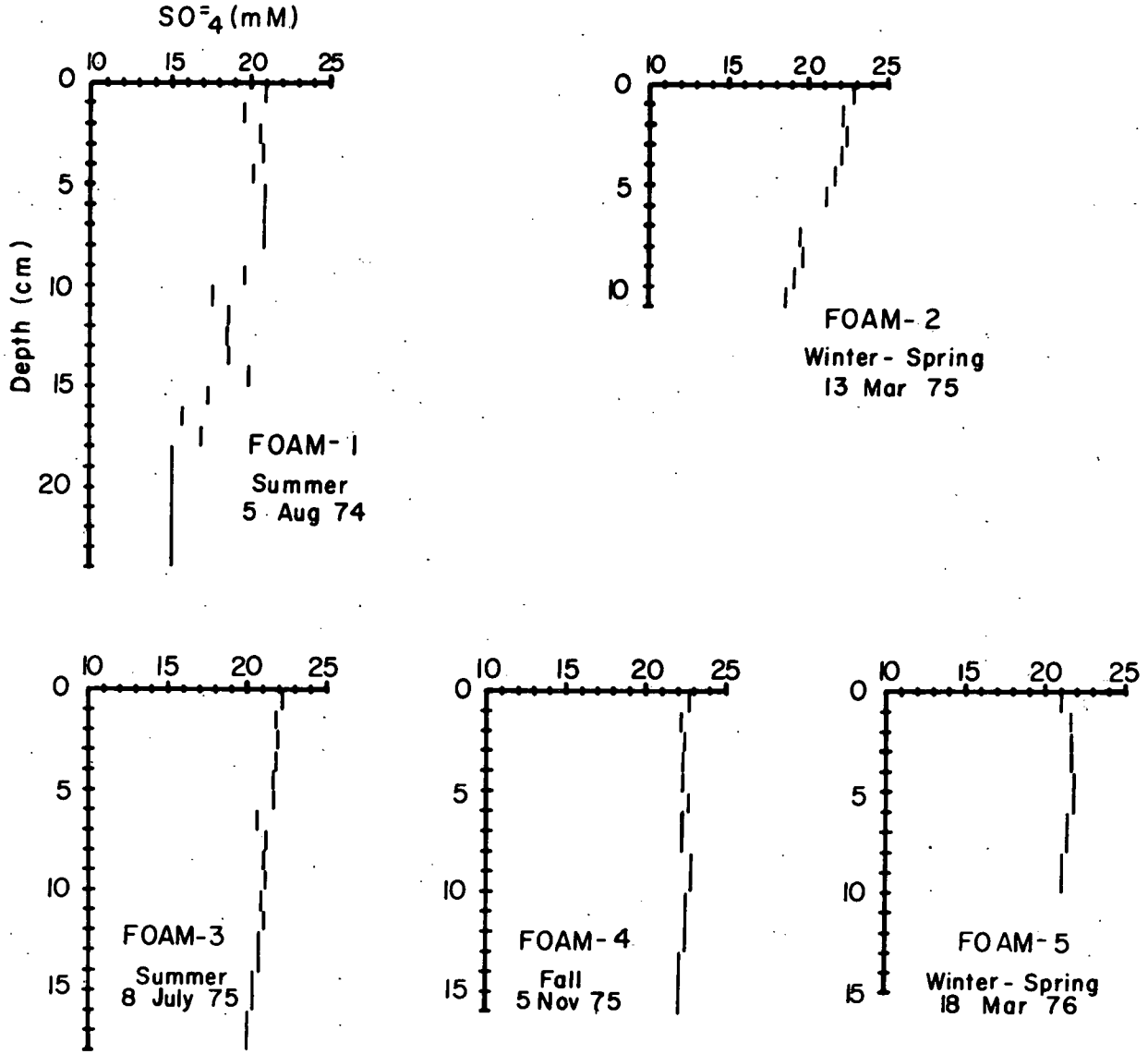

$SO^{=}_4$ (mM)
10 15 20 25
0
5
10
15
20
Depth (cm)
FOAM-1
Summer
5 Aug 74
FOAM-2
Winter-Spring
13 Mar 75
FOAM-3
Summer
8 July 75
FOAM-4
Fall
5 Nov 75
FOAM-5
Winter-Spring
18 Mar 76

Figure V-21

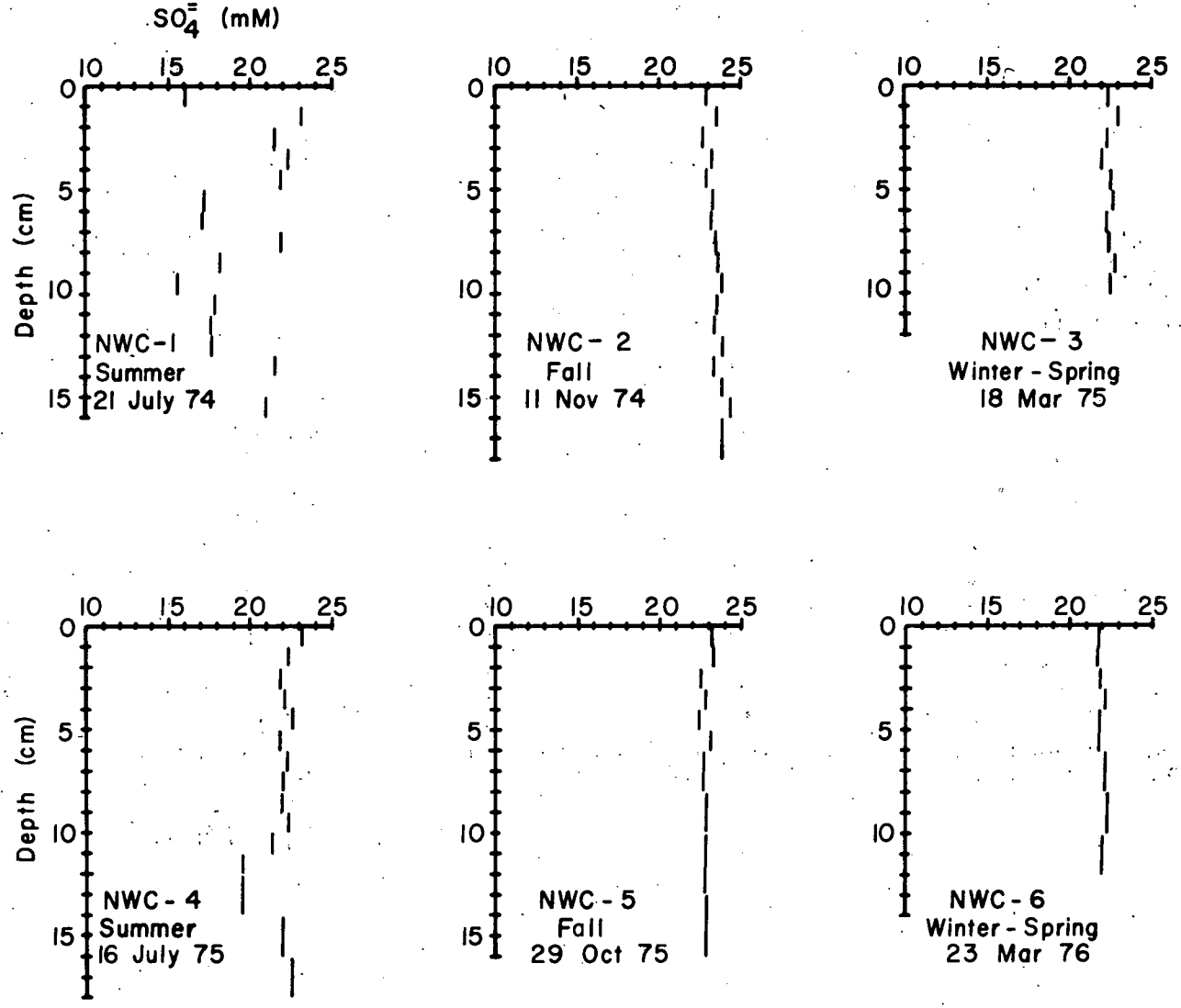

$SO_4^=$ (mM)
10 15 20 25
0
5
10
15
Depth (cm)
NWC-1
Summer
21 July 74
NWC-2
Fall
11 Nov 74
NWC-3
Winter-Spring
18 Mar 75
NWC-4
Summer
16 July 75
NWC-5
Fall
29 Oct 75
NWC-6
Winter-Spring
23 Mar 76

Figure V-22

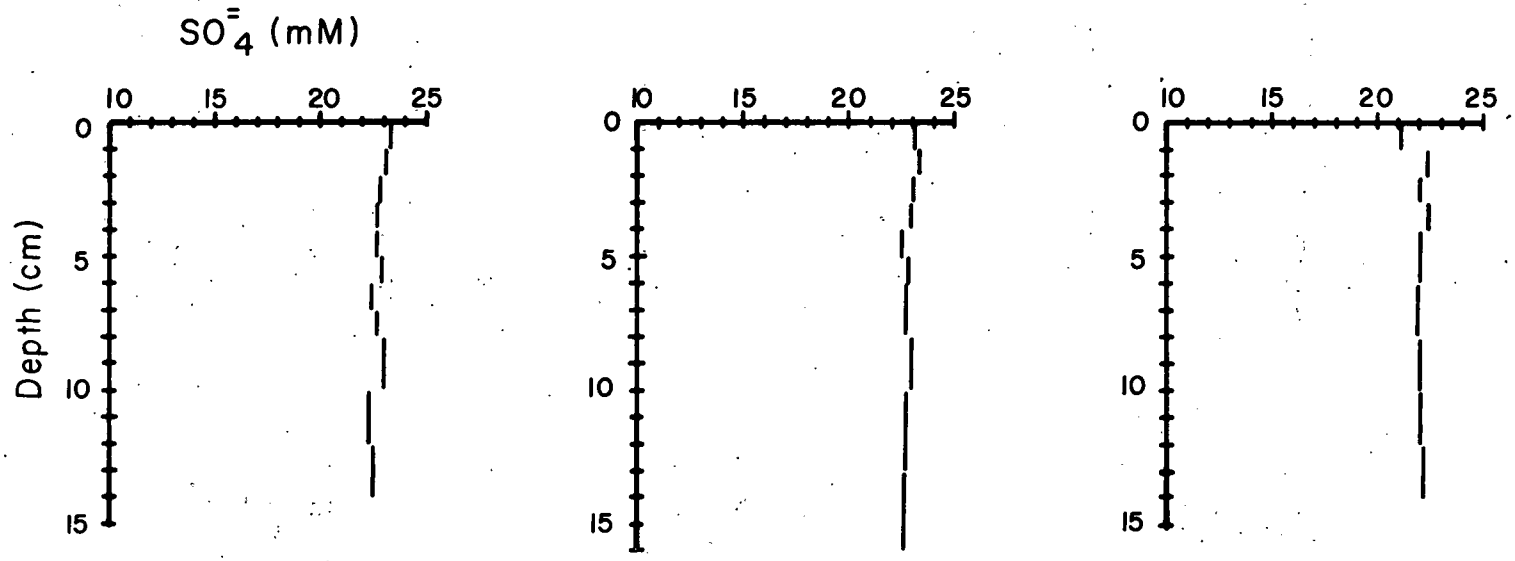

$SO_4^=$ (mM)
10
15
20
25
0
5
10
15
Depth (cm)
DEEP-1
Summer
23 July 75
DEEP-2
Fall
12 Nov 75
DEEP-3
Winter-Spring
13 Apr 76

Figure V-23

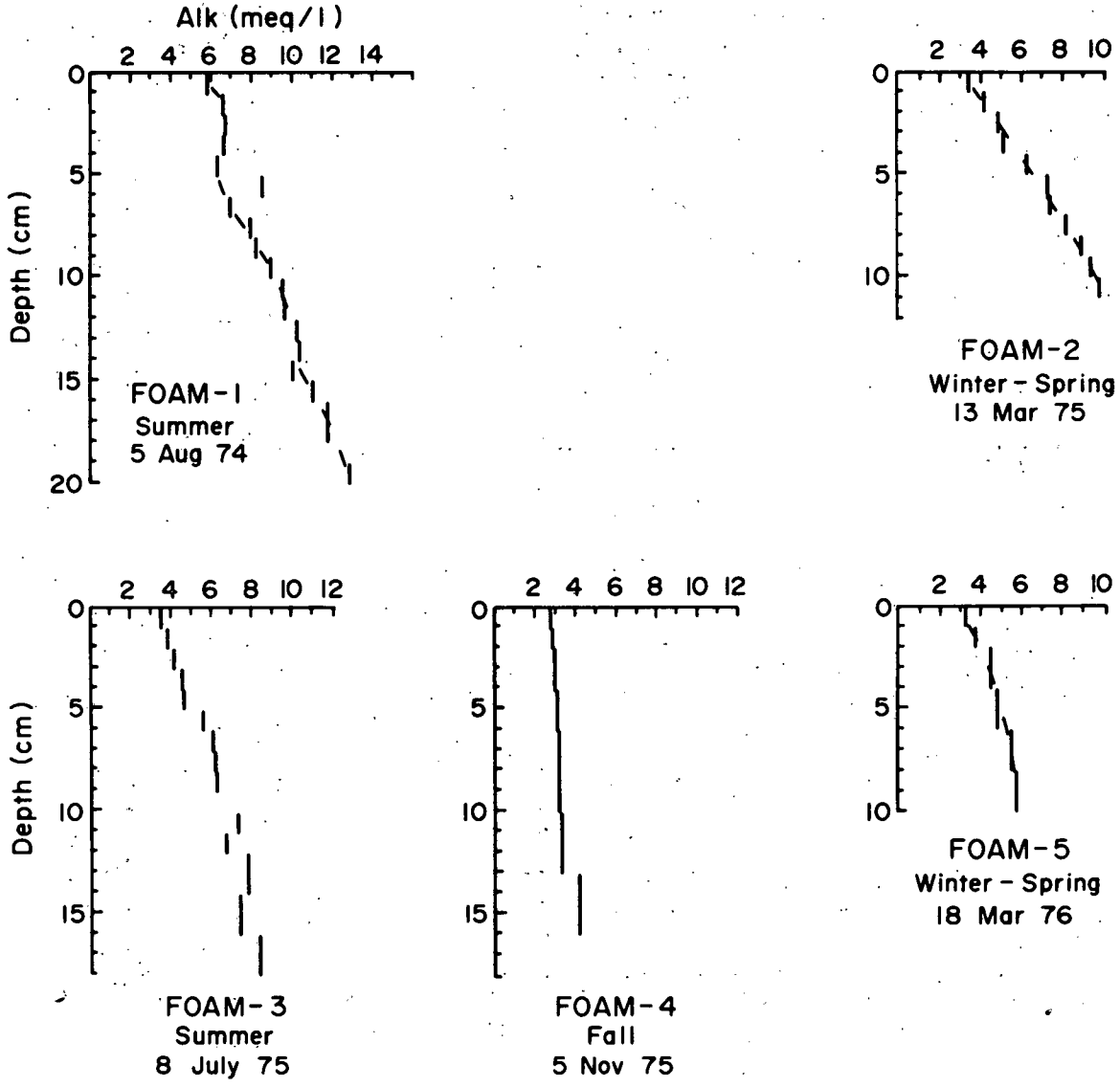

Alk (meq/l)
2 4 6 8 10 12 14
Depth (cm)
0
5
10
15
20
FOAM-1
Summer
5 Aug 74
2 4 6 8 10
0
5
10
FOAM-2
Winter - Spring
13 Mar 75
2 4 6 8 10 12
Depth (cm)
0
5
10
15
FOAM-3
Summer
8 July 75
2 4 6 8 10 12
0
5
10
15
FOAM-4
Fall
5 Nov 75
2 4 6 8 10
0
5
10
FOAM-5
Winter - Spring
18 Mar 76

Figure V-24

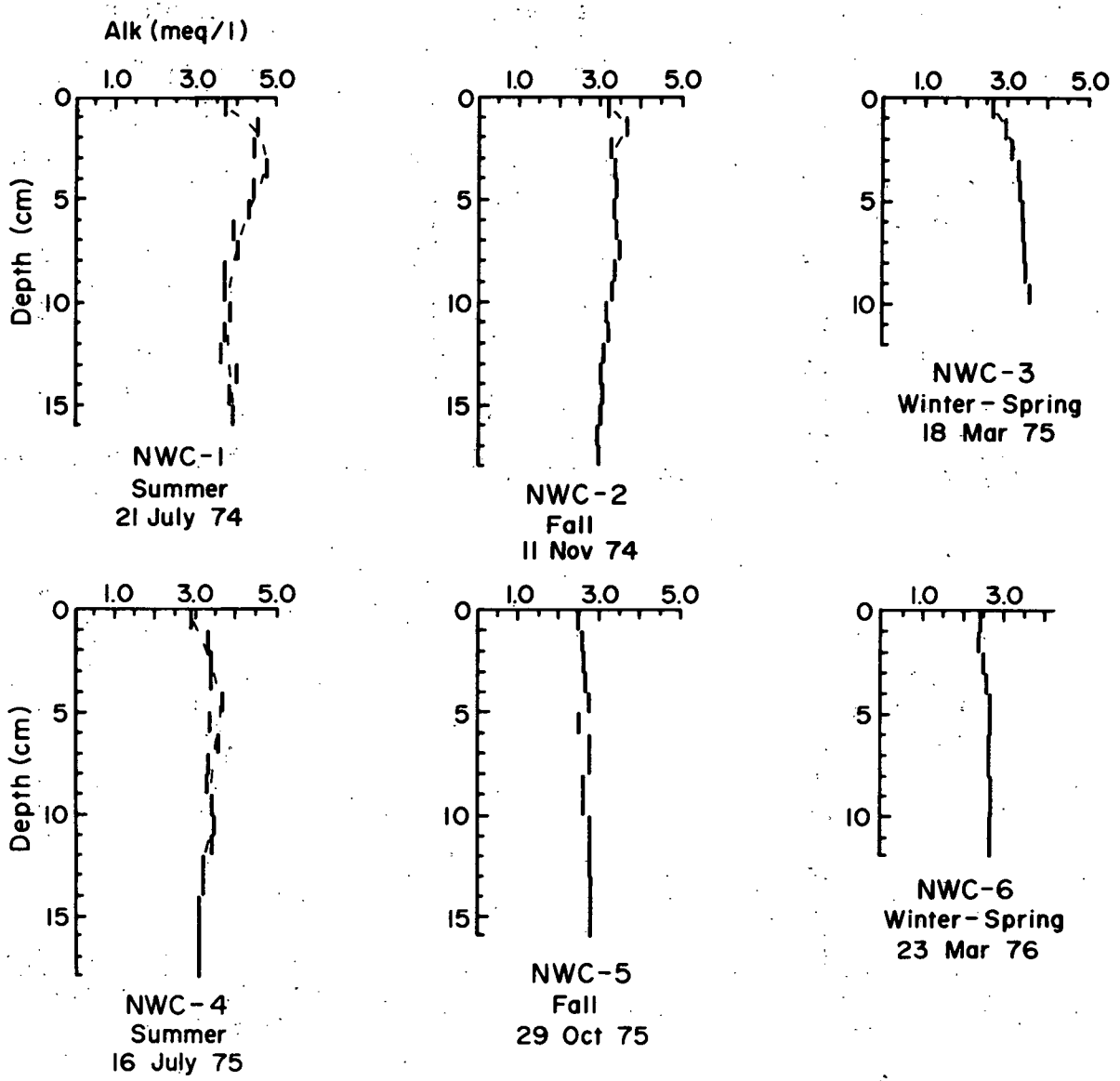

Alk (meq/l)
1.0
3.0
5.0
Depth (cm)
0
5
10
15
NWC-1
Summer
21 July 74
NWC-2
Fall
11 Nov 74
NWC-3
Winter-Spring
18 Mar 75
NWC-4
Summer
16 July 75
NWC-5
Fall
29 Oct 75
NWC-6
Winter-Spring
23 Mar 76

Figure V-25

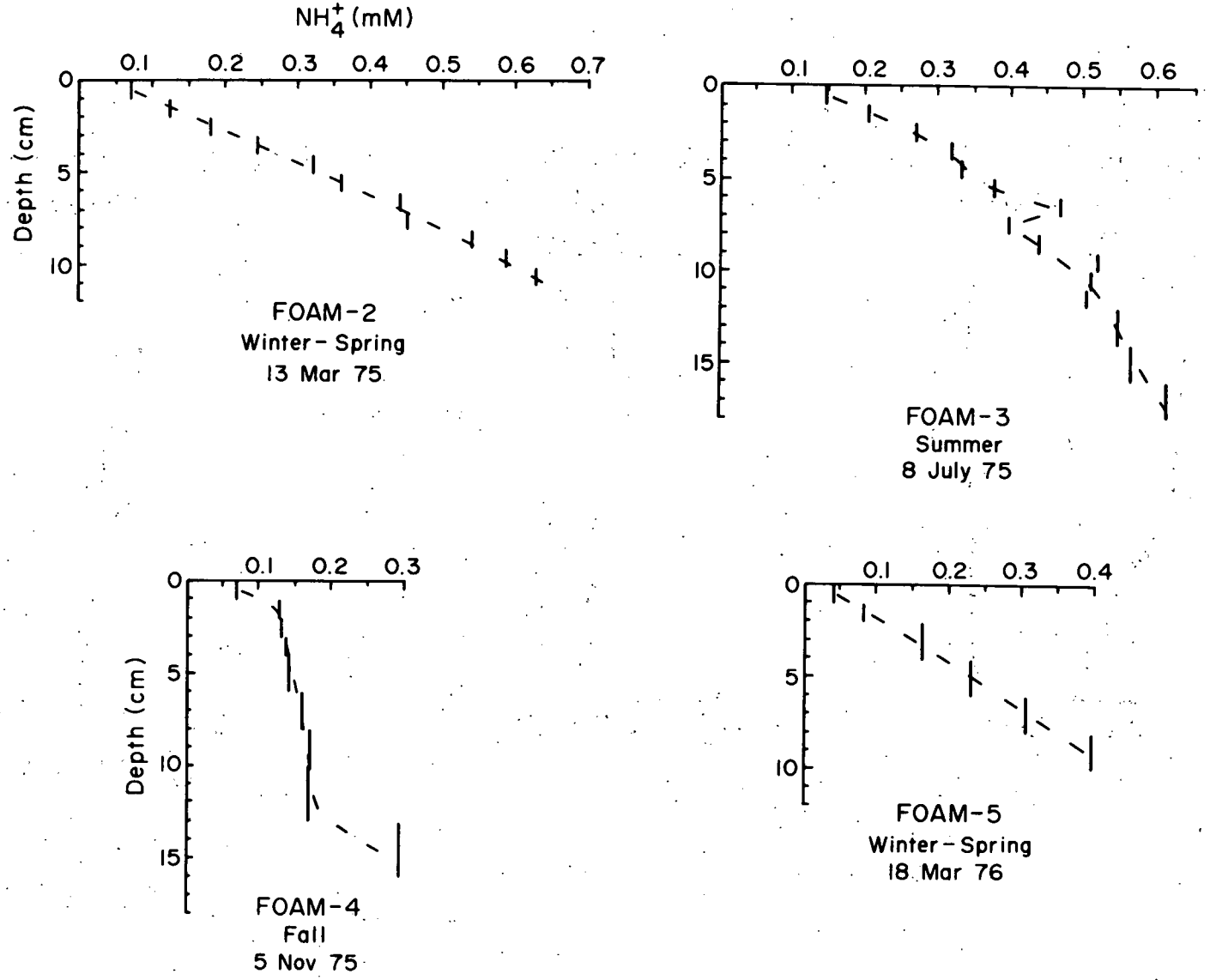

NH_4^+ (mM)
0.1
0.2
0.3
0.4
0.5
0.6
0.7
Depth (cm)
0
5
10
FOAM-2
Winter - Spring
13 Mar 75
0.1
0.2
0.3
0.4
0.5
0.6
0
5
10
15
FOAM-3
Summer
8 July 75
0.1
0.2
0.3
0
5
10
15
Depth (cm)
FOAM-4
Fall
5 Nov 75
0.1
0.2
0.3
0.4
0
5
10
FOAM-5
Winter - Spring
18 Mar 76

Figure V-27

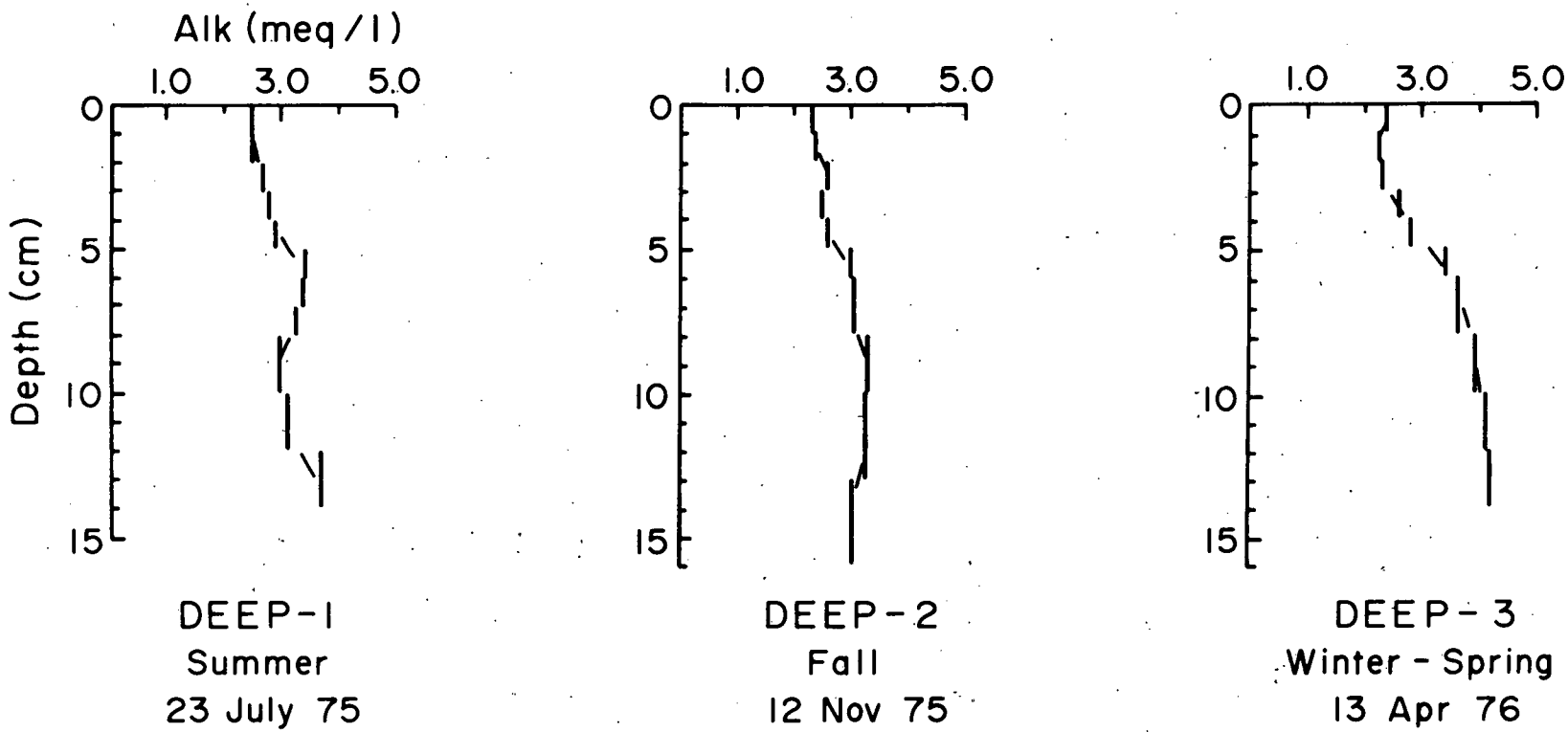

Alk (meq / l)
1.0
3.0
5.0
0
5
10
15
Depth (cm)
DEEP-1
Summer
23 July 75
DEEP-2
Fall
12 Nov 75
DEEP-3
Winter - Spring
13 Apr 76

Figure V-26

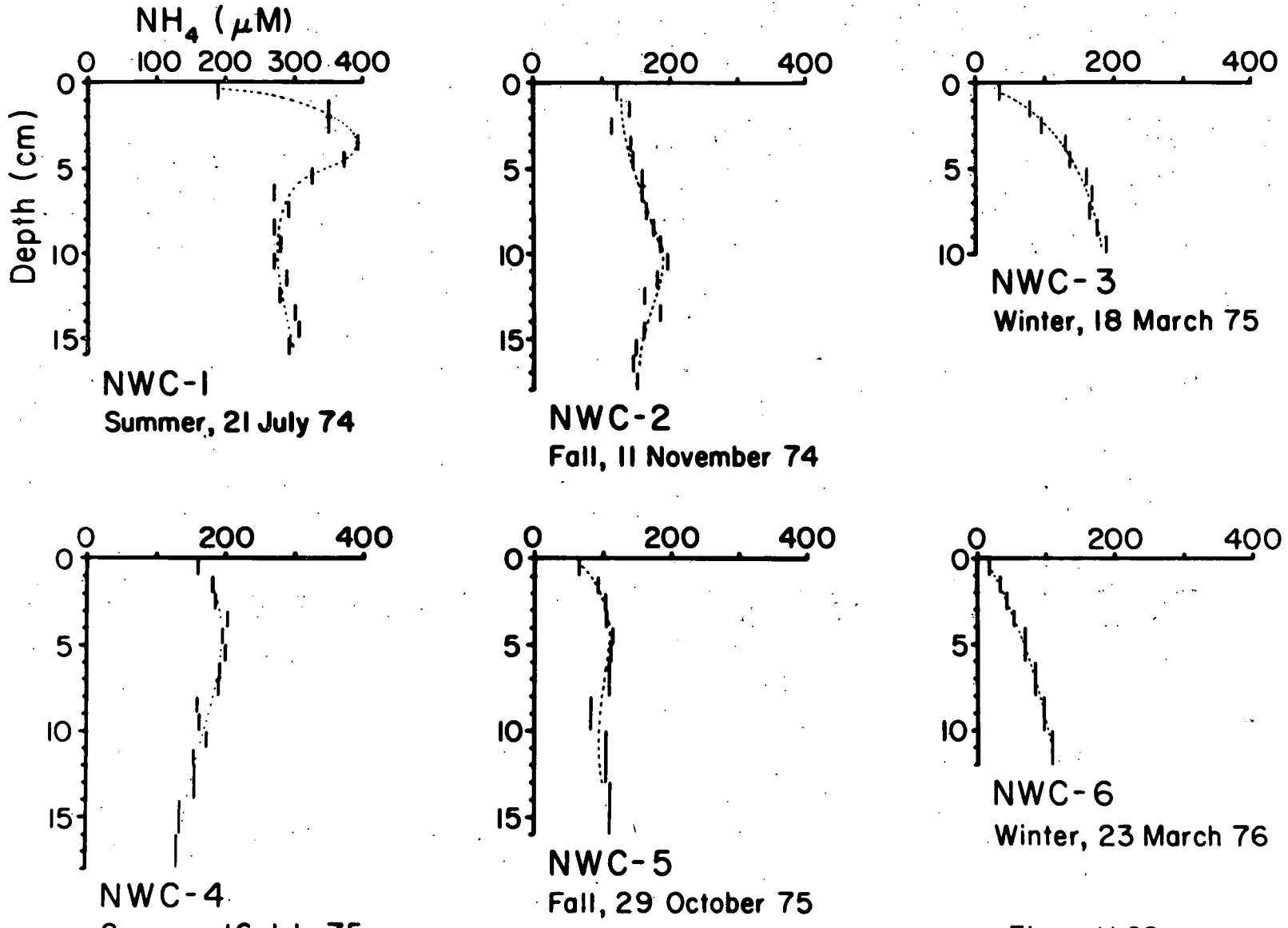

NH4 (μM)
0 100 200 300 400
Depth (cm)
0
5
10
15
NWC-1
Summer, 21 July 74
0 200 400
NWC-2
Fall, 11 November 74
0 200 400
NWC-3
Winter, 18 March 75
0 200 400
NWC-4
Summer, 16 July 75
0 200 400
NWC-5
Fall, 29 October 75
0 200 400
NWC-6
Winter, 23 March 76

Figure V-28

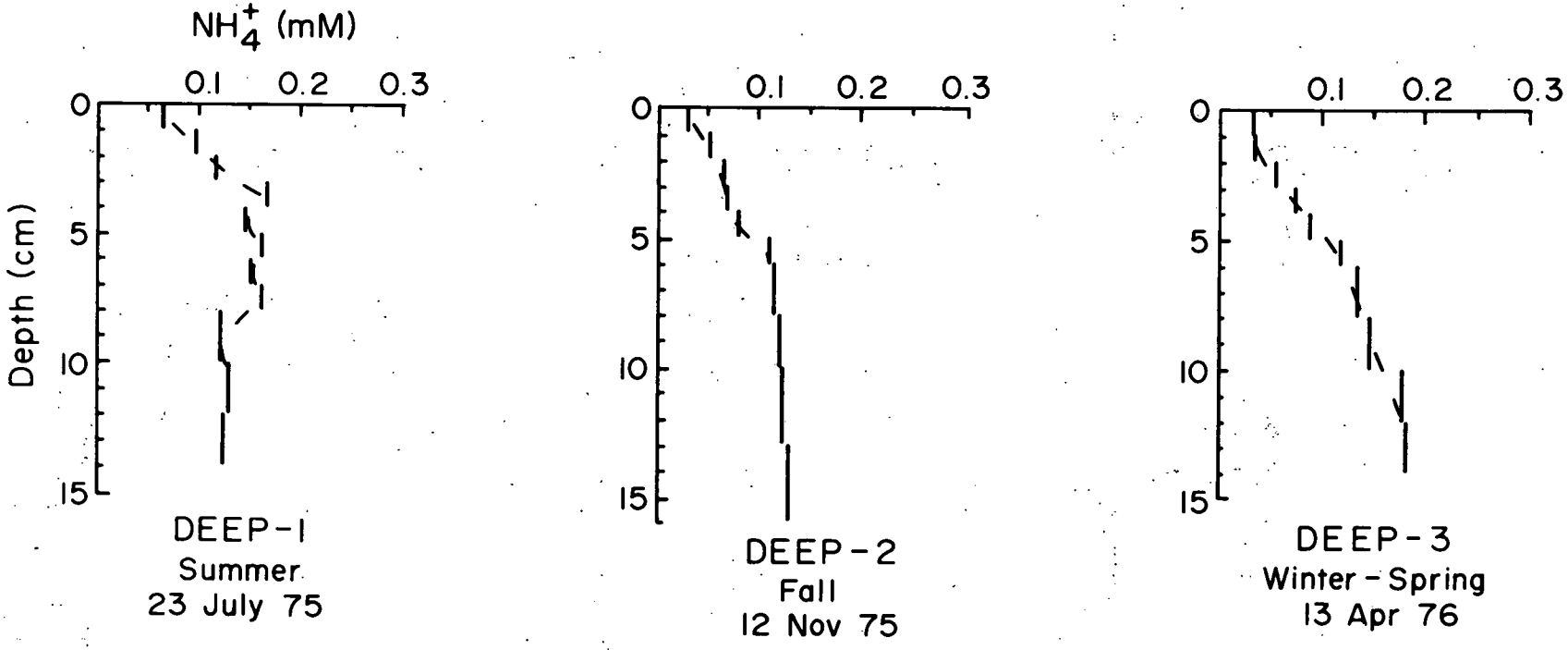

NH_4^+ (mM)
0.1
0.2
0.3
0
5
10
15
Depth (cm)
DEEP-1
Summer
23 July 75
DEEP-2
Fall
12 Nov 75
DEEP-3
Winter-Spring
13 Apr 76

Figure V-29

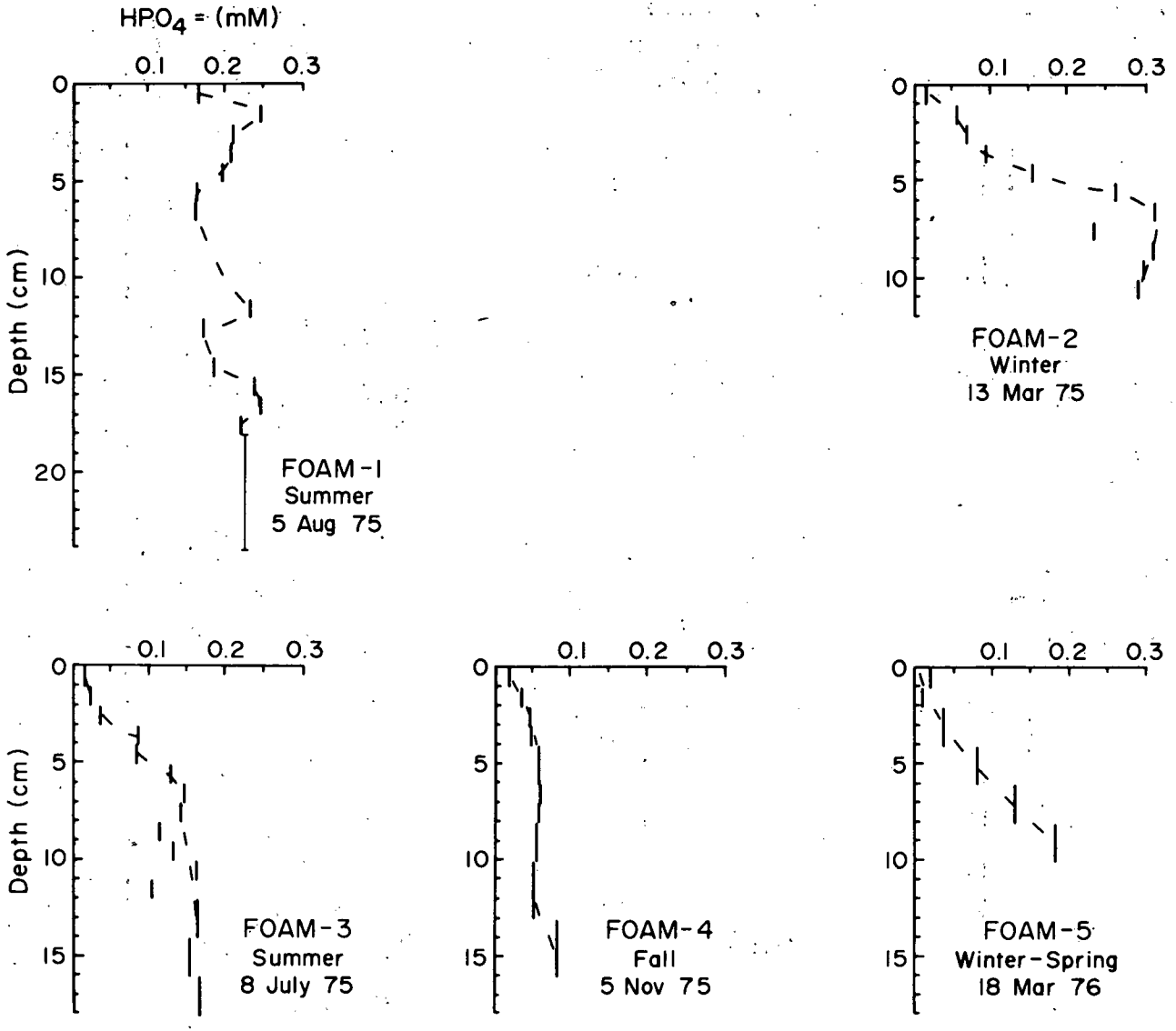

HPO_4 = (mM)
0.1
0.2
0.3
0
5
10
15
20
Depth (cm)
FOAM-1
Summer
5 Aug 75
FOAM-2
Winter
13 Mar 75
FOAM-3
Summer
8 July 75
FOAM-4
Fall
5 Nov 75
FOAM-5
Winter-Spring
18 Mar 76

Figure V-30

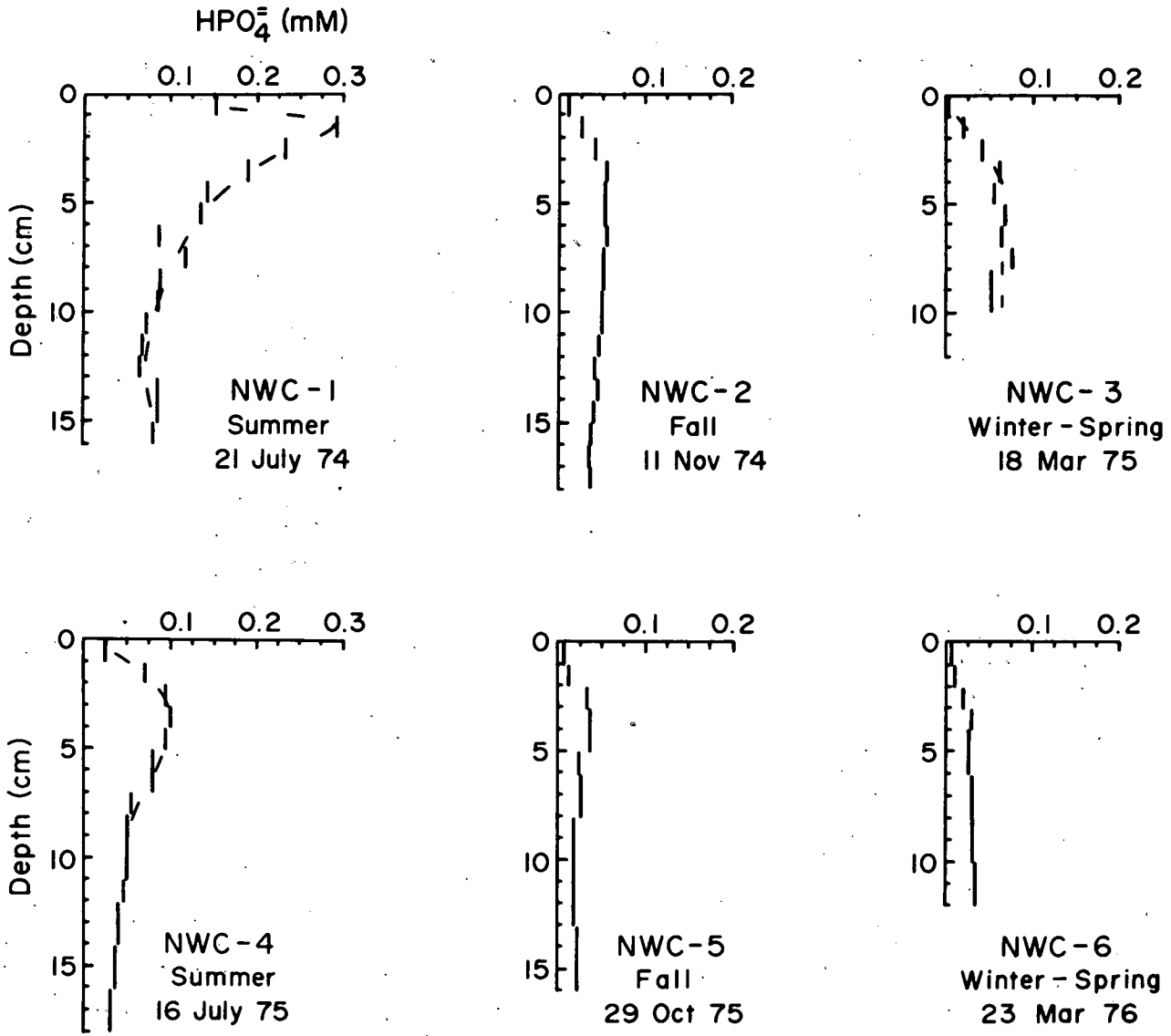

$HPO_4^=$ (mM)
0.1
0.2
0.3
Depth (cm)
0
5
10
15
NWC - 1
Summer
21 July 74
NWC - 2
Fall
11 Nov 74
NWC - 3
Winter - Spring
18 Mar 75
NWC - 4
Summer
16 July 75
NWC - 5
Fall
29 Oct 75
NWC - 6
Winter - Spring
23 Mar 76

Figure V-31

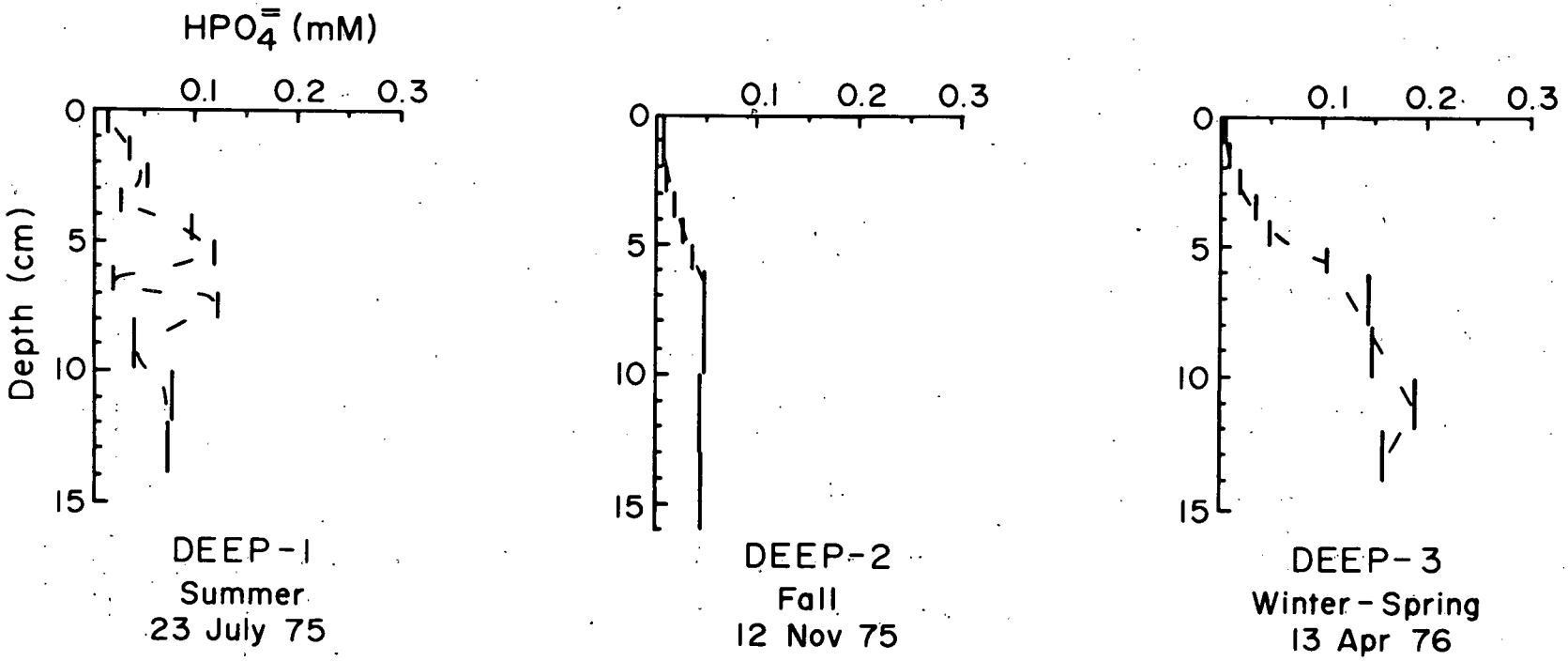

HPO4= (mM)
0.1
0.2
0.3
0
5
10
15
Depth (cm)
DEEP-1
Summer
23 July 75
DEEP-2
Fall
12 Nov 75
DEEP-3
Winter-Spring
13 Apr 76

Figure V-32

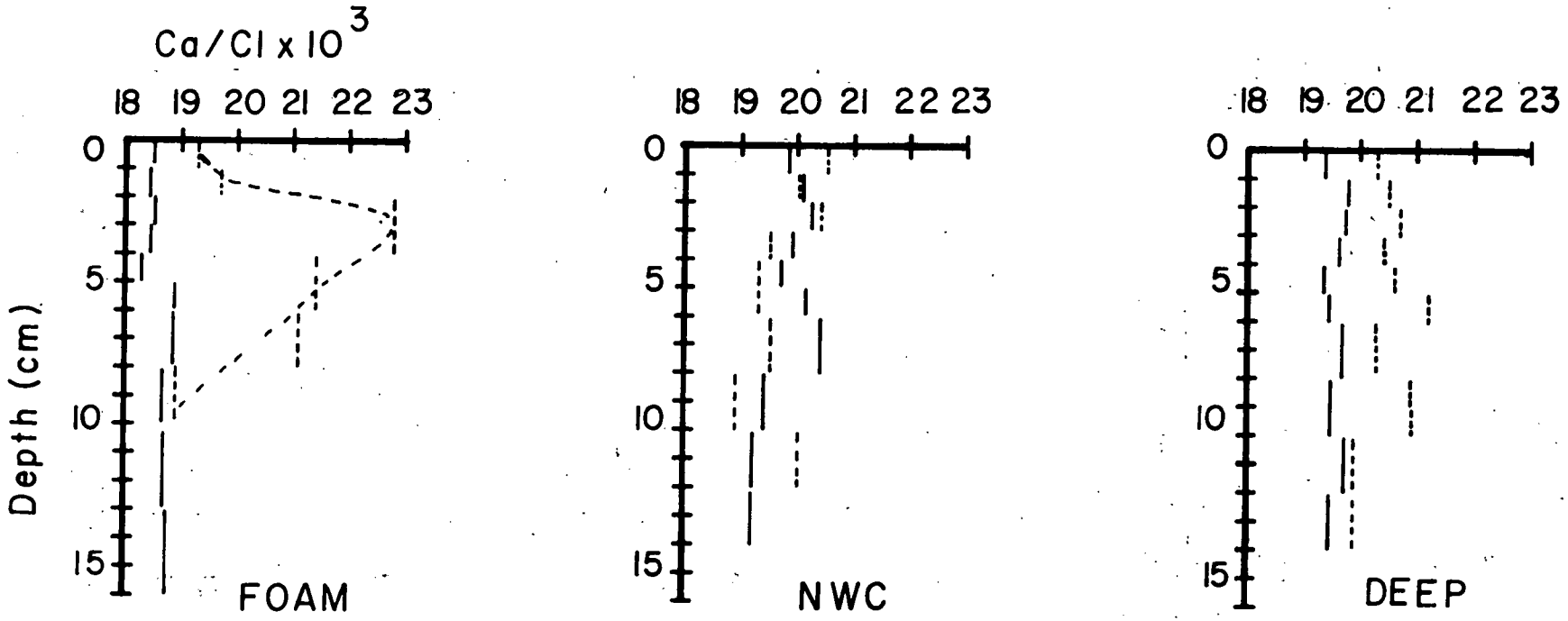


Figure V-33

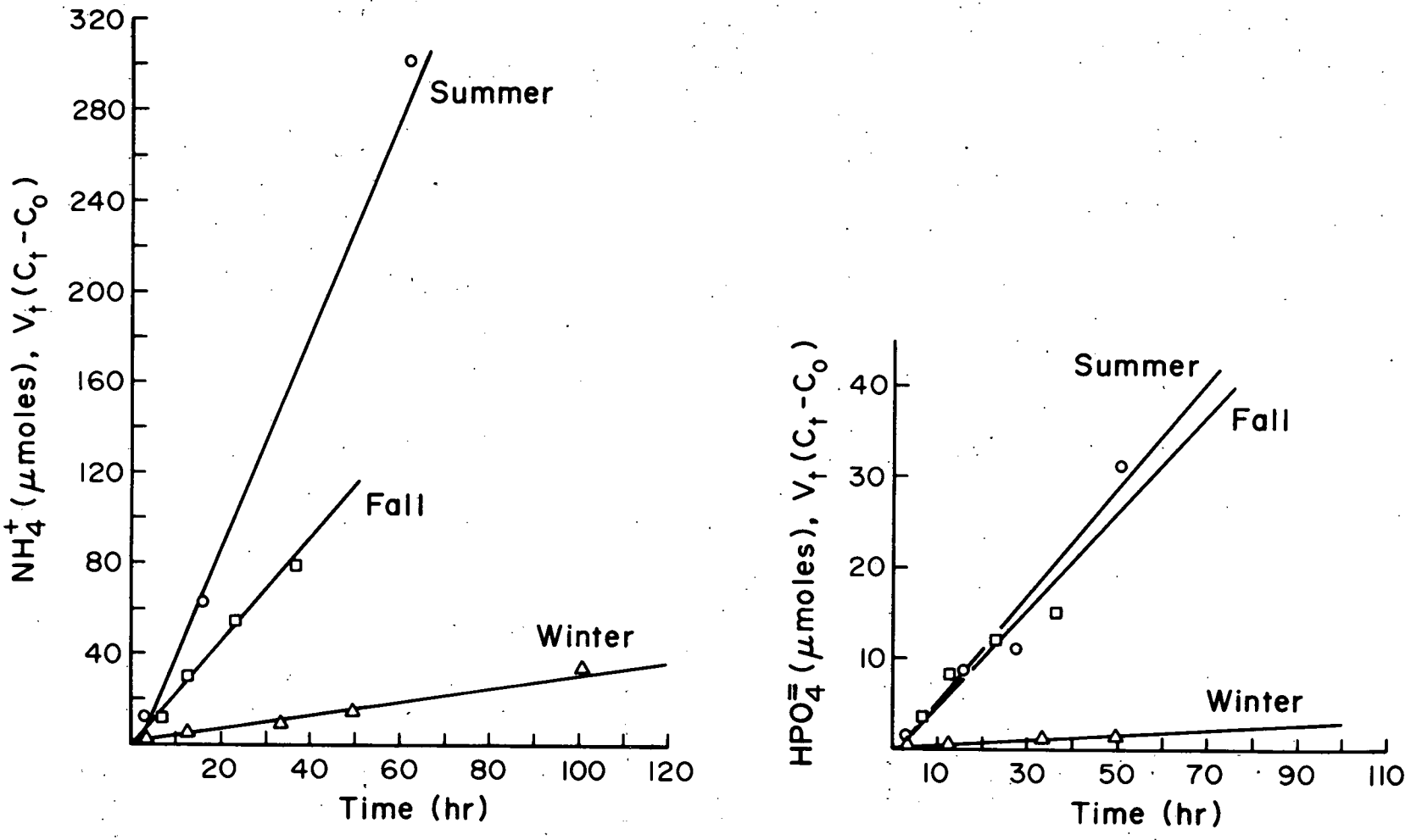

320
280
240
200
160
120
80
40
NH_4^+ (μmoles), $V_t(C_t-C_o)$
Summer
Fall
Winter
20
40
60
80
100
120
Time (hr)
40
30
20
10
$HPO_4^{=}$ (μmoles), $V_t(C_t-C_o)$
Summer
Fall
Winter
10
30
50
70
90
110
Time (hr)

Figure V-34

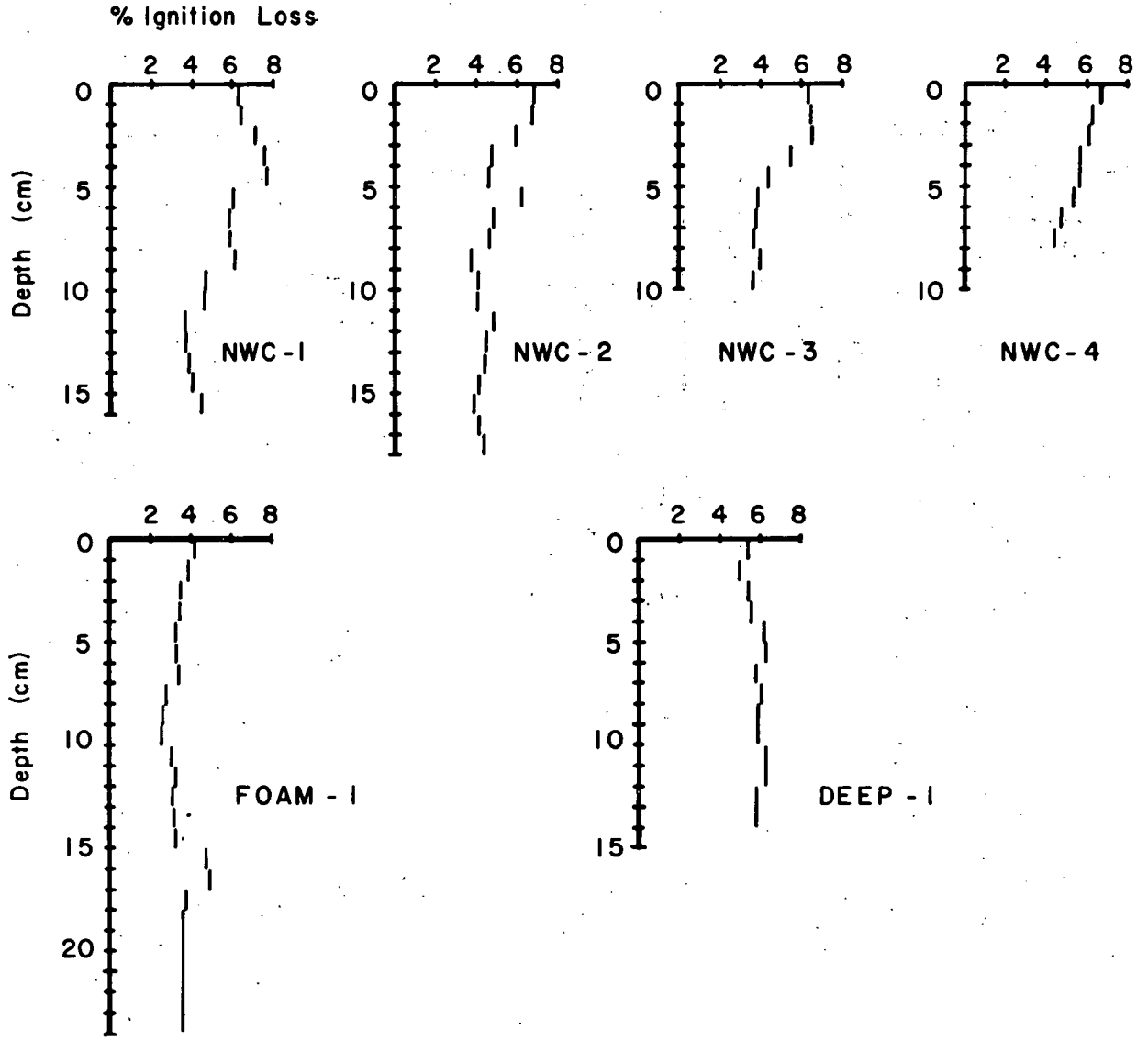

% Ignition Loss
2 4 6 8
0
5
10
15
Depth (cm)
NWC-1
NWC-2
NWC-3
NWC-4
20
FOAM-1
DEEP-1

Figure V-35

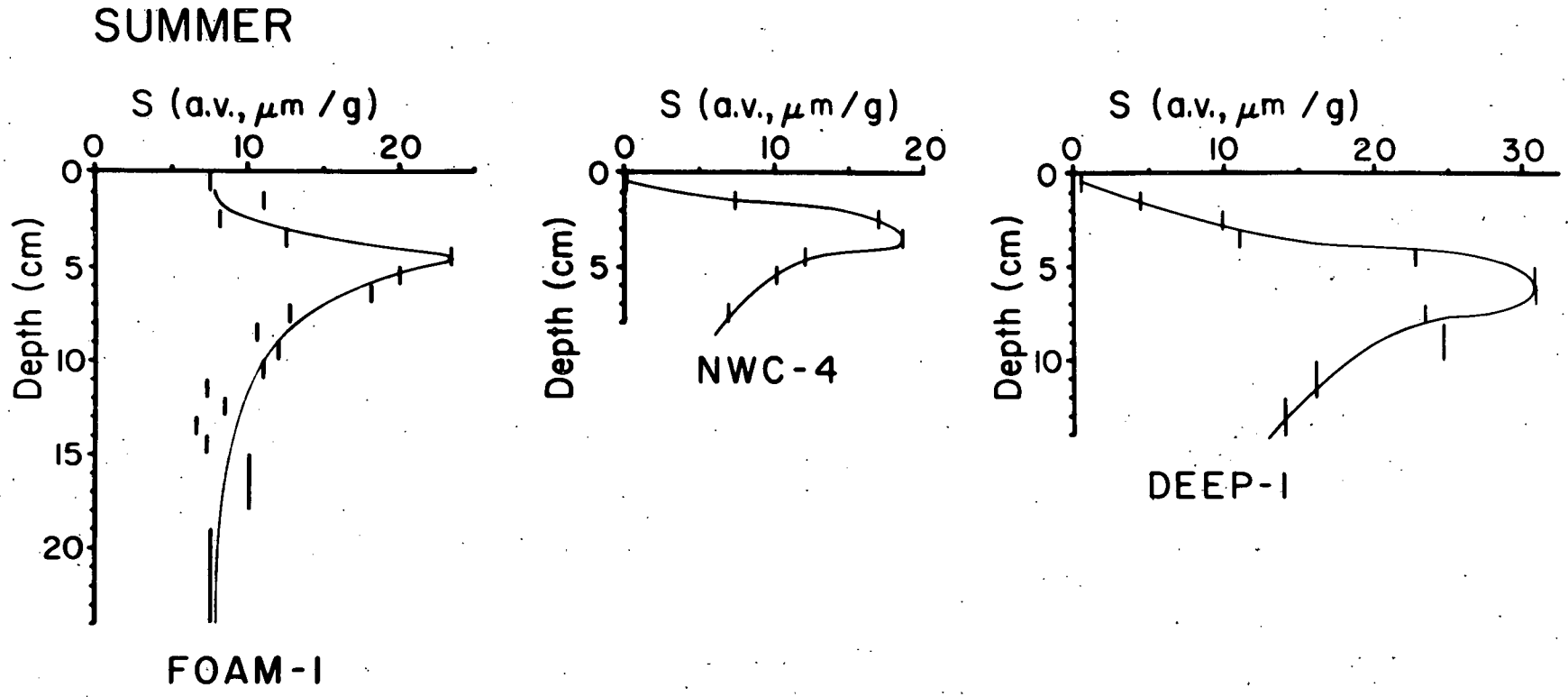

SUMMER
S (a.v., μm / g)
0
10
20
Depth (cm)
0
5
10
15
20
FOAM-1
(Goldhaber et al., 1977)
S (a.v., μm / g)
0
10
20
Depth (cm)
0
5
NWC-4
S (a.v., μm / g)
0
10
20
30
Depth (cm)
0
5
10
DEEP-1

Figure V-36

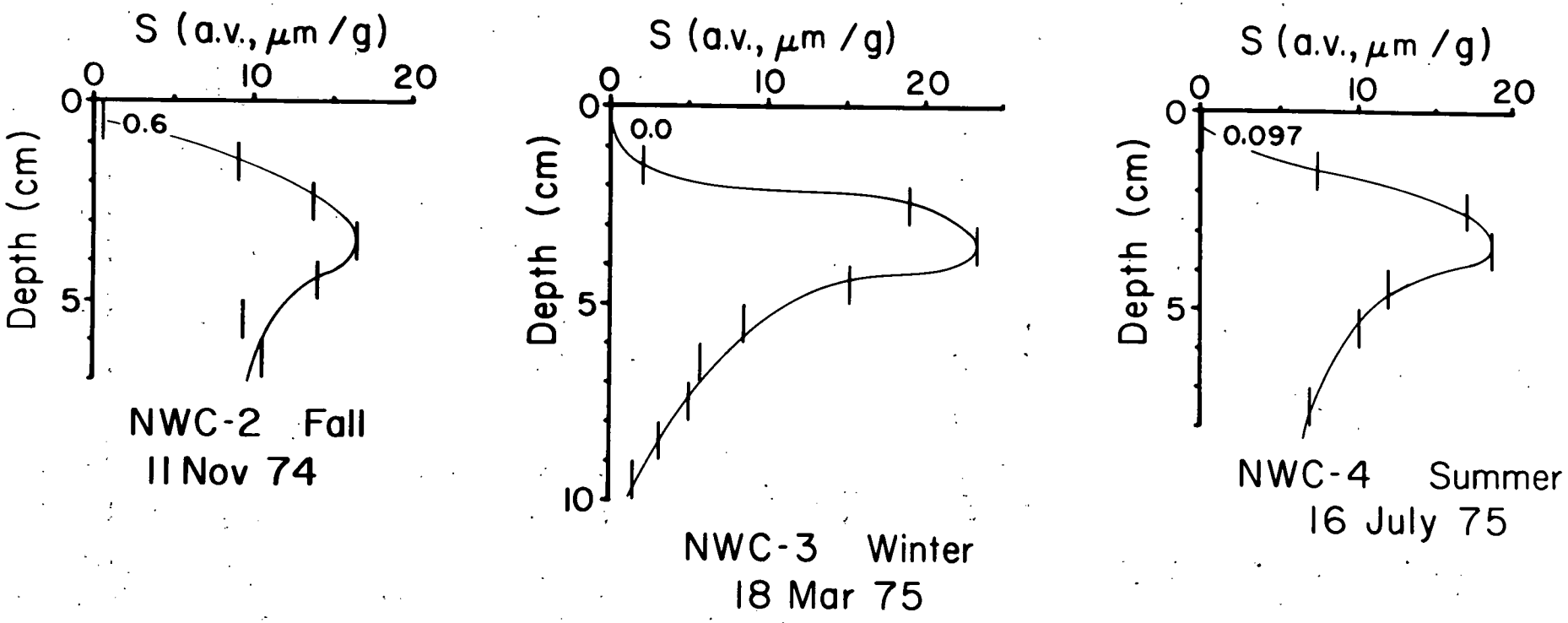

S (a.v., μm / g)
0
10
20
Depth (cm)
0
5
10
0.6
NWC-2 Fall
11 Nov 74
S (a.v., μm / g)
0
10
20
Depth (cm)
0
5
10
0.0
NWC-3 Winter
18 Mar 75
S (a.v., μm / g)
0
10
20
Depth (cm)
0
5
0.097
NWC-4 Summer
16 July 75

Figure V-37

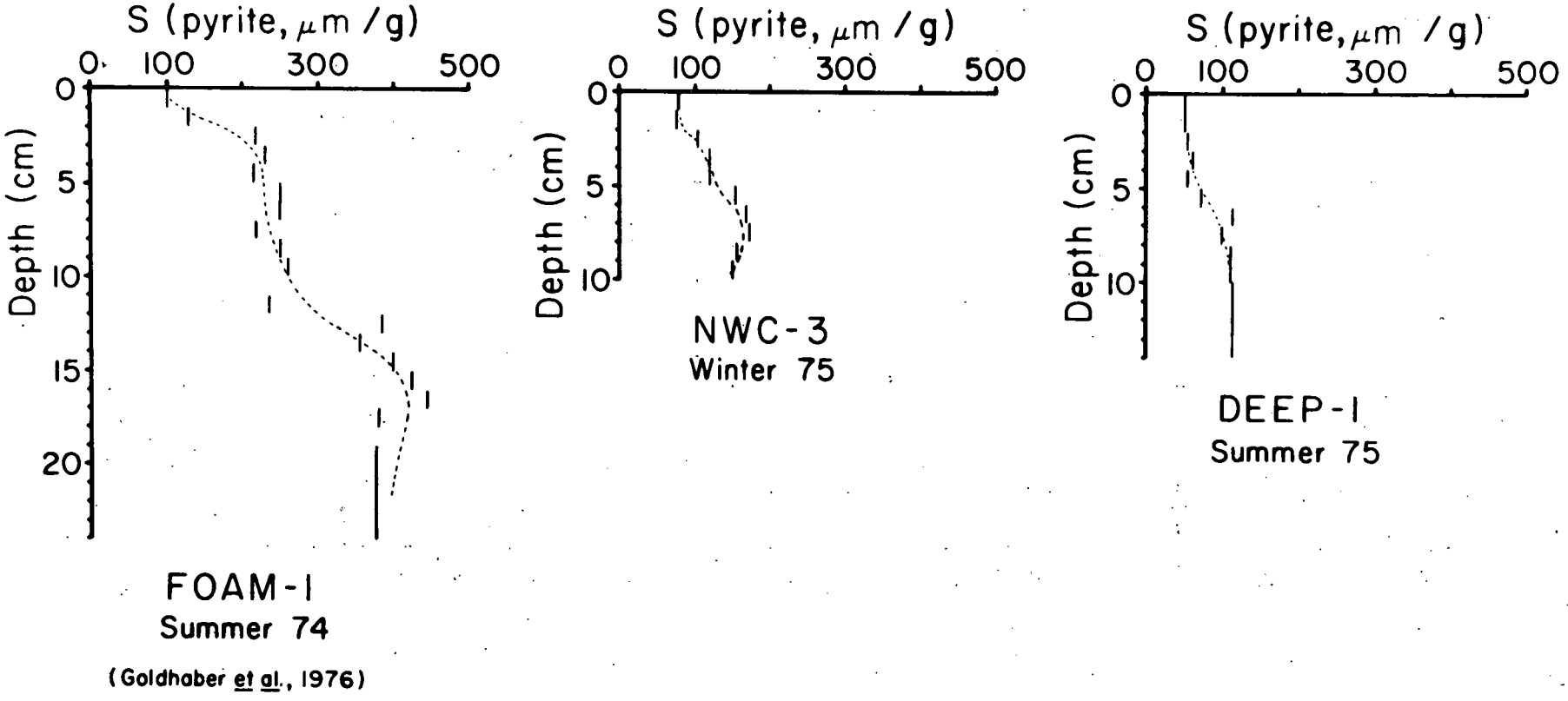

S (pyrite, μm / g)
0
100
300
500
Depth (cm)
0
5
10
15
20
FOAM-1
Summer 74
(Goldhaber et al., 1976)
S (pyrite, μm / g)
0
100
300
500
Depth (cm)
0
5
10
NWC-3
Winter 75
S (pyrite, μm / g)
0
100
300
500
Depth (cm)
0
5
10
DEEP-1
Summer 75

Figure V-38

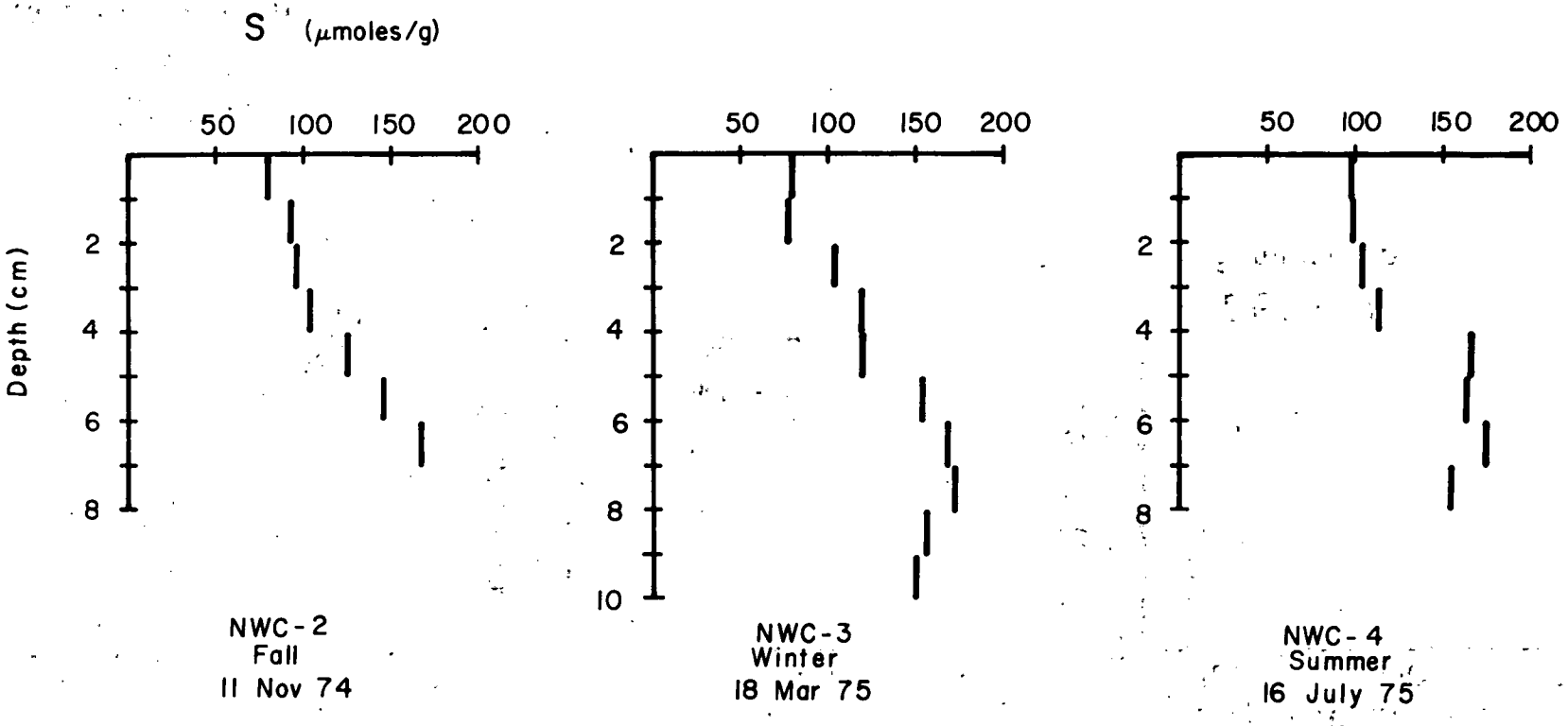

S (μmoles/g)
50
100
150
200
Depth (cm)
2
4
6
8
10
NWC-2
Fall
11 Nov 74
NWC-3
Winter
18 Mar 75
NWC-4
Summer
16 July 75

Figure V-39

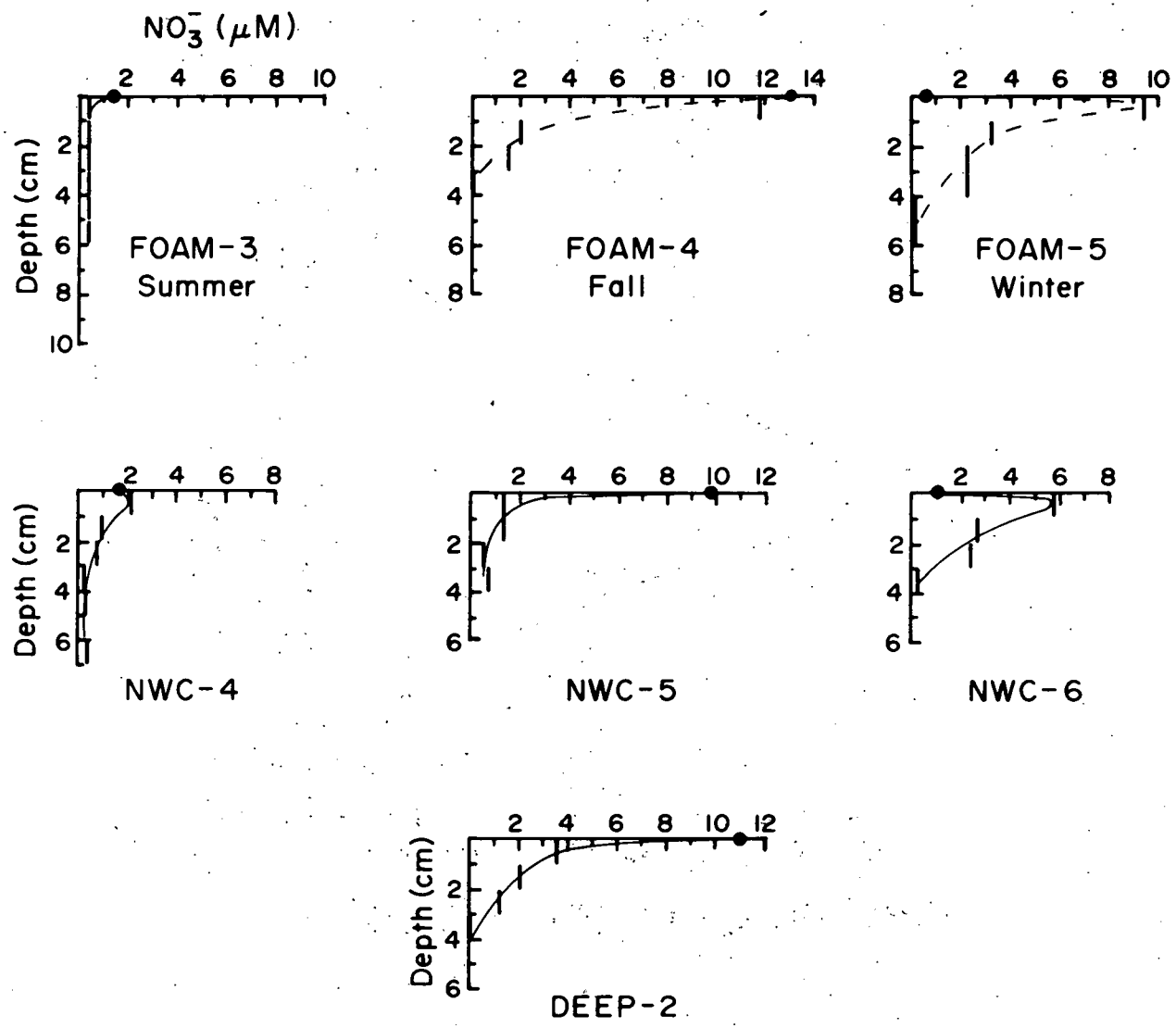

NO_3^- (μM)
Depth (cm)
FOAM-3
Summer
FOAM-4
Fall
FOAM-5
Winter
NWC-4
NWC-5
NWC-6
DEEP-2

Figure V-40

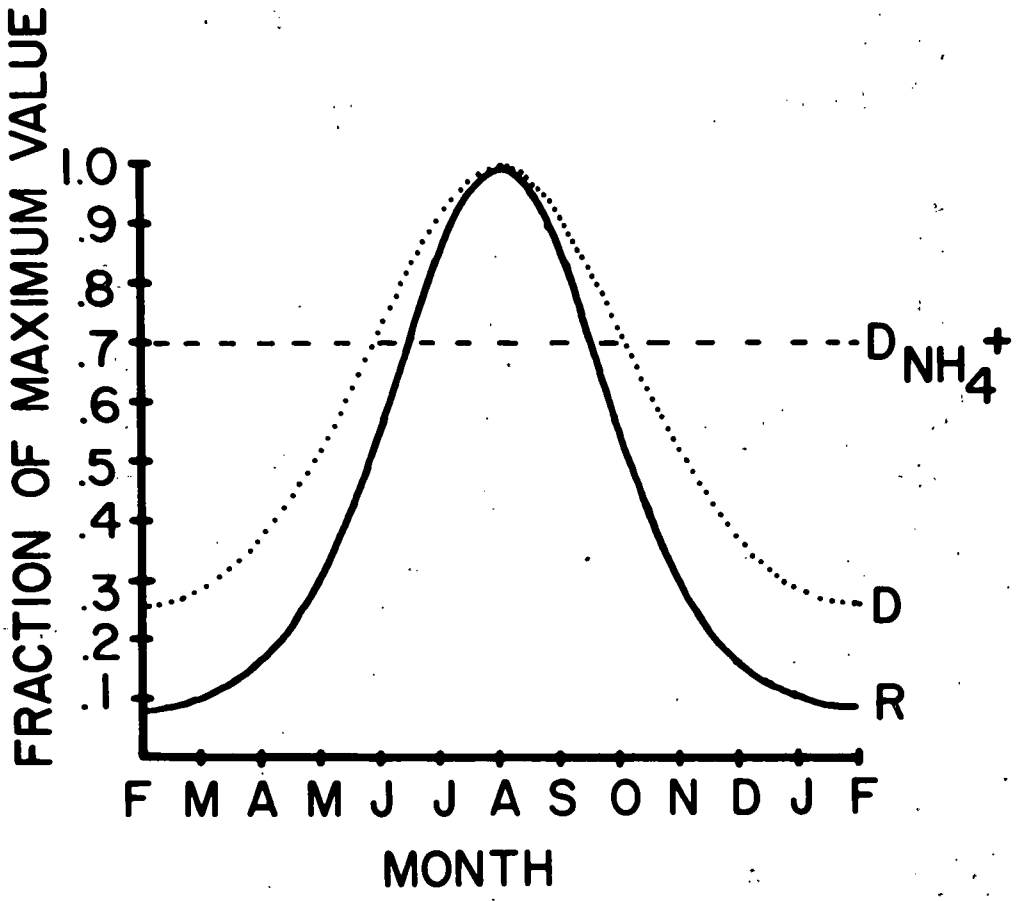

FRACTION OF MAXIMUM VALUE
1.0
.9
.8
.7
.6
.5
.4
.3
.2
.1
$D_{NH_4^+}$
D
R
F M A M J J A S O N D J F
MONTH

Figure V-41

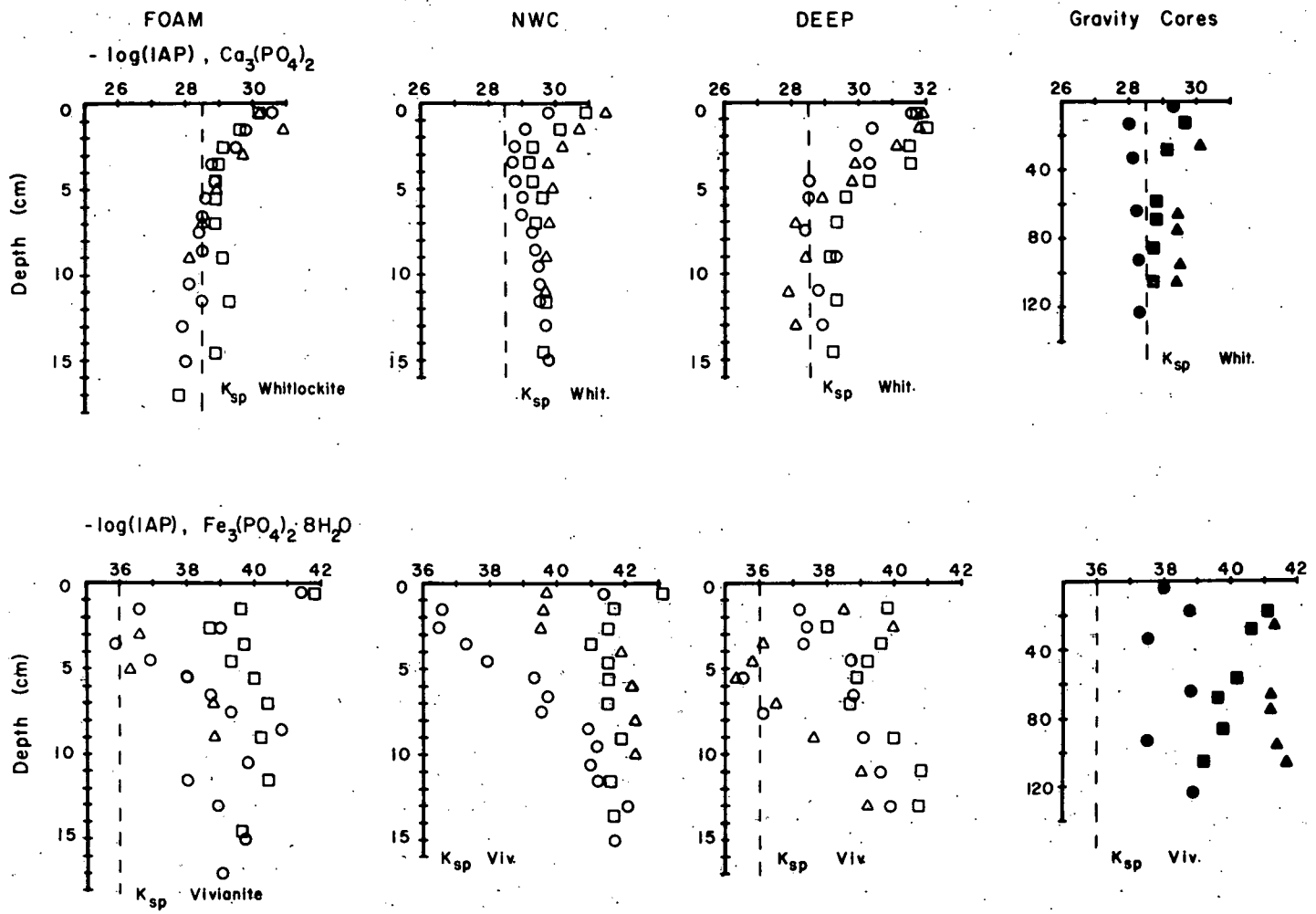

FOAM
NWC
DEEP
Gravity Cores
- log(IAP), $Ca_3(PO_4)_2$
Depth (cm)
K_{sp} Whitlockite
K_{sp} Whit.
K_{sp} Whit.
K_{sp} Whit.
- log(IAP), $Fe_3(PO_4)_2 \cdot 8H_2O$
K_{sp} Vivianite
K_{sp} Viv.
K_{sp} Viv.
K_{sp} Viv.

Figure V-42

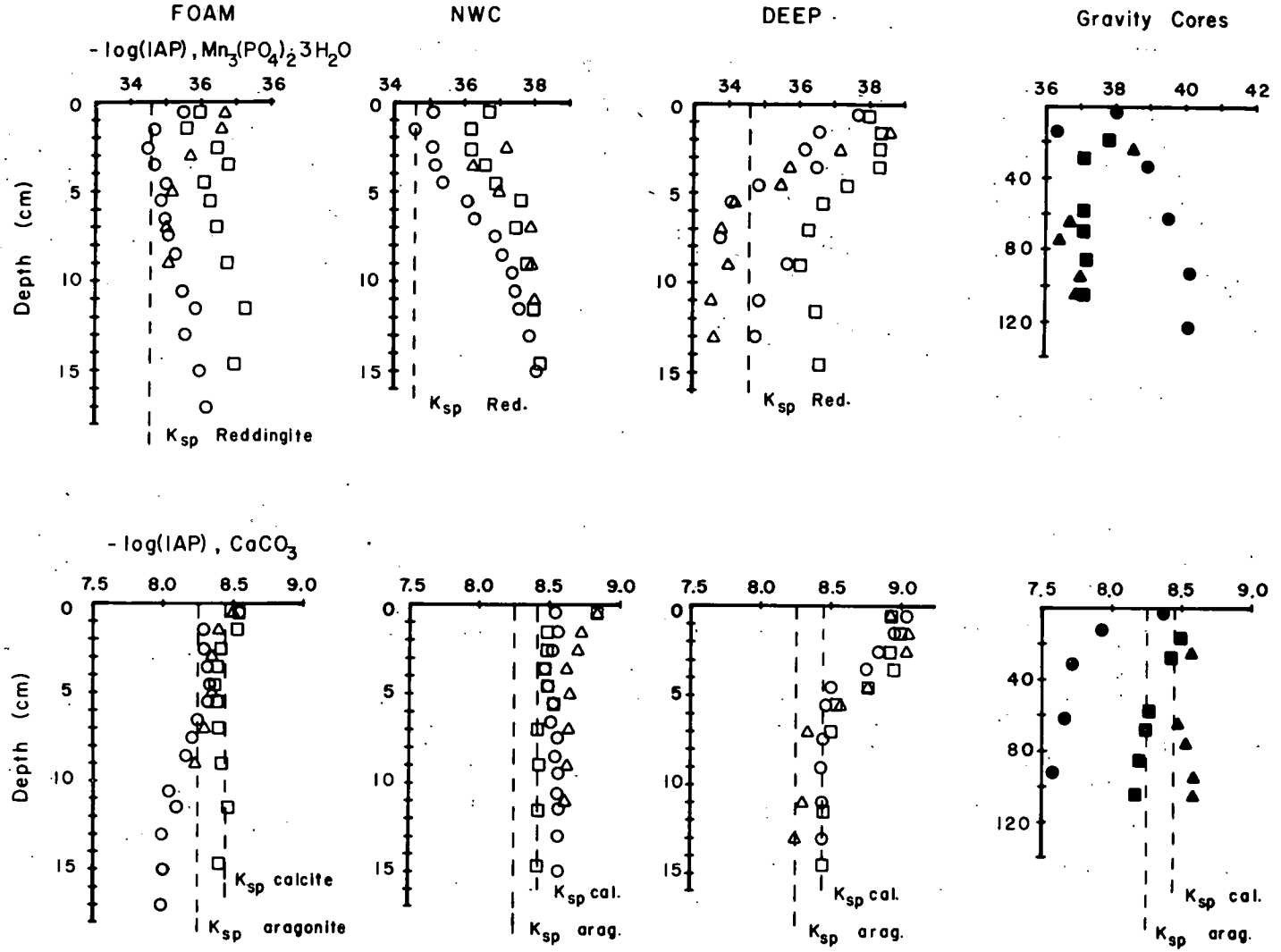

FOAM
NWC
DEEP
Gravity Cores
- log(IAP), $Mn_3(PO_4)_2 3H_2O$
Depth (cm)
K_{sp} Reddingite
K_{sp} Red.
K_{sp} Red.
- log(IAP), $CaCO_3$
K_{sp} calcite
K_{sp} aragonite
K_{sp} cal.
K_{sp} arag.
K_{sp} cal.
K_{sp} arag.
K_{sp} cal.
K_{sp} arag.

Figure V-43

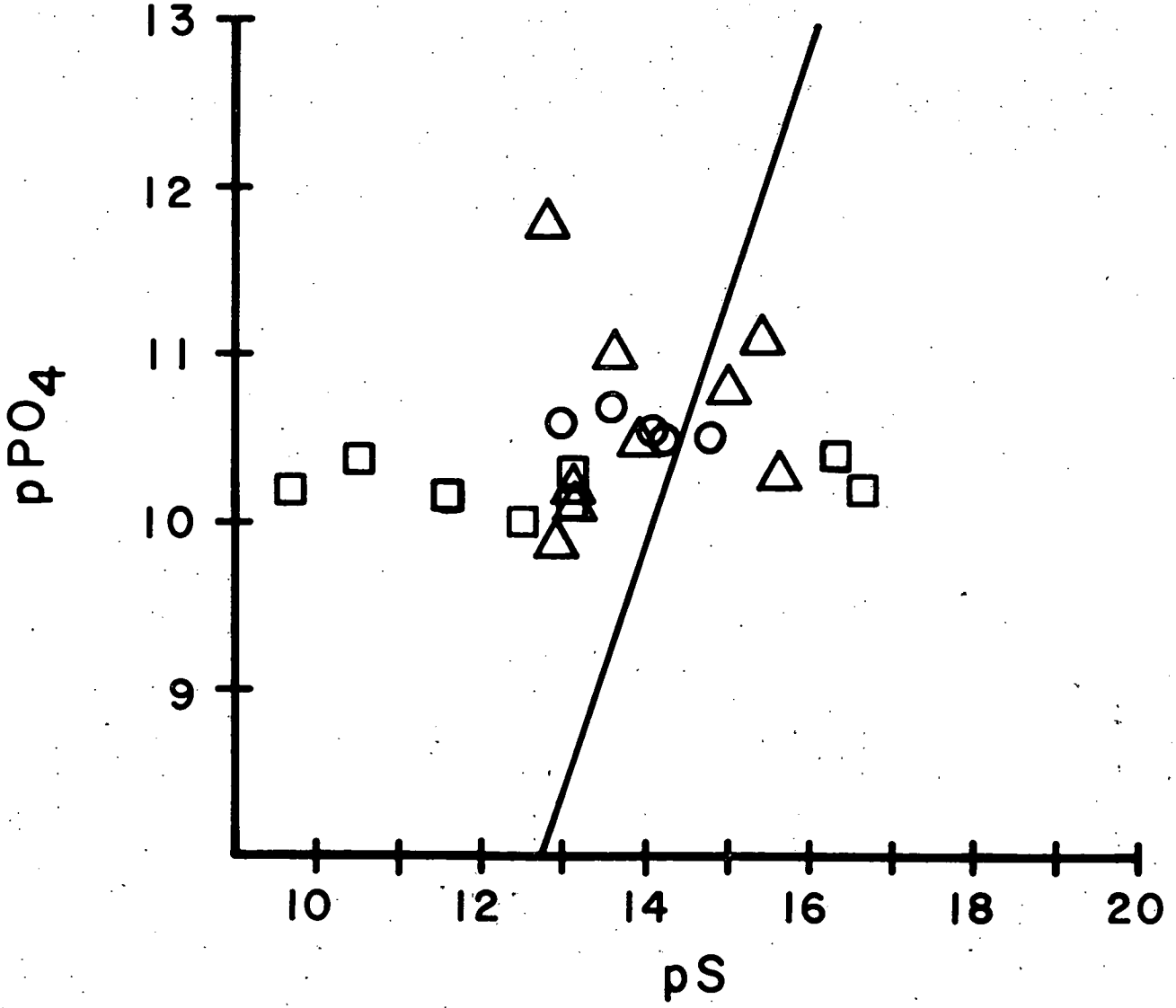


Figure V-44

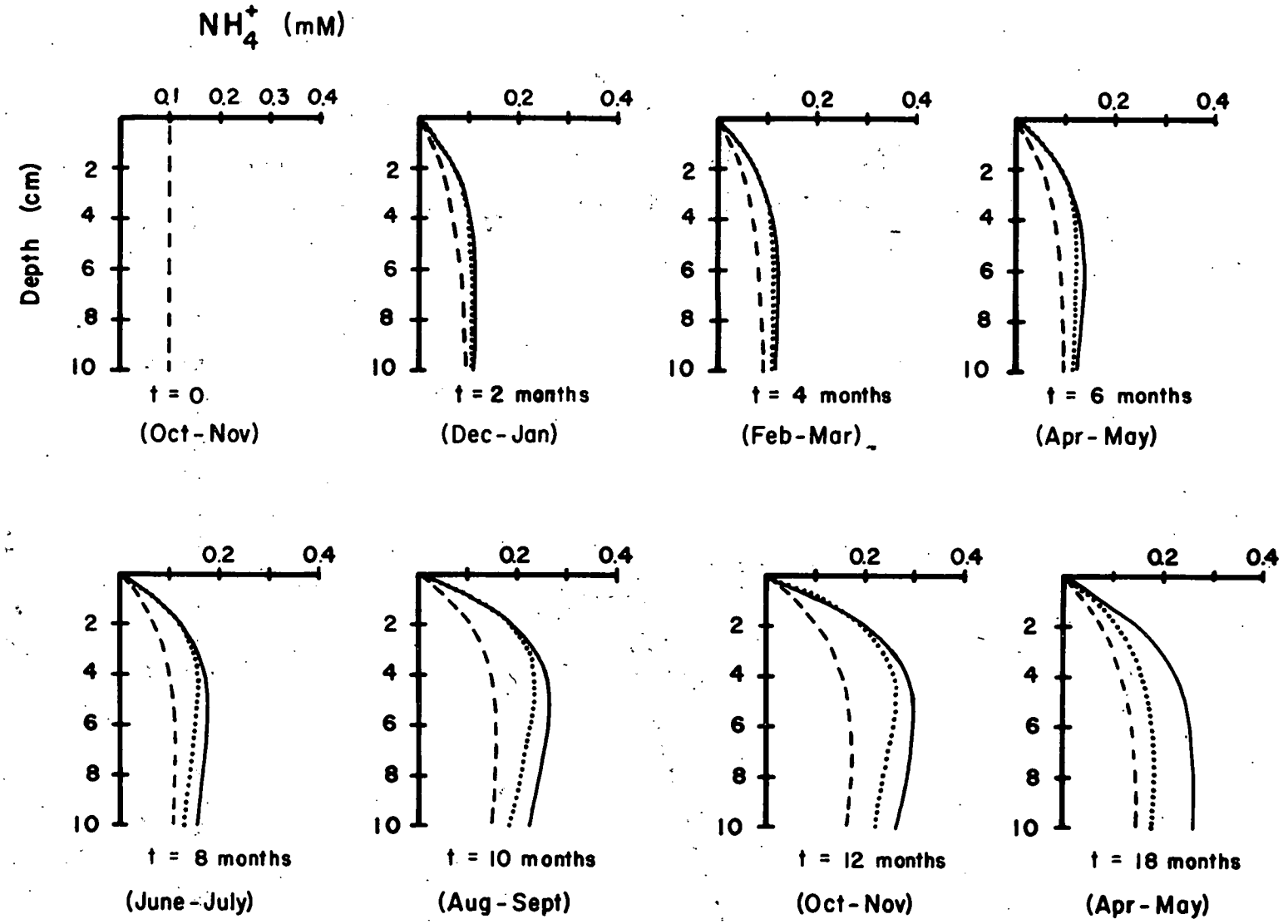
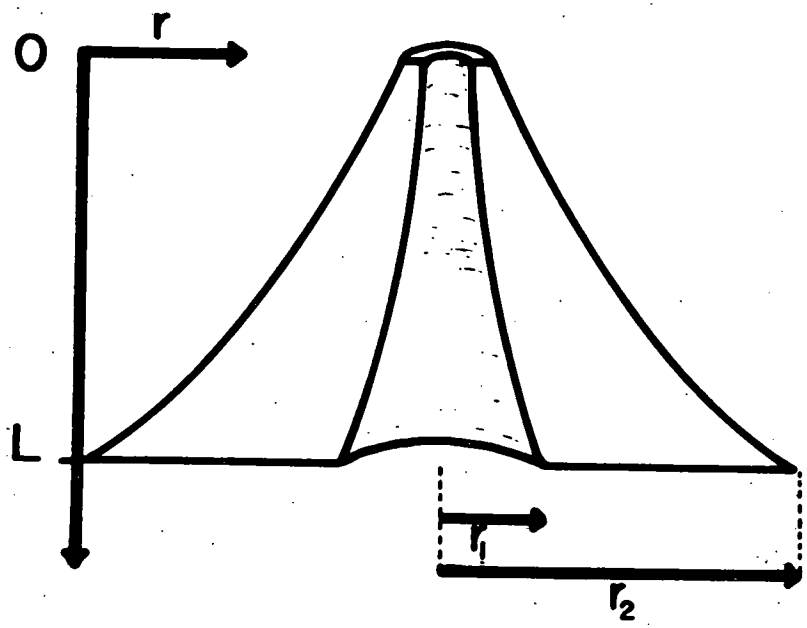
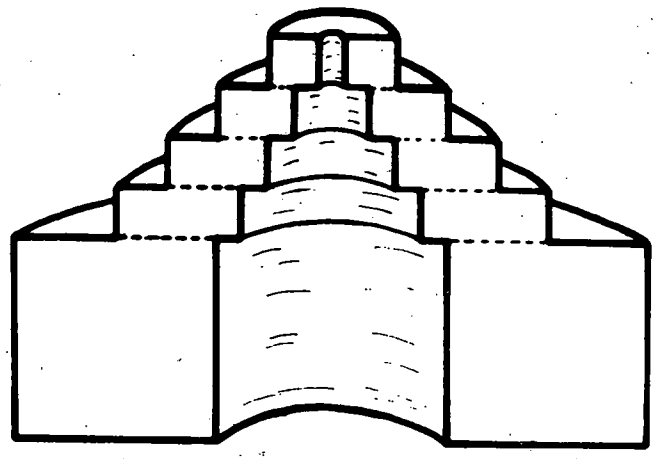

NH_4^+ (mM)
Depth (cm)
0.1 0.2 0.3 0.4
0.2 0.4
2
4
6
8
10
t = 0
(Oct - Nov)
t = 2 months
(Dec - Jan)
t = 4 months
(Feb - Mar)
t = 6 months
(Apr - May)
t = 8 months
(June - July)
t = 10 months
(Aug - Sept)
t = 12 months
(Oct - Nov)
t = 18 months
(Apr - May)

Figure V-45



A



B

Figure V-46

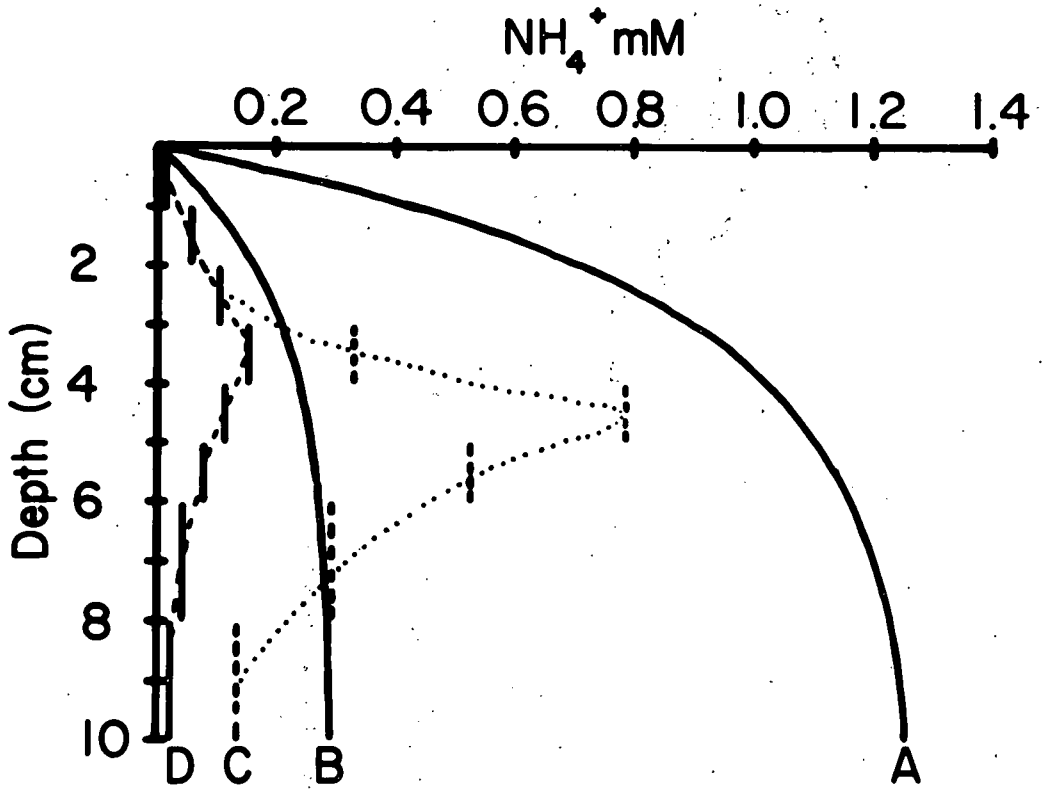


Figure V-47

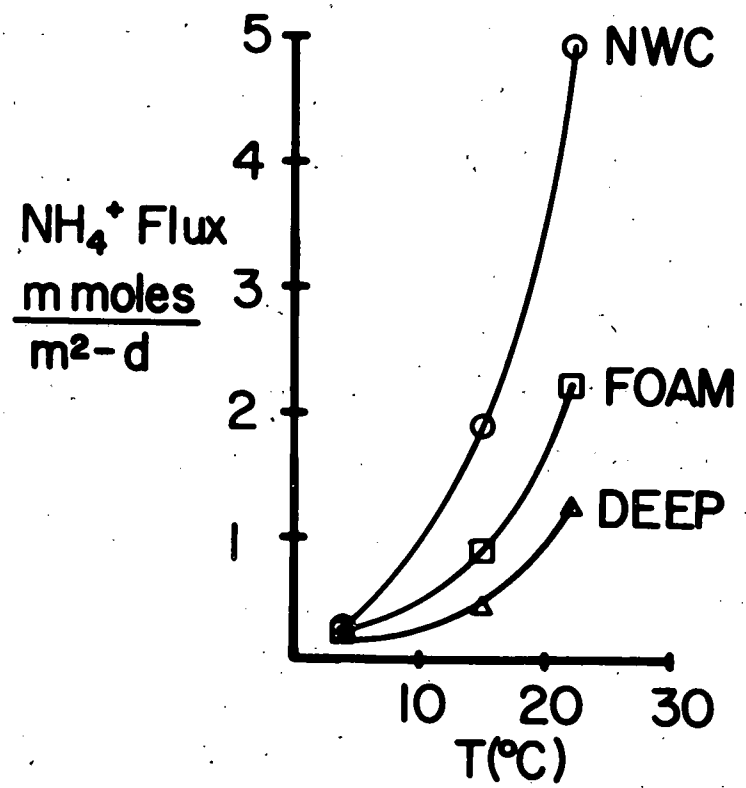


Figure V-48

CHAPTER VI

DIAGENETIC PROCESSES NEAR THE SEDIMENT-WATER INTERFACE OF LONG ISLAND SOUND, II: Fe AND Mn

Adsorption or coprecipitation with Fe and Mn-oxides are known to be important processes affecting the concentration or distribution of many metals in sea water and sediments (Goldberg, 1954; Krauskopf, 1956; Jenne, 1968). Because of this and because of the direct or indirect involvement of both Fe and Mn in the metabolic or biogeochemical activities of marine organisms, knowledge of the natural chemistry of these two elements is particularly essential to understanding marine sediment and water chemistry. Both Fe and Mn are relatively mobile under reducing, aqueous conditions but are rapidly precipitated when exposed to oxygenated, neutral-to-basic solutions. From thermodynamic predictions and observed kinetics of reaction, Fe is oxidized more easily and rapidly than Mn; these differences in properties often result in the segregation of the two metals from each other (e.g., Zapffe, 1931; Krauskopf, 1957; Stumm and Morgan, 1970). Near-shore, marine sediments are commonly reducing a few centimeters below the sediment surface and are overlain by oxygenated waters. Coupled with the oxidation-reduction

properties of Fe and Mn, and intense biological activity just beneath the sediment-water interface, these conditions promote the mobilization-reprecipitation of Fe and Mn in a sedimentary zone where potential interaction of these metals with other elements or living organisms in overlying water and sediment is greatest. In this report, diagenesis of Fe and Mn in the upper meter and especially the upper 10 cm of sediment from three distinct depositional environments of Long Island Sound is studied with the intention to investigate these processes. Particular attention is given to the role of macroorganisms in controlling transport and mediating reactions of Fe and Mn near the sediment surface.

Several kinds of measurements were made: (1) seasonal pore water and solid phase analyses, (2) direct flux measurements of Fe and Mn out of bottom sediment, (3) a series of oxidation-reduction experiments in the laboratory to investigate mobilization and precipitation reactions of Fe and Mn under different simulated natural conditions and (4) documentation of the abundance and composition of fauna and general sedimentary environment at each station.

Location and description of study area

The three stations chosen for study: FOAM, NWC, and DEEP, are located in predominately silt-clay regions of central Long Island Sound and lie in 9, 14, and 34 m of water respectively. The location, description, faunal analysis, and examples of x-radiographs of sediment at these stations

are given in detail in Chapter V and will not be repeated here. The three stations represent a general inshore-offshore transect running from FOAM to DEEP.

Sampling

Most bottom samples were obtained by SCUBA divers using specially constructed plexiglas box cores (Chapter V, Appendix I). The method of obtaining cores is described in Chapter V. Gravity cores were also taken at each station on one or more occasions as previously described. Box cores were taken in summer, fall, and winter-spring periods from 1974 to 1976; sampling was carried out over two year periods at FOAM and NWC and for one year at DEEP (Table V-2).

Treatment of cores

Pore water and sediment samples

The cores used for pore water or solid phase Fe and Mn analyses were the same used for the pore water analyses: alkalinity, $SO_4^=$, NH_4^+, $HPO_4^=$, pH, pS, $\%H_2O$, and solid phase analyses: FeS, FeS_2, percent organic matter, given in Chapter V. The treatment of cores is therefore identical. In brief summary: box cores were stored at 4°C for 3-5 hours after collection. Sediment was removed at 1 cm intervals under a N_2 atmosphere in a glove bag, placed in precut 10 cm long acetate-butyrate tube sections (4.5 cm O.D.), and squeezed using the method of Kalil and Goldhaber (1973) within 12-24 hours

after collection. Pore water was expressed first through a glass fiber pre-filter and secondly through 0.45 μm pore Millepore filters directly into plastic syringes without air contact. Gravity cores were processed in the same way except that the core was sectioned in 10 cm intervals by use of a hack saw and a miter box. Water taken from each end of a section was either kept separate and assigned to different 5 cm intervals or combined. In all cases, the first ~5 ml of pore water expressed was discarded and care was taken to avoid air contact during packing and squeezing operations to minimize oxidation reactions (Troup, Bricker, and Bray, 1974).

Pore water samples for Fe and Mn analysis were treated in the following way: 10 or 15 ml of pore water was passed rapidly from a syringe through a short section of Tygon tubing into a 10 or 15 ml pipet, depending on sample size. This sample was immediately drained into an acid-washed and distilled water rinsed 2 oz polyethylene wide-mouth bottle. The total transfer time was only slightly greater than the drain time of the pipet (~ 30 sec). The sample was titrated for alkalinity and acidified to pH 1-2 within 48 (occasionally 72) hours in the same 2 oz container (Chapter V). Care was taken to maintain the bottle upright prior to acidification to avoid loss of Mn and Fe to parts of the bottle wall which would not later be exposed to acidified solution. In order to determine whether Fe or Mn was permanently lost to the side of the bottle prior to acidification by this procedure, a series of experiments were performed.

Mixed Fe and Mn standards totaling 10 ml in volume and of concentration range ~ 30-60 μM (in 0.1 N HCl) were added to 2 oz bottles of the same type as used for samples. The pH was raised using Na_2CO_3 to ~ 8-9 and the samples allowed to sit. Within ~ 10 min the solutions became yellow-orange and flocs characteristic of Fe^{+3}-oxide formed. At various times over a period of several weeks, one of these bottles was opened and titrated using the same procedure and solutions as for normal alkalinity titration of pore water samples; the final pH after complete acidification was 1-2. Within a few hours these titrated solutions, like pore water samples, became clear in color. After sitting for a few days following acidification these standards were analyzed for Fe and Mn as described below. It was found that if acidification was performed within one-two weeks of sample precipitation, 100 ± 1% of the Fe and 100 ± 2% Mn was recovered. Distilled water blanks run through the same alkalinity titration procedure gave Fe and Mn blanks below detection limit for 10 ml samples.

In natural samples some loss of Fe and Mn in the transfer pipet is possible. There are several reasons to believe this is not a serious problem: (1) transfer time was short, < 45 sec; (2) pore water did not become yellow in color (precipitation of Fe) until several minutes (5-10) after transfer into the titration bottle; and (3) 10 and 15 ml samples taken from sediment intervals on either side of one another were either closely similar in Fe and Mn composition or part of a consistent concentration trend. Since the pipet wall and air exposed

surface area is different for the two sample sizes it is likely that irregular results would be obtained for different volumes of pore water if loss were a serious problem in the transfer time involved.

The sediment cake resulting from squeezing was retained in its butyrate tube, sealed with end caps and frozen. Ignition loss (475°C), % $CaCO_3$, acid volatile sulfide, and total non-volatile sulfur were measured on many samples (Chapter V). Fe, Mn, and Cu determinations were made as described below.

Flux samples

Two core boxes designed for measuring sediment to water fluxes were always taken; one contained only bottom water and acted as a blank, the other was filled with 10-15 cm of undisturbed bottom sediment and its overlying water (Chapter V). Both summer boxes (1975) were kept at 22°C, fall (1975) flux boxes at 15°C, and winter (1976) at 4°C. Processing of these boxes consisted of withdrawing water samples from each box at successive times and following the change in overlying water concentrations of selected, dissolved ions. The total initial water volume was determined and volumes removed at each sampling were measured. By correcting the concentration changes for volume differences between one sampling and the next, a flux of a given ion out of the sediment could be calculated as described below. The summer and fall boxes were periodically aerated.

Water samples were obtained by inserting a section of Tygon tubing attached to a syringe into a box and withdrawing a sample. This water was immediately filtered through 0.4 μm pore size Nuclepore filters directly into acid cleaned sample bottles. The contents of one bottle was acidified with HCl and one bottle was left unacidified and placed immediately into a refrigerator at 4°C. The acidified samples were later analyzed for Fe and Mn and the unacidified samples for NH_4^+ and $HPO_4^=$. pH and Eh of the water were occasionally checked by insertion of the appropriate electrode into a water sample.

After water sampling was complete, sediment in the flux boxes was sometimes sieved through a 1 mm mesh sieve for the contained animals (Chapter V).

Excretion experiments

The excretion rates of Mn and Fe by the common infauna: Yoldia limatula and Nephtys incisa were measured as follows. Yoldia (33 individuals) and Nephtys (13 individuals) were obtained by grab sampling at NWC. After freeing the animals of external sediment, all individuals from a given species were placed in a single 600 ml beaker and covered with sea water. When 5.5 hours had elapsed, this water was filtered (0.4 μm), acidified, and analyzed for Fe and Mn. These analyses were compared to blank values from sea water treated in the same way but without animals. Approximate excretion

rates, when detectable, were calculated from the differences between the samples with animals present versus blanks and normalized to the total dry tissue weights (shell-free) in each case.

Precipitation experiments

In order to determine the rate of loss of < 0.45 μm size Fe and Mn from water overlying the flux cores during flux measurements, two experiments were performed. After the last water sample was taken from the fall 1975 DEEP flux core, the core was allowed to sit for two more days at which time the remaining water was rapidly transferred to an identical but otherwise empty flux box maintained at 22°C. This water was sampled periodically to determine the rate of decrease of Fe and Mn in the water in the absence of an underlying sediment source. The experiment was repeated at a temperature of 4°C during winter 1976.

Reduction-decomposition experiments

In an attempt to recreate conditions affecting Fe and Mn mobilization or precipitation reactions during decomposition, two similar sets of experiments were done, one for each element. In the first, sediment from a salt marsh pan was collected near Guilford by Martens and Berner (1974), homogenized, and loaded into airtight glass jars which were immediately sealed. The jars were stored at 22° and opened sequentially for analysis of sulfate and methane in the pore water (Martens and Berner, 1974). Acidified samples of pore water

were made available to me by the investigators for Mn analysis. As the serial sulfate and methane analyses resulting from this experiment were shown to mimic in time the changes in pore water distributions with depth found in near shore Long Island Sound waters, analyses were made for Mn to see if the same held true for this element.

The second experiment involved analyses for Fe and $SO_4^=$ only and was set up in a similar fashion. In this instance, the effort was to recreate conditions which might be effective near the sediment-water interface. With the aid of M. B. Goldhaber, sediment from 20 to 50 cm in a core taken from the FOAM site was homogenized in a glove bag (He atmosphere) and divided into three 200 ml portions. Small quantities of one portion were loaded into a series of screw cap test tubes which were then sealed. To the second portion was added a quantity of glass beads which had been coated with mucus by the moon snail: Polinices duplicatus. The total dry weight of mucus added, as determined on a subsample of mucus coated beads, was ~0.1 g. The glass beads (silt size) acted simply as a carrier for the mucus during initial secretion by the organism and enabled the addition of fresh, wet mucus to the sediment while still allowing determination of the amount added by use of the subsample. The second portion was then loaded into a series of test tubes in the same way as the first. The same quantity of mucus coated glass beads was then mixed into the last remaining portion but, in addition, 12 g of freshly ground (<250 μm mesh) Georgia limonite (Wards Sci.) was also added. After homogenization,

this portion was loaded into test tubes and sealed. All test tube samples were then stored under a N_2 atmosphere and at various times thereafter placed in a centrifuge; the pore water was separated out, then removed using Eppendorf pipets and analyzed for $SO_4^=$ and Fe. The basic idea behind this experiment was: (1) to see if sediment taken from deep in a deposit could be reconstituted, in terms of increasing the rate of $SO_4^=$ reduction, upon the addition of mucus secretions by macrobenthos and (2) to see if mixing of reduced sediment, Fe-oxide and mucus such as might occur continuously in surface sediment, would result in a series of changes in chemistry similar to that observed near the sediment-water interface.

Oxidation experiments

The possibility that the oxidation of solid phase sulfides near the interface might result in the release of dissolved Fe^{++} or Mn^{++} was investigated in two separate experiments. In the first, done with the aid of M. B. Goldhaber, 281 g of sediment from the FOAM site taken from depth intervals: 10-11, 13-14, and 16-17 cm, was placed in a narrow-mouth reagent jar and covered with two liters of LIS sea water. To a second jar, 2.7 g of freshly ground (< 62 μm) pyrite was added and it was also covered with 2 liters of sea water. A third jar filled with sea water was used only as a blank. A large, glass-covered stirring bar was added to each, glass tubes passed through rubber stoppers were then placed into each jar, the jars sealed, and the solutions were

vigorously stirred and aerated by use of magnetic stirrers and by passing filtered (0.4 μm), water-saturated air through the glass tubes. The water in each jar was periodically sampled for Fe and $SO_4^=$ by inserting a section of Tygon tube attached to a syringe and withdrawing a quantity of water. This water was rapidly filtered through inline filters (0.4 μm, Nuclepore) attached to each syringe, the filtered water passed directly into a sample bottle, and acidified for later analysis.

The second set of experiments was similar to the first but in this case sediment taken from the 0-1, 1-2, 2-3, and 3-4 cm depth intervals of NWC-3 box core was used. In each case, a portion of sediment, still frozen following squeezing, was weighed and then placed in a narrow-mouthed, glass jar. Care was taken to remove visually oxidized portions of sediment. Sample 3-4 cm had become crumbly and was visually oxidized from storage and previous sampling so it was used only for the pyrite loss determination. A portion of the frozen sediment was dried for water analysis in order to determine the dry weight of sediment added to each jar. After covering with 1 liter of sea water, addition of stirring bars and aeration tubes, the samples were vigorously stirred and aerated. Periodic sampling of water and sediment in these and a blank jar was made as described above. The pH and alkalinity were measured on unacidified subsamples of jar water in addition to Fe and Mn analyses on acidified samples. Water and suspended sediment were removed

during stirring in order to maintain the solid/water ratio constant throughout the experiment. Water sampling was discontinued after 1 week but jars were allowed to sit for 4.5 months after which time the remaining sediment was collected, rinsed in distilled water and analyzed for pyrite sulfur in two of the samples (0-1 cm, 3-4 cm). Sediment from the sample intervals had been previously analyzed for acid volatile sulfur and pyrite sulfur prior to the beginning of the experiment (Chapter V).

Analytical techniques

General

pH and pH or Eh measurements were made in the glove bag by inserting the appropriate electrode directly into one end of the 10 cm squeezing section; electrodes were passed into the bag through a sealed port. The sediment immediately surrounding the electrodes was discarded before squeezing. A rugged, combination glass electrode with calomel reference was standardized at pH 7.414 and 7.0 and used for pH. Platinum (cleaned) and silver sulfide electrodes were used for Eh and pS measurements relative to the calomel reference of the pH electrode. The sulfide electrode was calibrated as described by Berner (1963). Both pH and pS came to stable readings in the time allowed; Eh did not, but it was not changing rapidly when readings were taken.

Water analyses

Fe analyses were made using the colorometric reagent Ferrozine (Stookey, 1970; Lewin and Chen, 1973). Samples were not boiled but were allowed to react for ~ 1 hour prior to color development. Sample size ranged from 1-10 ml for pore water to 45 ml for flux, oxidation, and precipitation experiments. Precision of analysis was ~ 1% in most cases. In the 0.02 μM range, precision was ~20% but in this range the analysis is quite close to background Fe in the reagents used and the results questionable in any case. Testing of the Ferrozine reagent on standard rock samples (GSP-1, BCR-1, G-2) indicated that this reagent reproduced the accepted analytical Fe content of those standards while several other methods of Fe analysis (e.g., AA, 2,2'-dipyridine) following recommended procedures, did not.

Mn analyses were made using flame Atomic Absorption by direct aspiration of samples. Precision was ~2-3%. Additional analyses using formaldoxime (Goto, Komatsu, and Furukawa, 1962) were made on some pore water samples and found to agree with AA analyses within ~5%. Pore water taken from the reduction experiment using marsh sediment was analyzed by use of formaldoxime only. It was found that if pore water samples from deep in the sediment were too large that low values of Mn were obtained by formaldoxime, probably as a result of $HPO_4^{=}$ and Ca^{++} interference (Henriksen, 1966). This interference could be eliminated by measuring successive dilutions of a

given sample; below a given dilution level a constant Mn concentration identical to that found by AA would be measured while at higher concentrations of sample a lower quantity of Mn would be determined. The measured concentration would decrease as sample size was increased. This problem occurred in only a few samples and was readily detected by routinely analyzing duplicates of two different sample volumes whenever interferences were likely.

Fall and winter Mn flux measurements and the oxidation-precipitation experiment Mn samples were measured by use of formaldoxime. Precision is ~ 2%.

Solid phase analyses

Solid phase analyses for Fe, Mn, and Cu were done as follows: weighed aliquots of ashed (475°) sediment were leached for 24 hours in hot 12 N HCl (30 ml), the solutions taken to near dryness, the residue picked up in hot 0.1-0.2 N HCl, and filtered through Whatman 42 paper. The resulting leachate was diluted to known volume and appropriate further dilutions analyzed for Fe using Ferrozine reagents and Mn and Cu using flame AA. Fe and Mn standards (in 0.1 N HCl) and the analytical techniques used were checked against analyses of totally dissolved standard rock samples (GSP-1, BCR-1, G-2) and found to have good agreement. No special attempt to determine the accuracy of the Cu analyses was made but serious matrix effects on AA

have apparently not been reported. Precision of all analyses is ~3%. Analyses of unashed sediment aliquots leached with hot aqua-regia gave good agreement with the ashed-sediment-HCl leach, indicating that pyrite was destroyed with the normal analytical procedure.

Total sulfur was determined on the oxidation experiment samples using a Leco Induction furnace as previously described (Chapter V). Yields of 84 ± 5% obtained by analyses of standards were used to correct the results to 100% yield.

Results

Pore water profiles, gravity cores

There are distinct inshore-offshore trends in the general nature of dissolved Fe and Mn pore water profiles (Figure VI-1). Because the cores were collected in different seasons the concentrations found in the upper sampling intervals cannot be readily compared as will be shown later when results from high resolution and seasonal sampling are presented. Below the upper 10-30 cm of sediment, the inshore-offshore trends are that dissolved Fe is generally highest at FOAM and lowest at DEEP. There is a tendency for dissolved Fe to increase with depth in sediment at NWC. The irregular nature of the profile at FOAM may result from sampling problems during squeezing or may be real; the higher values are assumed more likely to be correct if handling is the cause of the irregularity.

Dissolved Mn shows an opposite inshore-offshore trend to that of Fe. Pore water Mn is lowest at depth in the sediment at FOAM and highest at DEEP.

Sulfide and pH measures were not always made on the same gravity cores used for Fe and Mn pore water analyses but the general values of these parameters are relatively predictable deep in the sediment at each station based on other cores. These are listed in Appendix IV along with pore water analyzes. Sulfide levels are highest at FOAM (e.g., Goldhaber et al., 1977) and lowest at DEEP where they are below the detection limit of a sulfide electrode in the gravity core samples (but not in the box cores).

Pore water profiles, box cores

Pore water profiles of dissolved Fe and Mn obtained from box cores are illustrated in Figures VI-2-VI-7. There are several important seasonal and spatial trends in the data. At all stations, dissolved Fe reaches a maximum concentration in a 1 cm sampling interval 1 to 3 cm below the interface and decreases rapidly to lower concentrations on either side of the maximum. Decreases in concentration are generally more sharp toward the interface than below the maximum. The highest maximum concentrations are reached at FOAM and the lowest at NWC. There are distinct seasonal trends in concentration with lowest dissolved Fe found in fall cores. The highest dissolved Fe is found during winter at FOAM and DEEP but during summer at NWC. Concentrations

as high as 1 mM are measured, well over 10^5 times that of overlying water. As shown by data from NWC and FOAM, the general patterns are repeatable from year to year.

Dissolved Mn has a somewhat different seasonal and spatial pattern than does Fe (Figures VI-2-VI-4). At FOAM and NWC, Mn decreases exponentially below the interface during the summer and fall as determined by 1 cm sampling intervals. This means that a maximum in Mn concentration is reached in the top 0-1 cm at these times. During the winter, this maximum drops to a lower level in the sediment and Mn concentrations generally decrease below that found in warmer times. Like Fe, fall Mn concentrations decrease from those measured in summer.

At DEEP, the form of the Mn concentration profiles differs from that at FOAM and NWC, there is less of a tendency for exponentially decreasing values beneath the interface. During the summer, high Mn is found in the top few centimeters; these decrease to much lower levels in these same sampling intervals in winter. There is a tendency for a maximum to occur over an interval from 5-8 cm corresponding to an increase in organic matter at that depth (Chapter V). High concentrations of Mn occur deep in the sediment during winter and the profile decreases relatively smoothly toward the interface at that time. The lowest concentrations are measured in fall.

Solid phase

Total Fe and Mn concentrations from several box cores are plotted as a function of depth in Figures VI-8-VI-9. As determined at NWC (Figure VI-8) there is no seasonality detectable in solid phase distributions of Fe and Mn. At NWC, total Fe shows a tendency to decrease slightly with depth. There is considerable scatter in the data probably resulting from the irregular distribution of shell debris (Chapter V). The sharp decreases in Fe at discrete depths such as 5-6 cm in NWC-1 are related to the presence of distinct shell layers. Total Mn decreases exponentially below the sediment-water interface reaching a background concentration of ~500 μg/g-ash by 4-5 cm. The solid phase profile appears to be at steady state.

DEEP also has surface enrichment of Mn but less so than NWC. The Mn content passes through a minimum and then begins to increase again to depth. Fe has no surface enrichment but increases regularly with depth. Dilution by $CaCO_3$ is not significant at this station (Chapter V, Appendix IV).

Although $CaCO_3$ is present in abundance at FOAM (~30%, Goldhaber et al., 1977), correction of Fe and Mn analyses to a $CaCO_3$--free basis does not radically alter the profile shapes. Mn has no special surface enrichment at this station and below 10 cm begins to increase in concentration. Fe shows essentially the same kind of distribution. When corrected for $CaCO_3$ dilution, the concentration of Fe and Mn appear to decrease slightly towards the interface.

Cu profiles differ at the three stations (Figure VI-10). The FOAM profile is taken from Goldhaber et al. (1977) and represents results from a 1.0 N HNO_3 leach rather than 12 N HCl. At both FOAM and NWC, Cu is high in near surface sediment and after a zone of relatively constant values, or, after reaching a slight maximum, decreases steadily to depth. The DEEP station profile indicates constant or slightly increasing Cu levels to ~ 14 cm.

Precipitation experiments

The rates of decrease of dissolved Mn and Fe in water taken from the flux cores and allowed to sit in an otherwise empty flux box are compiled in Table VI-1. A minor decrease in Mn concentration occurs over a 12 hour period at 22°C and no decrease in dissolved Mn was detectable at 4° during 28 hours. Expressed as a first order reaction in Mn concentration, the rate constant for Mn decrease at 22° is 8×10^{-5}/min. Use of a first order equation is valid only if active surface area present for precipitation is in large excess (Lewis, 1976) otherwise Mn oxidation is autocatalytic and not first order (Hem, 1964; Morgan, 1967).

Starting Fe concentrations in the 4° experiment were near background and did not change. Dissolved Fe showed a rapid decrease in concentration at 22°C after separation of flux core water from the underlying sediment (Table VI-1). Fe precipitation kinetics can be expressed as first order (Stumm and Lee, 1961). After 12 hours the Fe concentration appeared to be asymptotic

to ~0.036 μM; this value was interpreted to be the colloidal or unreactive background rather than free dissolved Fe (see also Lewin and Chen, 1973). The asymptotic value was subtracted from all previous concentrations and the differences plotted on a semi-log scale against time (Figure VI-11). The slope gives a first order rate constant of $k = 7.5 \times 10^{-3}$/min. For comparison, data from an experiment at 10°C by Lewin and Chen (1973) on the rate of decrease of dissolved Fe in Puget Sound sea water was manipulated in a similar fashion. Their data for Fe concentration in a 4 liter bottle (similar volume to water in flux cores) with time is also plotted in Figure VI-11. The value they measured at 48 hours was assumed to be colloidal or unreactive background and has been subtracted from all preceding values to obtain the numbers used. A $k = 1.7 \times 10^{-3}$/min is calculated. These k values are remarkably similar and the difference is consistent with the temperature dependence of Fe precipitation rates of 10 times/15°C found by Stumm and Lee (1961). The salinities in both experiments are similar (~27-28‰).

Flux measurements

Fluxes of Fe and Mn were calculated as follows. The concentration, C_o, of either Mn or Fe at the time of first measurement in the blank box was determined. The volume of water overlying the sediment in the flux box at a given time, V_t, and the concentrations, C_t, of Mn or Fe in that water at the same time were also measured. The quantity $V_t(C_t - C_o)$ was then

plotted versus time, t, a line fit to the data and the amount of material entering the water per unit time determined as the slope. The basic assumption is that:

(1) $$\frac{dC}{dt} = AF = \mathfrak{F}$$

C: concentration in water overlying the core

F: constant flux out of sediment (assumes that the pore water concentration gradient and overlying water concentration do not change sufficiently during the time of measurement to influence the flux)

A: sediment area

For Fe this is a severe approximation since with precipitation:

(2) $$\frac{dC}{dt} = \mathfrak{F} - kC$$

k: first order rate constant

giving:

(3) $$C = \frac{\mathfrak{F}}{k} + (C_o - \frac{\mathfrak{F}}{k}) e^{-kt}$$

C_o: starting concentration in overlying water

This assumes k is constant, but because both pH and O_2 drop in the flux core water while it is in contact with the sediment sample, k actually decreases during the course of the flux sampling. For the period in which k is approximately constant:

(4) $\mathfrak{F} = \left(\frac{dC}{dt}\right) e^{kt} + k C_o$

If k is zero or if $C_o \sim 0$ and $t \sim 0$, then (1) holds.

The only way to evaluate (4) is to know the functional form of $\frac{dC}{dt}$ while k is constant. This was not done in this study because: (1) it was not known a priori what kind of dC/dt to expect at each station at each sampling time, (2) the sampling schedule of water in the flux core had to accommodate the measurement of several elements and (3) there is a limited quantity and number of samples taken. k was determined in the precipitation experiment to be significant for Fe so that at the normal 3-6 hour first sampling time the factor: $e^{kt} \sim 4\text{-}15$. Unfortunately since the derivative of C at time t is not known, the correction factor cannot be applied to the present data. It should be kept in mind that in general the calculated Fe flux could be 10X lower than actual. Note that at steady state $dC/dt = \mathfrak{F}/k$ but unfortunately the assumption of constant $\mathfrak{F}$ and k does not hold for long times because of changes in the chemistry of the core and the overlying water.

Because of the problem of precipitation, Mn and Fe data from all cores could not be treated in the same way. In some cases, precipitation obviously took place and points were eliminated from consideration. Fluxes were calculated assuming the linear model (1) in each case and using one to six sample points in addition to the bottom water value. The exact points used and comments are given with the actual flux data in Appendix V. Curves

illustrating types of time-concentration changes in Mn and Fe observed in the flux cores are shown in Figure VI-12. Examples of decreasing k (or increasing $\mathfrak{F}$) and precipitation are given. Once sufficient precipitation took place in core water it seems likely that Fe colloids building up on the filters used in sampling may have altered values of Fe and $HPO_4^=$ (Chapter V) in water which passed through.

The calculated fluxes are listed in Table VI-2. Measured Fe fluxes were lowest during winter and highest during fall. Mn flux is highest in summer, lowest in winter. The same pattern is observed at all stations.

Reduction-decomposition experiments

Marsh sediment.--Dissolved Mn versus the time of opening of sample jars (Table VI-3) is plotted in Figure VI-13. $SO_4^=$ (estimated from Martens and Berner, 1974) is also plotted to illustrate the approximate stage of decomposition as reflected by $SO_4^=$ reduction. Mn decreases rapidly and within two weeks is a constant concentration of ~ 10 μM.

Mucus-limonite.--The $SO_4^=$ and Fe concentrations in the FOAM mud, FOAM mud + mucus, and FOAM mud + mucus + limonite jars are plotted versus time of sampling in Figure VI-14. $SO_4^=$ did not decrease in concentration in the mud to which limonite was added while Fe increased regularly and then decreased. Sediment to which mucus only was added had a consistently greater $SO_4^=$ reduction than sediment without added mucus (0.02 $\frac{mM}{d}$ versus 0.0035 $\frac{mM}{d}$).

Oxidation experiments

The pyrite and FOAM sediment oxidation experiment shows little change in either $SO_4^=$ or Fe concentration in the pure pyrite and blank jar samples (Figure VI-15, Table VI-5). There is a slight increase in dissolved Fe at 5 and 43 hours in the pyrite sample. The sediment sample shows a distinct release of dissolved Fe which decreases with time. $SO_4^=$ has an apparent minor increase in concentration by 341 hours. The maximum release of Fe due to interstitial water remaining in the squeezed sediment is ~0.2 μmoles. The observed release at 5 hours is ~3.2 μmoles.

Fe is released in the same concentration-time pattern from suspended sediment taken from 0-1 cm at NWC (Figure VI-16) but not from the 1-2 and 2-3 cm samples. Mn, measured only in the water samples from the 0-1 cm jar, jumps rapidly above blank starting values and then decreases steadily with time. pH, which was low (7.77) at the start of the experiment due to build-up of CO_2 in the unfiltered stock water, increased during aeration to a final value of 8.01 in the blank jar and 7.89-7.92 in the suspended sediment jars (Table VI-6). The titration alkalinity dropped in the suspended sediment jars but not in the blank; the greatest drop is observed in the sample from 2-3 cm and the least in the 0-1 cm sample (Figure VI-17).

Measurement of total sulfur remaining after a 4.5 month period gave a loss rate of 50 ± 12 μmoles S/g/yr from the 0-1 cm and 3-4 cm sediment samples.

Excretion experiments

The measured excretion rates were very close to the blank values and are therefore of questionable accuracy. The results are (with respect to dry wt):

Nephtys:	0.01 μmoles/g-hr	Mn
	0.06 μmoles/g-hr	Fe
Yoldia:	0.05 μmoles/g-hr	Mn
	-0.007 μmoles/g-hr	Fe

It is likely that the negative change of Fe in the case of Yoldia resulted from precipitation on the large amount of shell surface present.

Discussion

The form of the pore water profiles of Fe and Mn found in Long Island Sound (LIS) is similar in basic features to those reported from other marine, sedimentary basins (e.g., Elderfield, 1976), particularly the southern Chesapeake Bay (Troup, 1974; Bricker and Troup, 1975; Holdren, Bricker, and Matisoff, 1975; Holdren, 1977). The exact shape of profiles from a given depositional environment reflect the depth dependent transport-reaction processes occurring there. It was shown in Chapter V that in LIS, biogenic transport of particles and solutions differs from one region to another and that these differences result insignificant changes in the way in which products of decomposition build-up in the upper meter of sediment.

The types of macrofauna present at FOAM, NWC, and DEEP reflect the decreasing physical disturbance of the bottom with increasing water depth in the Sound (McCall, 1976); FOAM is the most physically controlled station studied while NWC and DEEP have well established bottom communities but are populated by different functional groups. The type, intensity, and depth distribution of biogenic transport in the sediment at each station changes in accordance with these differences. Particle reworking and irrigation control the distribution in the sediment column of metabolizable organic particles and the build up or supply of interstitial metabolites. Because of this, the different reworking patterns at FOAM, NWC, and DEEP are associated with slightly different distributions of microbial decomposition activity with depth in the sediment, although the total integrated metabolic activity is not greatly different (Chapter V). These same transport processes can be expected to directly or indirectly influence the distribution of Fe and Mn in the sediment to a greater or lesser extent depending on the type and rate of reactions to which these metals respond. Transport and reaction controls on Fe and Mn at the three stations will now be considered in detail.

Production of dissolved Mn and Fe

Under reducing conditions, Mn-oxides are solubilized as Mn^{++} through both biogenic or abiogenic reactions (e.g., Krauskopf, 1957). The rate of Mn^{++} production as a function of depth in sediments can be assumed proportional

to the change in concentration of available Mn-oxide, for purposes of modeling pore water concentrations (Robbins and Callender, 1975; Holdren, Bricker, and Matisoff, 1975). Because Mn-oxides may act as terminal electron acceptors for some microbial metabolic pathways or as oxidants of reduced metabolic products of microbial metabolism (Mann and Quastel, 1946; Trimble and Ehrlich, 1968; Schweisfurth, 1968; Bromfield and David, 1976), in sediment zones rich in both bacterial populations and Mn-oxide, the rate of Mn^{++} production by Mn-oxide reduction may more properly (but sometimes less usefully) be viewed as proportional to the supply of metabolizable organic matter (Mann and Quastel, 1946). In some cases, the reduction of Mn-oxide by bacteria has been shown to be greatly accelerated by the presence of specific electron carriers such as methylene blue (Bromfield and David, 1976).

The possibility that Mn^{++} might be released as an intermediate reaction product by oxidation of reduced compounds such as MnS during biogenic or physical reworking of the upper few cm of sediment was investigated in the oxidation experiment. The apparent rapid increase of Mn^{++} in solution following sediment suspension and its steady decrease thereafter (Table VI-6) is more suggestive of a simple release of exchangeable Mn (Murata, 1939) followed by slow precipitation as Mn-oxide onto suspended particles than of release by oxidation. As in many previous studies, it is concluded that Mn reduction and to a lesser extent, exchange reactions during particle reworking, determine the production rate of Mn^{++} and that near the sediment-

water interface this rate is intimately related to the distribution of metabolizable organic matter.

Reduction of Fe-oxide and release of Fe^{++} takes place at a lower oxidation potential than Mn reduction. Like Mn, microorganisms are thought to have both indirect and direct roles in generation of Fe^{++}. The elimination of O_2 and decrease in pH brought about by aerobic metabolism promotes reducing conditions in which Fe^{++} is the stable Fe speciation and results in dissolution of Fe-oxides (Halvorson and Starkey, 1927). The release of reduced organic compounds during metabolism and the subsequent reduction of Fe^{+++} by these metabolic products is thought to play a major role in Fe^{++} production and mobilization of Fe in sediments (e.g., Bromfield, 1954; Berner, 1969). Several investigators have proposed and presented evidence that under certain conditions bacteria use ferric iron directly as an electron acceptor in place of O_2, NO_3^-, or $SO_4^=$ (Bétrémieux, 1951; Vishniac, 1965). Of the possible pathways, the indirect reduction of Fe through metabolic products is thought to be the most important for biogenic Fe^{++} formation in the absence of O_2 (Bromfield, 1954). This means that like Mn, the rate of Fe^{++} production should be related to the abundance of metabolizable organic matter rather than the presence of Fe-oxide per se, unless Fe-oxide becomes limiting.

An example of Fe^{++} release by reduction of Fe-oxide is provided by the mucus-limonite reduction experiment where conditions similar to those

occurring at the sediment-water interface were set up (Figure VI-14). The rate of Fe^{++} production, using the data from the first 100 days, is ~0.02 μM/day after which precipitation of Fe^{++} began to take place, probably as FeS. The excess Fe-oxide present presumably reacted with all free HS^- since no H_2S smell could be detected upon opening the tubes containing limonite and the starting sediment used in the experiment contained considerable quantities of HS^- (Goldhaber et al., 1977). One interesting result of this experiment is that $SO_4^=$ reducers appear to be inhibited by the presence of large amounts of limonite or else $SO_4^=$ is being returned continuously to solution by an unknown oxidation reaction. Addition of small quantities of mucus into sediment, as occurs continually near the sediment surface and around animals, increases the rate of sulfate reduction (Figure VI-14). Near the interface, this kind of process presumably increases the rate of Fe^{++} production by speeding decomposition reactions. Fe^{++} did not increase above control values in the present case of mucus addition because of the high levels of HS^- in the tubes (very strong H_2S smell) containing mucus + mud and mud only.

Unlike Mn, there is considerable evidence that Fe^{++} is also released under oxidizing conditions by the oxidation of FeS or FeS_2, as demonstrated by acid mine drainage (e.g., Stumm and Morgan, 1970) and acid sulfate soils (e.g., Hart, 1963; Bloomfield, 1972; van Breemen and Harmsen, 1975; Harmsen and van Breemen, 1975a). Because of the associated production of $SO_4^=$ during oxidation, the pH, particularly in the case of

pyrite oxidation, can become greatly depressed following reprecipitation of Fe. The appropriate reactions, in which the oxidation of Fe^{++} to Fe^{+++} is the rate determining step at low pH are (Singer and Stumm, 1970):

(5) $FeS_{2\,s} + 7/2\ O_2 + H_2O = Fe^{++} + 2\ SO_4^{=} + 2H^+$

(6) $Fe^{++} + 1/4\ O_2 = Fe^{+++} + 1/2\ H_2O$

(7) $Fe^{+++} + 3H_2O = 3\ H^+ + Fe(OH_3)$

(8) $FeS_2 + 14\ Fe^{+++} + 8\ H_2O = 15\ Fe^{++} + 2\ SO_4^{=} + 16\ H^+$

Pyrite oxidation is known to be slow in sea water (Harmsen, 1954; Hart, 1963) and in this study was found to be $\sim 50 \pm 12$ μmoles S/g/yr for LIS surface sediment under optimal oxidation conditions. At low pH the reaction is microbially mediated (e.g., Trudinger, 1971). Although at the high pH of sea water significant microbial catalysis might not be expected, Thiobacillus, sulfide-oxidizing bacteria, are readily cultured from marine surface muds (Vishniac and Santer, 1957). It seems reasonable to conclude that some Fe^{++} is produced near the sediment-water interface by oxidation of pyrite. At a rate of 50 μmole S/g/yr, Fe^{++} production could be ~ 0.05 μmoles/liter/day assuming 60% water content of sediment by weight. This is two to three times the minimum rate calculated for Fe^{++} release in the mucus + limonite experiment.

The oxidation experiments support the hypothesis that Fe^{++} is released near the interface by oxidation of sediment sulfides. In sediment from the top 0-1 cm, Fe is released into solution within a few hours, continues to increase in concentration for 10 hours, and then rapidly decreases; a similar result is obtained for sediment taken from depth at FOAM (Figures IV-14-IV-15). Ion exchange might account for the Fe release pattern but this seems unlikely since the particle surfaces become progressively coated with oxides which should inhibit exchange and, unlike Mn (ion exchange?), measurable increases in Fe release continue for 10 hours. Pure pyrite showed little Fe release nor did sediment from 1-2 and 2-3 cm at NWC. It seems likely that Fe was also released from the 1-2, 2-3 cm NWC samples but was not held in solution due to rapid precipitation onto particles suspended in the jars. The abundance of fresh organic matter in the top 0-1 cm interval (see Chapter V) or slight differences in the nature of that material, may have aided in maintaining Fe^{++} in solution in the 0-1 cm jar for a long enough time to be observed (e.g., Moore and Maynard, 1929; Rashid and Leonard, 1973; Picard and Felbeck, 1976).

The amount of Fe released from the top NWC sample, at least 4 μmoles in 10 hours, could not have been supplied by pyrite oxidation at the measured average pyrite oxidation rate. It is possible that a much faster pyrite oxidation rate was in effect initially and that use of the average rate is misleading. Another possibility is that oxidation of FeS causes at least

part of the observed Fe release. The oxidation of FeS is much more rapid than that of FeS_2 and takes place readily at high pH (e.g., Harmsen, 1954; Hart, 1963). FeS oxidation releases $SO_4^=$ into solution (Bloomfield, 1972) so that the overall reaction:

(9) $4FeS + 8O_2 = 4Fe^{++} + 4SO_4^=$

(10) $4Fe^{++} + O_2 + 10H_2O = 8H^+ + Fe(OH_3)$

can result in formation of a ferrous intermediate and acid production. The total acid production is less than that of pyrite oxidation. Acid volatile sulfide measurements at NWC (Chapter V) show that FeS increases with depth but pyrite is relatively constant in the top 4 cm. This suggests that if oxidation of FeS takes place, acid production should result in a greater reduction of alkalinity in samples taken from deeper in the sediment. As illustrated in Figure VI-16, alkalinity did decrease to a greater extent in samples with large amounts of FeS.

It is possible to determine whether the observed decrease in alkalinity is consistent with the small effect on the pH of jar water. Because of vigorous aeration, the experimental jars can be considered to be held at constant CO_2 content (by the end of the experiment) so that if the carbonic acid system is controlling pH, the relation:

(11) $pH_1 - pH_2 = \log Alk_1 - \log Alk_2$

describes to a good approximation the expected change in H^+ activity related to change in carbonate alkalinity (~ titration alkalinity). This assumes $a_H >> K_2'$ where a_H = activity H^+ and K_2' = second, apparent dissociation constant of H_2CO_3 in sea water. With the observed change in alkalinity in the 2-3 cm jar a pH change of ~ 0.19 units is expected, the measured value is 0.12. Considering the measurement errors and the approximations involved in this calculation, agreement seems good so that the small change in pH is not inconsistent with acid production and the observed lowering of alkalinity.

There are several problems with interpreting the changes observed in the oxidation experiments as resulting from the dissolution of FeS. The first is that ~ 4X too much Fe is observed in solution (0-1 cm, NWC sample) as can be accounted for by the total amount of FeS (~ 0.6 μmoles) added. This discrepancy could be explained by possible interferences in measuring FeS in the presence of Fe^{+++} as explained in Chapter V. The more critical problem is that the observed decrease in alkalinity in the samples from 1-2 cm and 2-3 cm requires ~ 3-4X the quantity of FeS actually added if the oxidation reaction as written is stoichiometrically correct. There should be little interference on FeS measurement in these latter samples. The release of additional, perhaps organic, acids or oxidation of other reduced species seems likely.

In summary, Fe^{++} may be released by oxidation of both FeS and FeS_2 present near the sediment-water interface. A destruction of alkalinity is associated with this reaction. The experimental results are consistent with

but do not unequivocally prove this expectation. As will be shown later, field measurements are also suggestive of solid phase sulfide oxidation as a source of Fe^{++} and alkalinity decrease.

Precipitation reactions and equilibrium controls

Both Fe^{++} and Mn^{++} form insoluble phases with anions commonly produced during anaerobic metabolism: $HPO_4^{=}$, HCO_3^{-}, and HS^{-}. The likelihood that a specific solid phase is forming in sediment and influencing the dissolved concentration of Fe and Mn can be determined in two ways: (1) direct analysis of solid phase components or (2) inferring the existence or absence of a given phase by calculating the equilibrium saturation state of pore water with respect to it. There are significant problems in both of these approaches. Direct analysis by x-ray or wet chemical techniques is impossible for any but the most abundant phases and, in the case of wet chemical analyses, often involves operational definitions of a component. Equilibrium calculations are limited by analytical uncertainties (e.g., speciation, abundance) which become magnified in importance during calculation, by kinetic effects, by the fact that sediments are open systems and near the interface are often nonsteady state, and by lack of thermodynamic information on any but a few pure well crystallized end-member phases. Despite these drawbacks the use of both approaches: direct measurement and equilibrium calculation, has been shown to place useful limits on the possible reactions controlling Fe

and Mn pore water chemistry (e.g., Bray, 1973; Troup, 1974; Holdren, 1977).

The common end-member phases of Fe likely to form in anoxic marine sediment are: $Fe_3(PO_4)2 \cdot 8H_2O$ (vivianite), $FeCO_3$ (siderite), and FeS, Fe_3S_4, FeS_2 (mackinawite, greigite, pyrite) (Nriagu and Dell, 1974; Troup, 1974; Bricker and Troup, 1975; Rickard, 1969; Berner, 1967, 1970). Direct measurement demonstrates the existence of Fe-sulfides at all stations in LIS (Chapter V, Appendix IV). In order to determine whether thermodynamic calculations are in agreement with direct measurement and predict saturation of Fe^{++} with respect to specific sulfide phases it is necessary to determine the ion activity of Fe^{++} in the pore water. This was done for Fe^{++} and other ions measured in this study using an ion-pairing electrostatic model written and developed by Holdren (1977) as described in Chapter V. The range of the total activity coefficient for Fe^{++} calculated by this model for LIS pore waters is: 0.14-0.19. The pS values in summer box cores (1975) were estimated from the Eh measurement using the conversion equation of Berner (1963); these are considered extremely approximate but gave reasonable values based on subsequent direct pS measurements at each station. pS values for FOAM and NWC gravity cores were obtained from different cores than the actual Fe^{++} analyses (Appendix IV). Calculation of the IAP's (ion activity product) for several sulfide phases as a function of depth in sediment at FOAM, NWC, and DEEP, assuming the reactions and K_{sp} values given in Table VI-7, demonstrates that in some cases pore waters are

close to saturation with respect to one or more common sulfide phases (Figure VI-18). But, in general, pore waters at NWC and DEEP tend to be undersaturated with respect to the less stable Fe-sulfides despite the presence of these compounds in the solid phase (Chapter V). This is probably not due simply to inaccurate measurement of pS since total H_2S is < 20 μM in the upper 20 cm at NWC (based on methylene blue measurements, Goldhaber, personal communication) and at the Fe concentration present, total H_2S should be ~ 40 μM for equilibrium saturation with FeS. The conclusions are that either the measured Fe^{++} is too low, that the pore waters are in equilibrium with another sulfide phase in between greigite and pyrite in stability, or that transport or additional reactions other than sulfide formation are controlling Fe^{++}. At FOAM there is apparent supersaturation in some cases with respect to even the least stable amorphous sulfide suggesting that: (1) the analytical concentrations of Fe are too high due to contamination, (2) Fe^{++} is complexed by organics (e.g., Nissenbaum et al., 1971) and is unreactive to HS^- but not to the Ferrozine reagent used in analysis or (3) polysulfide formation increases the solubility (Gardner, 1974, although no data on Fe per se are given).

The IAP for Fe-sulfide at depth in sediment decreases offshore and is lowest ($S^=$ below detection) in the gravity core at DEEP. One possible explanation for the inshore-offshore decrease of IAP is that the lower HS^-

concentrations building up at NWC and DEEP due to biogenic transport (Chapter V) decrease the rate of Fe-sulfide formation deep in the sediment. The result of this would be that Fe-sulfide on particle surfaces at these stations may be better crystallized or more pyrite-like than at FOAM. Pore waters would then be in equilibrium with a more stable sulfide phase at offshore stations with the most stable present at DEEP. Another of the many possibilities is that pore water concentrations are responding to a phase other than the common sulfides at these stations.

$FeCO_3$ is distinctly undersaturated at most depths at all stations (Figure VI-17) although near-saturation may occur in a thin band in the upper ~ 5 cm corresponding to the zone where Fe^{++} production is dominant. Since total titration alkalinity was used, the IAP as calculated is a maximum. It seems likely that Fe-carbonate is not forming in central LIS sediments.

It was demonstrated in Chapter V that a pure vivianite-like phase could be forming in the upper few centimeters of sediment during at least some times of the year at all stations. The equilibrium boundary between $Fe_3(PO_4)_2 \cdot 8H_2O$-FeS occurs between 2-8 cm depth (Chapter V--Figure V-44). Below this depth pore waters are generally grossly undersaturated with respect to pure vivianite (Chapter V).

In the upper 0-2 cm of sediment Fe^{++} is rapidly oxidized and precipitated as Fe-oxide. This reaction is rapid and can be described by first order kinetics such that (Stumm and Lee, 1961):

$$(12) \quad \frac{dC}{dt} = k_o \frac{(O_2)}{(H^+)^2} (Fe^{++})$$

Since there is a gradient in both pH and O_2 as the interface is approached, the rate of precipitation becomes hundreds of times higher as sea water is intersected than just fractions of a centimeter below the interface. It was shown earlier that at normal (O_2) and (H^+) values of sea water $\frac{k_o(O_2)}{(H^+)^2}$ $\sim 2\text{-}8 \times 10^{-3}$/min. In the presence of abundant particle surfaces near the sediment-water interface, the effective value of k_o must be even higher than in overlying water.

In summary, consumption reactions affecting Fe^{++} concentrations at FOAM, NWC, and DEEP include a zone of Fe-oxide and Fe-phosphate formation in the upper few centimeters of sediment underlain by a more extensive zone of sulfide precipitation. (The possibility that phases other than the common sulfides are influencing Fe solubility at depth cannot be excluded.) The thickness of the upper zone change seasonally. Pore waters at depth appear to be in or near equilibrium with more stable sulfide phases in deeper water stations where the build-up of HS^- is lowered by biogenic transport (Chapter V).

The end-member of Mn phases likely to form in anoxic sediment include: $Mn_3(PO_4)_2\ 3H_2O$ (reddingite), $MnCO_3$ (rhodochrosite), and MnS, MnS_2 (alabandite, hauerite) (Tessenow, 1974; Nriagu and Dell, 1974; Holdren, Bricker and Matisoff, 1975; Holdren, 1977). The appropriate

reactions and representative K_{sp}'s are listed in Table VI-7. The thermodynamic stabilities of reddingite and alabandite are poorly known.

It was demonstrated in Chapter V that except at DEEP, pore waters were undersaturated with respect to pure $Mn_3(PO_4)_2\,3H_2O$. Summer (DEEP-1) and winter (DEEP-3) box cores at DEEP have zones below 4 cm in which pore waters are close to saturation with a reddingite-like phase. During the fall, the lowering of pore water concentrations by irrigation and burrowing activity results in considerable undersaturation at that time at all stations. Because of the large uncertainty in the accepted K_{sp} for reddingite and the tendency for formation of mixed phases (Tessenow, 1974) it cannot be said with any certainty that Mn-phosphates are not forming at NWC and FOAM.

Within the range of uncertainty in the K_{sp} for MnS and MnS_2, it is possible for both these sulfides to be present in LIS sediments but like Fe, the stability of the sulfide phase controlling solubility must increase in offshore sediment (Figure VI-19). Mn-sulfides are not commonly reported as occurring in marine sediments and this seems to be the chief argument against sulfide acting as a major control on Mn^{++} pore water concentrations (Holdren, 1977).

$MnCO_3$ (rhodochrosite) is believed to be forming in many marine environments and to act as an important control on pore water Mn^{++} concentrations (Li, Bischoff, and Mathieu, 1969; Calvert and Price, 1971; Holdren, Bricker, and Matisoff, 1975; Holdren, 1977). IAP calculation indicates that at FOAM

the pore water samples taken from box cores are very near saturation with $MnCO_3$ below ~4 cm during the summer and winter but are undersaturated during the fall (Figure VI-19). The same pattern is found at DEEP (Figure VI-19), suggesting that during winter and summer, pore waters at DEEP could be in equilibrium with both rhodochrosite and reddingite. NWC box cores are undersaturated (~5-10X) with respect to rhodochrosite. Gravity cores indicate that deeper pore waters are slightly (~5X) undersaturated at NWC and DEEP and are undersaturated to a greater extent at FOAM. Part of this discrepancy could be due to not having pH values on the exact same gravity cores at NWC and FOAM for which alkalinity and Mn were obtained but because of the slight variation in pH, this should not be a major problem.

It seems likely that below a few centimeters depth Mn, like Fe, comes into fairly rapid equilibrium with solid phase components although at present these components are unknown. Evidence that Mn concentrations respond rapidly to the build up of reactive anions comes in the present study from the marsh sediment decomposition experiment (Figure VI-13). The experimental results suggest that the implicit assumption that precipitation kinetics are fast enough to make equilibrium calculations, as done above, may be a fairly good one. The time variation in concentration of Mn^{++} in that experiment mimics the depth variation observed at all stations, particularly FOAM and NWC, indicating that the concept of precipitation-adsorption-equilibrium control of Mn^{++} concentration at depth is basically correct. Of course,

in the Sound, the concentrations of anions which might enter into reactions with Mn are controlled by a combination of transport and decomposition processes distinct to each station (Chapter V). This emphasizes that although an ion may be in equilibrium or have a set mass action relation with a given phase, the magnitude of its concentration may be set by other factors. An example of this in the present case, is the general increase of Mn^{++} concentration in sediment offshore (Figure VI-1). The increase may be related to the general decrease in HCO_3^- (assuming for the sake of argument $\sim MnCO_3$ equilibrium at all stations) which in turn is controlled by transport-decomposition processes related to the presence of specific macrobenthos (Chapter V).

Seasonality of pore water profiles

The Mn and Fe pore water profiles follow a definite seasonal pattern of change which is repeatable in general characteristics from year to year as demonstrated at FOAM and NWC (Figure VI-2-VI-7). Both the shape of the Mn profiles and the seasonal changes observed, mimic the general depth-time distribution of decomposition reactions outlined in Chapter V. Production-decomposition reactions which follow the initial warming of overlying water and input of organic matter from the winter-spring plankton bloom, result in the reduction and release of large quantities of Mn^{++} into solution. The depth dependence of this release in the sediment is consistent with the depth dependence of the rates of decomposition determined at each station

(Chapter V): strongly exponential at both FOAM and NWC and initially exponential but then relatively constant at DEEP. Note that in general the release of Mn^{++} is better correlated with the rates of decomposition as a function of depth than with changes in solid phase Mn distributions (Figure VI-8-VI-9) although the presence of decreases in Mn-oxide obviously places limits on the quantity of Mn^{++} produced. Even the slight maximum in Mn^{++} at DEEP in the 5-7 cm interval is associated with a measured increase in $SO_4^{=}$ reduction rates at that depth (see Figure VI-16, Chapter V).

During the fall, Mn^{++} concentrations drop to lower concentrations down the length of the DEEP-2 box core and down to at least the upper 10 cm at FOAM and NWC. As outlined in detail in Chapter V, this results from a decrease in production rates, due to depleted organic sources and slightly colder water, and the increased influence of biogenic transport: particle reworking and irrigation, which flushes the sediment at that time. Horizontal diffusion into burrows at depth and homogeneous mixing near the interface are largely responsible for this decrease (Chapter III, V).

In the winter, Mn^{++} concentrations drop to their lowest level of the year, particularly in the top few centimeters. The shapes of winter profiles reflect the increased dominance of molecular diffusion, abiogenic reactions, and the lower production rates at this time. At DEEP, where Mn^{++} is relatively high throughout the core, there is diffusion of Mn^{++} from depth into the mixed zone which was depleted of Mn^{++} during the fall.

The lower attenuation of decomposition rates with depth at this station also promoted the build up of decomposition products during the winter since, in the absence of biogenic transport, even at the lowered production rate, molecular diffusion cannot keep the concentration at fall values. The basic similarity of the seasonal changes in Mn profiles to those observed for metabolic products such as NH_4^+ attests to the intimate involvement of Mn^{++} mobilization with microbial decomposition processes.

Fe^{++} has a similar seasonal pattern to that of Mn^{++} but with some distinct differences. The maximum in Fe^{++} concentration commonly occurs deeper in the sediment than the Mn^{++} maximum, a finding consistent both with the relative oxidation potentials at which these metals are reduced and with the more rapid oxidation and precipitation kinetics of Fe^{++} as sea water pH values are approached. The minimum Fe concentrations are generally found during the fall. It was shown in Chapter III that Fe^{++} profiles like that occurring during the fall at FOAM and NWC could be reproduced in the lab by simply allowing Yoldia limatula, a deposit-feeding bivalve, to rework sediment whereas, in its absence, profiles like that of the summer or winter are formed. These findings are consistent with the interpretation that relatively high biogenic diffusion and low production are responsible for the formation of fall type profiles. The fall Fe^{++} maximum at DEEP is slightly larger than the summer maximum although the integrated Fe^{++} present in the upper 10 cm is clearly the lowest of the year. This difference between stations reflects the absence of intensive

near surface mixing by interface-dwelling animals at DEEP compared to NWC (Chapter IV), and apparently to FOAM as well.

Unlike Mn, the maximum Fe^{++} concentration is found during the winter at both FOAM and DEEP and reaches concentrations as high as 1 mM (Figures VI-5-VI-7). This is not true at NWC where the maximum is in the summer. An additional clue that production sources of Fe^{++} might be somewhat different than Mn^{++} comes from the similarity of Fe^{++} profiles at all stations while at DEEP the Mn^{++} profiles are clearly different from FOAM and NWC. At DEEP, the winter maximum in Fe^{++} is associated with a slight concavity in the alkalinity profile (see Figure V-26, Chapter V) although no such concavity is found at FOAM where alkalinites are much higher, making small differences hard to detect. Similar decreases in alkalinity which mimic Fe^{++} maxima can be produced in the laboratory when macrofauna are removed from sediment (Chapter III) and were found during the winter at the New Haven Dump site (paper in preparation). These observations together with the fact that a net decrease in FeS occurs in the top 2 cm at NWC during the winter and the findings of the oxidation experiment described previously, indicate that oxidation of solid phase Fe-sulfides, both FeS and FeS_2, is a major source of Fe^{++} in the sediment. Since this production reaction can be entirely abiogenic, its existence would not only explain such observations as small decreases in alkalinity but would explain the large increase in Fe^{++}

during times of the year when biological activity is lowest. The completely abiogenic reduction of Fe-oxide is a relatively slow reaction and it therefore seems unlikely that reduction is responsible for the observed winter increase.

It is concluded that Fe^{++} production is, unlike Mn^{++} production, due to two sources which vary in importance seasonally: (1) the biogenic reduction of Fe-oxide and (2) the abiogenic (or biogenic) oxidation of Fe-sulfides (a metabolic product). During the summer, the microbial reduction of Fe-oxides dominates and Fe^{++} is relatively high; at some stations, such as NWC, it is the highest of the year while at others the high production of HS^- must rapidly fix Fe^{++} as solid phase (Chapter V), thereby preventing excessive build-up of concentration. Biogenic transport may also act to lower Fe^{++} concentrations at this time. In the fall, the depletion of the spring influx of organics and the lower temperatures result in a decrease in Fe^{++} production by reduction of Fe-oxide. The increased biogenic reworking (effective diffusion) during late summer and early fall prevent build-up of pore water constituents from any sediment source. If oxidation of sulfides is an Fe^{++} source, this increase in effective diffusion rate might explain the lack of Fe^{++} build-up in pore water during the fall despite increased oxidation. At high rates of oxidation, the rate of reaction (6) may also become too fast relative to reaction (5) or (9) to measure an increase in standing concentration, or, extensive formation of oxide coatings on aggregate particles (fecal pellets) might also act to protect

interior sulfides from further oxidation. (See Chapter III, p. 181 for discussion of a specific case.) During the winter, a portion of the Fe-sulfide formed earlier in the year is lost by oxidation, and in the process alkalinity is lowered and Fe^{++} released to solution. At the reduced rates of diffusion, Fe^{++} builds up in selected horizons as a reaction intermediate prior to reprecipitation.

Flux of Mn and Fe into overlying water

The flux of Mn out of sediment and into the overlying water varies seasonally in a regular fashion and is a strong function of temperature (Figure VI-20, Table VI-2). It is also evident that the magnitude of the flux is dependent on the depositional environment. In LIS, the Mn flux is higher at offshore than inshore stations and is highest at NWC, a protobranch dominated bottom area (see Chapter V). Unlike NH_4^+ flux rates, Mn flux can be approximated by a simple straight line correlation with temperature over the range in which it was measured, but, if it is assumed that the flux does not become negative, then the temperature dependence must be a strong exponential. Both FOAM and DEEP show a tendency for exponential dependence and the winter pore water profiles suggest that the Mn^{++} flux is never negative. This means that either a linear function broken into two parts such that $T < 4^{\circ}C$, $F = 0$ and $T \geq 4^{\circ}C$, $F = mT + b$ or an exponential function of the Arrhenius type used (with stated reservations) previously to describe NH_4^+ flux:

$F = F_o \exp(\frac{-E}{RT})$ (T = absolute temperature, E = activation energy, R = 1.987,

F_o = constant pre-exponential factor), can be used to fit the data. Both these approaches were tried and were found to produce the same yearly average flux if T = 22 - 10 cos ωt ($\omega = 2\pi$, t = time in years, T in degrees C). The linear equations are for $T \geq 4^oC$, F = mmoles/m^2-day:

$F = 0.0834T - 0.286$ FOAM

$F = 0.323T - 1.18$ NWC

$F = 0.284T - 1.25$ DEEP

The corresponding apparent activation energies and pre-exponential factors are:

$A = 28.1$ Kcal, $F_o = \exp(48.61)$ FOAM

$A = 50.4$ Kcal, $F_o = \exp(88.38)$ NWC

$A = 57.0$ Kcal, $F_o = \exp(99.6)$ DEEP

The resulting yearly average Mn fluxes are: 0.67, 2.7, and 2.2 mmoles/m^2-day at FOAM, NWC, and DEEP respectively.

In the case of NH_4^+ flux it was shown that the apparent activation energy agreed well with that found for the temperature dependence of the rate of $SO_4^=$ reduction (Chapter V); this derives from the dependence of flux on the rate of production and therefore metabolic activity. The apparent activation energy of Mn flux is much higher. The reason for this may arise from the catalytic nature of Mn-oxide reduction when certain organic electron carriers are present (Mann and Quastel, 1946; Bromfield and David, 1976). This can be expressed through reactions such as:

(13) $R - H + MnOOH + 2H_2CO_3 \rightarrow Mn^{++} + R + 2HCO_3^- + 2H_2O$

(MnO_2)

where R-H is any of many possible reduced organic electron carriers. Presumably in the presence of bacteria R is quickly regenerated to R-H to complete the cycle.

Graham, Bender, and Klinkhammer (1976) report Mn fluxes from Narragansett Bay R.I. taken in June-July, 1975. They obtained an average for this time of about 0.4 mmoles/m^2-day which is lower than that measured at any LIS station. No information was given on the depositional environment so direct comparison with stations in the present study is not possible, nevertheless, the values obtained are not grossly dissimilar to those found at FOAM. Elderfield (1976) estimated a range of fluxes from near shore sediment of 0.003-0.3 mmoles/m^2-day based on pore water profile data of Calvert and Price (1972). He implies that this flux is to surface sediment and that it does not represent Mn which actually escapes into overlying water. If it is assumed that the Mn does escape, these are in general significantly lower than the yearly average fluxes calculated in this study.

It was found in Chapter V that use of Fick's First Law (Cartesian coordinate model) and molecular diffusion coefficients predicted the NH_4^+ flux to within a factor of ~ 2. By considering both $HPO_4^=$ and NH_4^+ fluxes, it was demonstrated that use of a stochastic diffusion coefficient of $\sim 1 \times 10^{-5}$ cm^2/sec due to biogenic reworking and allowance for excretion by macrofauna

resulted in good agreement between observed and predicted rates during the summer period; the biogenic diffusion coefficient was lower during the fall and molecular diffusion and excretion dominated winter fluxes. In order to evaluate how well molecular diffusion and Fick's First Law (in vertical dimension) predict the observed Mn fluxes in LIS it is necessary to calculate concentration gradients. For the winter profiles and the fall DEEP-2 profile this can be done by assuming that: $C = a_o + a_1x + a_2x^2$ over the top two centimeters. The constant a_o = sea water Mn concentration and is taken as zero. Integration of the concentration equation over the intervals 0-1 cm and 1-2 cm and simultaneous solution of the resulting equations using the average concentration in each interval yields a_1 and a_2 (Chapter V). The flux at x = 0 is then:

$$(14) \quad F = - \varphi D \left(\frac{\partial C}{\partial x}\right)_{x = 0}$$

φ = porosity = 1

D = molecular diffusion coefficient

To estimate D_{Mn}, the infinite dilution values at 22°, 15°, and 4° were calculated from the data of Li and Gregory (1974) and these were multiplied by 0.37, the tortuosity-sediment factor calculated from the in situ $SO_4^=$ diffusion coefficient determined by Goldhaber et al. (1977) at FOAM relative to infinite dilution D_{SO_4} of Li and Gregory (1974). The appropriate D's are

equal to 2.4, 2.0, and 1.4×10^{-6} cm^2/sec. The predicted winter fluxes at all stations and fall flux at DEEP determined in this way are listed in Table VI-2.

Because the highest Mn^{++} concentration occurs in the top 0-1 cm interval at all other times, it is impossible to calculate the concentration gradient exactly. One approach would be to assign the average 0-1 cm value to a depth of 0.5 cm and calculate a linear gradient to obtain a minimum flux. Another approach, which will be used here, is to consider the top 0-1 cm as a discrete slab 1 cm thick in which Mn^{++} is produced at a constant rate R. On its upper boundary, the slab contacts water having sea water Mn concentration and on its lower boundary it contacts water having the average value of Mn^{++} in the 1-2 cm interval. Because of the small thickness, 1 cm, the slab will attain steady state very rapidly so that the steady state transport-reaction equation describing the pore water Mn^{++} concentration, C, in the top centimeter (no compaction):

$$(15) \quad \frac{\partial C}{\partial t} = 0 = D \frac{\partial^2 C}{\partial x^2} + R$$

$$x = 0, \; C = C_o$$

$$x = 1, \; C = C_1$$

is a good approximation. Adsorption drops out of this formulation at steady state (Berner, 1976b). The solution is:

$$(16) \quad C = C_o + (C_1 - C_o + \frac{R}{2D}) x - \frac{Rx^2}{2D}$$

Since the average concentration, $\bar{C}$, is known in the interval 0-1, then by integration:

$$(17) \quad R = 12\,D\,(\bar{C} - \frac{C_o}{2} - \frac{C_1}{2})$$

and the concentration gradient at x = 0 is readily calculated:

$$(18) \quad (\frac{\partial C}{\partial x})_{x=0} = C_1 - C_o + \frac{R}{2D} = 6\bar{C} - 2C_1 - 4C_o$$

The depth at which the maximum concentration is obtained is calculated to be:

$$(19) \quad x_{max} = - \frac{C_o - C_1 - \frac{R}{2D}}{\frac{R}{D}}$$

demonstrating that if $C_1 > C_o$, the maximum concentration occurs above 0.5 cm. The remaining fluxes: summer at all stations and fall at NWC and FOAM, were calculated using this model. An example of the results are for DEEP-1, $R = 2.0 \times 10^{-6}$ μM/sec, $x_{max} = 0.35$ cm. Additional values of R will be discussed below. In general, the fluxes predicted by the 1 cm slab model are ~2X that calculated by assigning the average 0-1 cm concentration to 0.5 cm. The predicted fluxes are listed in Table VI-2.

In all cases, the predicted winter flux is higher than the measured flux. The predicted summer and fall fluxes at FOAM are larger than measured, although fall flux measurements are very close to predicted. These results suggest that either Mn is precipitating at the sediment-water interface and not escaping into the overlying water during the winter and at FOAM, or

that Mn is being lost from the flux core water in those cases due to precipitation. The measured summer and fall fluxes at NWC and DEEP are much higher than the calculated flux. Appropriate effective diffusion coefficients to account for the discrepancies are $6 \times 10^{-}$ cm^2/sec (NWC, summer), 6×10^{-6} cm^2/sec (NWC, fall) 11×10^{-6} cm^2/sec (DEEP, summer), and 9.7×10^{-6} cm^2/sec (DEEP, fall). Like NH_4^+ and $HPO_4^=$ fluxes, the effective diffusion coefficients cluster near $0.5 - 1 \times 10^{-5}$ cm^2/sec and are higher than the assumed molecular values. As shown in results, the rate of Mn excretion by bottom organisms is not significant in these calculations so no further correction is required.

The horizontal diffusion model developed in Chapter V predicts that when the rate of Mn production is high at depth in the sediment, the radial flux into burrows will become a significant contribution to the overall flux out of the sediment. It seems reasonable that the consistently higher effective diffusion coefficient calculated for DEEP can be explained in part by the high Mn production rate at depth and diffusion into the many dwelling burrows characteristic of this station. This Mn would be rapidly irrigated into overlying water (e.g., Chapter II). Based on the FOAM and winter flux results, there is some loss due to precipitation at the sediment surface or in the flux core water. This will also add to variation in the calculated value of effective D for any reactive ion, in this case Mn^{++}.

At an overlying water concentration of ~0.2 μM, the measured flux rates predict a minimum residence time of Mn in water of 0.7-2.5 days during the summer, assuming a 20 m water column (see p. 349, Chapter V). The 0.7 day residence time corresponds to a first order reaction rate of $\sim 1 \times 10^{-3}$/min which is considerably higher than observed for Mn removal in the lab. High resuspension rates and abundant reactive surface area in the form of Mn, Fe-oxide coated particles are presumably responsible for this rapid scavenging of Mn^{++} (e.g., Lewis, 1976).

The seasonality of the measured Fe flux is different than Mn: highest fluxes are observed in fall and lowest in winter. It was demonstrated in the results section that depending on the flux of Fe, that the precipitation kinetics, filtering effects (scavenging of Fe^{++} by Fe colloids trapped on filter), and too few samples shortly after core collection, can cause the calculation of Fe fluxes at least 10X too low. The measured fluxes are therefore absolute minima and the observed seasonality could easily be more apparent than real. In fact, stripping of other ions such as Mn or $HPO_4^{=}$ from flux core water by Fe released from sediment could lower the measured flux of those ions as well.

Predicted Fick's Law Fe fluxes were calculated by first determining diffusion coefficients from the data of Li and Gregory (1974) and Goldhaber et al. (1977) in the same way as was done for Mn, giving: 2.4, 2.1, and 1.5×10^{-6} cm^2/sec at 22°, 15°, and 4°C respectively. The concentration gradients were approximated by either the simple equation: $C = a_o + a_1x + a_2x^2$

using only the top two sample points as done for Mn, or, if the concentration were slightly concave upward, then the linear equation $C = a_o + a_1 x$ was used instead. The predicted fluxes are listed in Table VI-2. Except during the fall, the predicted fluxes are larger than measured. In the fall, the measured fluxes are several hundred times the predicted. Because the measured fluxes must be minima, the fall discrepancy suggests: (1) the analytical values obtained for the pore water near the interface are too low; since O_2 is present in the pore water no amount of anoxic handling can prevent precipitation in samples from this zone once they are removed from the sediment source. However, samples from the top 0-1 cm never turned yellow, suggesting qualitatively that Fe^{++} was as low as measured. (2) Fe^{++} is released along burrow walls or during reworking so that its concentration does not build up in pore water but it is irrigated out of sediment and observed as flux. Because Fe^{++} can be generated by oxidation this is a reasonable possibility and would correspond to micro-acid mine drainage (see Chapter II for actual example). In this respect Fe^{++} has a source in addition to reduction reactions, unlike the other materials whose flux was measured, and the odd seasonality would be at least partially explained since reworking is known to superficially oxidize the sediment most completely during the fall (Rhoads, Aller, and Goldhaber, 1977).

Beyond the possible explanations for the Fe-flux patterns it is important simply to demonstrate that Fe^{++} escapes into overlying water from sediment

during normal diagenesis. It is not uncommon to read comments in the pore water literature that Fe^{++} does not get past the interface; this conclusion seems to be based largely on the low standing-crop of dissolved Fe in near shore waters rather than actual flux measurements. The fall fluxes demonstrate that Fe^{++} fluxes can be of the same magnitude as Mn^{++}. Lewin and Chen (1973) found evidence for transient Fe^{++} in near-shore Puget Sound waters, a finding consistent with Fe^{++} supply from the bottom. Because of the rapid disappearance of Fe^{++} from the dissolved state, the bottom flux might be conceptually pictured as a colloid flux.

A maximum Fe residence time of ~ 0.2 days, is calculated, assuming a 20 m water column, a sea water value of 0.01 μM and the FOAM fall flux value. This corresponds to a first order removal constant of $\sim 3 \times 10^{-3}$/min which is of the same magnitude as that found in the lab. Because of the uncertainty in the flux, which may be higher, and the true dissolved Fe concentration in sea water, which may be lower, this residence time is an upper limit.

The high flux of both Mn and Fe out of bottom sediment can be expected to play a major role in controlling water chemistry of the estuary (e.g., Turekian, 1976). Continual scavenging of Fe and Mn-oxide seeking elements, such as Zn, Cu, Co, Ra . . . , by coprecipitation or by adsorption on colloids and freshly coated particles, must take place. This sweeping-out process will maintain low standing concentrations of many metals even in the presence

of significant natural or anthropogenic inputs into the basin. What percentage of this Mn or Fe flux which escapes to the open ocean remains to be found out.

Rough limits on the proportion of the Mn flux that might be lost from near-shore deposits like LIS and contribute to deep-sea deposits can be estimated in the following way (see also Turekian, 1977). The accumulation rate of excess Mn in deep-sea sediments has been most recently calculated by Elderfield (1976) to be 0.2-2.0 $\mu g/cm^2/yr$. The average annual flux of Mn from LIS sediment is $\sim 4\text{-}5 \times 10^{-3}$ $\mu g/cm^2/yr$ (2-2.5 $mmoles/m^2/day$). Assuming that shelf areas make up $\sim 7\%$ of the seafloor and that of this, 10% has a Mn flux comparable to LIS (i.e., 0.7% of seafloor), then a maximum of about 6% of the annual Mn flux from such near-shore sediment would have to be lost to the deep-sea to supply the maximum estimate of excess Mn accumulation of 2.0 $\mu g/cm^2/yr$. This proportion is subject to change depending on exactly what estimates of the excess Mn accumulation rate or shelf area are used in the calculation (Turekian, 1977). The salient conclusion is that a rather small percentage need be lost in order to account for the average excess Mn accumulation observed in the deep-sea. This small percentage is consistent with the previous calculation of a short residence time for Mn in the water column implying that loss of a large percentage to the open ocean is unlikely. Labeyrie, Livingston, and Bowen (1976) have suggested on the basis of ^{55}Fe inventories in near-shore sediment that seaward mobilization of Fe is also likely.

Solid phase distributions

The redistribution of solid phase components, particularly redox sensitive metals such as Mn, in the sediment column during early diagenesis has been recognized and modeled for many years (e.g., Murray and Irvine, 1895; Lynn and Bonatti, 1965; Manheim, 1965; Bender, 1971; Bonatti et al., 1971; Robbins and Callender, 1975; Harmsen and Van Bremeen, 1975b; Elderfield, 1976). In LIS, earlier work demonstrated the enrichment of Mn near the interface of sediments in the offshore central Sound (Thomson, Turekian, and McCaffrey, 1975). Data from the present study demonstrate that the form of this enrichment differs from one region of the Sound to another (Figures VI-8-VI-9) and that the depth distributions of other metals: Fe, Cu, and, from additional studies, U (Thomson, Turekian, and McCaffrey, 1975; Aller and Cochran, 1976; Chapter IV; Benninger et al., 1976 and in preparation), differ as well.

The highest surface enrichment of Mn and the most rapid attenuation of its concentration with depth is found at NWC (Figure VI-8). This concentration curve is steady state and persists in the presence of intensive near interface mixing of particles by protobranch bivalves which inhabit NWC. It was shown earlier (Chapter III) that solid phase curves of this type could be readily formed in the lab from initially homogenized samples of NWC sediment on time scales of a month. It is possible to place limits on

the rate of Mn dissolution in the field at NWC by use of ^{234}Th (24 day half life) profiles at this station (Aller and Cochran, 1976). The effective particle diffusion coefficient in the upper 4 cm at NWC reaches a maximum value of 1×10^{-6} cm^2/sec (Chapter IV, Aller and Cochran, 1976). The distribution of solid phase Mn in the upper 4 cm can then be described by a steady state transport-reaction equation of the form:

$$(20) \quad \frac{\partial C}{\partial t} = 0 = D_B \frac{\partial^2 C}{\partial x^2} - R$$

C = Mn concentration in particles

R = reaction term

D_B = particle diffusion coefficient

x = space coordinate, origin at interface, positive axis into sediment

Low sedimentation rates (Benninger et al., 1976 and in preparation) allow advection to be ignored. Because of the depth dependence of decomposition at NWC (Chapter V), the reaction term will be taken as the form $R = R_o e^{-\alpha x}$. With the boundary conditions:

$$x = L, \quad \left(\frac{\partial C}{\partial x}\right)_L = 0$$

$$x = L, \quad C = C_L$$

and the additional condition:

$$C_o = \frac{\int_0^1 C dx}{\int_0^1 dx} = \text{Mn concentration in top 1 cm.}$$

Then:

$$(21)\quad C = C_o + \frac{R_o}{\alpha D_B} e^{-\alpha} - \frac{R_o}{2\alpha D_B} e^{-\alpha L} - \frac{R_o}{\alpha D_B} + \frac{R_o x}{\alpha D_B} e^{-\alpha L} + \frac{R_o}{\alpha^2 D_B} e^{-\alpha x}$$

and:

$$(22)\quad R_o = \frac{C_L - C_o}{\frac{e^{-\alpha}}{\alpha D_B} - \frac{e^{-\alpha L}}{2\alpha D_B} - \frac{1}{\alpha D_B} + \frac{L}{\alpha D_B} e^{-\alpha L} + \frac{1}{\alpha^2 D_B} e^{-\alpha L}}$$

The boundary conditions for L = 4 cm are met best by the solid phase Mn profile of NWC-2 fall box core. Taking C_o = 1326 μg/g-ash, C_L = 522 μg/g-ash, $D_B = 1 \times 10^{-6}$ cm^2/sec, and L = 4 cm, the best fit to the data is obtained with α = 1. The model produced solid phase profile is shown in Figure VI-21. These values predict that $R = (2.6 \times 10^{-5})\, e^{-x}$ μmoles/g-sec over the top 4 cm of sediment at NWC. Since the range of D_B values measured at NWC is 0.2-1.2×10^{-6} cm^2/sec and varies seasonally (Chapter IV), it is clear that the values of R_o calculated can be about 5 X lower than the particular value calculated here, depending on D_B.

It was demonstrated earlier, in the flux section (equation 17) that the average value of R in the top 0-1 cm could be estimated from pore water profiles using a simple slab model to be: $\bar{R} = 12\, D\, (\bar{C} - \frac{C_o}{2} - \frac{C_1}{2})$

D = diffusion coefficient of pore water Mn

$\bar{C}$ = average pore water concentration of Mn in 0-1 cm interval

C_o = sea water Mn concentration.

C_1 = average Mn concentration in 1-2 cm interval

When values of D corresponding to molecular diffusion coefficients given previously are used, the average $\bar{R}$ calculated for the upper 0-1 cm at NWC (from NWC-4, NWC-5) is $2.5\text{-}4.3 \times 10^{-6}$ mmoles/l-sec. The flux calculations and previous modeling of pore water profiles indicated that the effective or biogenic diffusion coefficient of pore water in the upper few cm is $6\text{-}10 \times 10^{-6}$ cm^2/sec or 2-5 times the molecular diffusion coefficients. This would increase the calculated $\bar{R}$ to $7.5\text{-}22 \times 10^{-6}$ mM/sec. For comparison, the R value calculated using the ^{234}Th particle transport rate and the solid phase Mn profile, can be converted to an equivalent pore water reaction rate by use of the H_2O content profile. $\%H_2O = 75.9\, e^{-0.084x}$ in the upper 4 cm of NWC-2 (Appendix IV). The average $\bar{R}$ in the upper 0-1 cm can then be calculated from the solid phase reaction rate to be:

$$(23) \quad \bar{R} = \frac{R_o \int_0^1 (1.32\, e^{0.084x} + 1)\, e^{-x}\, dx}{\int_0^1 dx} = 4 \times 10^{-5} \frac{mM}{sec}$$

This compares extremely well with the range of $\bar{R}$ calculated from the pore water profiles if effective or biogenic diffusion coefficients are used. Considering the range of possible D_B (particles) or effective D (pore water) values, these calculations predict the same Mn dissolution rate in the top 0-1 cm of $\sim 1 \times 10^{-5}$ mM/sec ($\sim 3 \times 10^{-5}$ μmoles/g sed-sec) and indicate

excellent correspondence between pore water, solid phase, radiochemical, biological and flux data at this station.

The turnover time τ of the excess Mn present in the top 4 cm at NWC can be calculated by dividing the quantity of Mn above background (~ 520 μg/g) in the top 4 cm by the average R over that same interval:

$$(24) \qquad \tau = \frac{\sum_{0}^{4} \Delta Mn}{\frac{\int_0^4 R dx}{\int_0^4 dx}}$$

This gives τ = 35 days for the NWC-2 core, in agreement with the high mobility of Mn observed in the lab over time scales of a month (Chapter III).

The slight enrichment of Fe in surface sediment at NWC together with the observed flux of Fe out of the sediment indicate that Fe is also subject to redistribution in the solid phase. Unfortunately because of the high mineral background Fe concentration in the sediment it is hard to accurately detect the much smaller quantity of Fe which is diagenetically mobile. In the case of Mn at least 1000 μg Mn/g sediment is capable of redistribution in the top 4 cm against a background value of ~ 500 μg/g. If a similar quantity of Fe were mobilized it is harder to unequivocally document movement against a background of ~ 35 mg Fe/g sediment irregularly diluted by 5-10% $CaCO_3$.

Although any single profile is subject to question, the four solid phase Fe profiles measured at NWC indicate a consistent enrichment of Fe in the upper 0-3 cm of at least 2-3 mg/g relative to sediment lower in the deposit. This suggests that the absolute quantity of Fe which is free to move about is similar to that of Mn and that the production rate of Fe^{++} from solid phase is equal to or greater than the Mn rate calculated above.

The solid phase Mn profiles at FOAM and DEEP differ both qualitatively and quantitatively from NWC. FOAM has little surface enrichment of Mn compared to NWC but shows a definite increase below 10 cm after a minimum (Figure VI-9). This increase at depth is probably related to downward diffusion of Mn as would be expected from the pore water profiles (Holdren, 1977; Chapter III). On a carbonate free basis, Mn becomes as high as 1100 μg/g below 10 cm. This is significantly higher than at NWC suggesting that, like other products of decomposition such as HS^- which are trapped in the solid phase or pore water constituents such as NH_4^+ and $HPO_4^=$, the deeper sediment at FOAM is a relatively closed system allowing the permanent capture of ions like Mn which diffuse downward. The higher Mn may also represent a depositional event (rather than an integrated diffusion effect) which transported Mn-rich surface sediment from other bottom areas onto the FOAM-site. Evidence that this is a reasonable possibility comes from the laminated sediment layers commonly present below 10-12 cm at FOAM. In the depositional case, the low degree of biogenic reworking would allow the permanent retention of this

Mn once deposited because the build-up of reactive anions which occurs with a low level of biogenic transport, would reduce the solubility of common Mn-phases and prevent its further redistribution by diffusion. In fact, Mn^{++} would be continually supplied to the layer by diffusion from above if the deposited layer were thick enough.

If a depositional event similar to the hypothesized one for FOAM occurred at NWC or DEEP, it is unlikely that much of the chemistry of the deposited sediment would be preserved. If it were surface sediment rich in organic matter, Mn-oxide would be reduced through the process already described as the organics began to decompose. Assuming the newly deposited layer is inhabited by animals typical of NWC or DEEP, the Mn^{++} produced would be transported out of the sediment (by a combination of horizontal diffusion into burrows and particle reworking) and into overlying water (Chapter III). Because of biogenic transport, other products of decomposition would tend not to build-up to a high level, thereby raising the solubility of Mn^{++} and further increasing its diffusive loss to overlying water. Once released from the sediment, Mn is free to precipitate onto resuspended particles and either return to the seafloor where it would be concentrated in a surface layer or it can be transported to other regions of the estuary. The end-result of these events would be a diagenetic Mn profile typical of the station rather than of stochastic physical events. The differences between FOAM, NWC, and DEEP in such a hypothetical but highly possible case arise because of the

complete alteration of transport-decomposition processes at NWC and DEEP brought about by the stable presence of macrobenthos. Macrobenthos are also present at FOAM but are transient and do not bring about thorough, predictable reworking of sediment.

The average Mn^{++} production rates predicted for the 0-1 cm interval at FOAM by use of equation (17) are: $2.1\text{-}5.4 \times 10^{-6}$ mM/sec (FOAM-1, 3, 4). The molecular diffusion coefficients were used in this calculation. This is the same as predicted for NWC when molecular diffusion coefficients are used in both cases. The different fluxes of Mn^{++} out of the sediment at each station indicate that effective or biogenic diffusion is higher at NWC and the production rate required to maintain similar concentration gradients is accordingly higher.

The Fe profile at FOAM is similar to that of Mn. The same explanations given for the Mn solid phase profiles would apply to Fe with the modification that the quantity of Fe which could be diagenetically mobilized into the lower sediment by diffusion must be a smaller percentage of the total. Irregular dilution by up to 30% $CaCO_3$ prevents small changes in Fe by diagenetic redistribution from being readily identified.

The presence of large numbers of sedentary tube dwellers at DEEP gives rise to somewhat different internal transport processes and geometries of transport than are present at either NWC, where homogeneous reworking and vagile benthos dominate, or FOAM where physical disturbances prevent the extensive

development of any long-lived, deep-burrowing bottom fauna. The lining of tubes with surface sediment or the packing of mucus secretions into burrow walls results in the transport of interface material down distinct shafts in the sediment and promotes a general increase of decomposition at depth. The effect of even a small quantity of mucus on the rate of $SO_4^=$ reduction is demonstrated by the mucus-mud experiment (Figure VI-14). A specific example of the role of tubes in promoting decomposition and reactions, otherwise typical of the sediment-water interface, deep in sediments, is provided by Amphitrite ornata in Chapter II. At the same time as burrow construction increases the intensity and rate of many diagenetic reactions, it prevents the build-up of reaction products. This is accomplished through horizontal or radial diffusion into cylindrical biogenic shafts which are rarely farther apart than a few centimeters. The result of these processes is that the entire burrowed interval takes on average diagenetic properties similar to those near the sediment surface. The average geometry of the transport of pore water is radial in this mental construction (Figure V-46 of Chapter V). It is necessary to keep these basic processes in mind in order to explain the solid phase profiles at DEEP compared to FOAM and NWC.

Near the sediment-water interface at DEEP the Mn solid phase profile has a sharp decrease like that at NWC but then increases again to a fairly constant value below 5 cm. The profile cannot be explained by $CaCO_3$ dilution ($< 5\%$) or lithologic variation as suggested by constant ^{232}Th profiles

present mental picture. The solid phase profile is then invisioned as a steady state profile where Mn-oxide rich particles are biogenically transported from the surface to depth where Mn^{++} forms and is at least partially lost by horizontal diffusion and irrigation. Near the interface, Mn^{++} is lost predominately by vertical diffusion to the overlying water. A part of this loss is resupplied to the interface by fall-out composed of resuspended particles loaded with newly precipitated Mn-oxide. This supply maintains the interface at a high value and also provides high Mn particles for burrow linings or fill. At some critical depth where mixing cannot resupply the Mn lost by diffusion, there must be a minimum solid phase value; at DEEP this minimum is 2-3 cm. This depth in the sediment must be intimately related to the average distance between burrows below it and to the depth dependence of R (Mn^{++} production rate). If R is constant below 3 cm, then the average distance between burrows must be greater than ~ 6 cm in order to maintain a higher Mn-oxide concentration in the sediment beneath 3 cm at a given mixing or Mn-oxide supply rate. This assumes that no special reactions or hinderances to Mn^{++} diffusion occur at burrow walls.

The Mn^{++} production rate in the top 0-1 cm at DEEP compares well with that of NWC and is (equation 17): 2×10^{-6} mM/sec (DEEP-1) if a molecular diffusion rate is assumed or $\sim 1 \times 10^{-5}$ mM/sec if the effective diffusion coefficient obtained from the fluxes is assumed. Because a part of the Mn^{++} flux probably comes from dwelling burrows which tap deeper Mn^{++} pore water

(Chapter IV). The pore water profiles preclude the minimum Mn at 3 cm as resulting from a particularly strong reducing region such that Mn^{++} diffuses away from the 2-3 cm interval both toward the interface and to depth in the sediment. Instead, the following explanation is given. If it is assumed that Mn^{++} formation mimics the rate of decomposition (Chapter V), then Mn^{++} is produced in the sediment column at DEEP with a reaction rate of the form: $R = R_1 + R_o e^{-\alpha x}$. Near the interface, the Mn^{++} diffuses vertically toward the sediment surface where it is precipitated in part and in part lost to overlying water. A proportion of that lost to overlying water can be expected to return to the sediment surface based on the presence of excess ^{234}Th at DEEP (Chapter IV) and the residence times of Mn^{++} calculated previously. This Mn appears as the excess Mn near the interface (0-1 cm) and is mixed down continuously into the sediment. In the upper few centimeters mixing is relatively rapid: $D_B = 0.1 \times 10^{-6}$ cm^2/sec (Chapter IV), but below this depth particle reworking is more irregular and consists largely of the filling in of vacated dwelling burrows or tube formation with surface sediment. Because of the form of the Mn^{++} production function R (which results from the mixing process) Mn^{++} is produced at a high rate at depth as well. This Mn^{++} diffuses horizontally toward burrows rather than vertically and presumably is precipitated in part at the nearest inner burrow wall and in part escapes into overlying water. Mn-oxide incrusted burrows are a common feature of marine sediment (Chapter II, e.g., Buckley, Easton, and Johnson, 1974) a fact in support of the

sources, the use of the effective D at DEEP to estimate production rate is probably not as valid as using it at NWC where reworking and Mn^{++} production are more restricted to the upper few centimeters. The solid phase model can also be used to estimate Mn^{++} production although the model boundary conditions are not well met. Letting $D_B = 0.1 \times 10^{-6}$ cm^2/sec (Chapter IV), L = 2 cm, C_o = 753 μg/g, C_1 = 532 μg/g; then by equation (22), $R = (1.4 \times 10^{-6})$ e^{-x} μmoles/g-sec over the top 2 cm only. The average pore water Mn^{++} production rate, R, in the 0-1 cm interval is 4×10^{-7} mM/sec assuming a water content of 69.5% (Appendix IV). The solid phase model predicts a production rate at least 3X lower than the pore water model.

Fe must reflect the same transport regime as Mn. In the case of Fe, the pore water profiles indicate that transport of Fe^{++} is away from the interface below 3 cm and that Fe in the sediment should therefore increase with depth based on vertical diffusion alone. A portion of some of this Fe must be lost by horizontal diffusion at depth but the level of dissolved Fe^{++} is held so low by HS^- (pyrite equilibrium?) that horizontal loss from average sediment must be minimal. In special microenvironments such as tube walls, Fe^{++} will be generated and lost either by reduction of Fe-oxide or oxidation of sulfides (e.g., Chapter II). Compared to Mn^{++}, which is at high concentration deep in the sediment, loss of Fe^{++} through burrows must not be quantitatively significant to total solid phase Fe.

Near the sediment surface there is a net Fe loss. This is also in agreement with the pore water profile but not with the observed surface enrichment of Mn. If Mn is captured at the interface then Fe would also be expected to be concentrated there as observed at NWC. The explanation must be that both Fe^{++} and Mn^{++} are lost from the sediment into overlying water but that only a part of the Fe returns. DEEP station has lower resuspension rates than the shallower stations and its ^{234}Th inventory indicates less efficient scavenging of ^{234}Th by particles over this area of the Sound than NWC (Chapter IV). This means that the probability of both Fe and Mn escaping DEEP is higher than, for example, NWC. Other more efficient scavenging areas may supply more Mn to the water column than Fe so that particles returning to DEEP after resuspension in other areas may be much higher in Mn than Fe relative to average sediment. If only a portion of the lost metal is returned with a somewhat higher Mn/Fe ratio then it will be most easily detected in the case of Mn where the background concentration is low. Whatever the exact explanation, the profiles indicate redistribution of metals like Fe and Mn laterally in the Sound as well as vertically in the sediment. Bottom areas with high scavenging potential (particle resuspension, e.g., Aston and Chester, 1973), will tend to gain reactive elements at the sediment surface from regions of lower efficiency. Once mixed below the interface, however, particles are subjected to the internal transport-diagenetic regime of a bottom area so that final standing crop of an element deep in a deposit need not directly reflect initial input at the surface.

An increase in the concentration of metals like Cu, Zn, Hg, and Pb in the upper few centimeters of near shore marine sediment is commonly attributed to the influence of increased anthropogenic supply of these metals to sediments during the last 100 years (e.g., Chow et al., 1973; Thomson, Turekian, and McCaffrey, 1975). Although this explanation is reasonable, except for Mn, consideration of the effects of diagenetic redistribution and biogenic transport on the profiles is seldom taken into account in the interpretation. Measurement of sedimentary metal profiles on culturally polluted compared to pristine, lake basins have been used to try to determine whether diagenesis or anthropogenic sources are responsible for the observed increases (e.g., Schoettle and Friedman, 1974). Because the entire diagenetic regime is usually altered in the two cases due to different inputs of organic matter, the profiles from oligotrophic or pristine lakes are not really a valid diagenetic control. Metals such as Cu have been shown to be relatively soluble in oxygenated versus sulfide rich zones of water or sediment (e.g., Spencer and Brewer, 1971; Sasseville and Norton, 1975), which should result in redistribution by diffusion processes, and have been demonstrated to be diagenetically mobile in lab and field observations (e.g., Cline and Upchurch, 1973). Other observations, for example those of Bonatti, et al. (1971), indicate that metals like Cu are not mobile, at least over the length of their core sample. In the present study, it is possible to compare sediment profiles of Cu taken from the same estuary but from regions of the basin which vary

in the relative importance of possible diagenetic transport mechanisms.

Cu profiles at FOAM, NWC, and DEEP vary significantly in the upper 15 cm when the extent of the zone of constant or high Cu concentration is considered. The Cu profile obtained by Thomson, Turekian, and McCaffrey (1975) from a station midway between NWC and DEEP had Cu concentrations which increased slightly to a depth of 10 cm then decreased regularly. If it is assumed that at some depth at DEEP Cu begins to decrease (this is being tested), then all cores from LIS except NWC-2 have a lower Cu concentration in the upper few centimeters followed by a maximum and then a regular decrease. The inshore-offshore pattern then seems to be that the zone of high Cu is thicker but at a lower average concentration at offshore deep water stations than at nearshore ones. This trend is consistent with trends in the average depth of intensive biogenic particle reworking suggesting that the thickness and average concentration of the high Cu layer in LIS is controlled in part by biogenic mixing. If it is assumed that Cu in pore water profiles reaches a maximum concentration just below the sediment-water interface (see Sasseville and Norton, 1975), then Cu could move downward into the sediment as well as be released into overlying water. The decrease in Cu near the interface is consistent with release and the regular decrease in Cu at depth in the sediment would be in agreement with either biogenic particle reworking or downward pore water diffusive transport. The release of Cu from sediment is not overwhelmingly high since it was undetectable in flux core water samples

by flame AA, which, although not sensitive, would detect a flux of > 0.1 $\frac{\text{mmoles}}{m^2\text{-d}}$ over the collection timescales used.

The solid phase Cu profiles are consistent with an increased anthropogenetic supply which has been redistributed vertically in the sediment column predominately by biogenic particle reworking and to a lesser extent, diffusion. The resulting vertical profile is indicative of the benthic community which controls reworking at each station. When longer cores from each station are completely analyzed by the same technique, a comparison of standing crop versus sedimentation or reworking rates will demonstrate how homogeneous Cu supply is or whether it is being redistributed in the Sound by the flux-particle scavenging processes already described for Mn and Fe.

Because of reworking and diagenetic redistribution, the chronology of anthropogenic supply cannot be accurately determined; for example: based on ^{234}Th and ^{210}Pb particle mixing timescales of $0.1\text{-}1.0 \times 10^{-6}$ cm^2/sec and assuming no pore water diffusion, the profiles at NWC could be explained by increased supply over only the last ~ 10 rather than 100 years.

Modeling Mn pore water profiles

A number of steady state-transport-reaction models for Mn^{++} profiles in sediments have been proposed which adequately describe the observed concentration distribution in sediment (e.g., Michard, 1971; Calvert and Price, 1971; Robbins and Callender, 1975; Holdren, Bricker, and Matisoff,

1975; Elderfield, 1976; Holdren, 1977). These will not be repeated here as several of the most significant parameters which can be inferred from such models (e.g., Mn^{++} production rates, flux rates or establishment of equilibrium with a given solid phase), have already been estimated earlier from models specific to a given sediment zone, or, have been measured directly. The nonsteady-state model used to describe NH_4^+ distribution near the interface (Chapter V) can be used to show that the production rates calculated previously and the conclusion that Mn^{++} is being precipitated as a reduced phase at depth are consistent with the observed interstitial water profiles. This will be done by first assuming that only production and one dimensional diffusion of Mn^{++} are important and then inferring from deviations between observed and predicted what additional processes other than those assumed in the model and taking place. The equation to be solved is:

$$(25) \quad \frac{\partial C}{\partial t} = \frac{Df(t)}{1+K} \frac{\partial^2 C}{\partial x^2} + \frac{R_o g(t)}{1+K} e^{-\alpha x}$$

x = vertical dimension, positive axis into sediment, $x = 0$ at interface

C = pore water concentration

D = maximum value of effective diffusion coefficient attained during warmest time of year

K = Langmuir adsorption coefficient in linear range

$f(t)$, $g(t)$ = time dependent functions of form $f = f_o \exp\left(\frac{-E}{B + G\cos\omega t}\right)$

$R_o e^{-\alpha x}$ = depth dependent reaction term

The solution is given in Chapter V for the initial conditions:

$$t = 0,\ x \geq 0,\ C = mx + b$$

and the boundary condition: $x = 0,\ C = 0,\ t > 0$

For winter at NWC, or $T = 2^{\circ}$, the initial condition will be taken roughly as $C = 0.05\ \mu M$, $D = 1 \times 10^{-5}\ cm^2/sec$, $R_0 = 1 \times 10^{-5}\ mM/sec$, $\alpha = 1$, and f(t), g(t) as defined in Chapter V. The predicted June-July Mn^{++} profile is shown in Figure VI-22. Two values of K have been used: $K = 0$, $K = 2$. In the case of $K = 2$, it was assumed that Mn^{++} adsorption was of the same order as Ca^{++} (Murata, 1939; data of Norvell, 1975) which is $K_{Ca} \approx 1.8$ (Li and Gregory, 1974). K was applied to the effective diffusion coefficient term. The general shape and magnitude of the observed Mn^{++} concentrations are in fair agreement with the calculated distribution but there are some distinct differences as well. The measured July pore water concentrations at NWC attenuate more rapidly with depth than the calculated profiles and the observed maximum concentration is in the 0-1 cm interval rather than the 2-3 cm interval as calculated. These discrepancies can be explained by the failure to include precipitation of Mn^{++} with metabolic anions such as HCO_3^- in the model (e.g., Holdren, Bricker, and Matisoff, 1975), underestimation of R_o near the interface, and the possibility that K varies as a function of depth. Discrepencies can also be caused by not adequately describing transport in the sediment. Horizontal diffusion into irrigated burrows will

lower the concentration below that predicted by simple one dimensional diffusion and cause attenuation which in a one dimensional model would be interpreted as a precipitation reaction. The fact that solid phase Mn does not build up at depth at NWC as predicted by one dimensional diffusion (Holdren, 1977) suggests that both particle reworking and horizontal diffusion are playing a role.

This points out the problem of inferring reactions from vertical diffusion models in sediment zones which are well below the interface but in burrowed regions of a deposit. [Vertical diffusion models become good approximations either very near the interface, as shown by flux calculations and scale analysis, or below the bioturbated zone (Chapter V).] Because the Mn^{++} production rate as a function of depth is not accurately known at FOAM or DEEP (although R_o is) and because horizontal diffusion and irrigation dominates pore water profiles at DEEP no further attempt to model the exact distribution of pore water Mn^{++} at these stations beyond the calculations made earlier will be done here. It can be concluded from the present model calculations at NWC that the production rates determined earlier are capable of adequately accounting for much of the observed seasonal change in concentration but that an exact model which allows accurate calculation of solid phase distribution of Mn or inferrence of reaction rates below 4 cm, requires a two dimensional description of transport.

Summary

(1) Pore water profiles of Fe^{++} and Mn^{++} from three stations in Long Island Sound have general depth dependent concentration distributions similar to those reported from other sedimentary basins: concentrations rise above sea water values to a maximum below the interface and then decrease again lower in the deposit. Beyond these general features, specific qualities of the profiles reflect the internal transport-reaction regime effective at each station. These differ in a regular fashion along an inshore-offshore transect running from shallow to deeper water.

(2) The production of Mn^{++} in pore waters is directly related to the rate of reduction of Mn-oxides during the decomposition of organic matter, both as a function of depth in the sediment as well as seasonally. Fe^{++}, on the other hand, is produced both by the reduction of Fe-oxides and by abiogenic or biogenic oxidation of Fe-sulfides. The result of different sources for the two dissolved metals is a different seasonality of the interstitial water profiles. The seasonality of both Mn^{++} and Fe^{++} profiles are periodic and repeatable from year to year. During the summer, pore water Mn^{++} is highest of the year. At stations where rates of decomposition decrease exponentially with depth in the sediment so does Mn^{++} production; where decomposition is initially exponentially decreasing but becomes constant at depth, then Mn^{++} production does as well. In the fall, Mn^{++} concentrations are lowered in magnitude as a

result of both decreased production and a relative increase in the effect of biogenic transport processes which exchange sediment with overlying waters. During the winter, Mn^{++} profiles become controlled by molecular diffusion and lowered rates of production. Whereas in the summer and fall the highest Mn^{++} concentrations are often found in the 0-1 cm sampling interval, in the winter the lowest concentrations are found there. Mn^{++} production mimics very closely the seasonal and depth dependent patterns of NH_4^+ formation (Chapter V). Fe^{++} is also formed in abundance near the sediment-water interface during the early summer when the water first begins to warm. Because of the associated increase in sulfide production Fe^{++} does not always rise to its maximum yearly concentration at this time. In the fall, like many other ions whose source is in the sediment, Fe^{++} concentrations below the top few centimeters drop to their lowest value of the year. Unlike Mn^{++}, during the winter Fe^{++} may reach its maximum standing concentration of the year at some stations. This results from a net oxidation and loss of FeS and FeS_2 from surface sediment and an associated release of Fe^{++} which does not immediately depend on strongly temperature-controlled microbial metabolism.

(3) Both Mn^{++} and Fe^{++} react rapidly with anions formed during decomposition. Equilibrium calculations and direct measurement of solid phase sulfides indicate that away from oxidized portions of sediment Fe^{++} concentration is determined in part by the formation of FeS-FeS_2 while Mn^{++} concentrations appear to be related in some cases to the formation of $MnCO_3$.

Because of uncertainty in equilibrium constants of phosphate compounds and fairly high error in the measurement of pS, it is not possible to rule out the formation of Mn-sulfides or mixed Mn and Fe-phosphates.

(4) Although Mn^{++} and Fe^{++} may maintain a set mass action relation with a given solid phase, the overall magnitude of their concentrations are determined by transport processes within the sediment. Biogenic transport is important at all stations but increases in dominance offshore in deep water. The most inshore and shallow water station, FOAM, approximates the most closed system where much transport is by one dimensional (vertical) molecular diffusion. As the presence of macrobenthos becomes more predictable offshore, the sediment column becomes more open to exchange. The exact type of exchange processes are dependent on the kinds of animals present.

(5) At NWC, vagile benthos dominate and the sediment is relatively randomly and intensely reworked in the upper 15-20 cm and particularly the upper 4 cm. Excess Mn captured from the water column by resuspended particles is rapidly reworked into the bottom by protobranch bivalves and remobilized. The mean turnover time for all the excess Mn above the average sediment background is 35 days. The production rate of Mn^{++} in the top 0-1 cm at NWC is at least 1×10^{-5} mM/sec.

(6) Whereas Mn remobilization is concentrated mostly in the upper few centimeters at NWC, DEEP is characterized by relatively rapid reworking of particles to greater depths and the active Mn^{++} production region is

more spread out. Mn and organic rich particles are extracted from surface sediment and packed as burrow fill or tube-lining at depth where decomposition and remobilization occurs. Production rate is at least 0.2-1 x 10^{-5} mM/sec in the top 0-1 cm.

(7) The quantity of Fe^{++} being redistributed in the sediment is probably greater than Mn but less easily identified against the lithologic background.

(8) Both Mn^{++} and Fe^{++} escape into overlying water. The flux varies seasonally and is a function of depositional environment and the bottom community present. Like NH_4^+, Mn^{++} flux is highest in the summer and lowest in the winter. The seasonal range incompassing values at all stations is: 0.01-5 mmoles/m^2/day; the yearly average flux range is: 0.67-2.7 mmoles/m^2/day over most of the central Sound. Effective diffusion coefficients of 0.6-1 x 10^{-5} cm^2/sec can be used to account for the measured fluxes with the observed pore water concentration gradients. The high reactivity of Fe^{++} under oxygenated conditions caused major problems in measurement of its flux out of the bottom. Because of this it is not possible to say with certainty what the seasonality of the flux is; the present data indicate that fall is the time of highest Fe^{++} flux. The Fe^{++} flux can be of the same magnitude as the Mn^{++} flux: $\sim$ 1 mmole/m^2/day, and all indications are that measured values are minima. Because of its rapid precipitation rate (first order rate constant: k $\sim$ 8 x 10^{-3}/min in this study), the Fe^{++} flux may be conceptually

viewed as a colloid flux out of the bottom.

(9) The high mobility of Fe and Mn results in its redistribution vertically in the sediment column by diffusion and biogenic transport and laterally in the Sound by a combination of physical and biogenic processes.

(10) The same kinds of remobilization processes apparently influence the distribution of other metals such as Cu. The depth of penetration of high Cu into the sediment correlated well with the depth of biogenic reworking in different regions of the Sound. It appears that any anthropogentic increase in Cu supply to bottom sediment is subject to redistribution by particle reworking and diffusion within the sediment column and to loss from the oxygenated zone of sediment to overlying water.

(11) In both Chapter V and this chapter it has been shown that the presence of a well established bottom community radically influences diagenetic processes in marine sediment. Many of these effects are brought about by the complete alteration of transport processes in the sediment column by the reworking and irrigation activities of macroinfauna. Pore water diffusion becomes two dimensional and particles are randomly or specifically reorganized in the sediment. The depth in the sediment to which these activities are important, the geometry of diffusion and diagenetic reactions, and the chemistry of sediment leaving the bioturbated zone depend on the functional types of animals present in a given area and therefore both the depositional environment and subtle biological interactions.

Table VI-1

Precipitation Rate Experiment

Fe and Mn

Time (hours)	Mn µM	Fe µM
Temperature = 22°		
0	22.4	0.10
2.33	22.2	0.055
4.4	22.0	0.045
12.2	21.1	0.036
Temperature = 4°		
0	6.1	-
1.42	6.0	-
3.5	6.0	-
18.6	6.0	-
28.2	6.0	-

Table VI-2

Flux Measurements *
Fe and Mn

Station	Summer (22°)		Fall (15°)		Winter (4°)	
	Mn	Fe	Mn	Fe	Mn	Fe
FOAM	1.6	0.002	1.0	1.1	0.08	-
predicted:	2.9	0.1	1.1	0.004	0.38	0.001
NWC	5.8	0.014	3.9	0.049	0.03	-
predicted:	2.3	0.07	1.3	0.004	0.16	0.01
DEEP	5.2	0.03	2.7	0.63	0.013	-
predicted:	1.1	0.07	0.55	0.001	0.069	0.064

* All units mmoles/m^2/day

Estimated error for measured fluxes from slopes of concentration increase (when more than one point was used) is ∿10%.

Table VI-3

Decomposition Experiments - Marsh Sediment

Time (days)	Mn µM	$SO_4^{=}$ *
0	138	18
1	69	18.5
3	-	17.5
11	18	9.5
15	10	6
19	13	3
22	19	0.7
24	14	0.1
32	11	0
47	12	0
82	11	0

* $SO_4^{=}$ estimated from Martens and Berner (1974)

Table VI-4

Decomposition Experiments - Mud + Mucus + Limonite

Time (days)	Mud		Mud + Mucus		Mud + Mucus + Limonite	
	SO_4 mM	Fe µM	SO_4 mM	Fe µM	SO_4 mM	Fe µM
3	12.6	0.067	13.7	0.26	13.3	0.047
10	11.1	0.010	12.3	0.030	13.1	0.20
17	11.3	0.030	10.7	0.080	12.4	0.80
24	11.8	0.271	(14.5)	0.271	(14.6)	0.94
102	10.5	0.172	9.6	0.20	15.1	2.5
209	7.7	0.12	5.8	0.14	13.0	1.15

Numbers in parenthesis are left out of plot

Table VI-5

Oxidation Experiment - Pyrite - FOAM

Time (hours)	Blank		Pyrite		FOAM Sediment	
	SO_4 mM	Fe µM	SO_4 mM	Fe µM	SO_4 mM	Fe µM
0	20.2	0.066	20.2	0.066	20.2	0.084
5	21.1	0.081	20.1	0.21	19.9	1.60
43	20.6	0.098	20.6	0.13	20.5	0.22
116	21.8	0.075	21.2	0.084	21.8	0.150
192	21.7	0.075	21.2	0.084	22.1	0.129
341	21.2	0.075	21.7	0.084	22.8	0.142

Table VI-6

Oxidation Experiment - NWC Sediment

Time (hours)	Sample	pH	Alkalinity	Mn µM	Fe µM
0	Blank	7.77	2.28 (meq/l)		
	0-1 cm	7.77	2.28	0.1	0.01
	1-2 cm	7.75	2.28		0.01
	2-3 cm	7.77	2.28		0.01
3.5	Blank	7.82			
	0-1 cm	7.77	2.16	3.3	0.34
	1-2 cm	7.79	2.20		0.089
	2-3 cm	7.81	2.22		0.095
6.5	Blank	7.91			
	0-1 cm	7.81	2.14	0.97	2.23
	1-2 cm	7.82	2.16		0.045
	2-3 cm	7.82	2.18		0.051
10	Blank	7.92			
	0-1 cm	7.93	2.12	1.6	3.97
	1-2 cm	7.91	2.10		0.068
	2-3 cm	7.93	2.10		0.051
24	Blank	7.96			
	0-1 cm	7.88	2.10	0.61	1.17
	1-2 cm	7.89	2.08		0.063
	2-3 cm	7.91	2.06		0.058
31	Blank	8.01			
	0-1 cm	7.93	2.04	0.51	1.02
	1-2 cm	7.94	1.94		0.054
	2-3 cm	7.88	1.82		0.10
180.5	Blank	8.01	2.30		
	0-1 cm	7.92	2.04	0.3	0.37
	1-2 cm	7.93	1.84		0.092
	2-3 cm	7.89	1.46		0.053

Sample	Weight
0-1 cm	6.32 g
1-2 cm	6.88 g
2-3 cm	7.25 g

Table VI-7

Solubility Products at 25°C for Selected Sulfide and Carbonate Compounds

Reaction	Solubility Product	Reference
$FeS_{amorph} \rightleftarrows Fe^{++} + S^{=}$	$K_{sp} = 10^{-16.9}$	1
$FeS_{mack} \rightleftarrows Fe^{++} + S^{=}$	$K_{sp} = 10^{-17.5}$	1
$Fe_3S_{4\,greig.} \rightleftarrows 3Fe^{++} + 3S^{=} + S^{\circ}$	$K_{sp(FeS)} = 10^{-18.2}$	1
$FeCO_{3\,siderite} \rightleftarrows Fe^{++} + CO_3^{=}$	$K_{sp} = 10^{-10.2}$	2
$MnS_{alab.} \rightleftarrows Mn^{++} + S^{=}$	$K_{sp} = 10^{-12.9}$	3
	$K_{sp} = 10^{-15.2}$	4
	$K_{sp} = 10^{-17.8}$ *	5
$MnS_{2\,hauer.} \rightleftarrows Mn^{++} + S^{=} + S^{\circ}$	$K_{sp} = 10^{-20.6}$	5
$MnCO_3 \rightleftarrows Mn^{++} + CO_3^{=}$	$K_{sp} = 10^{-10.4}$	6

References: (1) Berner (1967); (2) Stumm and Singer (1966); (3) Robie (1966); (4) Kolthoff(1931); (5) Mills (1974); (6) Morgan (1967).

* = value plotted in Figure

Chapter VI

Figure Captions

Figure VI-1: Pore water Fe^{++} and Mn^{++} profiles from gravity cores at FOAM, NWC, and DEEP. Near interface region should not be compared because of different collection times of cores.

Figure VI-2: Seasonal change in pore water Mn^{++} profiles in box cores from FOAM.

Figure VI-3: Seasonal change in pore water Mn^{++} profiles in box cores from NWC.

Figure VI-4: Seasonal change in pore water Mn^{++} profiles in box cores from DEEP.

Figure VI-5: Seasonal change in pore water Fe^{++} profiles in box cores from FOAM.

Figure VI-6: Seasonal change in pore water Fe^{++} profiles in box cores from NWC.

Figure VI-7: Seasonal change in pore water Fe^{++} profiles in box cores from DEEP.

Figure VI-8: Distribution of Mn and Fe in solid phase at NWC showing lack of seasonal variation for Mn and ability to repeat gross features of solid phase distribution in separate samples.

Figure VI-9: Fe and Mn solid phase distribution at FOAM and NWC. Dashed lines represent concentration on a $CaCO_3$-free basis at FOAM.

Figure VI-10: Examples of solid phase Cu profiles at FOAM (Goldhaber et al., 1977), NWC, and DEEP. FOAM analyses were by a weaker leach than NWC and DEEP so concentration values are not directly comparable but relative concentration depth profiles should be.

Figure VI-11: Semi-log plot of dissolved Fe in sea water versus time after collection (Lewin and Chen, 1973; $T = 10^{\circ}$, triangles) or after separation of water from underlying sediment in flux core ($T = 22^{\circ}$, circles). See text for details of calculation.

Figure VI-12: Amount of Mn^{++} and Fe^{++} released from flux core sediment versus time after collection. Mn^{++} profiles are linear with time. The first point for NWC summer has been ignored because high water turbidity due to storm activity for a few days previous to collection increased precipitation loss in the core prior to settling out of particles after collection. The first Fe point for the same core is also ignored. The fall Fe^{++} shows the tendency for Fe^{++} to rapidly build up and then precipitate in the flux cores. The initial increase is taken as

an estimate of the flux. All fall cores showed the same type of Fe^{++} release-time pattern (Appendix V).

Figure VI-13: Concentration of Mn^{++} (open circles) as function of time in decomposition experiment using marsh sediment. $SO_4^=$ decrease during same period (Martens and Berner, 1974) is plotted as dashed line.

Figure VI-14: Concentration-time plots of $SO_4^=$ and Fe^{++} in the mucus + mud + limonite experiment. Triangles = mud + mucus + limonite; circles = mud only; squares = mud + mucus.

Figure VI-15: Fe^{++} concentration in overlying water versus time of resuspension in pyrite-FOAM sediment oxidation experiment. Squares = FOAM sediment; triangles = pyrite; circles = blank.

Figure VI-16: Fe^{++} concentration in overlying water versus time of resuspension of NWC sediment from 0-1 cm in oxidation experiment.

Figure VI-17: Alkalinity of overlying water versus time of resuspension of NWC sediment from different depth intervals (0-1 cm = circles; 1-2 cm = squares; 2-3 cm = triangles).

Figure VI-18: Plots of -logIAP for solid phases: FeS and $FeCO_3$ as a function of depth in sediment at FOAM, NWC, and DEEP. Box cores: open circles = summer (1975); open squares =

fall (1975); open triangles = winter (1976). Gravity cores: closed circles = FOAM, closed squares = NWC; closed triangles = DEEP.

Figure VI-19: Plots of -logIAP for solid phases: MnS and $MnCO_3$ as a function of depth at FOAM, NWC, and DEEP. Symbols as in Figure VI-18.

Figure VI-20: Mn^{++} flux out of bottom sediment at each station as a function of temperature (season).

Figure VI-21: Solid phase distribution predicted by transport-reaction model (solid line-circles at boundaries) compared to Mn distribution of core NWC-2 (vertical bars).

Figure VI-22: June-July pore water Mn^{++} profile predicted from transport-production model described in text. Starting profile: winter = 0.05 mM, dashed line. No adsorption = solid line. Adsorption with K = 2 = dotted line. Time = 122 days.

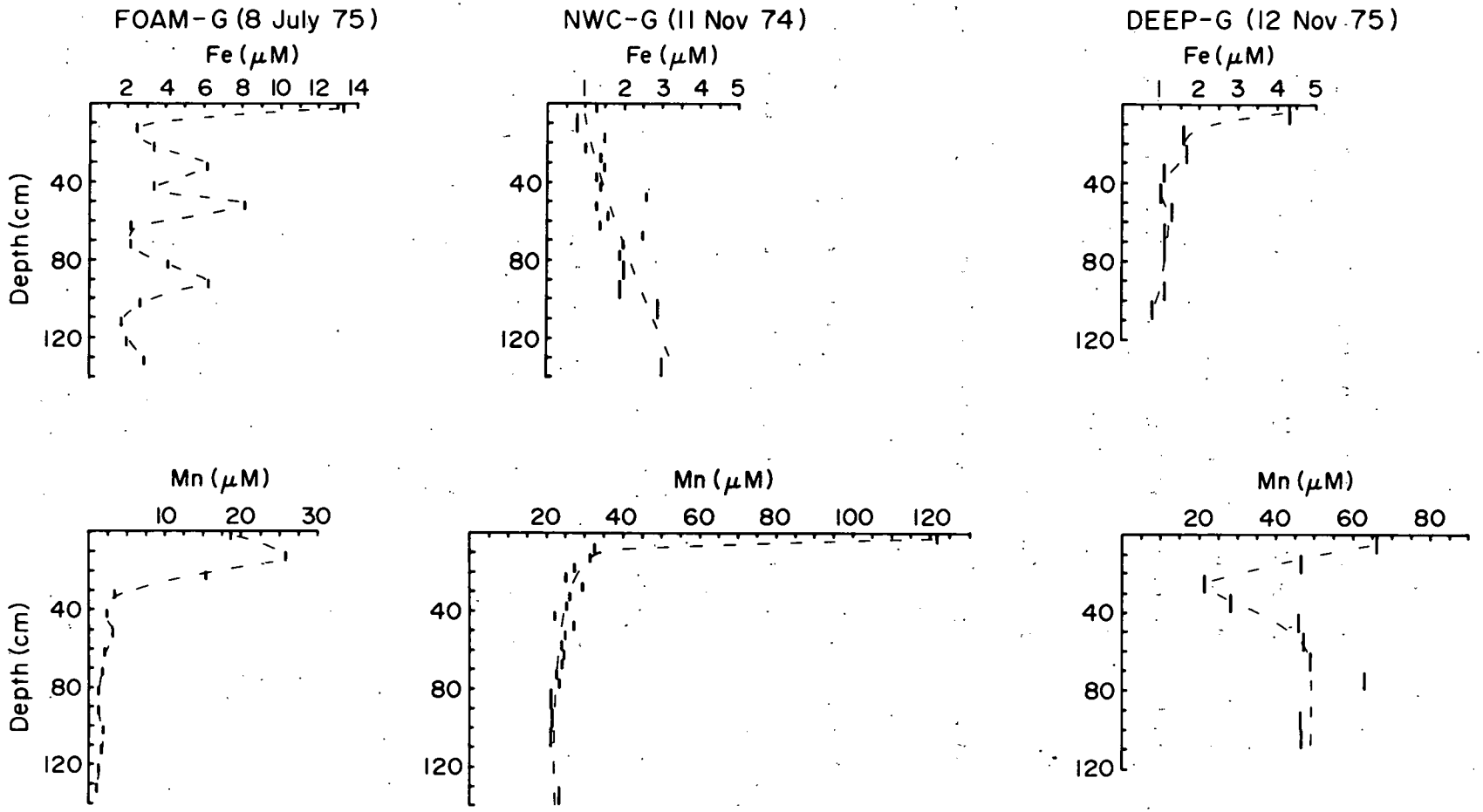

FOAM-G (8 July 75)
Fe (μM)
2 4 6 8 10 12 14
NWC-G (11 Nov 74)
Fe (μM)
1 2 3 4 5
DEEP-G (12 Nov 75)
Fe (μM)
1 2 3 4 5
Depth (cm)
40
80
120
Mn (μM)
10 20 30
Mn (μM)
20 40 60 80 100 120
Mn (μM)
20 40 60 80

Figure VI-1

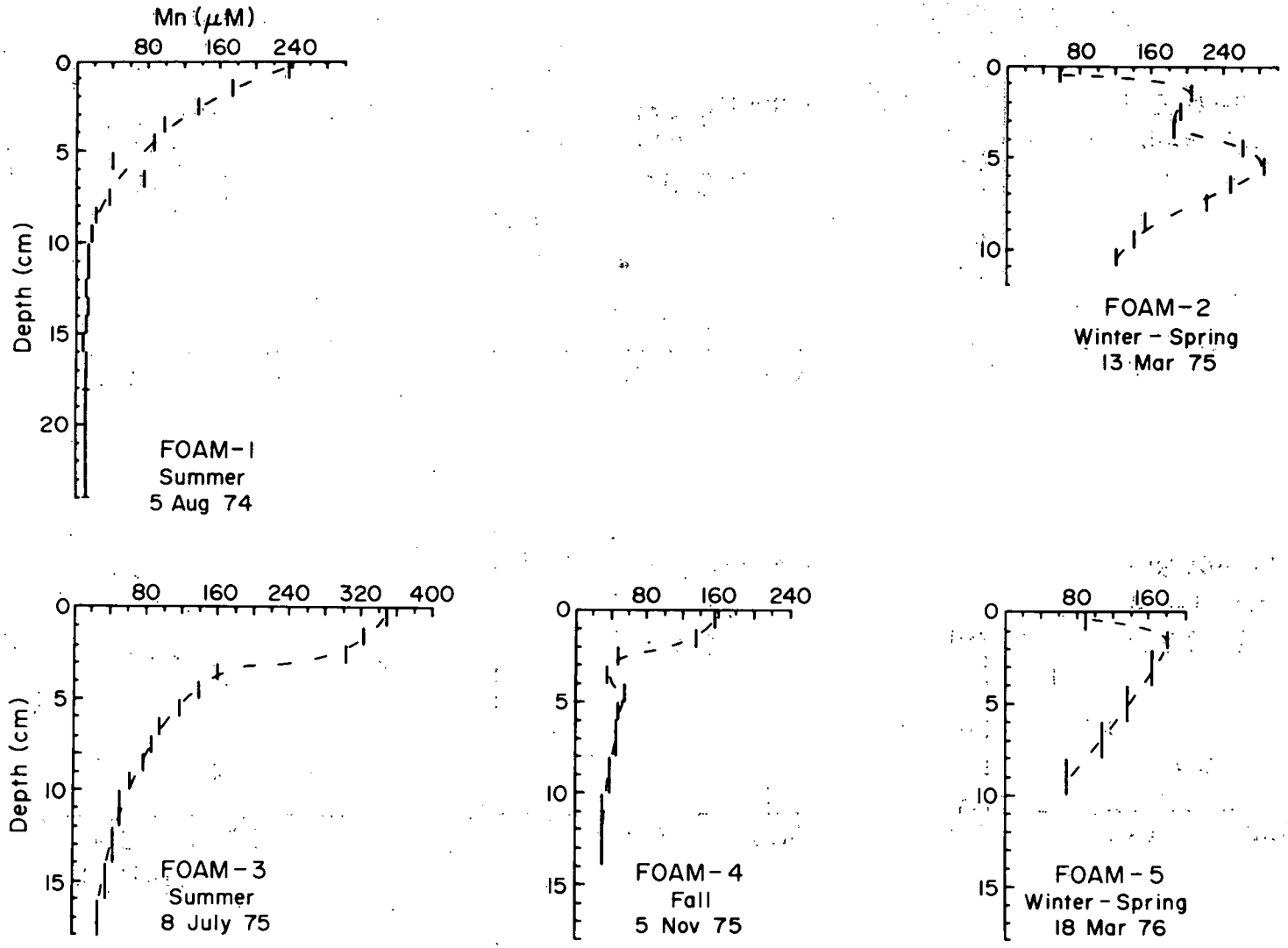

Mn (μM)
80
160
240
0
5
10
15
20
Depth (cm)
FOAM-1
Summer
5 Aug 74
FOAM-2
Winter - Spring
13 Mar 75
320
400
FOAM-3
Summer
8 July 75
FOAM-4
Fall
5 Nov 75
FOAM-5
Winter - Spring
18 Mar 76

Figure VI-2

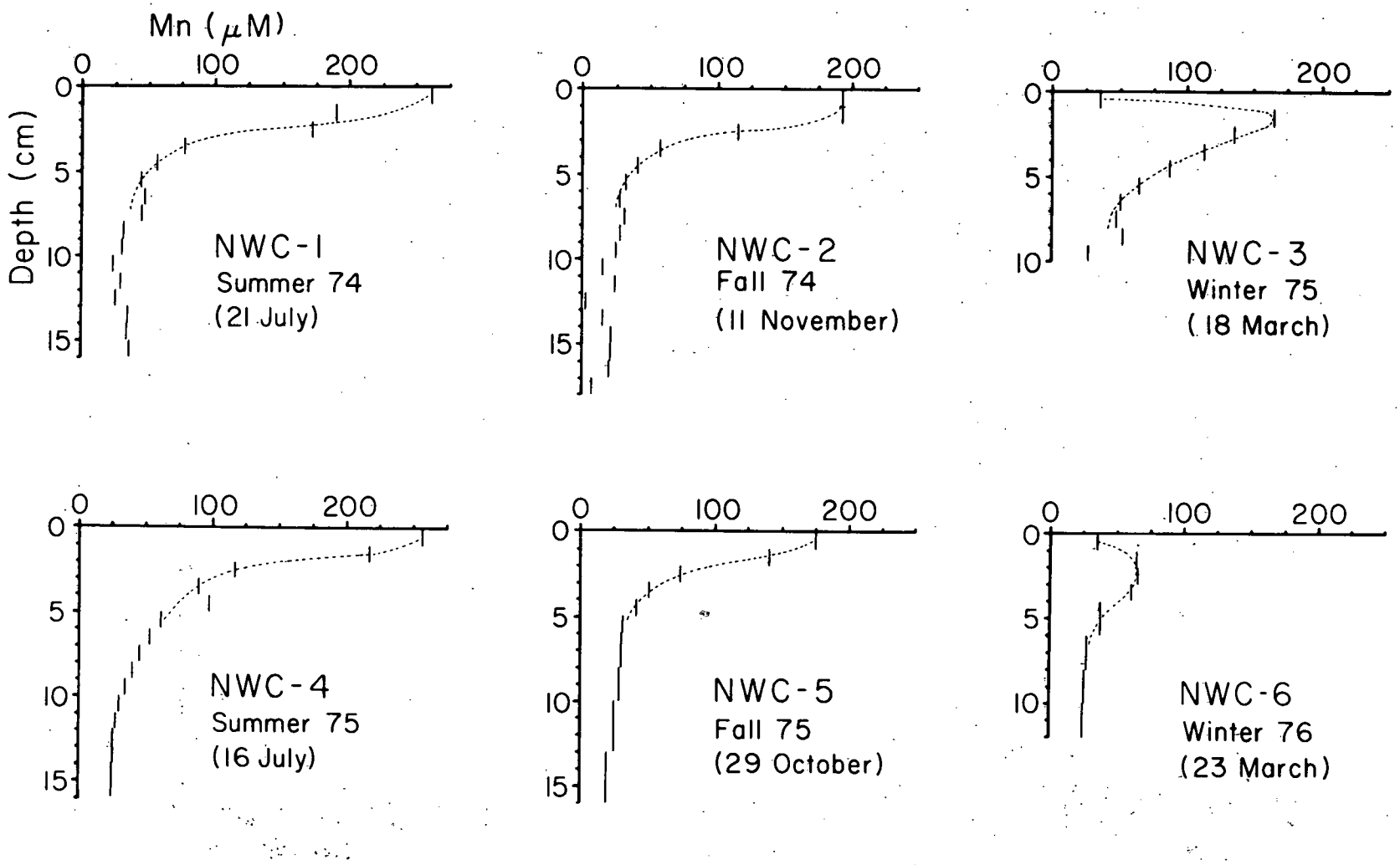

Mn (μM)
0
100
200
Depth (cm)
0
5
10
15
NWC-1
Summer 74
(21 July)
NWC-2
Fall 74
(11 November)
NWC-3
Winter 75
(18 March)
NWC-4
Summer 75
(16 July)
NWC-5
Fall 75
(29 October)
NWC-6
Winter 76
(23 March)

Figure VI-3

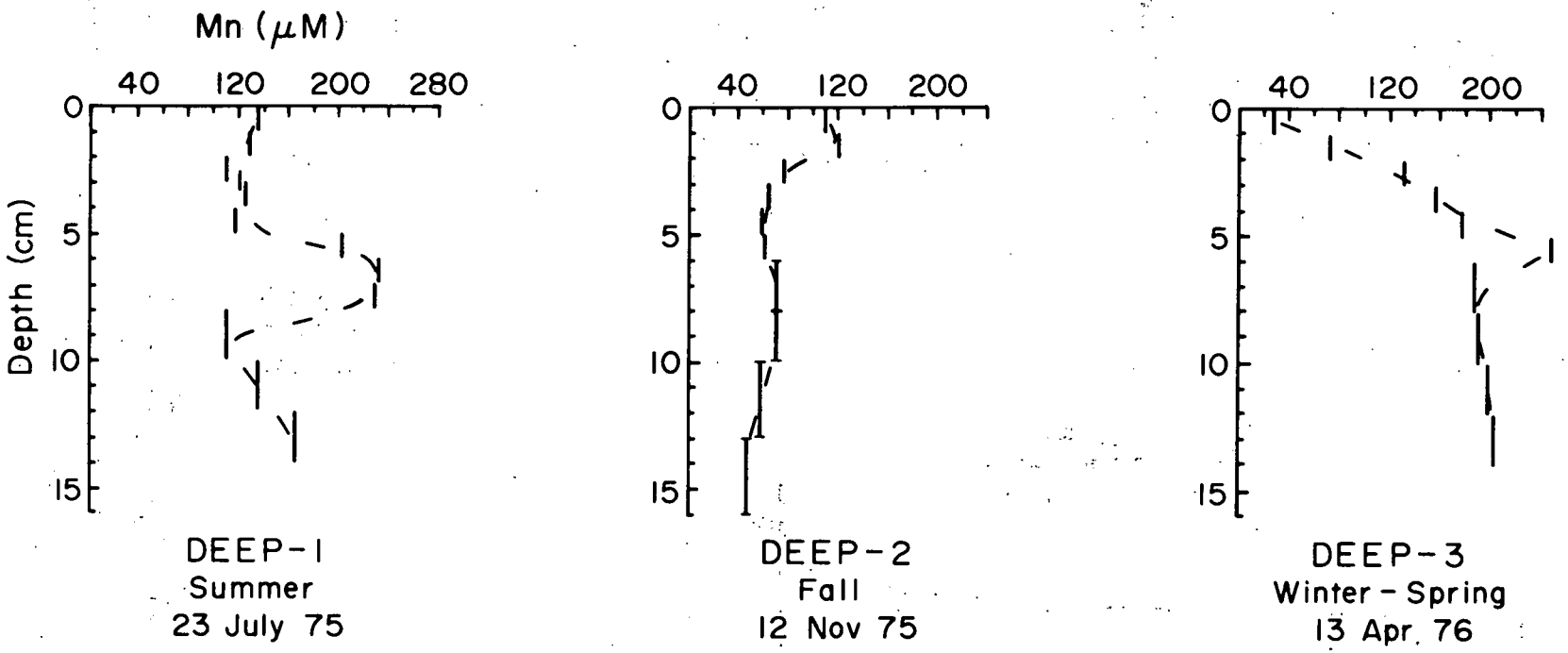

Mn (μM)
40
120
200
280
0
5
10
15
Depth (cm)
DEEP-1
Summer
23 July 75
40
120
200
DEEP-2
Fall
12 Nov 75
40
120
200
DEEP-3
Winter - Spring
13 Apr. 76

Figure VI-4

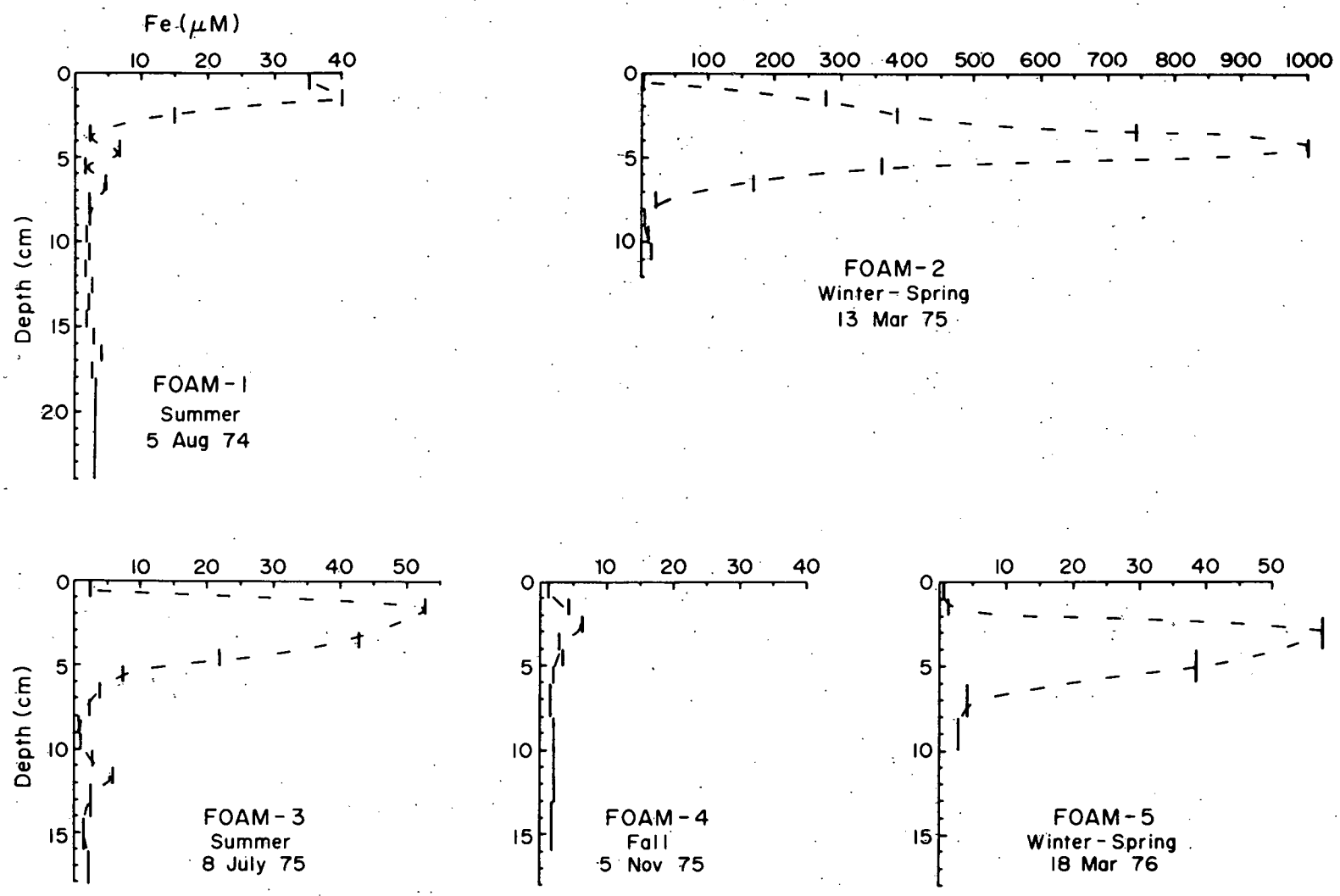

Fe (μM)
10 20 30 40
0
5
10
15
20
Depth (cm)
FOAM-1
Summer
5 Aug 74
100 200 300 400 500 600 700 800 900 1000
0
5
10
FOAM-2
Winter-Spring
13 Mar 75
10 20 30 40 50
0
5
10
15
Depth (cm)
FOAM-3
Summer
8 July 75
10 20 30 40
0
5
10
15
FOAM-4
Fall
5 Nov 75
10 20 30 40 50
0
5
10
15
FOAM-5
Winter-Spring
18 Mar 76

Figure VI-5

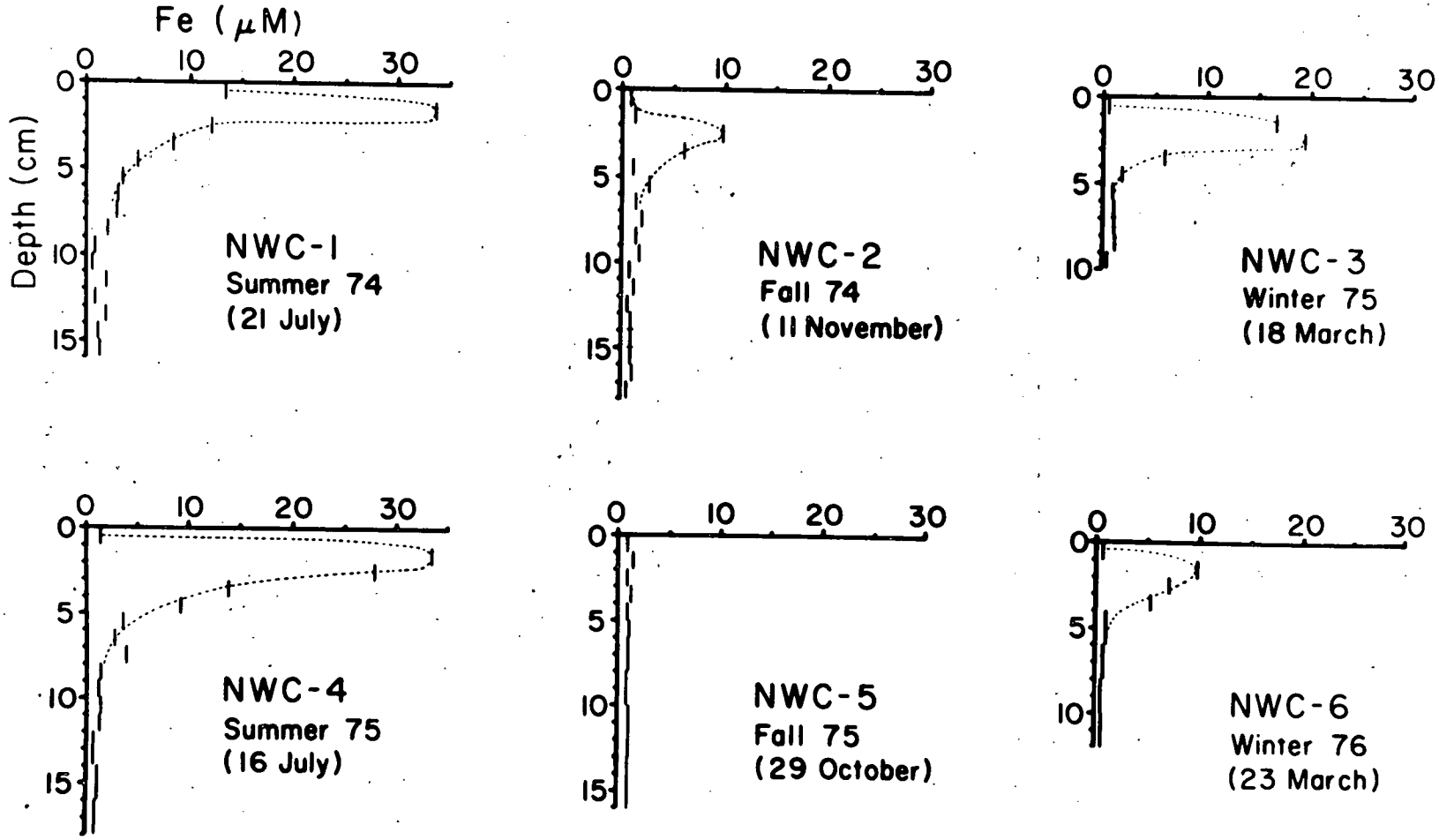

Fe (μM)
0 10 20 30
Depth (cm)
0
5
10
15
NWC-1
Summer 74
(21 July)
NWC-2
Fall 74
(11 November)
NWC-3
Winter 75
(18 March)
NWC-4
Summer 75
(16 July)
NWC-5
Fall 75
(29 October)
NWC-6
Winter 76
(23 March)

Figure VI-6

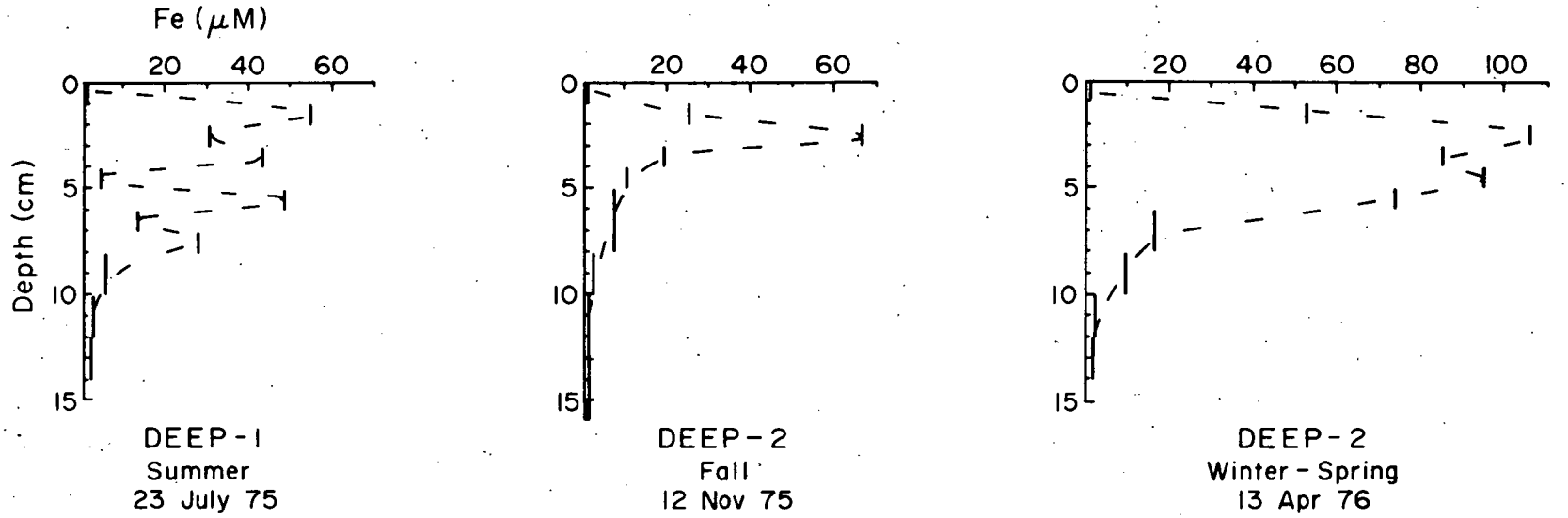

Fe (μM)
20
40
60
0
5
10
15
Depth (cm)
DEEP-1
Summer
23 July 75
20
40
60
0
5
10
15
DEEP-2
Fall
12 Nov 75
20
40
60
80
100
0
5
10
15
DEEP-2
Winter - Spring
13 Apr 76

Figure VI-7

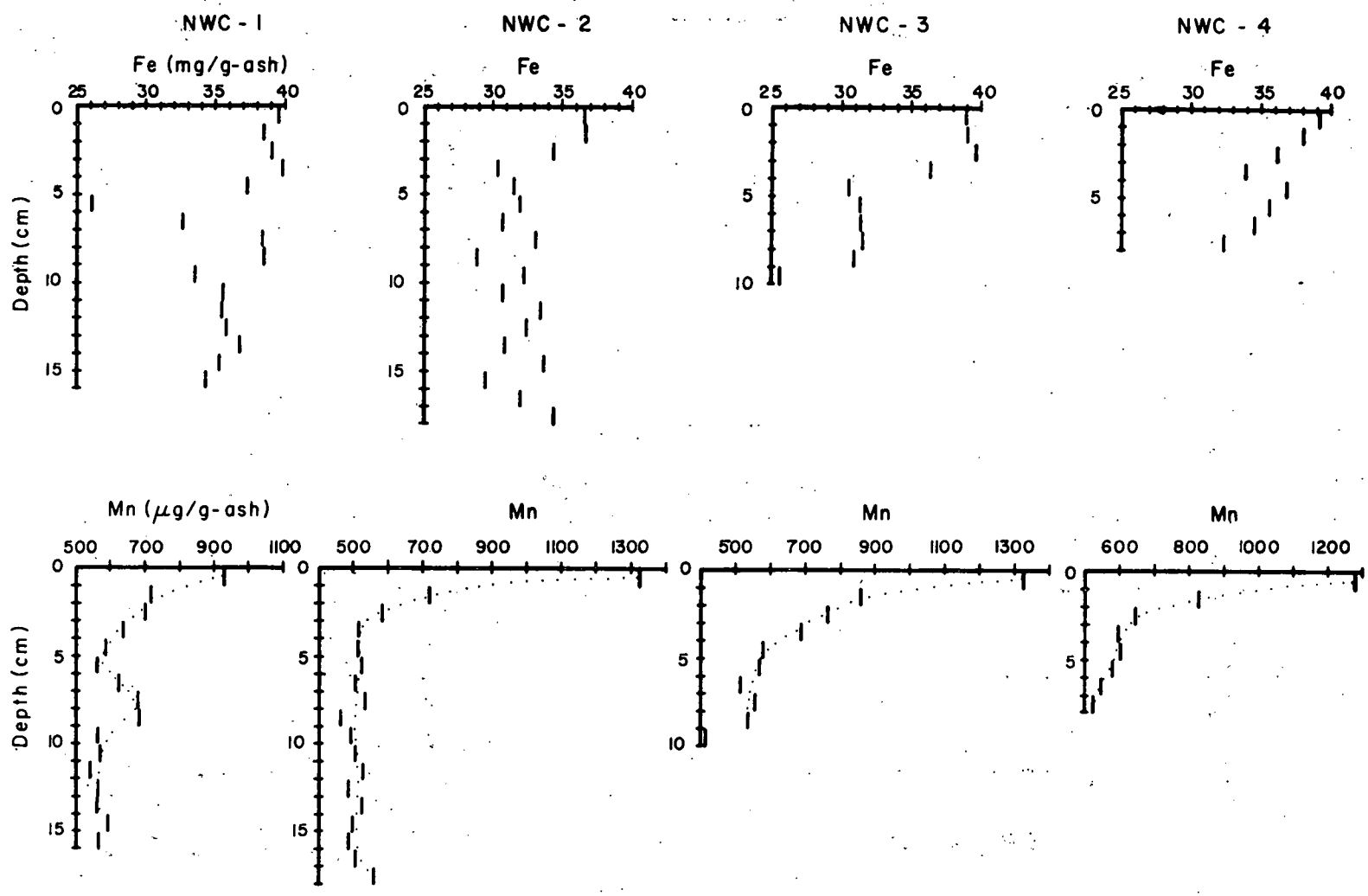

NWC - 1
Fe (mg/g-ash)
25 30 35 40
NWC - 2
Fe
25 30 35 40
NWC - 3
Fe
25 30 35 40
NWC - 4
Fe
25 30 35 40
Depth (cm)
0 5 10 15
Mn (μg/g-ash)
500 700 900 1100
Mn
500 700 900 1100 1300
Mn
500 700 900 1100 1300
Mn
600 800 1000 1200

Figure VI-8

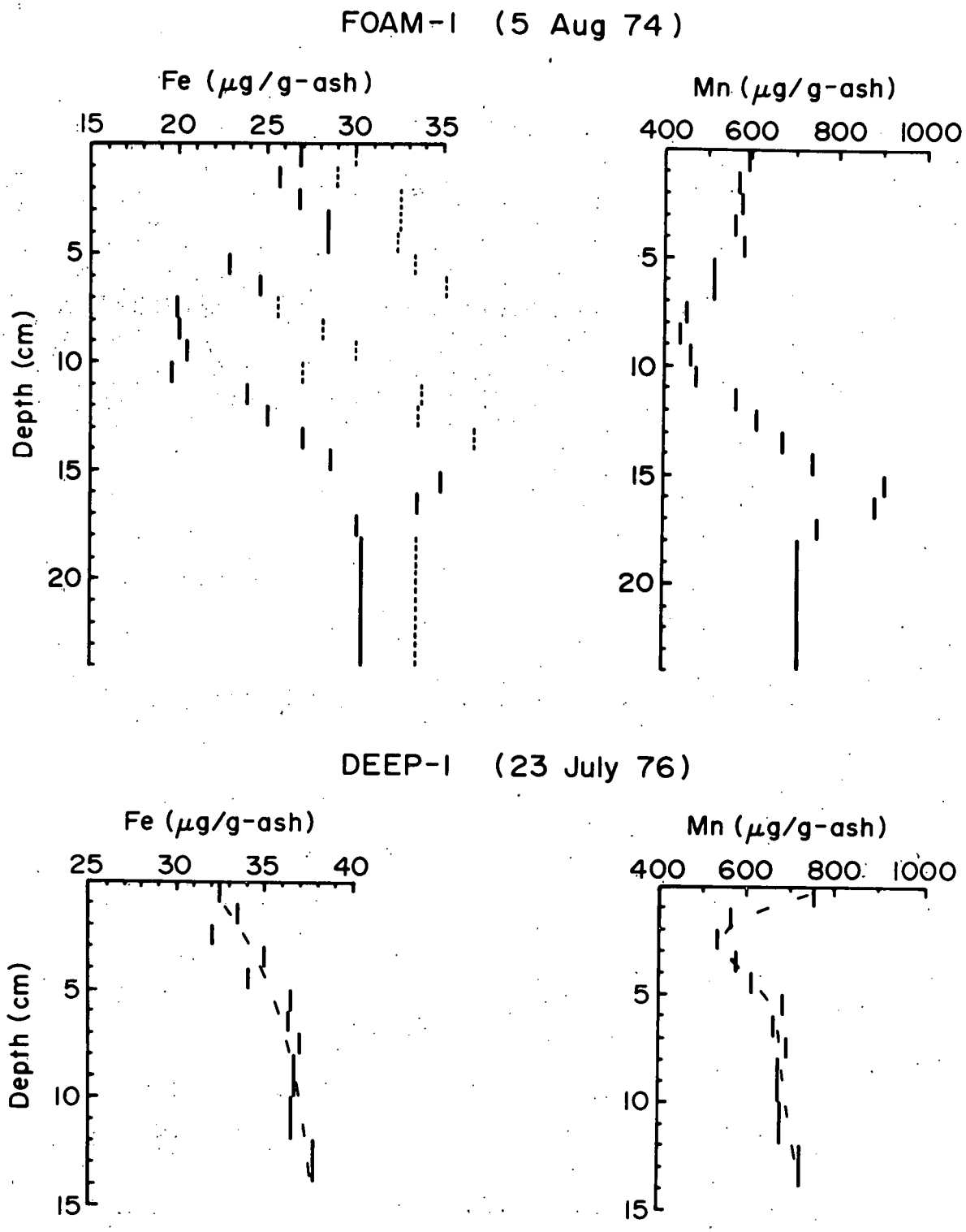

FOAM-1 (5 Aug 74)
Fe (μg/g-ash)
15 20 25 30 35
Mn (μg/g-ash)
400 600 800 1000
Depth (cm)
5
10
15
20
DEEP-1 (23 July 76)
Fe (μg/g-ash)
25 30 35 40
Mn (μg/g-ash)
400 600 800 1000
Depth (cm)
5
10
15

Figure VI-9

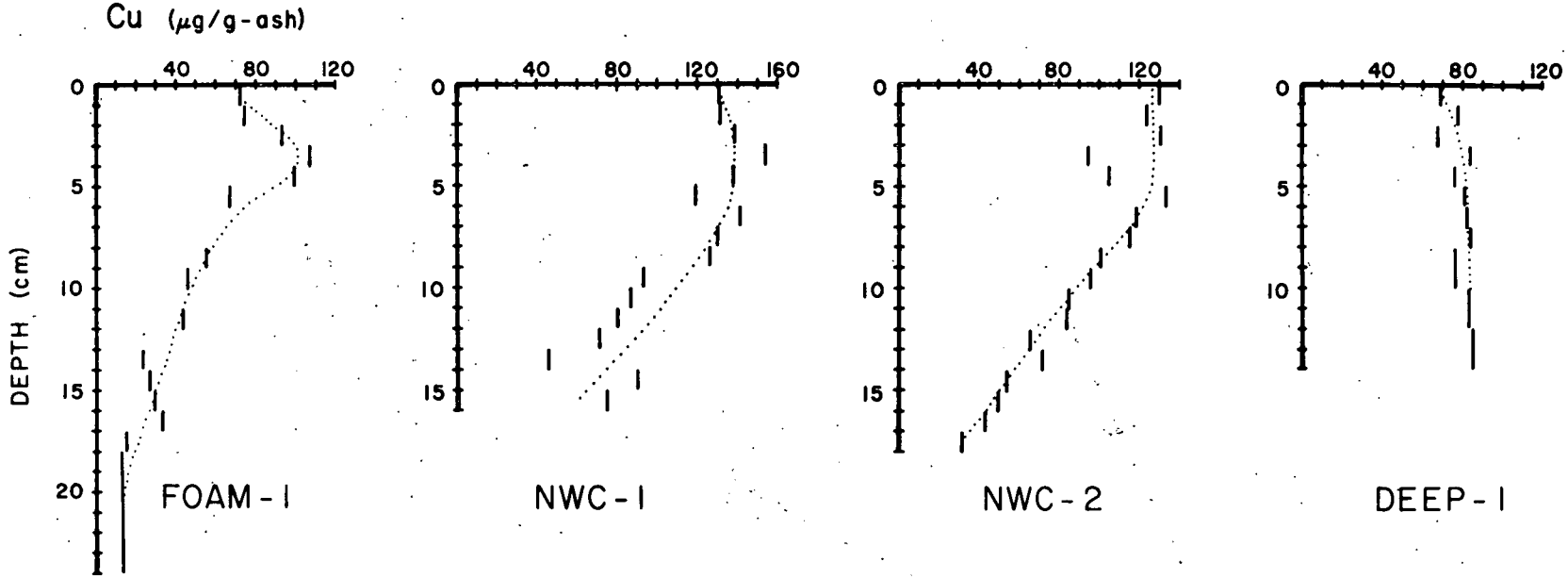


Figure VI-10

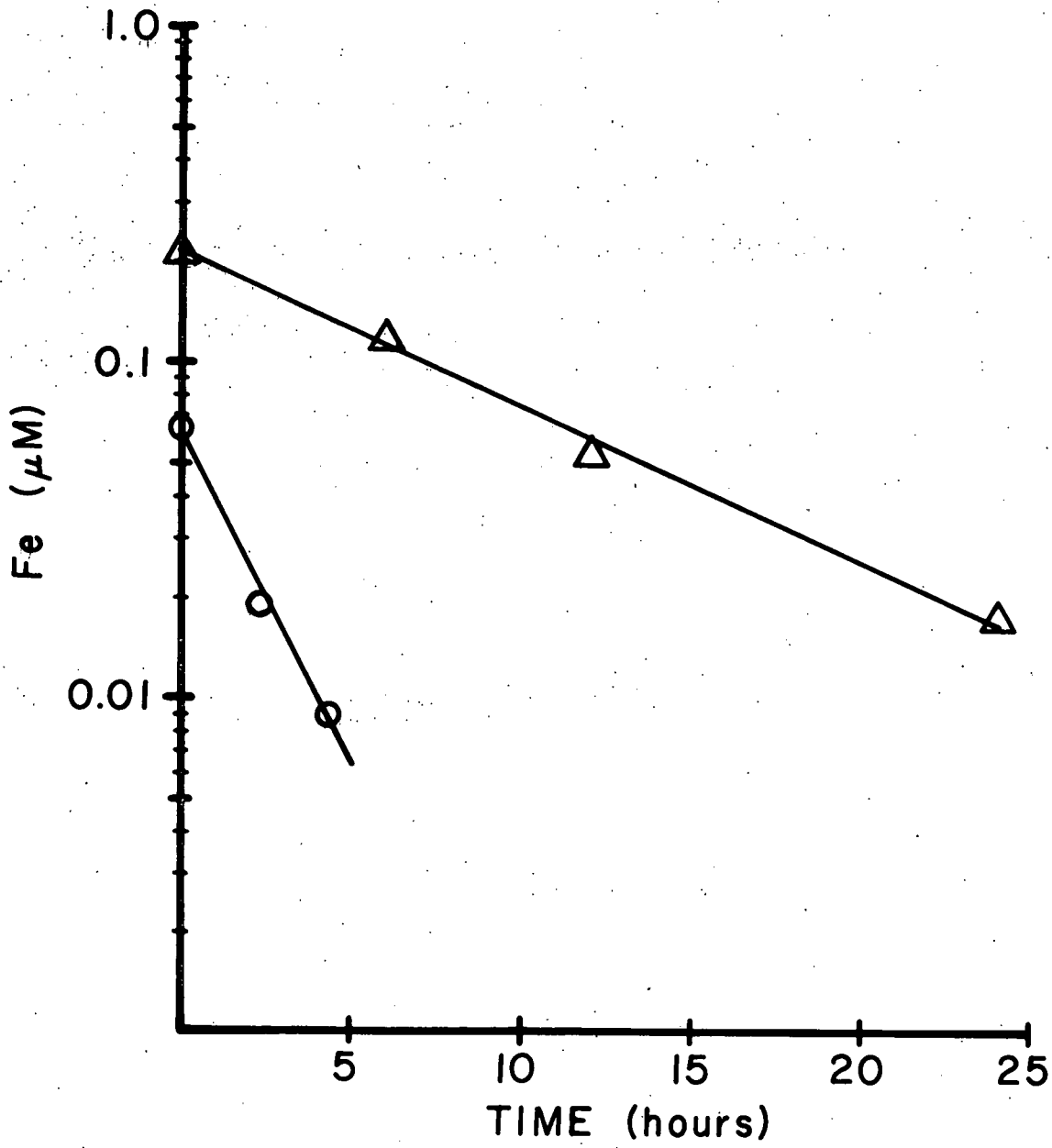
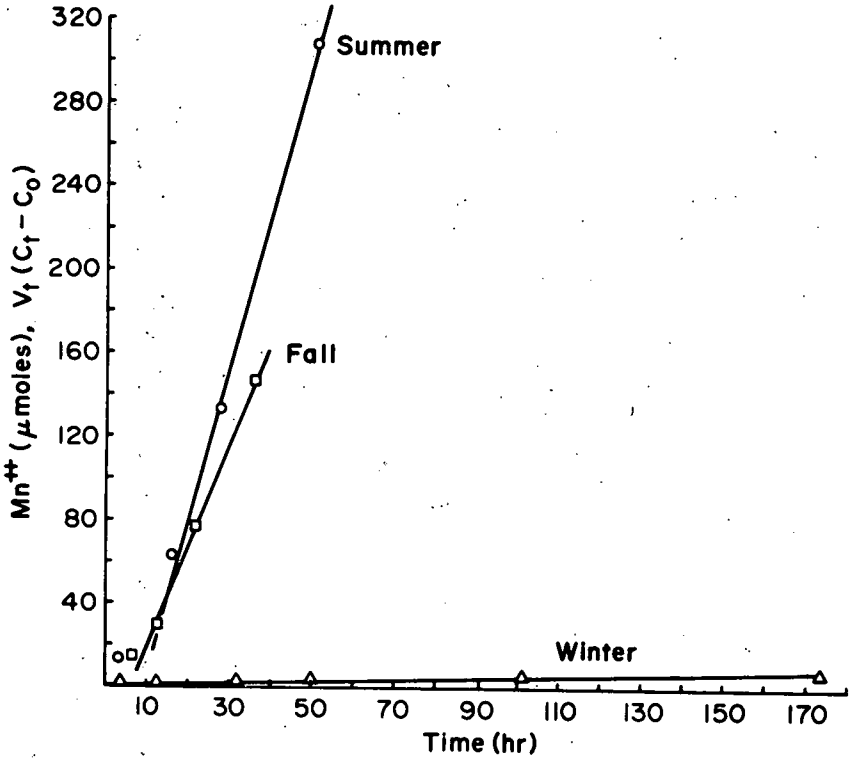


Figure VI-11


320
280
240
200
160
120
80
40
Mn++ (μmoles), Vf (Cf – Co)
Summer
Fall
Winter
10
30
50
70
90
110
130
150
170
Time (hr)

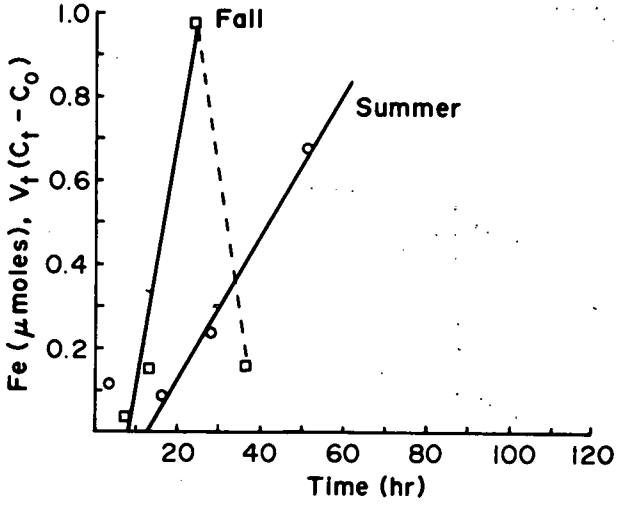

1.0
0.8
0.6
0.4
0.2
Fe (μmoles), Vf (Cf – Co)
Fall
Summer
20
40
60
80
100
120
Time (hr)

Figure VI-12

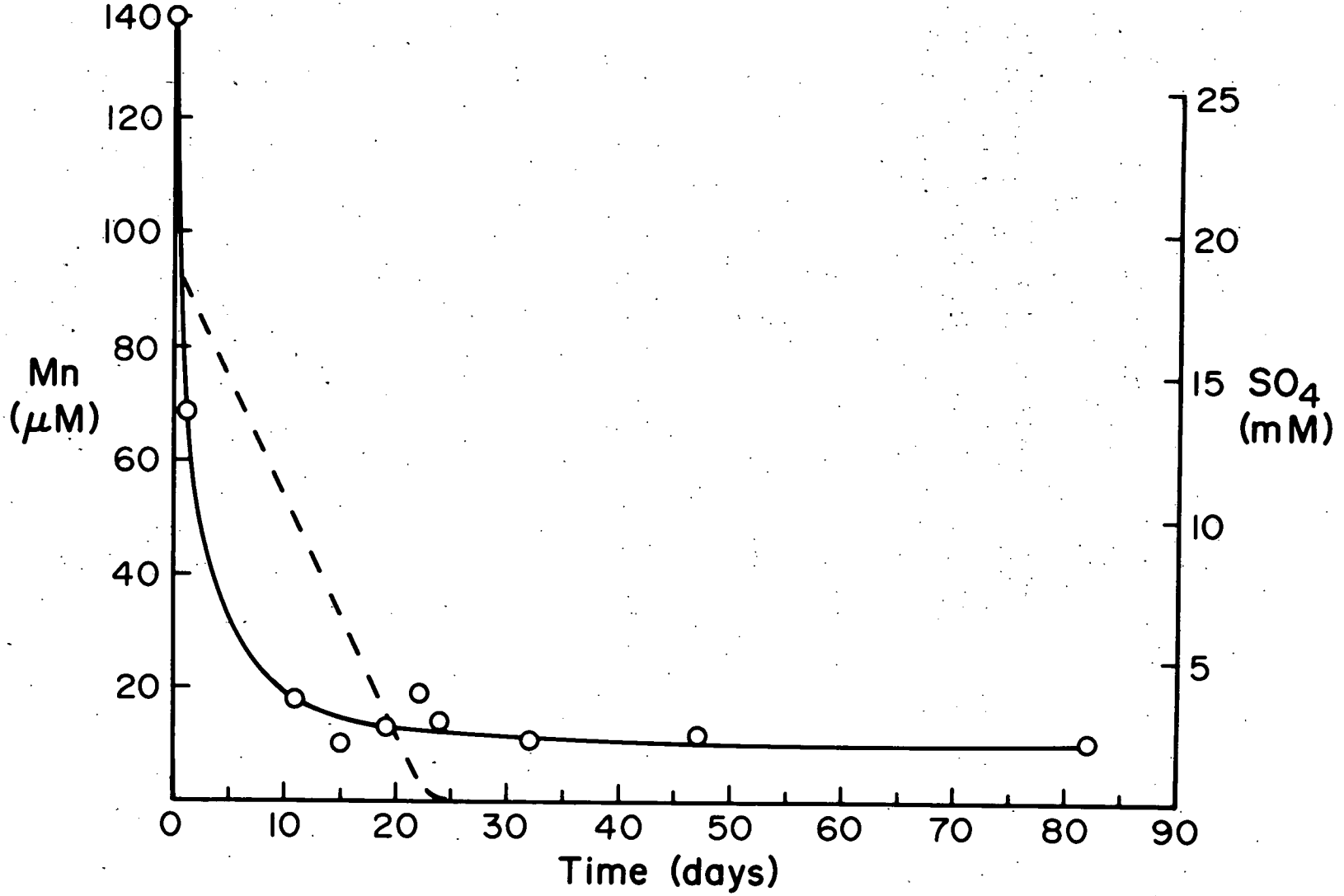

140
120
100
80
60
40
20
Mn
(μM)
25
20
15
10
5
SO4
(mM)
0
10
20
30
40
50
60
70
80
90
Time (days)

Figure VI-13

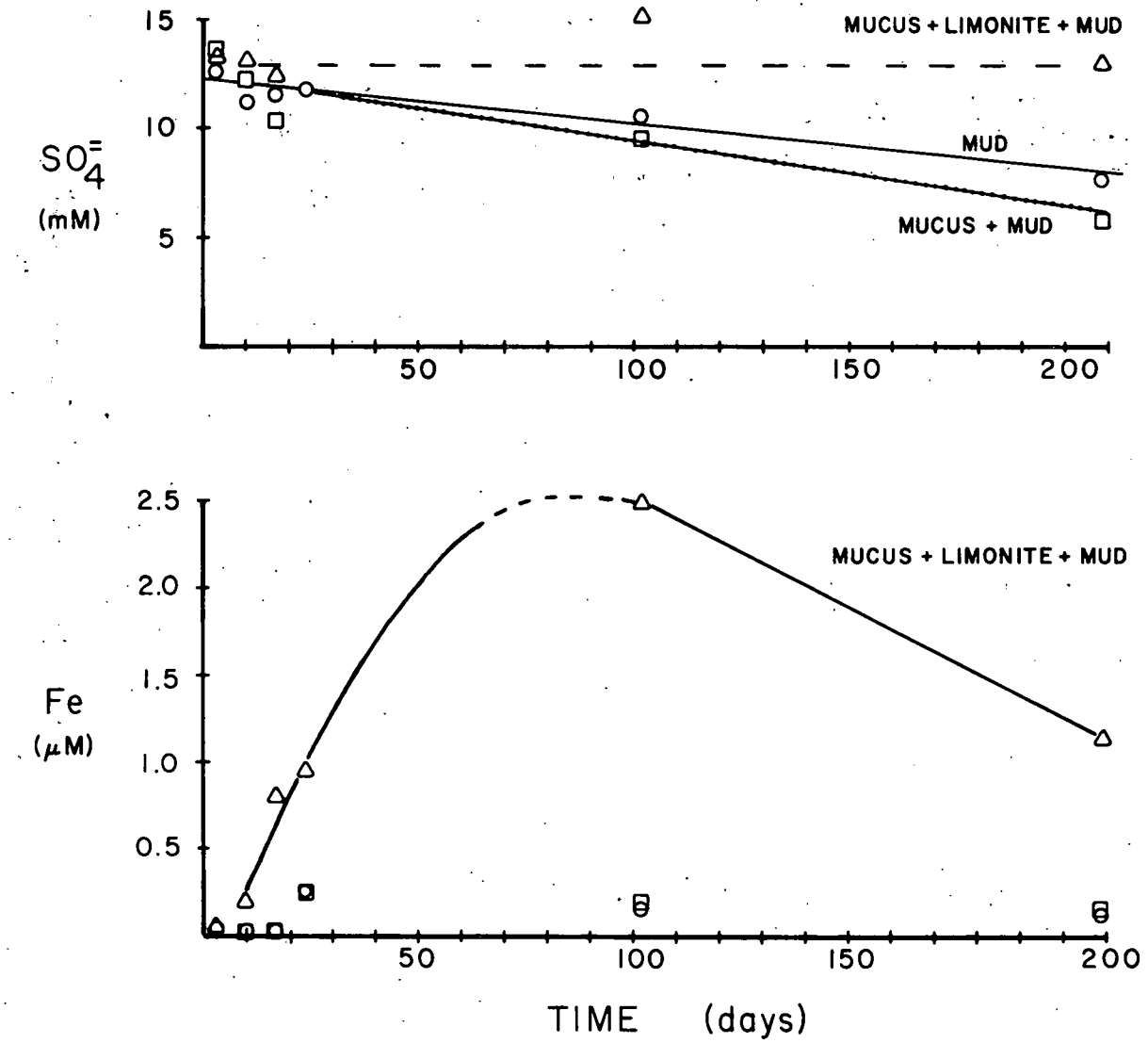

15
10
5
$SO_4^=$
(mM)
MUCUS + LIMONITE + MUD
MUD
MUCUS + MUD
50
100
150
200
2.5
2.0
1.5
1.0
0.5
Fe
(μM)
MUCUS + LIMONITE + MUD
50
100
150
200
TIME (days)

Figure VI-14

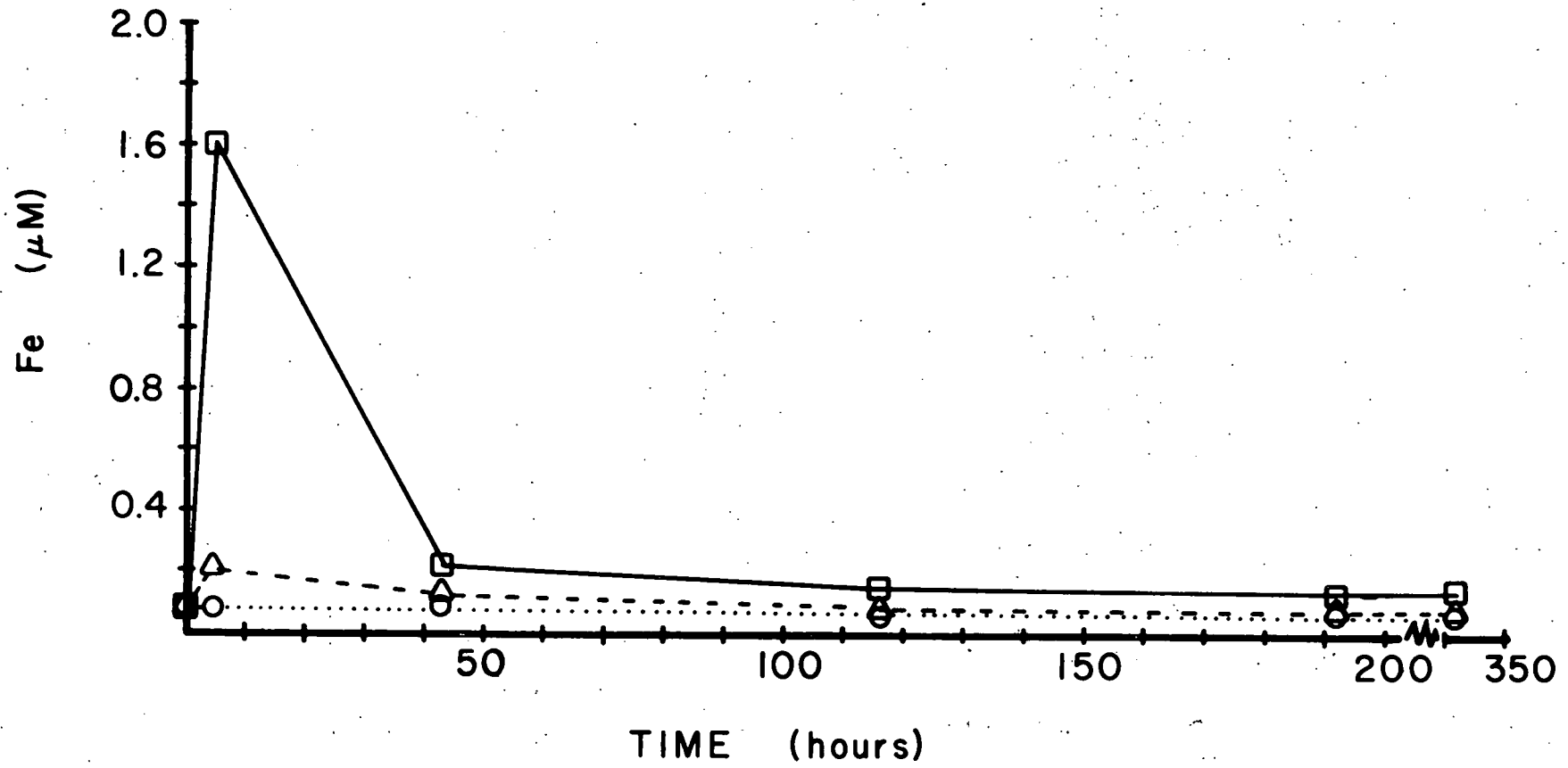


Figure VI-15

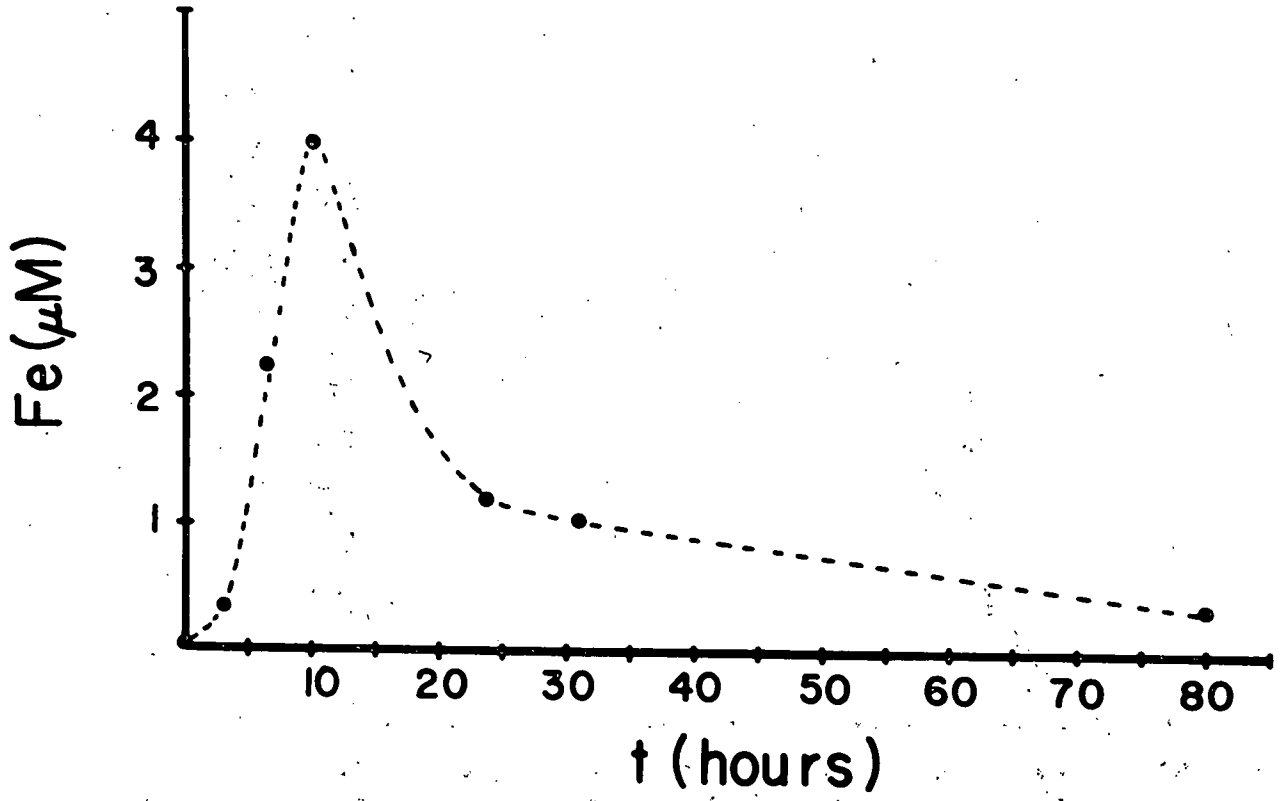


Figure VI-16

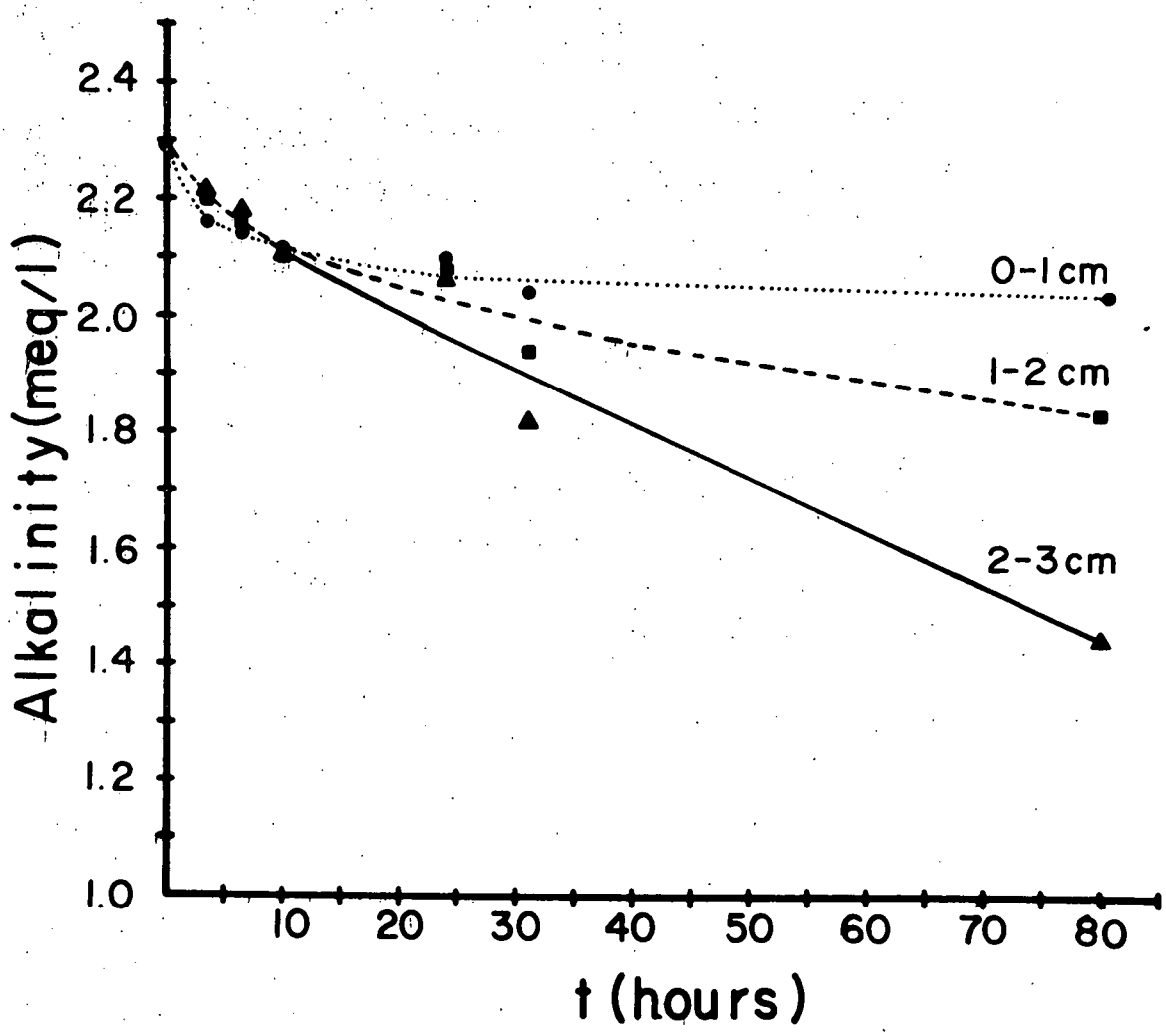

Alkalinity (meq/l)
2.4
2.2
2.0
1.8
1.6
1.4
1.2
1.0
10
20
30
40
50
60
70
80
t (hours)
0-1 cm
1-2 cm
2-3 cm

Figure VI-17

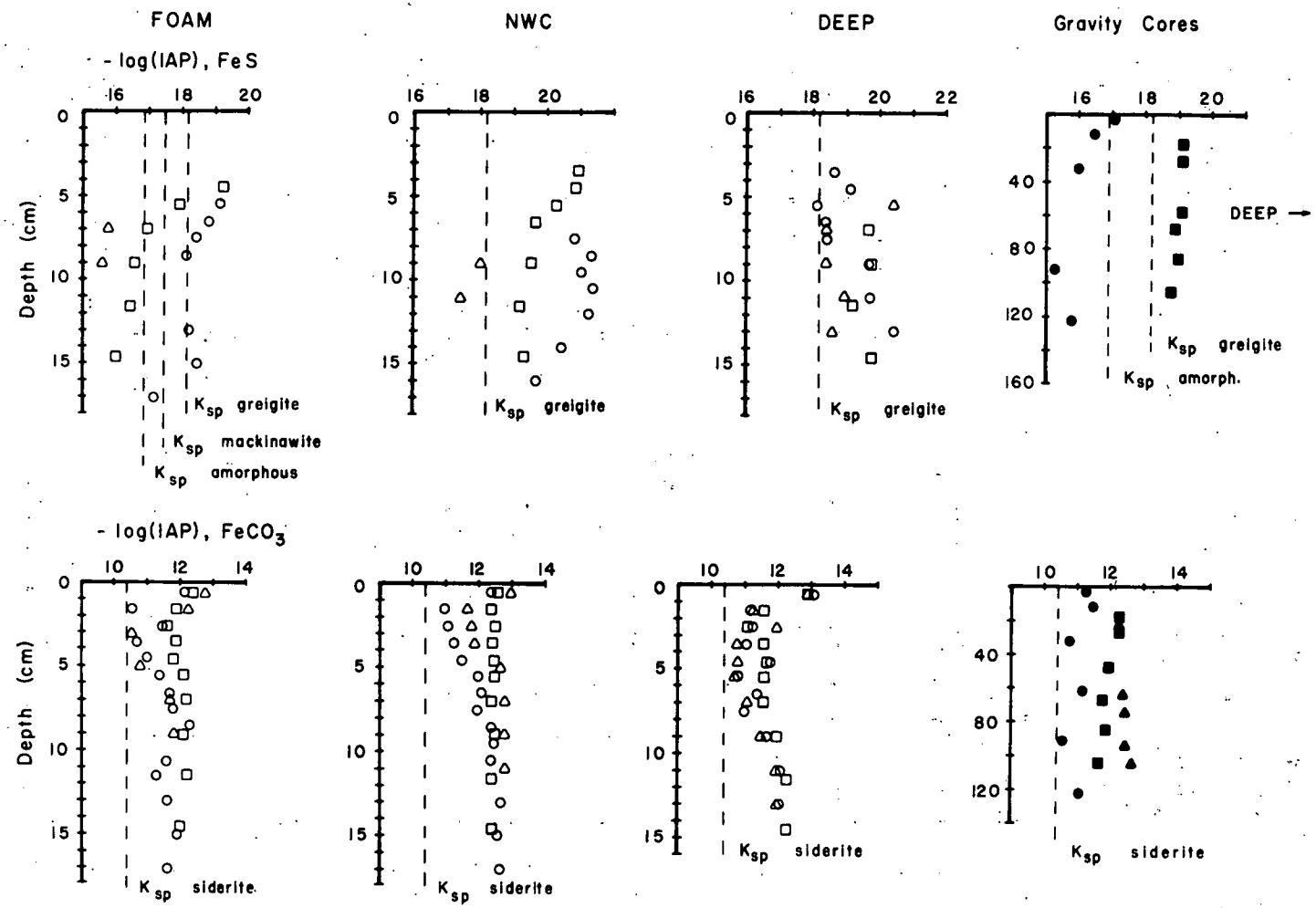

FOAM
NWC
DEEP
Gravity Cores
- log(IAP), FeS
Depth (cm)
Ksp greigite
Ksp mackinawite
Ksp amorphous
DEEP
Ksp greigite
Ksp amorph.
- log(IAP), FeCO3
Ksp siderite

Figure VI-18

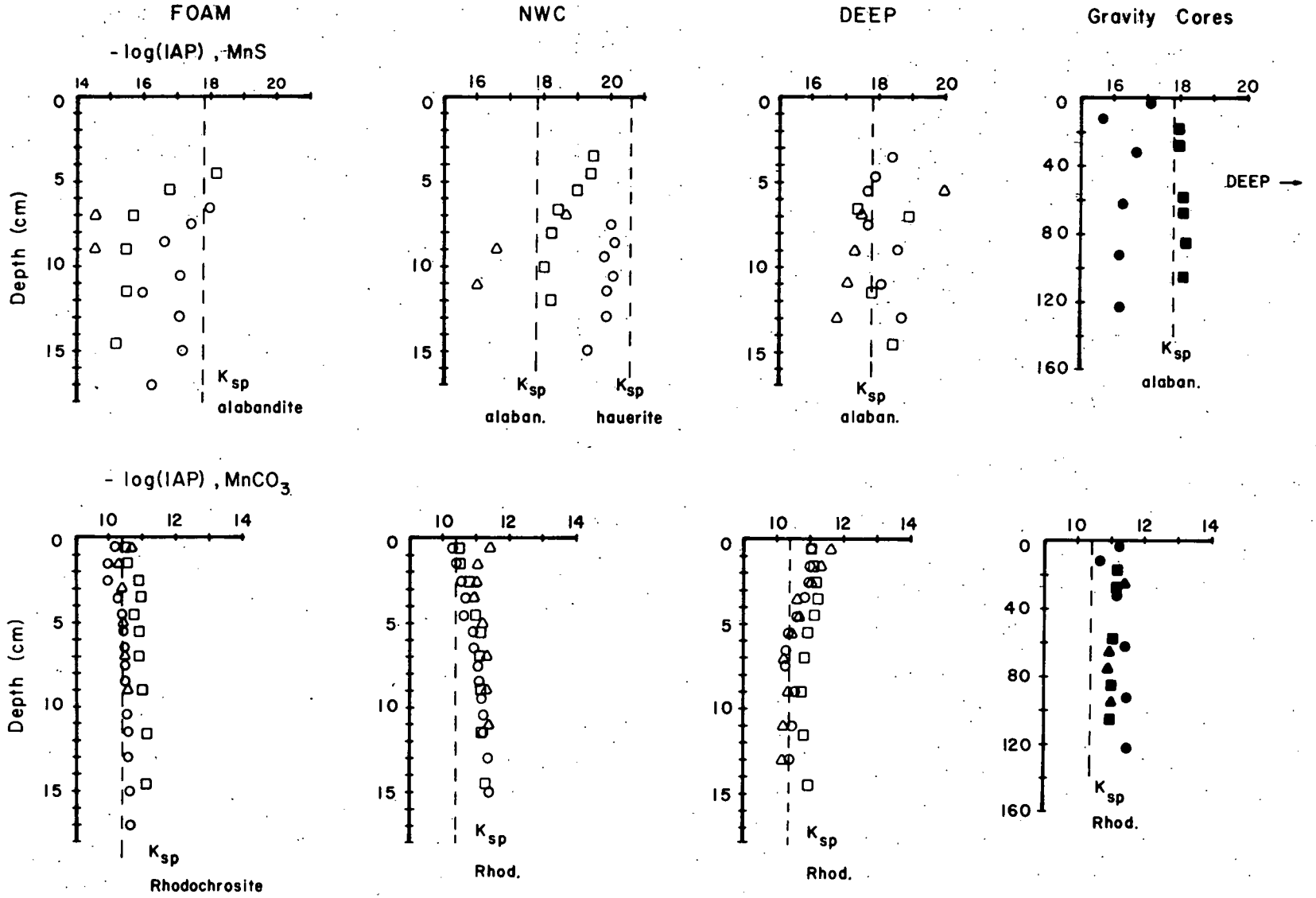

FOAM
NWC
DEEP
Gravity Cores
- log(IAP) , MnS
Depth (cm)
K sp
alabandite
alaban.
hauerite
DEEP
- log(IAP) , MnCO3
Rhodochrosite
Rhod.

Figure VI-19

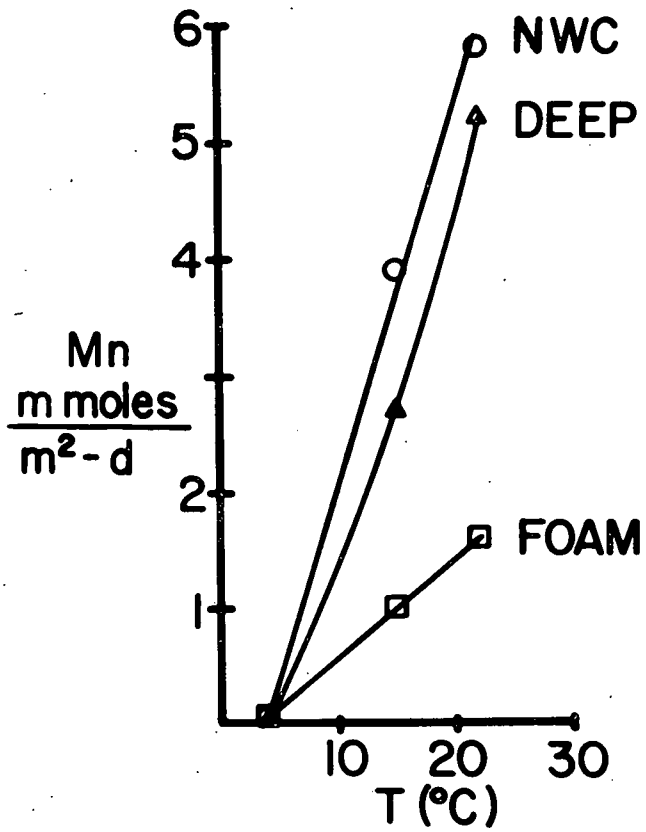


Figure VI-20

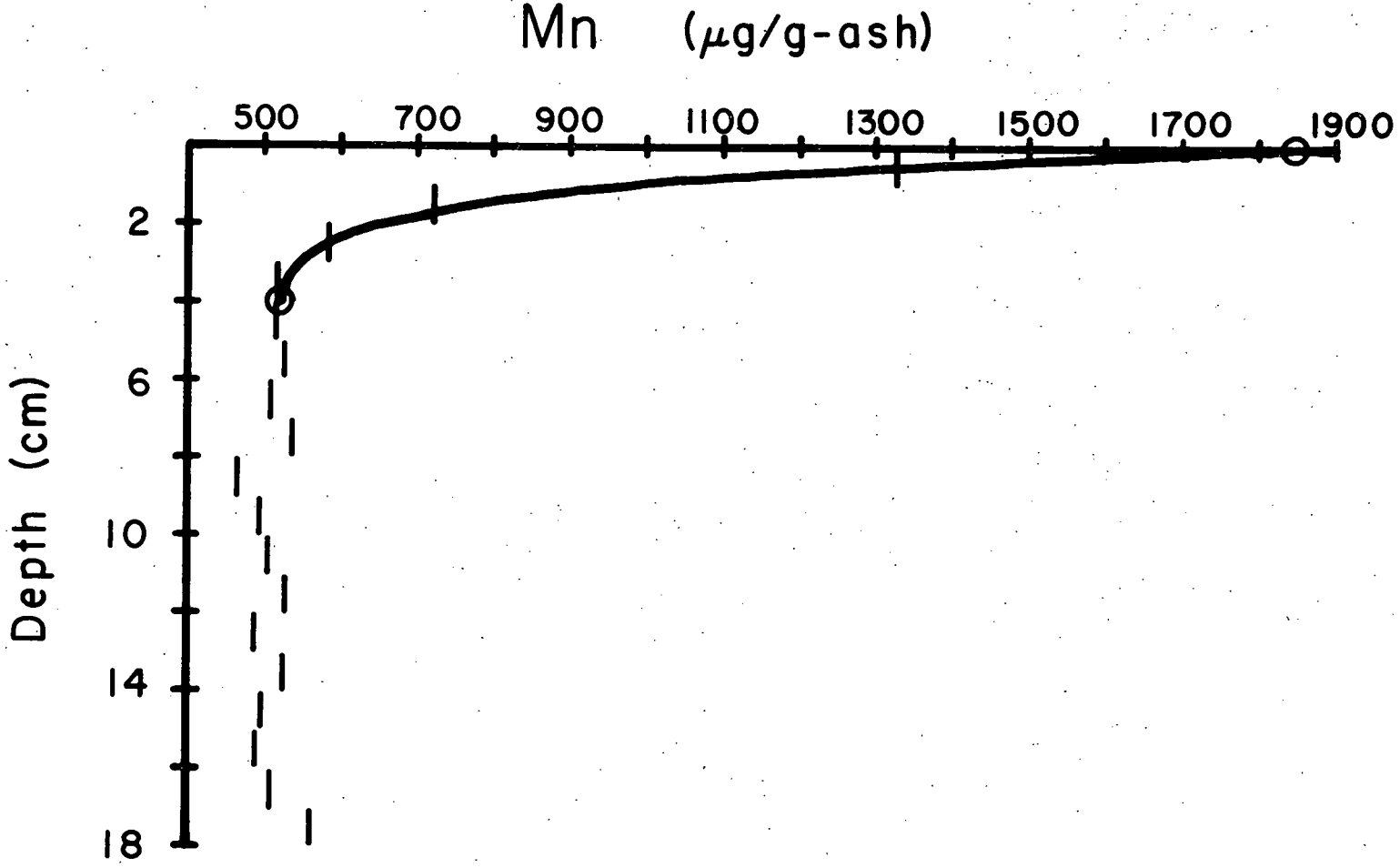

Mn (μg/g-ash)
500
700
900
1100
1300
1500
1700
1900
2
6
10
14
18
Depth (cm)

Figure VI-21

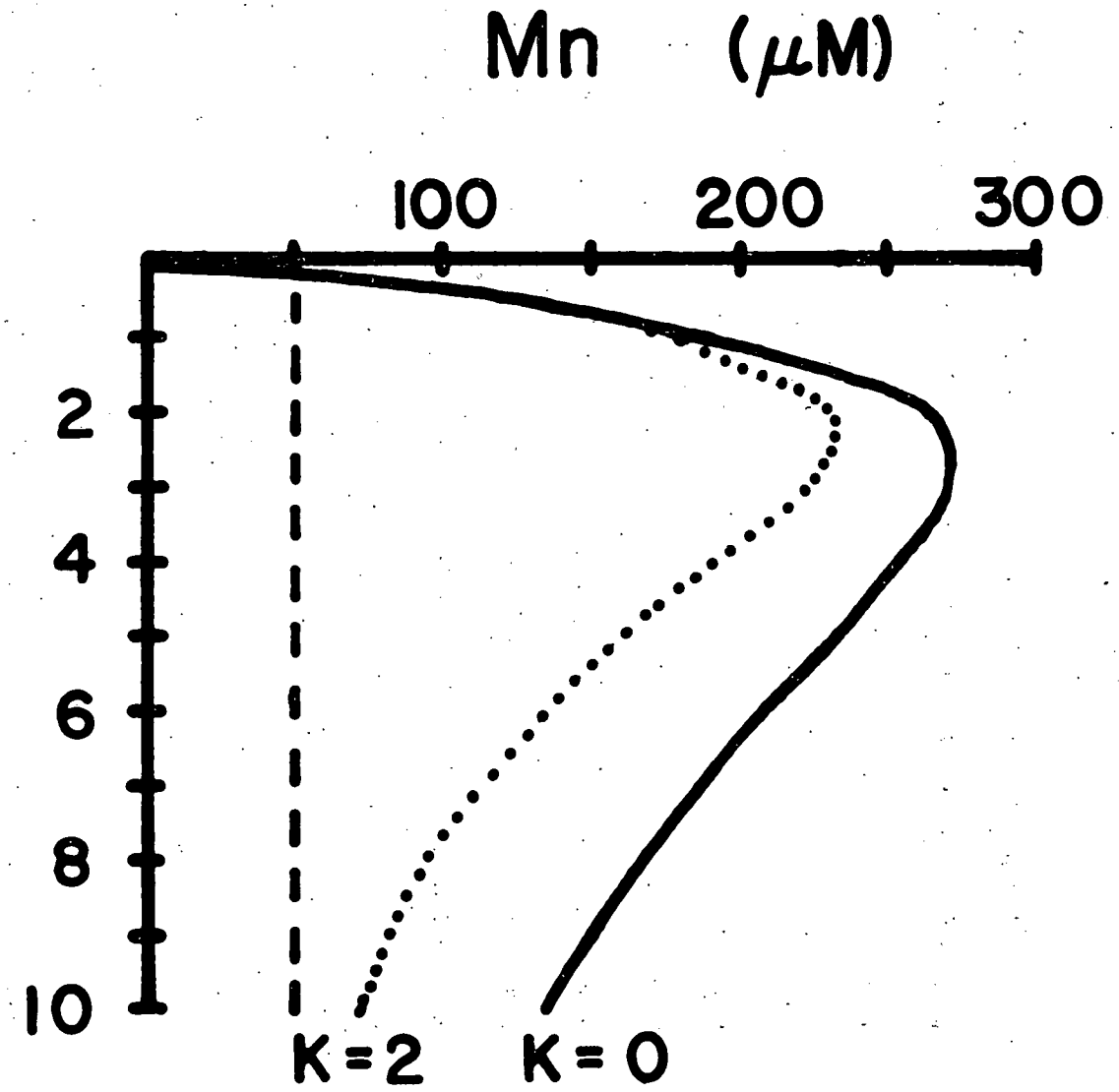


Figure VI-22

APPENDIX I

DESIGN AND USE OF DIVER-TAKEN BOX CORERS

The box corers designed and used during this study are constructed of clear acrylic plastic (Rohm and Haas "Plexiglas"). This material is relatively inert, rugged, lightweight, and transparent both to light and x-rays. The general design of the box corers is shown in Figure AI-1. Five types of hand-held box corers have been used, dimensions varying according to the data being collected. Four of the corers are described in Figure AI-1 and Table AI-1. The first three corers listed are used for routine x-ray study of sedimentary structures, geochemical analysis, and flux measurements; the largest corer is used for sampling burrows or simply large quantities of material. The fifth corer is of the same dimensions as the large corer but one of its longer sides is composed of independently removable 2.5 cm high slats. This latter corer was used to obtain horizontal x-ray slabs by pushing plexiglas trays horizontally into it through the slatted sides to obtain samples.

As shown in Figure AI-1, the bottom of the boxes are open with edges bevelled and sharpened to facilitate coring. In taking a sample, the diver pushes the box corer gently into the sediment to a depth of 10-25 cm.

The vent holes in the top then are plugged. Next, sediment on one side of the corer is scooped away by hand and the watertight base plate is slid into place underneath the box. The corer is then lifted out of the sediment while holding the base plate in place. Rubber straps are looped under the base plate and over the top of the box to secure the base plate and the sample is brought to the surface. Because each core box is watertight and is filled with sediment plus initial overlying water, careful transport of the core does not normally disturb the interface.

The x-ray corer described here collects a vertical section of the bottom 10-25 cm deep and 2.5 cm thick; similar samplers have been used since 1968 to study biogenic and other sedimentary structures (Rhoads and Young, 1970; Stanley, 1970). Radiography is done by placing a 20 x 25 cm or larger sheet of x-ray film (Kodak "AA Industrial") against one side of the core box and exposing it through the sediment, at 60 kv for periods of 2.5 to 3.5 min at a distance of 80 cm. X-radiographs of laminated sediments show that the coring process produces only slight distortion of laminae near the edges of the box. This demonstrates minimal disturbance of the sample by this coring method. If the core is radiographed within a few hours of collection many animals can be observed in life position (Aller and Cochran, 1976).

Chemical corers are used for studying interstitial water and sediment chemistry. They are also readily placed in aquaria where animals found in a core may be observed in their undisturbed life positions. For chemical

analysis of reduced sedimentary compounds, cores are placed into an anoxic (e.g., N_2) atmosphere such as that provided by a glove bag. The top of the box is removable so that once placed in an anoxic atmosphere the core is easily sampled for squeezing or centrifugation of pore water.

The undisturbed nature of the samples obtained by these boxes permits the study of fluxes of material between the sediment and the overlying water. A larger box than used for sediment chemistry (Table AI-1) is used in order that serial sampling of water overlying the core can be made and that a relatively large area of bottom is sampled.

Gaskets for the removable top are made of foam-rubber stripping, weather-stripping, silicone rubber, or neoprene foam. The bottom gasket is made of foam-backed floor covering material (Armstrong "Quiet-Step") glued to the base plate with the foam side exposed. This foam resists abrasion from sediment and the sharpened corer edge. The guide strip is then glued to the foam. Silicone sealant (Dow-Corning "Silastic") is used for cementing gaskets to the plastic. In sandy sediment a thicker, more pliable foam, such as 6.4 mm thick weather-stripping must be used for the base plate gasket for a watertight seal.

Bolts (size 10-32, 3.81 cm long) with wingnuts are used to hold the top plate to the core box. The holes for these bolts are outside of the gasket and are not threaded so that the bolts can be easily removed to prevent metal contamination when cores are stored or placed in an aquarium. Brass,

nylon, or stainless steel bolts can be used. The base plate is held on with large rubber bands or bands cut from a truck-size inner-tube. Rubber stoppers used to plug the vent holes in the top are fastened to the handle with loops of nylon cord.

Appendix I

Table AI-1. Dimensions of Box Corers

Inside Dimensions (cm)			Wall Thickness (mm)	Use
A	B	C		
25.2	29.2	2.5	6.2	x-ray sections
25.2	29.2	7.6	6.2	sediment chemistry
30.5	29.2	10.2	6.2/10.2	flux measurements
30.5	28.1	20.5	10.2	large samples, horizontal x-rays

Appendix I

Figure Caption

Figure AI-1: The hand-held, diver-operated box corer with details of construction. Dimensions A, B, and C for each corer type are given in Table AI-1. Vent holes use size 5 stoppers.

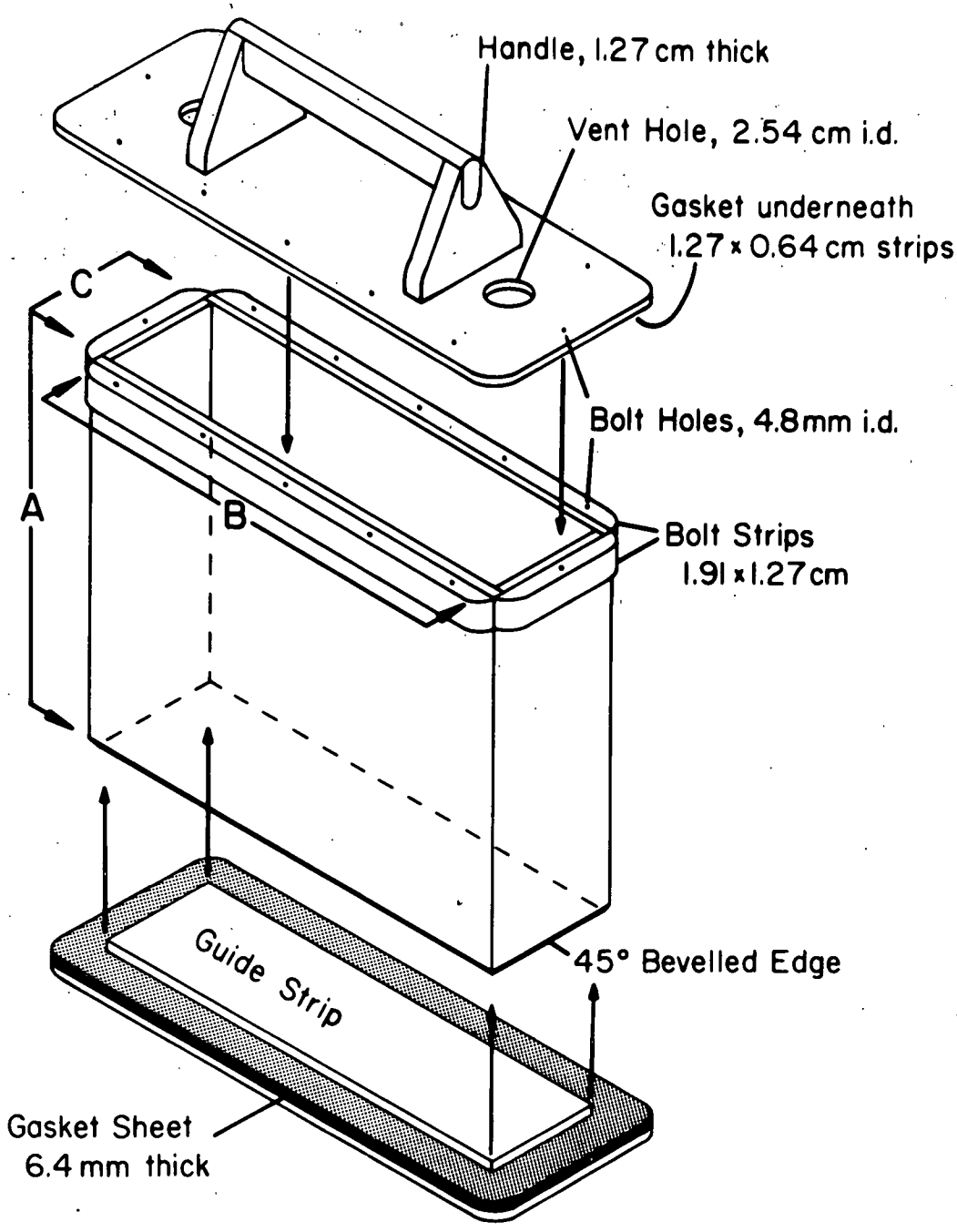

Handle, 1.27 cm thick
Vent Hole, 2.54 cm i.d.
Gasket underneath
1.27 × 0.64 cm strips
C
Bolt Holes, 4.8mm i.d.
A
B
Bolt Strips
1.91 × 1.27 cm
45° Bevelled Edge
Guide Strip
Gasket Sheet
6.4 mm thick

Figure AI-1

APPENDIX II

NOTES ON ANALYTICAL TECHNIQUES

The analytical techniques used in this study are generally adequately described in the text. However, modifications of the leuco-malachite green (LMG) method for determination of Mn (Fernandez, Sobel, and Jacobs, 1963; Strickland and Parsons, 1968) were extensive enough to require further explanation.

The reagents used (acetate buffer, KIO_4, leuco-malachite green) and the procedure followed were the same as those described by Strickland and Parsons (1968) with the following changes:

(1) 20 ml of acetate buffer were added to each sample rather than 15 ml. This insured proper pH when acidified samples were used.

(2) KIO_4 solution was always made-up the same day of use.

(3) Color development was allowed to take place at room temperature rather than in a bath. Absorbance readings were made after 2–6 hours of color development depending on sample salinity.

(4) Rather than a simple single standard addition (i.e., comparison of sample absorbance above blank with sample + standard absorbance), two

standard additions, one of 0.04 μg Mn and one of 0.08 μg Mn were made.

Mn in the sample was calculated as follows.

Let: ΔMn = amount of Mn in smallest standard addition

A_1 = absorbance of sample (above blank)

A_2 = absorbance of sample + ΔMn (above blank)

A_3 = absorbance of sample + $2\Delta Mn$ (above blank)

Setting:

$$x_1 = 0 \qquad y_1 = A_1$$

$$x_2 = \Delta Mn \qquad y_2 = 2A_2 - \frac{1}{2}A_1 - \frac{1}{2}A_3$$

$$x_3 = 2\,\Delta Mn \qquad y_3 = 4A_2 - 2A_1 - A_3$$

Then calculation of the line: $y = a_1x + a_o$ gives the Mn concentration in the sample as: $Mn = -a_o$.

The reason for calculating the concentration in this way instead of letting $y_1 = A_1$, $y_2 = A_2$, $y_3 = A_3$, is that the relation between absorbance versus time of color development is nonlinear. There is a more rapid increase in absorbance at higher Mn concentrations in a given time than at lower concentrations. This means that in general at any time, t, after beginning color development the absorbance is given by:

$$y = a_o + a_1x + a_2x^2 + \ldots$$

rather than the simple linear relation. It was found by many experiments with standards that the coefficient $a_2 \geq 0$. The usual result of assuming that the

relation is linear is to calculate a Mn concentration which is too low (see for example, Delfino and Lee, 1969), that is, the value calculated for a_1 is too large making $|a_o|$ small. If enough standard additions are made, the function, y could be accurately determined and a_o calculated. I compromised by first making ΔMn small and then assumed that the deviation from linearity Δy (i.e., ΔA) was small enough so that $\Delta y \propto \Delta Mn$.

The relations for y_1, y_2, and y_3 were then derived by iteration as follows. Assume first that A_2 and A_1 are related linearly and that only A_3 is too high. The predicted absorbance, A_3', assuming a linear relation between Mn added and absorbance is:

$$(1) \qquad A_3' = \frac{(A_2 - A_1)}{\Delta Mn} 2\Delta Mn + A_1$$

$$= 2A_2 - A_1$$

therefore, $\Delta A_3' = A_3 - A_3'$

Now, since $\Delta A \propto \Delta Mn$, set:

$$\Delta A_2 = \frac{\Delta A_3'}{2}$$

then the corrected absorbance, A_2', is:

$$(2) \qquad A_2' = A_2 - \Delta A_2$$

$$= 2A_2 - \frac{1}{2}A_1 - \frac{1}{2}A_3$$

which is y_2.

Recalculating (iteration) a new corrected A_3'' using A_2' in equation (1) gives:

(3) $$A_3'' = 4A_2' - 2A_1 - A_3$$

which is y_3.

Note that if $a_2 = 0$, i.e., the standard addition is linear, then the correction terms collapse to $y_1 = A_1$, $y_2 = A_2$, $y_3 = A_3$. (What has been approximated is the tangent to the curve y at $\Delta Mn = 0$).

By use of these formulas, good agreement ($\pm$ 5%) between the leuco-malachite green method and other Mn methods: formaldoxime and atomic absorption, is obtained. Otherwise, the LMG method as outlined by Strickland and Parsons tends to give low Mn values.

Contrary to the statement by Strickland and Parsons (1968) that a Fe correction should be made, I have found by experiments with standard rocks (GSP-1) and tap water that when both Mn and Fe are present, no correction is necessary if the internal standard addition method is used. Fe alone will catalyze the oxidation of leuco-malachite green but in the presence of Mn its role is to enhance the catalytic behavior of Mn rather than to simply add to the absorbance as background.

Delfino and Lee (1969) reported that the leuco-malachite green method gave unpredictable results in lake water analyses. I found that if determinations of standards were done in distilled water, the color development was often irregular. Repeatable (predictable) absorbances could be obtained by adding

a small quantity of Fe or 1 ml of Mn-free sea water to the distilled water -Mn standard samples. The reason either of these additions makes color development more regular is unknown.

APPENDIX III

MACROFAUNA (> 1 mm) SIEVED FROM FLUX CORE BOXES

Sediment from flux cores was gently sieved through a 1 mm mesh sieve. The residue remaining on the sieve was stored in formalin (rose bengal added) for a few days after which it was transferred into ethanol or isopropanol (rose bengal added) solutions. Samples were picked for macrofauna and the animals sorted and identified. Data are reported in Table AIII-1 for the five cores analyzed in this way.

Table AIII-1 - Faunal Samples (≥ 1 mm)

SAMPLE:	FOAM Flux Box 17 Nov 1975		FOAM Flux Box 19 Mar 1976		NWC Flux Box 23 Mar 1976		DEEP Flux Box 12 Nov 1975		DEEP Flux Box 14 Apr 1976	
Species	No./ sample	No./m^2	No./ sample	No./m^2	No./ sample	No./m^2	No./ sample	No./m^2	No./ sample	No./m^2
Bivalvia:										
Mulinia lateralis	8	269	1	34	-	-	20 (<2 mm)	672	11	369
Pitar Morrhuana	-	-	-	-	-	-	8	269	7	235
Tellina agilis	3	101	1	34	-	-	-	-	-	-
Macoma tenta	1	34	1	34	1	34	2	67	-	-
Nucula annulata	4	134	-	-	-	-	1 (∿1 mm)	34	-	-
Yoldia limatula	-	-	1	34	8	269	-	-	-	-
Gastropoda:										
Nassarius trivitatus	1	34	1	34	-	-	-	-	-	-
Retusa sp.	1	34	-	-	-	-	-	-	-	-
Polychaeta:										
Spiochaetopterus oculatus	-	-	1	34	-	-	-	-	1	34
Pherusa affinis	-	-	-	-	-	-	7 (large)	235	4 (large)	134
Pista palmata	-	-	-	-	-	-	-	-	1	34
Melinna cristata	-	-	-	-	-	-	2	67	-	-
Clymenella sp.	8	269	4	134	-	-	3	101	-	-
Nephtys incisa	1	34	4	134	7	235	5	168	3	101
Sigambra tentaculata	-	-	-	-	-	-	1	34	-	-
Phyllodoce sp.	1	34	-	-	-	-	-	-	-	-

Table AIII-1 - Faunal samples (≥ 1 mm) (continued)

SAMPLE:	FOAM Flux Box 17 Nov 1975		FOAM Flux Box 19 Mar 1976		NWC Flux Box 23 Mar 1976		DEEP Flux Box 12 Nov 1975		DEEP Flux Box 14 Apr 1976	
Species	No./ sample	No./m^2	No./ sample	No./m^2	No./ sample	No./m^2	No./ sample	No./m^2	No./ sample	No./m^2
Crustacea:										
Ampelisca sp.	72	2417	1	34	-	-	-	-	-	-
Pagurus sp.	-	-	1	34	-	-	-	-	-	-
Cumacean A.	1	34	-	-	-	-	-	-	-	-
Ostracoda A.	1	34	-	-	-	-	-	-	-	-
Hydrozoa:										
Corymorpha pendula	-	-	-	-	-	-	-	-	2	67

NH_4^+ (Kjeldahl): J. K. Rosenfeld (FOAM-2)

NO_3^-: J. K. Rosenfeld

$CaCO_3$: M. B. Goldhaber (FOAM-1)

B. Brockett (DEEP-1)

FeS: M. B. Goldhaber, A. Ruggiero (FOAM-1)

Cu, FeS_2: M. B. Goldhaber (FOAM-1)

For the sake of completeness, data for FOAM-1 and FOAM-2 published in Goldhaber et al., 1977 is also listed here.

APPENDIX IV

BOX CORE AND GRAVITY CORE DATA FROM LONG ISLAND SOUND

Symbols:

meq/l = milliequivalents/liter

M = moles/liter

mM = millimoles/liter

μM = micromoles/liter

μm = micromoles

g = gram; in the case of solid phase metal analyses this is grams of ash where ash refers to residue from ignited sample (organic free)

( ) = refers to questionable analysis

Additional Analysts:

$SO_4^=$: M. B. Goldhaber, A. Ruggiero (FOAM-1, NWC-1, NWC-2)
J. K. Rosenfeld (FOAM-2, FOAM-G)

Alkalinity: M. B. Goldhaber (FOAM-1, NWC-1)

H_2S: M. B. Goldhaber (FOAM-1)

Table AIV-1

BOX CORE: FOAM-1; August 5,1974; T = ∿ 20°

	Pore water						Solid Phase						
Depth (cm)	$\Sigma.H_2S$ (μM)	$SO_4^=$ (mM)	Alk (meq/l)	$HPO_4^=$ (μM)	Mn (μM)	Fe (μM)	Organic matter (%)	$CaCO_3$ (%)	S-FeS (μm/g)	S-FeS_2 (μm/g)	Fe (mg/g)	Mn (μg/g)	Cu* (μg/g)
0-1	-	20.9	5.8	161	237	35.3	4.17	10.3	7.5	90	28.0	599	64.5
1-2	-	19.6	6.6	243	174	40.1	3.87	11.1	11	110	25.8	573	65.7
2-3	-	20.6	6.7	207	136	15	3.46	17.8	8.1	180	26.9	581	74.0
3-4	-	20.8	6.6	204	98.8	2.3	3,44	12.5	12	200	28.5	567	96.2
4-5	-	20.2	6.3	193	87.7	6.8	3.22	10.8	23	190	28.5	588	88.9
5-6	-	20.9	8.5	160	40.2	1.8	3.24	31.6	20	170	22.9	520	45.9
6-7	-	20.9	6.9	157	76.2	4.8	3.39	(30)	18	180	24.7	518	-
7-8	22	20.9	7.9		37.7	2.3	2.79	22.2	13	170	20.0	455	-
8-9	63	(13.9)	8.2		22.0	2.3	2.62	29.0	11	180	20.1	440	39.3
9-10	91	19.7	8.9		18.6	1.8	2.57	31.5	12	180	20.6	465	31.3
10-11	87	17.7	9.5		15	2.3	3.05	27.4	11		19.7	477	-
11-12	75	18.7	9.6	230	16	1.6	3.28	29.1	7.2	170	24.0	569	29.4
12-13	73	18.6	10.2	168	12	2.7	3.07	25.2	8.4	210	25.2	614	-
13-14	131	18.7	10.3		14	2.1	3.10	26.3	6.6	260	27.2	671	17.2
14-15		20.0	10.0	181	13	1.9	3.25	23.4	7.2	310	28.7	747	20.0
15-16		17.4	11.0	235	8.2	2.9	4.78	19.6	10	343	35.0	906	24.0
16-17	143	15.8	11.7	243	11	4.1	4.89	14.4	10	381	33.7	885	27.6
17-18	134	17.0	11.7	217	11	2.7	3.66	12.4	10	334	30.2	757	13.6
18-24	287	15.2	12.8	223	11	3.2	3.53	9.6	7.5	340	30.5	711	11.7

*Cu analyses of 1.0N HNO_3 leach, Fe and Mn are from 12N HCl leach.

Table AIV-2

BOX CORE: FOAM-2; T = 3.0 - 3.5°C

Depth (cm)	Pore water H_2O (%)	pH	$H_2S^{\dagger}$	$SO_4^{=}$ (mM)	NH_4^{+} (μM)	NH_4^{+*} (μM)	$HPO_4^{=}$ (μM)	Mn (μM)	Fe (μM)	Alk (meq/l)
0-1	56.4	7.36		22.8	71.2	84	12.6	59.0	3.85	3.47
1-2	50.2	7.17		22.2	124	135	52	204	278	4.25
2-3	49.8	7.09		22.4	181	240	65	193	385	4.96
3-4	50.9	7.00		22.1	245	264	91	185	743	5.16
4-5	54.7	6.92		21.7	322	283	151	262	1022	6.31
5-6	53.9	6.96		21.1	361	328	258	286	363	7.39
6-7	39.6	7.14		-	442	407	309	249	170	7.43
7-8	38.5	7.33		19.5	453	514	231	221	24.9	8.24
8-9	37.5	7.45		19.7	542	530	308	155	5.4	9.00
9-10	38.7	7.55		19.1	590	652	294	142	11	9.51
10-11	36.9	7.53		18.6	631	628	288	122	16	9.95

* NH_4^{+} analysis on 5 ml samples by J. Rosenfeld using Kjeldahl distillation, good correspondence with phenol-hypochlorite method (0.1-0.2 ml) is found.

† H_2S detectable by smell below 9 cm.

Table AIV-3

BOX CORE: FOAM-3; July 8, 1975; T = 18°C

	Pore water										
Depth (cm)	H_2O (%)	pH	Eh (mv)	Cl^- (M)	$SO_4^=$ (mM)	Alk (meq/l)	NH_4^+ (μM)	NO_3^* (μM)	$HPO_4^=$ (μM)	Mn (μM)	Fe (μM)
0-1	48.2	7.25	425	0.434	22.2	3.42	145	0.4	13	348	2.5
1-2	42.4	7.47	95	0.434	21.8	3.72	205	0.4	20	322	52.6
2-3	40.8	7.43	75	0.427	21.9	4.06	269	0.4	32	303	(6.5)
3-4	39.9	7.34	105	0.432	21.8	4.48	318	0.4	82	159	42.8
4-5	39.9	7.31	65	0.429	21.6	4.56	331	0.4	80	138	21.7
5-6	41.9	7.27	5	0.434	21.7	5.56	378		124	117	7.3
6-7	43.7	7.30	-100	0.436	20.6	6.00	468		142	94.1	3.8
7-8	45.9	7.34	-115	0.436	21.2	6.07	398		137	85.2	2.3
8-9	45.9	7.39	-140	-	21.0	6.10	439		109	76.4	0.77
9-10	49.2	7.41	-155	0.436	21.1	-	520		127	60.4	0.91
10-11	55.7	7.43	-135	0.437	20.8	7.24	509		159	50.1	2.7
11-12	60.0	7.41	-165	0.436	21.0	6.62	504		100	50.1	6.8
12-14	62.4	7.49	-135	0.438	20.7	7.73	547		159	41.7	2.3
14-16	55.3	7.49	-135	0.440	20.3	7.39	565		149	33.7	1.3
16-18	48.7	7.55	-165	0.437	20.0	8.31	614		163	24.4	2.0
Bottom water:							2.0	1.36	2.8		

* NO_3^- concentration at background for this core.

Table AIV-4

BOX CORE: FOAM-4; November 5, 1975; T = 14-14.5°C

	Pore water											
Depth (cm)	H_2O (%)	pH	pS	Cl^- (M)	Ca^{++} (mM)	$SO_4^=$ (mM)	Alk (meq/l)	NH_4^+ (mM)	NO_3^- (μM)	$HPO_4^=$ (μM)	Mn (μM)	Fe (μM)
0-1	51.6	7.37	-	0.427	7.90	22.7	2.64	71.4	11.8	17	157	1.3
1-2	46.6	7.37	-	0.430	7.93	22.2	2.80	130	2.0	33	135	4.3
2-3	44.8	7.46	-	0.430	7.96	22.4	2.94	133	1.5	45	48.4	6.4
3-4	42.1	7.48	-	0.431	7.96	22.3	2.95	139	0.0	46	35.7	2.9
4-5	41.3	7.49	13.1	0.430	7.87	22.3	3.05	143	-	55	54.6	3.4
5-6	40.8	7.47	11.6	0.429	8.11	22.7	3.03	143	0.0	55.1	47.1	2.0
6-8	40.3	7.43	10.5	0.431	8.14	22.3	3.15	161		55.6	45.5	1.6
8-10	40.6	7.42	10.2	0.432	8.08	22.8	3.11	173		52	38.2	2.0
10-13	49.9	7.35	10.1	0.436	8.14	22.5	3.25	170		48	30.4	2.0
13-16	54.9	7.31	9.8	0.439	8.23	22.1	4.17	296		79	30.4	2.7
Bottom water:								0.3	13.0	1.2		

Table AIV-5

BOX CORE: FOAM-5; March 18, 1976; T = 2.2°C

Depth (cm)	Pore water H_2O (%)	pH	pS	Cl^- (M)	Ca^{++} (mM)	$SO_4^=$ (mM)	Alk (meq/l)	NH_4^+ (μM)	NO_3^- (μM)	$HPO_4^=$ (μM)	Mn (μM)	Fe (μM)
0-1	54.8	7.34	-	0.410	7.90	21.0	3.26	39.6	9.4	16.6	89.3	0.50
1-2	46.2	7.37	-	0.415	8.17	21.6	3.71	79.1	3.2	(6.6)	181	1.3
2-4	41.1	7.25	-	0.422	9.63	21.7	4.56	160	2.2	29.8	164	58.8
4-6	41.2	7.25	16.3	0.428	9.15	21.8	4.82	227	0	77.7	137	38.5
6-8	45.6	7.25	9.7	0.431	9.08	21.4	5.48	302	-	127	109	4.04
8-10	47.3	7.34	9.5	0.432	8.17	21.1	5.78	393	-	180	69.2	2.81
Bottom water								0.1	0.5	0.68		

Table AIV-6

BOX CORE: NWC-1; July 21, 1974; T = 20°C

	Pore water							Solid phase			
Depth (cm)	H_2O (%)	$SO_4^=$ (mM)	Alk (meq/l)	NH_4^+ (μM)	$HPO_4^=$ (μM)	Mn (μM)	Fe (μM)	Organic Matter (%)	Fe (mg/g)	Mn (μg/g)	Cu (μg/g)
0-1	72.8	(16.0)	3.7	190	153	261	13.3	6.32	39.5	929	130
1-2	64.9	23.2	4.5	349	294	189	33.7	6.43	38.5	718	131
2-3	65.4	21.5	4.4	349	235	172	12.1	7.17	39.1	702	138
3-4	66.3	22.3	4.7	392	190	76.8	8.30	7.60	39.8	639	154
4-5	67.7	21.9	4.4	370	144	56.4	4.89	7.72	37.3	588	138
5-6	61.8	(17.2)	4.3	326	135	43.9	3.46	6.03	26.1	566	119
6-7	59.2	(17.1)	3.9	270	87	47.0	3.04	5.92	32.7	627	141
7-8	61.5	21.9	4.0	290	119	44.2	2.94	5.91	38.4	680	130
8-9	65.1	(18.2)	3.7	270	89	31.9	2.13	6.13	38.5	686	126
9-10	64.0	(15.6)	3.7	278	87	30.2	0.82	4.75	33.6	566	93
10-11	55.6	(17.9)	3.8	269	74	23.7	0.66	4.62	35.6	570	87
11-12	55.7	(17.6)	3.7	287	69	29.3	1.88	3.72	35.5	543	80
12-13	54.1	(17.7)	3.6	277	67	25.7	0.82	3.76	35.8	568	71
13-14	54.9	21.5	4.0	299	87	34.2	1.83	3.82	36.8	560	46
14-15	54.9	(19.9)	3.8	304	87	33.9	1.15	4.01	35.3	596	90
15-16	55.4	21.0	3.9	289	81	36.2	1.3	4.52	34.3	568	85

Table AIV-7

BOX CORE: NWC-2; November 11, 1974; T = 13.2°

	Pore water								Solid phase						
Depth (cm)	H_2O (%)	pH	$SO_4^=$ (mM)	Alk (meq/l)	NH_4^+ (μM)	$HPO_4^=$ (μM)	Mn (μM)	Fe (μM)	Organic Matter (%)	$CaCO_3$ (%)	S-FeS (μm/g)	S-FeS_2 (μm/g)	Fe (mg/g)	Mn (μg/g)	Cu (μg/g)
0-1	72.7	7.42	22.9	3.16	122	13	193	0.77	6.81	3.82	0.6	80	36.6	1326	130
1-2	66.5	7.47	23.5	3.62	141	28.8	193	1.2	6.79	5.78	9.04	93	36.7	721	123
2-3	62.4	7.35	22.7	3.24	115	43.6	116	9.76	5.97	5.33	13.7	96	34.3	583	130
3-4	56.1	7.40	23.2	3.36	142	55.3	57.7	5.98	4.83	7.05	16.5	104	30.3	518	95
4-5	54.6	7.58	22.9	3.37	145	54.3	40.8	1.1	4.61	7.76	14.0	125	31.5	516	105
5-6	55.2	7.51	23.3	3.32	158	54.8	31.1	2.61	6.24	7.51	9.36	146	31.9	526	133
6-7	52.8	7.51	23.2	3.38	158	55.8	27.1	1.3	4.94	6.69	10.6	168	30.7	509	118
7-8	49.2	7.47	23.4	3.46	164	53.0	30.8	1.9	4.75	6.66			33.1	538	115
8-9	47.1	7.62	23.6	3.32	175	52.7	27.7	1.3	3.87	9.61			28.8	464	101
9-10	49.9	7.55	23.8	3.28	185	50.5	25.5	1.6	4.12	7.34			32.2	494	96
10-11	50.4	7.58	23.5	3.16	195	52.1	14.9	0.73	4.70	8.49			30.8	504	85
11-12	49.7	7.58	23.3	3.19	181	48.7	24.0	1.1	4.80	4.69			33.4	529	84
12-13	51.3	7.57	22.8	3.02	162	42.6	2.4	0.52	4.50	5.89			32.4	489	66
13-14	53.1	7.49	23.3	3.00	184	46.8	15.3	0.84	4.43	4.97			30.4	526	72
14-15	50.9	7.44	23.8	3.04	159	41.5	20.8	0.84	4.16	6.40			33.7	499	54
15-16	54.2	7.47	24.3	3.00	150	39.7	20.6	0.84	3.93	5.71			29.4	489	50
16-17	52.5	7.47	23.8	2.92	146	36.7	19.5	0.97	4.09	4.47			32.0	508	43
17-18	53.6	7.47	23.8	2.98	151	38.3	7.5	0.52	4.42	3.93			34.4	561	32

Table AIV-8

BOX CORE: NWC-3; March 18, 1975; T = 3°C

	Pore water								Solid phase				
Depth (cm)	H_2O (%)	pH	$SO_4^=$ (mM)	Alk (meq/l)	NH_4^+ (μM)	$HPO_4^=$ (μM)	Mn (μM)	Fe (μM)	Organic matter (%)	S-FeS (μm/g)	S-FeS_2 (μm/g)	Fe (mg/g)	Mn (μg/g)
0-1	72.2	7.34	22.4	2.61	34	2.5	35.7	0.48	6.36	0.00	83	38.9	1325
1-2	65.8	7.51	23.0	2.93	78	20	165	16.6	6.48	2.1	79	39.0	860
2-3	63.4	7.55	22.3	3.09	94.2	42	135	19.3	6.48	19.0	103	39.6	763
3-4	61.3	7.49	22.0	3.23	129	63	113	5.9	5.55	23.3	119	36.4	689
4-5	51.6	7.44	22.5	3.29	136	58	86.8	1.8	4.37	15.2	119	30.5	579
5-6	47.1	7.46	22.6	3.31	160	69	63.7	0.97	3.85	8.45	153	31.3	569
6-7	46.6	7.41	22.3	3.39	167	65	50.4	1.1	3.79	5.71	168	31.3	517
7-8	48.6	7.50	22.4	3.41	165	78	47.5	1.1	3.66	4.99	172	31.5	553
8-9	48.4	7.43	22.8	3.44	176	52	52.2	1.2	3.99	3.18	156	30.8	537
9-10	42.9	7.43	22.5	3.55	188	52	26.9	0.57	3.61	1.7	150	25.5	414

Table AIV-9

BOX CORE: NWC-4, July 16, 1975, T = 19°C

	Pore water											Solid phase				
Depth (cm)	H_2O (%)	pH	Eh (mv)	Cl^- (M)	$SO_4^=$ (mM)	Alk (meq/l	NH_4^+ (μM)	NO_3^- (μM)	$HPO_4^=$ (μM)	Mn (μM)	Fe (μM)	Organic matter (%)	S -FeS (μm/g)	S $-FeS_2$ (μm/g)	Fe (mg/g)	Mn (μg/g)
0-1	71.6	7.32	235	0.443	23.2	2.89	160	2.1	26	257	1.4	6.71	0.097	98	39.1	1277
1-2	64.2	7.25	135	0.442	22.3	3.27	182	0.9	72.8	217	33.5	6.31	7.36	98	38.0	823
2-3	62.6	7.29	105	0.438	21.9	3.32	186	0.7	96.8	117	27.8	6.15	16.9	103	36.2	645
3-4	-	7.33	110	0.438	22.1	3.35	203	0.2	102	89.7	13.8	5.72	18.6	113	33.9	597
4-5	55.9	7.27	125	0.438	22.6	3.65	195	0.3	97.3	98.3	9.20	5.63	12.0	165	36.8	601
5-6	54.5	7.27	5	0.438	21.8	3.32	199		82.4	61.9	3.6	5.38	10.1	163	35.6	580
6-7	-	7.27	45	0.437	22.3	3.52	191	0.3	81.9	53.3	2.7	4.88	-	174	34.5	548
7-8	52.7	7.25	-50 ±35	0.437	22.0	3.30	190		57.9	45.0	3.9	4.46	6.86	154	32.3	524
8-9	50.3	7.27	-45	0.437	21.9	3.25	160		52.0	40.0	1.4					
9-10	48.0	7.23	-55	0.436	22.3	3.39	162		51	34.6	1.2					
10-11	-	7.23	-45	0.437	21.6	3.40	173		52	30.6	1.4					
11-12	51.2	7.23	-55	0.436	(19.5)	3.36	155		49	28.0	1.3					
12-14	54.2	7.23	-55	0.437	(19.5)	3.16	156		41	25.5	0.68					
14-16	53.8	7.21	-75	0.438	22.0	3.04	138		38	24.8	1.1					
16-18	54.1	7.19	-105	0.439	22.5	3.01	135		34	-	0.82					
Bottom water:							2.4	1.36	1.6							

Table AIV-10

BOX CORE: NWC-5; October 29, 1975; T = 16.4°C

Depth (cm)	H_2O (%)	pH	pS	Cl^- (M)	Ca^{++} (mM)	$SO_4^=$ (mM)	Alk (meq/l)	NH_4^+ (μM)	NO_3^- (μM)	$HPO_4^=$ (μM)	Mn (μM)	Fe (μM)
	Pore water											
0-1	67.4	7.37	-	0.438	8.26	23.2	2.43	64.9	1.3	6.8	175	0.86
1-2	62.4	7.44	-	0.440	8.41	23.3	2.55	92.2	1.3	14	141	1.4
2-3	58.0	7.44	-	0.440	8.47	22.5	2.60	103	0.5	35	74.6	0.86
3-4	55.3	7.46	14.3	0.440	8.32	22.8	2.63	104	0.7	38	51.0	1.2
4-5	54.1	7.43	14.1	0.440	8.23	22.4	2.76	115		38	41.3	0.91
5-6	54.9	7.43	13.6	0.436	8.35	23.1	2.48	112		26	31.5	1.1
6-8	54.4	7.46	13.0	0.43	8.35	22.7	2.74	111		29	30.9	1.0
8-10	54.8	7.49	12.8	0.443	8.17	22.8	2.58	81.6		20	29.3	0.86
10-13	57.9	7.43	12.5	0.443	8.08	22.8	2.74	104		21	25.3	1.1
13-16	58.6	7.47	12.6	0.446	8.11	22.9	2.79	111		24	19.7	1.0
Bottom water:								0.2	9.8	2.5		

Table AIV-11

BOX CORE: NWC-6; March 23, 1976; T = 3.2°C

	Pore water											
Depth (cm)	H_2O (%)	pH	pS	Cl^- (M)	Ca^{++} (mM)	$SO_4^=$ (mM)	Alk (meq/l)	NH_4^+ (μM)	NO_3^- (μM)	$HPO_4^=$ (μM)	Mn (μM)	Fe (μM)
0-1	68.2	7.11	-	0.416	8.10	21.8	2.39	18.6	5.8	7.0	35.7	0.59
1-2	61.4	7.24	-	0.416	7.90	21.7	2.36	33.4	2.6	12.3	64.4	9.63
2-3	60.0	7.22	-	0.418	8.10	22.1	2.49	42.2	2.4	23.7	65.3	6.99
3-4	58.7	7.31	-	0.419	7.76	22.2	2.56	53.4	0.2	31.2	61.0	5.28
4-6	55.3	7.29	-	0.417	7.62	21.8	2.61	68.9		29.6	37.3	0.92
6-8	56.7	7.30	13.2	0.423	7.83	22.2	2.60	83.4		31.9	27.1	0.68
8-10	57.9	7.31	11.1	0.425	7.62	22.3	2.66	96.5		33.6	25.1	0.55
10-12	54.1	7.29	10.5	0.426	8.10	22.0	2.64	107		35.1	24.2	0.59
Bottom water								0.9	1.0	1.05		

Table AIV-12

BOX CORE: DEEP-1; July 23, 1975; T = 18.5°C

	Pore water										Solid phase						
Depth (cm)	H_2O (%)	pH	Eh (mv)	Cl^- (M)	$SO_4^=$ (mM)	Alk (meq/l)	NH_4^+ (μM)	$HPO_4^=$ (μM)	Mn (μM)	Fe (μM)	Organic matter (%)	$CaCO_3$ (%)	S-FeS (μm/g)	S-FeS_2 (μm/g)	Fe (mg/g)	Mn (μg/g)	Cu (μg/g)
0-1	69.5	6.88	75 ±10	0.446	23.3	2.49	62.9	12	135	0.77	5.37	5.1	0.62	50	32.6	753	68.3
1-2	53.7	6.97	0	0.448	23.1	2.47	95	34	128	54.6	4.98	4.3	4.43	50	33.6	567	77.8
2-3	56.3	7.06	-30 ±40	0.448	22.8	2.65	115	51	109	30.4	5.40	4.6	9.92	53	32.2	532	66.4
3-4	57.5	7.12	-43 ±38	0.449	22.7	2.77	165	26	125	46.2	5.47	3.5	11.0	62	35.1	579	80.4
4-5	56.8	7.37	-83 ±27	0.446	22.7	2.88	144	96	117	4.55	6.19	-	22.7	56	34.2	611	75.4
5-6	55.0	7.33	-100 ±40	0.446	22.9	3.40	160	117	202	48.3	6.25	-	30.7	72	36.6	684	80.3
6-7	55.2	7.31	-108 ±23	0.446	22.4	3.37	150	(19)	231	13.1	5.89	0.0	30.8	115	36.5	663	81.5
7-8	53.7	7.38	-95 ±55	0.448	22.7	3.22	160	121	228	27.9	6.02	-	23.3	100	37.1	696	84.0
8-10	54.4	7.43	-80 ±40	0.448	23.0	2.95	120	39	110	5.44	5.87	-	24.6	112	36.8	677	76.0
10-12	52.2	7.39	-90 ±30	0.447	22.3	3.09	128	77	135	2.5	6.26	2.1	16.0	115	36.7	679	83.0
12-14	49.3	7.35	-70 ±30	0.447	22.5	3.69	123	73	165	2.2	5.89	-	13.9	115	37.9	727	84.7

Table AIV-13

BOX CORE: DEEP-2; November 12, 1975; T = 14°C

	Pore water											
Depth (cm)	H_2O (%)	pH	pS	Cl^- (M)	Ca^{++} (mM)	$SO_4^=$ (mM)	Alk (meq/l)	NH_4^+ (μM)	NO_3^- (μM)	$HPO_4^=$ (μM)	Mn (μM)	Fe (μM)
0-1	70.6	7.05	-	0.441	8.11	23.1	2.29	27.2	3.5	6.9	109	1.0
1-2	59.0	6.96	-	0.441	8.29	23.3	2.32	48.6	2.0	5.7	120	25.2
2-3	58.6	7.00	-	0.441	8.26	23.0	2.56	62.7	1.2	9.6	76.1	66.4
3-4	57.8	7.00	-	0.443	8.26	22.9	2.45	65.0	0.0	17	64.6	19.5
4-5	59.1	7.16	-	0.442	8.08	22.5	2.57	77.7		25.3	59.3	10.7
5-6	57.6	7.33	-	0.441	8.14	22.8	2.98	108		34.9	61.0	7.86
6-8	57.3	7.34	13.9	0.442	8.26	22.7	3.01	111		47.1	70.1	7.54
8-10	54.4	7.43	13.5	0.442	8.17	22.9	3.24	117		47.5	69.7	2.7
10-13	54.3	7.41	12.7	0.442	8.29	22.7	3.20	120		41.7	56.4	1.5
13-16	49.7	7.43	13.2	0.443	8.17	22.6	2.99	127		44.5	46.2	1.5
Bottom water:								0.1	11.0	1.15		

Table AIV-14

BOX CORE: DEEP-3; April 13, 1976; T = 5.8°C

Depth (cm)	Pore water H_2O (%)	pH	pS	Cl^- (M)	Ca^{++} (mM)	$SO_4^=$ (mM)	Alk (meq/l)	NH_4^+ (μM)	$HPO_4^=$ (μM)	Mn (μM)	Fe (μM)
0-1	69.1	7.04	-	0.415	8.03	21.1	2.36	31.3	5.16	27.1	0.87
1-2	63.8	6.91	-	0.418	8.14	22.3	2.21	33.2	8.75	71.4	52.3
2-3	62.6	6.91	-	0.422	8.32	22.0	2.28	52.1	18.5	131	106
3-4	60.5	7.17	-	0.422	8.20	22.4	2.54	72.0	34.6	157	85
4-5	59.3	7.11	-	0.424	8.29	22.0	2.76	86.1	49.4	177	95
5-6	57.7	7.21	15.6	0.431	8.55	22.0	3.36	116	103	249	73.5
6-8	54.3	7.44	12.9	0.423	8.17	21.9	3.58	132	143	187	16.2
8-10	54.5	7.28	12.7	0.423	8.58	22.0	3.88	144	147	190	9.14
10-12	53.6	7.42	12.6	0.430	8.11	22.0	4.06	176	190	198	2.03
12-14	52.5	7.43	12.2	0.431	8.14	22.2	4.12	175	158	202	1.90
Bottom water:								0.7	1.21		

Table AIV-15

GRAVITY CORES: FOAM-G; July 8, 1975; October 14, 1975

Pore water (July 8, 1975)									(October 14, 1975)	
Depth (cm)	pH	Ca^{++} (mM)	$SO_4^{=}$ (mM)	Alk (meq/l)	NH_4^{+} (μM)	$HPO_4^{=}$ (μM)	Mn (μM)	Fe (μM)	Depth (cm)	pS
0-5	7.36	8.26		3.88	0.253	42	18.8	13.3	0-5	11.5
5-10			19.4							
10-15	7.47	7.96		9.04	0.618	156	25.9	2.5	10-15	10.2
15-20			16.9							
20-25		7.59		13.42	0.981	219	15.5	3.4	30-35	10.2
25-30			13.0							
30-35		6.92		19.44	1.15	224	3.5	6.24	60-65	9.7
35-40	↓		10.9							
40-45		6.64		20.86	1.45	215	2.5	3.4	90-95	9.4
45-50			8.8							
50-55		8.85		25.66	1.56	250	3.3	8.2	120-125	9.4
55-60			7.5							
60-65	7.4	6.30		26.12	1.58	234	2.2	2.2		
65-70			4.9							
70-75		6.15		27.58	1.76	219	2.0	2.2		
75-80			3.6							
80-85		6.00		29.28	1.82	242	1.5	4.7		
85-90			2.7							
90-95		5.88		30.58	1.90	239	1.5	6.3		
95-100	↓		1.6							
100-105		5.85		32.74	2.15	245	2.0	2.7		
105-110			0.8							
110-115		5.88		34.0	2.12	245	1.8	1.7		
115-120			0.4							
120-125		5.87		34.80	2.23	252	1.5	2.0		
125-130			0.1							
130-135		5.37		35.00	2.41	261	1.3	2.9		
135-140			0.4							

Table AIV-16

GRAVITY CORES: NWC-G; November 11, 1974; September 16, 1975; October 29, 1975

Pore water (Nov. 11, 1974)								Sept. 16, 1975		Oct. 29, 1975		
Depth (cm)	Ca^{++} (mM)	$SO_4^{=}$ (mM)	Alk (meq/l)	NH_4^{+} (μM)	$HPO_4^{=}$ (μM)	Mn (μM)	Fe (μM)	Depth (cm)	pH	Depth (cm)	pH	pS
0-5	8.31	22.4	3.40	183	58.3	122	1.3	3-8	7.30	30-35	7.38	12.5
5-10	-	22.8	3.21	193	35.5	32.6	0.8					
10-15	7.39	22.1	3.19	192	34.9	31.7	0.8	18-23	7.13	50-55	7.37	12.5
15-20	8.21	(23.2)	3.44	220	37.6	27.7	1.5					
20-25	7.78	21.9	3.75	261	54.0	25.3	1.0	43-48	7.14	80-85	7.36	12.4
25-30	7.78	21.9	4.21	299	71.5	29.7	1.4					
30-35		22.0	4.46	317	74.2	26.2	1.5	68-73	7.18	110-115	7.33	12.6
35-40	8.10	22.0	5.00	354	81.6	25.5	1.3					
40-45	8.06	22.0	5.08	381	79.5	22.2	1.4	78-83	7.15	150-155	7.30	12.9
45-50		21.6	5.26	400	92.7	27.3	2.6					
50-55		21.9	5.70			25.1	1.3	88-93	7.12			
55-60	7.76	21.2	5.98	428	97.8	24.2	1.6					
60-65		21.5	6.01			25.0	1.4	93-98	7.21			
65-70	7.98	21.5	6.15	458	98.6	24.4	2.5					
70-75	8.13	-	6.42	464	103	23.0	2.0	98-103	7.20			
75-80	8.11	21.1	6.68			23.7	1.9					
80-90		20.1	6.60	489	109	21.7	2.0					
90-100	7.66	19.8	7.16	515	109	21.9	1.9					
100-110	7.98	19.6	7.62	574	115	21.5	2.9					
130-140	8.21	17.7	9.66			23.7	3.0					

Table AIV-17

GRAVITY CORE: DEEP-G; November 12, 1975

	Pore water									
Depth (cm)	pH	pS	Cl^- (M)	Ca^{++} (mM)	$SO_4^=$ (mM)	Alk (meq/1)	NH_4^+ (μM)	$HPO_4^=$ (μM)	Mn (μM)	Fe (μM)
0-10		-	0.444	7.78	22.3	3.96	186	53.1	66.3	4.34
10-20	7.22	-	0.447	8.03	22.7	3.72	159	39.4	46.8	1.6
20-30	7.23	-	0.447	7.96	22.8	3.44	159	27.4	21.7	1.7
30-40		-	0.441	8.03	22.4	3.58	156	36.9	28.6	1.1
40-50		-		7.96	22.1	3.95		53.3	46.1	1.0
50-60		-	0.444	8.08	22.1	4.02	163	59.6	47.6	1.3
60-70	7.25	-	0.447	7.93	22.5	3.95	151	57.4	49.5	1.1
70-80	7.20	-		8.03	22.5	4.08	152	66.6	63.2	1.1
90-100		-	0.446	8.08	22.3	3.59	104	54.0	46.6	1.1
100-110		-		8.16	22.4	3.44	95.8	61.5	46.8	0.8

APPENDIX V

FLUX CORE DATA

The t = 0 values given in the data Tables (AV-1-3) represent the initial blank flux box analyses. In some cases not all the data points collected from a flux experiment were used in calculation of the fluxes (see p. 443). When fewer than the total were used in any given case, the particular data used are indicated by asterisks. The justification for ignoring certain points is as follows.

The suspended particle concentration in the water at NWC (July 16, 1975) was extremely high following a storm. The first sampling point was ignored in this case for Mn and Fe since it was thought that as particles settled out the loss due to precipitation would decrease and a more accurate flux rate would be calculated.

The FOAM (March 10, 1976) flux core became slightly disturbed due to a mishap; the resulting resuspension of the surface caused a rapid increase in Mn and $HPO_4^{=}$ in the water overlying the core. A similar increase may have occurred in the case of NH_4^{+} but it could not be delineated from the usual linear (with time) increase. In the case of $HPO_4^{=}$ and Mn, the flux was calculated from the rate of concentration increase above the initial background caused by the disturbance.

Only the first sample (relative to blank) was used in calculation of fall Mn and Fe fluxes at FOAM and DEEP due to the subsequent Fe precipitation in the water overlying the core. For this same reason only the first three points were used for the NWC fall flux calculation.

The first Mn sample at DEEP (July 23, 1975) was used to calculate the summer Mn flux at that station. This was done because the time dependence of the Mn increase in the core water indicated a decreasing Mn flux with time or possible precipitation loss (p. 442). It was decided that the most accurate flux estimate in this case would be to use only the first sample in calculating the rate of Mn increase above sea water concentrations. The initial Fe concentration was too close to background in the summer sample to use just the first sample point in the calculation of Fe flux. This does not necessarily mean that the Fe flux is low (p. 443).

Summer and fall flux boxes were periodically aerated.

Table AV-1

Flux Core Data: FOAM

t (hours)	V_t (liters)	NH_4^+ (μM)	$HPO_4^=$ (μM)	Mn^{++} (μM)	Fe^{++} (μM)
Summer (07/08/75					
0		1.98	1.20	0.2	0.018
5.5	5.31	2.66	1.49	2.00	0.039
16	4.99	6.23	1.88	2.37	0.027
29	4.62	16.6	2.18	6.37	0.081
54	4.30	-	3.36	23.5	0.064
Fall (11/17/75)					
0		0.32	2.81	0.2	0.09
5.6	5.15	1.4	2.87	1.62*	1.6*
23.3	4.78	3.9	3.05	1.8	.02
35.9	4.41	8.93	3.37	3.3	.04
50.8	4.06	13.4	3.59	3.8	.01
Winter-Spring (03/18/76)					
0		0.10	0.68	0.2	-
3	5.97	0.79	1.21^{δ}	2.2^{δ}	-
12.75	5.49	1.58	1.15^{δ}	2.1^{δ}	-
25.25	5.01	3.43	1.23^{δ}	2.0^{δ}	-
48.42	4.54	4.75	1.23*	$2.2^{*\dagger}$	
74.75	4.12	7.38	1.21*	2.9^{*}	-
99.75	3.64	10.0	1.32*	4.1^{*}	-

† = concentration assigned as t = 0 for flux calculation

* = points used in calculation

$^{\delta}$ = resuspension

Table AV-2

Flux Core Data: NWC

t (hours)	V_t (liters)	NH_4^+ (μM)	$HPO_4^=$ (μM)	Mn^{++} (μM)	Fe^{++} (μM)
Summer (07/16/75)					
0		2.4	1.63	0.07	.047
3	5.92	4.58*	1.88*	(2.3)	.066
16	5.58	13.8 *	3.22*	11.3*	.063*
27.5	5.24	-	3.75*	24.2*	.091*
50.5	4.90	64.0*	8.02*	62.7*	.18 *
Fall (10/29/75)					
0		0.2	2.46	1.3†	.032
6.75	4.58	2.6	3.27	2.7	.039*
12.75	4.21	7.3	4.33	8.0	.068*
23	3.84	14.5	5.56	21.3	.287*
35.75	3.48	23.2	6.78	43.7	.077
Winter-Spring (03/23/76)					
0		0.9	1.05	0.07	
3.25	5.34	1.3	1.09	0.34	
12.25	4.98	1.4	1.15	0.43	
33.25	4.61	3.0	1.28	0.62	
49.50	4.24	4.4	1.36	0.84	
100.75	3.87	9.9	-	1.46	
172.75	3.50	-	-	2.22	

† considered high

Table AV-3

Flux Core Data: DEEP

t (hours)	V_t (liters)	NH_4^+ (μM)	$HPO_4^=$ (μM)	Mn^{++} (μM)	Fe^{++} (μM)
Summer (07/23/75)					
0		0.36†	1.15†	0.2†	0.01†
6	5.62	5.4	2.61	7.1*	0.029
22	5.28	6.1	3.34	14.0	0.086
35	4.95	16.0	4.27	18.0	0.13
47.5	4.61	18.4	4.92	24.8	0.37
Fall (11/12/75)					
0		0.14	2.55	0.24	0.018
6.33	4.44	2.6	2.88	4.95*	1.13*
25.33	4.08	4.9	3.04	5	0.14
31.33	3.69	5.8	3.11	5.5	0.14
48.83	3.33	10.1	3.29	6.1	0.063
Winter-Spring (04/13/76)					
0		1.21	0.694	0.16	-
29	3.07	2.25	0.896	0.86	-
48	2.64	3.79	0.996	0.89	-
73	2.21	7.81	1.24	1.16	-
99	1.78	11.8		2.00	-

† = collected at 23m

REFERENCES

Abd-el-Malek, Y. and S. G. Rizk, 1963, Bacterial sulphate reduction and the development of alkalinity. J. Appl. Bact. 26, Part I: 7-13, Part II: 14-19, Part III: 20-26.

Allen, J. A., 1962, Preliminary experiments on the feeding and excretion of bivalves using Phaeodactylum labelled with ^{32}P. J. Mar. Biol. Ass. U.K. 42, 609-623.

Aller, R. C. and R. E. Dodge, 1974. Animal-sediment relations in a tropical lagoon Discovery Bay, Jamaica. J. Mar. Res. 32, 209-232.

Aller, R. C. and J. K. Cochran, 1976, $^{234}Th/^{238}U$ disequilibrium in near-shore sediment: particle reworking and diagenetic time scales. Earth Planet. Sci. Lett. 20, 37-50.

Allman, M. and D. F. Lawrence, 1972, Geological Laboratory Techniques. Arco Publ. Co., N.Y., 336 pp.

Anderson, D. Q., 1939, Distribution of organic matter in marine sediments and its availability to further decomposition. J. Mar. Res. 2, 225-235.

Applequist, M. D., A. Katz, and K. K. Turekian, 1972, Distribution of mercury in the sediments of New Haven (Conn.) Harbor. Environ. Sci. Techn. 6, 1123-1124.

Aston, S. R. and R. Chester, 1973, The influence of suspended particles on the precipitation of iron in natural waters. Estuarine and Coastal Mar. Sci. 1, 225-231.

Ayers, J., 1959, Hydrography of Barnstable Harbor, Massachusetts. Limnol. Oceanogr. 4, 448-462.

Bass Becking, L. G. M., I. R. Kaplan, and D. Moore, 1960, Limits of the natural environment in terms of pH and oxidation-reduction potentials. J. Geol. 68, 243-284.

Bender, M. L., 1971, Does upward diffusion supply the excess manganese in pelagic sediments? J. Geophys. Rev. 76, 4212-4215.

Benninger, L. K., 1976, The uranium-series radionuclides as tracers of geochemical processes in Long Island Sound. Ph.D. Dissertation, Yale University, New Haven, Connecticut, 151 pp.

Benninger, L. K., D. M. Lewis, and K. K. Turekian, 1975, The use of natural Pb-210 as a heavy metal tracer in the river-estuarine system. In: T. M. Church (ed.), Marine Chemistry in the Coastal Environment. ACS Symp. Series, 18, 202-210.

Benninger, L. K., R. C. Aller, J. K. Cochran, and K. K. Turekian, 1976, Lead-210 geochronology of contemporary nearshore sediments: status and problems. EOS, Trans. Am. Geophy. Union 57, 931-932.

Ben-Yaakov, S., 1973, pH buffering of pore water of Recent anoxic marine sediments. Limnol. Oceanogr. 18, 86-94.

Berger, W. H. and G. R. Heath, 1968, Vertical mixing in pelagic sediments. J. Mar. Res. 26, 134-143.

Berner, R. A., 1963, Electrode studies of hydrogen sulfide in marine sediments. Geochim. Cosmochim. Acta 27, 563-575.

Berner, R. A., 1964a, An idealized model of dissolved sulfate distribution in recent sediments. Geochim. Cosmochim. Acta 28, 1497-1503.

Berner, R. A., 1964b, Distribution and diagenesis of sulfur in some sediments from the Gulf of California. Mar. Geol. 1, 117-140.

Berner, R. A., 1967, Thermodynamic stability of sedimentary iron sulfides, Am. Jour. Sci. 265, 773-785.

Berner, R. A., 1969, Migration of iron and sulfur within anaerobic sediments during early diagenesis. Am. Jour. Sci. 267, 19-42.

Berner, R. A., 1970, Sedimentary pyrite formation. Am. Jour. Sci. 268, 1-23.

Berner, R. A., 1971, Principles of Chemical Sedimentology, McGraw-Hill, Inc., New York, 240 pp.

Berner, R. A., 1974a, Kinetic models for the early diagenesis of nitrogen, sulfur, phosphorous and silicon in anoxic marine sediments. In: E. D. Goldberg (ed.), The Sea, Vol. 5, Marine Chemistry. John Wiley and Sons, N.Y. 427-450.

Berner, R. A., 1974b, Iron sulfides in Pleistocene deep Black Sea sediments and their Paleo-oceanographic significance, In: The Black Sea-Geology, Chemistry and Biology, AAPG Memoir 20, 524-531.

Berner, R. A., 1976a, The benthic boundary layer from the viewpoint of a geochemist. In: I. N. McCave (ed.), The Benthic Boundary Layer. Plenum Publ. Corp., N.Y. 33-55.

Berner, R. A., 1976b, Inclusion of adsorption in the modeling of early diagenesis. Earth Planet. Sci. Lett. 29, 333-340.

Berner, R. A. 1976c, The solubility of calcite and aragonite in sea water at atmospheric pressure and 34.5‰ salinity. Am. Jour. Sci. 276, 713-730.

Berner, R. A., M. R. Scott, and C. Thomlinson, 1970, Carbonate alkalinity in the pore waters of anoxic marine sediments. Limnol. Oceanogr. 15, 544-549.

Bétrémieux, R., 1951, Étude expérimentale de l'évolution du fer et du manganese dans les sols. Ann. Agron. Paris 2, 193-295.

Bhat, S. G., S. Krishnaswamy, D. Lal, Rama, and W. S. Moore, $^{234}Th/^{238}U$ ratios in the Ocean. Earth Planet. Sci. Lett. 5, 483-491.

Billen, G., 1975, Nitrification in the Scheldt Estuary (Belgium and the Netherlands). Estuarine and Coastal Mar. Sci. 3, 79-90.

Bloomfield, C., 1972, The oxidation of iron sulphides in soils in relation to the formation of acid sulphate soils and of ochre deposits in field drains. J. Soil Sci. 23, 1-16.

Bokuniewicz, H. J., 1976, Estuarine sediment flux evaluated in Long Island Sound. Ph.D. Dissertation, Yale University, New Haven, Connecticut, 170 pp.

Bokuniewicz, H. J., J. Gebert, and R. B. Gordon, 1976, Sediment mass balance of a large estuary, Long Island Sound. Estuarine and Coastal Mar. Sci. 4, 523-536.

Bonatti, E., D. E. Fisher, O. Joensuu, and H.S. Rydell, 1971, Postdepositional mobility of some transition elements, phosphorous, uranium and thorium in deep sea sediments. Geochim. Cosmochim. Acta 35, 189-201.

Boyle, E., R. Collier, A. T. Dengler, J. M. Edmond, and A. C. Ng, 1974, On the chemical mass-balance in estuaries. Geochim. Cosmochim. Acta 38, 1719-1728.

Bray, J. T., 1973, The behavior of phosphate in the interstitial waters of Chesapeake Bay sediments. Ph.D. Dissertation, The Johns Hopkins University, Baltimore, Md. 149 pp.

Bray, J. T., O. P. Bricker, and B. N. Troup, 1973, Phosphate in interstitial waters of anoxic sediments: oxidation effects during sampling procedure. Science 180, 1362-1364.

Bricker, O. P. and B. N. Troup, 1975, Sediment-water exchange in Chesapeake Bay. In: L. E. Cronin (ed.), Estuarine Research, 1. Chemistry, Biology and the Estuarine System. Academic Press, N.Y. 3-27.

Broecker, W. S., A. Kaufman, and R. M. Trier, 1973, The residence time of thorium in surface sea water and its implications regarding the rate of reactive pollutants. Earth Planet. Sci. Lett. 20, 35-44.

Bromfield, S. M., 1954, Reduction of ferric compounds by soil bacteria. J. Gen. Microbiol. 11, 1-6.

Bromfield, S. M. and D. J. David, 1976, Sorption and oxidation of manganous ions and reduction of manganese oxide by cell suspensions of a manganese oxidizing bacterium. Soil Biol. Biochem. 8, 37-43.

Bubnova, N. P., 1972, The nutrition of the detritus-feeding mollusks Macoma balthica (L.) and Portlandia arctica (Gray) and their influence on bottom sediments. Oceanology 12, 899-905.

Buckley, H. A., A. J. Easton, and L. R. Johnson, 1974, Iron and manganese encrustations in Recent sediments. Nature 249, 436-437.

Calvert, S. E., 1964, Factors affecting distribution of laminated diatomaceous sediments in the Gulf of California. In: T. H. van Andel and G. G. Shor (eds.), Marine geology of the Gulf of California. Am. Assoc. Petroleum Geol. Mem. 3, 311-330

Calvert, S. E. and N. B. Price, 1972, Diffusion and reaction profiles of dissolved manganese in the pore waters of marine sediments. Earth Planet. Sci. Lett. 16, 245-249.

Carriker, M. R., 1967, Ecology of estuarine benthic invertebrates: a perspective. In: A. H. Lauff (ed.), Estuaries. AAAS, 442-487.

Carritt, D. E. and S. Goodgal, 1954, Sorption reactions and some ecological implications. Deep Sea Res. 1, 224-243.

Carslaw, H. S. and J. C. Jaeger, 1959, Conduction of Heat in Solids, Clarendon Press, Oxford, 510 pp.

Cherdyntsev, V. V. 1971, Uranium-234. Keter Press, Jerusalem, Israel, 234 pp.

Chow, T. J., K. W. Bruland, K. K. Bertine, A. Soutar, M. Koide, and E. D. Goldberg, 1973, Lead pollution: records in southern California coastal sediments. Science, 181, 551-552.

Claypool, G. E. and I. R. Kaplan, 1974, The origin and distribution of methane in marine sediments. In: I. R. Kaplan (ed.), Natural Gases in Marine Sediments. Plenum Press, N. W. 99-139.

Cline, J. T. and S. B. Upchurch, 1973, Mode of heavy metal migration in the upper strata of lake sediment. Proc. 16th Conf. Great Lakes Res., Intern. Assoc. Great Lakes Res., 349-356.

Conover, S. A. M., 1956, Oceanography of Long Island Sound, 1952-1954. IV. Phytoplankton. Bull. Bingham Oceanogr. Coll. 15, 62-112.

Cowan, I. R., 1965, Transport of water in the soil-plant-atmosphere system. J. Appl. Ecol. 2, 221-239.

Coyer, P. E. and C. P. Mangum, 1973, Effect of temperature on active and resting metabolism in polychaetes. In: W. Wieser (ed.), Effects of Temperature on Ectothermic Organisms. Springer-Verlag, N.W. 173-180.

Crank, J., 1956, The Mathematics of Diffusion. Clarendon Press, Oxford, 347 pp.

Cullen, D. J., 1973, Bioturbation of superficial marine sediments by interstitial meiobenthos. Nature 242, 323-324.

Dales, R. P., 1955, Feeding and digestion in terebellid polychaetes. J. Mar. Biol. Ass. U.K. 34, 55-79.

Dales, R. P., 1957, Some quantitative aspects of feeding in sabellid and serpulid fan worms. J. Mar. Biol. Ass. U.K. 36, 309-316.

Dales, R. P., 1961a, Oxygen uptake and irrigation of the burrow by three terebellid polychaetes: Eupolymnia, Thelepus, and Neoamphitrite. Physiol. Zool. 34, 306-311.

Dales, R. P., 1961b, Observations on the respiration of sabellid polychaete Schizobranchia insignis. Biol. Bull. 121, 82-91.

Dales, R. P., 1964, The coelomocytes of the terebellid polychaete Amphitrite johnstoni. Quart. J. Micro. Sci. 105, 263-279.

Dales, R. P., 1969, Respiration and energy metabolism in annelids. In: M. Florkin and B. Scheer (eds.), Chemical Zoology, Vol. IV. Academic Press, N. Y. 93-109.

Dales, R. P., C. P. Mangum, and J. C. Tichy, 1970, Effects of changes in oxygen and carbon dioxide concentrations on ventilation rhythms in onuphid polychaetes. J. Mar. Biol. Ass. U.K. 50, 365-380.

Dalyell, J. G., 1853, The Powers of the Creator Displayed in the Creation. Vol. 2. London, John Van Woorst. 327 pp.

Dapples, E. C., 1942, The effect of macro-organisms upon near-shore marine sediments. J. Sed. Pet. 12, 118-126.

Darwin, C. R., 1894, The Formation of Vegetable Mould Through the Action of Worms, with Observations on Their Habits. J. Murray, London. (First printing 1881). 328 p.

Davis, R. B., 1974, Stratigraphic effects of tubificids in profundal lake sediments. Limnol. Oceanogr. 19, 466-488.

Dean, W. E. Jr., 1974, Determination of carbonate and organic matter in calcareous sediments and sedimentary rocks by loss on ignition: comparison with other methods. J. Sed. Pet. 44, 242-248.

Degobbis, D., 1973, On the storage of sea water samples for ammonia determination. Limnol. Oceanogr. 18, 146-150.

Delfino, J. J. and G. F. Lee, 1969, Colorimetric determination of manganese in lake waters. Environ. Sci. Techn. 3, 761-764.

Driscoll, E. G., 1975, Sediment-animal-water interaction, Buzzards Bay, Massachusetts. J. Mar. Res. 33, 275-302.

Duff, E. J., 1971, Orthophosphates. Part IV. J. Chem. Soc. A. 1971, 921-926.

Eagle, R. A., 1973, Benthic studies in the south east of Liverpool Bay. Estuarine and Coastal Mar. Sci. 1, 285-299.

Einsele, W., 1938, Über chemische und koloidchemische Vorgänge in Eisenphosphatsystemen unter limnochemischen und limnogeologischen Geisichtspunkten. Arch. Hydrobiol. 33, 361-387.

Elderfield, H., 1976, Manganese fluxes to the oceans. Mar. Chem. 4, 103-132.

Emerson, S., 1976, Early disgenesis in anaerobic lake sediments: chemical equilibria in interstitial waters. Geochim. Cosmochim Acta 40, 925-934.

Emery, K. and S. C. Rittenberg, 1952, Early diagenesis of California basin sediments in relation to origin of petroleum. Bull. Am. Assoc. Petroleum Geol. 36, 735-806.

Ensminger, L. E. and J. E. Gieseking, 1942, Resistance of clay-adsorbed proteins to proteotytic hydrolysis. Soil Sci. 53, 205-209.

Fanning, K. A., and M. E. Q. Pilson, 1974, Diffusion of dissolved silica out of deep-sea sediments. J. Geophys. Res. 79, 1293-1297.

Fenchel, T., 1970, Studies on the decomposition of organic detritus derived from the turtle grass Thalassia testudinum. Limnol. Oceanogr. 15, 14-20.

Fernandez, A. A., C. Sobel, and S. L. Jacobs, 1963, Sensitive method for the determination of submicrogram quantities of manganese and its application to human serum. Anal. Chem. 35, 1721-1724.

Forstner, H. and K. Rutzler, 1969, Two temperature-compensated thermistor current meters for use in marine ecology. J. Mar. Res. 27, 263-271.

Frankenberg, D. and K. L. Smith Jr., 1967, Coprophagy in marine animals. Limnol. Oceanogr. 12, 443-450.

Frey, R. W., 1970a, Environmental significance of Recent marine lebensspuren near Beaufort, North Carolina. J. Paleo. 44, 507-519.

Frey, R. W., 1970b, Trace fossils of Fort Hays Limestone Member of Niobrara Chalk (Upper Cretaceous), west-central Kansas. Kansas Univ. Paleont. Contr., Art. 53, 41 pp.

Gardner, L. R., 1973, Chemical models for sulfate reduction in closed anaerobic marine environments. Geochim. Cosmochim. Acta 37, 53-68.

Gardner, L. R., 1974, Organic versus inorganic trace metal complexes in sulfidic marine waters--some speculative calculations based on available stability constants. Geochim. Cosmochim. Acta 38, 1297-1302.

Gardner, W. R., 1960, Dynamic aspects of water availability to plants. Soil Sci. 89, 63-73.

Garrels, R. M. and C. L. Christ, 1965, Solutions, Minerals and Equilibria, Harper and Row Publ. Inc., N.Y., 450 p.

Gieskes, J. M. and W. C. Rogers, 1973, Alkalinity determination in interstitial waters of marine sediments. J. Sed. Pet. 43, 272-277.

Goldberg, E. D., 1954, Marine geochemistry. 1. Chemical scavengers of the sea. J. Geol. 62, 249-265.

Goldhaber, M. B., 1974, Equilibrium and dynamic aspects of the marine geochemistry of sulfur, Ph.D. Dissertation, University of California, Los Angeles, 399 pp.

Goldhaber, M. B. and I. R. Kaplan, 1975a, Apparent dissociation constants of hydrogen sulfide in chloride solutions. Mar. Chem. 3, 83-104.

Goldhaber, M. B. and I. R. Kaplan, 1975b, Controls and consequences of sulfate reduction rates in recent marine sediments. Soil Sci. 119, 42-55.

Goldhaber, M. B., R. C. Aller, J. K. Cochran, J. K. Rosenfeld, C. S. Martens, and R. A. Berner, 1977, Sulfate reduction, diffusion and bioturbation in Long Island Sound sediments: report of the FOAM group. Am. Jour. Sci. 277, 193-237.

Gordon, D. C. Jr., 1966. The effects of the deposit feeding polychaete Pectinaria gouldii on the intertidal sediments of Barnstable Harbor. Limnol. Oceanogr. 11, 327-332.

Gordon, R. B. and C. C. Pilbeam, 1974, Environmental consequences of dredge spoil disposal in Long Island Sound: Geophysical studies, 1 October 1972-30 September 1973, Rep. to U.S. Army Corps of Engineers, New England Division, Waltham, Mass.

Goto, K., T. Komatsu, and T. Furukawa, 1962, Rapid colorimetric determination of manganese in waters containing iron. Anal. Chim. Acta 27, 331-334.

Graber, R., 1975, $CaCO_3$ saturation in anoxic sediments. Senior Thesis, Yale University, New Haven, Connecticut. 23 pp.

Grassle, J. F. and J. P. Grassle, 1974, Opportunistic life histories and genetic systems in marine benthic polychaetes. J. Mar. Res. 32, 253-284.

Grill, E. V. and F. A. Richards, 1964, Nutrient regeneration from phytoplankton decomposing in sea water. J. Mar. Res. 22, 51-69.

Guinasso, N. L. Jr. and D. R. Schink, Quantitative estimates of biological mixing rates in abyssal sediments. J. Geophys. Res. 80, 3032-3043.

Gunkel, W. and C. H. Oppenheimer, 1963, Experiments regarding the sulfide formation in sediments of the Texas Gulf Coast. In: C. H. Oppenheimer and C. Thomas (eds.), Symposium on Marine Microbiology, C. C. Thomas, Publisher, 674-683.

Hale, S. S., 1975, The role of benthic communities in the nitrogen and phosphorus cycles of an estuary. In: Mineral Cycling in Southeastern Ecosystems. Proc. Symp. at Augusta, Georgia, May 1-3, 1974. ERDA Symp. series. 291-308.

Hallam, A., 1960, Kulindrichnus langi, a new trace-fossil from the Lias. Palaeont. 3, 64-68.

Halvorson, H. O. and Starkey, R. L., 1927, Studies on the transformations of iron in nature. Part II. Concerning the importance of micro-organisms in the solution and precipitation of iron. Soil Sci. 24, 381-402.

Hargrave, B. T., 1970, The effect of a deposit-feeding amphipod on the metabolism of benthic microflora. Limnol. Oceanogr. 15, 21-30.

Harmsen, G. W., 1954, Observations on the formation and oxidation of pyrite in the soil. Plant and Soil 5, 324-348.

Harmsen, K. and N. Van Breemen, 1975b, A model for the simultaneous production and diffusion of ferrous iron in submerged soils. Soil Sci. Soc. Am. Proc. 39, 1063-1068.

Harmsen, K. and N. Van Breemen, 1975a, Translocation of iron in acid sulfate soils: II. Production and diffusion of dissolved ferrous iron. Soil Sci. Soc. Am. Proc. 39, 1148-1153.

Harris, E., 1959, The nitrogen cycle in Long Island Sound. Bull. Bingham Oceanogr. Coll. 17, 31-65.

Harris, E. and G. A. Riley, 1956, Oceanography of Long Island Sound, 1952-1954. VIII. Chemical composition of the plankton. Bull. Bingham Oceanogr. Coll. 15, 315-323.

Hart, M. G. R., 1963, Observations on the source of acid in empoldered mangrove soils: II. Oxidation of soil polysulfides. Plant and Soil 19, 106-114.

Hartwig, E. O., 1974, Physical, chemical, and biological aspects of nutrient exchange between the marine benthos and the overlying water. U. of Calif.--Instit. of Marine Resources Ref. No. 74-14, Sea Grant Publication No. 40. 174 pp.

Haven, D. S. and R. Morales-Alamo, 1966, Aspects of biodeposition by oysters and other invertebrate filter feeders. Limnol. Oceanogr. 11, 487-498.

Hayes, F. R., 1964, The mud-water interface. In: H. Barnes (ed.), Oceanogr. Mar. Biol. Ann. Rev. 2, 121-145.

Hein, J. R. and G. B. Griggs, 1972, Distribution and scanning electron microscope (SEM) observations of authigenic pyrite from a Pacific deep-sea core. Deep Sea Res. 19, 133-138.

Hem, J. D., 1964, Deposition and solution of manganese oxides. U. S. Geol. Survey Water-Supply Paper. 1667-B. 42 pp.

Henriksen, A., 1966, An automated modified formaldoxime method for determining low concentrations of manganese in water containing iron. Analyst 91, 647-651.

Hertweck, G., 1970, The animal community of a muddy environment and the development of biofacies as effected by the life cycle of the characteristic species. In: T. P. Crimes and J. C. Harper (eds.), Trace Fossils, Geol. J. Spec. Issue No. 3, 235-242, Liverpool, Seel House Press.

Hoar, W. S., 1966, General and Comparative Physiology. Prentice-Hall, Inc., Inglewood Cliffs, N.J., 815 pp.

Hoffmann, R. J. and C. P. Mangum, 1970, The function of coelomic cell hemoglobin in the polychaete Glycera dibranchiata. Comp. Biochem. Physiol. 36, 211-228.

Hofmann, H. J., 1971, Precambrian fossils, pseudofossils, and problematica in Canada Geol. Surv. Canada, Bull. 189, 146 pp.

Holdren, G. R. Jr., O. P. Bricker, and G. Matisoff, 1975, A Model for the control of dissolved manganese in the interstitial waters of Chesapeake Bay, in T. M. Church (ed.), Marine Chemistry in the Coastal Environment (ACS Symposium Series 18), American Chemical Society, Wash., D.C., 364-381.

Holdren, G. R. Jr., 1977, Distribution and behavior of manganese in the interstitial waters of Chesapeake Bay Sediments during early diagenesis. Ph.D. Dissertation, The Johns Hopkins University, Baltimore, Md., 191 pp.

Holliday, L. M. and P. S. Liss, 1976, The behaviour of dissolved iron, manganese and zinc in the Beaulieu Estuary, S. England. Estuarine and Coastal Mar. Sci. 4, 349-353.

Howard, J. D. and C. A. Elders, 1970, Burrowing patterns of haustoriid amphipods from Sapelo Island, Georgia. In: T. P. Crimes and J. C. Harper (eds.), Trace Fossils, Geol. J. Spec. Issue No. 3, 243-262, Liverpool, Seel House Press.

Howard, J. D., 1975, The sedimentological significance of trace fossils. In: R. W. Frey (ed.), The Study of Trace Fossils. Springer-Verlag, New York. 131-146.

Hult, J. E., 1969, Nitrogenous waste products and excretory enzymes in the marine polychaete Cirriformis spirobranchia (Moore). Comp. Biochem. Physiol. 31, 15-24.

Imboden, D. M., 1975, Interstitial transport of solutes in non-steady state accumulating and compacting sediments. Earth Planet Sci. Lett. 27, 221-228.

Jacobsen, V. H., 1967, The feeding of the lugworm, Arenicola marina (L.). Quantitative studies. Ophelia 4, 91-109.

Jacobson, R. L. and D. Langmuir, 1974, Dissociation constants of calcite and $CaHCO_3^+$ from 0 to 50°C. Geochim. Cosmochim. Acta 38, 301-318.

Jenne, E. A., 1968, Controls on Mn, Fe, Co, Ni, Cu, and Zn concentrations in soils and water: significant role of hydrous Mn and Fe oxides. Trace Inorganics in Water, Adv. in Chem. Series 73, 337-387.

Johannes, R. E., 1968, Nutrient regeneration in lakes and oceans. Adv. Microbiol. Sea 1, 203-212.

Jones, J. D., 1955, Observations on the respiratory physiology and on the haemoglobin of the polychaete genus Nephthys, with special reference to N. hombergii (Aud. et M. Edw.). J. Exptl. Biol. 32, 110-125.

Jørgensen, B. B. and T. Fenchel, 1974, The sulfur cycle of a marine sediment model system. Mar. Biol. 24, 189-201.

Jørgensen, B. B., 1977, The sulfur cycle of a coastal marine sediment (Linfjorden, Denmark). Manuscript, in press.

Jørgensen, C. B., 1966, Biology of suspension feeding. Intern. Series Monogr. Pure and Applied Biology 27. Pergamon Press. 357 pp.

Jumars, P. A. and K. Fauchald, 1977, Between-community contrasts in successful polychaete feeding strategies. In: B. C. Coull (ed.), Ecology of Marine Benthos, Belle W. Baruch Library in Marine Science No. 6, U. of S. Carolina Press, Columbia (in press).

Kalil, E. K. and M. Goldhaber, 1973, A sediment squeezer for removal of pore waters without air contact. J. Sed. Pet. 43, 553-557.

Kamp-Nielsen, L., 1974, Mud-water exchange of phosphate and other ions in undisturbed sediment cores and factors affecting the exchange rates. Arch. Hydrobiol. 73, 218-237.

Kaplan, I. R., K. O. Emery, and S. C. Rittenberg, 1963, The distribution and isotopic abundance of sulphur in recent marine sediments off southern California. Geochim. Cosmochim. Acta 27, 297-331.

Kessick, M. A. and J. J. Morgan, 1975, Mechanism of autoxidation of manganese in aqueous solution. Environ. Sci. Techn. 9, 157-159.

Kester, D. R. and R. M. Pytkowicz, 1967, Determination of the apparent dissociation constants of phosphoric acid in seawater. Limnol. Oceanogr. 12, 243-252.

Kharkar, D. P., K. K. Turekian, and K. K. Bertine, 1968, Stream supply of dissolved silver, molybdenum, antimony, selenium, chromium, cobalt, rubidium, and cesium to the oceans. Geochim. Cosmochim. Acta 32, 285-298.

Kinne, O., 1967, Physiology of estuarine organisms with special reference to salinity and temperature: general aspects. In: G. H. Lauff (ed.), Estuaries, AAAS Conference on Estuaries, Jekyll Island, 1964. 525-540.

Klawe, W. L. and L. M. Dickie, 1957, Biology of the bloodworm, Glycera dibranchiata Ehlers, and its relation to the bloodworm fishery of the Maritime Provinces. Bull. Fish. Res. Bd. Can. 115, 1-37.

Kolthoff, I. M., 1931, The solubilities and solubility products of metallic sulfides in water, J. Phys. Chem. 35, 2711-2721.

Kraeuter, J. N., 1976, Biodeposition by salt-marsh invertebrates. Mar. Biol. 35, 215-223.

Krause, H. R., 1959, Biochemische Untersuchungen über den postmortalen Abbau von totem Plankton unter aeroben und anaeroben Bedingungen, Archiv. fur Hydrobiol. 24, 297-337.

Krauskopf, K. B., 1956, Factors controlling the concentration of thirteen rare metals in sea water. Geochim. Cosmochim. Acta 9, 1-32.

Krauskopf, K. B., 1957, Separation of manganese from iron in sedimentary processes. Geochim. Cosmochim. Acta 12, 61-84.

Labeyrie, L. D., H. D. Livingston, and V. T. Bowen, 1976, Comparison of the distributions in marine sediments of the fallout derived nuclides ^{55}Fe and $^{239, 240}Pu$: a new approach to the chemistry of environmental radionuclides. ERDA/IAEA International Symposium on Transuranium Nuclides in the Environment, San Francisco, 17-21 Nov. 1975, in press.

Lai, T. M. and M. M. Mortland, 1961, Diffusion of ions in bentonite and vermiculite. Soil Sci. Soc. Am. Proc. 25, 353-357.

Latimer, W. M., 1952. Oxidation Potentials Prentice-Hall, N.Y. 392 pp.

Levinton, J., 1972, Stability and trophic structure in deposit-feeding and suspension-feeding communities. Am. Naturalist 106, 472-486.

Levinton, J. S. and R. K. Bambach, 1975, A comparative study of Silurian and recent deposit-feeding bivalve communities. Palebiology 1, 97-124.

Lewin, J. and C. Chen, 1973, Changes in the concentration of soluble and particulate iron in sea water enclosed in containers. Limnol. Oceanogr. 18, 590-596.

Lewis, D. M., 1976, The geochemistry of manganese, iron, uranium, lead-210, and major ions in the Susquehanna River. Ph.D. Dissertation, Yale University, New Haven, Connecticut. 272 pp.

Li, W. C., D. E. Armstrong, J. D. H. Williams, R. F. Harris, and J. K. Syers, 1972, Rate and extent of inorganic phosphate exchange in lake sediments. Soil Sci. Soc. Amer. Proc. 36, 279-285.

Li, Y.-H. and S. Gregory, 1974, Diffusion of ions in sea water and in deep-sea sediments. Geochim. Cosmochim. Acta 38, 703-714.

Li, Y.-H., J. L. Bischoff and G. Mathieu, 1969, The migration of manganese in the Arctic Basin sediments. Earth Planet. Sci. Lett. 7, 265-270.

Lindroth, A., 1938, Studien über die respiratorischen Mechanismen von Nereis virens Sars. Zool. Bidr. Uppsala 17, 367-497.

Linville, H. R., 1903, The natural history of some tube-forming annelids (Amphitrite ornata, Diopatra cuprea). In: G. H. Parker (ed.), Mark Anniv. Vol., Henry Holt and Co., N.Y., 227-235.

Lyman, J., 1965, Apparent dissociation constants of carbonic acid, Appendix Tables VI-VII. In: J. P. Riley and G. Skirrow (eds.), Chemical Oceanography, Vol. 1, Academic Press, N.Y., 651.

Lynn, D. C. and E. Bonatti, 1965, Mobility of manganese in diagenesis of deep-sea sediments. Mar. Geol. 3, 457-474.

MacGinitie, G. E., 1939, The method of feeding of Chaetopterus. Biol. Bull. 77, 115-118.

Mangum, C. P., 1963, Studies of speciation in maldanid polychaetes of the North American Atlantic coast--III. Intraspecific and interspecific divergence in oxygen consumption. Comp. Biochem. Physiol. 10, 335-349.

Mangum, C. P., 1964, Activity patterns in metabolism and ecology of polychaetes. Comp. Biochem. Physiol. 11, 239-256.

Mangum, C. P., S. L. Santos, and W. R. Rhodes, Jr., 1968, Distribution and feeding in the onuphid polychaete, Diopatra cuprea (Bosc). Mar. Biol. 2, 33-40.

Mangum, C. P. and W. Van Winkle, 1973, The response of aquatic invertebrates to declining oxygen conditions. Amer. Zool. 13, 529-541.

Mangum, C. P. and L. E. Burnett, 1975, The extraction of oxygen by estuarine invertebrates. In: F. J. Vernberg (ed.), Physiological Ecology of Estuarine Organisms. Belle W. Baruch Library in Marine Science, No. 3., U. of S. Carolina Press, Columbia. 147-163.

Manheim, F. T., 1965, Manganese-iron accumulations in the shallow marine environment. Narragansett Marine Lab. Univ. Rhode Island Occasional Publ., 3, 217-276.

Manheim, F. T., 1970, The diffusion of ions in unconsolidated sediments. Earth Planet. Sci. Lett. 9, 307-309.

Mann, P. J. G. and J. H. Quastel, 1946, Manganese metabolism in soils. Nature 158, 154-156.

Martens, C. S . and R. C. Harriss, 1970, Inhibition of apatite precipitation in the marine environment by magnesium ions. Geochim. Cosmochim. Acta 34, 621-625.

Martens, C. S. and R. A. Berner, 1974, Methane production in the interstitial waters of sulfate-depleted marine sediments. Science 185, 1167-1169.

Matisoff, G., O. P. Bricker, G. R. Holdren, Jr., and P. Kaerk, 1975, Spatial and temporal variations in the interstitial water chemistry of Chesapeake Bay Sediments. In: T. M. Church (ed.), Marine Chemistry in the Coastal Environment. ACS Sympsoium Series 18, 343-363.

McCall, P. L., 1976, The influence of disturbance on community patterns and adaptive strategies of the infaunal benthos of central Long Island Sound. Ph.D. Dissertation, Yale University, New Haven, Connecticut 198 pp.

McIntosh, W. C., 1894, On certain homes or tubes formed by annelids. Ann. Mag. Nat. Hist. ser. VI, 13, 1-18.

Mead, A. D., 1897, The early development of marine annelids. J. Morph. 13, 227-326.

Meek, B. D., A. L. Page, and J. P. Martin, 1973, The oxidation of divalent manganese under conditions present in tile lines as related to temperature, solid surfaces, micro-organisms, and solution chemical composition. Soil Sci. Soc. Am. Proc. 37, 542-548.

Michard, G., 1971, Theoretical model for manganese distribution in calcareous sediment cores. J. Geophys. Res. 76, 2179-2186.

Mills, K. C., 1974, Thermodynamic data for inorganic sulfides, selenides, and tellurides. Butterworths, London. 845 pp.

Molina, B. F., 1974, A rapid and accurate method for the analysis of calcium carbonate in small samples. J. Sed. Pet. 44, 589-590.

Moore, D. G. and P. C. Scruton, 1957, Minor internal structures of some recent unconsolidated sediments. Amer. Assoc. Petroleum Geol. Bull. 41, 2723-2751.

Moore, E. S. and J. E. Maynard, 1929 a,b,c, Solution, transportation, and precipitation of iron and silica. Econ. Geol. 24, Part I: 272-303, Part II: 365-402, Part III: 506-527.

Moore, H. B., 1931a, The muds of the Clyde Sea area. III. Chemical and physical conditions; rate and nature of sedimentation; and fauna. J. Mar. Biol. Ass. U.K. 17, 325-358.

Moore, H. B., 1931b, The specific identification of faecal pellets. J. Mar. Biol. Ass. U.K. 17, 359-365.

Morgan, J. J., 1964, Chemistry of aqueous manganese II and IV. Ph.D. Dissertation, Harvard University, Cambridge, Massachusetts.

Morgan, J. J., 1967, Chemical equilibria and kinetic properties of manganese in natural waters. In: S. P. Faust and J. V. Hunter (eds.), Principles and Applications of Water Chemistry, John Wiley and Sons, N.Y. 561-622.

Morse, J. W. and R. A. Berner, 1972, Dissolution kinetics of calcium carbonate in sea water. II. A kinetic origin for the lysocline. Am. Jour. Sci. 272, 840-851.

Mortimer, C. H., 1941, The exchange of dissolved substances between mud and water. I and II. J. Ecol. 29, 280-329.

Mortimer, C. H., 1971, Chemical exchanges between sediments and water in the great lakes--speculations on probable regulatory mechanisms. Limnol. Oceanogr. 16, 387-404.

Mortland, M. M. and A. R. Wolcott, 1965, Sorption of inorganic nitrogen compounds by soil materials. In: W. V. Bartholomew and F. E. Clark (eds.), Soil Nitrogen, Agronomy 10, 150-197.

Murata, K. J., 1939, Manganese in river and ocean muds. Am. Jour. Sci. 237, 725-735.

Murray, J. and R. Irvine, 1895, On the manganese oxides and manganese nodules in marine deposits. Trans. Roy. Soc. Edinburgh 37, 721-742.

Murray, J. W., 1975, The interaction of metal ions at the manganese dioxide-solution interface. Geochim. Cosmochim. Acta 39, 505-519.

Muskat, M., 1934, The flow of compressible fluids through porous media and some problems in heat conduction. Physics 5, 71-94.

Muzii, E. O., 1968, A coating membrane in the calcareous tube of serpulids. Pubbl. Staz. Zool. Napoli. 36, 135-137.

Myers, A. C., 1972, Tube-worm-sediment relationships of Diopatra cuprea (Polychaeta: Onuphidae). Mar. Biol. 17, 350-356.

Myers, A. C., 1973, Sediment reworking, tube building, and burrowing in a shallow subtidal marine bottom community: rates and effects, Ph.D. Dissertation, U. of Rhode Island, Kingston, R.I. 117 pp.

Nakai, N. and M. L. Jensen, 1964, The kinetic isotope effect in the bacterial reduction and oxidation of sulfur. Geochim. Cosmochim. Acta 28, 1893-1912.

Nelson, H. M., 1952, Temperature distribution with simultaneous platten and dielectric heating. Brit. Jour. Appl. Phys. 3, 79-86.

Nesis, K. I., 1965, Aspects of the food structure of marine biocoenosis. Oceanology 5, 96-107.

Newell, R. C., 1965, The role of detritus in the nutrition of two marine deposit feeders, the protobranch Hydrobia ulvae and the bivalve Macoma balthica. Proc. Zool. Soc. Lond. 144, 25-45.

Newell, R. C., 1970, Biology of intertidal animals. Elseivier, N. Y. 555 pp.

Neyman, A. A., 1968, Limits to the application of the 'trophic group' concept in benthic studies. Oceanology 8, 149-155.

Nissenbaum, A., M. J. Baedecker, and I. R. Kaplan, 1971, Studies on dissolved organic matter from interstitial water of a reducing marine fjord. Advances in Organic Geochemistry. 427-440.

Nõmmik, H., 1965, Ammonium fixation and other reactions involving a nonenzymatic immobilization of mineral nitrogen in soil. In: W. V. Bartholomew and F. E. Clark (eds.), Soil Nitrogen, Agronomy 10, 198-258.

Norton, S. A. and D. R. Sasseville, 1975, Flux of nutrients by diffusion through the lake sediment-hypolimnion interface for 9 lakes in Maine, U.S.A. Int. Ver. Theor. Angew. Limnol. Verh. 19, 372-381.

Norvell, W. A., 1974, Insolubilization of inorganic phosphate by anoxic lake sediment. Soil Sci. Soc. Amer. Proc. 38, 441-445.

Nriagu, J. O., 1972, Stability of vivianite and ion pair formation in the system $Fe_3(PO_4)_2$-H_3PO_4-H_2O, Geochim. Cosmochim. Acta 36, 459-470.

Nriagu, J. O. and C. I. Dell, 1974, Diagenetic formation of iron phosphates in recent lake sediments, Am. Mineral. 59, 934-946.

Olson, S., 1964, Phosphate equilibrium between reduced sediments and water. Verh. Internat. Verein. Limnol. 15, 333-341.

O'Malley, K. L. and R. C. Terwilliger, 1975, Aspects of nitrogen metabolism in the terebellid polychaete Pista pacifica Berkeley. Comp. Biochem. Physiol. 52A, 367-369.

Oppenheimer, C. H., 1960, Bacterial activity in sediments of shallow marine bays. Geochim. Cosmochim. Acta 19, 244-260.

Parfitt, R. L., R. J. Atkinson, and R. St. C. Smart, 1975, The mechansm of phosphate fixation by iron oxides. Soil Sci. Sco. Am. Proc. 39, 837-641.

Pettibone, M. H., 1963, Marine polychaete worms of the New England region. 1. Aphroditidae through Trochochaetidae. U.S. Nat. Mus. Bull. 227, 1-356.

Picard, G. L. and Felbeck, G. T., 1976, The complexation of iron by marine humic acid. Geochim. Cosmochim. Acta 40, 1347-1350.

Pinck, L. A., R. S. Dyal, and F. E. Allison, 1954, Protein-montmorillonite complexes, their preparation and the effects of soil micro-organisms on their decomposition. Soil Sci. 78, 109-118.

Pomeroy, L. R., E. E. Smith, and C. M. Grant, 1965, The exchange of phosphate between estuarine water and sediments. Limnol. Oceanogr. 10, 167-172.

Presley, B. J., 1971, Techniques for analyzing interstitial water samples. Part I: Determination of selected minor and major inorganic constituents. Initial Rep. Deep Sea Drilling Project. V. 7, part 2, 1749-1755.

Presley, B. J. and I. R. Kaplan, 1968, Changes in dissolved sulfate, calcium, and carbonate from interstitial water of near-shore sediments. Geochim. Cosmochim. Acta 32, 1037-1048.

Prosser, C. L. and F. A. Brown, 1961, Comparative Animal Physiology. W. B. Saunders, Co., Philadelphia-London 688 pp.

Pruden, G. and C. Bloomfield, 1968. The determination of ferrous sulphide in soil, in the presence of ferric oxide. Analyst 93, 532-534.

Purdy, E. G., 1964, Sediments as substrates. In: J. Imbrie and N. D. Newell (eds.), Approaches to Paleoecology, Wiley, N.Y. 238-271.

Rashid, M. A. and J. D. Leonard, 1973, Modifications in the solubility and precipitation behavior of various metals as a result of their interaction with sedimentary humic acid. Chem. Geol. 11, 89-97.

Renfro, W. C., 1973, Transfer of ^{65}Zn from sediments by marine polychaete worms. Mar. Biol. 21, 305-316.

Rhoads, D. C., 1963, Rates of sediment reworking by Yoldia limatula in Buzzards Bay, Massachusetts and Long Island Sound. J. Sed. Pet. 33, 723-727.

Rhoads, D. C., 1967, Biogenic reworking of intertidal and subtidal sediments in Barnstable Harbor and Buzzards Bay, Massachusetts. J. Geol. 75, 461-476.

Rhoads, D. C., 1974, Organism-sediment relations on the muddy sea floor. In: H. Barnes (ed.), Oceanogr. Mar. Biol. Ann. Rev. 12, 263-300.

Rhoads, D. C. and D. J. Stanley, 1965, Biogenic graded bedding. J. Sed. Pet. 35, 956-963.

Rhoads, D. C. and D. K. Young, 1970, The influence of deposit-feeding organisms on sediment stability and community trophic structure. J. Mar. Res. 28, 150-178.

Rhoads, D. C. and A. Michael, 1974, Summary of benthic biologic sampling in central Long Island Sound and New Haven Harbor (prior to dredging and dumping), July 1972-August, 1973, Rep. to U.S. Army Corps. of Engineers, New England Division, Waltham, Mass.

Rhoads, D. C., R. C. Aller, and M. B. Goldhaber, 1977, The influence of colonizing macrobenthos on physical properties and chemical diagenesis of the estuarine seafloor. In: B. C. Coull (ed.), Ecology of marine benthos. Belle W. Baruch Library in Marine Science, No. 6., U. of S. Carolina Press, Columbia (in press).

Richards, F. A., 1965, Anoxic basins and fjords. In: J. P. Riley and G. Skirrow (eds.), Chemical Oceanography, Vol. 1, Academic Press, N.Y. 611-645.

Richter, R., 1927, Die fossilien Fährten und Bauten der Würmer, ein Überblick über ihre biologischen Grundformen und deren geologische Bedeutung. Paläont. Zeitschr. 9, 193-240.

Rickard, D. T., 1969, The chemistry of iron sulfide formation at low temperatures. Stockholm. Contr. Geology 20, 67-95.

Rickard, D. T., 1974, Kinetics and mechanism of the sulfidation of goethite. Am. Jour. Sci. 274, 941-952.

Rickard, D. T., 1975, Kinetics and Mechanism of pyrite formation at low temperatures. Am. Jour. Sci. 275, 636-652.

Riley, G. A., 1956a, Oceanography of Long Island Sound, 1952-1954. II. Physical oceanography. Bull. Bingham Oceanogr. Coll. 15, 15-46.

Riley, G. A., 1956b, Oceanography of Long Island Sound, 1952-1954. IX. Production and utilization of organic matter. Bull. Bingham Oceanogr. Coll. 15, 324-344.

Rittenberg, S. C., K. O. Emery, and W. L. Orr, 1955, Regeneration of nutrients in sediments of marine basins, Deep Sea Res. 3, 23-45.

Robbins, J. A. and E. Callender, 1975, Diagenesis of manganese in Lake Michigan sediments. Amer. Jour. Sci. 275, 512-533.

Robbins, J. A. and D. N. Edgington, 1975, Determination of recent sedimentation rates in Lake Michigan using Pb-210 and Cs-137. Geochim. Cosmochim. Acta 39, 285-304.

Robie, R. A., 1966, Thermodynamic properties of minerals. In: S. P. Clark Jr. (ed.), Handbook of physical constants, Geol. Soc. Mem. 97, 437-458.

Röder, H., 1971, Gangsysteme von Paraonis fulgens Levinsen 1883 (Polychaeta) in ökologischer, ethologischer und aktuopaläontologischer Sicht. Senckenbergiana maritima 3, 3-51.

Rosenfeld, J. K. and R. A. Berner, 1976. Ammonia adsorption in nearshore anoxic sediments. Abstracts with prog. Geol. Soc. Am. Annual Meeting 8, 1076.

Rowe, G. T., C. H. Clifford, K. L. Smith, Jr., P. L. Hamilton, 1975, Benthic nutrient regeneration and its coupling to primary productivity in coastal waters. Nature 255, 215-217.

Sanders, H. L., 1956, Oceanography of Long Island Sound, 1952-1954. X. The biology of marine bottom communities. Bull. Bingham Oceanogr. Coll. 15, 345-414.

Sanders, H. L., 1958, Benthic studies in Buzzards Bay. I. Animal-sediment relationships. Limnol. Oceanogr. 3, 245-258.

Sasseville, D. R. and S. A. Norton, 1975, Present and historic geochemical relationships in four Maine lakes. Limnol. Oceanogr. 20, 699-714.

Schäfer, W., 1956, Wirkungen der Benthos-Organismen auf den jungen Schichtverband. Senckenbergiana leth. 37, 183-263.

Schäfer, W., 1962, Aktuo-Paläontologie. Frankfurt am Main, Waldemar Kramer, 666 p. (Ecology and paleoecology of marine environments, G. Y. Craig (ed.), I. Oertel (trans.), Univ. of Chicago Press, 1972, 568 p.)

Schoettle, M. and G. M. Friedman, 1974, Effect of man's activities on distribution of trace elements in sub-bottom sediments of Lake George, New York. Sedimentology 21, 473-478.

Schwarz, A., 1932, Der tierische Einfluss auf die Meeressedimente (besonders auf die Beziehungen zwischen Frachtung, Ablagerund und Zusammensetzung von Wattensedimenten). Senckenbergiana 14, 118-172.

Schweisfurth, R., 1968. Untersuchungen über manganoxydierende und reduzierende Mikroorganismen. Mitl. Int. Verein. Theor. Angen. Limnol. 14, 179-186.

Scott, J. W., 1909, Some egg-laying habits of Amphitrite ornata Verrill. Biol. Bull. 17, 327-340.

Scott, J. W., 1911, Further experiments on the methods of egg-laying in Amphitrite. Biol. Bull. 20, 252-265.

Seilacher, A., 1951, Der Röhrenbau von Lanice conchilega (Polychaeta). Senckenbergiana 32, 267-280.

Seilacher, A., 1964, Biogenic sedimentary structures. In: J. Imbrie and N. Newell (eds.), Approaches to Paleoecology. Wiley, N.Y., 296-316.

Seilacher, A., 1967, Bathymetry of trace fossils. Mar. Geol. 5, 413-428.

Shishkina, O. V., 1964, Chemical composition of pore solutions in oceanic sediments. Geochem. Internat. 3, 522-528.

Shokes, R. F., 1976, Rate dependent distributions of ^{210}Pb and interstitial sulfate in sediments of the Mississippi River delta. Tech. Rep. Ref. 76-1-T. Office Naval Res.

Sholkovitz, E., 1973, Interstitial water chemistry of the Santa Barbara Basin sediments. Geochim. Cosmochim. Acta 37, 2043-2073.

Siever, R., K. C. Beck, and R. A. Berner, 1965, Composition of interstitial waters of modern sediments. J. Geol. 73, 39-73.

Sillén, L. G. and A. E. Martell, 1964, Stability constants of metal-ion complexes. Special Publication #17. The Chemical Society, London, Burlington House, 754 pp.

Simpson, S., 1957, On the trace-fossil Chondrites. Geol. Soc. London, Quart. Jour. 112, 475-499.

Singer, P. C. and W. Stumm, 1970, Acidic mine drainage--the rate determining step. Science 167, 1121-1123.

Solorzano, L., 1969, Determination of ammonia in natural waters by the phenolhypochlorite method. Limnol. Oceanogr. 14, 799-801.

Sorokin, Yu. I., 1962, Experimental investigation of bacterial sulfate reduction in the Black Sea using S^{35}. Mikrobiologiya 31, 402-410.

Spencer, D. W. and P. G. Brewer, 1971, Vertical advection diffusion and redox potentials as controls on the distribution of manganese and other trace metals dissolved in waters of the Black Sea. J. Geophys. Res. 76, 5877-5892.

Stanley, S. M., 1970, Relation of shell form to life habits in the Bivalvia. Geol. Soc. Am. Mem. 125, 296 pp.

Stookey, L. L., 1970, Ferrozine--a new spectrophotometric reagent for iron. Anal. Chem. 42, 779-781.

Strickland, J. D. H. and T. R. Parsons, 1969, A practical handbook of sea water analysis. Canada Fish. Res. Bd. Bull. 167, 311 pp.

Stumm, W. and G. F. Lee, 1961, Oxygenation of ferrous iron. Ind. Eng. Chem. 53, 143-146.

Stumm, W. and P. C. Singer, 1966, J. Sanitary Engineering Div. Am. Soc. Civil Engineers, Proc. Paper 4920.

Stumm W. and J. J. Morgan, 1970, Aquatic Chemistry, John Wiley and Sons, N.Y. 583 pp.

Swedmark, B., 1964, The interstitial fauna of marine sand. Biol. Rev. 39, 1-42.

Sweeney, R. E. and I. R. Kaplan, 1973, Pyrite framboid formation: laboratory synthesis and marine sediments. Econ. Geology. 68, 618-634.

Syers, J. K., R. F. Harris, and D. E. Armstrong, 1973, Phosphate chemistry in lake sediments. J. Environ. Quality 2, 1-14.

Teal, J. M. and J. Kanwisher, 1961, Gas exchange in a Georgia salt marsh. Limnol. Oceanogr. 6, 388-399.

Tessenow, U., 1972, Lösungs-, Diffusions- und Sorptionsprozesse in der Oberschicht von Seesedimenten. I. Arch. Hydrobiol. Suppl. 38, 353-398.

Tessenow, U., 1974, Lösungs-, Diffusions-, und Sorptionsprozesse in der Oberschicht von Seesedimenten. IV. Arch. Hydrobiol. Suppl. 47, 1-79.

Thomson, J., K. K. Turekian, and R. J. McCaffrey, 1975, The accumulation of metals in and release from sediments of Long Island Sound. In: L. E. Cronin (ed.), Estuarine Research, 1. Chemistry, Biology and the Estuarine System, Academic Press, 28-44.

Thorstenson, D. C., 1970, Equilibrium distribution of small organic molecules in natural waters. Geochim. Cosmochim. Acta 34, 745-770.

Thorstenson, D. C. and F. T. Mackenzie, 1974, Time variability of pore water chemistry in recent carbonate sediments, Devil's Hole, Harrington Sound, Bermuda. Geochim. Cosmochim. Acta 38, 1-19.

Tietjen, J. H., 1969, The ecology of shallow water meiofauna in two New England estuaries. Oecologia 2, 251-291.

Trimble, R. B. and H. L. Ehrlich, 1968, Bacteriology of manganese nodules. III. Reduction of MnO_2 by two strains of nodule bacteria. Appl. Microbiol. 16, 695-702.

Troup, B. N., 1974, The interaction of iron with phosphate, carbonate and sulfide in Chesapeake Bay interstitial waters: A thermodynamic interpretation. Ph.D. Dissertation, The Johns Hopkins University, Baltimore, Md., 114 pp.

Troup, B. N., O. P. Bricker, and J. T. Bray, 1974, Oxidation effect of the analysis of iron in the interstitial water of recent anoxic sediments, Nature 249, 237-239.

Trudinger, P. A., 1971, Microbes, metals and minerals. Miner. Sci. Eng. 3, 13-25.

Turekian, K. K., 1976 The fate of metals in estuaries. In: C. B. Officer and P. J. Hart (eds.), Estuaries, geophysics and the environment. Geophysics Research Board, National Academy of Sciences, Washington, D.C. (in press).

Turekian, K. K., 1977, The fate of metals in the oceans. Geochim. Cosmochim. Acta (in press).

Turekian, K. K., J. K. Cochran, D. P. Kharkar, R. M. Cerrato, J. R. Vaisnys, H. L. Sanders, J. F. Grassle, and J. A. Allen, 1975, Slow growth rate of a deep-sea clam determined by ^{228}Ra chronology. Proc. Nat. Acad. Sci. 72, 2829-2832.

Turpaeva, E. D., 1957, Food interrelationships of dominant species in marine benthic biocoenoses. In: B. N. Nikitin (ed.), Trans. Inst. Okeanol., Mar. Biol. Acad. Sci. USSR Press 20, 137-148. (Published in U.S. by Am. Inst. Biol. Sci., Washington, D.C.).

Vaccaro, R. F., 1965, Inorganic nitrogen in sea water. In: J. P. Riley and G. Skirrow (eds.), Chemical Oceanography, Vol. 1, Academic Press, N.Y., 365-408.

Van Breemen, N. and K. Harmsen, 1975, Translocation of iron in acid sulfate soils: I. Soil morphology, and the chemistry and mineralogy of iron in a chronosequence of acid sulfate. Soil Sci. Soc. Am. Proc. 39, 1140-1148.

Vanderborght, J. P., R. Wollast, and G. Billen, 1976, Kinetic models of diagenesis in disturbed sediments. Part I. Mass transfer properties and silica diagenesis. Limnol. Oceanogr., in press.

Van Straaten, L. M. J. U., 1952, Biogene textures and the formation of shell beds in the Dutch Wadden Sea. I, II. Koninkl. Nederl. Akad. Van Wetenschappen. Proc. Series B 55, 500-516.

Vishniac, W., 1965, Bacterial ecologies in limonite. In: M. Florkin (ed.), Life Sciences and Space Research, vol. 3, Wiley, N.Y. 139-141.

Vishniac, W. and M. Santer, 1957. The thiobacilli. Bact. Rev. 21, 195-213.

Vosjan, J. H., 1974, Sulphate in water and sediment of the Dutch Wadden Sea. Neth. J. Sea Res. 8, 208-213.

Waksman, S. A., 1933, On the distribution of organic matter in the sea bottom and the chemical nature and origin of marine humus. Soil Sci. 36, 125-147.

Waksman, S. A. and M. Hotchkiss, 1938, On the oxidation of organic matter in marine sediments by bacteria. J. Mar. Res. 1, 101-118.

Walker, K. R. and R. K. Bambach, 1974, Feeding by benthic invertebrates: classification and terminology for paleoecological analysis. Lethaia, 7, 67-78.

Watson, A. T., 1890, The tube-building habits of Terebella littoralis. J. R. Micr. Soc. 1890, 685-689.

Wells, G. P. and R. P. Dales, 1951, Spontaneous activity patterns in animal behaviour: The irrigation of the burrow in the polychaetes Chaetopterus variopedatus Renier and Nereis diversicolor O. F. Muller. J. Mar. Biol. Ass. U.K. 29, 661-680.

Whitlatch, R. B. and R. G. Johnson, 1974, Methods for staining organic matter in marine sediments. J. Sed. Pet. 44, 1310-1312.

Whitlatch, R. B., 1974, Food--resource partitioning in the deposit-feeding polychaete Pectinaria gouldii. Biol. Bull. 147, 227-235.

Yamanouchi, T., 1927, Some preliminary notes on the behavior of the holothurian, Caudina chilensis (J. Müller). Sci. Rep. Tohoku Univ. (ser. 4) 2, 85-91.

Yingst, J. Y., 1974, The utilization of organic detritus and associated micro-organisms by Parastichopus parvimensis, a benthic deposit-feeding holothurian. Ph.D. Dissertation, U. of S. California, Los Angeles. 154 pp.

Yingst, J. Y., 1977, The relationship of adenosine triphosphate measurements to patterns of micro--and meiofaunal abundance in marine sediment. Mar. Biol. (in press).

Yonge, C. M., 1954, Feeding mechanisms in the invertebrata., Tab. Biologicae, 21, 25-45.

Young, D. K., 1971, Effects of infauna on the sediment and seston of a subtidal environment. Vie et Milieu. Supp. 22, 557-571.

Zapffe, C., 1931, Deposition of manganese. Econ. Geol. 26, 799-832.

Ziegelmeier, E., 1952, Beobachtungen über den Röhrenbau von Lanice conchilega (Pallas) im Experiment und am natürlichen Standort. Helgol. Wiss. Meeresuntersuch. 4, 107-129.

Ziegelmeier, E., 1969, Neue Untersuchungen über die Wohnröhren-Bauweise von Lanice conchilega (Polychaeta, Sedentaria). Helgol. Wiss. Meeresuntersuch. 19, 216-229.

Zobell, C. E. and D. Q. Anderson, 1936, Vertical distribution of bacteria in marine sediments. Bull. Amer. Ass. Petroleum Geol. 20, 258-269.

Zobell, C. E. and S. C. Rittenberg, 1948, Sulfate reducing bacteria in marine sediments. J. Mar. Res. 7, 602-617.

Zola, H., 1967, Sugar phosphate polymers in polychaete tubes and in mineralized animal tissues. Comp. Biochem. Physiol. 21, 179-183.

Zottoli, R. A. and M. R. Carriker, 1974, External release of protease by stationary burrow-dwelling polychaetes. J. Mar. Res. 32, 331-342.